

University Library



Author/Filing Title NORWOOD, A.

Class Mark T

Please note that fines are charged on ALL
overdue items.

FOR REFERENCE ONLY

0403272157





Rapid
Manufacturing
Research Group



Loughborough
University

Faculty of Engineering


Wolfson School of Mechanical and Manufacturing Engineering

Thermal Fatigue of Rapid Tooling Materials

Author

Andrew John Norwood

Thesis to be submitted to Loughborough University for the Degree of Doctor of
Philosophy

	Loughborough University Pilkington Library
Date	JAN 2007
Class	T
Acc No.	04032721572

Contents

Contents	i
Abstract	ix
Acknowledgements	x
Glossary	xi
Nomenclature	xiv
List of Figures	xv
List of Tables	xx
Chapter 1: Introduction and Literature Review	1
1.1 Introduction	1
1.2 Aims	2
1.3 Objectives	3
1.4 Die-Casting and Pressure Die-Casting	3
1.5 Gravity Die-Casting	4
1.6 Pressure Die-Casting	5
1.6.1 Cold Chamber Die-Casting	5
1.6.2 Hot Chamber Die-Casting	6
1.7 Alloys Used for Die-Casting	8
1.7.1 Zinc Alloys	8
1.7.2 Magnesium Alloys	9
1.7.3 Copper Alloys	9
1.7.4 Aluminium Alloys	9
Chapter 2: Die-Casting Dies	12
2.1 Die Design	12
2.2 Conventional Tooling Materials	14
2.2.1 Hot Work Tool Steels	14
2.3 H13 Die Heat Treatment	18
2.3.1 Annealing of H13 Tool Steel	19
2.3.2 Hardenability and Martensite Formation	20
2.3.3 Tempering of H13 Tools Steel	20
Chapter 3: Die Failure	22
3.1 Failure Modes for Dies	22
3.1.1 Erosion	22
3.1.1.1 Oxidation	22
3.1.1.2 Chemical	22
3.1.2 Wear	
3.1.2.1 Abrasive Wear	22
3.1.2.2 Adhesive Wear	23

3.1.3	Thermal Fatigue	24
3.1.4	Cracking of Metals by Thermal Fatigue	24
3.2	Initiation of Cracks	27
3.2.1	Fatigue Fracture	27
3.2.1.1	Initiation of Micro Cracks	29
3.2.1.2	Propagation of Micro Cracks	31
3.3	Key Factors for Improving Thermal Fatigue Life of a Material	31
3.4	Die Life Expectancy	33
3.4.1	Determining Die Failure	34
3.5	Thermal Fatigue Testing	34
3.5.1	Wallace Thermal Fatigue Test	36
3.5.2	Glenny Thermal Fatigue Test	41
3.5.3	Persson Thermal Fatigue Test	42
3.6	Temperature within a Pressure Die-Casting Tool	45
3.7	Crack Detection and Measurement	46
3.7.1	Optical	46
3.7.2	Liquid	46
3.7.3	Magnetic	46
3.7.4	Ultrasonic	47
3.7.5	Gamma Radiography and X-ray Radiography	47
3.7.6	SEM and TEM	47
Chapter 4:	Prototype / Low Volume Tooling for High Pressure Die-Casting	48
4.1	Introduction	48
4.2	Indirect Tooling Methods	48
4.2.1	Cast Tools	49
4.2.2	Metacopy	50
4.2.3	Keltool	51
4.2.4	Rapid Solidification Process	51
4.3	Direct Tooling Methods	52
4.3.1	Laminate Tooling	53
4.3.2	Selective Laser Sintering and Direct Laser Sintering	54
4.3.2.1	Selective Laser Sintering (SLS, 3D Systems)	55
4.3.2.2	DirectMetal Laser Sintering (DMLS, EOS GmbH)	57
4.3.3	Other Tooling Methods	59
4.4	Hypothesis	61
4.5	Methodology	62

Chapter 5:	Initial Work	65
5.1	Selection of Test Materials	65
5.2	Reference Specimen H13	65
5.3	Indirect Die Materials	66
	5.3.1 Metalcopy 5507	66
	5.3.2 Metalcopy Janalloy	68
	5.3.3 Metalcopy Cu	69
5.4	Direct Die Materials	70
	5.4.1 Laminate H13	70
	5.4.2 3D Systems RapidSteel™	71
	5.4.3 EOS GmbH DirectSteel 20µm	73
5.5	Density of the Test Materials	74
	5.5.1 Methodology	74
	5.5.2 Results	76
	5.5.3 Review of Results	76
5.6	Thermal Conductivity Experiment	77
	5.6.1 Methodology	77
	5.6.1.1 Test Apparatus	77
	5.6.1.2 Specimen Preparation	78
	5.6.1.3 Test Procedure	80
	5.6.2 Results	81
	5.6.3 Review of Results	82
 Chapter 6:	 Establishing the Thermal Fatigue System (Parameters, Equipment and Specimens)	 85
6.1	Tool Temperature Recording	85
	6.1.1 Aim	85
	6.1.2 Methodology	85
	6.1.3 Mould Design	85
	6.1.4 Cast Alloy	86
	6.1.5 Die Casting Machine Parameters	87
	6.1.6 Tool Temperature Experiment One	88
	6.1.6.1 Methodology	88
	6.1.6.2 Results	90
	6.1.7 Tool Temperature Experiment Two	91
	6.1.7.1 Methodology	91
	6.1.7.2 Results	91
6.2	Design of Thermal Fatigue Specimen and Apparatus	93
	6.2.1 Specimen	93
	6.2.2 Design of Thermal Fatigue Apparatus	94

6.3	Cooling Tank	95
6.4	Reproducing the Thermal Cycle	97
6.4.1	Manufacturing of H13 Specimens	97
6.4.2	H13 Heat Treatment	97
6.4.3	Thermal Cycle Methodology	97
6.4.4	Thermal Profile when Heating Specimens in a Fluidised Bed	98
6.4.4.1	Results	99
6.4.5	Thermal Profile when Heating Specimens in Aluminium	102
6.4.5.1	Methodology	102
6.4.5.2	Results	102
6.4.5.3	Conclusion	103
6.4.6	Thermal Profile when Heating Specimens in Air in the Furnace	104
6.4.6.1	Methodology	104
6.4.6.2	Results	104
6.4.7	Temperature Simulation Conclusion	106
6.5	Specimen Manufacture	107
6.5.1	Vertical Laminate and Horizontal Laminate Specimen Manufacture	107
6.5.2	Amdry 790 Specimen Manufacture	108
6.5.3	Final Machining	108
6.5.4	Hardness	108
Chapter 7:	Thermal Fatigue Experiment	111
7.1	Aim	111
7.2	Thermal Fatigue Test Methodology	111
7.3	Optical Examination Methodology	111
7.4	H13 Thermal Fatigue Methodology	114
7.4.1	H13 Thermal Fatigue Results	114
7.4.1.1	Initial Signs of Cracking	114
7.4.1.2	Hardness	114
7.4.1.3	Number of Cracks	114
7.5	Metalcopy 5507 Thermal Fatigue Methodology	116
7.5.1	Metalcopy 5507 Thermal Fatigue Results	116
7.5.1.1	Initial Signs of Cracking	116
7.5.1.2	Hardness	116
7.5.1.3	Number of Cracks	116
7.5.1.4	Crack Length	117
7.6	Metalcopy Janalloy Thermal Fatigue Methodology	118
7.6.1	Metalcopy Janalloy Thermal Fatigue Results	118

	7.6.1.1	Initial Signs of Cracking	118
	7.6.1.2	Hardness	119
	7.6.1.3	Number of Cracks	119
	7.6.1.4	Crack Length	120
7.7		Metalcopy Cu Thermal Fatigue Methodology	121
	7.7.1	Metalcopy Cu Thermal Fatigue Results	121
	7.7.1.1	Initial Signs of Cracking	121
	7.7.1.2	Hardness	122
	7.7.1.3	Number of Cracks	122
	7.7.1.4	Crack Length	123
7.8		Vertical Laminate Thermal Fatigue Methodology	124
	7.8.1	Vertical Laminate Thermal Fatigue Results	124
	7.8.1.1	Initial Signs of Cracking	124
	7.8.1.2	Hardness	124
	7.8.1.3	Number of Cracks	124
	7.8.1.4	Crack Length	125
7.9		Horizontal Laminate Thermal Fatigue Methodology	127
	7.9.1	Horizontal Laminate Thermal Fatigue Results	127
	7.9.1.1	Initial Signs of Cracking	127
	7.9.1.2	Hardness	128
7.10		Amdry 790 (Solid) Thermal Fatigue Methodology	128
	7.10.1	Amdry 790 (Solid) Thermal Fatigue Results	128
	7.10.1.1	Initial Signs of Cracking	128
	7.10.1.2	Hardness	129
	7.10.1.3	Number of Cracks	129
	7.10.1.4	Crack Length	130
7.11		Vertical RapidSteel 2.0 Thermal Fatigue Methodology	131
	7.11.1	Vertical RapidSteel 2.0 Thermal Fatigue Results	131
	7.11.1.1	Initial Signs of Cracking	131
	7.11.1.2	Hardness	131
7.12		Horizontal RapidSteel 2.0 Thermal Fatigue Methodology	131
	7.12.1	Horizontal RapidSteel 2.0 Thermal Fatigue Results	131
	7.12.1.1	Initial Signs of Cracking	131
	7.12.1.2	Hardness	131
	7.12.1.3	Number of Cracks	132
	7.12.1.4	Crack Length	132
7.13		EOS DirectSteel 20µm Thermal Fatigue Methodology	134
	7.13.1	EOS DirectSteel 20µm Thermal Fatigue Results	134
	7.13.1.1	Initial Signs of Cracking	134
	7.13.1.2	Hardness	134

	7.13.1.3	Number of Cracks	134
	7.13.1.4	Crack Length	135
Chapter 8:	Post Thermal Fatigue Analysis		137
8.1	Specimen Sectioning and Mounting		137
8.2	H13 Post Thermal Fatigue Results		138
	8.2.1	Crack Initiation and Propagation	138
	8.2.2	EDX Analysis	139
8.3	Metalcopy 5507 Post Thermal Fatigue Results		140
	8.3.1	Crack Initiation and Propagation	140
	8.3.2	EDX Analysis	144
8.4	Metalcopy Janalloy Post Thermal Fatigue Results		145
	8.4.1	Crack Initiation and Propagation	145
	8.4.2	EDX Analysis	147
8.5	Metalcopy Cu Post Thermal Fatigue Results		148
	8.5.1	Crack Initiation and Propagation	148
	8.5.2	EDX Analysis	150
8.6	Vertical Laminate Post Thermal Fatigue Results		151
	8.6.1	Crack Initiation and Propagation	151
	8.6.2	EDX Analysis	153
8.7	Horizontal Laminate Post Thermal Fatigue Results		155
	8.7.1	Crack Initiation and Propagation	155
	8.7.2	EDX Analysis	157
8.8	Amdry 790 Post Thermal Fatigue Results		157
	8.8.1	Crack Initiation and Propagation	157
	8.8.2	EDX Analysis	158
8.9	Horizontal RapidSteel 2.0 Post Thermal Fatigue Results		161
	8.9.1	Crack Initiation and Propagation	161
	8.9.2	EDX Analysis	162
8.10	EOS DirectSteel 20µm Post Thermal Fatigue Results		164
	8.10.1	Crack Initiation and Propagation	164
	8.10.2	EDX Analysis	166
Chapter 9:	Discussion		167
9.1	Overview		167
9.2	The Thermal Cycle of an Aluminium Pressure Die Casting Tool		170
9.3	Reproducing the Temperature Profile of an Aluminium Pressure Die Casting Tool		171
	9.3.1	Effect of Material Structure on Thermal Fatigue	172
9.4	Comparison of Material Performance		175

9.4.1	Initial Signs of Cracking	176
9.4.2	Number of Cracks	176
9.4.3	Crack Length	178
9.4.3.1	Average Crack Length	180
9.5	The Relationship between Material Properties and Thermal Fatigue Life	183
9.5.1	Hardness	183
9.5.2	Density	184
9.5.3	Thermal Conductivity	186
9.5.4	The Effect of the Material Properties and Thermal Fatigue Properties	188
9.5.4.1	Crystal Structure	188
9.5.4.2	Thermal Expansion	188
9.5.4.3	Modulus of Elasticity	189
9.5.4.4	Elongation	190
9.5.4.5	Ultimate Tensile Strength	191
9.5.4.6	Yield Strength	191
9.5.4.7	Poisson's Ratio	192
9.5.5	The Effect of Material Properties on Fatigue Resistance Overview	193
9.5.5.1	Category 1 H13 Tool Steel	193
9.5.5.2	Metalcopy Janalloy, Metalcopy 5507, Metalcopy Cu and RapidSteel 2.0 Materials	194
9.5.5.3	EOS DirectSteel 20µm, Vertical Laminate and Amdry 790 Materials	195
9.6	Methods to Improve Thermal Fatigue Resistance	195
Chapter 10:	Conclusions	197
Chapter 11:	Recommendations for Further Work and the Contribution of this Work to the Body of Knowledge	199
11.1	Recommendations for Further Work	199
11.2	Contribution to the Body of Knowledge	200
References		201

Appendix i	Material Thermal Conductivity and Density	I
Appendix ii	Thermocouple and Temperature Paint Calibration and H13 Heat Treatment	XI
Appendix iii	Bonded Laminate Manufacture	XXV
Appendix iv	Material Flatness	XXXVIII
Appendix v	Thermal Fatigue Experiment Graphs	XLIV
Appendix vi	Papers	LXI

Abstract

Within the field of rapid prototyping a range of metal materials and production techniques have emerged. One field of application which has been addressed is for elevated temperature applications, namely die-casting.

This thesis will investigate a range of rapid tooling materials available at the commencement of the work for use in aluminium pressure die casting.

A series of experiments were conducted to answer the following research questions:-

- To what extent can rapid tooling materials resist thermal cycling and be used as a solution for aluminium pressure die casting?
- If the thermal profile of an aluminium pressure die cast tool can be obtained, can it be simulated? Can the thermal properties, failure mode, and life expectancy of rapid tooling metal materials be determined?
- From the data obtained, is it possible to predict how other rapid tooling or like-materials would behave when subjected to thermal fatigue and can their suitability as a die casting tool material be determined?

The experiments conducted showed that the surface temperature of a die could be obtained from a H13 steel tool running on an aluminium pressure die-casting machine. It was important to determine the temperature profile of the production process to gain an accurate thermal cycle to be simulated. An experimental apparatus was designed and manufactured to simulate the thermal cycle. The apparatus only simulated thermal fatigue as it is the main cause of die failure and determines die life.

Thermal cycling of the materials was conducted to evaluate their performance in die-casting. Crack data was obtained by halting the thermal fatigue test, at predetermined intervals, to examine the specimens optically and measure any cracks. The mechanics / mode of crack initiation and propagation were determined by examining the microstructure of the material after thermal fatigue testing. Understanding these mechanisms may allow material improvements to be made with the aim of increasing their thermal fatigue resistance.

The research highlighted limitations when employing rapid tooling materials in elevated temperature applications. The research demonstrates an assessment method for rapid tooling materials. In addition, the results indicate how a material's composition and structure affect its performance at elevated temperatures. The thermal fatigue test could lead to a new generation of rapid prototyping and tooling materials designed to work at elevated temperatures.

Acknowledgements

I would like to thank Professor Phillip Dickens for giving me the opportunity, guidance, support and motivation throughout the course of this PhD.

I wish to express thanks to all those who have assisted me in my research. This extends from the support received from the technical staff at the Wolfson School of Mechanical and Manufacturing Engineering at Loughborough University, my additional supervisors Dr Rupert Soar and Dr Russell Harris and industrial collaborators (EOS GmbH, 3D Systems, Wiba, IVF Production Engineering Research Inst and Warwick University).

Special recognition goes to Mr Rodney Springthorpe, Mr Robert Temple and Mr Andrew Sandaver whose knowledge, technical skills and assistance have helped me greatly throughout this PhD.

I wish to thank my Mum, Dad and Mr Darren Watts for final proof reading of my thesis.

In addition, I wish to express my appreciation to my family - Mum, Dad, Jenny, Laura, Alice and Sophie. All of who helped me through the years and have given encouragement and the determination to complete this thesis. Particular thanks go to my darling baby daughter Sophie Heather who always has a smile when I need one.

This leaves two family members unmentioned, my beloved Susan whose support, patience and love has driven me and enabled me to complete this thesis and finally, I dedicate this thesis in the memory of my sister Heather Lorraine who tragically died of non-Hodgkin's lymphoma on April 20th 2001 aged 27. We miss you so much.

Glossary

Austenitic Region	–	Region between 912°C and 1,394°C where carbon in steel dissolves into a face-centred cubic structure.
Austenite	–	Face centred cubic solid solution containing up to 2wt% interstitial carbon.
Bainite	–	Microstructure of discrete rounded carbide dispersed in ferrite, obtained by low-temperature isothermal transformation.
Biscuit	–	Excess metal in the shot sleeve of a cold chamber die casting machine. It is part of the casting and is removed from the die with the casting.
Blowholes	–	A blister that has ruptured and may produce a void.
Bolster	–	A tool, or reinforcing part, which supports the backer which, in turn, supports a die against the pressure.
Carbide	–	A compound of carbon with one or more metallic elements.
Craze Cracking	–	Network of cracks often formed in thermal fatigue.
DMLS	–	DirectMetal Laser Sintering.
DXF	–	Data Exchange File, a two-dimensional graphics file format supported by virtually all PC based CAD products.
Eutectic (simple)	–	A thermally reversible reaction (two components are soluble in each other in liquid state, but are insoluble in each other in the solid state).
Eutectoid	–	A thermally reversible reaction (change from one solid structure too another).
Ferrite	–	Body centred cubic solid solution of iron with up to 0.2 % wt. of carbon.
Gate	–	Passage for molten metal that connects the runner with the die cavity.
Gooseneck	–	Spout connecting a metal chamber with a nozzle in the die, through which molten metal is forced. It is the injection mechanism in a hot chamber die casting machine.
Grain	–	Crystals whose geometric shape has been distorted by contact with adjacent crystals so their growth is impeded.
HPDC	–	High Pressure Die Casting.

Hydrogen Embrittlement	–	Absorption of hydrogen at high temperature. It results in hydrogen gas in the atomic structure of the metal. The gas flows to the points of high stress and causes the formation of microscopic cracks.
Hypo-eutectoid	–	A steel with lower carbon content than the eutectoid composition.
Inclusion	–	Usually non-metallic particles contained in metal. In steel they may consist of simple or complex oxides, sulphides, silicates and sometimes nitrides of iron, manganese, silicon, aluminium and other elements. In general they are detrimental to mechanical performance but much depends on the number, their size, shape and distribution.
Insert	–	Segment of a tool with a cavity that is placed in the tool or die; this contains the component geometry.
Isothermal Transformation	–	Transformation with time by holding at a specific temperature.
Lattice	–	The space arrangement of atoms in a crystal structure.
Notch Sensitivity	–	The ability of a metal to withstand the increased stress at a notch.
Pearlite	–	A microstructure of ferrite and lamella carbide of eutectic composition.
Phase	–	A physically homogeneous part of a material system.
Phases	–	Different metal grains in an alloy.
Plunger	–	Ram or piston, which forces molten metal into a die.
Precipitate	–	A precipitated solid substance in suspension or after settling or filtering.
Pro-eutectoid	–	Precipitation from hypoeutectic austenite above the eutectoid temperature.
Rapid Manufacturing	–	The direct use of layer manufacturing technologies to produce final products.
Rapid Prototyping	–	Additive layer-by-layer prototyping technology.
Rapid Tooling	–	Method of fabricating tools quickly or using a rapid prototyping process. Rapid tooling may be direct or indirect methods: In direct methods, the part fabricated by the RP machine itself is used as the tool. In indirect methods, the part fabricated by the RP machine is used as a pattern in a secondary process.
Sintering	–	The process of bonding adjacent surfaces of particles in a powder by heating.

SLS

– Selective laser sintering.

Toggle Clamp

– Linkage employed to mechanically multiply pressure when locking the dies of a casting machine.

Nomenclature

A	Cross sectional area	mm ²
α	Coefficient of thermal expansion	m / m·K
ΔL	Change in length	mm or m
ΔT	Temperature difference	°C, °F, °K
$\Delta T / \Delta L$	Thermal gradient	°K / m
E	Modulus of elasticity	N / m ²
Ω	Electrical resistivity	$\mu\Omega\text{m}$
G	Giga	$\times 10^9$
GPa	Giga Pascals	N / m ² $\times 10^9$
k	Kilo	$\times 10^3$
K	Thermal Conductivity	W / m·K
kN	Kilo Newton	N $\times 10^3$
L _o	Original length	m
M	Mega	$\times 10^6$
μ	Micro	$\times 10^{-6}$
M _s	Martensitic start	no units
MPa	Mega Pascals	N / m ² $\times 10^6$
ρ	Density	g / cm ³
Q	Heat passing through	°K
Q / A	Heat Flux	°K / m ²
Ra	Surface roughness Average	μm
T	Degrees Centigrade / Fahrenheit / Kelvin	°C / °F / °K
ν	Poisson's ratio	no units
P	Pressure	kgf / cm ²
<	Less than	no units
>	Greater than	no units
+ / -	Plus or minus	no units
≈	Approximately equal to	no units

List of Figures

Figure 1 - 1	Gravity die-casting	5
Figure 1 - 2	Cold chamber machine (Dynacast, 2004)	5
Figure 1 - 3	Cold chamber die set (Dynacast, 2004)	6
Figure 1 - 4	Hot chamber machine diagram illustrates the plunger mechanism, which is submerged in molten metal (Dynacast, 2004)	7
Figure 1 - 5	Hot chamber die set (Dynacast, 2004)	7
Figure 2 - 1	Typical die design	12
Figure 2 - 2	Die designs (NADCA, 2006)	13
Figure 2 - 3	Tempering chart (Timken, 2004)	21
Figure 3 - 1	Thermal shock (Badger Metals, 2003)	24
Figure 3 - 2	Extrusions and intrusions bands (University of Groningen, 2006)	28
Figure 3 - 3	Thermal fatigue specimen and test equipment (Wallace et.al., 2000)	37
Figure 3 - 4	(A) Fluidised bed test equipment (Glenny et.al., 1959); (B) Thermal fatigue test specimen (measurements in inches)	41
Figure 3 - 5	(A) Location of the four temperature measurement probes; (B) Casting; (C) Schematic of the probe (Persson et.al., 2004 ^b)	42
Figure 3 - 6	Typical temperature profiles; (A) Whole temperature profile; (B) Close-up (Persson et.al., 2004 ^b)	43
Figure 3 - 7	Schematic of Persson thermal fatigue test (Persson, 2004)	43
Figure 3 - 8	Persson thermal fatigue test equipment (Persson, 2004)	44
Figure 4 - 1	Metalcopy process	50
Figure 4 - 2	RSP process (RSP Tooling, 2004)	52
Figure 4 - 3	3D model of die halves	53
Figure 4 - 4	Individual DXF file output (profile of one laminate)	53
Figure 4 - 5	DTM (now 3D Systems Vanguard) laser sintering system (3D Systems, 2004)	56
Figure 4 - 6	3D DTM (now 3D Systems) LaserForm™ sintering and infiltration furnace (3D Systems, 2004)	56
Figure 4 - 7	EOS M250 sintering machine	57
Figure 4 - 8	EOS M250 sintering process	58
Figure 5 - 1	(A) Vertical orientation; (B) Horizontal orientation	72
Figure 5 - 2	Stanton Unimatic model C.L.1	75
Figure 5 - 3	Average material density	76
Figure 5 - 4	Guarded hot plate assembly	77
Figure 5 - 5	Cussons thermal conductivity apparatus model P5687	78
Figure 5 - 6	Self clamping specimen stack inside the dewar vessel	78

Figure 5 - 7	Specimen geometries	79
Figure 5 - 8	Thermal conductivity average results	82
Figure 6 - 1	(A) Moving half of the tool; (B) Clutch housing casting (Supplied by Dyson and Kemlows)	86
Figure 6 - 2	CAD image of 'Dyson' clutch housing	86
Figure 6 - 3	Frech DAK 125 SDV	87
Figure 6 - 4	Casting machine process cycle	88
Figure 6 - 5	Aluminium blow out through thermocouple holes	89
Figure 6 - 6	Location of the thermocouples and temperature paint on the moving half of the tool	89
Figure 6 - 7	Screen dump of LabVIEW data logging software	90
Figure 6 - 8	Graph showing tool surface temperature during casting (biscuit area)	90
Figure 6 - 9	Section of figure 6 - 8 showing tool surface temperature during casting (biscuit area)	91
Figure 6 - 10	Tool temperature review	92
Figure 6 - 11	Aluminium pressure die casting thermal cycle	92
Figure 6 - 12	Disc design (dimensions in mm)	93
Figure 6 - 13	Multiple specimen test arrangement	94
Figure 6 - 14	Thermal fatigue apparatus design	95
Figure 6 - 15	Thermal fatigue apparatus X - Z	95
Figure 6 - 16	Water temperature recording (1hr thermal cycling period)	96
Figure 6 - 17	Tank design; (A) Empty quench tank; (B) Quench tank with agitator on	96
Figure 6 - 18	Thermocouple location in specimen	98
Figure 6 - 19	Graphite air distributor design	99
Figure 6 - 20	Fluidised bed temperature	99
Figure 6 - 21	Fluidised bed temperature profile	100
Figure 6 - 22	Fluidised bed with heated air temperature	101
Figure 6 - 23	Fluidised bed with heated air temperature profile	101
Figure 6 - 24	Aluminium build up after one cycle	102
Figure 6 - 25	Aluminium thermal fatigue temperature	103
Figure 6 - 26	Aluminium temperature profile	103
Figure 6 - 27	Furnace experiment one temperature profile	104
Figure 6 - 28	(A) Furnace temperature profile; (B) Temperature profile from die experiments	104
Figure 6 - 29	Maximum temperature	105
Figure 6 - 30	Furnace experiment two temperature profile	105
Figure 6 - 31	(A) Single fatigue cycle; (B) Desired thermal cycle from die experiments	106
Figure 6 - 32	Furnace experiment two reversed temperature profile	106
Figure 6 - 33	Position of hardness measurements	108

Figure 6 - 34	Specimen hardness before thermal fatigue testing	110
Figure 7 - 1	Example of crack picture and measurement	112
Figure 7 - 2	Example of crack log sheet with specimen in position with cracks 1 - 4 identified	113
Figure 7 - 3	Specimen 2 S2-180K-1-x4	115
Figure 7 - 4	Specimen 4 S4-220K-1-8-x2	115
Figure 7 - 5	Metalcopy 5507 S1-10K-1-x4	116
Figure 7 - 6	Metalcopy 5507 number of cycles versus number of cracks	117
Figure 7 - 7	Metalcopy 5507 number of cycles versus average crack length with maximum - minimum crack length of all cracks	117
Figure 7 - 8	Metalcopy 5507 number of cycles versus total crack length	118
Figure 7 - 9	Metalcopy Janalloy S1-1,500-12-x1	118
Figure 7 - 10	Metalcopy Janalloy number of cycles versus number of cracks	119
Figure 7 - 11	Metalcopy Janalloy number of cycles versus average crack length with maximum - minimum range crack length of all cracks	120
Figure 7 - 12	Metalcopy Janalloy number of cycles versus total crack length	121
Figure 7 - 13	Metalcopy Cu specimen 1 S1-7K-8-x3	121
Figure 7 - 14	Metalcopy Cu number of cycles versus number of cracks	122
Figure 7 - 15	Metalcopy Cu number of cycles versus average crack length with maximum - minimum crack length of all cracks	123
Figure 7 - 16	Metalcopy Cu number of cycles versus total crack length	123
Figure 7 - 17	Vertical laminate specimen 2 S2rs-3K-1-x3	124
Figure 7 - 18	Vertical laminate number of cycles versus number of cracks	125
Figure 7 - 19	Vertical laminate number of cycles versus average crack length with maximum - minimum range	126
Figure 7 - 20	Vertical laminate number of cycles versus total crack length	126
Figure 7 - 21	Horizontal laminate machining defects	127
Figure 7 - 22	Horizontal laminate specimen 3 S3-500-1-x2	127
Figure 7 - 23	Horizontal laminate specimen 1 S1rs-3K-5-x2	128
Figure 7 - 24	Amdry 790 S3rs-3K-5-x5	128
Figure 7 - 25	Amdry 790 number of cycles versus number of cracks	129
Figure 7 - 26	Amdry 790 number of cycles versus average crack length with maximum - minimum range	130
Figure 7 - 27	Amdry 790 number of cycles versus total crack length	130
Figure 7 - 28	Horizontal RapidSteel 2.0 specimen 1 S1-50K-4-x3	131
Figure 7 - 29	Horizontal RapidSteel 2.0 number of cycles versus number of cracks	132
Figure 7 - 30	Horizontal RapidSteel 2.0 number of cycles versus average crack length with maximum - minimum range	133
Figure 7 - 31	Horizontal RapidSteel 2.0 number of cycles versus total crack length	133

Figure 7 - 32	EOS DirectSteel 20µm specimen 4 S4-500-2-x2	134
Figure 7 - 33	EOS DirectSteel 20µm number of cycles versus number of cracks	135
Figure 7 - 34	EOS DirectSteel 20µm number of cycles versus average crack length with maximum - minimum range	136
Figure 7 - 35	EOS DirectSteel 20µm number of cycles versus total crack length	136
Figure 8 - 1	(A) H13-S1-300K-2-x40 crack tip; (B) H13-S1-300K-3-x40	138
Figure 8 - 2	H13 specimen 1, S1-300K-1-x1000 (close up specimen 1, S1-300K-1-x3000)	139
Figure 8 - 3	H13 EDX analysis	140
Figure 8 - 4	Metalcopy 5507 S3-25K-6-x20 showing crack propagating through matrix	141
Figure 8 - 5	Metalcopy 5507 reference specimen S5-25K-3-x20 over etched to reveal structure in the stainless steel	141
Figure 8 - 6	Metalcopy 5507 S3-25K-11-x500	142
Figure 8 - 7	Crack tip showing growth in the matrix and through the steel	142
Figure 8 - 8	Metalcopy 5507 S3-25K-9-x10K	143
Figure 8 - 9	Metalcopy 5507-S3-25K-1	143
Figure 8 - 10	Metalcopy 5507 EDX analysis	144
Figure 8 - 11	(A) Reference specimen S5-0K-2-x10 (not etched); (B) Specimen 3 S3-5K-8-x10 (not etched)	145
Figure 8 - 12	Reference specimen S5-0K-12-x40	145
Figure 8 - 13	(A) Metalcopy Janalloy specimen 3 S3-5K-4-x20K; (B) Metalcopy Janalloy specimen 3 S3-5K-5	146
Figure 8 - 14	(A) Metalcopy Janalloy specimen 3 S3-5K-3-x25K; (B) Metalcopy Janalloy specimen 3 S3-5K-8	147
Figure 8 - 15	Metalcopy Janalloy EDX analysis	148
Figure 8 - 16	(A) Reference specimen 5 S5-0K-3-x20; (B) Specimen 1 S1-25K-8-x40	148
Figure 8 - 17	Reference specimen 5 S5-0K-13-x10K	149
Figure 8 - 18	(A) Metalcopy Cu specimen 1 S1-25K-92; (B) Metalcopy Cu specimen 1 S1-25K-89	149
Figure 8 - 19	Metalcopy Cu specimen 1 S1-25K-91	150
Figure 8 - 20	Metalcopy Cu EDX analysis	151
Figure 8 - 21	Vertical laminate reference specimen 5 S5-5K-4-x20	152
Figure 8 - 22	(A) Vertical laminate specimen 1 S1-5K-5-x20; (B) Vertical laminate reference specimen 5 S5-5K-5-x5	152
Figure 8 - 23	(A) Vertical laminate specimen 1 S1-5K-12-x20; (B) Vertical laminate specimen 1 S1-5K-4-x20	153
Figure 8 - 24	(A) Vertical laminate specimen 1 S1-5K-85; (B) Vertical laminate specimen 1 S1-5K-86	153

Figure 8 - 25	Vertical laminate SEM element spot line	154
Figure 8 - 26	Vertical laminate elemental change across braze	154
Figure 8 - 27	Vertical laminate specimen 4 S4-5K-82	154
Figure 8 - 28	Vertical laminate EDX analysis	155
Figure 8 - 29	Horizontal laminate specimen 5 S5-5K-1-x5	155
Figure 8 - 30	Horizontal laminate specimen 1 S1-5K-9-x5	156
Figure 8 - 31	Horizontal laminate specimen 1 S1-5K-5-x5	156
Figure 8 - 32	Amdry 790 specimen 1 S1-100K-1-x5	157
Figure 8 - 33	Amdry 790 specimen 1 S1-110K-2-x20	157
Figure 8 - 34	Amdry 790 specimen 3 S3-110K-1-x5	158
Figure 8 - 35	(A) S3-110K-1-x10; (B) S3-110K-1-x20; (C) S3-110K-1-x40	158
Figure 8 - 36	Amdry 790 specimen 3 S3-110K-3	159
Figure 8 - 37	Amdry 790 specimen 3 S3-110K-4	159
Figure 8 - 38	Amdry 790 specimen 3 EDX test 1	160
Figure 8 - 39	Amdry 790; (A) Specimen 1 S1-110K-14; (B) Specimen 1 S1-110K-16	160
Figure 8 - 40	Reference specimen 5; (A) S5-0K-1-x5; (B) S5-0K-1-x20; (C) S5-0K-1-x40	161
Figure 8 - 41	Specimen 5; (A) S5-0K-5-x40; (B) S5-0K-1-x40	161
Figure 8 - 42	Horizontal RapidSteel 2.0 specimen 1 S1-100K-5-x5	162
Figure 8 - 43	Horizontal RapidSteel 2.0 specimen 1; (A) S1-100K-6-x20; (B) S1-110K-7-x40	162
Figure 8 - 44	Horizontal RapidSteel 2.0 specimen 1 EDX analysis area test 1	163
Figure 8 - 45	Horizontal RapidSteel 2.0 specimen 1 EDX analysis test 1	163
Figure 8 - 46	Horizontal RapidSteel 2.0 specimen 1 EDX analysis area test 2	164
Figure 8 - 47	EOS DirectSteel 20 μ m specimen 5 S5-5K-4-x10	164
Figure 8 - 48	EOS DirectSteel 20 μ m specimen 5 S5-5K-3-x40	165
Figure 8 - 49	EOS DirectSteel 20 μ m specimen 1 S1-5K-9-x10	165
Figure 8 - 50	EOS DirectSteel 20 μ m specimen 1 S1-5K-87	166
Figure 8 - 51	EOS DirectSteel 20 μ m EDX analysis	166
Figure 9 - 1	Number of cycles versus initial number cracks (log scale)	176
Figure 9 - 2	Number of cycles versus initial the total number of cracks (log scale)	177
Figure 9 - 3	Number of cycles versus the final total number of cracks (log scale)	178
Figure 9 - 4	Number of cycles versus initial total crack length (mm) (log scale)	179
Figure 9 - 5	Number of cycles versus final total crack length (mm) (log scale)	180
Figure 9 - 6	Number of cycles versus initial average crack length (mm) (log scale)	181
Figure 9 - 7	Number of cycles versus final average crack length (mm) (log scale)	181
Figure 9 - 8	Number of cycles versus hardness (HRb) (log scale)	183

List of Tables

Table 1 - 1	Alloys melt temperature versus number of shots (Clegg, 1991)	8
Table 1 - 2	Alloy properties (NADCA, 2006)	9
Table 1 - 3	Characteristics of die casting alloys (NADCA, 2006)	10
Table 1 - 4	Aluminium alloys (Bartley, 1992)	10
Table 1 - 5	LM24 composition	11
Table 2 - 1	Chemical composition and material data of hot work tool steels (Oberg et.al., 1996)	16
Table 2 - 2	Material properties of H11, H12 and H13	17
Table 2 - 3	The most commonly used materials for dies working at elevated temperatures (ASM, 1998)	18
Table 3 - 1	Material classification (ASM, 1996)	29
Table 3 - 2	Steel compositions	38
Table 3 - 3	Ferrous materials	40
Table 3 - 4	Non-ferrous materials	40
Table 3 - 5	Thermal cycles (Persson, 2003)	44
Table 3 - 6	Crack detection methods and resolution (ASM, 1996)	46
Table 4 - 1	RapidSteel™ material data (DTM, 1999)	55
Table 4 - 2	EOS GmbH material data (EOS GmbH, 2005 material data sheet)	58
Table 5 - 1	H13 reference (Oberg, E., et.al., 1996, Shackelford and Alexander, 2001, MatWeb, 2004) and EDS % Wt. composition	65
Table 5 - 2	H13 material properties (Shackelford and Alexander, 2001, Mat web, 2004, Timkin Latrobe Steel, 2004)	66
Table 5 - 3	316L reference (Azom, 2006, Shackelford and Alexander, 2001) and EDS composition	66
Table 5 - 4	Metalcopy 5507 bonding material EDS composition	66
Table 5 - 5	Metalcopy 5507 EDS composition	67
Table 5 - 6	Material properties of 316L grade of stainless steel (Azom, 2006, Sandmeyer Steel, 2005, Matweb, 2004, Shackelford and Alexander, 2001)	67
Table 5 - 7	Material properties of pure silver (Shackelford and Alexander, 2001, Goodfellow, 2005, Environmental Chemistry 2005, Matweb, 2004)	68
Table 5 - 8	Metalcopy Janalloy 316L EDS composition	68
Table 5 - 9	Metalcopy Janalloy bonding material EDS composition	68
Table 5 - 10	Metalcopy Janalloy EDS composition	69
Table 5 - 11	316L EDS composition	69
Table 5 - 12	Metalcopy Cu bonding material EDS composition	69

Table 5 - 13	Metalcopy Cu EDS composition	69
Table 5 - 14	Material properties of pure copper (Shackelford and Alexander, 2001, Goodfellow, 2005, Environmental Chemistry, 2005, Matweb, 2004)	70
Table 5 - 15	Composition of Amdry 790 (Sulzer Metco (UK) Ltd., 1998)	70
Table 5 - 16	Vertical laminate EDS and Vertical laminate H13 EDS composition	71
Table 5 - 17	Material properties of pure nickel (Goodfellow, 2005, Environmental Chemistry 2005, Matweb, 2004)	71
Table 5 - 18	Chemical composition and EDS analysis of phosphor bronze (MatWeb, 2004)	71
Table 5 - 19	RapidSteel™ 2.0 material, bonding material and steel EDS compositions	72
Table 5 - 20	Material data for 90 Cu, 10 Sn phosphor bronze (MatWeb, 2004, Efunda, 2005, Goodfellow, 2005)	73
Table 5 - 21	Material properties of RapidSteel™ 2.0 (DTM Corporation, 1999)	73
Table 5 - 22	Material properties of EOS GmbH materials (supplied by EOS GmbH)	74
Table 5 - 23	EDS analysis of EOS GmbH DirectSteel 20µm	74
Table 5 - 24	Thermal conductivity of 99.9% pure iron	81
Table 5 - 25	Thermal conductivity of H13 tool steel	82
Table 6 - 1	LM24 die-cast properties	86
Table 6 - 2	Casting parameters	88
Table 6 - 3	Specimen hardness prior to thermal fatigue	109
Table 7 - 1	Magnification and conversion factors	113
Table 7 - 2	Metalcopy Janalloy crack initiation rate	120
Table 7 - 3	Vertical laminate crack initiation rate	125
Table 9 - 1	Initial material performance	182
Table 9 - 2	Final material performance	182
Table 9 - 3	Overall thermal fatigue results	183
Table 9 - 4	Initial material performance versus hardness	184
Table 9 - 5	Final material performance versus hardness	184
Table 9 - 6	Overall material performance versus hardness	184
Table 9 - 7	Initial material performance versus density	184
Table 9 - 8	Final material performance versus density	185
Table 9 - 9	Overall material performance versus density	185
Table 9 - 10	Initial material performance versus infiltrant density	185
Table 9 - 11	Final material performance versus infiltrant density	185
Table 9 - 12	Overall material performance versus infiltrant density	186
Table 9 - 13	Powder material and bonding material densities and differences	186

Table 9 - 14	Initial material performance versus thermal conductivity	187
Table 9 - 15	Final material performance versus thermal conductivity	187
Table 9 - 16	Overall material performance versus thermal conductivity	187
Table 9 - 17	Initial material performance versus thermal expansion	188
Table 9 - 18	Final material performance versus thermal expansion	188
Table 9 - 19	Overall material performance versus thermal expansion	188
Table 9 - 20	Initial material performance versus modulus of elasticity	189
Table 9 - 21	Final material performance versus modulus of elasticity	189
Table 9 - 22	Overall material performance versus modulus of elasticity	190
Table 9 - 23	Initial material performance versus elongation	190
Table 9 - 24	Final material performance versus elongation	190
Table 9 - 25	Overall material performance versus elongation	190
Table 9 - 26	Initial material performance versus ultimate tensile strength	191
Table 9 - 27	Final material performance versus ultimate tensile strength	191
Table 9 - 28	Overall material performance versus ultimate tensile strength	191
Table 9 - 29	Initial material performance versus yield strength	192
Table 9 - 30	Final material performance versus yield strength	192
Table 9 - 31	Overall material performance versus yield strength	192
Table 9 - 32	Initial material performance versus poisson's ratio	193
Table 9 - 33	Final material performance versus poisson's ratio	193
Table 9 - 34	Overall material performance versus poisson's ratio	193

Chapter 1: Introduction and Literature Review

1.1 Introduction

It has been identified the die casting industry is seeking innovative methods of die manufacture and increased die performance to maintain a competitive edge in today's market. In addition they are seeking a method to validate dies and produce prototype / short run tooling using identical cast alloy and process to obtain the correct geometric shape and material properties that occurs in the production part (Rooks, 2002^b, Soar, 2000). Traditional prototyping techniques do not use a metal die or represent the process; hence, a prototype component is not a true representation of the production component. A means of manufacturing a cost effective tool capable of resisting the environment is required - a problem requiring a solution.

The first stage off the investigation researched die casting to determine the process's, and alloys cast. Die casting is a process where molten metal is poured / injected into a permanent die (chapter 1). The investigation showed pressure die casting is considered the most detrimental due to the cycle times and temperatures as this produces rapid thermal cycling (Persson et.al., 2004^a, Wallace and Schwam, 1999). Aluminium pressure die casting was seen to be the most commercial process with more occurrences of die failure. It was considered advantageous to choose the most commercial process as the research could have a larger impact on industry. Plus, if a tool material performs well with the aluminium die casting process it is likely to have an increased performance in casting processes with a longer cycle time and lower melting point alloys.

The second stage of the investigation was to ascertain the current die designs, current die materials and their heat treatment to determine how these affect die failure (chapter 2). A tooling solution must be able to generate the same features of a typical die. It was also evident that geometries such as sharp corners and large change in cross section increases die failure and may influence specimen design. The importance of current material alloying was seen to have a significant affect as did heat treatment. It was evident that conventional materials used carbide forming elements to improve material properties and increase die life. However, these materials do fail and there was a need to understand how current materials fail and to see how a material initiated and propagated cracks. Pressure die casting subjects a tool material to an aggressive environment of wear, erosion and thermal fatigue (chapter 3). The literature research showed thermal fatigue is the main cause of die failure, however, it also highlighted that existing test methods did not simulate die casting since the thermal cycles and number of cycles to initiate cracking were not comparable. In addition, information on the thermal cycle within a tool was sparse. The research showed that certain material properties are considered to improve or aid die life. Chapter 3 then continued to discuss crack detection and measurement techniques as thermal fatigue is seen as the main cause of die failure.

Now that an understanding of the die casting process, die design, materials and main cause of tool failure had been established the next stage was to review the rapid tooling processes as they may provide the solution to prototype / low volume tooling for pressure die casting. However, the materials have mainly been used in low temperature tooling applications, (Radstok, 1999, Segal and Campbell, 2001, Klocke et.al., 1995).

These potential tooling methods could provide the industry with:

- Economically viable short run tooling
- Short run tooling for a new niche market
- Prototype tooling under production conditions allowing components to be assessed for fit, function and mechanical properties
- Tool design verification under production conditions to assess tool geometry, part geometry (shrinkage, warping etc.) filling, cooling channels effectiveness / placement and allows design iterations

A literature review of rapid tooling techniques and materials was conducted (chapter 4). It was clear that many rapid tooling materials are constructed from two different alloys and have different microstructures to typical alloys. It was also evident that the material properties were less than favourable (chapters 4 and 5). In addition, previous projects and papers (IMI RADICAL project, IMS Project and the Sony Ericsson project) (Hague, 2001, Harris et.al., 2003^a, Harris et.al., 2003^b, Harris et.al., 2004, Norwood et.al., 2001, Norwood and Soar, 2001, Norwood et.al., 2004, Norwood and Dickens, 2005) showed, that the rapid tooling materials are not capable of withstanding the environment for long periods of time and suffer from thermal fatigue, otherwise known as heat checking or heat cracking. There is a need to understand how and why this failure occurs to improve rapid tooling materials for high temperature applications. This is a hole in the body of knowledge and one that requires an answer; hence, it was decided to thermally fatigue the materials as this is the most detrimental tool failure mode; to answer the research question.

This research would enable the thermal fatigue life for these materials to be determined. The information obtained would give an understanding of the crack initiation and propagation of the materials and enable future material development to improve the thermal fatigue resistance of these material types.

1.2 Aims

The research programme was designed to study the principle mode of failure (thermal fatigue) of high pressure die casting tools. The aim of this work was to determine the mechanism of failure in rapid tooling materials that are subjected to harsh die casting environments and to analyse the material performance, mode of failure and suitability for the application.

1.3 Objectives

The objective of this work was to determine the life expectancy of current rapid tooling materials and their failure mode leading to a method of comparing the materials to predict how similar materials would behave if subjected to thermal fatigue and how thermal fatigue resistance could be improved. This was achieved by:

- Identifying a common die casting process, suitable prototype / low volume tooling materials, die failure modes, thermal fatigue test methods, crack initiation / propagation modes, and a means of crack detection / measurement.
- Determining the temperature in a pressure die casting tool for aluminium parts.
- Simulating the temperature profile of the surface of a die by designing an experiment and manufacturing a test apparatus. (To accomplish this several factors had to be taken into account; specimen geometry, heating and cooling method, and mediums, cycle time etc.).
- Determining the number of cycles to initiate cracks and to observe crack growth by conducting a series of thermal fatigue experiments on rapid tooling materials.
- Understanding how the cracks initiate and propagate through the materials allowing the mode of failure to be established and comparisons made between the performance of different materials.

1.4 Die-Casting and Pressure Die-Casting

In this chapter casting processes and the alloys used are reviewed to determine the process conditions in terms of cycle time, process temperature, thermal gradient etc.

Die-casting is a manufacturing process enabling the production of dimensionally accurate near net shape components with little or no post processing (Liu et.al., 2000). Typically, the cast alloys are zinc, magnesium, aluminium and copper alloys. The advantages of die-casting are:

- The ability to produce near net shapes with closer tolerances than achievable with other mass production casting and forming processes (Oberg et.al., 1996)
- High rates of production with little or no machining required (Oberg et.al., 1996)
- Thinner wall sections possible compared with other casting methods (1mm) (DeGarmo, 1988. Oberg et.al., 1996)
- The production of durable, dimensionally stable parts with good surface finish (3.2 - 0.4 Ra (μm) (DeGarmo, 1988, Oberg et.al., 1996, Street, 1986)
- Dies are capable of producing thousands of identical components within the specified tolerances (DeGarmo, 1988)
- The ability to integrate fastenings, such as bosses and studs, in the die casting to improve assembly productivity (DeGarmo, 1988)
- Less material waste than other processes, for example, machining (DeGarmo, 1988, Oberg et.al., 1996, Street, 1986)

Where many components are required, die-casting is an efficient, cost effective process, it can produce shapes that are not easily machinable or alternatively have to be made as an assembly (Street, 1986). The benefit is significant savings in cost and labour as an assembly line is not required.

Die-casting can be described as a method of producing multiple components, usually non-ferrous, from permanent dies. Processes include gravity die-casting and cold / hot chamber pressure die-casting.

Prior to the development of die-casting all casting processes were based upon expendable moulds in which the metal was cast and when solidified, the mould was destroyed and the casting removed. Sand and investment casting are examples of the expendable mould processes. These processes also produce components of near net shape requiring little or no post machining, and eliminate excessive material waste and finishing costs compared to component manufacture using machining processes. Permanent moulds were introduced where high volumes, reduced shrinkage, improved surface finish, etc., were required (DeGarmo, 1988, Oberg et.al., 1996, Street, 1986).

In die-casting, thousands of components can be manufactured before excessive tool wear / thermal fatigue leads to tool failure. The components produced seldom require finishing with the exception of runners and risers when manufactured by the gravity die casting process (Ray, 1987).

1.5 Gravity Die-Casting

Gravity die-casting employs reusable moulds commonly machined from grey cast iron, tool steel, graphite etc. The mould halves have to be aligned accurately, which can be achieved by employing a bolster in which the die is located or by hinging the mould to ensure accurate and repeatable mould closure. For aluminium die casting the mould is preheated with a gas lance (200°C - 250°C) to reduce the thermal shock on the tool and then molten metal poured into the pouring cup and the mould is filled under gravity alone. The molten metal flows along the runner and fills the component cavity and the risers. The risers allow gas to escape and contain surplus molten metal to feed the component cavity as solidification occurs (Figure 1 - 1). After solidification, the mould is opened and the casting removed, the process is then repeated. Common casting materials are aluminium, magnesium and copper based alloys and the use of graphite moulds enables iron and steel to be cast.

The process produces dimensional accuracy within 0.13mm - 0.25mm over 600mm (DeGarmo, 1988). Selectively heating (cartridge heaters), cooling (cooling channels) or altering the wall thickness of the mould allows directional solidification to be promoted producing near defect free castings. It is possible to produce complex castings using gravity die casting with the use of sand cores or retractable cores to create internal geometries.

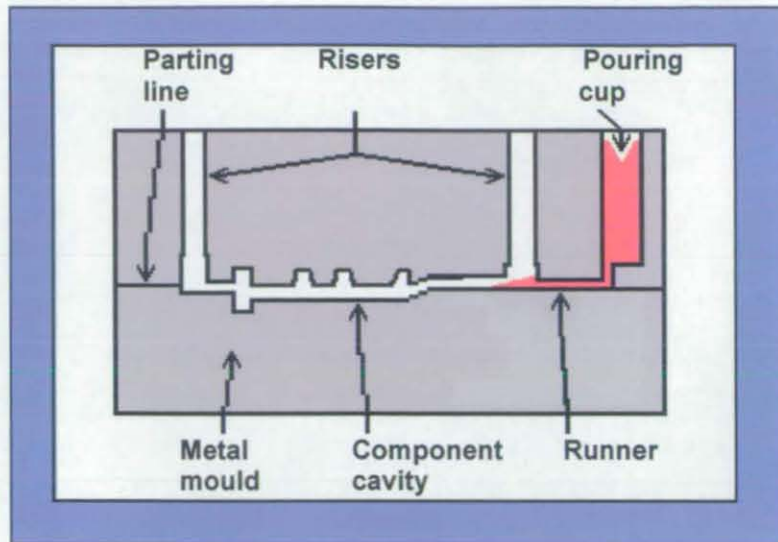


Figure 1 - 1 Gravity die-casting

1.6 Pressure Die-Casting

Pressure die-casting differs from gravity die-casting in that molten metal is forced into a metal die under pressure. It is held under pressure during solidification improving the component's dimensional accuracy, uniformity, repeatability and creating a finer grain structure (Ray, 1987). Pressure die-casting machines require large clamping forces to maintain mould closure during the injection cycle. The forces can stretch 150mm diameter tie bars by 1.15mm on a typical 500 ton machine (Oberg et.al., 1996).

1.6.1 Cold Chamber Die-Casting

Figure 1 - 2 illustrates a cold chamber die-casting machine. Metal is melted in a separate furnace and a measured amount of molten material is transported to the chamber shot sleeve of the machine, usually manually, however, robotic arms are also used.

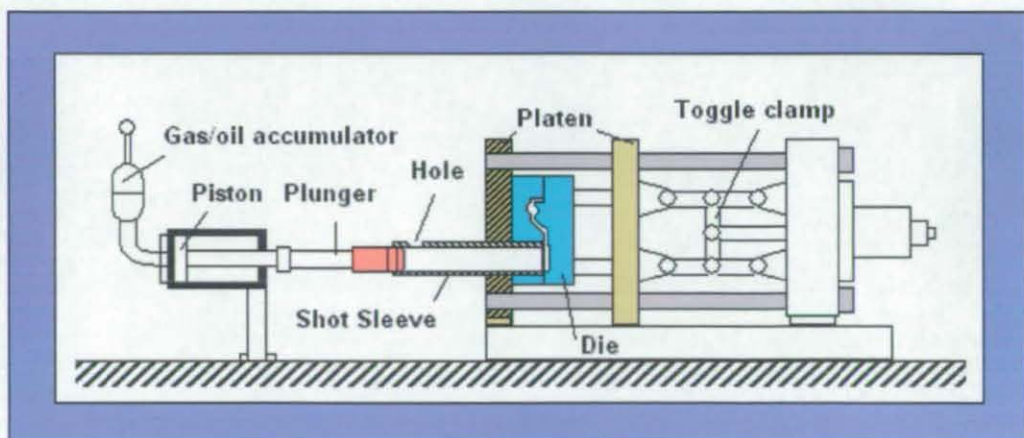


Figure 1 - 2 Cold chamber machine (Dynacast, 2004)

The molten material is forced into the die via a hydraulic plunger / piston (Figure 1 - 3) in three controlled phases producing high quality castings.

- Phase one is termed take up and slowly pushes the aluminium towards the die with minimum turbulence
- Phase two is the injection phase (filling of the die cavity) and has to be is fast enough to prevent chilling whilst the alloy is filling the die. The speed of this phase is approximately 10m/s and typically takes 0.05 - 0.1 seconds; however, velocities can be as high as 100m/s (Chen, 2005). During this phase any gases are expelled via machined vents in the die and through the parting line
- Phase three is the compaction phase, as the alloy solidifies in the cavity it begins to shrink away from the surface of the die. The force applied to the alloy ($50 - 70\text{N/mm}^2$) reduces this effect and reduces the size of inclusions and porosity caused by air, trapped during injection

The process can be used with zinc, magnesium, aluminium and copper based alloys. The cold chamber process has a longer cycle time compared to the hot chamber process because the molten metal has to be transferred to the shot chamber (DeGarmo, 1988).

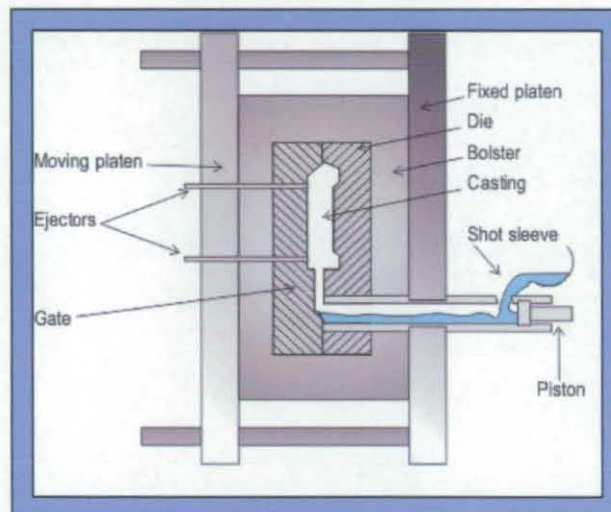


Figure 1 - 3 Cold chamber die set (Dynacast, 2004)

1.6.2 Hot Chamber Die-Casting

Figure 1 - 4 illustrates the hot chamber machine. The term gooseneck refers to the area of the machine that is submerged in a pool of molten metal.

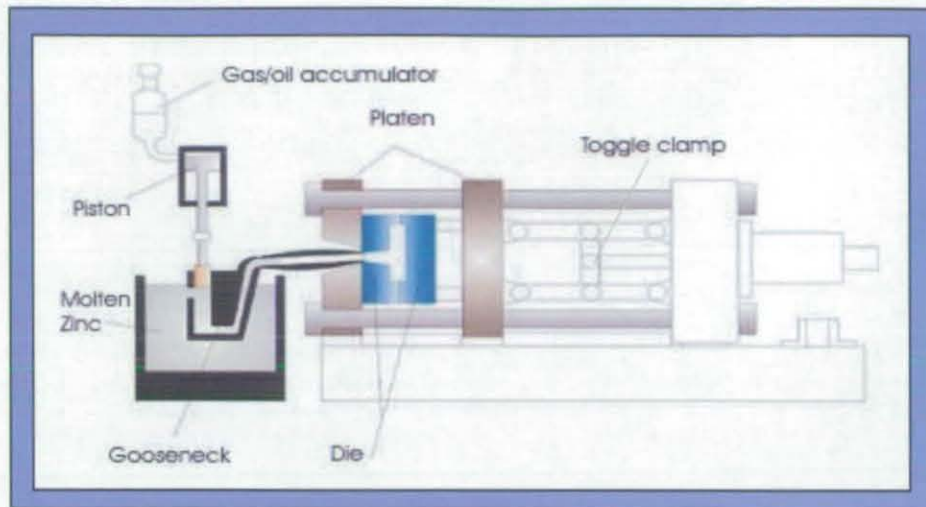


Figure 1 - 4 Hot chamber machine diagram illustrates the plunger mechanism, which is submerged in molten metal (Dynacast, 2004)

Molten metal fills the gooseneck on each cycle; the metal is then forced out of the gooseneck by a mechanical plunger / piston into the die cavity where it solidifies, the die is then opened and the part is ejected and die lubricant applied to the surface to aid part release (Figure 1 - 5). Hot chamber die casting machines are fast and the metal is injected from the same chamber in which it is melted.

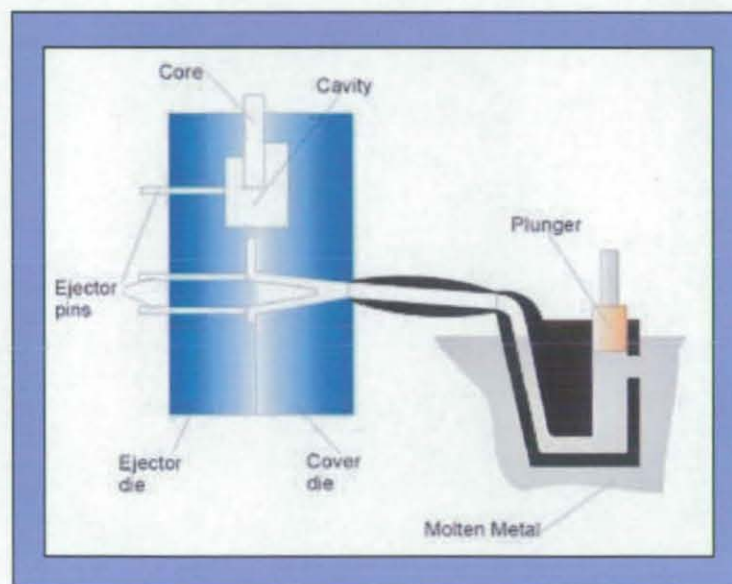


Figure 1 - 5 Hot chamber die set (Dynacast, 2004)

The processes discussed are all common commercial die casting processes. They all subject steel dies to fluctuating temperatures due to the injection of molten metal and then rapid cooling by part ejection and the application of die lubricant. This process causes the die to thermally fatigue and eventually fail, the rate of failure is dependent upon the type of alloy being cast i.e. alloys with high melting point have a greater thermal shock on steel dies. Thermal fatigue is costly for die casters, due to down time, loss of production, conducting die repairs etc. Obtaining

an understanding of how materials perform and fail when subjected to thermal fatigue is important for die casters (Wallace, 1997 and 2000). Dies could be manufactured with die life in mind, for example short run production is becoming increasingly popular and an alternative tooling solution and alternative cheaper materials may be beneficial.

The die casting process with a high thermal fatigue temperature profile, i.e. a process with the greatest fluctuating temperature range and fastest cycle time, is the most detrimental to a die. Hot chamber die casting has the fastest cycle time of the processes due to the lower melting point alloys used (zinc and magnesium) and the automated gooseneck injection system. Since zinc alloys and magnesium alloys have low melting points and processing temperatures, the thermal shock the tool is subjected to is lower. This is reflected in the life expectancy of dies in terms of the number of shots they can take (Table 1 - 1). Gravity die casting typically has slower pouring and solidification times and hence, a slower cycle time. The dies are generally not water cooled and not sprayed with a water based die lubricate, so the thermal profile is not as great as cold chamber pressure die casting. The cold chamber pressure die-casting process, however, can cast aluminium alloys which are injected at 700°C - 750°C depending on the die geometry. The die is typically water cooled and the surface sprayed with water based die lubricant causing thermal shock. It has a fast cycle time and unlike gravity die casting, the tools are subjected to high pressures and increased wear. Cold chamber pressure aluminium die-casting is deemed the worst common casting process in terms of thermal cycle (temperature gradient, speed) and hence, die life. If a material can withstand this thermal cycle then it could be assumed that it can withstand the thermal cycles of the other die casting processes giving a longer die life.

Alloy type	Die life (number of shots)	Pouring temperature (°C)
Aluminium based	100,000	700
Magnesium based	300,000	670
Zinc based	1,000,000	420

Table 1 - 1 Alloys melt temperature versus number of shots (Clegg, 1991)

1.7 Alloys Used for Die-Casting

The alloys used in modern die-casting techniques are zinc, magnesium, copper and aluminium alloys. Each has a particular advantage depending upon the final product environment, geometry, mechanical properties and the quantity requirements (Table 1 - 2 and Table 1 - 3).

1.7.1 Zinc Alloys

Zinc alloys are one of the simplest alloys to cast because of their low melting point and their fluidity in the molten state enabling very intricate shapes to be made. Components can typically be made to closer tolerances and thinner wall sections than when using aluminium. Zinc alloys offer good mechanical properties with high ductility and high impact strength (Table 1 - 2). Die life is good (1,000,000 shots) due to the low casting temperatures of 400°C - 425°C. The hot chamber die casting process lends itself to simple automation and high production rates and the quality of surface finish is high allowing ease of plating and other finishing process.

1.7.2 Magnesium Alloys

Magnesium has an excellent strength (Table 1 - 2) to weight ratio and is the lightest alloy commonly cast, with a density of only 1.74g/cm^3 at 20°C . Magnesium can be cast using either the hot or cold pressure die-casting processes and since it does not dissolve iron, the die life is better than that of aluminium. Magnesium has a lower specific heat and faster solidification rate than aluminium making production, typically, 50% faster. Magnesium, however, has to be processed in an atmosphere of argon, CO_2 , and 2% SF_6 , (Sulphur Hexafluoride) gas or fluxes to prevent oxidation and to exclude oxygen from the surface of the molten metal. The alloys melting temperature is 650°C .

1.7.3 Copper Alloys

These alloys possess high hardness, high corrosion resistance and the highest mechanical properties of alloys cast. They offer excellent wear resistance and dimensional stability, with strength approaching that of steel parts. Typically they are cast at 900°C (NADCA, 2006).

1.7.4 Aluminium Alloys

Aluminium alloys are the most common materials used for die-casting (Davey and Hinduja, 1990) (USA and Europe) because of their high dimensional stability for complex shapes and thin wall sections. They offer corrosion resistance, good mechanical strength (Table 1 - 2), even at high temperatures, and have high thermal and electrical conductivities (NADCA, 2006).

Material Properties	Aluminium	Copper	Magnesium	Zinc
Tensile strength, psi x 1000	47	55	34	41
Yield strength, psi x 100 (0.2 pct offset)	23	30	23	—
Shear strength, psi x 1000	28	37	20	31
Fatigue strength, psi x 1000	20	25	14	7
Elongation, pct in 2 in.	3.50	15	3.0	10
Hardness (Brinell)	80	91	63	82
Specific gravity	2.71	8.30	1.80	6.60
Weight, lb/cu. in.	0.098	0.305	0.066	0.24
Melting point (liquid), $^\circ\text{C}$	600	910	650	400
Thermal conductivity, CG5	0.23	0.21	0.16	0.27
Thermal expansion, in./in./ $^\circ\text{F} \times 10^6$	12.1	12.0	15.0	15.2
Electrical conductivity, pct of copper standard	27	20	10	27
Modulus of elasticity, psi x 10^6	10.3	15	6.5	—
Impact strength (Charpy), ft/lb	3.0	40	2.0	43.0

Table 1 - 2 Alloy properties (NADCA, 2006)

Characteristics of Die Casting Alloys				
	Aluminium	Copper	Magnesium	Zinc
Dimensional stability	Good	Excellent	Excellent	Good
Corrosion resistance	Good	Excellent	Fair	Fair
Casting ease	Good	Fair	Good	Excellent
Part complexity	Good	Fair	Good	Excellent
Dimensional accuracy	Good	Fair	Excellent	Excellent
Die cost	Medium	High	Medium	Low
Machining cost	Low	Medium	Low	Low
Finishing cost	Medium	Low	High	Low
<i>Chart does not intend to compare metals. Its purpose is to show the most advantageous characteristics of each specific metal.</i>				

Table 1 - 3 Characteristics of die casting alloys (NADCA, 2006)

Table 1 - 4 shows a list of aluminium alloys that are used in cold chamber pressure die casting.

Alloy	Freezing range (°C)	Typical Pouring temperature (°C)	Fluidity
LM 2	570 - 525	615 - 700	Good
LM 6	575 - 565	725	Excellent
LM 9	575 - 550	710	Good
LM 12	625 - 525	710	Fair
LM 13	560 - 525	700	Good
LM 20	575 - 565	-	Excellent
LM 24	580 - 520	700	Good
LM 26	580 - 520	700	Good
LM 27	605 - 525	710	Good
LM 28	675 - 520	735	Fair
LM 29	770 - 520	830	Fair
LM 30	650 - 505	760	Good
LM 31	615 - 570	620 - 650	Fair

Table 1 - 4 Aluminium alloys (Bartley, 1992)

The most popular materials are aluminium-silicon-copper alloys, such as LM24 (the composition is shown in Table 1 - 5). Casting temperatures are typically in the region of 650°C - 750°C.

Material	Percentage (%)
Copper	3.0 - 4.0
Magnesium	0.3 Max
Silicon	7.5 - 9.5
Iron	1.3 Max
Manganese	0.5 Max
Nickel	0.5 Max
Zinc	3.0 Max
Lead	0.2 Max
Tin	0.2 Max
Titanium	0.2 Max
Aluminium	Remainder

Table 1 - 5 LM24 composition

The alloy selection is based on the component and the required material properties, i.e. thermal expansion, corrosion resistance, ductility, tensile strength, hardness, heat treatability etc. However, an important factor is the fluidity and castability of the alloy especially for a complex component with thin wall sections (1mm). The most widely cast aluminium alloy for cold chamber casting is LM24, which 'is essentially a pressure die casting alloy, for which it has excellent casting characteristics and is generally a little simpler to die cast than higher silicon containing alloys' (Bartley, 1992).

The next issue to be addressed is the different mould types to determine the general geometry and typical features of a die. From this assessment, features can be incorporated into a specimen design.

Chapter 2: Die-Casting Dies

2.1 Die Design

Die design and material selection is crucial as it affects the performance and the life of dies. A small radius (0.5mm - 1mm) or a large change in the die thickness can cause accelerated thermal fatigue as they act as stress concentrators / crack initiators. Dies must be designed to minimise these features although it is not always possible. The die material and correct heat treatment process is also crucial in prolonging die life.

Dies must also be robust enough to withstand the high pressures applied to them, designed to enable adequate fill rate (speed at which the die is filled with molten metal) and rapid air expulsion through vents. To ensure sound castings are produced it is essential that the gates and vents be positioned correctly.

Pressure die casting dies (Figure 2 - 1) are made of alloy tool steels with at least two sections called the fixed die half and the moving die half. The steels most generally used are low carbon steel-chromium-vanadium and tungsten steels; known as hot work tool steels. The fixed die half is typically the female and is mounted on the side through which the molten metal is injected. The moving die half is typically the male half to which the casting usually shrinks onto and hence, contains the ejectors to push the casting off the die and is mounted on the moveable platen of the machine.

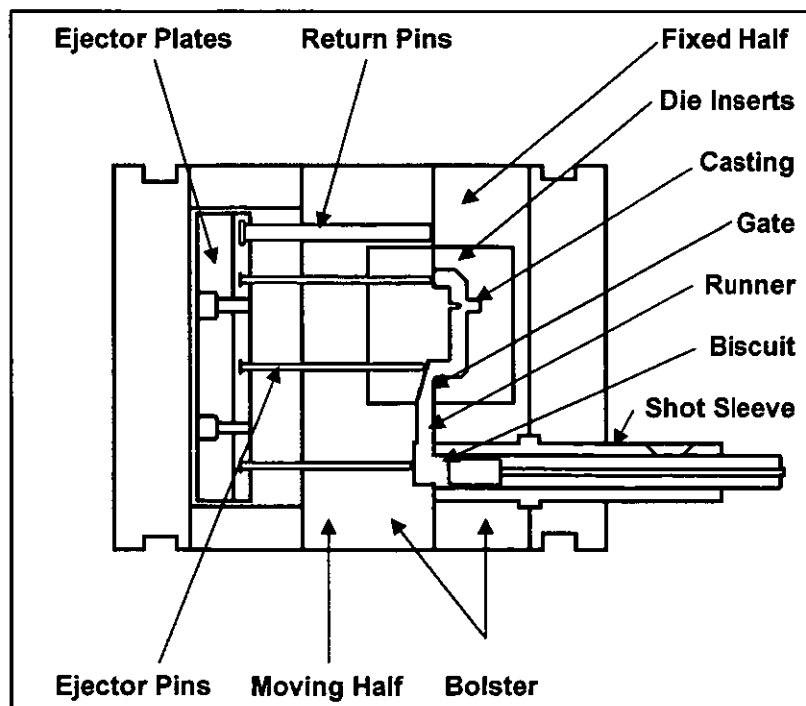


Figure 2 - 1 Typical die design

The fixed half is designed to contain the shot sleeve and biscuit (excess metal in the shot sleeve of a cold chamber die casting machine) through which molten metal enters the die cavity. The moving half usually contains the ejector pins / plates, runners (passage ways) and gates (inlets), which route molten metal to the cavity (or cavities) within the die. Ejection occurs when pins connected to the ejector plate move forward to force the casting off the die; this generally occurs as part of the opening stroke of the machine. Placement of ejector pins must be carefully arranged to prevent the ejection force resulting in deformation of the casting. Pins attached to the ejector plate return it to its casting position as the die closes (some are pushed and some driven). Dies are classified as: single cavity, multiple cavity, combination and unit dies as shown in Figure 2 - 2.

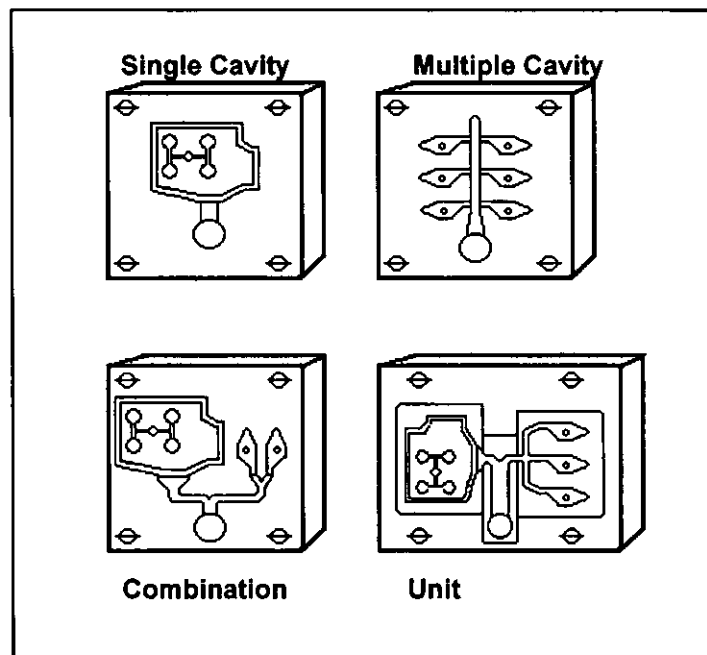


Figure 2 - 2 Die designs (NADCA, 2006)

A single cavity die consists of a single component. Multiple cavity dies have several cavities, which are all identical. If a die has cavities of different shapes, it is called a combination or family die. A combination die is used to produce several parts for an assembly. Unit dies might be used for several parts for an assembly, or for different customer's components. One or more unit inserts are assembled in a common holder and connected by runners to a common biscuit hole; this permits simultaneous filling of all cavities. These replaceable units are designed to be readily removed from the main die frame without the labour intensive removal of the standard frame from the die-casting machine. However, unit dies limit the use of core slides.

Any new tool manufacturing process, such as rapid direct tooling and indirect tooling, must be able to match current tooling design in terms of cavity geometries (deep narrow cavities, small radiuses), die size etc.

A specimen for examining thermal fatigue properties should contain a small radius and varying cross section as these are the most detrimental features in terms of inducing stress in a die. It is also necessary to study current tooling materials and their properties to understand their performance and to select a suitable reference material. In addition, the method of heat treatment needs to be ascertained to enable the reference specimen to have similar properties to that of a die.

2.2 Conventional Tooling Materials

There are many grades of material that are used to produce tooling for the manufacturing industry. Different applications favour certain materials and factors, such as material cost, production run, temperature, forces, die design and material being formed; all play a role in material selection. 'The materials used in tooling are probably the single most critical aspect of manufacture' (Dandy, 1995).

Commercially available materials suited for casting tools include maraging steels, high speed tool steels, hot work tool steels, shock resisting, mould and special-purpose tool steels. These materials are capable of withstanding high loading, elevated temperatures and / or rapidly changing temperatures; they also have good wear resistance and resistance to thermal fatigue.

Material selection in die-casting requires knowledge of the extent and types of forces, the operating conditions, cost etc. (Oberg et.al., 1996). Tool steels are generally heat-treatable making them adaptable to the desired application by altering the material properties. Other factors to be considered are surface hardening, machinability, resistance to de-carbonisation, hot hardness, wear resistance, creep strength, ductility (% elongation), oxidation resistance, low thermal expansion coefficient and high thermal conductivity (Davis, 1995, Allsop and Kennedy, 1983, Norström, 1982). Hot work tool steels are generally used in the manufacture of aluminium pressure die casting dies (Zhu et.al., 2003).

2.2.1 Hot Work Tool Steels

Hot work steels, called group H, have been developed to withstand the combination of heat, pressure and abrasion. Group H steels have a medium carbon content (0.35 - 0.45%). H10 – H19 hot work steels contain chromium, H21 - H26 tungsten and H41 - H43 molybdenum and generally have a low carbon content (Table 2 - 1) (Krauss, 1990, Roberts et.al., 1998). Typically H11, H12 and H13 are used for the manufacture of pressure die cast tooling.

They have good resistance to softening at elevated temperatures due to their medium chromium content and the addition of carbide forming elements such as molybdenum, tungsten and vanadium.

The low carbon and low total alloy contents promote toughness at the normal working hardness of 40HRc - 55HRc. Increasing the tungsten and vanadium alloying elements promotes greater

hot strength at the expense of toughness. Vanadium is added to promote wear resistance and silicon improves oxidation resistance at temperatures up to 800°C (ASM, 1998).

Chromium hot work steels can all be deep hardened; air hardening balances the alloy contents resulting in low distortion during hardening. Since the alloy has a low carbon content, it can also be water-cooled without cracking.

The advantage of H11 over conventional high strength steels is its ability to resist softening during continued exposure to temperatures up to 540°C whilst at the same time retaining moderate toughness and ductility (% elongation). Since H11 has a secondary hardening characteristic it can be tempered at high temperatures, resulting in near complete relief of hardening stresses, which enhances toughness and high strength (ASM, 1998).

Additional benefits of H11, H12, and H13 are ease of forming and working, good weldability, relatively low thermal conductivity, low thermal expansion and resistance to corrosion.

Chromium hot work steels are especially well adapted to hot die work of all kinds, particularly dies for the extrusion of aluminium and magnesium, as well as die casting dies, forging dies, mandrels and hot shears.

Hot-Work Tool Steels																		
Chemical Composition and Material Data																		
AISI	Group			Chromium Types					Tungsten Types						Molybdenum Types			
	Type			H10	H11	H12	H13	H14	H19	H21	H22	H23	H24	H25	H26	H41	H42	H43
% Chemical Elements	C			0.4	0.35	0.35	0.35	0.4	0.4	0.35	0.35	0.35	0.45	0.25	0.5	0.65	0.6	0.55
	W			1.5	5	5	9	11	12	15	15	18	1.5	6
	Mo			2.5	1.5	1.5	1.5	8	5	8
	Cr			3.25	5	5	5	5	5	3.5	2	12	3	4	4	4	4	4
	V			0.4	0.4	0.4	1	1	1	2	2
	Co		
Heat Treatment Data	Hardening Temperature Range °C			1010-1038	996-1024	996-1024	996-1038	1010-1038	1093-1204	1093-1204	1093-1204	1093-1260	1093-1232	1149-1260	1177-1260	1093-1191	1121-1218	1093-1191
	Tempering Temperature Range °C			538-649	538-649	538-649	538-649	538-649	538-704	593-677	593-677	649-816	565-649	565-677	565-677	565-649	565-649	565-649
	Approx Tempered Hardness, (HRc)			56-39	54-38	55-38	53-38	47-40	59-40	54-36	52-39	47-30	55-45	44-45	58-43	60-50	60-50	58-45
Relative Ratings and Properties ('A' = greatest - 'D' = Least)																		
Characteristics in Heat Treatment	Safety in Hardening			A	A	A	A	A	B	B	B	B	B	B	B	C	C	C
	Depth of Hardening			A	A	A	A	A	A	A	A	A	A	A	A	A	A	A
	Resistance to Decarburisation			B	B	B	B	B	B	B	B	B	B	B	B	C	B	C
	Stability of shape in heat treatment	Quench medium	Air or salt	B	B	B	B	C	C	C	C	C	C	C	C	C	C
			Oil	D	D	D	D	D	D	D	D	D	D
Service Properties	Machinability			C/D	C/D	C/D	C/D	D	D	D	D	D	D	D	D	D	D	D
	Hot Hardness			C	C	C	C	C	C	C	C	B	B	B	B	B	B	B
	Wear Resistance			D	D	D	D	D	C/D	C/D	C/D	C/D	C	D	C	C	C	C
	Toughness			C	B	B	B	C	C	C	C	D	D	C	D	D	D	D

Table 2 - 1 Chemical composition and material data of hot work tool steels (Oberg et.al., 1996)

The most important properties required of materials for die-casting tools are resistance to thermal fatigue and to softening at elevated temperatures. Resistance to softening is required to withstand the erosive action of molten metal under high injection pressures and velocities. Additional properties that influence selection of materials for die casting dies are impact resistance, thermal conductivity, machinability and weldability (Table 2 - 2). Availability and cost are additional factors.

Properties	H11	H12	H13
Hardening Temp (°C)	996-1024	996-1024	996-1038
Annealing Temp (°C)	538-649	538-649	538-649
Hardness (HRc)	38-54	38-55	38-53
Impact Resistance (J)	18J @ 25°C	7J @ 25°C, 16J @ 500°F	14J @ 25°C
Thermal Conductivity (W/mK)	24.57 @ 216°C	23 @ 204°C	28.55 @ 416°C
Thermal Expansion (mm/mm/°C x10 ⁻⁶)	9.8 @ 100°C 13.7 @ 600°C	9.8 @ 100°C 13 @ 600°C	10.7 @ 100°C 13.1 @ 600°C

Table 2 - 2 Material properties of H11, H12 and H13

The performance of die casting dies is related to the casting temperature of the work metal, thermal gradients within the dies and the frequency of exposure to high temperature. Tool steels of increasingly higher alloy content are required as the casting temperature increases.

Hot-work tool steels are the most popular materials for die casting dies, in particular H13. Other widely used hot work tool steels include H11, H12, H20, H21 and H22, Din 1.2367 (Thytherm 2367) for high temperature aluminium die-casting $\approx 750^{\circ}\text{C}$ (ASM, 1992).

There are a number of considerations to be addressed when selecting a die material. In order to resist failure, the die material should have a uniform microstructure, no internal defects, good machinability, good surface finish (Novovic et.al., 2004), good response to heat treatment, good toughness, resistance to wear and resistance to thermal fatigue (Table 2 - 3). Such considerations limit the material choice for die manufacture.

H13 is commonly used in industry for the manufacture of aluminium pressure die casting dies (Sjoström and Bergström, 2004, Xiaoxia et.al., 2004, Zhu et.al., 2003). The heat treatment of the material is important as incorrect heat treatment can result in premature die failure. It is therefore necessary to understand the heat treatment of the material to obtain the desired material properties (Worbye, 1985). Understanding the heat treatment may also be beneficial in determining how failure occurs.


Resistance to			
 Increased Resistance	Wear	Thermal Softening	Catastrophic Fracture (Impact Strength, Toughness)
	H26	H26	
	H23	H24	
	H24, A2	H23	H12
	H19, H14	H19	H11
	H21	H21	H10, H13
	H10, H12	H14	A9
	H13		
	A9	H10	H14
	A8		
	H11		A8
		H11	H19, A2
		H12	
		H13, A8	
		A9	H21, H23
			A6
			H24
			H26

Table 2 - 3 The most commonly used materials for dies working at elevated temperatures (ASM, 1998)

2.3 H13 Die Heat Treatment

H13, like many hot work tool steels, has a high chromium (5%) and vanadium (1%) content; these elements control carbide formation. The elements are distributed between carbides and the austenitic matrix during solidification, annealing, hot work and austenitising for hardening. During hardening, the alloy carbides formed in austenite are retained and the austenite matrix transforms to martensite. When tempered further, alloy element partitioning occurs as retained austenite transforms and fine alloy carbides precipitate in tempered martensite. The strength and wear resistance are provided by the chemical elements in the microstructure (retained carbides, tempered martensite and the carbides formed when tempered).

M_7C_3 carbide is mostly found in chromium rich alloy steels, having a hexagonal lattice structure; the carbide is resistant to dissolution at higher temperatures and is hard and abrasion resistant. H13 contains M_7C_3 carbides in equilibrium with austenite at 870°C.

To minimize distortion in complex tools, a double preheat should be employed. Heating should occur at a rate that does not exceed 222°C per hour up to 621°C - 677°C; the temperature is then allowed to stabilise before it is raised to 816°C - 871°C and again allowed to stabilise. For tools not requiring double reheat, the second temperature range can be used as a single preheating treatment. The tool should be soaked for 1 hour per 25mm section thickness.

The tool is then heated rapidly to the austenitising temperature, 982°C - 1032°C, typically in a vacuum furnace, an inert atmosphere furnace (argon) or a salt bath. For maximum toughness, 982°C should be used and for maximum hardness and resistance to thermal fatigue cracking and wear 1032°C, is used. Soaking should occur at this temperature for 15 - 60 minutes depending upon the section. Previous work has shown that different austenising temperatures in the tool steel hardening treatment can result in differences in thermal stability (Sjoström and Bergström, 2004).

The tool is then quenched in air, pressurised gas or warm oil. Tools with a thickness of up to and including 125mm will typically through harden when cooled, in still air, from the austenitising treatment. Sections greater than 127mm in thickness require accelerated cooling by the use of forced air, pressurised gas, or an interrupted oil quench to obtain maximum hardness, toughness and resistance to thermal fatigue cracking.

For pressurised gas quenching, a minimum quench rate of approximately 28°C per minute to below 538°C is required to obtain the optimum properties in the steel. For oil, quench until black, about 482°C, then cool in still air to between 51°C - 66°C.

2.3.1 Annealing of H13 Tool Steel

Annealing is required to alter the microstructure into a condition suitable for machining. The annealing treatment produces a uniformly dispersed microstructure of spheroidised carbides in a matrix of ferrite. In addition, annealing refines coarse grained structures, which may have formed during high temperature processing, i.e. laser cutting, and is achieved by heating the part just above its upper critical temperature and cooling slowly in the furnace allowing recrystallisation to occur.

The coarse particles are primary M_7C_3 carbides, which form during melting and are dispersed during hot work. The finer spheroidised particles are a result of secondary low temperature precipitation.

Annealing is achieved by heating just to the temperature where all ferrite transforms to austenite ($\approx 800^\circ\text{C} - 900^\circ\text{C}$). The material should not be subjected to a heat up rate exceeding 222°C per hour to 857°C - 885°C, the temperature should be held for 1 hour per 25mm of maximum thickness and for a minimum of 2 hours. It should then be cooled slowly in the furnace at a rate not exceeding 28°C per hour to 538°C. Cooling to ambient temperature can be continued in the furnace or in air.

Carbide particles are retained and spheroidised, and the austenite transforms to ferrite and additional spheroidised carbides on cooling. If tool steels are annealed at too high a temperature, the alloy carbides dissolve and the enriched austenite may form carbides on austenitic grain boundaries or transform to pearlite or martensite on cooling. Slow cooling from

the annealing temperatures is essential to ensure that the austenite transforms to ductile ferrite spheroidised carbide microstructures instead of pearlite or martensite.

2.3.2 Hardenability and Martensite Formation

The hardenability of the majority of tool steels is excellent (Oberg et.al., 1996), oil, air or salt quenching is sufficient to produce the required microstructures and properties. Martensite forms in tool steels when cooling conditions and hardenability are sufficient to prevent diffusion controlled transformation to pro-eutectoid carbides, pearlite and bainite. The matrix austenite composition dictates the morphology (lath or plate formation) of the martensite microstructure (ASM, 1992, 1996, 1997).

The retained austenite is present in thin sheets between the parallel martensite laths of the H13 steel. There are many crystallographic variants of martensitic laths formed in a given austenite grain, however, all austenite retained in an austenite grain has the same orientation despite its appearance within the martensite. The austenite retained after quenching can be transformed to carbides and ferrite during high temperature tempering.

2.3.3 Tempering of H13 Tool Steel

Tempering is the final stage of heat treatment for tool steels the aim being to improve toughness. Although, secondary hardening or precipitation of alloy carbides at high tempering temperatures is of great importance. Double or triple tempering stages are applied to tool steels to ensure that toughness is improved after micro-structural changes are introduced by the initial tempering steps; H13 is typically double tempered. In turn, retained austenite transforms to martensite, which is subsequently tempered (ASM, 1992, 1996, 1997).

Tempering should be conducted immediately after quenching. The typical tempering temperature range is 538°C - 621°C (Figure 2 - 3). The temperature should be held for 1 hour per 25mm of thickness and for 2 hours minimum and then air cooled to ambient temperature. The process is repeated for double tempering. To maximize toughness and tool performance, a third temper is often used as a stress relief mechanism after all finish machining, grinding, and electro discharge machining (EDM) have been completed on the tool.

The formation of alloy carbides during tempering requires the diffusion of carbide forming elements to be substitutionally diffused through the body centred cubic iron lattice of the tempered martensite. The slow diffusion results in short diffusion distances and in fine closely spaced alloy carbide precipitates. In turn, this inhibits carbide coarsening during high temperature service.

The composition of the alloy carbides, which form during tempering are very sensitive to the specific alloying elements present.

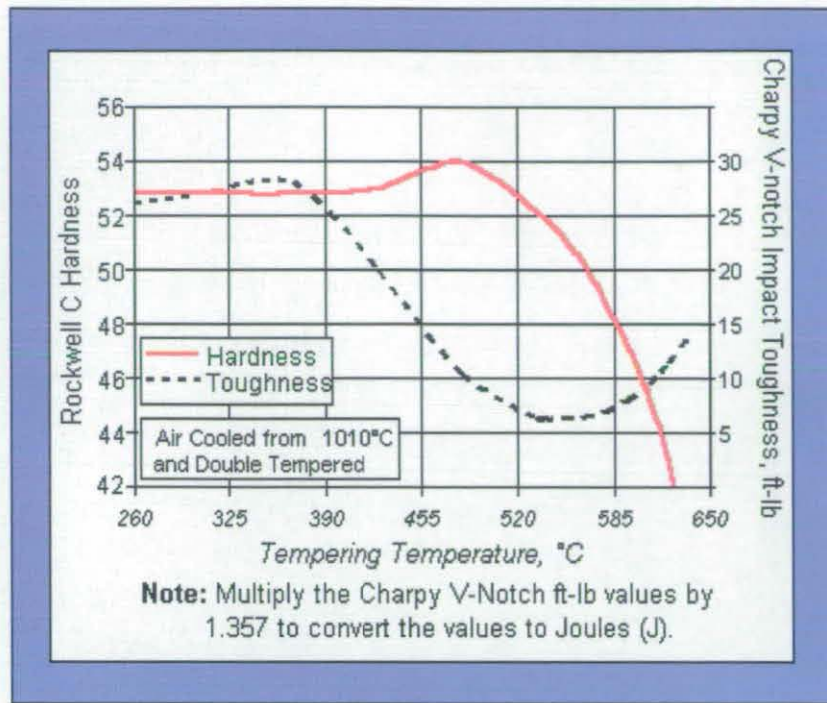


Figure 2 - 3 Tempering chart (Timken, 2004)

Retained austenite transforms to ferrite and cementite during tempering. In highly alloyed steels the austenite has an increased stability and does not transform until temperatures in excess of 500°C are reached; this can lead to coarse inter-lath carbides. Double tempering tends to spheroidise and produce less harmful interlath carbides formed by the transformation of retained austenite (ASM, 1992, 1996, 1997).

All aspects of hardening and heat treatment have an effect on the thermal fatigue performance of materials and hence, die life. For reference specimens it is essential that the correct heat treatment schedule is followed to obtain a representative comparison.

Chapter 3: Die Failure

3.1 Failure Modes for Dies

During high pressure die casting of aluminium the die has to withstand severe operating conditions such as high pressure and rapid temperature fluctuations and over time, tool failure occurs (Gulizia et.al., 1999, Sjoström and Bergström, 2004). There are three basic categories of failure associated with die casting dies (Schwam, et.al., 2004).

- Erosion
- Wear
- Thermal fatigue

3.1.1 Erosion

During die casting, as molten metal is injected into the cavity at high speed, erosion occurs.

3.1.1.1 Oxidation

If an oxide film adheres to the surface it prevents metal to metal contact and wear is reduced. However, if it is a brittle oxide, it can break off and act as an abrasive. Oxides occupy larger volumes than the metal being replaced allowing oxide peeling / cleaving action to start. The oxide can also be removed / washed away by the molten metal during die filling (Danzer et.al., 1983, Sundqvist et.al., 1997).

3.1.1.2 Chemical

Fatigue strength is reduced substantially by exposure to corrosive media such as moist air, electrolyte solution, or more aggressive substances. This causes corrosion of the surface which increases the surface roughness and provides more sites for crack initiation (Weroński and Hejwoski, 1991). Also aluminium dissolves iron in the die and has a similar effect.

3.1.2 Wear

Wear of die-casting dies is a significant problem due to their high cost. Wear is caused by solid particles in the molten alloy; these can be in the form of solidified aluminium, inclusions, hypereutectic silicon, dross, oxide from the ladle (Joshi et.al., 2004). The wear resistance of H13 tool steel is affected by heat treatment (Bahrami et.al., 2004).

3.1.2.1 Abrasive Wear

Abrasive wear occurs when a harder material cuts into a softer material. The hard material may be one of the mating materials or a foreign body between the mating surfaces (aluminium flash).

There are three levels (1) low stress abrasion (scratching); (2) high stress abrasion (grinding); (3) gouging abrasion where sizable gouges or grooves are formed.

3.1.2.2 Adhesive Wear

Adhesive wear is the most commonly found in moving machinery. At low stresses small junctions are formed at contact points and small fragments of metal become detached with movement. At higher stresses larger junctions are formed which can cause seizure.

Another form of adhesive wear is the interaction between the die steel and the alloy causing the formation of intermetallic phases that adhere to the die surface. This is also known as soldering (Sundqvist and Hogmark, 1993, Chen et.al., 1999, Chen and Jahedi, 1999, Xiaoxia et.al., 2004, Yu et.al., 1995, Persson et.al., 2001). This is caused by iron and aluminium reacting with each other to form binary iron aluminium intermetallic phases (Klarenfjord, 2005). These phases then react further with the molten aluminium to form ternary iron-aluminium-silicon intermetallic phase (Chen, 2005, Shanker, 2000^a, Shanker, 2000^b, Shanker and Apelian, 1997).

Previous work has shown (Shankar and Apelian, 1999, Gopal et.al., 2000) the mechanism of adhesion in die casting to be as follows:

Stage 1	Erosion of grain boundaries on the die surface
Stage 2	Pitting of the die surface
Stage 3	Formation of binary iron aluminium compounds
Stage 4	Formation of pyramid shaped structures of ternary iron-aluminium-silicon phases
Stage 5	Adherence of aluminium onto the pyramids of intermetallic phase
Stage 6	Flattening, merging and straightening of erosion pits and intermetallic phase

The problems can be reduced by employing die coatings; surface engineering methods (physical vapour deposition (Srivastava, 2003, Persson et.al., 2001, Gulizia et.al., 2001)), nitriding (Joshi et.al., 2004) and lubricants, however, these are not permanent solutions but do prolong die life. Eventually the intermetallic phases have to be removed by polishing, although, this results in loss of production and excessive polishing can damage the die reducing its life and ultimately, effect component geometry (Jahedi and Fraser, 2001).

Typically a combination of the above die failure modes is common place with erosion and wear modes leading to a defective surface finish on the die. These act as stress concentrators and crack initiation sites eventually leading to tool failure by thermal fatigue (Zhu et.al., 2003, Zhu et.al., 2002). Thermal fatigue is the most important failure mode in die casting (Mitterer et.al., 2000).

3.1.3 Thermal Fatigue

Fatigue wear occurs when a surface is stressed and unstressed. Fatigue is greatly affected by surface conditions such as microstructure, hardness, surface finish (Novovic, et.al., 2004), residual stresses etc.

'In actual die casting, the dominant tool failure mechanism is thermal fatigue cracking. The formation of the cracks is associated with accumulation of the local plastic strain that occurs during each casting cycle. Initial crack growth is facilitated by oxidation of the crack surfaces, and proceeding growth is facilitated by this oxidation in combination with crack filling of cast material, and by softening of the tool material' (Persson, 2003). Figure 3 - 1 shows the stress associated with thermal or heat cracking. Initially molten metal contacts the die and causes the surface temperature to increase above that of the interior of the die (Schwam, et.al., 2004).

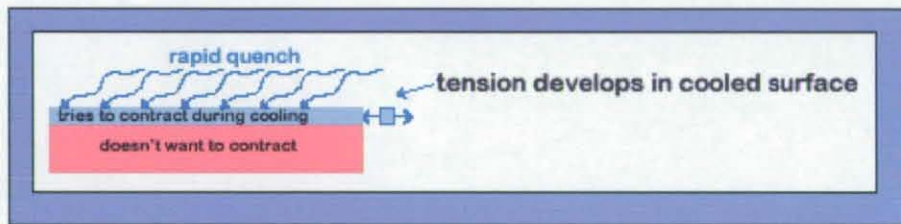


Figure 3 - 1 Thermal shock (Badger Metals, 2003)

The die face starts to expand; however, the cooler underlying layer resists this expansion creating a temporary compressive stress layer (Srivastava, 2003, Srivastava et.al., 2004). When the casting is removed, the die surface starts to cool and as it does, the surface shrinks or contracts. The surface cools more quickly than the interior of the die, which places the sub-surface of the die into residual tensile stress, which is made worse by the application of die lubricant (Olive, 2005). During further cycling, the die surface is subjected to alternating compressive and tensile stresses that result in some plastic deformation (Bendyk et.al., 1970). Continued cycling reduces the yield strength of the tool causing increased residual tensile stresses to develop and cracks to initiate. This type of cracking is more prevalent in aluminium and brass die casting because of the higher temperatures and resulting thermal shock by the molten metal. The heat cracking performance is improved by tool steel selection, proper heat treatment and preventative maintenance measures (Badger Metals, 2003).

3.1.4 Cracking of Metals by Thermal Fatigue

Thermal fatigue is typically a failure mechanism involving fluctuating temperatures. When certain materials are subjected to rapid heating and cooling, thermal gradient cracking may occur (thermal shock). The thermal gradient produces strain, which is related to the materials coefficient of expansion. Failure occurs when the thermally induced stress exceeds the strength of the material. In metals the thermal fatigue mechanism often results in the gradual formation of a network of cracks and is termed 'craze cracking' or 'heat cracking'. However, thermal

fatigue can occur under uniform temperatures caused by internal constraints such as differing grain orientation or anisotropy of the thermal expansion coefficient.

The composition and structure is as influential in thermal fatigue as it is in mechanical fatigue. Increasing the strength of the material through carbide formation and solid solution strengthening increases the resistance of the material to repeated strains. The ability to withstand microstructural change and oxidation is also crucial (Weroński and Hejwoski, 1991). Thermal properties are also important, such as the coefficient of thermal expansion (low values offer improved resistance to fatigue), specific heat and heat conductivity (higher values are generally preferential) (Norström, 1982, Weroński and Hejwoski, 1991, Worbye, 1985).

When a material with high thermal conductivity is thermally cycled it heats up and cools quicker creating a large thermal shock (heating and cooling rapidly inducing stress in a material) (Weroński and Hejwoski, 1991). In addition, if a material is constructed of dissimilar metals then, the differing thermal conductivities may induce internal stresses.

Thermal conductivity can be described as the ability of a solid to transmit heat; it is a measure of heat flow through a material (Material Testing Services, 2004). It relates heat flow (the flow of heat energy per unit area, per unit time) to the temperature gradient. The temperature gradient describes a temperature difference per unit distance.

Thermal conductivity is defined as:

$$K = (Q/A)/(\Delta T/\Delta L) \quad \text{Equation 3 - 1}$$

Where:

K	=	Thermal conductivity of the specimen
Q	=	Heat passing through
A	=	Cross sectional area of the specimen
(Q/A)	=	Heat flux
ΔT	=	Temperature difference
ΔL	=	Length
$(\Delta T/\Delta L)$	=	Thermal gradient

The measurement of thermal conductivity always involves the measurement of the heat flux and the temperature difference. The measurement of the heat flux is carried out by measuring the electrical power entering the heater and is then called absolute. Where the flux measurement is carried out indirectly it is called comparative. Other methods exist and are usually transient in nature (Anter Corporation, 2004).

Ferritic steels have higher thermal conductivities and lower coefficients of expansion than austenitic steels. However, at elevated temperatures (800°C) their thermal conductivities are similar. High thermal conductivity reduces the thermal gradient and a lower coefficient of expansion is beneficial (Norström, 1982, Weroński and Hejwoski, 1991, Worbye, 1985).

In general, a material with a low Young's modulus and high yield stress is advantageous as the elastic element of the strain is high and the plastic element low during thermal cycling (Norström, 1982, Weroński and Hejwoski, 1991, Worbye, 1985). Both high strength and high ductility (% elongation) are desirable to resist thermal fatigue, however, high strength typically equates to low ductility (% elongation), hence, a compromise has to be made to achieve optimum properties (Norström, 1982, Sjoström and Bergström 2004, Worbye, 1985).

Rutz et.al. (1996) discovered that the density of a material can affect the thermal fatigue performance. The higher the density of a material the better the thermal fatigue resistance.

Woodford and Mowbray's (1974) thermal fatigue experiment investigated the effect of chemistry and structure on fatigue performance. They discovered that carbides played an important role in thermal fatigue and that cracks progressed between them. They graded the materials either by type and morphology of carbides or by environmental effects. In terms of grain size, fine grains impede crack initiation in thermal fatigue and coarse grains impede crack propagation. Hence, the as-cast structure is ideal since it has small grains on the outside and large ones in the centre. It was also found that directional solidification improves the resistance to thermal fatigue. However, the effect of heat treatment resulted in anomalies and it was not clear, which structural feature was most influential.

Another factor affecting thermal fatigue is, of course, the cycle time or time spent either subjected to hot or cold conditions. The maximum temperature in the thermal fatigue cycle is considered the most important since it is related to the reduction in the mechanical properties (yield point) and higher deformation. The temperature also affects the way in which the crack initiates and grows; high temperatures can cause re-crystallisation relaxation of stresses by creep etc. (Weroński and Hejwoski, 1991, Worbye, 1985).

Surface roughness or notch effect, as it is otherwise known, also plays a role. However, it is less significant in isothermal fatigue at ambient temperature. Decreasing the surface roughness from 0.63µm to 0.16µm has been shown to increase the thermal fatigue resistance of materials by 40 - 50%. Polishing increases the fatigue life in isothermal fatigue three to four times but only doubles it under thermal fatigue conditions (Weroński and Hejwoski, 1991). 'The mode of cracking, and therefore its rate, depends primarily on the actual combination of three independent, important variables describing the thermal cycle. (1) the maximum temperature in the cycle, (2) the strain amplitude, and (3) the hold time' (Weroński and Hejwoski, 1991). A moderate maximum temperature and low strain amplitude with no restraints initiate

transgranular fatigue whereas a high maximum temperature and a high strain cause the crack pattern to be a mixture of transgranular and intergranular cracking.

The surface temperature of a die however, is dependent upon the casting temperature of the metal, size of the casting, geometry of the casting and the thermal properties of the die material. In turn, longer holding times at peak temperature increase the risk of tempering the die steel (Worbye, 1985).

To improve the life of dies the materials should have (Worbye, 1985):

- Low coefficient of thermal expansion to reduce the thermal stresses
- High hot yield strength, since a small plastic strain amplitude results in a low thermal fatigue damage
- High resistance to tempering
- High creep strength
- Good ductility (% elongation) to resist plastic strain without cracking

Essential variables can be used to evaluate fatigue resistance between materials, however, there is a slight variation depending upon the literature source (Equation 3 - 2, Equation 3 - 3 and Equation 3 - 4).

Thermal fatigue resistance = yield strength x thermal conductivity / (elastic modulus x coefficient of thermal expansion) (White, 2005) Equation 3 - 2

Thermal fatigue resistance = yield strength x thermal conductivity x (1 - Poisson's ratio) / (elastic modulus x coefficient of thermal expansion) (Hansen, 2006) Equation 3 - 3

Thermal fatigue resistance = thermal conductivity x tensile fracture strength / (elastic modulus x coefficient of thermal expansion) (Askeland, 1994, Schwam et.al., 2004) Equation 3 - 4

The higher the value from each of the equations above then the better the thermal fatigue resistance (White, 2005).

3.2 Initiation of Cracks

3.2.1 Fatigue Fracture

Fatigue failure will naturally occur in a component that is subjected to repeated or fluctuating stress or strains having maximum values less than the tensile strength of the material (ASM, 1975).

Any feature, which increases stress concentrations, may enhance the likelihood of fatigue failure. Superficial flaws, discontinuities of the metal such as blowholes, microstructure defects (inclusions), local concentrations of stress such as notches, scratches, pits, sharp corners or

other causes of discontinuity, are all stress raisers and increase the likelihood of fracture (Simons, 1972).

The fatigue process is a three-step mechanism:

- Crack nucleation at the surface of the component
- Slow crack growth through the cross section of the component
- Catastrophic failure when the remaining cross section cannot support the load

The fatigue mechanism begins with plastic deformation as metal grains are distorted by a process of slipping along the crystal planes, 'like a pile of books sliding over each other when pushed sideways' (Simons, 1972).

During fatigue, slip is concentrated into narrow bands where crystals within the metal are distorted elastically with the distortion increasing proportionally as stress increases. If the stress is removed, the material will return to its original shape. However, if the stress is increased and the yield point reached (the point at which the elastic limit of the material is reached) then the material will not return to its original shape when the stress is removed; this region is known as 'plastic deformation' (Higgins, 1991) where the atoms in the lattice structure de-bond allowing the layers or planes of atoms to slide over each other. Within these bands extrusions and intrusions develop as shown in Figure 3 - 2 (Cottrell and Hull, 1957); this is the first stage of crack development from an intrusion and leads to crack propagation down the slip plane. After one or two crystals, the influence of the slip band is lost and the crack changes direction and orientates perpendicular to the applied stress. During the second stage the crack propagates a small amount with each stress cycle leaving an imprint of striations on the fracture surface similar to the marks left on sand by a receding tide and eventually failure results.

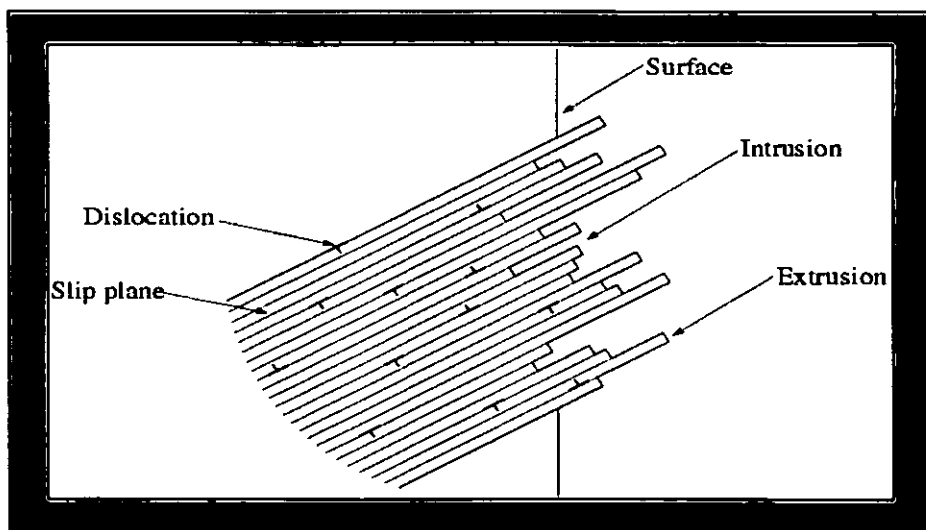


Figure 3 - 2 Extrusions and intrusions bands (University of Groningen, 2006)

Other factors that affect the fatigue characteristics of a material are:

- Surface condition: generally metals having a highly polished surface will be less affected by fatigue (Simons, 1972) due to reduced stress concentrators. However, surface treatments cause residual stresses, which enhance crack nucleation (ASM, 1996)
- Heat treatment and cold working: which influence fatigue resistance and hardness (Bendyk, et.al., 1970, Sjoström and Bergström, 2004, Simons, 1972, Worbye, 1985)
- High tensile strength and greater hardness: of a steel or other metals results in improved fatigue resistance in most cases (Bendyk, et.al., 1970, Simons, 1972)
- Temperature: affects fatigue strength and fatigue limit, especially where martensitic steels are involved (Bendyk, et.al., 1970, Simons, 1972)
- Cleavage of a non-metallic inclusion: a hard precipitate, or opening of holes also initiate fracture. The size, dispersion and type of particles have an influence on fatigue characteristics (ASM 1996, Worbye, 1985, ASM, Fine and Chung, 1980)

During a thermal fatigue cycle there is a tensile and a compressive mode. The tensile mode is generally more destructive in a fatigue test. In compression, when cracks try to propagate, they will find it difficult to do so. The reason for this is the friction between the fracture surfaces when the specimen is compressed. In tension, when cracks try to propagate, the fracture surfaces separate and there is no friction between them so the cracks find it easier to propagate (Andarifar, 2004).

3.2.1.1 Initiation of Micro Cracks

The type of material plays a role in fatigue characteristics. Pure metals contain no alloying constituents and can contain single or polycrystalline crystals. However, many materials are alloyed to improve their properties and they may, therefore, contain large second phase particles and have multiple phases and grain boundary phases as well as phases within the grain. A method has been used to classify materials based upon their structure as shown in Table 3 - 1 (Hertzberg, 1996).

Physical Properties	Increasing Tendency for Brittle Fracture
Electron bond	Metallic → Ionic → Covalent
Crystal structure	Close packed crystals → Low-symmetry crystals
Degree of order	Random solid → Short range order → Long range order

Table 3 - 1 Material classification (ASM, 1996)

Crystal structure is extremely important since it influences flow and fracture. The crystal structure in metals that results in poor fracture toughness is the body centred cubic lattice structure. This is because there is a limited number of slip systems in comparison to other metal crystal structures like face centred cubic or hexagonal close packed. When a metal is subjected to stress, it can deform elastically and plastically because planes of atoms that make-up the lattice structure can move. If a crystal structure can allow planes of atoms to move relative to

each other (slip), it will not cleave or separate the planes of atoms. If the slip systems are limited in number (as with the body centred cubic structure) or become ineffective, the planes of atoms will break bonds and separate instead of slip. As planes of metal atoms separate by cleavage, cracks and brittle fracture behaviour results. Metals like austenitic stainless steel, copper and aluminium have face centred cubic structures (FCC). Metals like titanium and tin have hexagonal close pack (HCP) lattice structures with increased slip systems operative at even low temperatures - so they don't exhibit brittle fracture behaviour.

At the microstructural level, fracture paths in alloys can occur through the grains termed 'transgranular' or along the grain boundaries termed 'intergranular'. However, associated failure modes are dimpled rupture, ductile striation formation, cleavage and intergranular failure. In turn, crack initiation has been observed to occur along slip bands, in grain boundaries, in second phase particles and in inclusion or second phase interfaces with the matrix phase (ASM, 1996). The type of crack initiation depends, simply, upon which provides the easiest path. Weak brittle precipitates also tend to play a dominant role in crack initiation.

Grain boundaries are particularly susceptible to fatigue crack initiation as slip is discontinuous across grain boundaries and many slip systems must be in action to prevent grains pulling apart (ASM, 1996).

There are differing opinions (ASM, 1996), on the sequence of events and modes of initiation of fatigue cracks. Fine and Chung (1980), describe it as cyclic plastic deformation in a metal that occurs by dislocations either emerging at the surface or piling up against obstructions. If the former occurs then slip bands eventually become cracks in the centre of the grains. The resistance to this decreases the larger the grain size. Dislocation pile-up on the other hand, can occur at any obstruction for instance at grain boundaries, inclusions, oxides, precipitates, etc. The consequence of the pile-ups is increased elastic strain energy, which leads to the initiation of micro cracks. From these, cracks can form along the slip band by, de-cohesion along the grain boundary or cracking of a second phase particle in the matrix or at the grain boundary. If there are no precipitates at the grain boundaries of a precipitation hardened alloy, then plastic flow at low plastic strains may be present in the area and cause crack initiation to occur. It must be noted that not all inclusions cause fatigue cracks as a cracked second phase inclusion must transfer to the matrix to start a fatigue crack (Fine and Chung 1980).

Notch sensitivity is another factor affecting crack initiation; if a material is notch sensitive then a small surface intrusion or extrusion can lead to crack initiation. The degree to which a material is notch sensitive is considered to increase with yield stress although this is not a general rule (Fine and Chung, 1980, Reimann and Brisbane, 1973).

3.2.1.2 Propagation of Micro Cracks

A crack must have initiated and grown in order to be detected and the degree to which detection can be achieved is dependent upon the resolution of the equipment. Venkataraman et.al., (1990, 1991) detected cracks of 1µm or less.

Not all micro cracks that form necessarily grow since a micro crack may initiate in an inclusion but the stress required to transfer and continue the crack growth in the matrix may be larger than the stress required to initiate it in the inclusion (Chang et.al., 1979). In a two phase alloy or composite, a crack may initiate in a non-continuous phase and be unable to transfer and continue into the continuous phase. If a crack initiates from a notch, pit, scratch etc. the stress reduces as the crack grows away from the defect and may stop. Grain boundaries can also prevent crack growth (ASM, 1996).

The number of micro cracks that form is dependent upon the stress or plastic strain amplitude. At high amplitudes many cracks form and combine across grain boundaries; this is the most common form of crack growth. At low amplitudes individual micro crack growth occurs (ASM, 1996, Ewing and Humfrey 1903).

The usual method of micro crack propagation in metals is by plastic deformation except when there are high levels of grain boundary embrittlement (ASM, 1996, Forsyth, 1979).

3.3 Key Factors for Improving Thermal Fatigue Life of a Material

From the literature researched it was found that certain material properties are important to improve thermal fatigue resistance, these are:

- High hardness and hot hardness are important and are related to mechanical strength, the greater the hardness the greater the yield and tensile strength. A loss of hardness reduces thermal fatigue life (ASM, 2001, Bendyk, et.al., 1970, Novovic et.al., 2004, Schwam, et.al., 2004, Simons, 1972, Sjöström and Bergström 2004)
- A high density increases fatigue endurance level. In infiltrated materials or cast materials density is extremely important as reduced porosity improves thermal conductivity and fatigue life (Rutz, 1996)
- A high thermal conductivity reduces the thermal gradient through a material so the materials surface tensile and compressive stresses are reduced, increasing fatigue endurance level. (Askeland, 1994, Norström, 1982, Olive, 2005, Schwam et.al., 2004, Weroński and Hejwoski, 1991, Worbye, 1985)
- A low thermal expansion will reduce the stress in a material (Norström, 1982, Schwam et.al., 2004, Weroński and Hejwoski, 1991, Worbye, 1985). Basically, a low coefficient of

thermal expansion minimises dimensional change and reduces thermal shock (Askeland, 1994)

- A low elastic modulus results in lower stress at a given strain level. A material with a low Young's modulus is advantageous as the plastic component of the strain is small in a typical thermal cycle (Askeland, 1994, Norström, 1982, Schwam et.al., 2004 Weroński and Hejwoski, 1991, Worbye, 1985)
- High elongation at break allows a material to accumulate plastic deformation before fracture occurs. (reduced by non metallic inclusions (oxides, sulphides, coarse carbides)) (Bendyk, et.al., 1970, Norström, 1982, Norström, 1989, Weroński and Hejwoski, 1991, Simons, 1972, Sjoström and Bergström 2004, Worbye, 1985)
- High ultimate tensile strength is favourable to increase thermal fatigue resistance. So when plastic deformation occurs the higher the ultimate tensile strength the greater the resistance to thermal fatigue. A high ultimate tensile strength usually goes hand in hand with a high yield strength which is also a desired property (Askeland, 1994, Bendyk, et.al., 1970, Norström, 1982, Weroński and Hejwoski, 1991, Simons, 1972, Sjoström and Bergström 2004, Worbye, 1985)
- High toughness is advantageous as it is the ability of a material to resist shock loading (reduced by coarse grain size, grain boundary precipitation of large carbides (bainite or pearlite as appose to martensite) and the presence of trace elements causing temper embrittlement) (Bendyk, et.al., 1970, Norström, 1982, Norström, 1989, Weroński and Hejwoski, 1991, Schwam et.al., 2004 Simons, 1972, Sjoström and Bergström 2004, Worbye, 1985)
- A high yield strength is important as during a thermal cycle the elastic component of the strain is large. In turn, during the compression part of the thermal cycle the increase in temperature can lower the yield strength of the material and the compressive strain may become plastic. During the tensile part of the cycle the thermal stress is larger than the yield strength and reverse plastic deformation may occur. After sufficient number of cycles the localised plastic deformation will create a fatigue crack (Badger Metals, 2001, Worbye, 1985, Schwam, et.al., 2004)
- High resistance to annealing to prevent a reduction in materials mechanical properties (yield strength, ultimate tensile strength etc.) (Persson, 2003, Schwam, et.al., 2004, Worbye, 1985)
- Heat treatment alloys that can be hardened through carbide formation increase the capacity to withstand repeated strains. They also retard the rate of softening by resisting

grain coarsening and provide hardness retention, good creep and thermal fatigue resistance. The decrease in hardness and strength of carbon steels during tempering is largely due to the coarsening of Fe_3C . However, excess alloying produces large carbide particles on the grain boundaries in the quenched and tempered steel causing increased brittleness resulting in gross cracking. (Bendyk, et.al., 1970, Schwam, 1994, Simons, 1972, Sjöström and Bergström 2004, Weroński and Hejwoski, 1991, Woodford and Mowbray, 1974)

- High creep strength increases thermal fatigue life. A material under constant load may be stretched and eventually fail, even though the stress is less than the yield strength. Hence, a high creep strength is advantageous to resist this (Askeland, 1994, Worbye, 1985)
- Resistance to oxidation at elevated temperatures. Oxidation is referred to as an instability and can cause crack initiation (Schwam, 1994, Weroński and Hejwoski, 1991)

3.4 Die Life Expectancy

The life of a die in terms of number of parts which can be made under production conditions will depend upon the alloy used, the product features required and the tolerances to be maintained on those features. The required surface finish and the final specifications for the cast surface have an important impact on die life. Typically, an aluminium die will produce 100,000 - 150,000 castings, a magnesium die 3 - 5 times more and a zinc die can typically produce an unlimited number.

Cracking initiates and propagates from the outside-in. It is a metallurgical principle that a crack cannot propagate into or through a layer of compressive stress unless the effective yield strength of the steel is exceeded (Badger Metals, 2001).

Although cracking is only one of the factors that cause die failure it can accelerate the time to failure, since, there is a greater chance of the additional failure modes to taking affect, i.e. adhesion in the crack could lead to ejection problems and allow further degradation of the die by material removal. Over time the problem will increase and the die will inevitably become inoperable.

Heat cracking occurs over a period of time as a result of strain cycling, the number of cycles required to initiate a crack range from thousands to millions of cycles depending upon the strain levels.

Thermal fatigue is the main cause for the reduction of the life of a die and consequently it is important to understand how a material behaves. There are no standard test procedures; this has led to researchers (Wallace et.al., 1997, Howes, 1973) developing and conducting their own experiments.

3.4.1 Determining Die Failure

Determining when a die has failed is case dependent, for example, a tool could be classed as failed for the following reasons:

- The severity of a crack or cracks impairing die operation and productivity
- The severity of a crack or cracks impairing the performance of the component in terms of aesthetics, geometry, surface finish, component tolerances etc.

Post processing operations could rectify some component defects but this is dependent upon the component specifications and the cost of post processing versus die repair. In some circumstances a die could be considered to have failed at the first sign of a crack, for example, a small hairline on a component may be unacceptable.

3.5 Thermal Fatigue Testing

To understand how a material behaves when subjected to thermal fatigue it is important to simulate the process thermal cycle in which it is to be used. This is achieved by assessing the process and developing a test that simulates the process temperature cycle (heating rate, cooling rate, temperature difference, mean temperature, cycle duration etc.).

There are several forms of thermal fatigue test, i.e. various forms of heating and cooling, for example forced convection methods, conduction methods by immersion in liquids, radiation, quartz lamp (Hartman, 1985), induction, (Taira et.al., 1979, Fissolo et.al., 1996, Persson et.al. 2005) resistance (Kawamoto et.al., 1966), immersion in fluidised solids (fluidised bed) etc.

The forced convection method involves subjecting the specimen to a blast of hot or cold gas with suitable velocity and pressure. The problem with this method is that large quantities of fuel are required to test specimens with a moderate size flame, which is typically followed by an air blast and hence, it is expensive (Glenny et.al., 1959). An additional drawback is the flow over the specimen needs to be uniform, to maintain constant heat transfer coefficients. An alternative technique is to heat a localised area of the specimen by a flame followed by an air blast to cool it, but this does not reproduce the thermal cycles very well.

Immersion in liquid is a common method used to induce fatigue damage and is carried out by immersing specimens in molten metals or salts. During immersion, heat transfer occurs by conduction. The specimen and molten medium contact layers initially reach a common temperature established by the ratio of their thermal conductivities. The large temperature gradient that occurs at the surface layer of the test piece during this time causes high stress generation but this method causes the specimen to be heated rapidly. The heat up rate is reduced if heating occurs by convection because of the low conductivity of air and hence, a lower initial thermal gradient results. A material can be affected by the difference between heating methods due to the extent and dispersal of the stresses (Glenny et.al., 1959).

There is also a limited choice of liquids available to heat specimens since the melting point must be higher than the final temperature of the specimen interface to prevent heat transfer problems caused by brief freezing of the liquid to the specimen surface. The metal or salts present may also cause corrosion / erosion affects.

Rapid cooling of specimens into liquids such as water, brine etc. result, initially, in localised boiling and vapour on the specimen surface. As the specimen cools the vapour begins to dissipate causing sporadic contact between the specimen surface and the liquid; this hinders the heat transfer and may not provide an acceptable thermal shock.

Heating or cooling of a specimen can be achieved by radiation, however, in order to obtain the required heating, rate it is necessary that the radiating surface be set at a higher temperature to achieve the desired specimen surface temperature. For example, Glenny et.al. (1959) states that to achieve rapid heating to 1000°C a radiating surface of 1400°C is required. After initial heating in a furnace, set at 1400°C, the specimen would have to be transferred, once the surface temperature reaches 1000°C, to a second furnace set at 1000°C. It may be difficult to determine the heat transfer coefficient using this method of heating. However, if it is required that the specimen surface reaches a certain temperature then this method could be used. Quartz lamps are typically more economical at lower temperatures because they offer uniform heating over different areas of the specimen. However they do have slow cooling rates and forced cooling is required when they are used (ASM, 1996).

Induction heating is achieved by allowing electric currents (eddy currents) to flow in the surface of a metal; this is achieved by an alternating magnetic field applied to a metal object. The alternating magnetic field is applied to the metal specimen to be heated by means of a 'work coil'. The coil can be configured and shaped to best suit the specimen shape and size. The alternating magnetic field causes electric currents (eddy currents) to flow in the surface of the metal and these currents produce heat due to the electrical resistance of the metal. Induction heating allows good control of heating rate and maximum temperature. However, as with radiation heating the heat input needs to be varied in order to first achieve the desired heating rate and then to maintain the desired temperature. Castelli and Ellis (1993) used a series of three independently controlled coils allowing a systematic approach to temperature modification at localised points along the specimen; this approach allows complex specimen geometries to be used but it is expensive (ASM, 1996).

Resistance heating is the oldest and simplest method of electric metal heating and melting. The two basic types are direct and indirect resistance heating. Direct resistance heating is where metal is clamped to electrodes in the walls of a furnace and charged with electric currents. Electric resistance generates heat, which melts the metal. Indirect resistance heating is where a current is passed through a wire coil to generate resistance and heat. This is then transferred to the metal by radiation, convection, or conduction.

The use of fluidised solids (fluidised beds) has been used extensively to heat and cool specimens. It consists of a container with a porous bottom through which a gas can flow to fluidise a powder. This method is discussed in more detail later in this chapter, section 3.5.2.

3.5.1 Wallace Thermal Fatigue Test

The Wallace dunk test has been used widely at Case Western Reserve University (CWRU) to measure the thermal fatigue resistance of die steels. The test measures average maximum crack length and total crack area on the four corners of a specimen after a set number of cycles of immersion into a bath of molten aluminium at 730°C. The specimen is internally water-cooled and has a high thermal gradient with sharp corners of radius 0.01" (0.254mm) (Figure 3 - 3). The test has been used for 30 years and the results correlate well with the service performance of die-casting die materials (Wallace et.al., 1997).

The specimen dimensions are 50.8mm x 50.8mm x 117.8mm (2"x2"x7") with a Ø38.1mm (Ø1.5") hole in the centre for internal water-cooling. The outer surface of the specimen is sprayed with a water-based lubricant before entering the aluminium. Water is passed through the specimen at 85 gallons (USA gallons) (321.76 litres) per minute. The molten aluminium is maintained at 730°C and the specimen is immersed for 12 seconds, removed and air cooled for 24 seconds, and then sprayed with die lubricant for a further 4 seconds. Wallace's procedure involves 5,000 thermal cycles, then a measure of the cracking pattern, it is then repeated every 5000 cycles up to a total of 15,000 cycles and then termination of the test occurs.

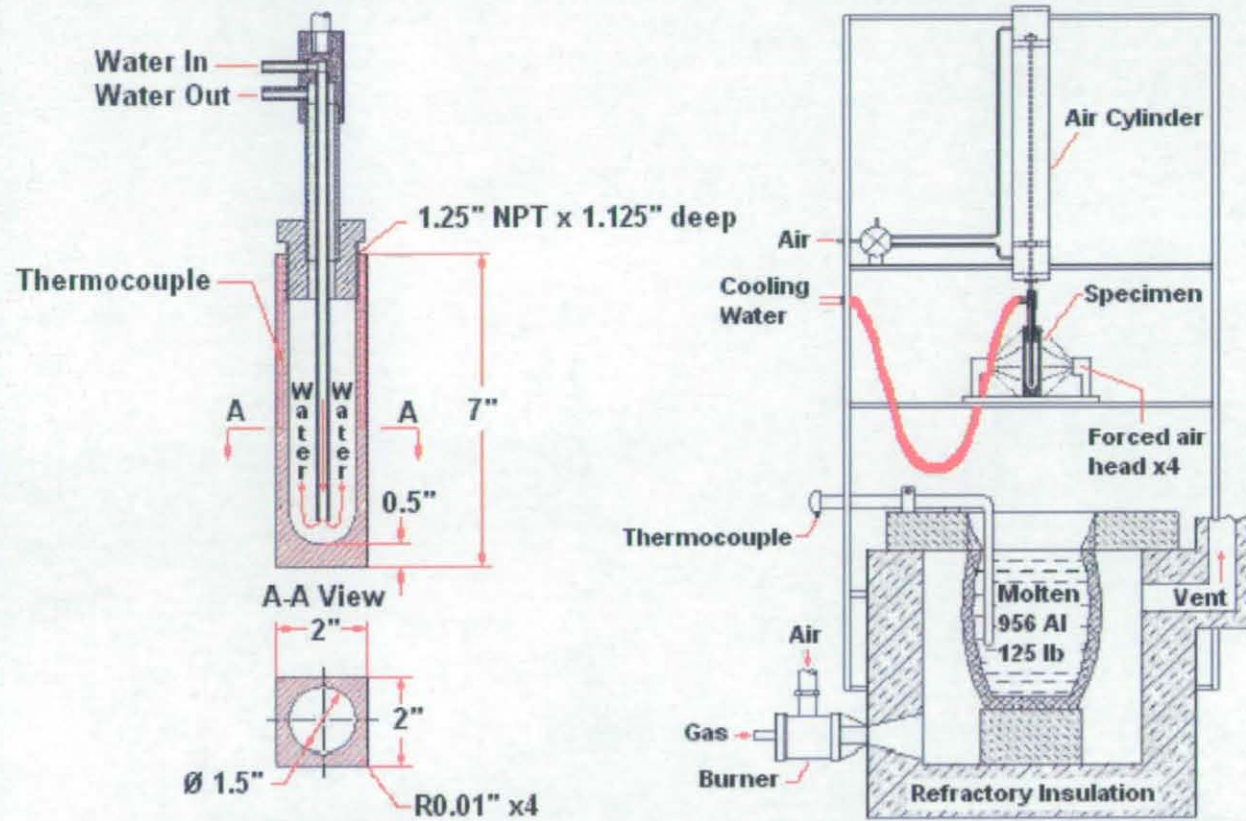


Figure 3 - 3 Thermal fatigue specimen and test equipment (Wallace et.al., 2000)

Wallace has tested many die materials and surface treatments with the aim of improving die life. In the die casting industry, premium grade H13 is used to produce dies and hence, all materials studied are compared to it (Wallace et.al., 2000).

Table 3 - 2 shows the composition of five commercially available steels that were tested using the Wallace dunk test. The aim was to investigate:

- The heat treatments of the steels to optimise the required properties
- Various austenitising temperatures and cooling rates to determine their influence on properties
- The effect of variation in Electro Discharge Machining (EDM) of the die steels on their properties (Wallace et.al., 1997)

Elements (% Wt.)	Steels				
	P.G. H13	H-11	K	Q	C
C	0.40	0.35	0.38	0.37	0.26
Si	1.00	0.85	0.21	0.30	0.85
Mn	0.35	0.38	0.42	0.63	0.90
P	0.025	0.016	0.01	0.015	0.019
S	0.001	0.003	0.002	0.001	0.001
Cr	5.25	4.81	5.20	2.46	10.94
Mo	1.50	1.82	1.85	2.22	0.94
V	1.00	0.31	0.51	0.84	0.50
Cu	0.08		0.03	0.22	0.05
Ni	0.15	0.45	0.03		0.95
W			0.01		0.90

Table 3 - 2 Steel compositions

The results of the experiments showed that K steel had the highest thermal fatigue resistance followed by Q, H13, H11 and C. The results also showed a small effect of hardness on the thermal fatigue resistance. As hardness increased from 45HRc to 48HRc there was an improvement in thermal fatigue resistance. Higher austenitising temperatures also resulted in increased thermal fatigue resistance; this was due to the higher temperatures resulting in reduced carbide levels and also a strengthening of the matrix (Wallace et.al., 1997).

Wallace also found the effect of EDM on thermal fatigue resistance is dependent upon the EDM process. In order to prevent a reduction of thermal fatigue resistance it is important to follow several steps: (1), Reducing the amperage of the arc on the final cuts, (2), Removal of the recast layer by polishing, (3), Tempering the un-tempered martensite layer.

The toughness of the steel gave an indication of the resistance to gross cracking. Again, K steel was better than H13, H11, Q and C steels in this respect.

Wallace concluded that the thermal fatigue resistance of all the steels tested was significantly affected by the heat treatment and processing. Faster cooling from the austenitising temperature improved both the thermal fatigue resistance and toughness of the die steels. A higher austenitising temperature without significant grain growth and a higher hardness up to 48HRc increased the thermal fatigue resistance but lowered the toughness to some extent.

Wallace conducted further thermal fatigue tests on other aluminium die casting tooling materials (Table 3 - 3 and Table 3 - 4). The Wallace dunk test was used to compare the materials to enable guidelines to be drawn up for selective use of high alloy tool steels, refractory metals and other non-ferrous high temperature die materials. Wallace concluded that a few of the most recently developed die steels show an improvement in thermal fatigue resistance compared to premium grade H13. The steels, however, required quenching from the austenitising temperature and a double temper to attain the properties. The alloying elements were very similar to that of H13 and they had sufficient toughness to be employed as die inserts. The tool steels, similar to H19 and H21, had improved thermal fatigue resistance and could be used as small inserts although these materials have low toughness and may be prone to gross cracking. The nickel copper alloys and refractory metals suffer little or no thermal fatigue cracking and hence, offer considerable promise for better die performance. Copper based alloys and refractory metals (metals with high thermal conductivity and heat diffusivity) can be employed to act as heat dissipaters from areas within a die and increase productivity. Low temperature diffusion coatings of nitriding and carbonising reduced the formation of thermal cracks compared to uncoated H13 (Wallace et.al., 2000).

Material	C	Mn	Si	S	P	Cr	Mo	V	Ni	Cu	W	Ti	Co	Fe
H13	0.40	0.35	1.00	0.005	0.025	5.25	1.50	1.00						Bal.
Bohler W303	0.38	0.40	0.40	0.005	0.01	5.00	2.80	0.65						Bal.
Thyssen E38K (mod H11)	0.38		1.00	0.005	0.015	5.3	1.30	0.40	0.60					Bal.
Thyssen 2367 (mod H13)	0.37			0.001	0.009	5.00	3.00	0.60	0.01					Bal.
Unddeholm Over Supreme	0.39	0.40	1.00	0.001	0.01	5.20	1.40	0.90						Bal.
Kind TQ1	0.35	0.43	0.40	0.001	0.01	5.20	1.80	0.55						Bal.
Kind RPU	0.38	0.40	0.40	0.001	0.01	5.2	2.80	0.60						Bal.
Uddeholm QRO-90	0.37	0.63	0.30	0.001	0.015	2.46	2.22	0.84		0.2				Bal.
Dunn-Marlok C-1650	0.01						4.50		14			0.30	10.5	Bal.
Allvac C-300	0.006	0.05	0.08	6e ⁻⁴		0.20	4.82		18.8		0.02	0.58	9.44	Bal.
Crucible SS446	0.20	1.50	1.00	0.03	0.04	25.00			0.25					Bal.
H21 Bohler W100	0.29	0.30	0.25	0.001	0.009	2.70		3.50			8.5			Bal.

Table 3 - 3 Ferrous materials

Material	C	W	Mo	Fe	Ni	Ti	Zr	Cu	Be	Cr	Nb
CMW-Anviloy 1150		90.00	4.00	2.00	4.00						
Allvac 718L	0.01		3.10	18.20	53.8	0.93				17.90	5.06
CSM-PM Mo			100								
Brush-QMAX Copper Beryllium					0.02			Bal.	2.00		
Brush-Nybril 360 Nickel Beryllium					Bal.	0.50			2.00		
Brush-Nybril-FX1 Nickel Beryllium					Bal.	0.50		12.50	1.00		

Table 3 - 4 Non-ferrous materials

3.5.2 Glenny Thermal Fatigue Test

Glenny designed a fluidised bed thermal fatigue test to evaluate materials for turbine blades. A fluidised bed consists of a container holding a bed of powder (in Glenny's case, aluminium oxide sand), supported on a filter. When air or gas is passed through the filter and the powder, a pressure difference is created across the bed. The pressure difference is increased by greater air / gas flow until it is equal to the hydrostatic weight of the bed. The bed then expands at which point the powder particles lose contact with one another and it becomes fluid like, increasing the pressure further, making the powder appear to boil. Heat transfer in a fluidised bed is achieved through elements that heat the powder particles through the gas boundary layers covering the particles; these particles then transfer heat to one another aided by the gas flow. It is also possible to cool the material using a fluidised bed (Van Heerden et.al., 1953) giving rise to a controllable thermal fatigue medium (Figure 3 - 4 A).

In the work by Glenny the specimens employed were tapered discs (Figure 3 - 4 B), which permitted a convenient method of evaluating thermal fatigue behaviour because the cracks initiated at the edges and were easily measured. During the test, the disc specimens were subjected to alternate heating and cooling shocks by transferring them between hot and cold fluidised beds of aluminium oxide sand. The specimens in the early work were designed to represent the thickness and edge radius of a typical turbine blade (Glenny et.al., 1959).

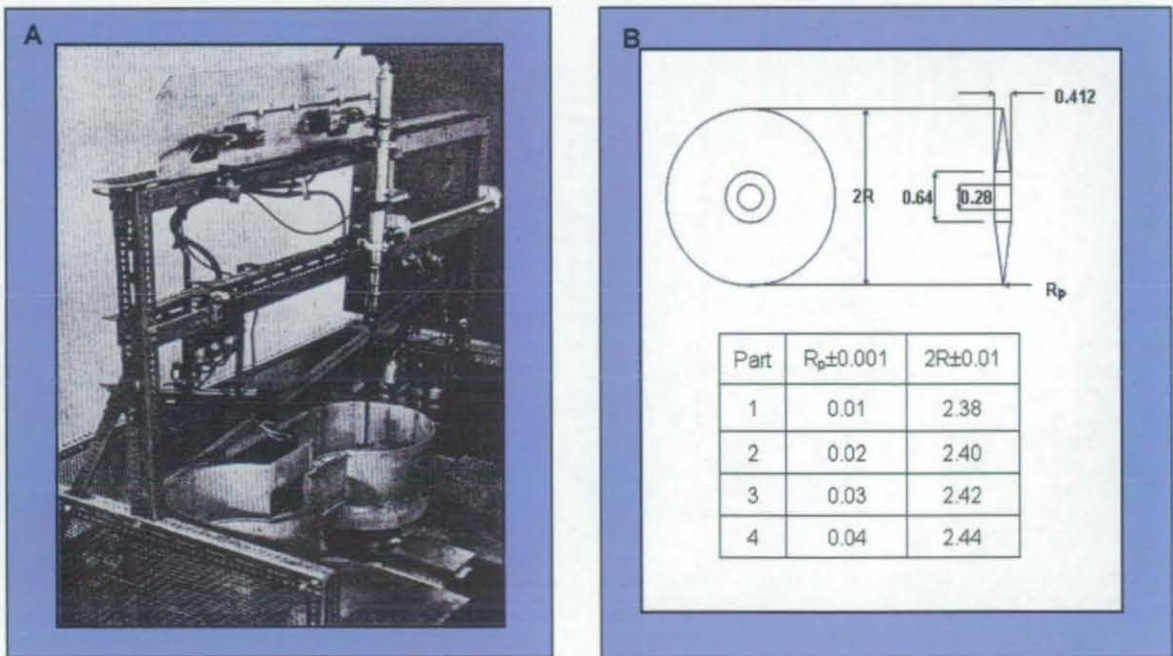


Figure 3 - 4 (A) Fluidised bed test equipment (Glenny et.al., 1959); (B) Thermal fatigue test specimen (measurements in inches)

Mowbray and McConnelee, (1976) conducted a study of the Glenny specimen shape and method of heating and cooling to determine the stress and strain on the disc. In the tests the cooling bath was held at 21°C for an exposure time of 4 minutes. The hot bath temperature was

varied between 815°C and 1035°C with exposure times of 1 or 4 minutes. The material tested was a cast cobalt-base super alloy, FSX414.

In the initial seconds of each shock the maximum temperature change developed at the discs extremities and in turn the maximum strain also occurred at this location.

3.5.3 Persson Thermal Fatigue Test

Persson (2003, 2004) investigated the thermal fatigue temperature profiles and conditions of brass pressure die casting and developed a test method. The method developed to measure the die's surface temperature during casting was achieved by placing four probes in a production die for tube couplings. The probes had a diameter of 16mm which housed a small cylindrical test disc behind which k type thermocouples (with thin wires of Ø0.13mm) were spot welded to the back of the discs. The thickness of the discs were 0.25mm, 0.5mm, 2mm and 5mm (Figure 3 - 5).

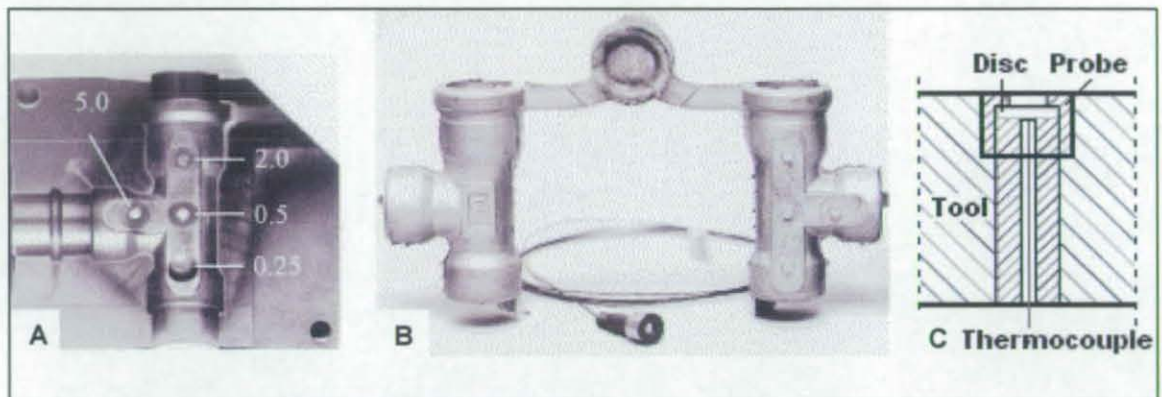


Figure 3 - 5 (A) Location of the four temperature measurement probes; (B) Casting; (C) Schematic of the probe (Persson et.al., 2004^b)

The temperature of the molten brass was 980°C and was used with a cycle time of 30 seconds during which the die was closed for 10 seconds and opened for 20 seconds. Water at 20°C circulated continually in the die and the die surfaces were lubricated. The shot weight of each casting was 1.6kg with a peak casting pressure of 164MPa.

During the first few cycles (less than 20) the tool ramped up from room temperature to a steady state of 300°C. Persson et.al., (2004^b) described a typical die surface temperature cycle as follows: 'When the 980°C melt makes contact with the tool, the tool material is heated within about 0.35 seconds from around 300°C to a maximum temperature of around 750°C at a surface depth of 0.25mm'. 'Until the tool is opened, cooling occurs by heat conduction into the bulk of the tool. Die opening and simultaneous cast ejection give rise to an additional heat loss through irradiation and convection' (Figure 3 - 6).

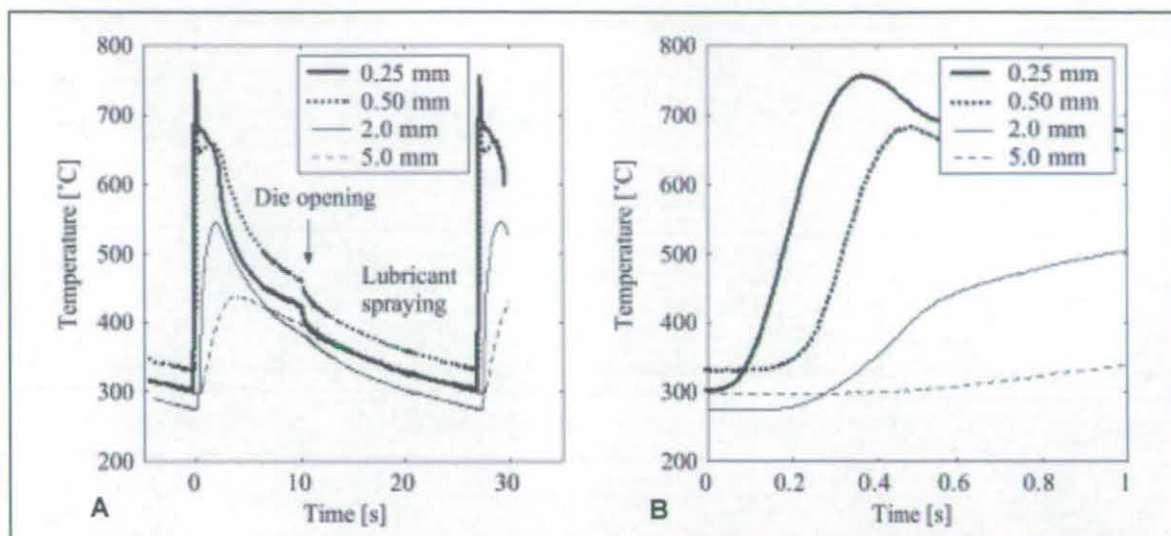


Figure 3 - 6 Typical temperature profiles; (A) Whole temperature profile; (B) Close-up (Persson et.al., 2004^b)

Persson (2003) and Persson et.al., (2004^a, 2004^b, 2005) developed a thermal fatigue test to simulate the temperature found in his previous work. This enabled thermal fatigue cracking of tool materials to be evaluated. Thermal fatigue cracking was produced on the surface of a test rod by simulating the rapid alternating temperature conditions using cyclic induction heating and internal cooling of the hollow cylindrical test rods ($\varnothing 10\text{mm}$, length 80mm with a $\varnothing 3\text{mm}$ cooling channel in the centre). Surface strain was also measured using a non-contact laser speckle technique (Figure 3 - 7 and Figure 3 - 8).

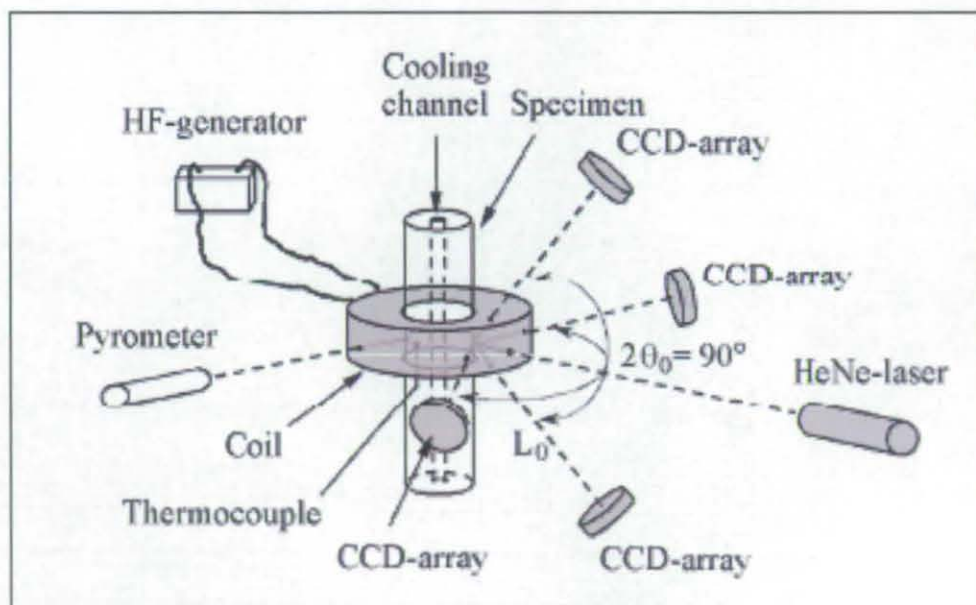


Figure 3 - 7 Schematic of Persson thermal fatigue test (Persson, 2004)



Figure 3 - 8 Persson thermal fatigue test equipment (Persson, 2004)

In a typical test, the induction unit (25kW, 3 MHz) heated approximately 20mm of the middle of the test rod. The cooling channel was continually supplied with silicon oil (2.5 litres / minute) at 60°C and cooled externally with argon or air. The external cooling also decreased oxidation. During the test a pyrometer and a k-type thermocouple measured the specimen temperature (Persson, 2003).

Three temperature profiles were represented to simulate various die casting temperature conditions (Table 3 - 5).

Maximum Temperature (°C)	Minimum Temperature (°C)	Heating Time (s)	Total Cycle Time (s)	External Cooling
600	170	0.2	11.2	Argon or Air
700	170	0.3 - 0.4	14.3 - 14.4	Argon or Air
850	170	2.2 - 2.5	26.2 - 26.5	Argon or Air

Table 3 - 5 Thermal cycles (Persson, 2003)

Some of Persson's, (2003) findings, when thermal-fatigue testing hot work tool steel grades QRO 90 and Supreme and Hotvar 700°C, were that a typical crack network occurred after 10,000 cycles with considerable softening of the tool materials. Persson estimated the tensile stresses during the test never exceeded the yield strength of the steel. However, numerous cracks formed within the low cycle fatigue range.

Low-cycle fatigue occurs at a relatively small numbers of cycles, or stress applications. The numbers of cycles may be in the tens, hundreds, or even thousands of cycles. Low-cycle fatigue conditions prevail when considerable plastic deformation occurs (Persson, et.al., 2004^b). There

is no exact dividing line between low-cycle and high-cycle fatigue, however, many define low cycle fatigue as that occurring in 50,000 cycles or less (Oberg, et.al., 1996).

High-cycle fatigue occurs at relatively large numbers of stress cycles and is not accompanied by plastic deformation instead it is dominated by elastic deformation (Persson, et.al., 2004^b).

It is believed that the results of Persson's work were due to the presence of stress raising defects that may have caused the tensile strength to exceed the tool steel yield stress during thermal fatigue with gradual softening reducing the yield strength. Hence, the material was subjected to cyclic stresses that caused accumulation of plastic strains after a certain number of cycles. It was also noted that crack length and crack density had a tendency to decrease with higher tool steel hardness. Persson, (2003) states that a higher hardness reduces the accumulation of plastic strain in the surface layer. Persson's later work was based on the thermal fatigue testing of hot work steel with Physical Vapour Deposition (PVD) coatings, Persson, (2003) and Persson et.al., (2005).

It is important to design a thermal fatigue test to simulate the environment / process to establish an accurate life expectancy of a material. Green and Munz, (1996), Merola et.al., (1996) and Hayashi et.al., (1998) show examples of thermal fatigue tests simulating different processes.

3.6 Temperature within a Pressure Die-Casting Tool

Bounds, (2000) investigated the thermal behaviour of the zinc pressure die casting process by measuring the temperature of the die to obtain the operating conditions. J type mineral insulated thermocouples were placed through the die block and die surface so that they would be in contact with the casting and additional thermocouples were positioned 2.5mm behind the die surface. The zinc solidus was at 380.4°C, the liquidus at 386.1°C and the casting alloy temperature, prior to injection, was 410°C. The report details a problem with the response rate of the thermocouples.

Aluminium pressure die casting research regarding die temperature is limited. However, Persson's, (2003) research estimated an aluminium die surface temperature to be 520°C. Srivastava, (2003) states that a typical die surface temperature reaches a maximum of 457°C and can be cooled to 107°C.

Research showed that on average the external surface temperature of the shot sleeve directly below the pouring hole reached 350°C whilst the internal temperature reached between 480°C and 500°C (Diecasting Times, 2004). The shot sleeve removes a significant amount of heat from the molten aluminium prior to injection. When injected, the aluminium formed a skin on impact with the die and the mass of the die cooled the metal so rapidly that the surface temperature never reached the aluminium pour temperature (Chen, 2003, Ghomashchi, 1995). This is confirmed by Oberg et.al, 1996 where it is stated 'Although the die is hot, metal entering the die is cooled quickly, producing layers of rapidly chilled, dense material about 0.015 in

($\approx 0.4\text{mm}$) thick in the metal having direct contact with the die cavity surface'; this is termed the skin effect.

3.7 Crack Detection and Measurement

Measurement and detection of fatigue cracks can be achieved using several techniques. The resolution of crack detection methods can range from $0.1\mu\text{m}$ - $500\mu\text{m}$ (Table 3 - 6).

Crack Detection Method	Method Resolution (μm)
Optical microscope	100 - 500
Liquid penetrant	25 - 250
Magnetic particle	500
Ultrasonics	50
Gamma radiography	2% of component thickness
Scanning electron microscope (SEM)	1
Transmission electron microscope (TEM)	0.1

Table 3 - 6 Crack detection methods and resolution (ASM, 1996)

3.7.1 Optical

The optical method is typically used to analyse and determine fatigue crack growth. It is normally conducted using a travelling microscope at 20 - 50x magnification. The crack length is measured over a number of cycles, at the same time the surface of the specimen can be observed and potential crack initiation sites detected (Marom and Mueller, 1971). The technique is simple and inexpensive and no calibration is required. In turn, accurate measurements can be performed provided no oxides or corrosion are present.

3.7.2 Liquid

The liquid penetrant method uses a liquid to flow into defects of a specimen by capillary action. Initially the specimen is degreased and dried thoroughly then covered with penetrant. The penetrant is left for a time to allow absorption into the specimen then the excess is wiped off and the developing agent is applied to the surface. The developing agent forms a powder on the surface of the specimen and draws the penetrant into it revealing the cracks; this method only reveals crack length information and cracks of $1\mu\text{m}$ in length and greater. The information gained from this technique depends upon the surface condition, such as roughness, porosity, crack morphology etc., of the specimens. The test can be applied to metals and non metals, magnetic and non magnetic materials (ASM, 1989).

3.7.3 Magnetic

The magnetic particle method requires material to be magnetised. Cracks set up a leakage field and can be detected by the application of fine magnetic particles over the surface of the specimen, which are attracted to the leakage field. The method can be used to determine crack length and is used as an inspection technique for structural components during service. However, the resolution is only 0.5mm (ASM, 1996).

3.7.4 Ultrasonic

Ultrasonic methods involve transmitting pulses of elastic waves (An elastic wave is a mechanical wave. In this wave, the force is directly proportional to the displacement, but is oppositely directed. This causes sinusoidal motion and the wave is a sine wave) through the specimen from a probe held on the surface. The resolution of the equipment is 50µm; this method is extensively used for crack measurement / detection, however, interpretation of the signals is required to determine the characteristics of the cracks detected (Coffey, 1980).

3.7.5 Gamma Radiography and X-ray Radiography

Gamma radiography and x-ray radiography are other methods of detecting cracks. The process emits radiation, which penetrates the specimen. If a crack is present it will allow the radiation to pass through more easily than in the solid material and this can be seen either on radiographic film or on real time imaging x-ray systems. Cracks can be magnified by positioning the film further away from the specimen, however, the use of the x-ray film method is difficult, initially, because voltage and amperage have to be determined to obtain high-resolution images; this will change depending upon the specimen size, thickness, density etc. Orientation is also a problem, false readings may occur if the crack is not at 90° to the x-ray beam. Real time x-ray units now overcome all of these problems and can even create 3D images of the specimen; however, this technique is expensive (ASM, 1996).

3.7.6 SEM and TEM

Microscopy methods include scanning electron microscope (SEM), and transmission electron microscope (TEM) etc. allowing the mechanisms for fatigue crack initiation and propagation to be established (ASM, 1996). The processes provide very high resolution and allow microstructural changes to be observed. SEM has a resolution of 1µm and the TEM 0.1µm. SEM also provides chemical analysis by using x-ray diffraction allowing chemical changes at the crack, in the specimen, to be determined. Energy dispersive spectroscopy (EDS) or Energy dispersive x-ray spectroscopy (EDXS) as it is also known allows an interaction between the energetic monochromatic electrons from an impinging electron beam to be determined. Characteristic x-rays are always of a specific energy or wavelength and can be used to identify the elements in a specimen (Gideon, 2004). The x-rays are characterised by their specific wavelength using a crystal diffraction grating. The most common instrument in use is an energy dispersive x-ray analyser (EDXA) attachment to the SEM; this is a doped wafer of silicon, which is used as a detector. The generated x-rays hit the silicon detector surface, which is doped with lithium. The penetration depth of the x-rays into the silicon is a direct function of the energy of the x-rays. A weak x-ray of a shallow penetration depth will generate a pulse of lower current than a more energetic x-ray of a longer penetration depth (Gideon, 2004).

Chapter 4: Prototype / Low Volume Tooling for High Pressure Die-Casting

4.1 Introduction

The main benefit of prototyping is design verification, allowing design flaws to be identified before a component goes into production (ÓDonnchadha and Tansey, 2004). The discoveries of errors or problems further along the developmental track, lead to greater cost to eliminate them; this is especially true for die-cast components where tooling costs can run into six figure sums.

Many production dies require rework ranging from simple modifications to a major overhaul; this may lead to additional costs in terms of a shorter tool life and delays in production resulting in loss of sales (Mueller, 1992).

Using rapid prototype processes (Upcraft and Fletcher, 2003) it may be possible to resolve the prototyping problem for pressure die casting and create a means for low volume - medium volume production, which at present is not available.

Several tooling techniques exist to produce prototype castings and prototype tooling for die-casting. Traditional processes include cast tooling (CSIRO, 2004), sand casting, investment casting, plaster mould casting etc. (Mueller and Thomas, 1992). Newer processes include, selective laser sintering (Levy and Schindel, 2002), spray metal tooling (Halford, 1999), Optoform (Bernard et.al., 2003), laser caving (Gildemeister, 2004), Metacopy, Keltool, (ÓDonnchadha and Tansey, 2004) Laminate tooling (Soar and Dickens, 2001) etc. Information on rapid prototyping processes can be found in alternative sources (Wohlers, 2004 and Wohlers, 2005).

These tooling techniques fall into two categories 'indirect' and 'direct tooling'. Indirect tooling refers to a tool, which is made using a rapid prototype part as a pattern for a secondary process as opposed to direct tooling, which is made directly by a rapid prototyping system (Hague and Reeves, 2000, Karapatis et.al., 1998).

4.2 Indirect Tooling Methods

Developments in rapid tooling technologies have been made in an effort to address the problem of producing accurate prototypes for pressure die casting by developing different methods of tool manufacture (Norwood and Soar, 2001), including cast tooling, rapid solidification process, metalcopy process etc. Many of these techniques have been used and reviewed for magnesium pressure die casting (Hague, 2001).

Processes such as sand casting, investment casting, plaster mould casting, etc., all require patterns to produce the moulds. The patterns are traditionally made from wood, however, many rapid prototyping techniques can be used to produce mould patterns for the die-casting industry (Rooks, 2002^a, Dickens et. al. 1995, Mueller, 1992, Wang et.al., 1999, Yan and Gu, 1996). Examples of these are:

- Quickcast process using stereolithography patterns for investment casting / plaster moulding (Jacobs, 1995, Hague et.al., 2001)
- Laser sintering process to produce sand or polymer (polystyrene, polyamide) patterns
- Thermojet to produce wax patterns
- Sanders to produce thermoplastic patterns
- Fused Deposition Modelling (FDM) process to produce wax or acrylonitrile butadiene styrene (ABS) patterns
- Laminated Object Manufacturing (LOM) to produce paper patterns

Traditional foundry techniques all produce castings that can be used for assessing the geometry and fit of components.

When assessing functionality, the prototype castings from the processes above have limitations since only production from an actual gravity die casting or pressure die casting tool can produce a part with precise die cast characteristics. Many prototyping methods cannot be used to cast the required alloys resulting in assumptions being made regarding component behaviour in terms of thermal conductivity, thermal expansion, mechanical properties, grain size, tolerances, draft angle, surface finish, porosity etc. (Soar, 2000).

A single-cavity metal prototype die is the most acceptable approach to determine product performance characteristics. Using certain rapid prototyping and rapid tooling techniques it may be possible to produce tooling that can be used to make castings using the desired process, a metal die and the desired casting alloy to ensure that the correct component properties are obtained.

4.2.1 Cast Tools

The cast tooling process is a simple indirect process requiring a pattern. The parting line is chosen and a soft negative is created in the shape of the tool. From this a ceramic tool is made in which the H13 die halves are cast. Secondary machining of the die is required to finish it and to add features such as runners, ejectors etc. The cast inserts are fitted into a bolster and can be run in a pressure die-casting press. Components can be produced using any type of die cast alloy (Armstrong, 2004).

Rapid prototyping techniques are generally quicker than traditional pattern making techniques, however, they have drawbacks. Their dimensional tolerance, stepping caused by the layer-by-layer manufacture and the maximum build size are limitations (Feenstra et.al., 2002).

4.2.2 Metalcopy

This technique has been developed by the Swedish company Prototol AB (previously known as Wiba AB). The technique is commercially termed 'Metalcopy' (Wohlers, 2003). The tool material consists largely of steel powder with a low melting point alloy bonding material.

The Metalcopy process involves the use of powder binder mixtures to produce metal tooling. The process starts with a primary master pattern of the part, typically manufactured via a rapid prototyping route. A silicone negative is cast from this, which is used to produce a green part consisting of a mixture of steel powder and binder; this is sintered and infiltrated with a low melting point alloy filling the pores between the metal powder grains (Figure 4 - 1) (Norwood and Dickens, 2005). The parts may require machining depending upon their application. The technique may provide time and cost advantages when compared with traditional tool production techniques dependent upon geometrical complexity. Initial tools have proved the possibility of producing pressure die-cast tooling and prototype castings (Harris et.al., 2003^a, 2003^b and 2004).

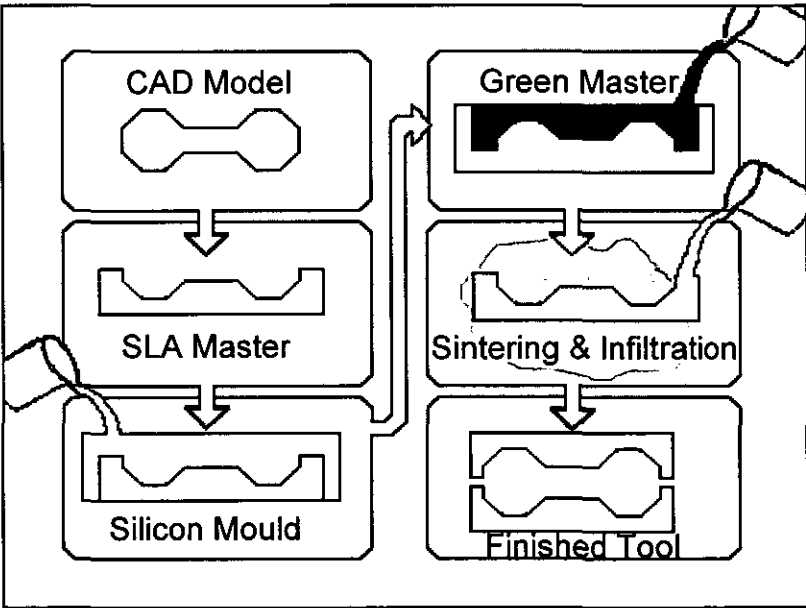


Figure 4 - 1 Metalcopy process

Main Advantages

- Good finish

Main Disadvantages

- Tolerance
- Size

- Several process steps
- Expensive infiltrant
- Heterogeneous material

4.2.3 Keltool

The Keltool process has been used to produce injection mould tools where hundreds of thousands of components have been produced (Dickens, 1999). The process is similar to the Metalcopy process and initially requires the manufacture of a master pattern typically from stereolithography. From this a negative silicone rubber soft mould is made and then a steel powder (grade A-6) in a binder is poured into the silicone mould. When set it is removed and placed in a furnace to melt and remove the binder to form a green part, which is then impregnated with copper (Zhou and He, 1999). Tools are approximately 70% A6 steel and 30% copper.

These tool or inserts require parting lines, core pins, ejector pins etc. to be machined in and heat treatment may be required. Up to 45HRc can be achieved.

Main Advantages

- Good finish

Main Disadvantages

- Tolerance
- Size
- Several process steps
- Expensive infiltrant
- Heterogeneous material

4.2.4 Rapid Solidification Process

The Rapid Solidification Process (RSP) begins with a pattern being created, ceramic is then poured and created from this pattern. Moulds are created by spraying molten steel from a crucible through a nozzle onto the ceramic negative as shown in Figure 4 - 2. As the metal is sprayed, the ceramic pattern is rotated and tilted to create an even coverage. With RSP Tooling, a pattern of the tool being developed is generated from a CAD solid model (Wohler, 2002).

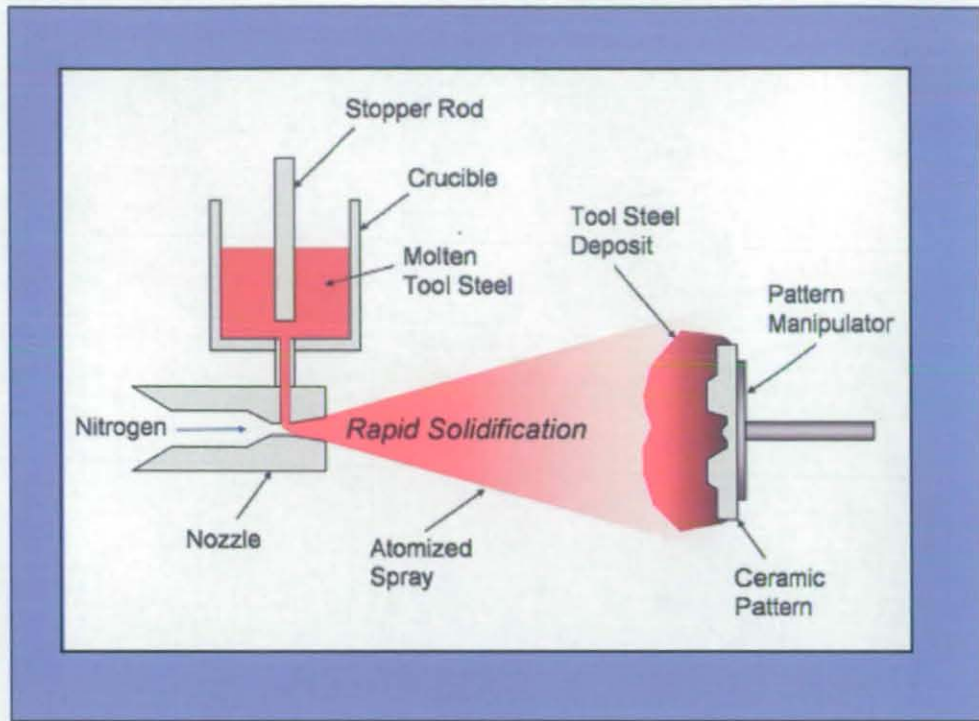


Figure 4 - 2 RSP process (RSP Tooling, 2004)

Post processing is required for the removal of over spray, ejectors, runners gates, cooling channels etc. An RSP tool insert can be sprayed in two hours from a CAD file. However, size is limited with a maximum diameter of 152.4mm by 101.6mm thick (Knirsch et.al., 2002).

It has been reported that RSP tools made of H13 do not require heat treatment and tools made of H13 appear to have a 25% increase in life expectancy over standard machined tools from high grade forged H13 (RSP Tooling, 2004).

Main Advantages

- Good strength

Main Disadvantages

- Tolerance
- Size (deep cavities not possible)
- Requires machining

4.3 Direct Tooling Methods

The direct tooling method is where metal die cavities are manufactured by an additive layer by layer approach.

4.3.1 Laminate Tooling

Laminate tooling (Himmer et.al., 1999, Himmer et.al., 2003, Gibbons et.al., 2003) the technique uses commercial grade metals (Obikawa, 1999, Norwood, 2001, Norwood 2002^a, Norwood 2002^b and Dickens, 1997).

The die halves shown Figure 4 - 3 require slicing (Tyberg and Bohn, 1998, Kulkarni and Dutta, 1996) to generate the 2D CAD data (Tata et.al., 1998) required for cutting the profiles of each laminate. A slicing subroutine in Delcam's Power-Shape 3D Package (Delcam, 2004) enables automatic slicing of the 3D tool and outputs individual 2D, DXF or IGES files.

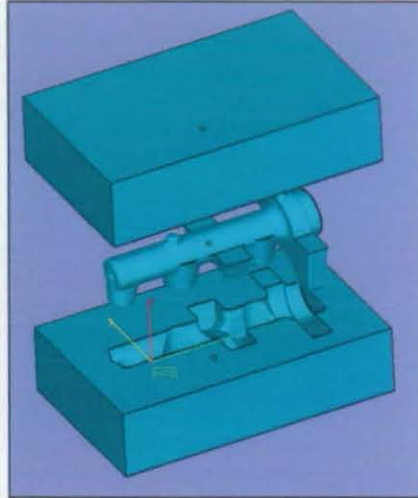


Figure 4 - 3 3D model of die halves

The 2D data shown in Figure 4 - 4 can then be transferred directly to any automated cutting process: water jet, laser (Rooks, 2002^b), plasma etc.

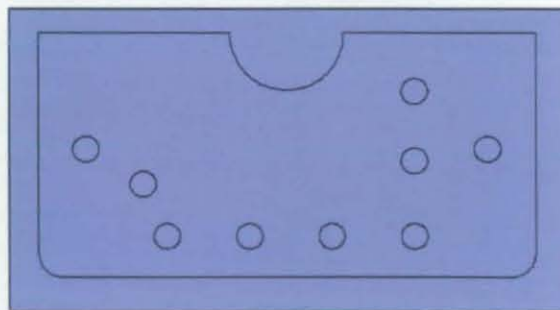


Figure 4 - 4 Individual DXF file output (profile of one laminate)

The cut laminates require cleaning prior to assembly; this can be effectively achieved by finishing or tumbling. Both processes are fast although finishing allows the laminate stack order to be maintained. Once clean the laminates are stacked, aligned and bolted or bonded together. The tool then requires finishing by electro discharge machining (EDM) or high speed machining can be employed.

Laminate tooling has produced several tools or parts for different applications, such as:

- Blanking tool and die set (Yokoi et.al., 1984)
- Polyurethane foam moulding tool (Dickens, 1996)
- Specimen products (spanner and wheel) (Obikawa, 1999)
- Metal forming dies (Walczyk and Hardt, 1994, Walczyk and Hardt, 1996, Walczyk, 1998)
- Injection moulding dies (Glozer, 1992, Bryden and Pashby, 1999, CRDM, 2005)
- Aluminium die casting tool (Soar and Dickens, 1998^a, Soar and Dickens 1998^b)
- Bonded laminate steel tools (Bryden et.al., 2000, Bryden et.al., 2001, Bryden and Pashby, 2001, Wimpenny et.al., 2003)

Injection mould tools have been manufactured and tested with favourable results (Glozer, 1992).

The next logical transition was to transfer the technology to high pressure die casting (HPDC). However, there are additional problems associated with the die-casting process:

- Higher injection speeds and forces
- Thermal shock (thermal fatigue)
- Ingress of the aluminium between the laminates

The laminate tooling process has the benefit of producing castings using the desired tool material, casting process and casting alloy. An additional benefit is that the scale of the tool is limited only by the size of a laser cutting machine bed. Tooling has been manufactured and tested for both gravity and pressure die-casting producing prototype parts and low volume manufacturing quantities (500 - 2000 parts) (Norwood and Soar, 2001).

Main Advantages

- Complex geometries possible

Main Disadvantages

- Time consuming
- Tolerance
- Several process steps
- Bonding required
- Machining required
- Heterogeneous material

4.3.2 Selective Laser Sintering and Direct Laser Sintering

Both the selective laser sintering (3D Systems) and the DirectMetal laser sintering (EOS GmbH) processes produce metal tools less than 370mm x 320mm x 445mm and 250mm x 250mm x

215mm respectively. The main difference between the processes is that selective laser sintering uses polymer coated metal powder to form green parts that require sintering and infiltration with a low melting point alloy, whereas the direct laser sintering process produces a tool directly without binder and infiltration (Norwood and Soar, 2001). Both tooling methods have been used for pressure die-casting to produce prototype components. For additional metal laser sintering information, refer to Wohlers 2003, Agarwala et.al., 1995^a, Agarwala et.al., 1995^b, Klocke et.al., 1995.

4.3.2.1 Selective Laser Sintering (SLS, 3D Systems)

The selective laser sintering machine was originally developed by DTM corporation and now 3D Systems (2004). The following metals are currently used:

- LaserForm™ ST100 - polymer coated stainless steel (iron balance, chromium 12 - 14%, manganese 1%, silicon 1%) with an organic binder (2 - 3%) and has similar material characteristics to P20 tool steel, infiltrated with bronze 46%. The bronze used is phosphor bronze D C52400 (90% Cu, 10% Sn)
- LaserForm™ ST200 - polymer coated metal mixture (iron balance, chromium 10 - 30%) with an organic binder (1 - 5%), infiltrated with bronze 46%. The bronze used is phosphor bronze D C52400 (90% Cu, 10% Sn)

However, at the commencement of this research only RapidSteel™ (Dalgarno and Stewart, 2001) materials were available:

- RapidSteel™ 1.0 - 1080 steel with Cu bonding material (Stewart et.al., 1999)
- RapidSteel™ 2.0 - austenitic 316 stainless steel 60%, Phosphor Bronze D C52400 40% (90% Cu, 10% Sn)

RapidSteel™ 2.0 was the latest material development at the beginning of this work with improved material properties (Table 4 - 1). The base material was changed from 1080 carbon steel to 316 stainless steel with a powder size of 34µm reducing layer thickness from 100µm to 75µm. The binder material was also modified to eliminate the need for the cross-linking stage, hence, reducing the processing time and increasing the accuracy (Pham et.al., 2000).

Material	Density (g/cm ³)	Hardness (HRc and HRb)	Ultimate Tensile Strength (MPa)	Yield Strength (MPa)	Modulus of Elasticity (Young's Modulus) (GPa)	Thermal Conductivity (W/m-K)	Thermal Expansion (mm/mm/°C x 10 ⁻⁶)
RapidSteel™ 1.0 (DTM)	8.23	75.3HRc	475	225	210	184 @ 100°C, 91 @ 200°C	14.4
RapidSteel™ 2.0 (DTM)	7.5	99 - 103.5HRb	580	413	413	23 @ 100°C, 28 @ 200°C	14.6

Table 4 - 1 RapidSteel™ material data (DTM, 1999)

Using the sliced data from the STL file, a 25 or 100 watt (material dependent) CO₂ laser selectively scans a layer of the object on the polymer coated powder as shown in Figure 4 - 5. The system works by automatically depositing a layer of powdered material across the build platform by means of a precision roller mechanism. The build material is typically heated to 100°C - 130°C and the build area to ≈172°C. A CO₂ laser is then used to heat the material and fuse it together creating a green part (Dimov et.al., 2001, Bak, 2003). The operation is repeated layer after layer until the component is completed. The part is then removed from the build envelope and the excess powder removed (Pham et.al., 1999).

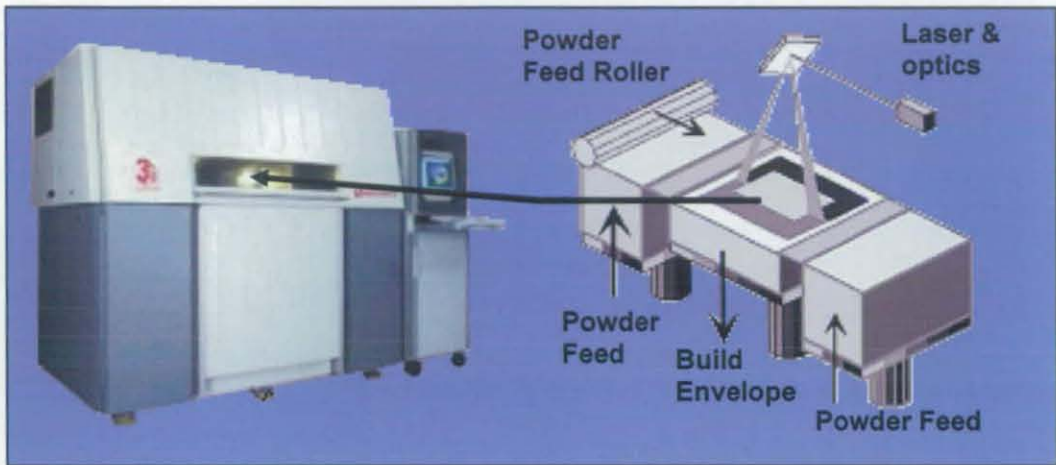


Figure 4 - 5 DTM (now 3D Systems Vanguard) laser sintering system (3D Systems, 2004)

Parts require a secondary operation as the metal is not fully dense. The metal powder is coated in nylon, which bonds it together. This structure requires infiltrating with bronze or copper to achieve a fully dense material; this is achieved by using an oven as shown in Figure 4 - 6 (Juster, 1994). The nylon is burnt out during the process and replaced with the bonding material by capillary action.



Figure 4 - 6 3D DTM (now 3D Systems) LaserForm™ sintering and infiltration furnace (3D Systems, 2004)

The components to be sintered are placed in a graphite crucible in the oven and the infiltrate placed by the component; it is then surrounded by alumina powder for covering and supporting the components in the oven. The oven has pre-set programmes that automatically sinters the parts in an inert atmosphere of nitrogen. Once molten, the infiltrate material is drawn by capillary action into any voids producing an infiltrated component with a resultant density of $\approx 99.5\%$. RapidSteel 1.0 requires one furnace cycle to debind and infiltrate however RapidSteel 2.0 requires two furnace cycles, one to debind and sinter the second to infiltrate (Dalgarno and Stewart, 2001).

Main Advantages

- Complex geometries possible

Main Disadvantages

- Machine takes a long time to heat up and cool down
- Infiltration is required
- Warpage may occur during infiltration cycle
- 370mm x 320mm x 445mm build area
- Heterogeneous material

4.3.2.2 DirectMetal Laser Sintering (DMLS, EOS GmbH)

The DirectMetal laser-sintering machines EOSINT M (Behrendt and Shellabear, 1995) (M250 and M270) manufactured by EOS GmbH (Figure 4 - 7) work in a similar manner to the selective laser sintering process.



Figure 4 - 7 EOS M250 sintering machine

Figure 4 - 8 shows how the sintering machine operates. Powder from a feed container is drawn across the build area with a powder slide (blade) to form a layer. A 200W CO₂ laser with a wave

length of 10.6µm and a spot size of 0.3mm (Khaing et.al., 2001) follows the 2D profile of the slice file to sinter the required area. The process is repeated until the component is produced.

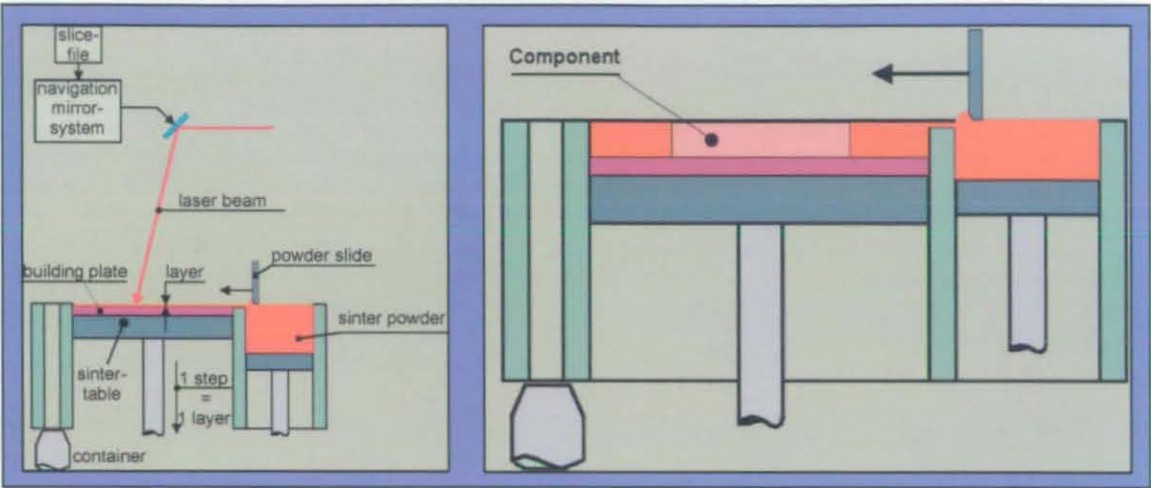


Figure 4 - 8 EOS M250 sintering process

The process uses the following metal materials:

- EOS DirectSteel 20µm (Steel based matrix containing Ni)
- EOS DirectSteel 50µm (Steel based matrix containing Ni)
- EOS DirectSteel H20 (Alloy steel containing Cr, Ni, Mo, Si, V and C) (available from quarter 1, 2004)
- EOS DirectMetal 20µm (bronze based metal)

Data for these materials is limited (Table 4 - 2). However, recent compression testing of EOS DirectSteel 50µm showed inconsistencies in the performance of the material (Dalgarno and Goodridge, 2004). Tests conducted by Storch et.al., (2003) revealed EOS DirectSteel 20µm to have brittle behaviour and the material properties were sensitive to build orientation.

Material	Chemical Composition	Density (g/cm ³)	Porosity (%)	Hardness (HRb)	Ultimate Tensile Strength (MPa)	Yield Strength (MPa)	Modulus of Elasticity (Young's Modulus) (GPa)	Thermal Conductivity (W/m-K)	Thermal Expansion (mm/mm/°C x 10 ⁻⁶)
DirectSteel 50µm	Steel based matrix containing Ni	-	-	-	-	-	-	25	18.1
DirectSteel 20µm	Steel based matrix containing Ni	6.3 - 7.6	2	94	600	400	130	13 @ 50°C	9 @ 50°C
DirectSteel H20	Alloy steel containing Cr, Ni, Mo, Si, V and C	7 - 7.8	< 0.5	109 - 113	1100	800	180	15 @ 50°C 18 @ 200°C	13 (100°C - 250°C) 14 (250°C - 400°C) 15 (400°C - 550°C)
DirectMetal 20µm	Bronze based metal	6.3 - 7.6	8	64	400	200	80	30 @ 50°C	18 @ 50°C

Table 4 - 2 EOS GmbH material data (EOS GmbH, 2005 material data sheet)

The parts are built directly onto a plate, which can be an integral part of the component / tool or a support structure can be built to aid component removal. However, the support structure has to be removed by machining.

Main Advantages

- No infiltration required

Main Disadvantages

- 250mm x 250mm x 215mm build area

Rapid tooling technology as discussed so far enabled the die-caster to produce prototype high pressure die-cast components. The majority of the rapid tooling processes discussed, use materials with 'similar' material characteristics to tool steels 'according' to the manufacturers. This enables prototype pressure die-cast components to be produced from the desired process, using the desired casting alloys, allowing cast components and tool designs to be evaluated and tested prior to the manufacture of production tooling. However, they are all in direct competition with high speed machining, which has increasing manufacturing speeds.

4.3.3 Other Tooling Methods

There are other rapid tooling methods these include, ProMetal, Solidica-Ultrasonic Consolidation, LaserCaving, EcoTool, Controlled Metal Build-up (CMB), ARCAM, Sprayform, Laser Engineered Net Shaping (LENS), Laser Consolidation, however, they were not studied in this research due to problems associated with obtaining / manufacturing specimens.

ProMetal: The process uses inkjet print heads to jet a binder onto the surface of metal powder. Layer by layer, the machine builds metal parts in 316L or 420 stainless steel. A furnace cycle burns out the binder and brings the parts to full density using a bronze infiltrant. The final part consists of about 60% steel and 40% bronze (ProMetal, 2006).

Solidica-Ultrasonic Consolidation: The process combined ultrasonic seam welding and layered manufacturing process. The process uses metal tape and ultrasonic vibration to bond the metal tape together. No inert environment is required or preparation of the metal prior to bonding. During bonding localised shear forces break up oxides and pressure creates internal stresses at the interfaces to set up elastic / plastic deformation and diffusion. The process is combined with machining to achieve a good surface finish (Solidica, 2006).

LaserCaving: This employs a laser to ablate the surface of a piece of metal to produce a tool, however, the process is time consuming and deep tools / deep cavities can not be manufactured due to the focal length of the laser.

EcoTool: The process is similar to aluminium-filled epoxy tooling. However, it uses a steel powder and binder which hardens at room temperature. It is then infiltrated in a similar manner to MetalCopy and Keltool (Castle Island's, (2006)).

CMB: The controlled metal build up (CMB) combines laser deposition welding and milling in order to build up, modify and repair moulds and dies. The process deposits a layer of weld in the desired area and a 3 axis high speed milling machine removes the excess material which insures accuracy.

ARCAM: Is similar to laser sintering of metal. The process fuses metal powders layer by layer to form strong metal parts using electron beam technology. The parts are nearly 100% dense, however, the surface finish is rough. It is reported that parts produced in H13 result in properties that are identical to parts machined from H13 stock (Wohler, 2002).

Sprayform: Employs twin wire metal arc guns that are robotically controlled to spray carbon steel onto the surface of a ceramic pattern. The ceramic patterns are made using a special freeze-casting process that ensures stability and accuracy of the ceramic. The build area is 760mm x 1015mm x 250 mm. Sprayform has been used to produce production dies for sheet metal stampings, injection moulding and composite lay-up tooling however class A finishes are not achievable (Wohler, 2002).

Laser Engineered Net Shaping (LENS): The process is a laser cladding process which injects metal powder into a pool of molten metal created by a focused laser beam. Parts are built layer by layer. LENS offers functionally grade material manufacture, however, the surface finish of components are poor and post machining is required. There are three companies that have commercialised the LENS process, Optomec, POM and Trumpf.

- **Optomec:** The process manufactures metal parts directly from CAD. The process produces components, made out of difficult-to-process materials such as titanium alloys. It can be used to repair components such as injection mould inserts. (Wohlers, 2002). The process is conducted in an inert atmosphere of argon. A 750W Nd:YAG laser is employed which traces the cross section of the part melting the powder as it is fed from the delivery nozzle (Optomec, 2006 and Wohlers, 2002)
- **POM:** Is similar to Optomec the main difference is it employs a 750W CO₂ laser instead of a 750W Nd:YAG laser (POM, 2006)
- **Trumpf:** Uses the POM system combined with a 5 axis control and closed loop feed back system to control feed rates. In addition the system offers up to four powder feeds (Trumpf, 2006)

Laser Consolidation: The process is similar to LENS using a 500W Nd:YAG laser with fibre optic delivery. The process, however, produces a significant better surface finish than other powder systems. The process is not yet commercial and is only offered as a service (Accufusion, 2006).

4.4 Hypothesis

The literature review has shown that high pressure die casting is an important process for making aluminium parts and that LM24 is the most widely used material in the cold chamber process.

The dies are normally made from hot working steels and H13 tool steel is the most common material for this. However, the dies are subjected to extreme conditions and this can lead to failure of the tool due to a number of reasons. It has been shown that thermal fatigue is the predominant cause of tool failure and the extent of this is highly dependent on the tool material, tool design, heat treatment of the tool and the die casting process parameters.

Several methods have been suggested for evaluating the thermal fatigue resistance of tool materials but, there is little sound basis for these and they do not fully represent the die casting conditions. A major unknown factor is the temperature of the tool surface during casting.

There are several processes that can be used for assessing cracks in a sample but optical microscopy is the fastest, simplest and cheapest.

In recent years a number of rapid tooling processes have been suggested as methods to manufacture prototype or short run tooling for high pressure die casting of aluminium. However, there is no authoritative information available on the materials fatigue resistance of these materials. The literature review has already shown that thermal fatigue resistance of a material is highly dependant on its structure and composition.

There are several types of rapid tooling materials, made with varying processes and different materials, many containing multiple materials; this is likely to have a major effect on thermal fatigue properties and die life.

The literature suggests that a suitable die material needs the following properties for good resistance to fatigue and thermal fatigue:

- High density (Rutz, 1996)
- Materials with high thermal conductivities to reduce thermal gradient (Norström, 1982, Weroński and Hejwoski, 1991, Worbye, 1985)
- Materials with a low thermal expansion to reduce stress (Norström, 1982, Schwam et.al., 2004, Weroński and Hejwoski, 1991, Worbye, 1985)

- Low elastic modulus (bulk) (Norström, 1982, Weroński and Hejwoski, 1991, Worbye, 1985)
- Low elastic modulus (rigidity) (Norström, 1982, Weroński and Hejwoski, 1991, Worbye, 1985)
- Low elastic modulus (Young's) (Norström, 1982, Weroński and Hejwoski, 1991, Worbye, 1985)
- High elongation at break (%) (ductility) (Bendyk, et.al., 1970, Norström, 1982, Weroński and Hejwoski, 1991, Simons, 1972, Sjoström and Bergström 2004, Worbye, 1985)
- High tensile strength / toughness (a compromise as it is not possible to have high strength with the toughness) (Bendyk, et.al., 1970, Norström, 1982, Weroński and Hejwoski, 1991, Simons, 1972, Sjoström and Bergström 2004, Worbye, 1985)
- High yield strength (Badger Metals, 2001, Worbye, 1985)
- High resistance to annealing (Persson, 2003, Worbye)
- High hardness (Bendyk, et.al., 1970, Novovic et.al., 2004, Simons, 1972, Sjoström and Bergström 2004)
- High creep strength (Worbye, 1985)
- Resistance to oxidation (Weroński and Hejwoski, 1991)

However, many rapid tooling materials are constructed from two different alloys such as stainless steel powder and phosphor bronze and have different microstructure to typical alloys. Generally rapid tooling materials do not meet the desired material properties or have a mismatch due to the different materials. It was believed that all of the rapid tooling materials would have poor thermal fatigue properties and not be suitable as die casting tool materials.

Therefore, it was decided to subject a selection of rapid tooling materials to thermal fatigue testing in order to validate this assumption and to compare them against each other. It was expected that the analysis of the materials would enable an understanding of the key material properties that prevent thermal fatigue.

4.5 Methodology

Die casting was chosen as the application because it is a high temperature application requiring a prototype / low volume tooling solution.

Aluminium (LM24) cold chamber pressure die casting was chosen as the representative process because it is the most common high volume casting process, has one of the highest casting temperatures, fastest cycle time and tool failure rate.

The choice of rapid tooling materials to be tested was driven by their accessibility through research projects being undertaken at the time of this work since funds were not available to purchase a complete set.

It was necessary to understand the compositions of each of the tooling materials that would be thermally fatigued as comprehensive data was not available for most of them. This was to be undertaken by EDS analysis.

It was also necessary to determine the tooling materials density and thermal conductivity as these properties have been shown to affect thermal fatigue (Norström, 1982, Rutz et.al., 1996, Weroński and Hejwoski, 1991, White, 2005, Worbye, 1985).

Other material properties that also affect thermal fatigue resistance such as tensile, percentage elongation, Young's modulus, toughness etc., were not evaluated due to the difficulty in obtaining specimens from the suppliers and time constraints.

Before a thermal fatigue test could be designed it was necessary to determine the temperature cycle within an aluminium die casting tool. At this point within the research this information was sparse.

A program of work was designed to determine these temperatures using thermocouples in the tool and the results of this were validated with temperature sensitive paints.

The next stage was to determine the shape and size of the thermal fatigue specimen. It was decided to employ Glenn's sample shape as it met several requirements.

- It is small unlike Wallace's sample. This will reduce power requirements and heat loss from the furnace and several samples can be tested simultaneously
- Glenn's sample has a small radius and changing cross section (typical features in a die)
- There was no need to polish the samples to analyse them as in Wallace's tests. This could remove small cracks or cracks that have just initiated and change the surface roughness and affect future crack initiation
- Persson's sample makes it difficult to measure crack length as it only shows surface cracking
- Glenn's sample has no water flowing through it unlike Wallace's and Persson's test. Rapid tooling materials may be porous and could be dangerous if water contacts molten aluminium or furnace elements

Both Wallace and Persson have designed thermal fatigue tests which are designed to test materials suitability for die-casting. The author of this work believed that neither Wallace's or Persson's tests were representative of pressure die-casting. Wallace's test dunks the specimen into molten aluminium at 730°C for 12 seconds and heats the specimen to 635°C and cracks occur in H13 die steel at 15,000 cycles. This is not a correct temperature profile as dies do not heat up to 635°C and are not subjected to that temperature for 12 seconds and H13 dies do not typically initiate cracking until 100,000 cycles. Persson's test caused cracking of die steel at 20,000 when tested at 600°C, again not representing the die casting temperature profile.

Glenny's thermal fatigue test was designed to test materials for turbine blade suitability and not die casting. This is reflected in the cycle times which can be as high as four minutes heating and four minutes cooling.

Due to previous tests not meeting the desired requirements a new test method had to be designed. Hence, once the specimen shape (Glenny's) had been determined and the apparatus built it was possible to manufacture H13 specimens to reproduce the temperature cycle within the tool. This involved several tests with different heating mediums.

Once the test design was complete the rapid tooling specimens were manufactured. For each rapid tooling process five thermal fatigue specimens were manufactured and their initial hardness recorded. Four specimens were tested and one was used as reference for each material.

The main experimental work subjected the specimens to the designed thermal fatigue test and periodically the specimen's were optically examined and hardness tested. Optical analysis was chosen as it was available to the author and it is quick, simple and has an accuracy of 0.001mm. The hardness tests were conducted to determine if the materials had softened during thermal fatigue. The following data was planned to be recorded:

- Number of cycles to initiate cracking
- Crack growth rate
- Number of cracks
- Hardness

After obtaining the thermal fatigue data optical, SEM and EDS (chapter 3, section 3.7.6) analysis was planned to examine the cracks and microstructure in more detail to determine the mode of crack initiation and propagation.

Chapter 5: Initial Work

5.1 Selection of Test Materials

The choice of rapid tooling materials to test in the experimental program was largely dependent upon those available in the rapid prototyping industry at the commencement of this research and the obtainability. These included Metalcopy 5507, Metalcopy Janalloy, Metalcopy Cu, Laminate steel, EOS DirectSteel 20µm, RapidSteel™ 2.0. Regarding the choice of material as a reference, previous background research detailed in chapter 2 revealed H13 to be the main tooling material for aluminium pressure die casting for a number of reasons but mainly because of hot working properties of this material.

The experimental plan was also important and several factors required initial research to enable the development of a thermal fatigue test. A procedure was also required to obtain data and to monitor the specimens during the test. Finally, the specimens required post examination to determine crack initiation, crack propagation, etc.

5.2 Reference Specimen H13

The material for the specimens was provided by Bohler and the material specifications can be seen in Table 5 - 1. Using a scanning electron microscope (SEM) (Leo 1350 VP FEG) and an energy dispersive spectroscopy (EDS) (EDAX) (chapter 3, section 3.7.6) chemical analysis it was possible to measure the energy and intensity distribution of x-ray signals generated by an electron beam strike on the surface of a specimen. The elemental composition at a point, along a line or in a defined area, can be easily examined to a high degree (0.1 % Wt.). The energy dispersive spectrometer analysis (EDS) composition is shown in Table 5 - 1. It must be noted that EDS cannot detect carbon and the analysis is conducted over a small area of a specimen so values may vary for a given material.

	Composition % Wt.						
	Fe	C	V	Si	Ni	Cr	Mo
H13 (reference)	Bal	0.32 - 0.4	1	1	-	5 - 5.25	1.33 - 1.5
H13 EDS	Bal.	-	1.3	1.2	0.1	5.3	1.3

Table 5 - 1 H13 reference (Oberg, E., et.al., 1996, Shackelford and Alexander, 2001, Matweb, 2004) and EDS % Wt. composition

H13 has the following material properties (Table 5 - 2).

Property	Value
Density (g/cm ³)	7.8
Thermal conductivity (W/m ^o K)	24.3
Coefficient of linear thermal expansion (m/m ^o C)	1.0 x 10 ⁻⁶
Elastic modulus (bulk) (GPa)	140.0
Elastic modulus (rigidity) (GPa)	81.0
Elastic modulus (Young's) (GPa)	210.0
Elongation at break (%)	9
Ultimate tensile strength (MPa)	1990
Yield tensile strength (MPa)	1650
Poisson's ratio	0.3
Annealing temperature (°C)	870.0
Melting point (°C)	1425
Hardness (HRb)	104 - 120

Table 5 - 2 H13 material properties (Shackelford and Alexander, 2001, MatWeb, 2004, Timkin Latrobe Steel, 2004)

5.3 Indirect Die Materials

5.3.1 Metalcopy 5507

Metalcopy 5507 was claimed to be stainless steel 316L powder (Table 5 - 3 powder material) in a matrix of silver (Table 5 - 4). There was limited material property data for this material and Prototal AB would not divulge the alloy composition. However, material data has been obtained from an EDS analysis (Table 5 - 5).

		Composition % Wt.									
		Fe	C	Mn	Si	P	S	Cr	Mo	Ni	N
316L reference	Min	Bal.	-	-	-	-	-	16.0	2.00	10.0	-
	Max	Bal.	0.03	2.0	0.75	0.045	0.03	18.0	3.00	14.0	0.10
316L EDS		Bal.	-	-	1	-	-	18.5	2.7	9.7	-

Table 5 - 3 316L reference (Azom, 2006, Shackelford and Alexander, 2001) and EDS composition

	Composition % Wt.							
	Ag	Fe	Mo	Cr	Ni	Si	Cu	Zn
Metalcopy 5507 bonding material EDS	Bal.	0.8	0.9	0.2	0.2	0.4	4.8	14.4

Table 5 - 4 Metalcopy 5507 bonding material EDS composition

	Composition % Wt.							
	Fe	Mo	Cr	Ni	Si	Ag	Cu	Zn
Metalcopy 5507 combined EDS	Bal.	1.7	12.5	6.7	0.5	15.2	2.7	7.9

Table 5 - 5 Metalcopy 5507 EDS composition

It should be noted that the materials were claimed to be 316L stainless steel powder with silver bonding material. However, from the EDS results it was clear that the bonding material was not pure silver.

This material was selected as a candidate as the powder was 316L stainless steel, which has good oxidation resistance in intermittent service to 870°C and in continuous service to 925°C. Grade 316L is also resistant to carbide precipitation and can be used in the temperature range 425°C - 860°C (Azom, 2006). 316L also has a high annealing temperature preventing softening at elevated temperatures. The 316L material properties can be seen in Table 5 - 6. The ultimate tensile strength and yield strength of this material are lower than those of H13. In turn the coefficient of thermal expansion of 316L is higher and its thermal conductivity lower than for H13.

Property	Value
Density (g/cm ³)	8.0
Thermal conductivity (W/m ² K)	18.9
Coefficient of linear thermal expansion (m/m/°C)	16.5 x 10 ⁻⁶
Elastic modulus (bulk) (GPa)	193
Elastic modulus (rigidity) (GPa)	83.0
Elastic modulus (Young's) (GPa)	215
Elongation at break (%)	40
Ultimate tensile strength (MPa)	515 - 558
Yield tensile strength (MPa)	170 - 290
Poisson's ratio	-
Annealing temperature (°C)	1010 - 1120
Melting point (°C)	1375 - 1400
Hardness (HRb)	95

Table 5 - 6 Material properties of 316L grade of stainless steel (Azom, 2006, Sandmeyer Steel, 2005, MatWeb, 2004, Shackelford and Alexander, 2001)

The Metalcopy 5507 matrix was primarily silver, which resists corrosion, has a high melting point and a high thermal conductivity, which are beneficial to thermal fatigue resistance. However, its annealing temperature is 600°C, which is lower than the processing temperature of LM24 ≈ 700°C. Silver, also has poor mechanical properties in comparison to 316L stainless steel (Table 5 - 7).

Property	Value
Density (g/cm ³)	10.5
Thermal conductivity (W/m ² K)	427
Coefficient of linear thermal expansion (m/m/°C)	19.7 x 10 ⁻⁶
Elastic modulus (bulk) (GPa)	104
Elastic modulus (rigidity) (GPa)	30
Elastic modulus (Young's) (GPa)	83
Elongation at break (%)	50
Ultimate tensile strength (MPa)	140
Yield tensile strength (MPa)	-
Poisson's ratio	0.4
Annealing temperature (°C)	600
Melting point (°C)	961
Hardness (HRb)	100

Table 5 - 7 Material properties of pure silver (Shackelford and Alexander, 2001, Goodfellow, 2005, Environmental Chemistry, 2005, MatWeb, 2004)

The points discussed above indicate that the material could withstand a degree of thermal fatigue but, it is unclear how the structure of the material would perform. Hence, Metalcopy 5507 was selected for thermal fatigue testing.

5.3.2 Metalcopy Janalloy

Metalcopy Janalloy is claimed to be identical to Metalcopy 5507 with 316L stainless steel powder in a matrix of silver. The difference was that the material was manufactured by Prototal AB in house and not by their supplier. However, the 316L EDS data was not identical to Metalcopy 5507, the most noticeable reductions are in the Fe and Cr content (Table 5 - 3 and Table 5 - 8). Differences in the bonding material composition were also evident. Increased Ag and Fe, no Mo, no Cr, no Ni, no Si, presence of Mg, reduced Cu, reduced Zn (Table 5 - 4 and Table 5 - 9). The overall EDS analysis of Metalcopy Janalloy can be seen in Table 5 - 10.

	Composition % Wt.									
	Fe	C	Mn	Si	P	S	Cr	Mo	Ni	N
316L EDS	Bal.	-	-	0.3	-	-	14.3	1.1	11.5	-

Table 5 - 8 Metalcopy Janalloy 316L EDS composition

	Composition % Wt.				
	Ag	Fe	Mg	Cu	Zn
Metalcopy Janalloy bonding material EDS	Bal.	1.6	1	3.2	11.3

Table 5 - 9 Metalcopy Janalloy bonding material EDS composition

	Composition % Wt.							
	Fe	Mo	Cr	Ni	Si	Ag	Cu	Zn
Metalcopy Janalloy combined EDS	Bal	0.5	7	8.5	0.1	17.4	2.7	7.3

Table 5 - 10 Metalcopy Janalloy EDS composition

The material was selected for the same reasons as Metalcopy 5507 and to determine if the thermal fatigue performance was similar.

5.3.3 Metalcopy Cu

Metalcopy Cu had the same powder material of stainless steel 316L as Metalcopy 5507 and Metalcopy Janalloy. However, the EDS analysis showed small differences in the alloying (Table 5 - 11). Table 5 - 12 shows the copper bonding material alloy and Table 5 - 13 shows the combined material composition. Table 5 - 14 shows the material properties of copper. When compared to the previous Metalcopy materials the thermal fatigue resistance could be impaired by the lower thermal conductivity, annealing temperature and higher Young's modulus. However, the material is corrosion resistant, has a higher hardness, higher tensile strength and a lower coefficient of linear thermal expansion than Metalcopy 5507 / Metalcopy Janalloy. Again without thermal fatigue testing it was uncertain how suitable this material would perform; hence it was selected for testing.

	Composition % Wt.									
	Fe	C	Mn	Si	P	S	Cr	Mo	Ni	N
316L EDS	Bal.	-	-	2.9	-	-	15.1	5	9.7	-

Table 5 - 11 316L EDS composition

	Composition % Wt.					
	Cu	Fe	Mo	Cr	Ni	Si
Metalcopy Cu bonding material EDS	Bal.	4.2	0.2	0.7	2.9	0.3

Table 5 - 12 Metalcopy Cu bonding material EDS composition

	Composition % Wt.					
	Fe	Mo	Cr	Ni	Si	Cu
Metalcopy Cu combined EDS	Bal.	2	12.8	7.8	0.7	24.9

Table 5 - 13 Metalcopy Cu EDS composition

Property	Value
Density (g/cm ³)	9.0
Thermal conductivity (W/m [°] K)	398
Coefficient of linear thermal expansion (m/m/°C)	16.5 x 10 ⁻⁶
Elastic modulus (bulk) (GPa)	140
Elastic modulus (rigidity) (GPa)	48
Elastic modulus (Young's) (GPa)	130
Elongation at break (%)	60
Ultimate tensile strength (MPa)	210
Yield tensile strength (MPa)	33.3
Poisson's ratio	0.3
Annealing temperature (°C)	405
Melting point (°C)	1085
Hardness (HRb)	110

Table 5 - 14 Material properties of pure copper (Shackelford and Alexander, 2001, Goodfellow, 2005, Environmental Chemistry, 2005, MatWeb, 2004)

5.4 Direct Die Materials

5.4.1 Laminated H13

Laminated H13 was selected as a candidate material as it is a tooling method, which employs commercial die material with excellent material properties (Table 5 - 2) in conjunction with a known brazing technique. As previously discussed, H13 has good thermal fatigue resistance. It is, however, unclear how the braze and indeed the laminate structure would perform when subjected to thermal fatigue, hence the material combination was selected for testing.

The nickel braze (Amdry 790) was commercially available and supplied by Sulzer Metco, The braze element data was provided by Sulzer Metco and is shown in Table 5 - 15. Table 5 - 15 also shows the EDS results (note boron cannot be detected by EDS) and highlighted an inconsistency in the iron content between the supplier's material data and the EDS analysis. It was expected that the small traces of Ti, Mo, Zr, P, S and Se would not be detected.

	Composition % Wt.											
	Ni	Si	B	Fe	C	Al	Ti	Mo	Zr	P	S	Se
Amdry 790	Bal.	3 - 4	1.5 - 2.2	1.5	0.06	0.05	0.50	0.05	0.05	0.02	0.02	0.005
EDS	Bal.	3.7	-	0.3	-	0.8	-	-	-	-	-	-

Table 5 - 15 Composition of Amdry 790 (Sulzer Metco (UK) Ltd., 1998)

Table 5 - 16 shows the EDS of the Vertical laminate structure and the H13 steel.

	Composition % Wt.					
	Fe	Mo	Cr	Ni	Si	V
Vertical laminate H13 EDS	Bal.	1	4.2	21.4	1.3	0.9
Vertical laminate combined EDS	7.6	0.4	0.5	Bal	8.1	0.2

Table 5 - 16 Vertical laminate EDS and Vertical laminate H13 EDS composition

Sulzer Metco had no mechanical data for Amdry 790 however, the material had a high percentage of nickel and its mechanical data is shown in Table 5 - 17. When compared with the bonding material materials of Metalcopy Cu, Metalcopy Janalloy and Metalcopy 5507 and the desired properties to resist thermal fatigue, nickel would have better resistance in terms of tensile strength, yield strength, annealing temperature, coefficient of liner expansion. However, it has a high Young's modulus and lower thermal conductivity, which may affect the thermal fatigue resistance of the material.

Property	Value
Density (g/cm ³)	8.9
Thermal conductivity (W/m ^o K)	90.9
Coefficient of linear thermal expansion (m/m/ ^o C)	13.3 x 10 ⁻⁶
Elastic modulus (bulk) (GPa)	180
Elastic modulus (rigidity) (GPa)	76
Elastic modulus (Young's) (GPa)	200
Elongation at break (%)	40
Ultimate tensile strength (MPa)	660
Yield tensile strength (MPa)	480
Poisson's ratio	0.3
Annealing temperature (^o C)	705
Melting point (^o C)	1455
Hardness (HV)	638 MN m ⁻² (over 120HRb)

Table 5 - 17 Material properties of pure nickel (Goodfellow, 2005, Environmental Chemistry, 2005, MatWeb, 2004)

5.4.2 3D Systems RapidSteel™

RapidSteel™ 1.0 was being phased out and replaced by RapidSteel™ 2.0 at the commencement of this research and was the only available metal from DTM / 3D Systems selective laser sintering process. The material is similar to Metalcopy in that the powder material is 316 stainless steel but it is infiltrated with 90% Cu / 10% Sn phosphor bronze. Table 5 - 18 shows the alloying data and the EDS results.

	Composition % Wt.	
	Cu	Sn
90/10PB	Bal.	10
EDS	Bal.	10.4

Table 5 - 18 Chemical composition and EDS analysis of phosphor bronze (MatWeb, 2004)

Many rapid tooling processes, like laser sintering, are layer manufacturing processes; it was thought that there could be differences in thermal fatigue properties depending upon the orientation of the specimens. It was decided to manufacture specimens in two different orientations. These were vertical and horizontal (Figure 5 - 1).

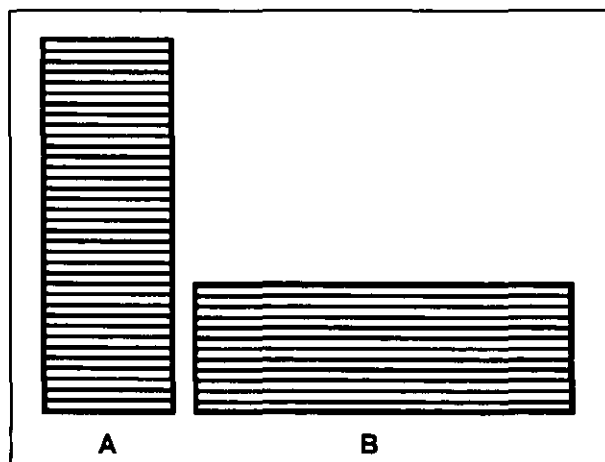


Figure 5 - 1 (A) Vertical orientation; (B) Horizontal orientation

Table 5 - 19 shows the alloy content of the RapidSteel™ 2.0 material, its bonding material and steel composition.

	Composition % Wt.				
	Fe	Cr	Si	Cu	Sn
Vertical RapidSteel™ 2.0 Steel	Bal	9	0.7	8.7	0.5
Vertical RapidSteel™ 2.0 bonding material EDS	1.7	0.1	0.3	Bal	10.4
Vertical RapidSteel™ 2.0 combined EDS	Bal	8.6	0.6	33.8	3.5
Horizontal RapidSteel™ 2.0 Steel	Bal	29	0.4	2.5	0.4
Horizontal RapidSteel™ 2.0 bonding material EDS	8.2	1.2	0.4	Bal	24.3
Horizontal RapidSteel™ 2.0 combined EDS	Bal	9.6	0.7	32.1	4.1

Table 5 - 19 RapidSteel™ 2.0 material, bonding material and steel EDS compositions

It should be noted that the composition of both the steel and the bonding material varied considerably depending upon the specific point chosen for analysis.

Comparing the desired material properties to resist thermal fatigue phosphor bronze has a significantly higher tensile strength than the other bonding materials. In comparison to Metacopy bonding materials it has a higher yield strength but not higher than nickel (Amdry 790), it has a good annealing temperature of 675°C. The Young's modulus is lower than nickel (Amdry 790) and similar to the copper bonding material. However, its thermal conductivity is low in comparison to the other bonding materials discussed (Table 5 - 20). The material was selected due to its reasonable mechanical properties (Table 5 - 20 and Table 5 - 21).

Property	Value
Density (g/cm ³)	8.8
Thermal conductivity (W/m ^o K)	50.0
Coefficient of linear thermal expansion (m/m/ ^o C)	18.4 x 10 ⁻⁶
Elastic modulus (bulk) (GPa)	-
Elastic modulus (rigidity) (GPa)	50.0
Elastic modulus (Young's) (GPa)	120
Elongation at break (%)	70
Ultimate tensile strength (MPa)	455 - 1014
Yield tensile strength (MPa)	193
Poisson's ratio	-
Annealing temperature (^o C)	675.0
Hardness (HRb)	55

Table 5 - 20 Material data for 90 Cu, 10 Sn phosphor bronze (MatWeb, 2004, Efunda, 2005, Goodfellow, 2005)

Property	Value
Density (g/cm ³)	7.5
Thermal conductivity (W/m ^o K)	23 @ 100 ^o C, 28 @ 200 ^o C
Coefficient of linear thermal expansion (m/m/ ^o C)	14.6 6 x 10 ⁻⁶
Elastic modulus (Young's) (GPa)	413
Elongation at break (%)	90
Ultimate tensile strength (MPa)	580
Yield strength (MPa)	413
Heat capacity (specific heat) (J/g ^o C)	339 - 418 @ 100-150 ^o C
Annealing temperature (^o C)	-
Melting point (^o C)	-
Hardness (HRb)	99 - 103.5

Table 5 - 21 Material properties of RapidSteel™ 2.0 (DTM corporation, 1999)

5.4.3 EOS GmbH DirectSteel 20µm

DirectSteel 20µm was a new material developed by EOS GmbH superseding DirectSteel 50µm at the commencement of this work, enabling 20 micron layers to be sintered. EOS GmbH also supply DirectMetal 20µm material (bronze based material containing nickel), however, the main limitation is its maximum operating temperature of 400^oC. EOS DirectSteel 20µm was selected as its maximum operating temperature is 800^oC and has superior material properties over DirectMetal 20µm (Table 5 - 22). The previous materials have been compared using their bonding material. EOS DirectSteel however, is an alloy and is not infiltrated. However, when comparing the material properties it does have the lowest thermal conductivity of all the materials. In comparison to Metacopy it has higher tensile strength and good yield strength but not as high as nickel (Amdry 790). When compared to phosphor bronze it has a lower tensile strength but higher yield strength. The material also has the lowest coefficient of linear thermal expansion in comparison to the other materials. These factors made it a suitable candidate material. EOS DirectSteel H20, however, is now available (Quarter 1, 2004 EOS GmbH, 2005),

which has much improved material properties and would have been the material of choice had it been available at the time.

Property	DirectMetal 20µm	DirectSteel 20µm	DirectSteel H20
Density (g/cm ³)	6.3 - 7.6	6.3 - 7.6	7 - 7.8
Thermal conductivity (W/m ^o K)	30	13 @ 50°C	15 - 18
Coefficient of linear thermal expansion (m/m ^o C)	18 x 10 ⁻⁶	9 x 10 ⁻⁶ @ 50°C	13 - 15x10 ⁻⁶
Elastic modulus (bulk) (GPa)	-	-	-
Elastic modulus (rigidity) (GPa)	-	-	-
Elastic modulus (Young's) (GPa)	80	130	180
Elongation at break (%)	-		
Ultimate tensile strength (MPa)	400	600	1100
Yield strength (MPa)	200	400	800
Poisson's ratio	-	-	-
Annealing temperature (°C)	-	-	-
Max operating temperature (°C)	400	800	1100
Hardness (HRb)	65	94	42

Table 5 - 22 Material properties of EOS GmbH materials (supplied by EOS GmbH)

EOS DirectSteel 20µm contains steel (alloy not divulged) alloyed with nickel. An EDS analysis was unable to determine a grade of steel as carbon cannot be detected. Using this technique, however, it is clear it was a plain carbon steel as it did not contain carbide forming elements and it was not a stainless steel as no chromium was evident. The material was an alloy of plain carbon steel, nickel and copper (Table 5 - 23).

	Composition % Wt.			
	Fe	Ni	Cu	P
EOS DirectSteel 20µm EDS	Bal.	26.3	9.3	1.3

Table 5 - 23 EDS analysis of EOS GmbH DirectSteel 20µm

5.5 Density of the Test Materials

The aim was to determine the density of each material, bonding material and powder.

5.5.1 Methodology

The density of a material is calculated by dividing its weight by its volume.

Weight / Volume = Density (g/cm³)

Equation 5 - 1

However, to determine the volume of specimen accurately it was necessary to weigh the specimens in air and in a beaker of water (300ml) and subtract one result from the other.

Archimedes principle states that the:

Weight of an object in air (g) - Weight of the same of the same object in water (g) = Weight of the water that the object displaces (g) Equation 5 - 2

As 1g of water occupies 1cm³ at 25°C (Oberg et.al., 1996) the volume of the object can be determined, hence:

Weight of an object in air (g) - Weight of the same of the same object in water (g) = Volume of that object (cm³) Equation 5 - 3

The water temperature was maintained at a constant 25.5°C throughout the test. The Stanton Unimatic, Model C.L.1 (Figure 5 - 2) scales were calibrated using several standard weights. Five specimens of each material were tested with the exception of Amdry 790 because insufficient braze material was available to manufacture five specimens.



Figure 5 - 2 Stanton Unimatic model C.L.1

The densities of all the specimens are shown in Appendix i, Figure 1, and the average densities for each material, bonding material and powder are shown in Figure 5 - 3.

5.5.2 Results

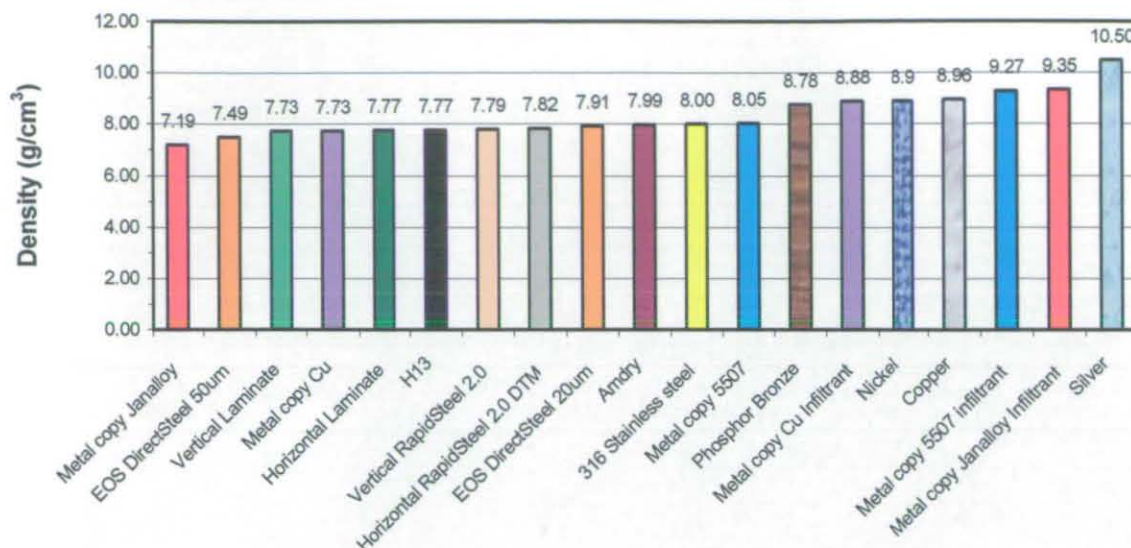


Figure 5 - 3 Average material density

5.5.3 Review of Results

The density of H13 was determined, from the experiments, to be 7.77g/cm^3 , which compared well with the standard value of 7.8g/cm^3 (MatWeb, 2004) - a difference of approximately 0.4%.

Metalcopy Janalloy was determined to have a density of 7.19g/cm^3 and a bonding material density of 9.35g/cm^3 (reference value of silver density is 10.49g/cm^3 MatWeb, 2004). The Metalcopy Janalloy specimens increased in weight suggesting that they were porous and would explain the reason for the variation in the density results (Appendix i, Figure 1); this may affect thermal fatigue of the material as any void acts as a stress raiser from which a crack can initiate. In turn, porosity can also affect thermal conductivity as the void or voids act as an insulator (s).

Metalcopy 5507 had a density of 8.05g/cm^3 and a bonding material density of 9.27g/cm^3 . Janalloy and Metalcopy 5507 should have identical had densities. The bonding material densities were similar differing by approximately 0.85%, however; their overall densities had a difference of approximately 10.7%. The likely cause of the difference was the porosity in the Metalcopy Janalloy.

Metalcopy Cu had a density of 7.73g/cm^3 and a bonding material density of 8.88g/cm^3 . The density value for Cu is 8.96g/cm^3 (MatWeb, 2004), approximately 0.9% difference.

Both laminate specimens had similar densities 7.3g/cm^3 and 7.7g/cm^3 with the nickel braze having a density of 7.99g/cm^3 (density of pure nickel is 8.88g/cm^3 , MatWeb, 2004).

The horizontal and vertical RapidSteel™ 2.0 specimens also had similar densities of 7.8g/cm^3 (DTM corporation, 1999, value 7.5g/cm^3). Although the density of the bonding material was not

tested it was infiltrated with phosphor bronze 90% Cu 10% Sn, which has a density of 8.78g/cm^3 (MatWeb, 2004).

The EOS DirectSteel 20 μm and 50 μm material is an alloy of Fe, Ni and Cu and had a density of 7.91g/cm^3 and 7.49g/cm^3 respectively (EOS (2005) value for DirectSteel 20 μm 6.3g/cm^3 - 7.6g/cm^3).

5.6 Thermal Conductivity Experiment

A series of experiments were required to test the thermal conductivity of the materials.

5.6.1 Methodology

5.6.1.1 Test Apparatus

The thermal conductivity test used was the guarded axial flow method manufactured by Cussons Technology. The test was chosen because it is a long established test method and produces the highest accuracy (Anter Corporation, 2005), (ASTM C 177 - 04, DIN 52612 or BS 874 - 2.1 and 3.1 test method). This steady state technique involves placing a solid specimen of fixed dimension between two temperature controlled plates. One plate is heated while the other plate is cooled, and their temperatures are monitored until they are constant. The steady state temperatures, the thickness of the specimen and the heat input are used to calculate the thermal conductivity (Figure 5 - 4).

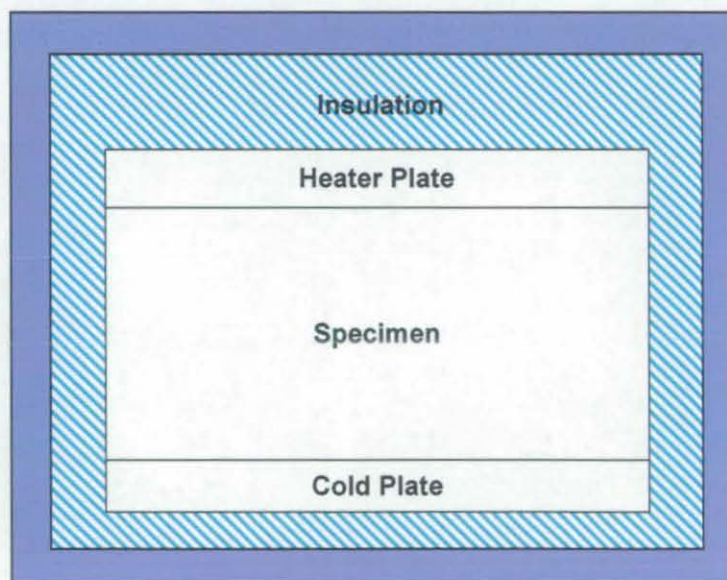


Figure 5 - 4 Guarded hot plate assembly

A steady state condition has to be achieved with this method of measurement. The test also requires the following to be recorded:

- The unidirectional heat flux in the metered region
- Temperatures of the hot and cold surfaces
- The dimensions of the specimens

The Cussons thermal conductivity apparatus Model P5687 (Figure 5 - 5) consists of a self clamping specimen stack assembly with an electric heat source in the dewar vessel (vacuum flask) (Figure 5 - 6), calorimeter base, dewar vessel enclosure (to ensure negligible loss of heat), and a constant water supply. Two mercury glass thermometers are provided to allow water inlet and outlet temperature readings. Four calibrated nickel chromium / nickel aluminium (type K) thermocouples were fitted and connected to a suitable potentiometer instrument to give accurate metal temperature readings.



Figure 5 - 5 Cussons thermal conductivity apparatus model P5687

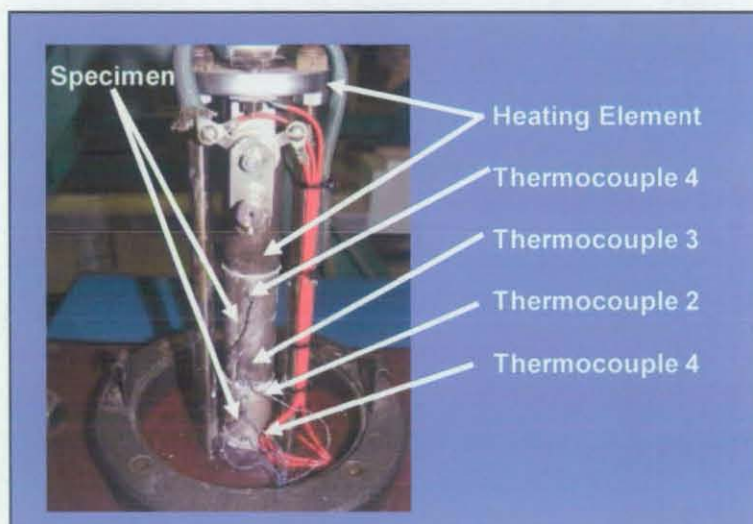


Figure 5 - 6 Self clamping specimen stack inside the dewar vessel

5.6.1.2 Specimen Preparation

A range of specimen lengths should be available depending upon the thermal conductivity of the material, for example when testing copper or aluminium (materials with high thermal conductivity), the specimen length needs to be longer in order to attain a noticeable temperature drop over the specimen length. Figure 5 - 7 shows three specimen sizes to suit the Cussons thermal conductivity apparatus. Specimen A and B need to be tested together so their overall length is sufficient (102mm) to test in the apparatus. The maximum specimen size is Ø25 with a

length of 102mm which is dictated by the Cussons thermal conductivity apparatus model P5687. Using two specimens is preferred as a reference specimen can be used to validate the test.

All the specimens in this experiment were machined to the dimensions shown in Figure 5 - 7 A because of the limited quantity of material available. The exception was the 99.9% pure iron which was used as the reference specimen for the thermal conductivity test as it was a pure material with a known thermal conductivity over a temperature range. The 99.9% pure iron was machined to the dimensions shown in Figure 5 - 7 B and used in every test.

The specimens were turned and the ends ground to an average surface roughness of $1\mu\text{m}$ (Ra) to ensure good surface contact and accurate specimen length (38mm \pm 0.01mm). Two $\varnothing 2\text{mm}$ holes were drilled to the centre of the specimens with hole centres of 25mm \pm 0.01mm.

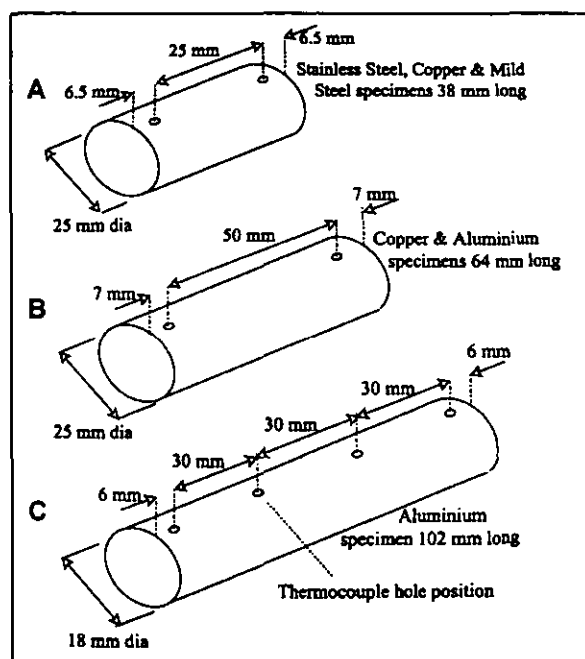


Figure 5 - 7 Specimen geometries

Five specimens of each of the following materials were chosen to ensure reproducibility:

- H13 tool steel (steel from Taylor Special Steels, cast number R0128)
- Metalcopy 5507 (Wiba / Prototal)
- Metalcopy 5507 bonding material (Wiba / Prototal)
- Metalcopy Janalloy (Wiba / Prototal)
- Metalcopy Janalloy bonding material (Wiba / Prototal)
- Metalcopy Cu (Wiba / Prototal)
- Metalcopy Cu bonding material (Wiba / Prototal)

- Vertical laminate braze bonded H13 tool steel (1mm thick H13 sheet 0.15mm braze thickness). Details of brazing process is discussed in Appendix iii, section iii.v (steel from Bohler Special Steels, braze supplied by Sulzer Metco)
- Horizontal laminate braze bonded H13 tool steel (Details of process and thickness of sheet and braze is discussed in Appendix iii, (steel from Bohler Special Steels, braze supplied by Sulzer Metco)
- Amdry 790 (laminate braze supplied by Sulzer Metco)
- Vertically built RapidSteel™ 2.0 (built by DTM Corporation)
- Horizontally built RapidSteel™ 2.0 (built by DTM Corporation)
- Vertically built EOS DirectSteel 50µm (built by EOS GmbH)
- Horizontally built EOS DirectSteel 50µm (built by EOS GmbH)
- Vertically built EOS DirectSteel 20µm (built by EOS GmbH)
- Horizontally built EOS DirectSteel 20µm (built by EOS GmbH)

5.6.1.3 Test Procedure

One test specimen was placed in the apparatus with one 99.9% iron reference specimen to ensure consistency between each test. The 99.9% iron reference specimen was placed in the lower position of the stack with Electrolube heat transfer compound (HTC10S), (supplied by RS Components), applied to the mating surfaces to ensure good contact. The clamp mechanism was applied and the thermocouple tips coated with Electrolube then inserted into the specimens and the dewar vessel replaced.

The water supply was turned on and adjusted to give a small regular flow of 0.5cc/sec – 1cc/sec. During the experiment adjustment of the flow was required to prevent the difference in temperature between the thermometers from exceeding 10°C in order to prevent excessive cooling.

The heat delivered to the specimen was controlled so that thermocouple 4 (T_4) was stable, at approximately 200°C. It was maintained at this temperature so the other thermocouples (T_1 , T_2 , and T_3) could stabilise at their independent temperatures.

During the test the following were recorded every 2 minutes for the duration of the test.

T_{in}	=	Temperature of water in (°C)
T_{out}	=	Temperature of water out (°C)
$T_1 - T_4$	=	Thermocouple temperatures (°C)

The test was run for a minimum of 600 seconds and upon completion the following were recorded:

M	=	Mass of water (kg or ml)
-----	---	--------------------------

s = Test duration (seconds)
Amp = Amperage (amps)

5.6.2 Results

The conductivity of each specimen was determined using the Fourier equation:

$$KA(\Delta T)/L = mS(T_{out}-T_{in}) \quad \text{Equation 5 - 4}$$

$$\text{Therefore } K = L(mS(T_{out}-T_{in}))/A(\Delta T) \quad \text{Equation 5 - 5}$$

Where:

K = Conductivity of the specimen (W/m²k)
L = Distance between thermocouples (m)
M = Mass of water (kg or ml)
s = Test duration (seconds)
m = Mass flow of cooling water (M/s)
S = Specific heat of water (J/kg°C)
T_{out} = Temperature of water out (°C)
T_{in} = Temperature of water in (°C)
A = Cross sectional area of the specimen (m²)
ΔT = Temperature change over length (°C)

The first specimens to be tested were the 99.9% pure iron reference specimens and the H13 specimens. Pure iron thermal conductivity varies with temperature from 69W/m²K at 125°C to 61.3W/m²K at 225°C (Efunda, 2005).

Both specimens were tested in the top position in the apparatus and at ≈200°C. Table 5 - 24 and Table 5 - 25 shows the results. The thermal conductivity of the 99.9% iron reference specimen is comparable to thermal conductivity data found in literature (Efunda, 2005).

Specimen	Test temperature (°C)	Thermal conductivity (W/m ² K)
Iron 99.9% pure 1	201.70	63.38
Iron 99.9% pure 2	204.40	64.35
Iron 99.9% pure 3	205.60	60.92
Iron 99.9% pure 4	208.77	61.89
Iron 99.9% pure 5	209.32	61.99
Average	205.96	62.51

Table 5 - 24 Thermal conductivity of 99.9% pure iron

Specimen	Test temperature (°C)	Thermal conductivity (W/m°K)
H13 1	211.72	25.88
H13 2	200.58	26.53
H13 3	200.65	25.42
H13 4	202.52	25.79
H13 5	203.00	25.48
Average	203.7	25.82

Table 5 - 25 Thermal conductivity of H13 tool steel

Appendix i, Table 1 to Appendix i, Table 16 show the values obtained during the tests and the calculations used to derive the thermal conductivity of the materials.

Figure 5 - 8 shows the average thermal conductivity for each specimen.

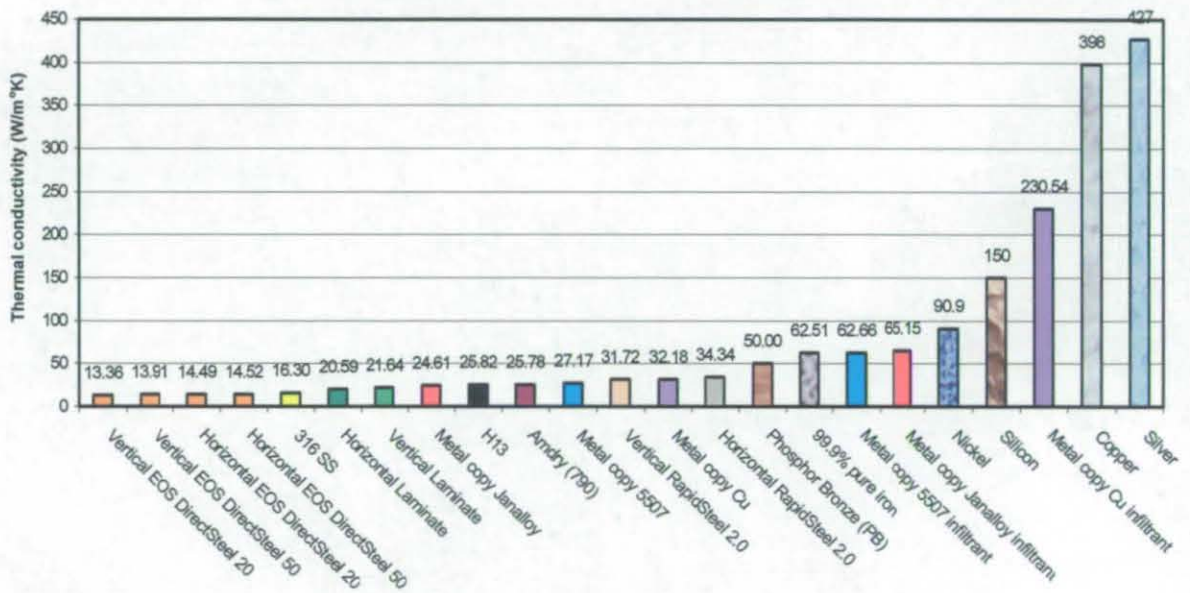


Figure 5 - 8 Thermal conductivity average results

5.6.3 Review of Results

The reference specimen of 99.9% pure iron had an average thermal conductivity of 62.51W/m°K at 205.96°C. This is a difference of only 0.24W/m°K (0.4%) from the value found by Efunda (2005). The results with iron showed the thermal conductivity apparatus was accurate and gave confidence in the test and results of the other materials.

Metalcopy 5507 and Metalcopy Janalloy were manufactured by the same process as discussed in section 4.2.2 but the silver bonding alloy (chemical composition) was different (section 5.3.1 and section 5.3.2). Metalcopy 5507 bonding material was manufactured by a supplier whilst Metalcopy Janalloy bonding material was made by Prototal AB. As expected the thermal conductivities of the infiltrated materials were similar 27.2W/m°K and 24.6W/m°K respectively, a difference of approximately 2.6W/m°K or approximately 10%. The thermal conductivity of their bonding material was also similar to one another 62.7W/m°K and 65.2W/m°K respectively, a

difference of $2.5\text{W/m}^{\circ}\text{K}$ or approximately 4%. The variation between the results may have been due to the slight differences in the chemical make up of the specimen and the formation of inclusions and porosity during manufacture. The experiment also showed that the bonding material (Metalcopy 5507 = $62.66\text{W/m}^{\circ}\text{K}$ and Metalcopy Janalloy = $65.15\text{W/m}^{\circ}\text{K}$) and the powder material (316 Stainless Steel = $16.3\text{W/m}^{\circ}\text{K}$) had dissimilar thermal conductivities (Figure 5 - 8), which was likely to be detrimental to their thermal fatigue performance.

Metalcopy Cu had a thermal conductivity of $32.2\text{W/m}^{\circ}\text{K}$ and was supposed to be infiltrated with copper but the infiltrant material only had a thermal conductivity of $230.5\text{W/m}^{\circ}\text{K}$ whereas pure copper, (99.9%) has a thermal conductivity, of $401\text{W/m}^{\circ}\text{K}$ (Hypertextbook, 2003). However, from EDS chemical analysis the bonding material was shown not to be pure copper and the method of manufacture may have caused inclusions and porosity. Metalcopy Cu had the largest difference between powder (316 stainless steel = $16.3\text{W/m}^{\circ}\text{K}$) and bonding material ($230.54\text{W/m}^{\circ}\text{K}$) thermal conductivity, of all the materials tested.

The laminated steel, RapidSteel 2.0 selective laser sintering and EOS DirectSteel $20\mu\text{m}$ direct laser sintering materials were built in two orientations to determine whether or not the build direction affected their thermal conductivities (vertical and horizontal).

The Vertical laminate steel specimens brazed with Amdry 790 gave similar results to those of the Horizontal laminate steel specimens brazed with Amdry 790, $21.6\text{W/m}^{\circ}\text{K}$ and $20.6\text{W/m}^{\circ}\text{K}$ respectively. The braze (Amdry 790) had a thermal conductivity of $25.8\text{W/m}^{\circ}\text{K}$, which is surprising as it contains over 90% Ni (confirmed by EDS, chapter 5, section 5.4.1), which has a thermal conductivity value of $90.7\text{W/m}^{\circ}\text{K}$ (Environmental Chemistry, 2005, Goodfellow, 2005). It was shown later that the specimens contained voids that were most probably formed when the braze powder was melted. The brazing process can cause gas entrapment. During brazing, flux can also be trapped causing voids or porosity in the specimen.

Build orientation did not have a major affect on the thermal conductivities of RapidSteel 2.0. The vertically built RapidSteel 2.0 had a thermal conductivity of $31.7\text{W/m}^{\circ}\text{K}$ and the horizontally built RapidSteel 2.0 had a thermal conductivity of $34.3\text{W/m}^{\circ}\text{K}$ (Figure 5 - 8), a difference of $2.6\text{W/m}^{\circ}\text{K}$ or approximately 7.5%. There is a discrepancy between the thermal conductivity recorded in the test and DTM Corporation, 1999 literature, which states RapidSteel 2.0 has a thermal conductivity of $28\text{W/m}^{\circ}\text{K}$. The difference may be due to inconsistent infiltration. Although the bonding material was not tested due to availability, it is phosphor bronze (90% Cu, 10% Sn) (DTM Corporation, 1999) with a thermal conductivity of $50\text{W/m}^{\circ}\text{K}$ (Hypertextbook, 2003). As with the Metalcopy materials there was a large difference between thermal conductivities of the powder and bonding materials.

The EOS DirectMetal materials were built in two orientations, vertically and horizontally. Two different layer thicknesses ($50\mu\text{m}$ and $20\mu\text{m}$) were also tested. The EOS DirectMetal materials had the lowest thermal conductivities (average $14.08\text{W/m}^{\circ}\text{K}$) with values between $13.4\text{W/m}^{\circ}\text{K}$ -

14.5W/m°K. In turn the values were very similar to the literature values for EOS of 13W/m°K (EOS, 2005).

The difference in thermal conductivity between bonding and powder material, of many of the materials, may affect thermal fatigue resistance because of induced internal stresses. (Weroński and Hejwoski, 1991).

Chapter 6: Establishing the Thermal Fatigue System (Parameters, Equipment and Specimens)

At the time of this research information on the temperature cycle within the aluminium pressure die casting tool during casting was sparse. It was, therefore, necessary to conduct experiments to determine this.

Tests were carried out to establish the temperature at the surface of a die. It was necessary to calibrate thermocouples and the temperature paints to verify the thermocouple readings (Appendix ii).

6.1 Tool Temperature Recording

6.1.1 Aim

To assess the performance of tool materials for thermal cycling applications such as aluminium pressure die-casting it was necessary to determine the thermal cycle of the process in order to conduct an accurate and comparative thermal fatigue experiment. A series of tests was conducted to establish the temperature profile of an aluminium pressure die-casting tool surface, under production conditions. The results were then used to determine the temperatures and cycle time for the thermal fatigue experiment.

6.1.2 Methodology

Obtaining a temperature profile was not a simple process because of the high pressures and speed of solidification in the pressure die casting process. The main problem was locating and securing the thermocouples in position on the surface of the die. They had to be located and secured, such that they resisted being pushed back into the bolster during injection, to prevent the aluminium escaping the cavity.

6.1.3 Mould Design

A typical industrial aluminium pressure die casting tool was required that could be modified to accommodate thermocouples. The tool needed to be manufactured from H13 tool steel (standard die material) to ensure the thermal characteristics of the tool were accurate.

A typical production H13 multi cavity (four) aluminium die cast tool was chosen. This was a tool for a clutch housing. The tool consisted of 5 inserts three on the moving half (Figure 6 - 1 (A)) and two on the fixed half; this arrangement made tool modification easier since they could easily be removed from the bolster and if damaged, replaced. The casting had a shot weight of 250g with runner and biscuit and all four components (Figure 6 - 1 (B)), and an individual component weighed 14g (Figure 6 - 2).

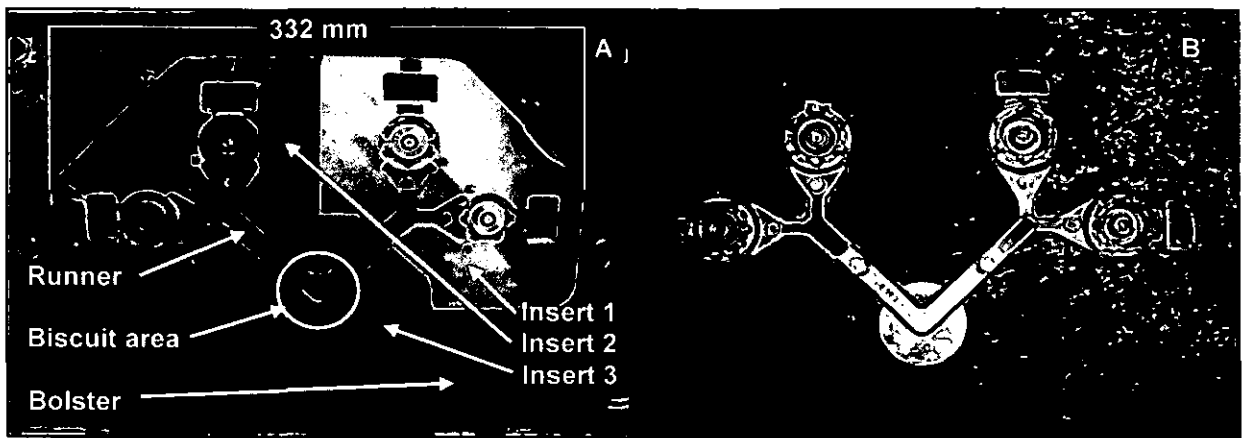


Figure 6 - 1 (A) Moving half of the tool; (B) Clutch housing casting (Supplied by Dyson and Kemlows)

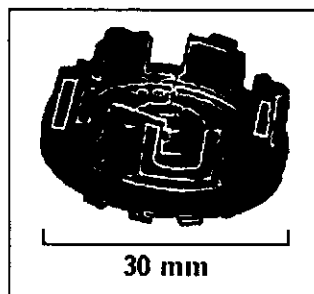


Figure 6 - 2 CAD image of 'Dyson' clutch housing

6.1.4 Cast Alloy

The casting alloy used was Al-Si8-Cu3 or LM24 (BS, 1490 / ASTM, B85-03). The alloy is commonly used for pressure die casting because its material properties are well suited for the process (Table 6 - 1).

Property	Value
0.2% Proof stress	150 N/mm ²
Tensile strength	180 N/mm ²
Elongation	1 - 3%
Impact resistance Charpy	3.4 Nm
Brinell hardness	85
Expansion coefficient	2.3 x10 ⁻⁵ N/mm ²
Shear strength	195 N/mm ²

Table 6 - 1 LM24 die-cast properties

Aluminium is prone to hydrogen absorption when molten, which can cause porous castings; this was resolved by modifying the alloy in the furnace by degassing. The aluminium was degassed by bubbling nitrogen through the molten alloy. The alloy also required fluxing (Foseco, Coverall 11); this separated the dross from the molten aluminium so that it rose to the surface creating a protective layer that hydrogen could not penetrate. The dross was only removed at the

beginning of the casting process. A sample of molten aluminium was taken in order to test the gas level using a hydrogen gas analyser, it was found to contain 0.15 - 0.25 cc of gas / 500g, which was within typical casting limits.

6.1.5 Die Casting Machine Parameters

The machine used had to be large enough to accommodate the size of the die and the shot weight. A Frech DAK 125 SDV cold chamber machine was used (Figure 6 - 3).



Figure 6 - 3 Frech DAK 125 SDV

The machine was set up to the values required when the die was in production. The parameters were provided by Kemlows Die Casting Products and are shown in Table 6 - 2 with the casting cycle shown in Figure 6 - 4. For consistency of die cooling, the automated die lubricator on the machine was utilised. The die lubricant (release agent) was Acheson DeltaCast 333 release 3, at $\approx 20^{\circ}\text{C} - 25^{\circ}\text{C}$; this was sprayed onto the die surface immediately prior to each shot, through six nozzles for three seconds.

As in production, the die was initially heated to approximately 150°C with a gas lance and 50 shots ran through to heat the die to the operating temperature.

Parameter	Value
Machine type	Frech DAK 125 SDV
Max piston velocity (1 st Phase)	0.15 m/s
Max piston velocity (2 nd Phase)	0.8 m/s
Start 2 nd phase	140mm
Start 3 rd Phase	270mm
Maximum shot chamber length	315mm
Maximum die closing force	125 tonne
Alloy	LM24
Pouring temperature	750°C
Initial temperature of die	180°C
Die coating material	DeltaCast 333 R3
Total cycle time	20- 24 seconds
Piston size	Ø 50mm
In gate velocity	2.48 m/s
Shot weight	250g
System pressure	105 bar

Table 6 - 2 Casting parameters

Operator Starting cycle 1-2 sec	Die Close 1sec	Ladling 5-8 sec	Injection 1 sec	Solidification 3 sec	Die Open 3 sec	Ejection 3 sec	Release Agent 3 sec
--	-----------------------------	---------------------------	---------------------------	--------------------------------	--------------------------	--------------------------	----------------------------------

Figure 6 - 4 Casting machine process cycle

6.1.6 Tool Temperature Experiment One

6.1.6.1 Methodology

Measuring the surface temperature was difficult and several attempts and test adaptations were conducted. An initial attempt to determine the surface temperature of a die resulted in an aluminium blow out causing considerable loss of time because the die had to be disassembled cleaned, repaired and re-assembled (Figure 6 - 5).

It was obvious from the first attempt that the thermocouples required relocation resulting in the machining of the bolster and the insert, to secure two calibrated mineral insulated k-type 0.25mm diameter end ground thermocouples by means of a collet. The size of the thermocouples was important because the smaller the diameter of the wire the faster the reaction speed. A compromise had to be made, if the thermocouple was too small it would be destroyed, and if it was too big its response rate would be too slow.

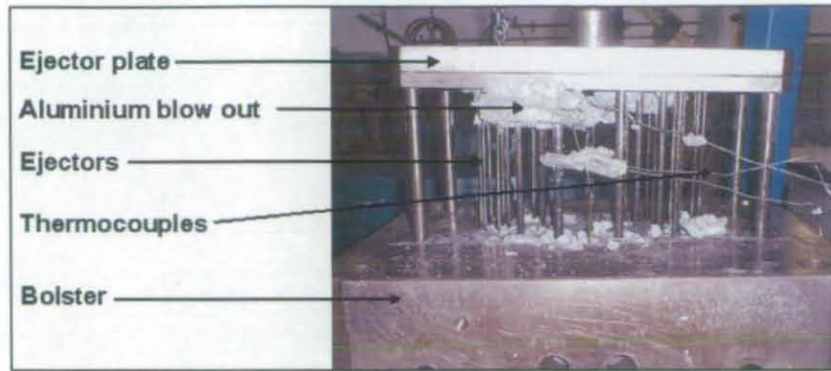


Figure 6 - 5 Aluminium blow out through thermocouple holes

The thermocouple tips were positioned at the die surface to allow direct contact with the molten aluminium as it entered the die. The temperature sensitive paints were placed in the biscuit and runner system of the aluminium die cast tool as these areas are typically subjected to the most heat (Figure 6 - 6). However, it was found that as the aluminium was being forced down the runners it washed the paints away. The location of the paints was changed to the over flow region of the die, to solve this problem (Figure 6 - 6).

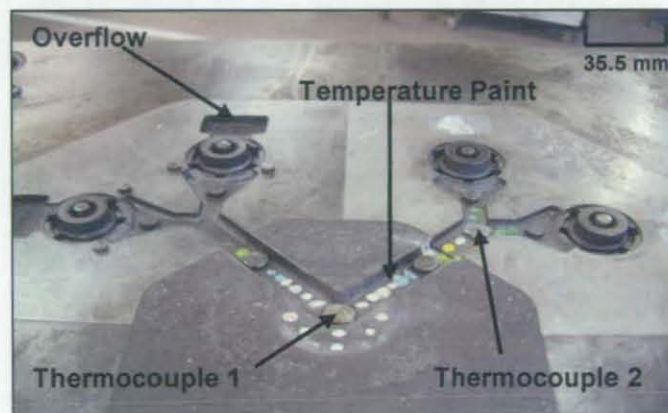


Figure 6 - 6 Location of the thermocouples and temperature paint on the moving half of the tool

The thermocouples were connected via a compensating cable to a computer data logger controlled by National Instruments LabVIEW™ version 5.1.1 software. It enabled several thermocouples to be connected at once. The data could also be loaded into Microsoft Excel. A screen dump of the software is shown in Figure 6 - 7.

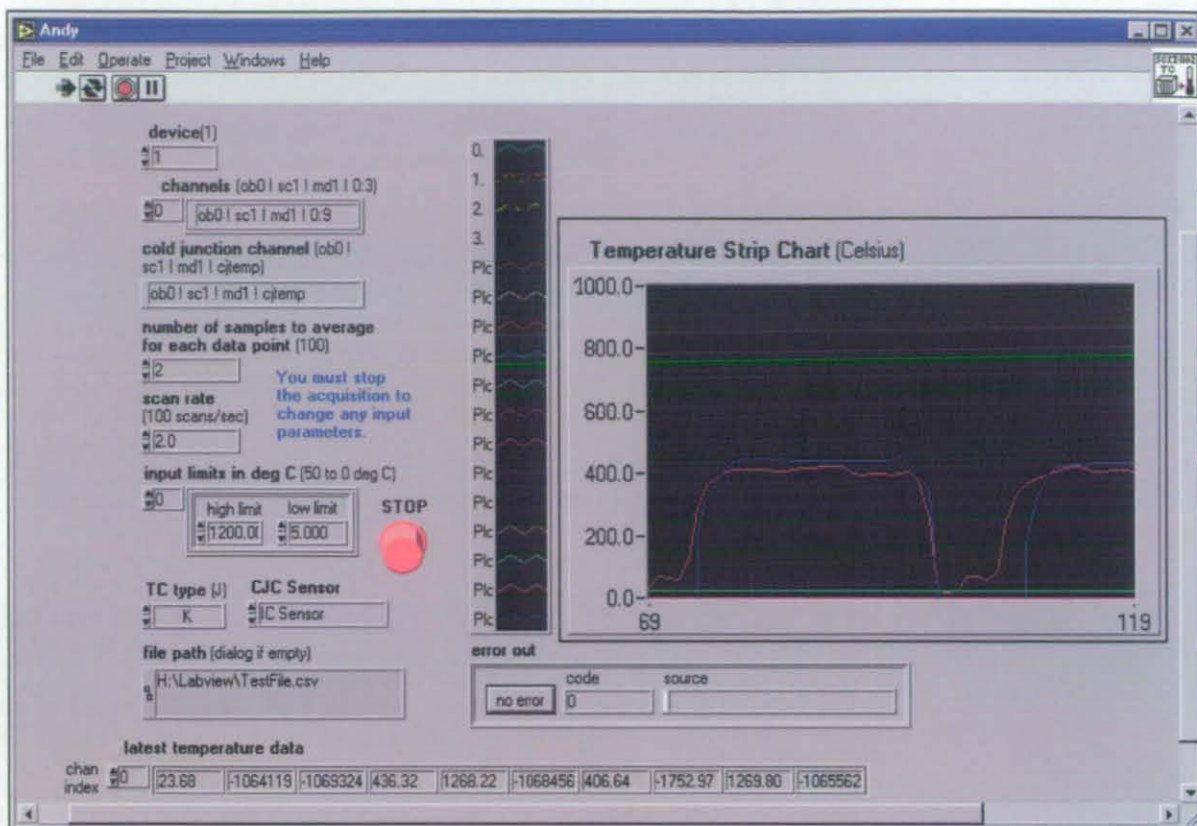


Figure 6 - 7 Screen dump of LabVIEW data logging software

6.1.6.2 Results

Figure 6 - 8 shows the results obtained from this test. Unfortunately the thermocouple in the runner failed when the die was warmed up to 250°C as it was directly next to the gas lance. The thermocouple in the hottest area (biscuit) survived and the test continued showing the surface temperature of the die reaching 350°C and cooling to between 150°C - 200°C with a typical cycle time of 20 - 24 seconds (Figure 6 - 9). However, the paints suggested that the surface temperature was between 399°C and 454°C.

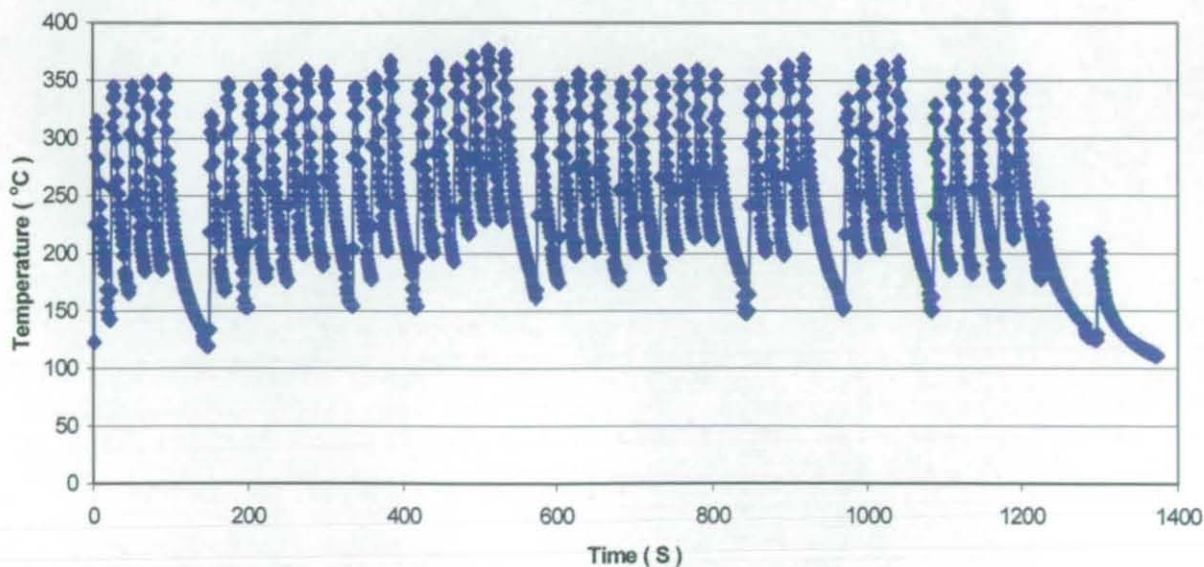


Figure 6 - 8 Graph showing tool surface temperature during casting (biscuit area)

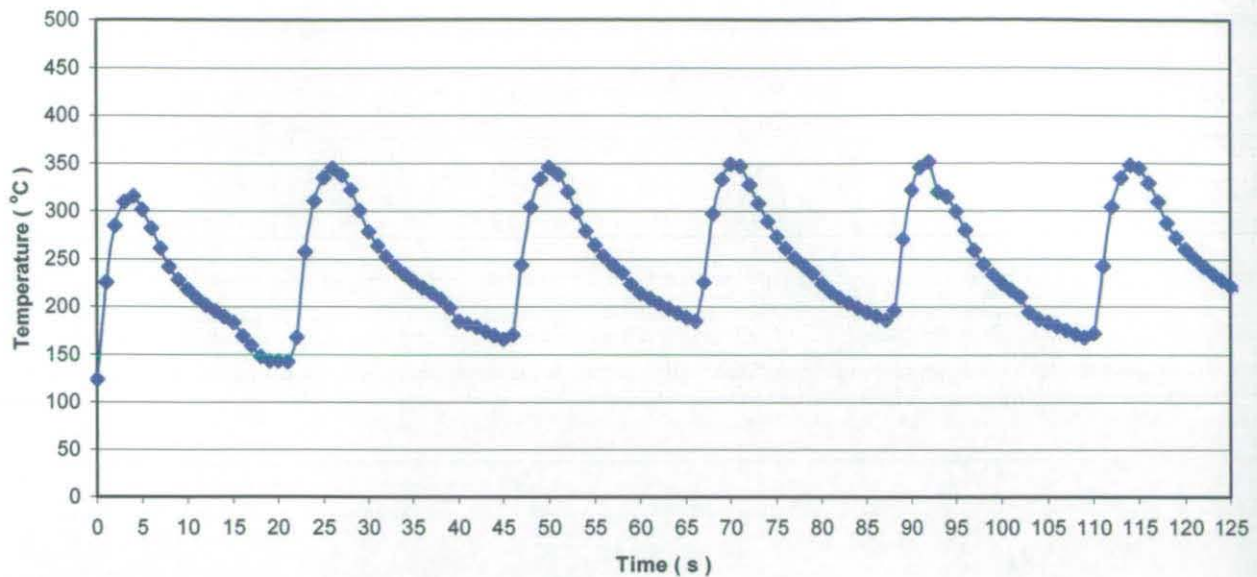


Figure 6 - 9 Section of figure 6 - 8 showing tool surface temperature during casting (biscuit area)

It was clear that reaction time of the thermocouples was too slow because of the large wire diameter and the insulation. Hence, the results obtained were not representative of the surface temperature in an aluminium pressure die-casting cycle because the thermocouples were not able to measure the temperature fast enough.

6.1.7 Tool Temperature Experiment Two

6.1.7.1 Methodology

To overcome the problem in the previous experiment several fibre glass insulated K type open ended thermocouples, with a wire diameter of 0.3mm, were adhered to the surface of the die. These thermocouples have a faster reaction time since they are open ended. There was, however, a question over their ability to survive the conditions long enough to enable a temperature reading to be obtained.

An additional problem was that the die could not be preheated as before since the thermocouples were fixed to the surface of the die with masking tape. However, a few shots were ran through the die to increase the temperature prior to applying the thermocouples.

6.1.7.2 Results

The results showed that on occasion the die temperature reached over 450°C but was typically between 400°C and 450°C (Figure 6 - 10). The paints verified this.

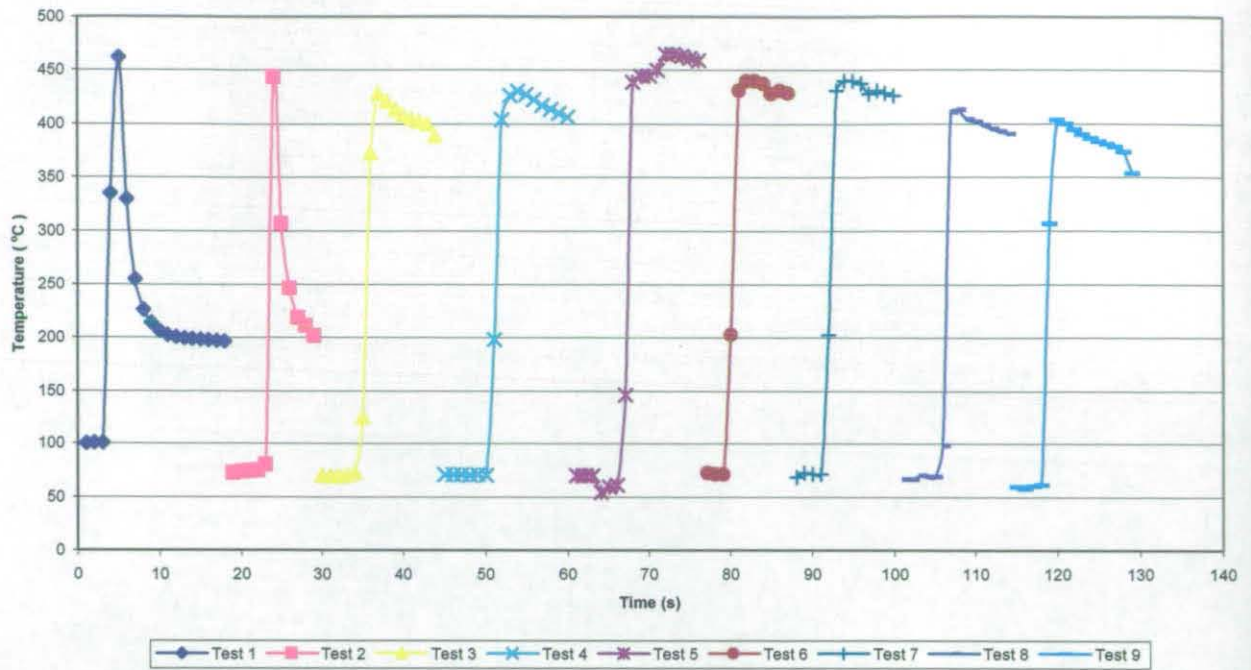


Figure 6 - 10 Tool temperature review

Unfortunately the cooling profile could not be obtained using the small thermocouples as they failed upon opening the die. However, the cooling profile could be obtained from Figure 6 - 9. Cooling occurred over a longer period of time (≈ 20 s) allowing the thermocouples to respond. This allowed the aluminium pressure die casting thermal cycle shown in Figure 6 - 11 to be determined.

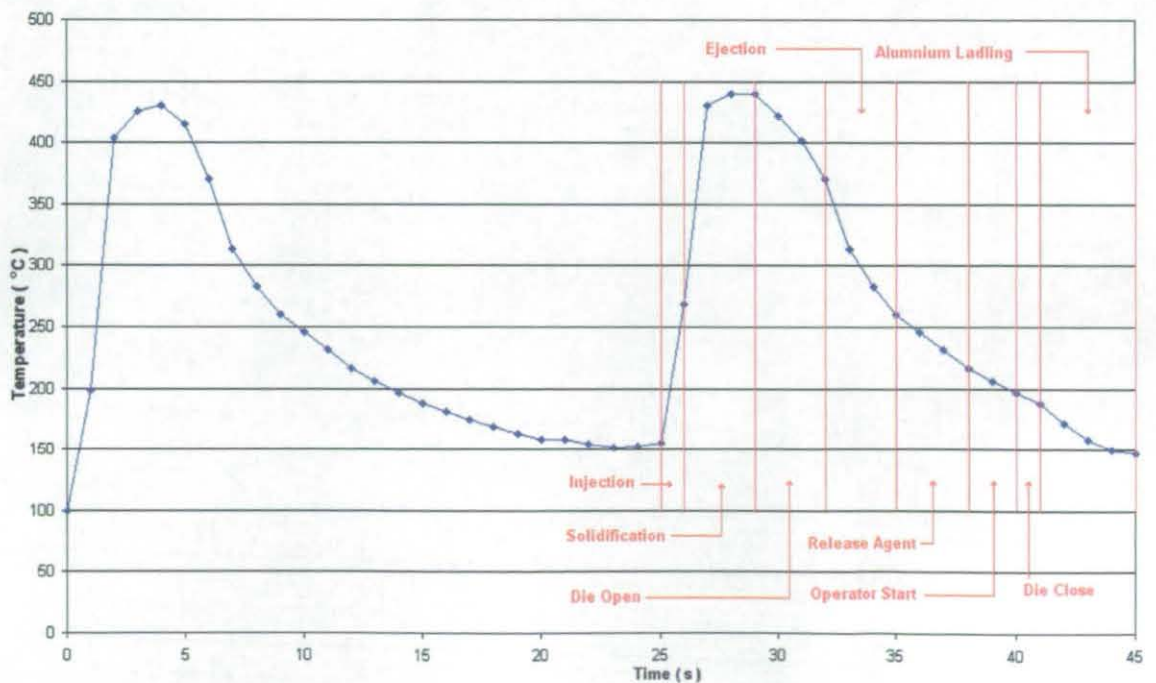


Figure 6 - 11 Aluminium pressure die casting thermal cycle

6.2 Design of Thermal Fatigue Specimens and Apparatus

It was considered to be inadvisable to use the Wallace dunk experimental procedure on rapid tooling materials because the procedure cools the specimen internally with pressurised water. Rapid tooling materials could contain flaws, voids / porosity etc., which could allow the water to leak and make contact with the molten aluminium (Wallace's heating medium) leading to a violent reaction. Wallace's specimens are designed to crack from the small radius.

At this point in time Persson's (2003, 2004), (Persson et.al., 2005) research had not been published.

6.2.1 Specimen

One of the advantages of the Wallace et.al., (1997), (Wallace et.al., 2000) specimen was that it had a small radius, which acts as a stress concentrator from which cracks initiate and propagate. This allowed crack initiation and propagation to be measured and recorded. Glenny et.al., 1959, however, used a disc shaped specimen with a small edge radius of 0.5mm. This is typically the smallest expected on a die. The specimen also had a change in cross section, which also occurs in dies, making it a suitable specimen geometry. The discs (Figure 6 - 12) were designed to initiate cracks at the edge radius (stress concentrator) and allow for ease of measurement. The specimen size was also relatively small (\varnothing 61mm) resulting in less energy to heat the specimens.

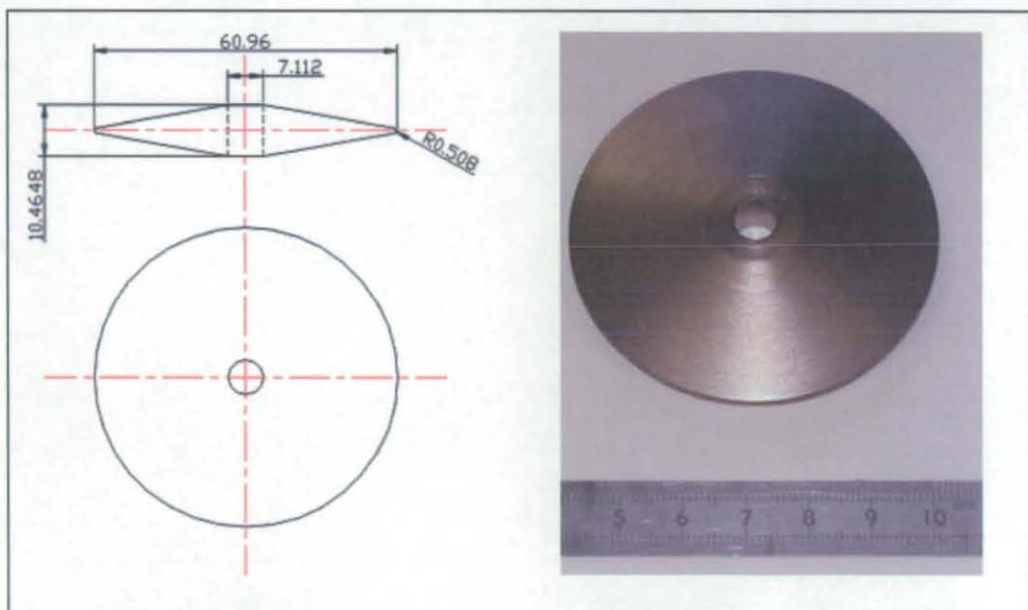


Figure 6 - 12 Disc design (dimensions in mm)

Using the disc shape it was possible to test several specimens simultaneously (Figure 6 - 13) allowing more accurate validation of the results in the same time that it would take to test one specimen using Wallace's method.

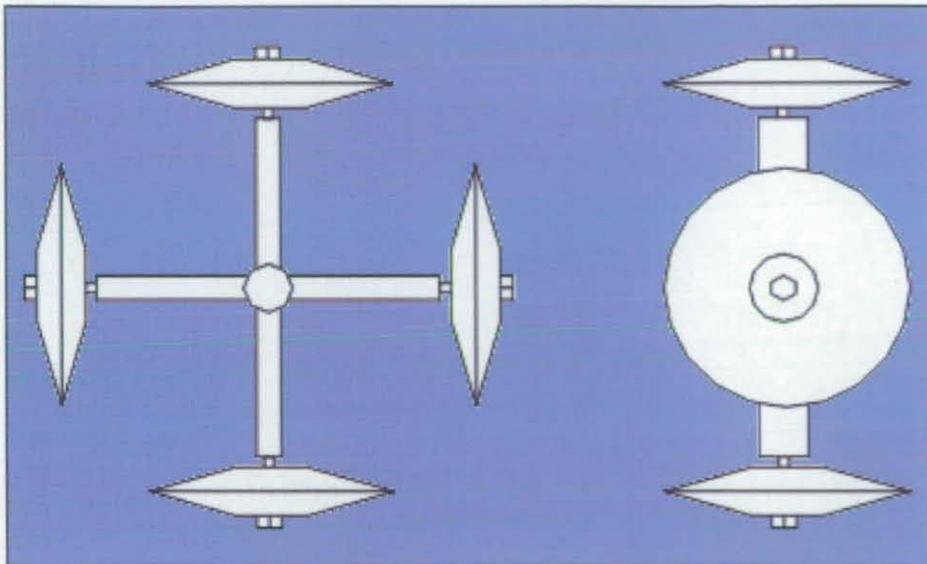


Figure 6 - 13 Multiple specimen test arrangement

6.2.2 Design of Thermal Fatigue Apparatus

In order to conduct accurate material evaluation, a reliable experimental apparatus and reproducible procedure needed to be developed for testing the thermal fatigue resistance of materials. An experiment was required to simulate the thermal conditions experienced by tool materials under high-pressure aluminum die casting conditions.

There are standard test procedures for fatigue testing but no standard test procedures were discovered for thermal fatigue at the commencement of this work. Hence, researchers (Glenny et.al., 1959, Howes, 1973, Wallace et.al., 1997, Mowbray and McConnelee, 1976) developed and conducted their own experiments for specific applications. Glenny's thermal fatigue test employs long cycle times, one to four minutes heating and four minutes cooling.

To conduct the thermal fatigue experiment a heating medium, a cooling medium and an automated transfer system were required. The transfer apparatus shown in Figure 6 - 14 was designed to be versatile allowing adjustments to be made in the positioning of the specimens. The basic design consisted of a steel frame with X and Z axis pneumatic actuators. An additional frame was fabricated connecting the Z piston to the specimen holder to prevent the heat being transferred and damaging the actuator and the electronics.

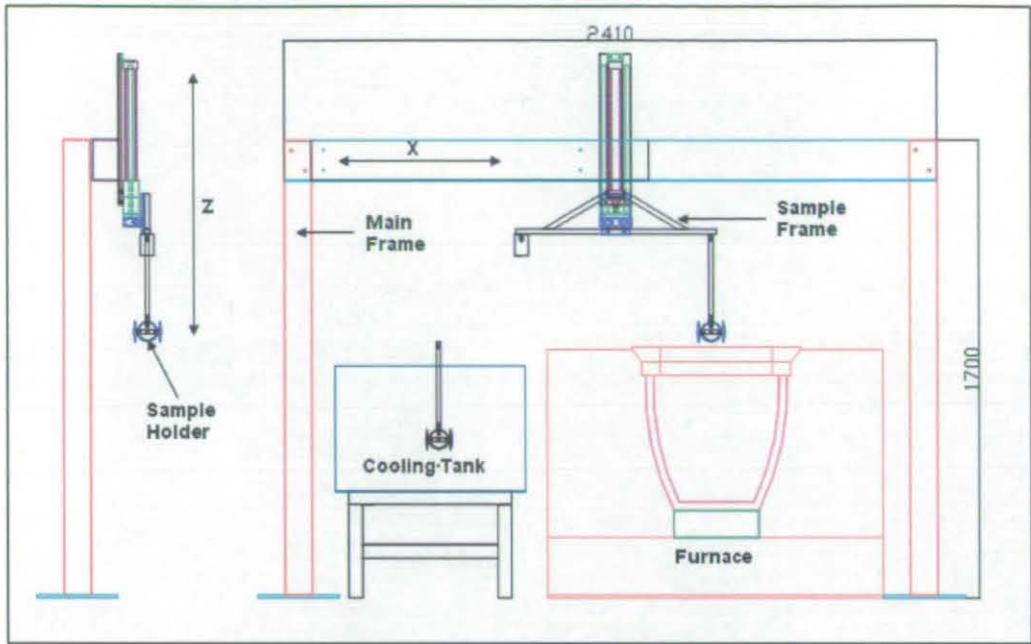


Figure 6 - 14 Thermal fatigue apparatus design

The assembled thermal fatigue apparatus is shown in Figure 6 - 15 with a furnace and cooling tank beneath.

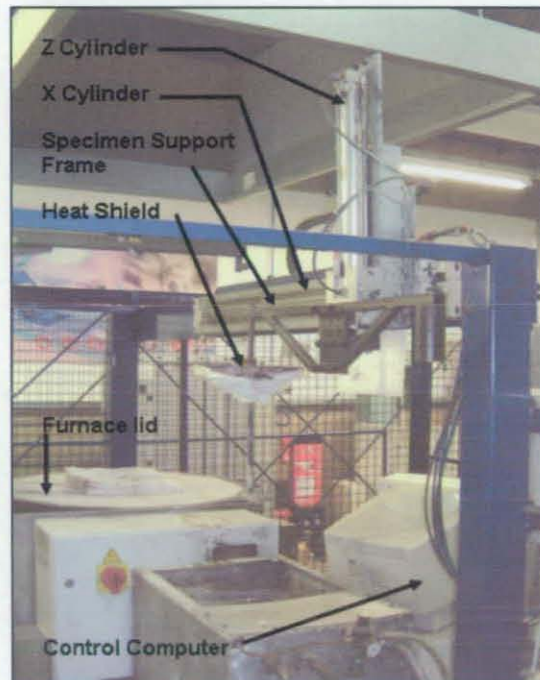


Figure 6 - 15 Thermal fatigue apparatus X - Z

6.3 Cooling Tank

Since dies have internal water / oil cooling channels and die casters use a water based lubricate to act as a coolant and release agent on the surface of the die, water was used to cool the specimen in the thermal fatigue experiments.

The cooling medium tank was designed to have constant cooling. The temperature was controlled through a series of copper pipes circling the edge of the tank; this was connected to a chiller system. Over a one hour thermal cycling period the tank maintained a steady water temperature between $\approx 11^{\circ}\text{C}$ - 14°C (Figure 6 - 16); this was tested using eight calibrated thermocouples placed in the water.

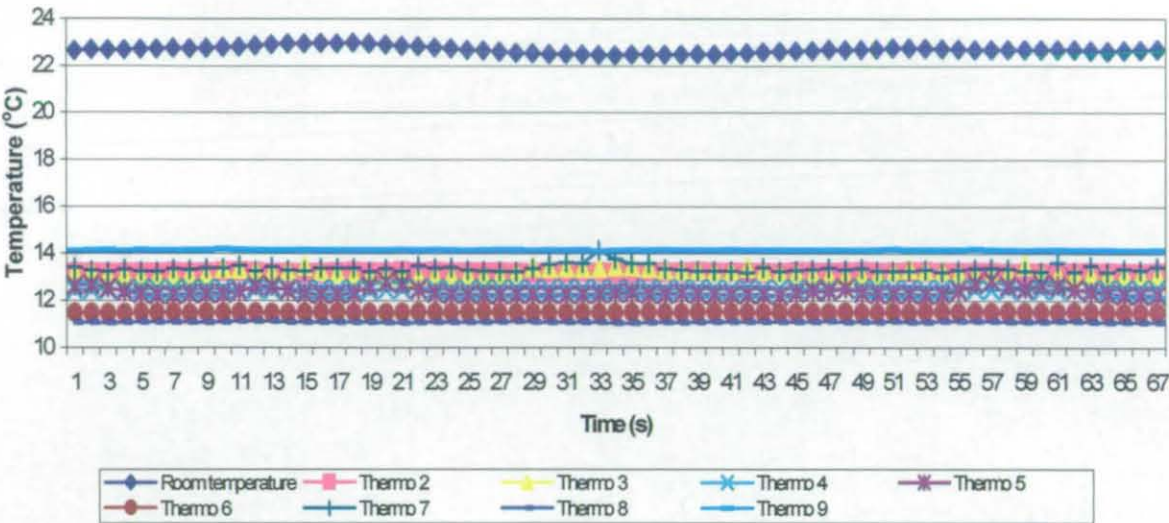


Figure 6 - 16 Water temperature recording (1hr thermal cycling period)

In order to obtain a constant level of water a float valve was positioned at the top of the water tank. A compressed air agitator was also installed in the tank to circulate the water around the cooling pipe array (Figure 6 - 17).

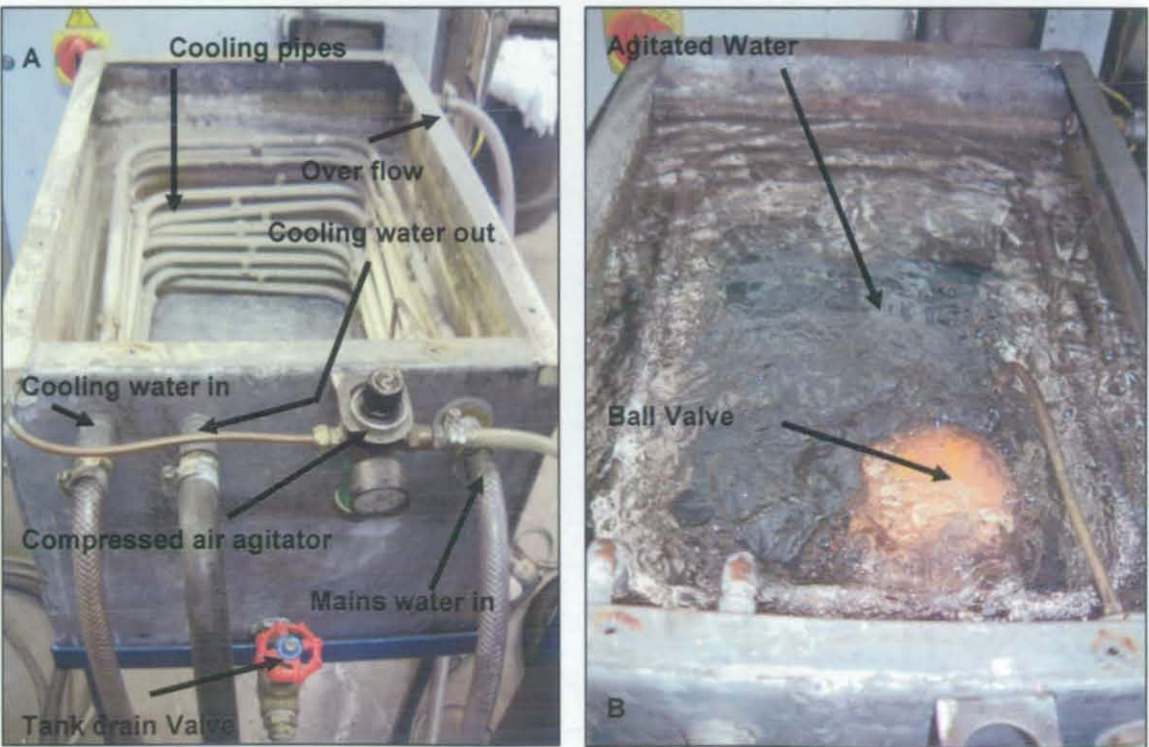


Figure 6 - 17 Tank design; (A) Empty quench tank; (B) Quench tank with agitator on

6.4 Reproducing the Thermal Cycle

6.4.1 Manufacture of H13 Specimens

In order to reproduce the thermal fatigue cycle of a die casting tool it was necessary to manufacture preliminary specimens for the trials. H13 (H13 supplied by Bohler Special Steels) specimens were manufactured for this purpose as this material can withstand the thermal cycle and would have a similar thermal conductivity to that of the H13 used in a die (similar rate of heat absorption and heat loss). In addition, it was necessary to test the specimens as their mass would affect the power required to achieve the temperature profile.

The H13 specimens were rough machined (1mm oversize), heat treated and finally CNC machined to size to ensure that the specimens were geometrically comparable.

6.4.2 H13 Heat Treatment

Heat treatment was conducted as discussed in chapter 2, section 2.3 but this is not a precise process and trials were necessary to determine a procedure to achieve the required hardness. Three additional specimens were made for this purpose and all the heat treatment work was conducted in a Carbolite furnace model: FFHT 1.1400 Prog, with an argon atmosphere (flow of 20 litres / minute) to prevent oxidation and to reduce de-carburising. For all the tests the furnace was initially heated to 750°C, with the argon flowing, prior to inserting the specimen into the furnace. Appendix ii Table 8 and Appendix ii Table 9 show the trial methods of hardening and tempering with the final method shown in Appendix ii Table 10.

Appendix ii Table 11 shows the hardness values obtained from the heat treatment methods. The hardness test was conducted using a Rockwell testing machine (Avery 6402). The heat treatment profile used for trial three was used for all the H13 thermal fatigue specimens as it achieved the desired hardness of between 43HRc and 45HRc.

6.4.3 Thermal Cycle Methodology

These tests were designed to determine the most suitable method of heating and cooling.

Three fibre glass insulated K type open ended thermocouples, with a wire diameter of 0.3mm were positioned at the edge of one specimen (Figure 6 - 18) in the cooling tank and in the furnace, each was calibrated and the data recorded as previously discussed.

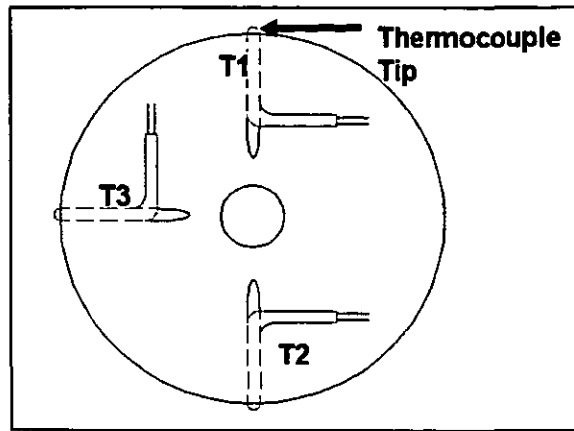


Figure 6 - 18 Thermocouple location in specimen

The furnace used for the tests was capable of operating between 20°C to 1200°C. The furnace was a laserform oven manufactured by DTM, now 3D systems. The furnace consisted of three sets of independently controlled elements, each with its own temperature feed back circuit. The furnace elements were controlled by a Eurotherm controller and by rheostats to power up or down depending upon whether heat was being lost or the correct temperature was obtained. Tests conducted with a calibrated thermocouple on the empty furnace showed that it could maintain temperature to within $\pm 10^\circ\text{C}$. This was also verified on the furnace control display.

The only alteration to the furnace was the manufacture of a furnace lid with a hole in the centre, to enable the specimens to be repeatedly placed in and out. Foundry cement, otherwise known as refractory, was used (Kerlite, Lafarge Refractories, supplied by Monolithics).

6.4.4 Thermal Profile when Heating Specimens in a Fluidised Bed

A fluidised bed was created, and positioned at the bottom of the furnace; this was connected to compressed air supplied through the hole at the base of the furnace and the flow controlled using a flow gauge. F0885 aluminium oxide sand with a maximum operating temperature of 900°C (supplied by Techne Ltd.) was then poured into the furnace and the air supply regulated to achieve a fluidised bed.

A graphite sheath was supplied by Ramsell SMC and 27, 2mm holes were drilled into it to allow the air to flow, which fluidised the bed of sand (Figure 6 - 19); this air distributor was used in all the experiments.

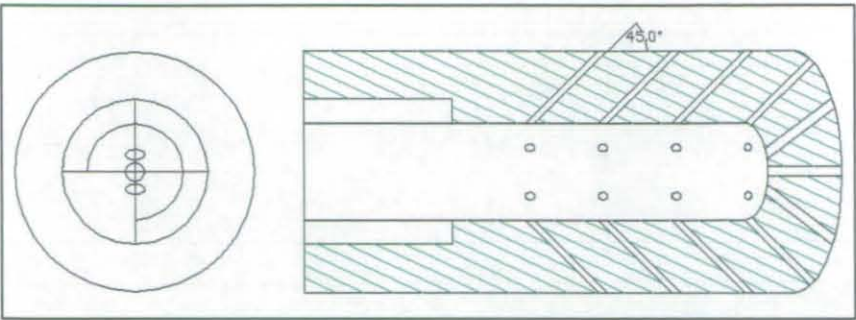


Figure 6 - 19 Graphite air distributor design

6.4.4.1 Results

After a series of preliminary tests it was found to be necessary to set the furnace at 1000°C in order to maintain the specimen edge radius temperature of 500°C - 550°C with the cycle time set to 30 seconds and the water temperature set and maintained below 20°C.

The method of heating was not ideal because at the start of each test the specimen edge radius heated to approximately 1000°C. This edge radius temperature eventually reduced and a stable profile attained at $\approx 575^\circ\text{C}$, after 3600 seconds or 120 cycles (Figure 6 - 20). The problem arose because the furnace was unable to maintain temperature once the cold compressed air was passed through the sand and in turn, the specimens were removing heat from the furnace on every cycle resulting in the system stabilising after one hour. An additional problem occurred over a period of time, when small quantities of the fluidised sand became airborne and were deposited on the thermal fatigue transfer apparatus causing severe wear over time and resulting in the replacement of the X axis cylinder.

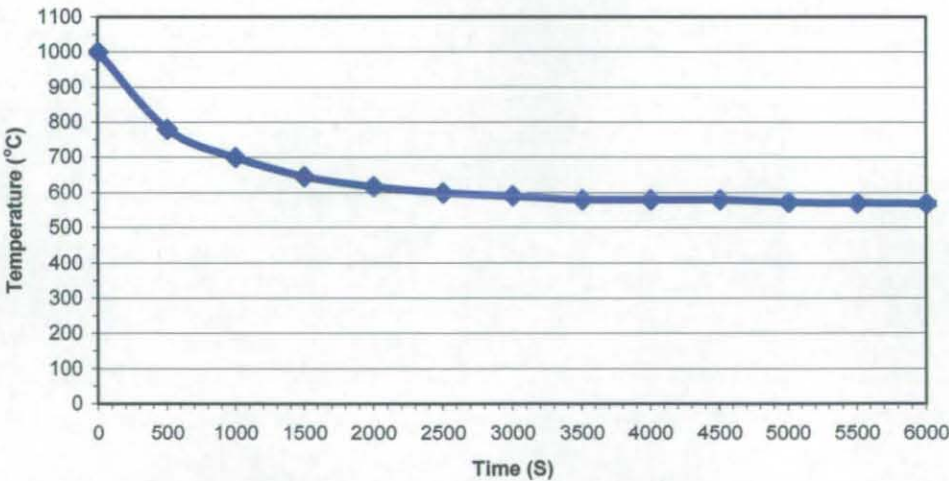


Figure 6 - 20 Fluidised bed temperature

The method created a heating cycle, which raised and lowered the specimen surface temperature from $\approx 50^\circ\text{C}$ to $\approx 550^\circ\text{C}$ (Figure 6 - 21); the temperature, however, could be altered by changing the length of time the specimens were placed in the furnace.

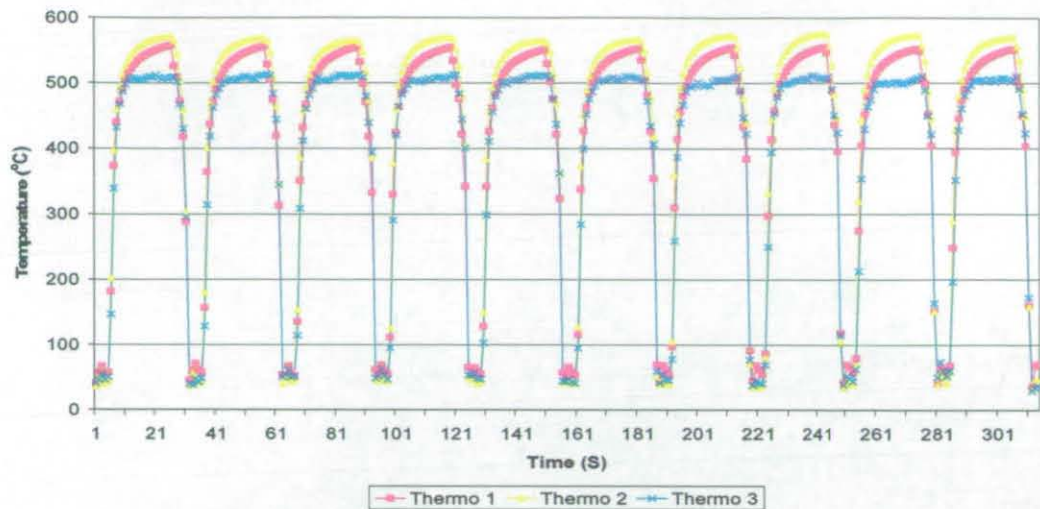


Figure 6 - 21 Fluidised bed temperature profile

The method was not representative because of the number of cycles (≈ 120 cycles in 3600 seconds) required to achieve a stable temperature profile. In addition, the specimens needed to be subjected to the same thermal cycle from the beginning of the test and not subjected to the elevated temperatures prior to stabilisation.

In an attempt to reduce the temperature loss in the fluidised bed the input air was pre-heated by placing a two layered rectangular network of $\varnothing 22\text{mm}$ stainless steel pipes in a Gallenkamp muffle furnace (20 - 1000°C). The furnace was set at 900°C and a calibrated thermocouple recorded the air input temperature for the fluidised bed to be $\approx 400^{\circ}\text{C}$.

The laserform oven temperature was reduced to 900°C and the water temperature remained below 20°C .

It was clear that heating the air was beneficial since the furnace temperature could be reduced and a higher maximum temperature of the thermal cycle $\approx 750^{\circ}\text{C}$ could be maintained (Figure 6 - 22).

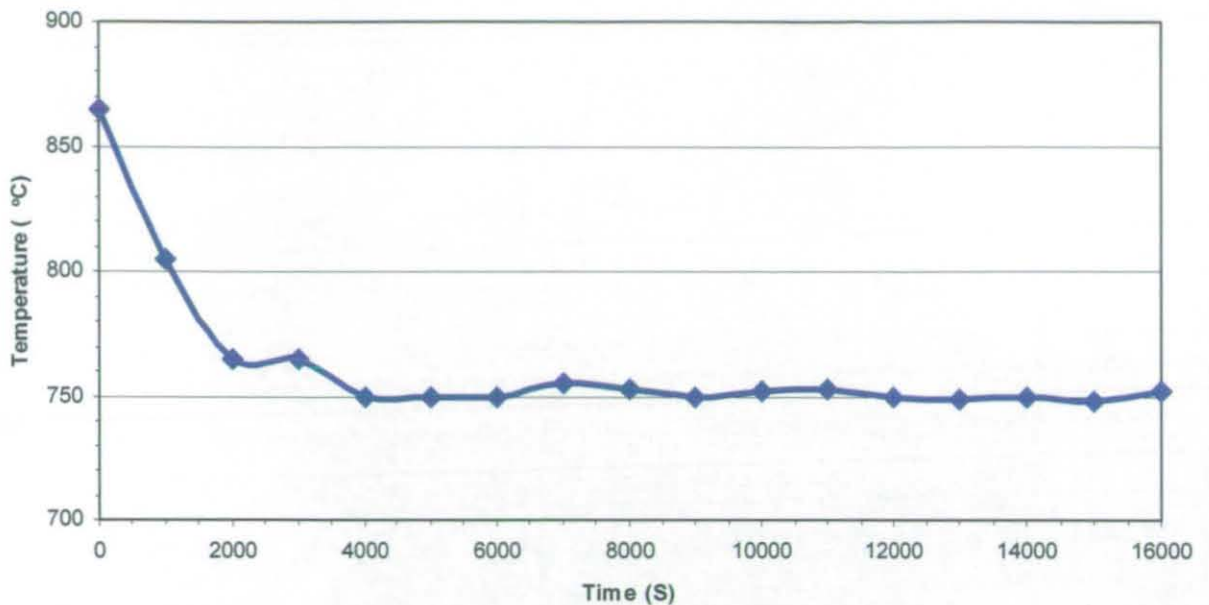


Figure 6 - 22 Fluidised bed with heated air temperature

It did however; take approximately 4,000 seconds, or 133 cycles, for the temperature to drop from 850°C to the steady temperature of 750°C Figure 6 - 23. Again the time to reach a steady state was not acceptable since the specimens would experience different thermal cycles at the initiation of each thermal fatigue test.

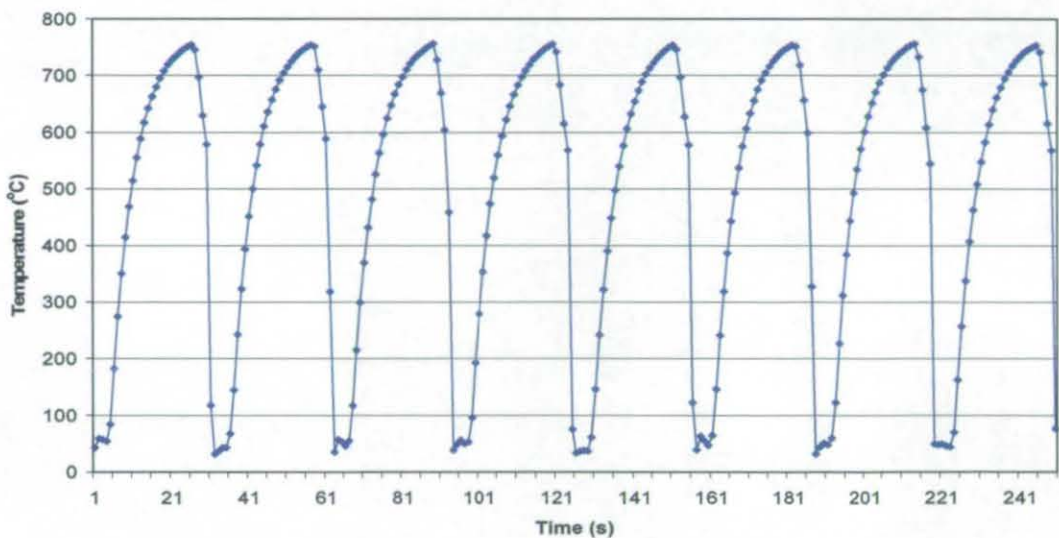


Figure 6 - 23 Fluidised bed with heated air temperature profile

Comparing the two fluidised bed methods showed that by heating the air and reducing the furnace temperature from 1000°C - 900°C, it was possible to maintain a hotter furnace temperature of 750°C rather than 600°C. However, both beds took a similar time, 4,000 seconds, to achieve a steady temperature state making them unsuitable as a means of heating the specimens. The time to heat the specimens to 500°C - 550°C was 6 - 7 seconds, and to achieve 700°C required 15 seconds. A further concern of the heated air and fluidised beds was reliability of the air distributor and loss of sand over a period of time, making it an unsuitable method for the test work.

6.4.5 Thermal Profile when Heating Specimens in Aluminium

6.4.5.1 Methodology

The experiment was conducted in an attempt to obtain a stable temperature profile. A 70kg capacity crucible was placed in the furnace and filled with LM24 aluminium. The furnace was set at 750°C and the cooling medium temperature was between $\approx 11^{\circ}\text{C}$ - 15°C .

A problem occurred during the process as the aluminium adhered to the specimens over time (Figure 6 - 24) and interfered with heat transfer to the specimens; the aluminium could cause chemical attack introducing additional thermal fatigue factors (see chapter 3).



Figure 6 - 24 Aluminium build up after one cycle

6.4.5.2 Results

The process maintained a stable temperature $\approx 720^{\circ}\text{C}$ from the beginning of the test $\pm 10^{\circ}\text{C}$ (Figure 6 - 25) with the surface of the specimens being subjected to $\approx 715^{\circ}\text{C}$ (Figure 6 - 26). The heating temperature, however, could not be lowered since the aluminium had to remain molten and hence, the thermal shock could not be reduced.

From the in die temperature experiments it was clear that the tool surface did not reach 600°C - 700°C so the aluminium furnace trial was unrepresentative.

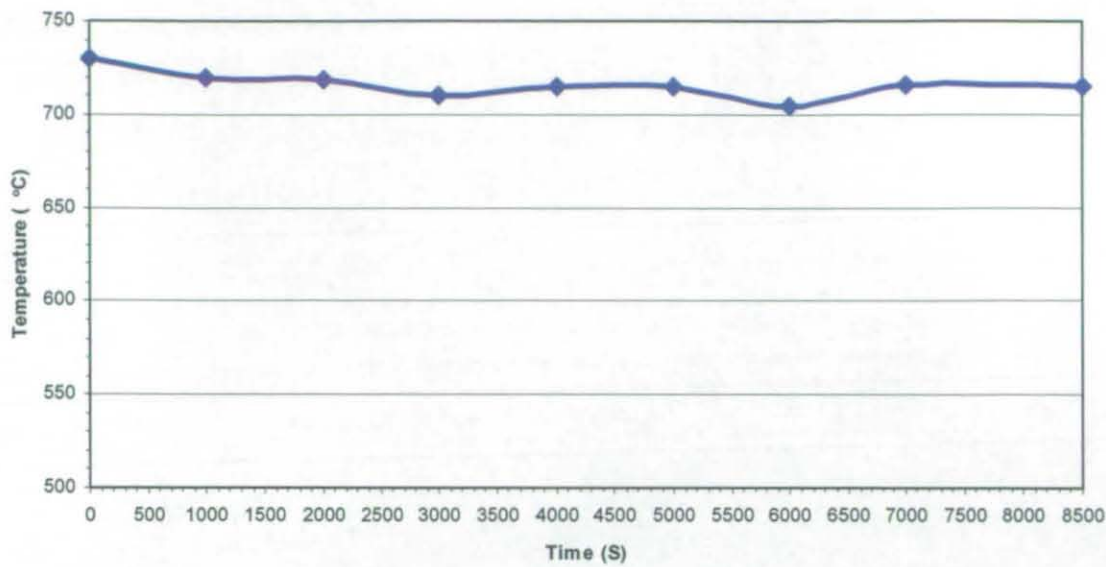


Figure 6 - 25 Aluminium thermal fatigue temperature

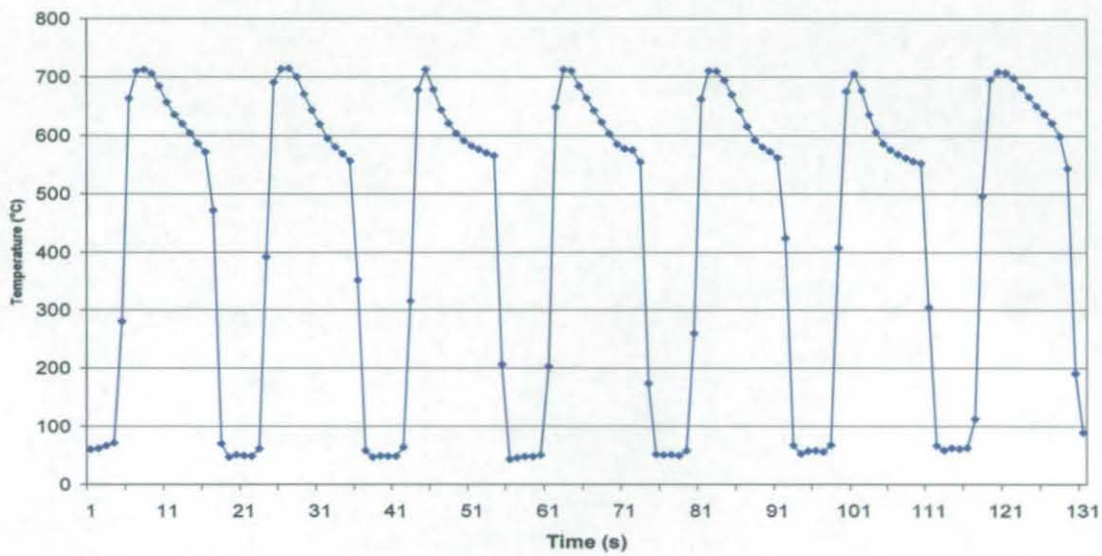


Figure 6 - 26 Aluminium temperature profile

6.4.5.3 Conclusion

The specimen surface was heated too quickly to over 600°C in 2 seconds, which was not representative as the in die surface test showed that it took approximately 2 seconds to reach only 400°C - 450°C. The maximum surface temperature obtained (over 700°C) was also too severe. In addition, using molten metals was not desirable because of the problem of solidification of the metal onto the specimens, which would affect the heat transfer and thermal profile.

6.4.6 Thermal Profile when Heating Specimens in Air in the Furnace

6.4.6.1 Methodology

The furnace was initially set at 900°C and the water was cooled to 20°C - 25°C; this ensured a constant thermal cycle with a maximum temperature of $\approx 425^{\circ}\text{C}$ and a 30 second cycle time (Figure 6 - 27).

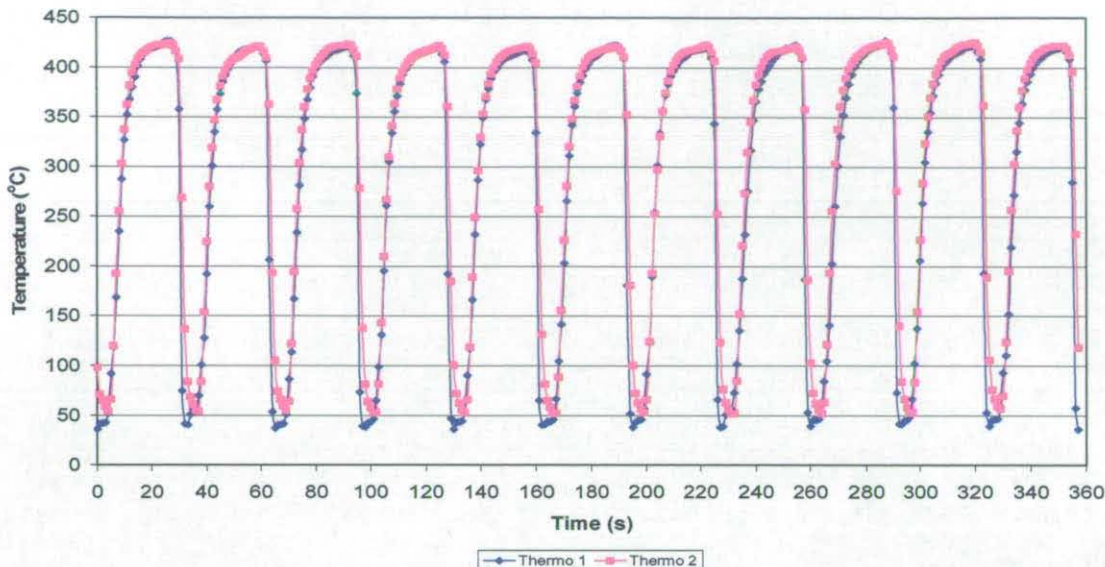


Figure 6 - 27 Furnace experiment one temperature profile

6.4.6.2 Results

Comparing the thermal cycle obtained (Figure 6 - 28 A) to the thermal profile from the die experiments (Figure 6 - 28 B), it is clear that the thermal cycles were not the same. The furnace heated the specimen to 425°C over a 10 second period and maintained it at 425°C for 15 seconds and cooling approximately 5 seconds, giving a total cycle time of 30 seconds. The surface of a die was heated to 425°C over a 5 second period with cooling occurred over 20 seconds, giving a total cycle time of 25 seconds.

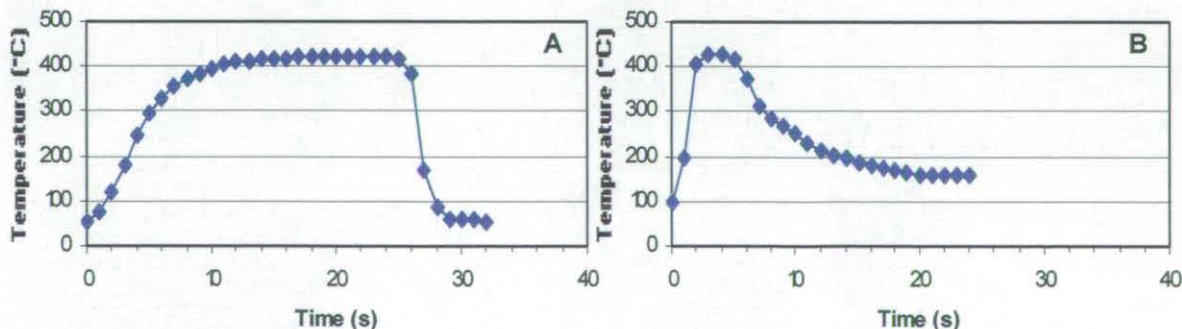


Figure 6 - 28 (A) Furnace temperature profile; (B) Temperature profile from die experiments

The temperature rates were not representative and the cycle time was too long. Changes to the cycle time and temperatures were required.

The cycle time was reduced to approximately 20 seconds and the furnace temperature rose to 1000°C. This achieved a temperature of 450°C - 480°C (Figure 6 - 29).

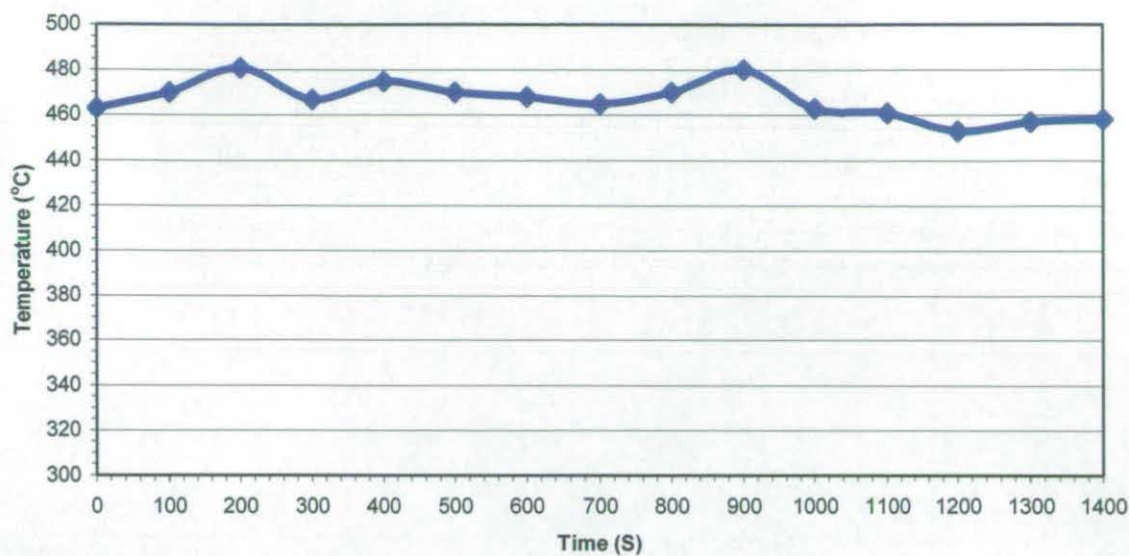


Figure 6 - 29 Maximum temperature

The specimens were heated in the furnace for 8 seconds, then removed from the furnace and transferred to the cooling medium within 5 seconds, immersed in water for 1 second, which was then followed by a 5 second transfer back to the furnace. The cycle achieved is shown in Figure 6 - 30 and a single cycle in Figure 6 - 31 A. It is clear that the thermal cycle was not comparable to the thermal cycle recorded in the die Figure 6 - 31 B. The thermal cycle took a minimum of 8 seconds to reach 400°C - 450°C.

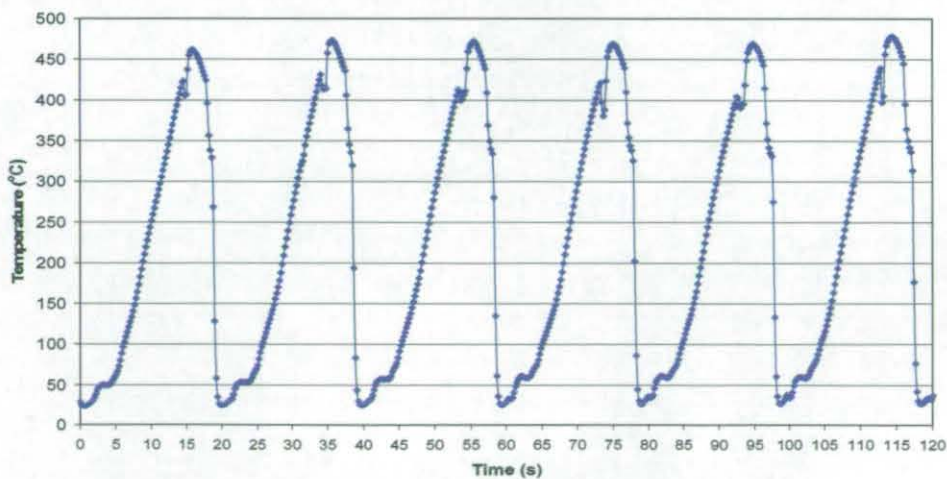


Figure 6 - 30 Furnace experiment two temperature profile

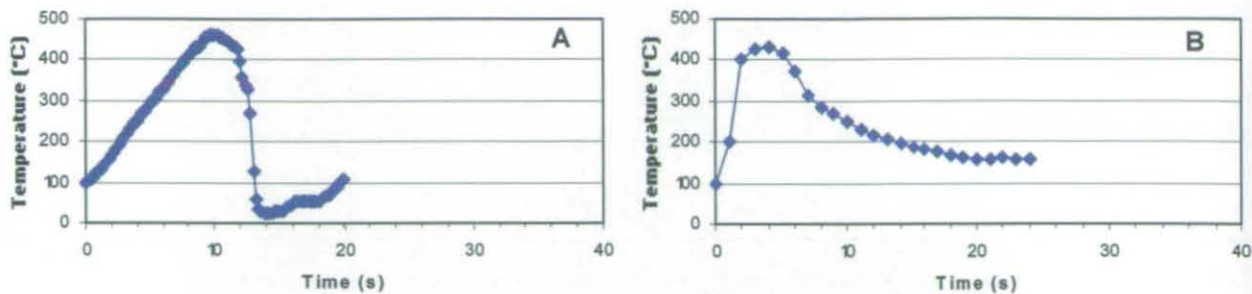


Figure 6 - 31 (A) Single fatigue cycle; (B) Desired thermal cycle from die experiments

Figure 6 - 32 shows the temperature profile when reversed; it can be seen, when comparing this to the actual die surface temperature Figure 6 - 31 B, that the reverse profile is similar. However, heating puts the material in tension and is generally more destructive due to the separation of the fracture surface. Cooling causes compression and it is harder for cracks to propagate between the fracture surfaces (Andarifar, 2004) so the profile is not a completely accurate representation.

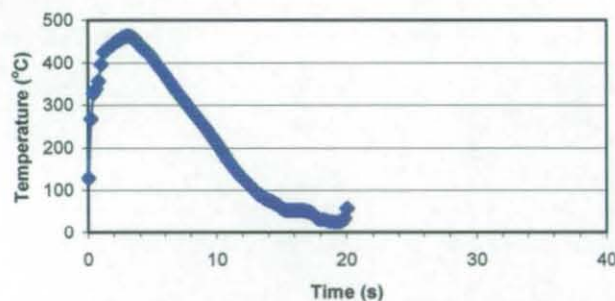


Figure 6 - 32 Furnace experiment two reversed temperature profile

The test showed that the desired temperature was achievable (400°C - 450°C), however, the heating rate was slow in comparison to the in die temperature experiments, the cooling rate was also too harsh. This would probably lead to a higher number of thermal fatigue cycles to initiate cracking.

6.4.7 Temperature Simulation Conclusion

It was clear that using the available equipment that none of the methods tested were able to simulate the temperature of the die surface.

The test apparatus was required to run non-stop for many hundred of thousands of cycles so it had to be durable. The fluidised bed and the aluminium heating methods both had problems with respect to their suitability as a means of heating the specimens. The fluidised bed experiments were not reliable due to loss of sand, aggressive wear on the pneumatic actuators and the time it took for the system to reach a stable temperature. The aluminium heating method was not chosen because the thermal cycle was too hot and aluminium adhered to the specimen surface affecting the thermal cycle. Both methods were investigated because

previous research of using these methods had been conducted by Wallace and Glenny but an alternative, improved, heating method was required.

This led to the most controllable, reliable and consistent method being adopted to simulate a thermal cycle. Although not simulating the die casting surface temperature, the materials would be subjected to the same temperatures experienced in a die. H13 specimens would also act as a reference and be used for comparison to assess the suitability of a material as a die material.

The furnace temperature simulation method in chapter 6, section 6.4.6 was the most controllable, reliable and consistent of all the methods tested. The profile in figure 6 - 37 was selected as it achieved the desired temperature. There were no problems cooling the specimens in water (note no water continually flowed inside the specimens as in Wallace's test) in a quench tank as this only cooled the surface and any excess water evaporated prior to dipping into the furnace.

6.5 Specimen Manufacture

The test program was designed to use four specimens for thermal fatigue testing with one control specimen. The control specimens were manufactured and treated in the same manner as the thermal fatigue specimens. For each of the test materials, H13, Metacopy 5507, Metacopy Janalloy, Metacopy Cu, Vertical laminate, Horizontal laminate, Amdry 790, Vertical RapidSteel 2.0, Horizontal RapidSteel 2.0, EOS DirectSteel 20 μ m, five specimens were used - making 50 specimens in total.

Both the EOS DirectSteel 50 μ m and the EOS DirectSteel 20 μ m specimens were built. However, only the EOS DirectSteel 20 μ m material was tested because the EOS DirectSteel 50 μ m was cracked after building and was unusable.

6.5.1 Vertical Laminate and Horizontal Laminate Specimen Manufacture

The sheet used to manufacture the laminate samples was H13 with a specified thickness of 1mm \pm 0.11mm. The sheets were laser cut to shape, 1mm x \varnothing 65mm for the horizontal profile; 1mm x 15mm x 65mm for the vertical profile. These were then finished to improve the flatness and roughness of the laminates. The laminates had an average flatness deviation of 0.048mm and an average roughness of 0.48 μ m Ra. The laminates were then cleaned in isopropanol alcohol followed by rinse and drying. One laminate was placed in the jig and dusted with braze powder (Amdry 790), another laminate was placed on top and the process repeated until the desired height of approximately 80mm was reached in the case of the vertical profile and 15mm for the horizontal profile; the jig lid was then closed. The lid had a dead weight and when closed it applied a uniform weight distribution on the laminate stack. The jig assemblies were placed in a furnace with an inert atmosphere of argon and the brazing conducted. After brazing the jig assemblies were removed and the brazed laminate stacks removed ready for final machining. Further information can be seen in Appendix iii.

6.5.2 Amdry 790 Specimen Manufacture

Amdry 790 was the brazing material used to bond the laminate specimens (Appendix iii). Thermal fatigue specimens of this material were tested alone to assess fatigue resistance and to determine whether or not the braze performed well on its own i.e. to answer the question is the fatigue resistance dependent upon the braze or a structure? The Amdry 790 brazing powder was placed in a ceramic crucible with a diameter of 65mm and heated until molten and then allowed to cool.

6.5.3 Final Machining

The external radius of the thermal fatigue specimen was designed to act as a stress raiser. A die designer typically avoids radii of less than 0.5mm, to prevent stress concentration points. However, sometimes component design prevents this approach and small radii are used. The external radius on each specimen was $0.5\text{mm} \pm 0.001$. All the specimens were rough cut on a standard lathe using carbide cutters and then machined to size on a Cincinnati Milacron Hawk 150 CNC lathe to the specified tolerances shown in Figure 3 - 4 (B).

One side of the specimen was machined and then the specimen was turned through 180° and the other side machined. On the final cut on each side, the specimen was machined with a new carbide tool tip to ensure accurate tolerances and identical surface roughness.

After machining, the specimens were measured by a shadowgraph (Isoma M 119G) and all were found to be within tolerance.

6.5.4 Hardness

Testing the specimens prior to thermal fatigue ensured each material set had similar hardness to each other. Each specimen was tested twice in different positions (Figure 6 - 33). Throughout the thermal fatigue testing programme specimens were hardness tested in the same manner to determine whether thermal fatigue was detrimental to the hardness of the material under test.

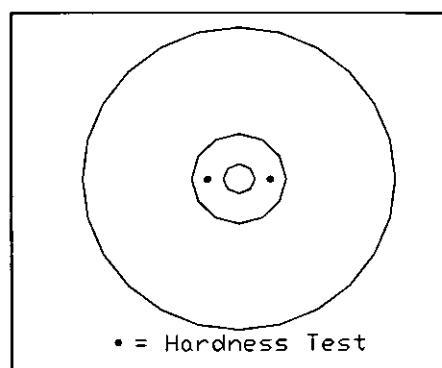


Figure 6 - 33 Position of hardness measurements

Figure 6 - 34 shows the results of the initial hardness tests. Table 6 - 3 shows that H13 had an average hardness of $\approx 114\text{HRb}$ ($\approx 44\text{HRC}$), Metalcopy 5507 $\approx 79.5\text{HRb}$ and Metalcopy Janalloy

had the lowest average hardness of $\approx 57\text{HRb}$. Metacopy Janalloy specimen 5 had a higher hardness in comparison to the other specimens, further tests showed the specimen to contain hard areas; this may have been due to areas that were rich in 316 steel and so there was not a uniform mixture of 316 steel powder and silver based bonding material. Metacopy Cu had an average hardness of 70.5HRb . The Vertical laminate, Horizontal laminate and H13 specimens had similar hardness to each other, 110HRb - 114HRb respectively. Amdry 790 had an average hardness of $\approx 88.5\text{HRc}$ but specimen 3 was harder than the rest, it was later found to be as a result of its microstructure (a result of the manufacturing method, i.e. how it cooled, and position in the bar (edge or centre may have had different cooling rates and hence, crystal structure / mechanical properties)). The Amdry 790 braze powder was put into a crucible and melted but on solidification and cooling it was possible that the material did not cool homogeneously, i.e. the top may have cooled faster than the bulk of the specimen.

Specimen	Average Hardness (HRb)
H13	114.0
Metacopy 5507	79.5
Metacopy Janalloy	57.1
Metacopy Cu	70.5
Vertical laminate	110.2
Horizontal laminate	113.4
Amdry 790	88.5
Vertical RapidSteel 2.0	84.4
Horizontal RapidSteel 2.0	83.6
EOS DirectSteel 20 μm	87.7

Table 6 - 3 Specimen hardness prior to thermal fatigue

Both the vertical RapidSteel 2.0 and horizontal RapidSteel 2.0 had similar hardness of $\approx 84\text{HRb}$ with EOS DirectSteel 20 μm exhibiting an average hardness of $\approx 88\text{HRc}$.

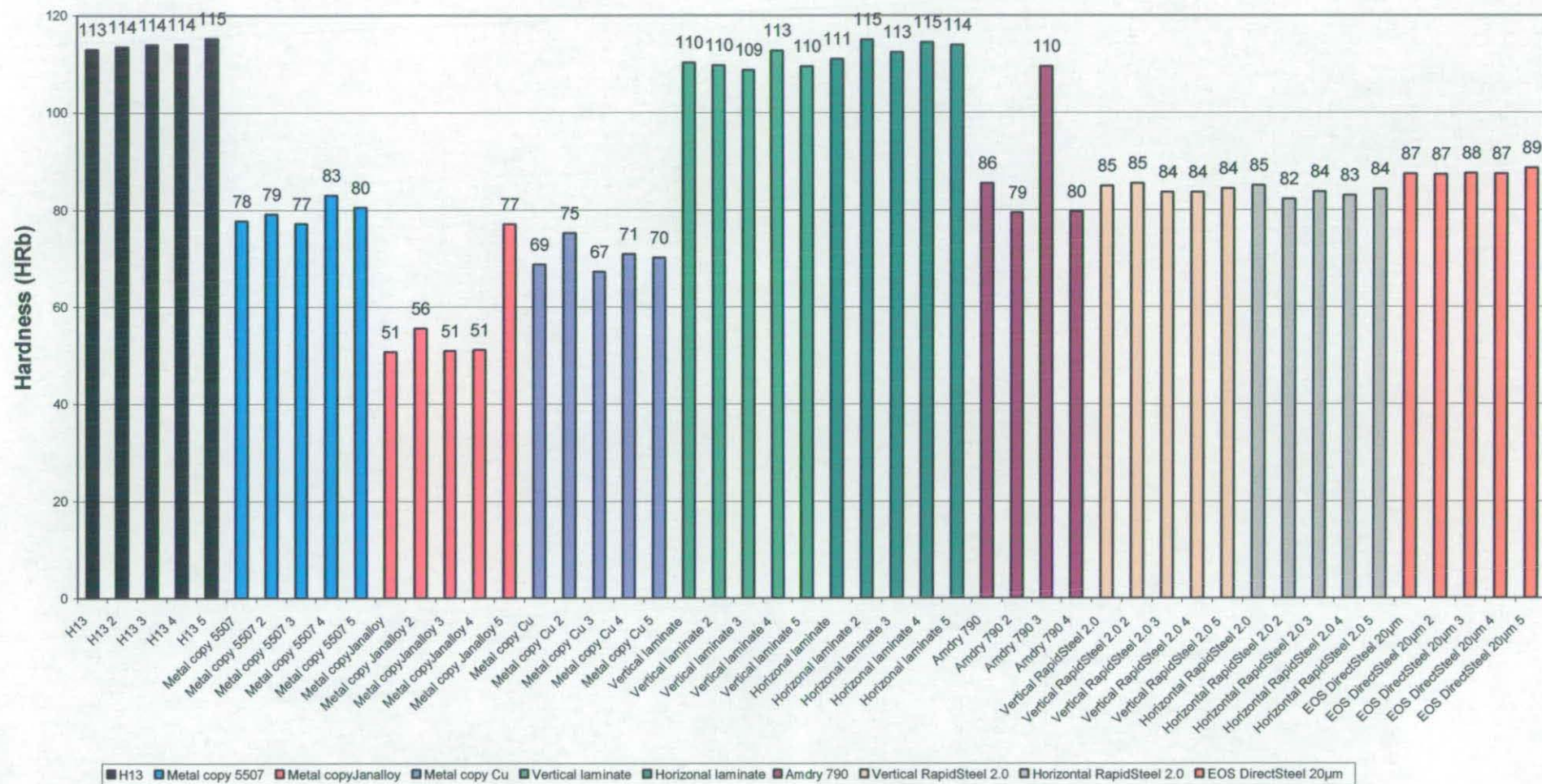


Figure 6 - 34 Specimen hardness before thermal fatigue testing

Chapter 7: Thermal Fatigue Experiment

7.1 Aim

To provide an understanding of how, when and why cracks in direct and indirect tooling materials initiate and their preferred direction of propagation.

7.2 Thermal Fatigue Test Methodology

During the thermal fatigue test on a material it was necessary to conduct periodic examinations consisting of a hardness test and observations of the specimens for signs of thermal fatigue (Maillot et.al., 2005) (each specimen was always re-positioned on the apparatus in the same place and with the same orientation after the examinations). The test was repeated until sufficient thermal fatigue cracking was evident and recorded or if the specimen was overwhelmed with cracks making analysis difficult. The number of cycles was increased in increments. If there was no prior knowledge of when thermal fatigue would initiate a crack, then the initial increments were small and increased if no cracking occurred. i.e. 50, 100, 200, 300, 400, 500, 1,000, 1,500, 2,000, 2,500, 3,000, 4,000, 5,000, 6,000, 7,000, 8,000, 9,000, 10,000, 15,000, 20,000, 30,000, 40,000 cycles etc.

After each set of cycles the specimens were wiped clean using Viakal (Proctor and Gamble) to remove mineral deposits (lime scale) and then optically inspected (Fissolo et.al., 1996).

7.3 Optical Examination Methodology

Optical examination of each specimen was conducted using a Nikon SMZ-2T Stereo Viewer. Any cracks were documented and their length measured, this process was repeated at each increment in the number of cycles to allow crack data to be obtained.

When a crack was detected it was referenced with a marker pen so that it could be recorded on the crack log sheet. A JPEG picture was taken of any crack using a JVC Colour Video Camera TK-C1481BEG and Win-TV image capture computer software. All pictures were taken at the same resolution. To prevent measurement errors a picture of the graticule was taken at set magnifications and measurement taken from the graticule.

If a crack was too large to be captured on one picture then several were taken along its length. These images were then imported into Microsoft Paint where they could be joined together and the crack length measured (Figure 7 - 1). Overlaying / joining the pictures could typically be achieved to within 1 - 2 pixels (Table 7 - 1).

The cracks were given a unique identity. First the specimen type was identified, second the specimen number, third the number of cycles, fourth crack number and fifth the magnification at

which the photograph was taken. For example, data for Metalcopy Cu-S2-180K-1-x4 was given as: Metalcopy copper, specimen number 2, 180,000 cycles completed, crack number 1, photograph taken at x4 magnification. For Metalcopy Cu-S2rs-200K-x1 the data was given as Metalcopy copper, specimen number 2 reverse side, 200,000 cycles completed, crack number 1, photograph taken at x1 magnification.

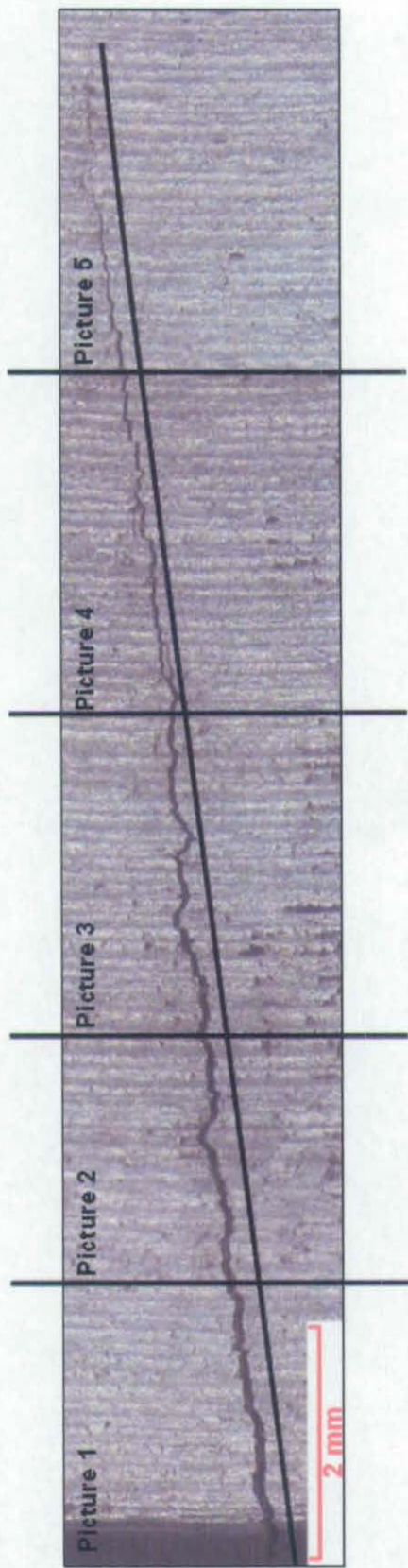


Figure 7 - 1 Example of crack picture and measurement

The measurement was achieved by drawing a line along the crack length and recording the number of pixels. The conversion factors are shown in Table 7 - 1.

Magnification	Number of pixels in 1mm	One pixel equates to (μm)
X1	105	10 μm
X2	207	5 μm
X3	308	3 μm
X4	414	2.4 μm
X5	526	2 μm
X6	616	1.6 μm

Table 7 - 1 Magnification and conversion factors

Once a crack had been identified it was recorded on a specimen crack log sheet (Figure 7 - 2) along with the specimen identification details, the number of cycles, the crack number etc. Rotational position was maintained with a score mark at the centre and on both sides of the specimen. The log sheet showed disc details for the front of the specimen and the back of the specimen allowing the cracks to be catalogued and making identification easier after further cycling (one sheet / specimen / set of cycles).

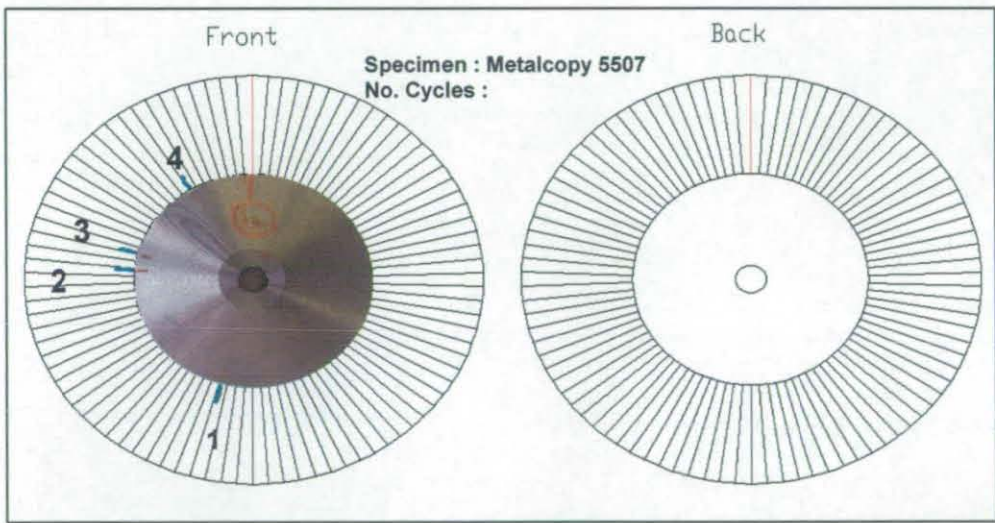


Figure 7 - 2 Example of crack log sheet with specimen in position with cracks 1 - 4 identified

In addition to crack monitoring the specimens were assessed for change in surface appearance and hardness.

7.4 H13 Thermal Fatigue Methodology

The number of thermal fatigue cycles for the H13 specimens were increased in increments of 10,000 up to 300,000. The reason for the large increments was because the material was a hot work steel having a metallurgy tailored to resist thermal and elevated temperature conditions. Therefore, cracks were not expected within 90,000 cycles.

7.4.1 H13 Thermal Fatigue Results

7.4.1.1 Initial Signs of Cracking

The first recorded sign of thermal fatigue cracking was seen on specimen 4 at 180,000 cycles.

7.4.1.2 Hardness

Specimen 3 exhibited a reduction in hardness between 120,000 and 130,000 cycles, specimen 4 at 190,000 cycles and specimen 2 and 3 at 220,000 (Appendix v Figure 1, and Figure 7 - 3).

Over the duration of the thermal fatigue test the reference specimen 5 maintained a hardness of 113HRb - 114HRb whilst the thermally fatigued specimens (1 to 4) exhibited a reduction in their hardness. At 220,000 cycles there was a noticeable drop in hardness from $\approx 112\text{HRb}$ to $\approx 107\text{HRb}$; this coincided with severe cracking in all the specimens with hundreds of cracks appearing at the radius (Figure 7 - 3) and gradually growing as the test continued to 300,000 cycles at which point the test was terminated.

7.4.1.3 Number of Cracks

The number of cracks made it impossible to catalogue them and hence, no data could be obtained from the specimens in terms of crack length, crack growth etc. However, H13 was the reference material and was only used as a material comparison. Typically an aluminium pressure die casting tool will suffer from fatigue cracking between 100,000 - 150,000 cycles depending upon the geometry of the die (Clegg, 1991). Signs of cracking in the test specimens began at approximately 180,000 cycles and severe cracking at 220,000 cycles. It must be noted that the experiment only took into account the thermal fatigue aspect of aluminium pressure die-casting and not other factors such as pressure, wear, adhesion, ingress, chemical attack etc., which occur during the casting process and promote crack initiation and crack growth in dies. The discrepancy found was probably a result of these additional factors but the experiment represented the thermal fatigue element of the process.

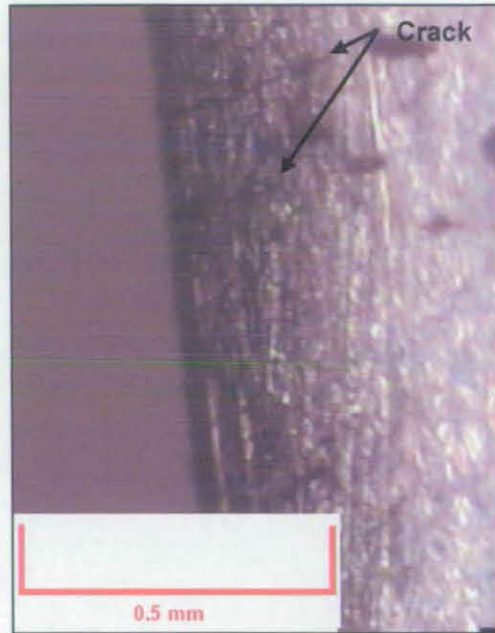


Figure 7 - 3 Specimen 2 S2-180K-1-x4

The thermal fatigue test however, produced cracking with the same characteristics pattern of the crazed cracking found in hot working dies (Figure 7 - 4) (Starling and Branco, 1997, Chinese Standard GB/T 15824 (1995)).

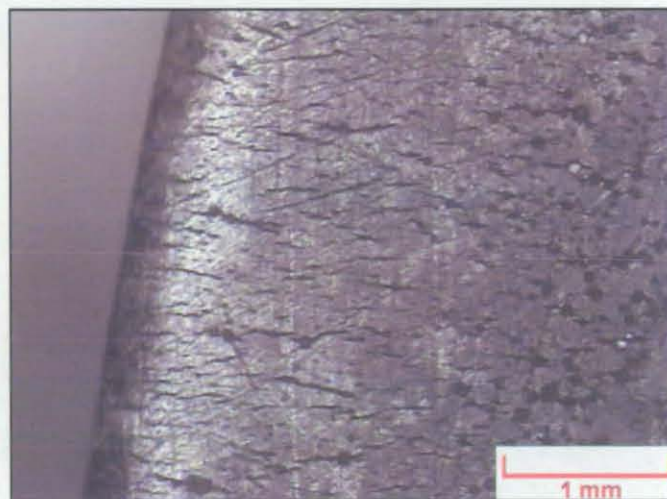


Figure 7 - 4 Specimen 4 S4-220K-1-8-x2

7.5 Metalcopy 5507 Thermal Fatigue Methodology

The thermal fatigue cycles for the Metalcopy 5507 specimens were increased in increments of 50 to 100, then increments of 100 to 500, followed by increments of 500 to 3000, then increments of 1,000 to 10,000 and finally increments of 3000 to 25,000. The small incremental changes were used because it was not clear when the material would fracture. Smaller increments were used initially but increased as the material exhibited resistance to cracking.

7.5.1 Metalcopy 5507 Thermal Fatigue Results

7.5.1.1 Initial Signs of Cracking

The first crack was observed on Metalcopy 5507 specimen 4 after 3000 cycles and measured as 0.44mm in length, however, this propagated from both sides of a surface defect in the material and not from the edge radius.

Initial signs of cracking from the specimen edge radius (Figure 7 - 5) were seen at 10,000 cycles on all specimens, with the exception of specimen 2 where nine cracks appeared between 13,000 to 16,000 cycles.



Figure 7 - 5 Metalcopy 5507 S1-10K-1-x4

7.5.1.2 Hardness

The hardness of the specimens and the reference specimen varied by a small amount over the course of the tests (Appendix v, Figure 2) and was probably due to the position of the indenter on the microstructure of the material, which consisted of steel balls in an alloy matrix of silver, copper and zinc. The average hardness of each of the Metalcopy 5507 specimens were similar $\approx 79\text{HRb}$.

7.5.1.3 Number of Cracks

Cracks initiated on specimen 4 at 3,000, specimen 1 and 3 at 10,000 and specimen 2 between 13,000 and 16,000. Over the duration of the test the number of cracks increased on specimen 1 and 2 but not to the same extent on specimens 3 and 4 (Figure 7 - 6).

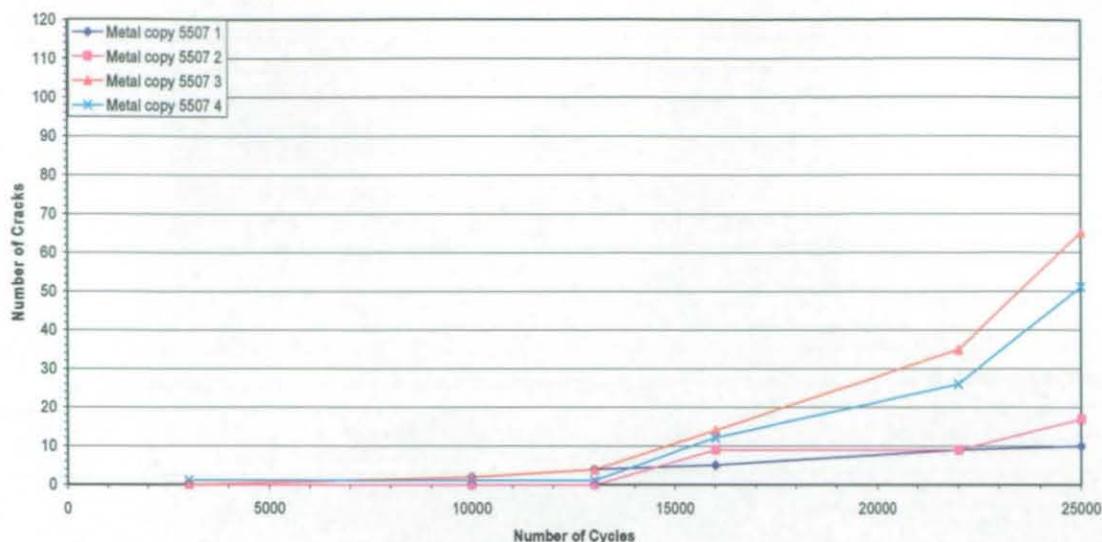


Figure 7 - 6 Metalcopy 5507 number of cycles versus number of cracks

The average number of cracks on each specimen increased at a rate of 0.09 / 500 cycles up to 13,000 cycles, it then increased to a rate of 1.2 cracks. After 25,000 cycles the average number of cracks in a specimen was ≈ 36 . It was clear that the number of cracks / specimen was variable with specimen 3 exhibiting 65 cracks and specimen 1 only 10 (Appendix v, Figure 3).

The total number of cracks during thermal fatigue cycling can be seen in Appendix v, Figure 4. The cracks initiated at 0.4 cracks / 500 cycles between 3,000 - 13,000, increasing to 5.46 cracks / 500 cycles to 25,000.

7.5.1.4 Crack Length

From Figure 7 - 7 it is clear that the average crack length did not increase rapidly (0.03mm / 500 cycles), which indicated that many new small cracks were initiating and propagating slowly. The low minimum crack length suggested this to be the case.

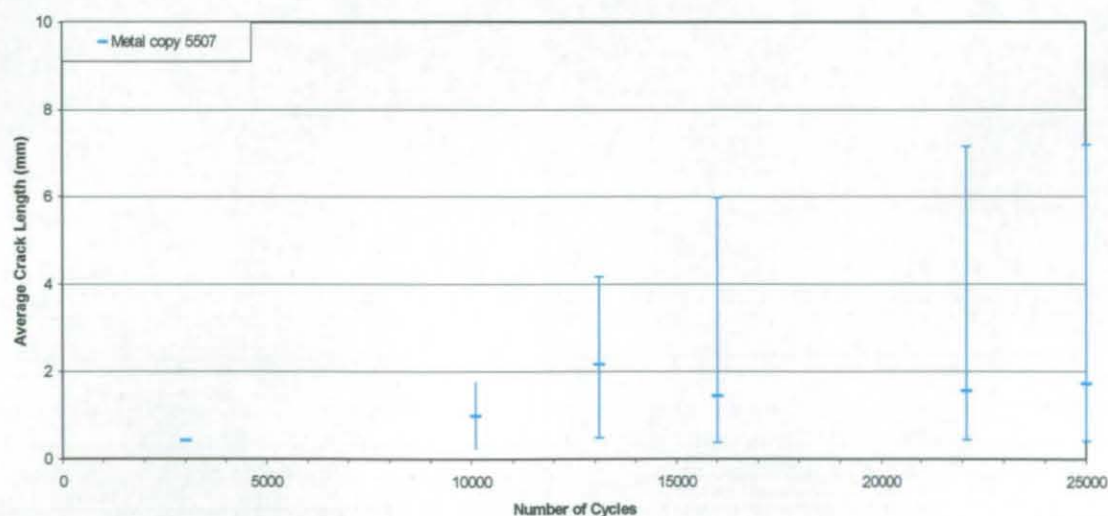


Figure 7 - 7 Metalcopy 5507 number of cycles versus average crack length with maximum - minimum crack length of all cracks

The specimen had a low average crack length and a high maximum crack length because there were only a few large cracks and many small ones initiating (Appendix v, Figure 5).

Initially the total crack length increased at a rate of 0.96mm / 500 cycles; this increased after 13,000 cycles to 5.79mm / 500 cycles and at 22,000 cycles it increased to 21.04mm / 500 cycles with a total crack length reaching 247.31mm after 25,000 cycles and (Figure 7 - 8).

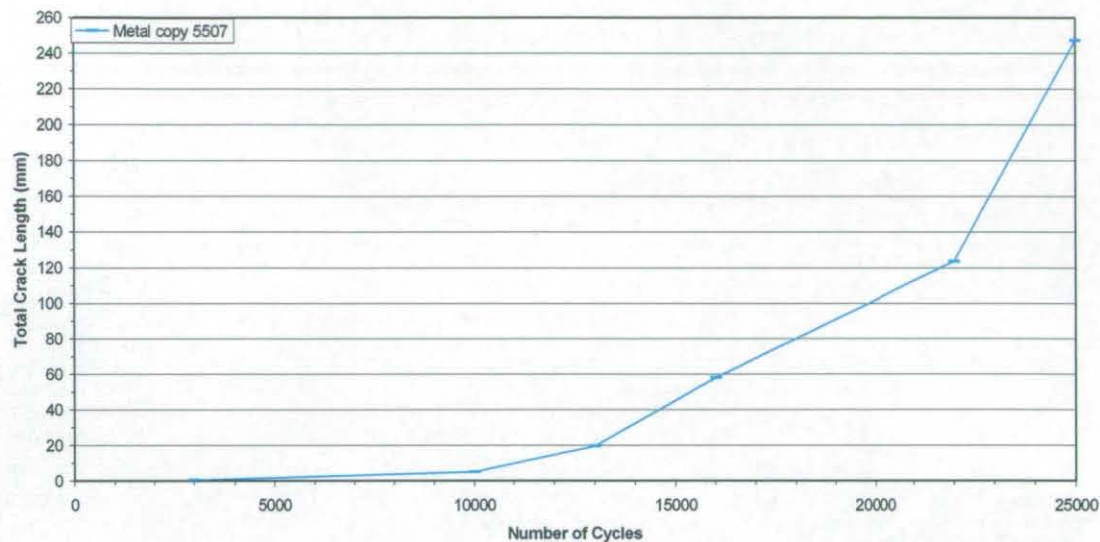


Figure 7 - 8 Metalcopy 5507 number of cycles versus total crack length

7.6 Metalcopy Janalloy Thermal Fatigue Methodology

The thermal fatigue cycles for the Metalcopy Janalloy specimens was increased in the same way as with Metalcopy 5507 up to 5,000 cycles and for the same reasons, given earlier. The test, however, was terminated after 5,000 cycles due to the abundance of cracks that formed. The thermal fatigue cycle was increased in increments of 50 to 100, then increments of 100 to 500, increments of 500 to 3,000 and finally increments of 1,000 to 5,000.

7.6.1 Metalcopy Janalloy Thermal Fatigue Results

7.6.1.1 Initial Signs of Cracking

Cracking initiated on all four specimens between 1,000 to 1,500 cycles ranging from 1 crack on specimen 2 to 6 cracks on specimen 1 (Figure 7 - 9).

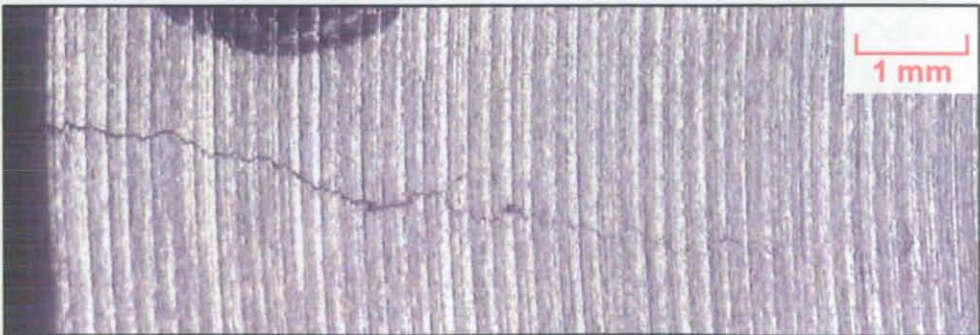


Figure 7 - 9 Metalcopy Janalloy S1-1,500-12-x1

7.6.1.2 Hardness

The hardness of the specimens and of the reference specimen tended to vary between $\approx 50\text{HRb}$ and $\approx 62\text{HRb}$ up to 3,000 cycles (Appendix v, Figure 6), the variance was most likely a result of the position of the indenter on the microstructure of the material. Again the structure consisted of steel balls in a matrix of silver and copper.

7.6.1.3 Number of Cracks

Figure 7 - 10 and Table 7 - 2 shows the number of cracks in the test specimens and rate of initiation. The cracks initiated between 1,000 and 1,500 cycles and their number increased between 1,500 and 2,000 cycles, after which the rate of initiation reduced but was then followed by a sharp increase in crack initiation for specimens 2, 3 and 4 between 2,500 and 3,000. The initiation of cracks in specimen 3 then reduced (0.25 cracks / 500 cycles) but in specimen 2 and 4 the number of cracks continued to increase at similar rates up to 4,000 cycles where they both reduced in rate to 0.5 cracks / 500 cycles. Specimen 1 on the other hand did not exhibit the same increase in crack numbers but at between 3,000 and 4,000 cycles more cracks became visible (2.5 cracks / 500 cycles).

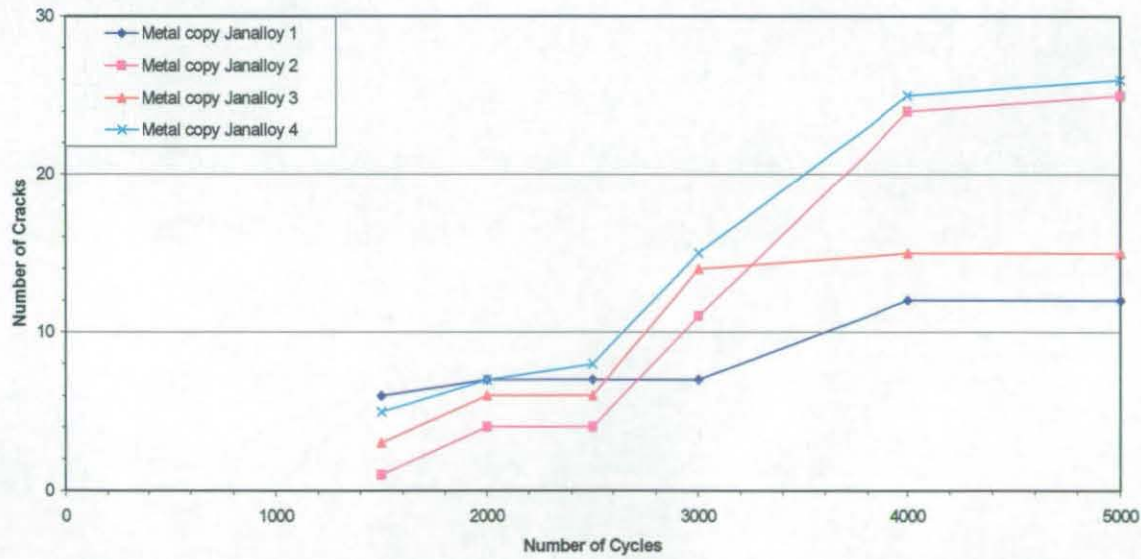


Figure 7 - 10 Metalcopy Janalloy number of cycles versus number of cracks

Specimen	Crack growth rate between 1,500 - 2,000 cycles	Crack growth rate between 2,500 - 3,000 cycles	Crack growth rate between 3,000 - 4,000 cycles	Crack growth rate between 4,000 - 5,000 cycles
1	1 crack / 500 cycles		2.5 cracks / 500 cycles	
2	3 cracks / 500 cycles	6.66 cracks / 500 cycles	6.66 cracks / 500 cycles	0.5 cracks / 500 cycles
3	3 cracks / 500 cycles	8 cracks / 500 cycles	0.25 cracks / 500 cycles	
4	2 cracks / 500 cycles	5.67 cracks / 500 cycles	5.67 cracks / 500 cycles	0.5 cracks / 500 cycles

Table 7 - 2 Metalcopy Janalloy crack initiation rate

The average number of cracks / specimen increased between 2,500 and 4,000 cycles and then became constant. The average crack initiation rate was 2.60 / 500 cycles (Appendix v, Figure 7).

The total number of cracks grew from 15 initially, to 25 over 500 cycles (5 cracks / 500 cycles). Between 2,500 and 4,000 cycles the crack numbers increased significantly to 76 (17 cracks / 500 cycles) and then reached 78 (1 crack / 500 cycles) (Appendix v, Figure 8).

7.6.1.4 Crack Length

Figure 7 - 11 shows the average crack length of the specimen with the maximum and minimum lengths. It is clear that the average crack length remained reasonably constant at approximately 4mm (0.08mm / 500 cycles). However, the maximum crack size grew from $\approx 8.5\text{mm}$ to $\approx 12\text{mm}$ over 3,500 cycles with an increase occurring after 2,500 cycles.

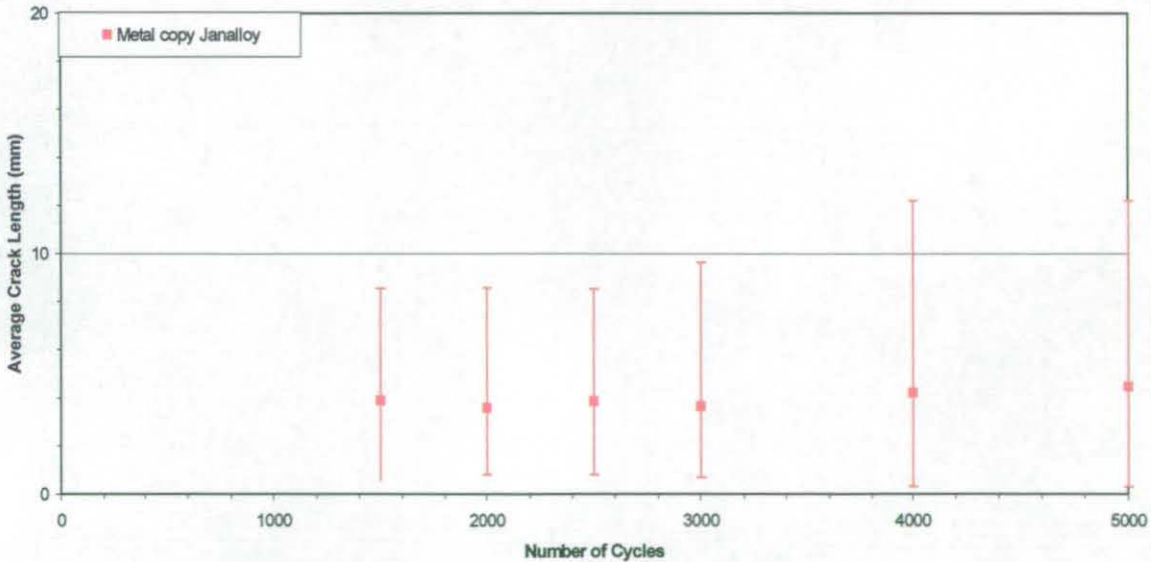


Figure 7 - 11 Metalcopy Janalloy number of cycles versus average crack length with maximum - minimum range crack length of all cracks

Between 3,000 and 5,000 cycles new cracks initiated (Appendix v, Figure 9) resulting in the average crack length remaining reasonably constant.

The initial total crack length of all four specimens at 1,500 cycles was over 50mm and increased at a rate of 18.9mm / 500 cycles; at 2,500 cycles the rate increased to 74.58mm / 500 cycles and at 4,000 cycles the rate reduced to 14.17mm / 500 cycles giving a total crack length of \approx 350mm after 5,000 cycles (Figure 7 - 12).

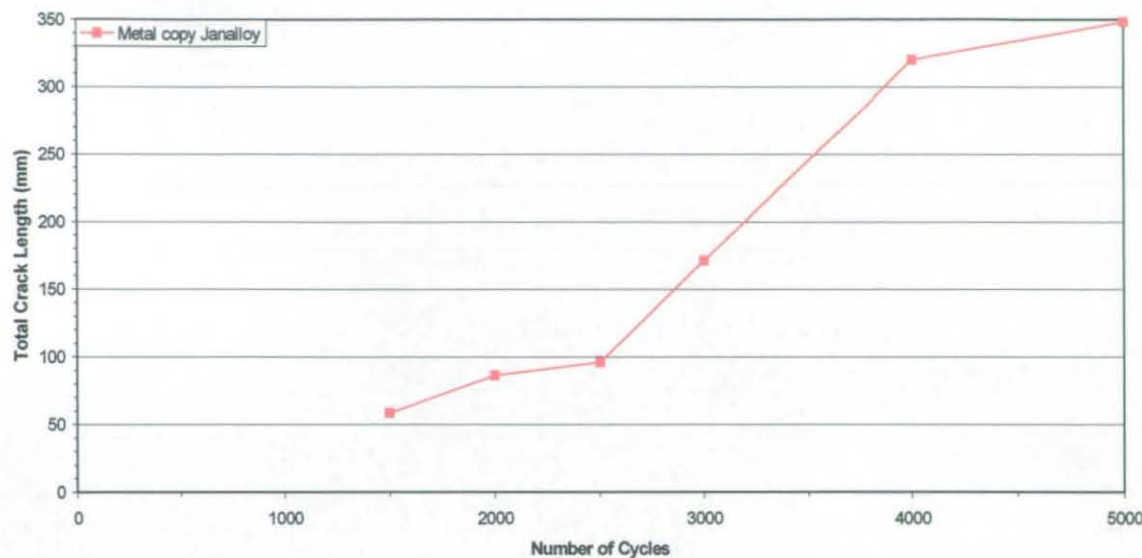


Figure 7 - 12 Metalcopy Janalloy number of cycles versus total crack length

7.7 Metalcopy Cu Thermal Fatigue Methodology

The thermal fatigue cycles for Metalcopy Cu were increased by increments of 50 up 500, increments of 500 up to 3,000, increments of 1,000 up to 10,000 and increments of 3000 up to 25,000.

7.7.1 Metalcopy Cu Thermal Fatigue Results

7.7.1.1 Initial Signs of Cracking

Cracks first initiated on specimen 1 between 6,000 and 7,000 cycles. Three cracks occurred, the largest measuring 1.08mm (Figure 7 - 13).

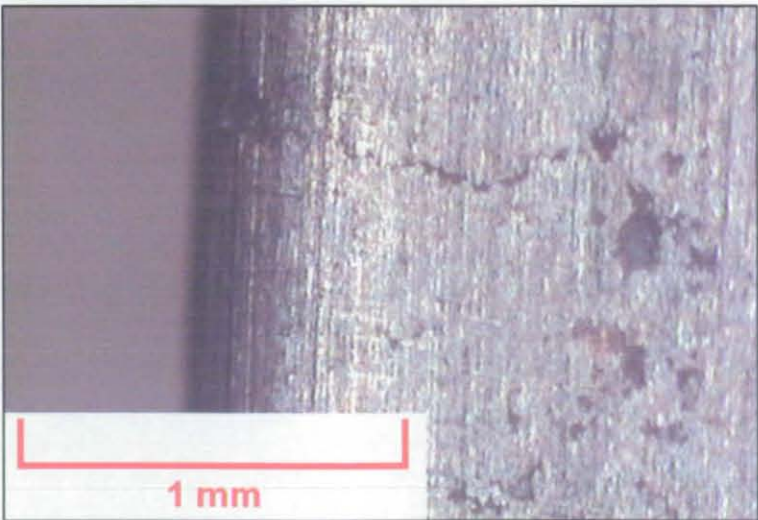


Figure 7 - 13 Metalcopy Cu specimen 1 S1-7K-8-x3

7.7.1.2 Hardness

The hardness of the specimens was reasonably constant throughout the experiment, between 68HRb and 78HRb, and the overall specimen average hardness was $\approx 70\text{HRb}$ (Appendix v, Figure 10).

7.7.1.3 Number of Cracks

Figure 7 - 14 shows that each specimen cracked in a different manner. Specimen 1 was the first to exhibit crack initiation and the number of cracks increased at a rate of 1.67 cracks / 500 cycles, at 10,000 cycles this decreased to 0.47 cracks / 500 cycles, giving a total of 27 cracks at 25,000 cycles. Specimens 2 and 3 did exhibit crack initiation but the number of cycles to initiate cracks and the rate of initiation were different and variable. Specimen 4 did not develop any cracks. The results show that there are inconsistencies and this may be due to the manufacturing process (poor infiltration versus good infiltration).

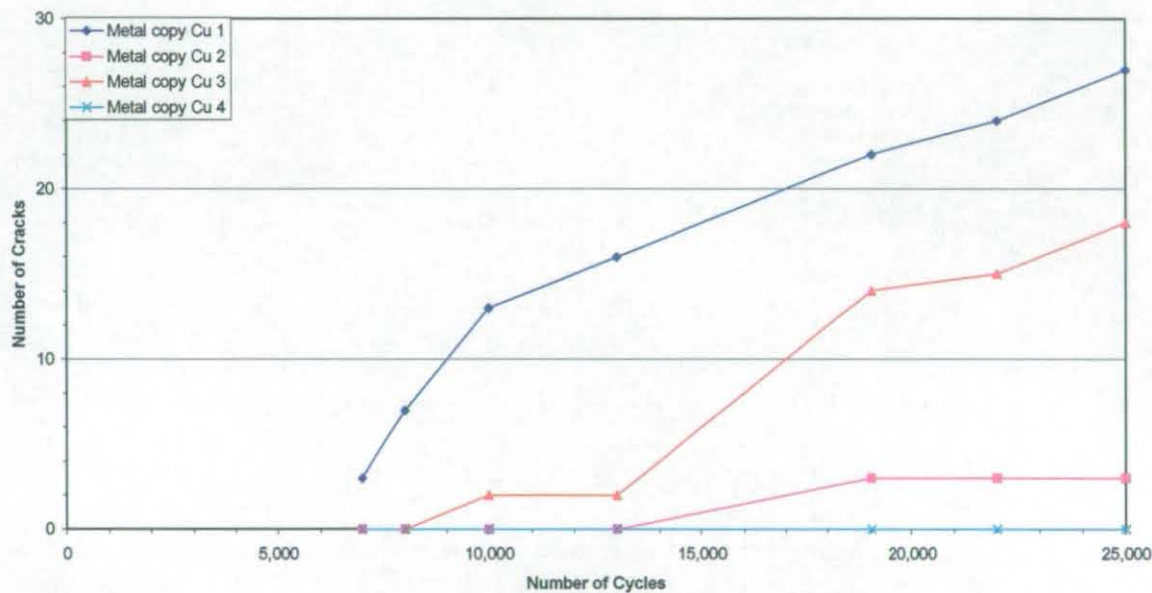


Figure 7 - 14 Metalcopy Cu number of cycles versus number of cracks

The average number of cracks slowly increased at a rate of 0.31 cracks / 500 cycles, however, there was a large difference between the maximum number of cracks on a specimen and the minimum. There was an increase in the average number of cracks between 13,000 and 19,000 cycles because specimen 1 and specimen 2 developed new cracks during this period (Appendix v, Figure 11).

The total number of cracks increased at a rate of 5.5 cracks / 500 cycles between 7,000 - 8,000 cycles; at 10,000 the increase was 1.1 cracks / 500 cycles and the specimens had a total of 48 cracks after 25,000 cycles (Appendix v, Figure 12).

7.7.1.4 Crack Length

Figure 7 - 15 shows the average crack length, which was initially 0.55mm at 7,000 cycles and increased to 1.72mm at 8,000 cycles (0.59mm / 500 cycles) because large cracks were initiating in specimen 1. The average crack length then levelled out between 8,000 and 10,000 cycles because specimen 1 and 3 only exhibited the initiation of small cracks. The average then increased between 10,000 and 13,000 cycles (0.15mm / 500 cycles) as a result of rapid growth in crack length, with few cracks initiating. Again the average crack length levelled out as new cracks initiated whilst others propagated (0.004mm / 500 cycles). The individual crack length over the number of cycles can be seen in Appendix v, Figure 13.

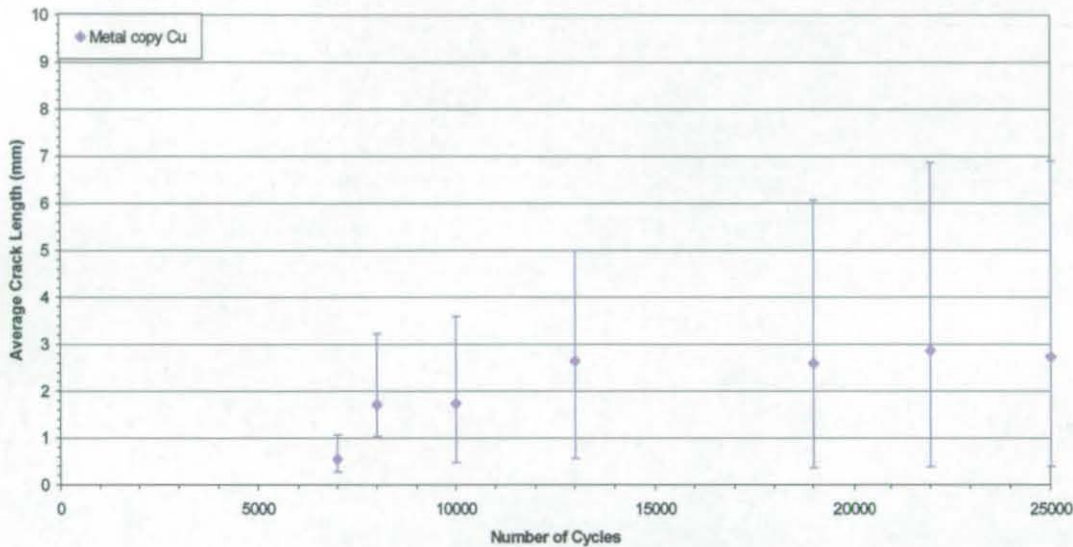


Figure 7 - 15 Metalcopu Cu number of cycles versus average crack length with maximum - minimum crack length of all cracks

The total crack length (Figure 7 - 16) increased at a rate of 3.96mm / 500 cycles from an initial 1.66 mm to a length of over 131.68mm at 25,000 cycles.

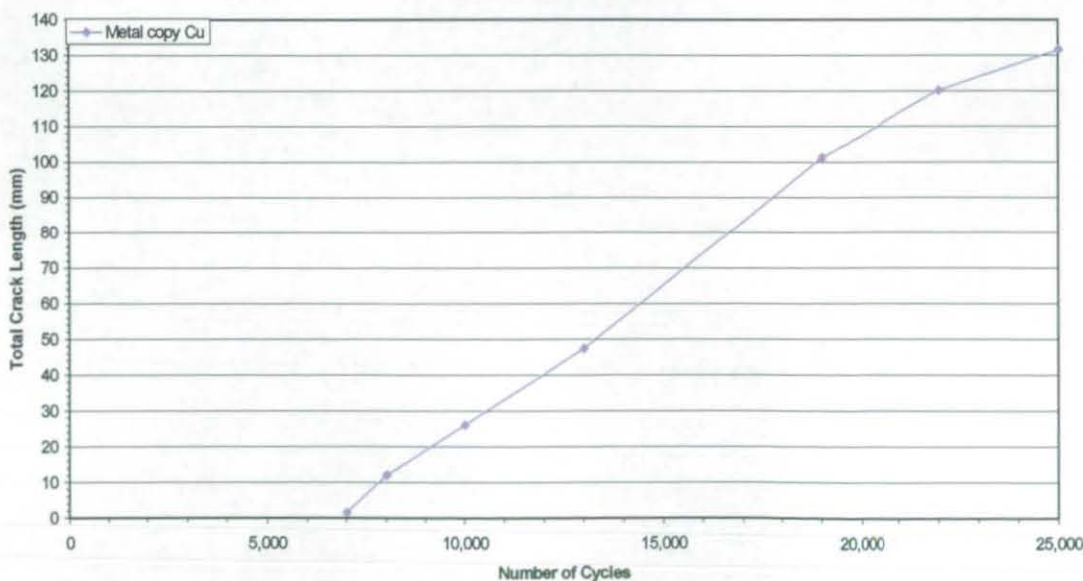


Figure 7 - 16 Metalcopu Cu number of cycles versus total crack length

7.8 Vertical Laminate Thermal Fatigue Methodology

The specimens were initially thermally fatigued for 100 cycles, since no signs of cracking occurred a further 400 cycles were conducted, then the thermal fatigue cycle was increased in increments of 500 to 5,000 cycles.

7.8.1 Vertical Laminate Thermal Fatigue Results

7.8.1.1 Initial Signs of Cracking

The first signs of cracking on the Vertical laminate specimens were observed on specimens 2 and 3 between 100 and 500 cycles. The cracks all initiated and propagated in the braze, an example is shown in Figure 7 - 17.



Figure 7 - 17 Vertical laminate specimen 2 S2rs-3K-1-x3

7.8.1.2 Hardness

The hardness of the specimens ranged from (108HRb - 115HRb) (Appendix v, Figure 14). It was possible that the difference in hardness was due to the structure of the composite material and how it was tested, i.e. whether the indenter was located on the H13 sheet, braze or a combination of both. The specimens, however, all had a comparable average hardness of $\approx 111\text{HRb}$, which equates to 39HRC.

7.8.1.3 Number of cracks

Figure 7 - 18 shows that a single crack initiated in the Vertical laminate specimens 2 and 3 between 100 and 500 cycles. Specimen 1 developed a crack between 500 and 1,000 cycles and specimens 2 and 3 developed their second cracks between 1,000 and 1,500.

When cracking occurred in all the specimens the rate of initiation was similar, at 3,000 / 3,500 cycles the rate increased. After 5,000 cycles specimen 1 had a total of 13 cracks, specimen 2, a total of 9 cracks and specimen 3 a total of 14 cracks after 5,000 cycles. Specimen 4 did not follow the same pattern but exhibited its first crack between 2,500 and 3,000 cycles and another between 3,000 and 3,500 cycles after which its crack initiation rates also increased to 2.5 cracks / 500 cycles (Figure 7 - 18 and Table 7 - 3).

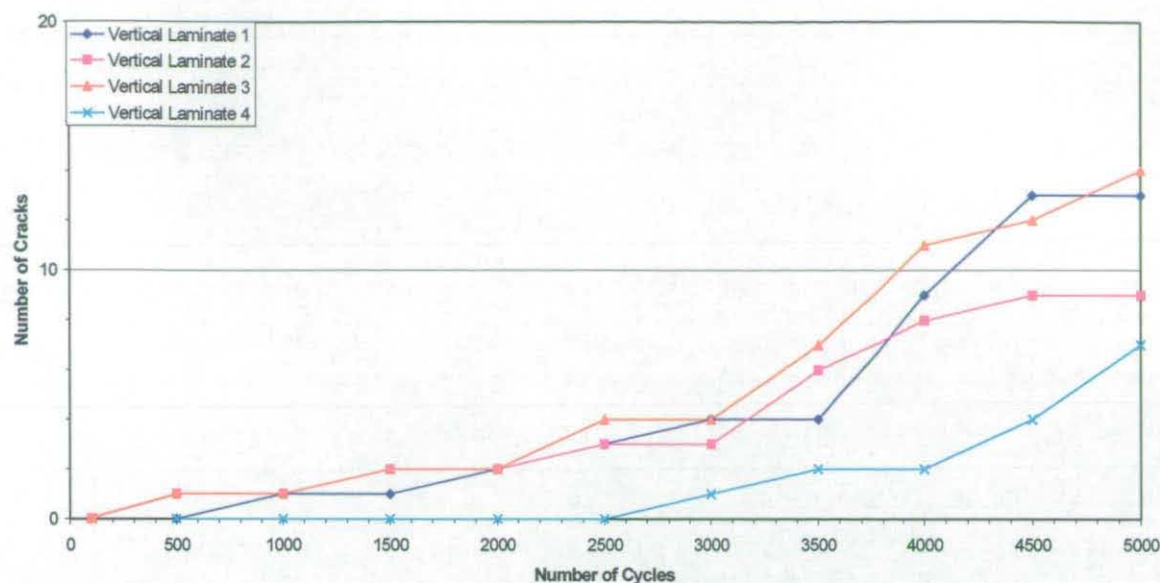


Figure 7 - 18 Vertical laminate number of cycles versus number of cracks

Specimen	Crack growth rate between 500 - 3,000 cycles	Crack growth rate between 3,000 - 4,000 cycles	Crack growth rate between 4,000 - 5,000 cycles
1	1 crack / 500 cycles	4.5 cracks / 500 cycles	4.5 cracks / 500 cycles
2	0.67 / 500 cycles	2.5 cracks / 500 cycles	0.5 cracks / 500 cycles
3	1.5 cracks / 500 cycles	3.5 cracks / 500 cycles	3.5 cracks / 500 cycles
4		1 crack / 500 cycles	2.5 cracks / 500 cycles

Table 7 - 3 Vertical laminate crack initiation rate

There was a steady increase in the rate of crack numbers in the specimens (0.5 cracks / 500 cycles) and a greater increase after 3,000 cycles (2 cracks / 500 cycles) (Appendix v, Figure 15). The total number of cracks increased by 2 every 500 cycles and then at 3,000 cycles increasing to a rate of 8.25 cracks / 500 cycles with a total of 45 cracks after 5,000 cycles (Appendix v, Figure 16).

7.8.1.4 Crack Length

Figure 7 - 19 shows the average crack length, which increased uniformly. From the gradient of the graph the average crack growth rate was calculated to be approximately 0.95mm / 500 cycles. However, the maximum crack length was increasing whereas the minimum was not, so smaller cracks formed in order to maintain a linear average crack length. The individual cracks initiated and the rate of crack growth is shown in Appendix v, Figure 17.

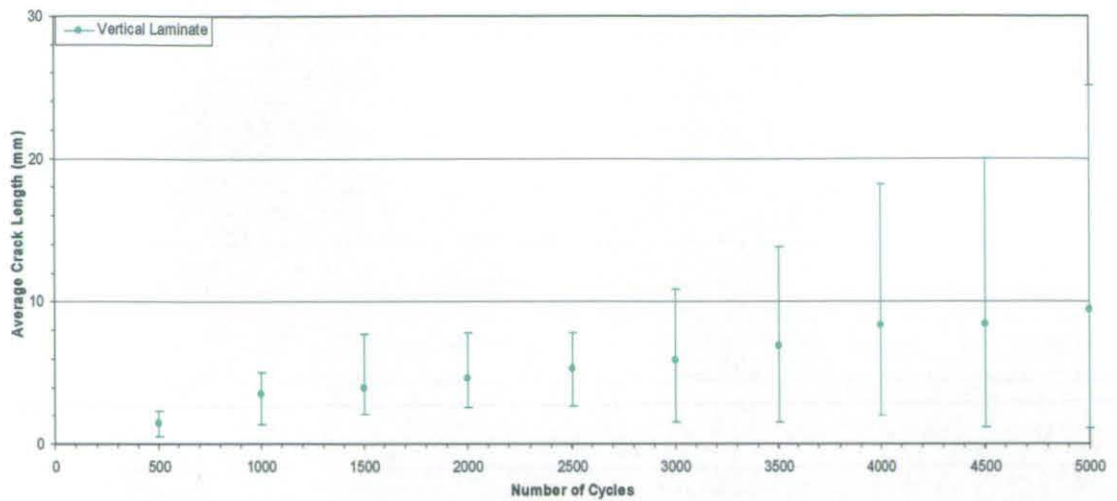


Figure 7 - 19 Vertical laminate number of cycles versus average crack length with maximum - minimum range

Figure 7 - 20 shows the total crack length of all the specimens over the course of the experiment. The rate at which the total crack length developed remained steady at approximately 13.57mm / 500 cycles up to 3,000 cycles and then increased to approximately 82.32mm / 500 cycles to a total crack length of 406.67mm after 5,000 cycles.

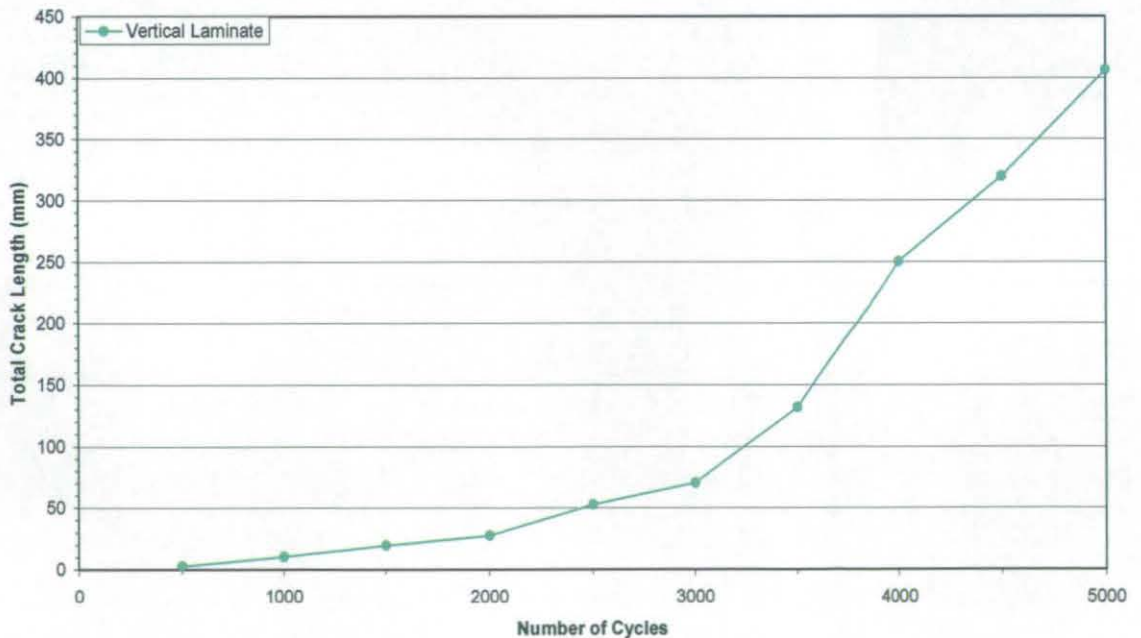


Figure 7 - 20 Vertical laminate number of cycles versus total crack length

7.9 Horizontal Laminate Thermal Fatigue Methodology

The thermal fatigue cycles were increased in increments of 500 to 2,000 and increments of 1,000 to 5,000. At 5,000 cycles the tests were terminated.

7.9.1 Horizontal Laminate Thermal Fatigue Results

7.9.1.1 Initial Signs of Cracking

The Horizontal laminate specimens failed in a different manner to the Vertical laminate specimens making data acquisition difficult. The mode of crack growth during the thermal fatigue test meant that no crack growth data could be recorded.

The interface between the H13 and braze was not uniform and the H13 laminate and braze had been removed in many places (Figure 7 - 21). At the braze / H13 interface, the H13 laminate became so thin during machining that it had simply been removed because of the cutting forces.



Figure 7 - 21 Horizontal laminate machining defects

As the test continued these areas thermally fatigued and the H13 was being removed (thin sections being fatigued easily) exposing more braze. Figure 7 - 22 shows a defect on specimen 3 after 500 cycles and Figure 7 - 23 shows the same defects over a larger area of the disc after 3,000 cycles.

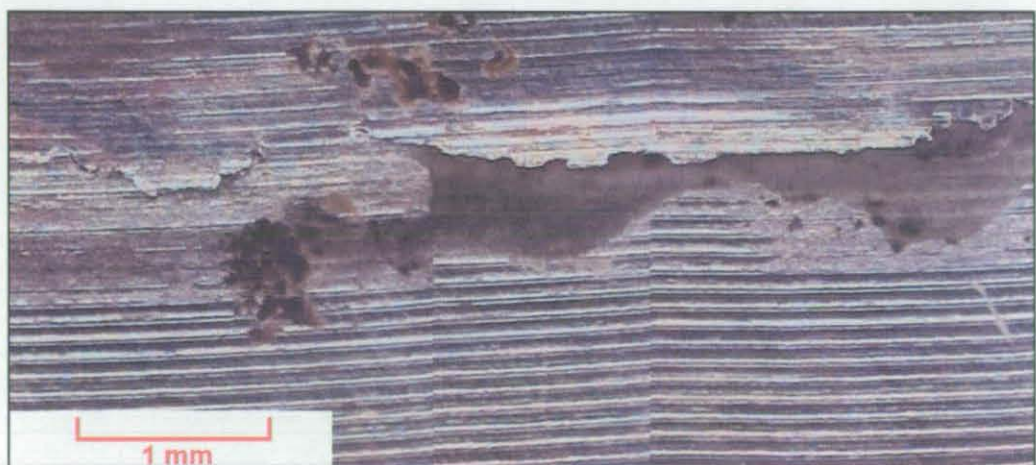


Figure 7 - 22 Horizontal laminate specimen 3 S3-500-1-x2

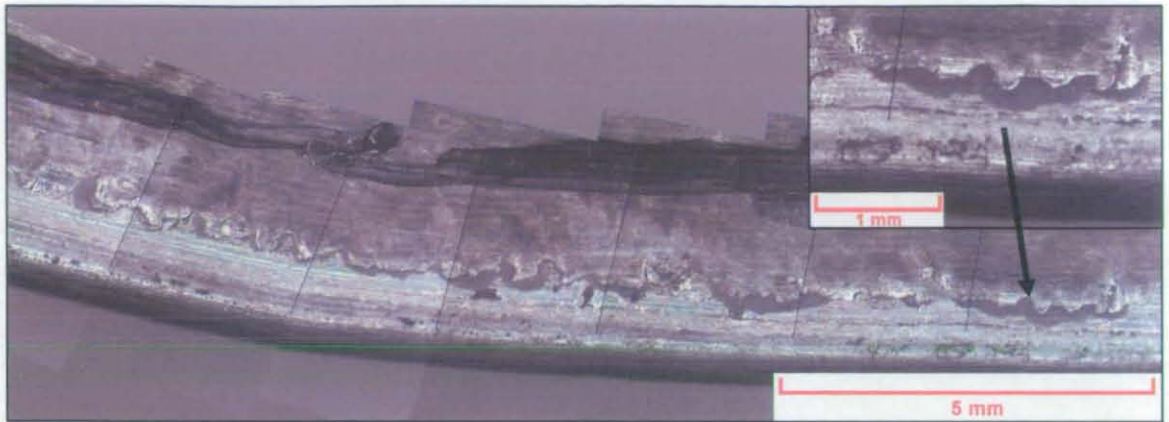


Figure 7 - 23 Horizontal laminate specimen 1 S1rs-3K-5-x2

7.9.1.2 Hardness

Each specimen exhibited a relatively stable hardness. The average hardness was $\approx 114\text{HRb}$ (Appendix v, Figure 18).

7.10 Amdry 790 (Solid) Thermal Fatigue Methodology

The thermal fatigue cycles were increased in increments of 500 up to 2,000 cycles, increments of 1,000 up to 10,000 cycles, increments of 5,000 up to 30,000, increments of 10,000 up to 50,000 and increments of 20,000 up to 110,000 at which point the tests were terminated.

7.10.1 Amdry 790 (Solid) Thermal Fatigue Results

7.10.1.1 Initial Signs of Cracking

Only three thermal fatigue specimens and one reference specimen were manufactured because of the availability and cost of braze. Initial cracks occurred at the edge radius between 2,000 - 3,000 cycles (Figure 7 - 24).

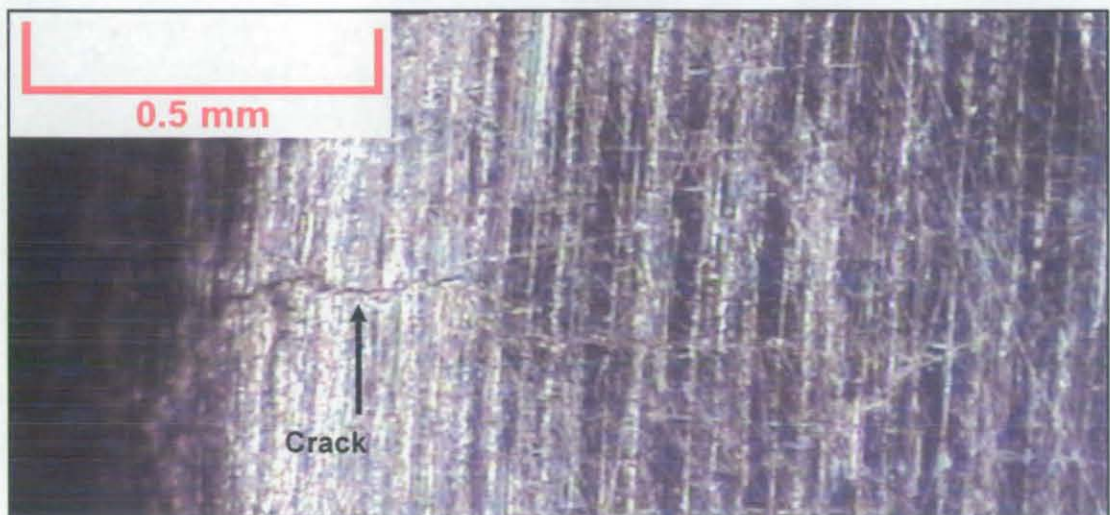


Figure 7 - 24 Amdry 790 S3rs-3K-5-x5

7.10.1.2 Hardness

The specimen hardness and the reference specimen had a hardness of approximately 83HRb (Appendix v, Figure 19). Specimens 1, 2 and 3 all maintained their hardness levels up to 50,000 cycles and then the hardness began to fall. The reference specimen hardness was constant. It must also be noted that specimen 3 had a higher hardness, approximately 112HRb, compared to specimens 1 and 2 which had hardness's in the 75HRb - 90HRb range. Post analysis showed that specimen three had a eutectic structure and was different to the other specimens and that could explain the difference.

7.10.1.3 Number of Cracks

Figure 7 - 25 shows that specimen 3 was the first to exhibit crack initiation with a total of 8 cracks between 2,000 - 3,000 cycles and specimen 1 initiated 4 cracks between 4,000 - 6,000 cycles. There was little change in crack initiation until 50,000 cycles when crack initiation significantly increased in specimen 1 to 0.38 cracks / 500 cycles and at 70,000 cycles increasing to 1.43 cracks / 500 cycles with a total of 133 cracks at 110,000 cycles. Specimen 3, however, only exhibited a small increase in the numbers of cracks to 14 (0.028 cracks / 500 cycles). Specimen 2, on the other hand, initiated 20 cracks between 10,000 and 90,000 cycles to a total of 44 after 110,000 cycles (0.55 cracks / 500 cycles).

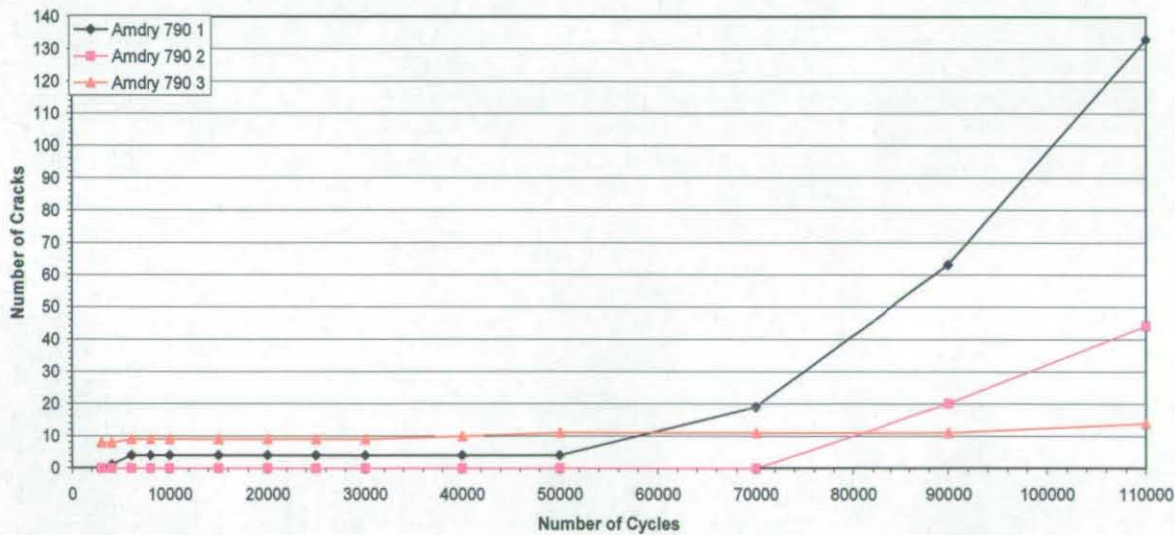


Figure 7 - 25 Amdry 790 number of cycles versus number of cracks

The average number of cracks on a specimen remained low (0.025 cracks / 500 cycles) up to 50,000 cycles, increasing to 0.13 cracks / 500 cycles up to 70,000 cycles and increasing again to 0.63 cracks / 500 cycles up to a total of 63.67 at 110,000 cycles (Appendix v, Figure 20).

The total number of cracks was 8 at 3,000 cycles rising slowly to 15 at 50,000 cycles (0.07 cracks / 500 cycles) but increasing faster to 30 cracks at 70,000 cycles (0.38 cracks / 500 cycles) with a further increase in rate to 180 cracks at 100,000 cycles (1.88 cracks / 500 cycles) (Appendix v, Figure 21).

7.10.1.4 Crack Length

Figure 7 - 26 shows how the average crack length remained low throughout the duration of the test reaching 1.58mm after 110,000 cycles (increasing at 0.005mm / 500 cycles). The minimum crack length remained low; however, the maximum rose steadily to 5.77mm after 110,000 cycles. The individual crack lengths are shown in Appendix v, Figure 22.

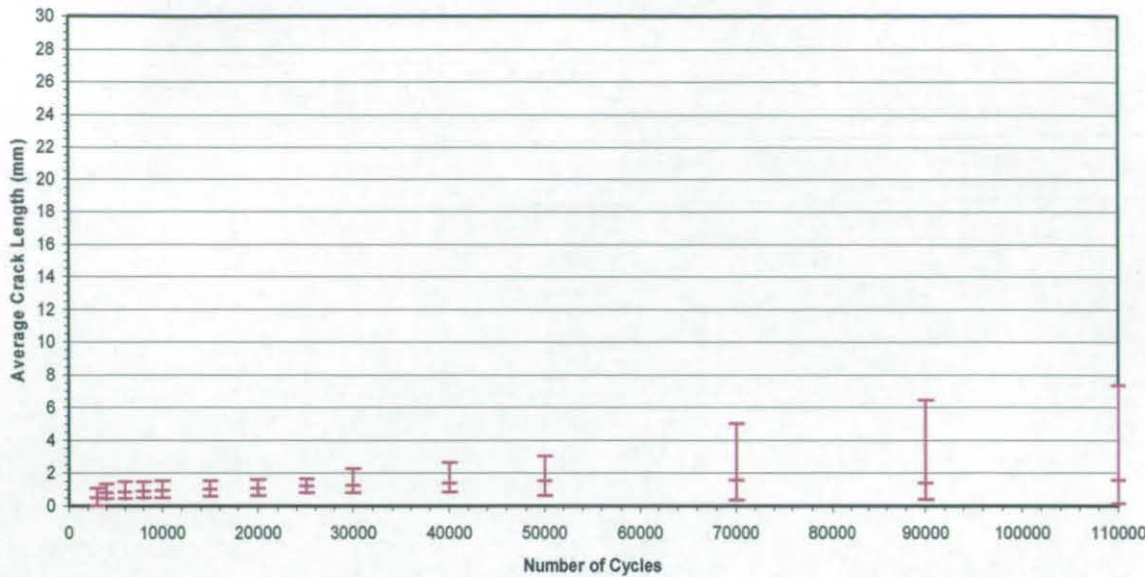


Figure 7 - 26 Amdry 790 number of cycles versus average crack length with maximum - minimum range

Figure 7 - 27 shows the total crack length in the specimens. The total crack length was 4.01mm at 3,000 cycles, and increased to 22.71mm at 50,000 cycles (0.2mm / 500 cycles) with a faster increase to 46.76mm at 70,000 cycles (0.6mm / 500 cycles), followed by a further increase to 302.13mm at 110,000 cycles (2.92mm / 500 cycles).

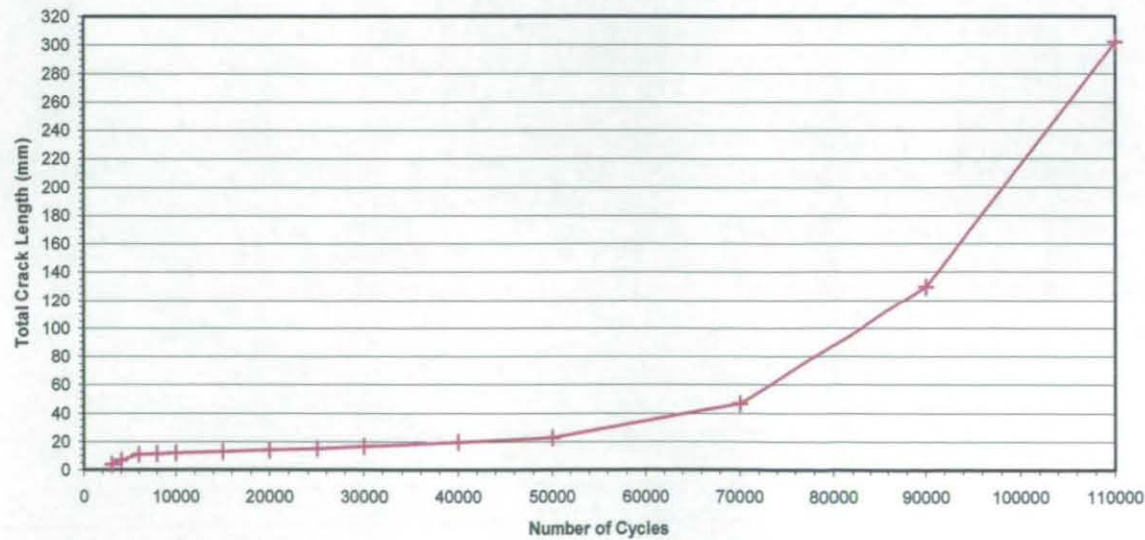


Figure 7 - 27 Amdry 790 number of cycles versus total crack length

7.11 Vertical RapidSteel 2.0 Thermal Fatigue Methodology

The thermal fatigue cycles were increased in increments of 500 to 3,000, increments of 1,000 to 10,000 s, increments of 3,000 to 40,000 and increments of 5,000 to 65,000.

7.11.1 Vertical RapidSteel 2.0 Thermal Fatigue Results

7.11.1.1 Initial Signs of Cracking

The tests were terminated prematurely because of the failure of the compressed air supply to the thermal fatigue apparatus. The specimens had remained in the furnace for over 8 hours causing severe degradation and destruction of the specimens, no cracks had initiated at this stage.

7.11.1.2 Hardness

The hardness had remained constant (Appendix v, Figure 23) with a specimen average hardness of $\approx 85.8\text{HRb}$. No further tests were conducted on these specimens.

7.12 Horizontal RapidSteel 2.0 Thermal Fatigue Methodology

The thermal fatigue cycles were increased in increments of 500 up to 3,000 cycles, increments of 1,000 up to 10,000 cycles, increments of 3,000 up to 40,000 cycles, increments of 5,000 up to 70,000 cycles and increments of 10,000 up to 100,000 cycles, the termination point of the test.

7.12.1 Horizontal RapidSteel 2.0 Thermal Fatigue Results

7.12.1.1 Initial Signs of Cracking

Initial cracks occurred at the edge radius at between 40,000 - 50,000 cycles (Figure 7 - 28).

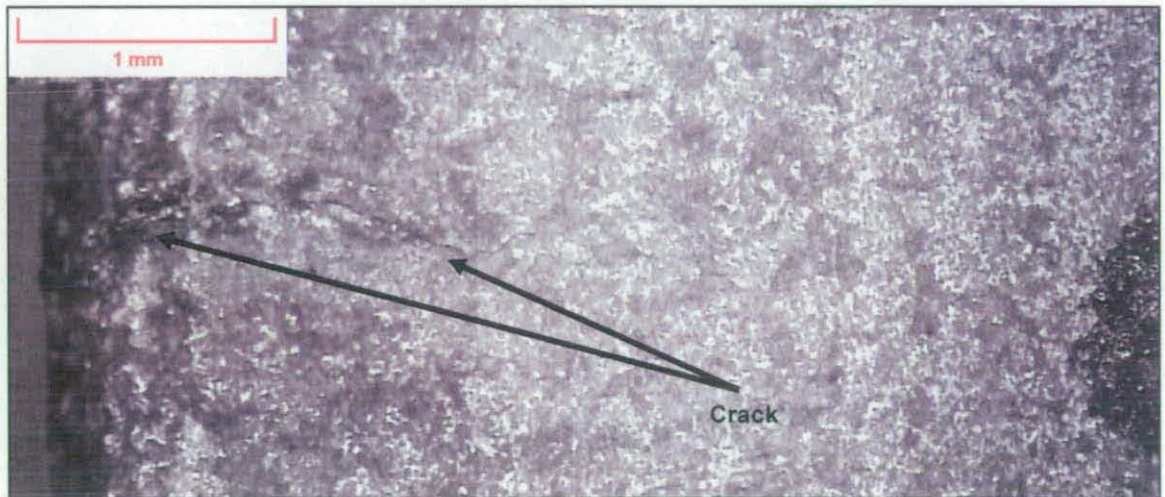


Figure 7 - 28 Horizontal RapidSteel 2.0 specimen 1 S1-50K-4-x3

7.12.1.2 Hardness

The specimens had similar hardness's to each another, which did not alter over the duration of the experiment. Specimen 1 had an average hardness of $\approx 84.5\text{HRb}$, specimen 2 $\approx 83\text{HRb}$, specimen 3 $\approx 86\text{HRb}$, specimen 4 $\approx 85\text{HRb}$ and specimen 5 $\approx 85\text{HRb}$ (Appendix v, Figure 24).

7.12.1.3 Number of Cracks

Figure 7 - 29 shows that specimen 1 was the first to initiate cracking, between 40,000 - 50,000 cycles, 14 cracks became visible and this rose to 20 cracks over the next 3,000 cycles. No further cracks developed up to 60,000 cycles but between 60,000 - 70,000 cycles there was a large increase to 39 cracks (approximate rate of 0.63 cracks / 500 cycles) after which no further cracks were detected up to 100,000 cycles. Specimens 2 and 4, however, exhibited crack initiation between 70,000 - 80,000 cycles. Specimen 2 had 12 cracks and specimen 4 only 3 but the rate of crack increase was similar in both cases. Specimen 3 showed the initiation of 9 cracks between 90,000 - 100,000 and again the rate of crack initiation was comparable (specimen 1 exhibited 0.63 cracks / 500 cycles, specimen 2 exhibited 0.45 cracks / 500 cycles, specimen 3 exhibited 0.45 cracks / 500 cycles and specimen 4 exhibited 0.48 cracks / 500 cycles).

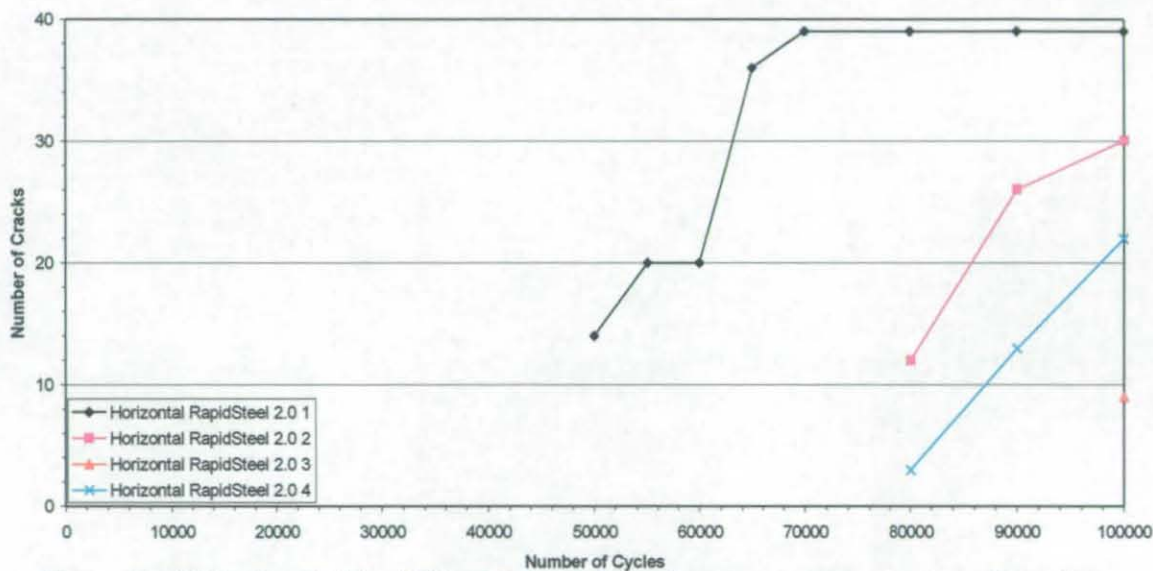


Figure 7 - 29 Horizontal RapidSteel 2.0 number of cycles versus number of cracks

The average number of cracks crack rate was 0.17 cracks / 500 cycles up to 80,000 cycles and increased to 0.29 cracks / 500 cycles up to 100,000 cycles (Appendix v, Figure 25).

The total number of cracks increased from 14 at 50,000 cycles to 54 cracks at 80,000 cycles (a rate of 0.67 / 500 cycles). The number of cracks increased to 100 after 100,000 cycles (a rate of 1.15 cracks / 500 cycles) (Appendix v, Figure 26).

7.12.1.4 Crack Length

Figure 7 - 30 shows the average crack length; initially it was 2.62mm at 50,000 cycles rising to 4.12mm over 10,000 cycles (a rate of 0.08mm / 500 cycles). The crack length then became nearly constant increasing by 0.13mm up to 100,000 cycles (a rate of 0.002mm / 500 cycles). Each individual crack, the number of cycles to initiation and propagation can be seen in Appendix v, Figure 27.

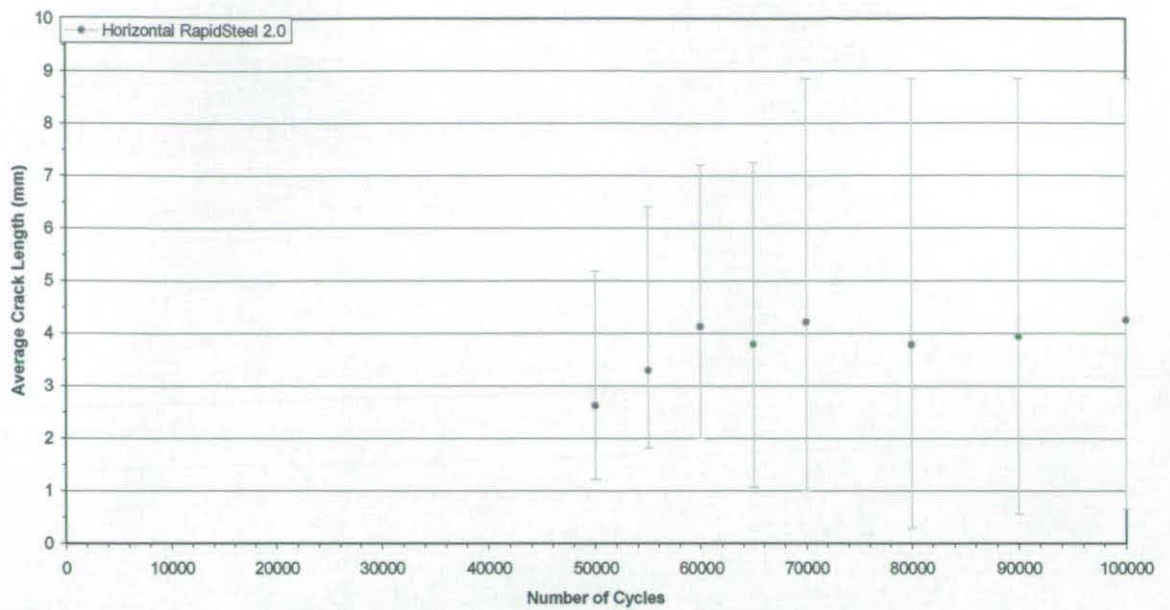


Figure 7 - 30 Horizontal RapidSteel 2.0 number of cycles versus average crack length with maximum - minimum range

Figure 7 - 31 shows the total crack length, which started at 36.66mm at 50,000 cycles and increased to 204.4mm at 80,000 cycles (a rate of 2.80mm / 500 cycles). The total crack length then grew to 424.97mm at 100,000 cycles (a rate of 5.51mm / 500 cycles).

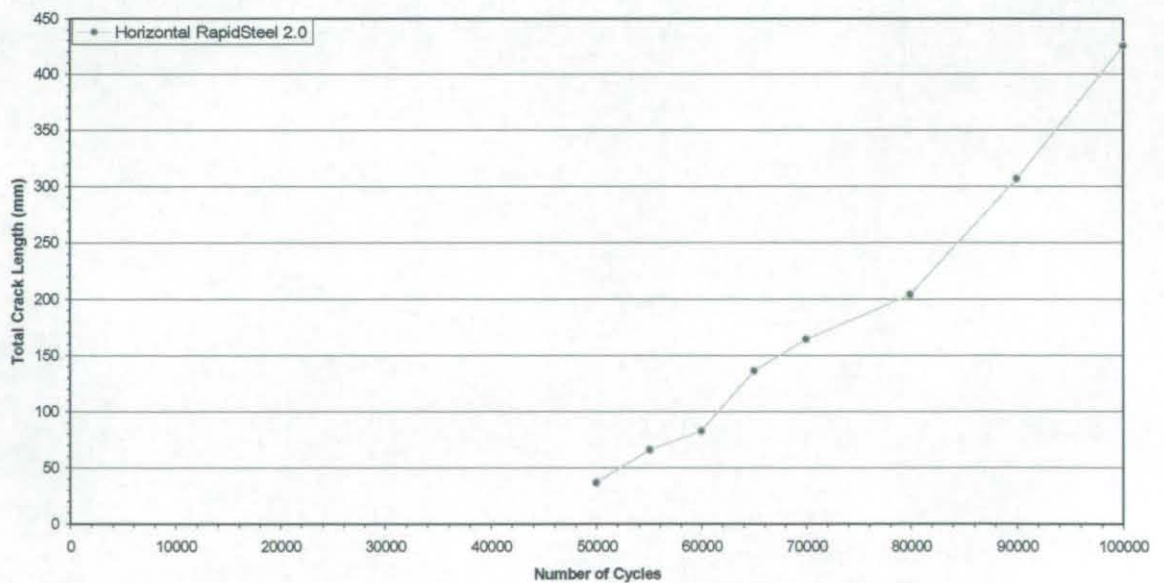


Figure 7 - 31 Horizontal RapidSteel 2.0 number of cycles versus total crack length

7.13 EOS DirectSteel 20 μ m Thermal Fatigue Methodology

The thermal fatigue cycles were increased in increments of 500 to 3,000 and increments of 1,000 up to 5,000, at which point the tests were terminated.

7.13.1 EOS DirectSteel 20 μ m Thermal Fatigue Results

7.13.1.1 Initial Signs of Cracking

Cracks initiated at the edge radius between 0 - 500 cycles (Figure 7 - 32).



Figure 7 - 32 EOS DirectSteel 20 μ m specimen 4 S4-500-2-x2

7.13.1.2 Hardness

The individual specimen hardness over the course of the thermal fatigue experiment were similar to each other between $\approx 88\text{HRb}$ and $\approx 89\text{HRb}$ (Appendix v, Figure 28).

7.13.1.3 Number of Cracks

Figure 7 - 33 shows the rate of crack initiation, all the specimens initiated cracks between 0 and 500 cycles; Specimen 1 exhibited 2 cracks initially, which increased at a rate of 2 / 500 cycles to 1,500 cycles after which no further cracks initiated. Specimen 2 crack initiation was slower (0.22 cracks / 500 cycles), 2 cracks were initially present, then between 1,000 and 1,500 one crack formed and between 4,000 and 5,000 cycles another formed, making a total of 4 cracks after 5,000 cycles. Specimen 3 initiated 4 cracks, then between 1,000 and 1,500 cycles a further crack initiated, between 1,500 and 2,500 cycles cracks initiated at a rate of 3 / 500, cycles which then slowed to a rate of 0.4 / 500 cycles making a total of 13 cracks after 5,000 cycles. Specimen 4 initiated 3 cracks then continued to initiate cracks at a rate of 6 / 500 cycles to 1,000 cycles slowing to 1 crack initiation every 500 cycles, making a total of 17 cracks at 5,000 cycles when the test was terminated.

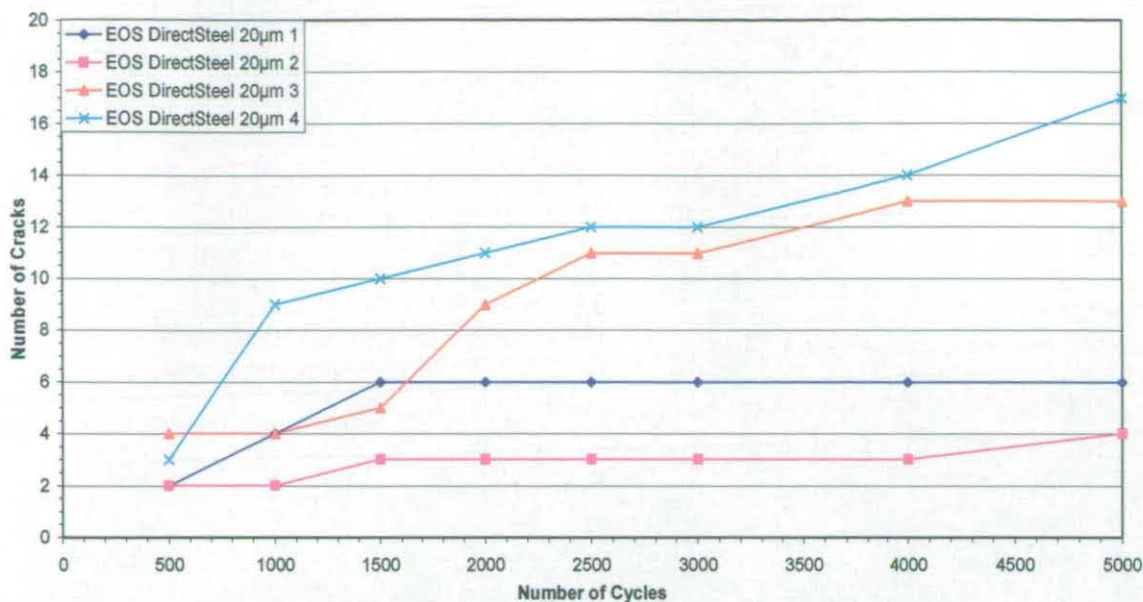


Figure 7 - 33 EOS DirectSteel 20µm number of cycles versus number of cracks

The average number of cracks / specimen increased at a rate of 1.5 cracks / 500 cycles between 500 and 2,000 cycles and then slowed to 0.46 cracks / 500 cycles (Appendix v, Figure 29).

The total number of cracks increased from 11 to 29 between 500 and 2,000 cycles, a rate of 6 cracks / 500 cycles. The rate then reduced to 1.83 cracks / 500 cycles until the experiment was terminated with a total of 40 cracks in all the specimens (Appendix v, Figure 30).

7.13.1.4 Crack Length

Figure 7 - 34 shows the average crack length remained relatively constant at approximately 6mm, increasing at a rate of 0.05mm / 500 cycles. However, it was apparent that there was a large maximum crack size starting at ≈ 14 mm and rising to ≈ 19 mm at 5,000 cycles. Small new cracks also initiated and maintained the constant average. Each crack and its length is shown in Appendix v, Figure 31.

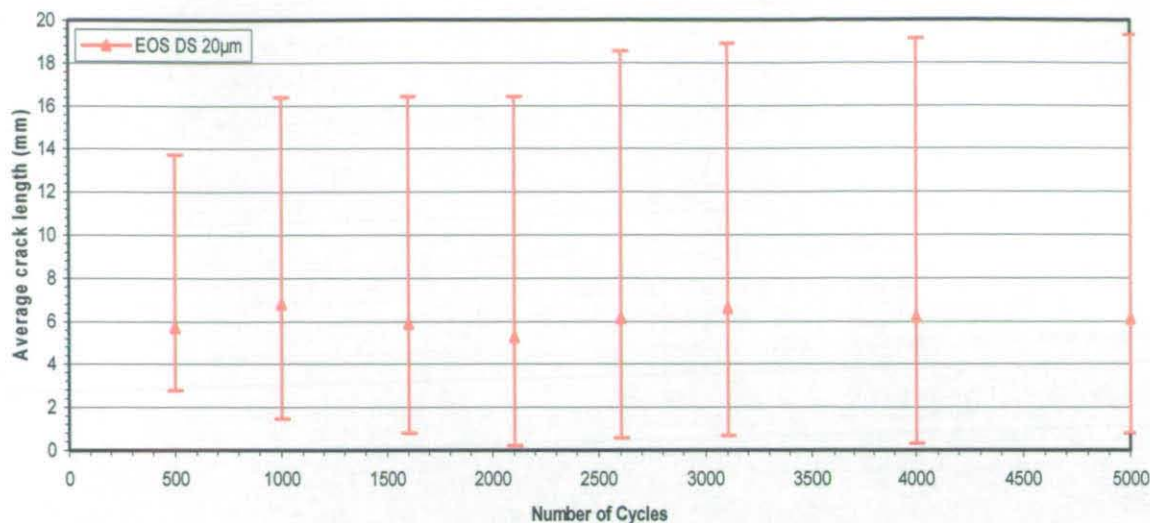


Figure 7 - 34 EOS DirectSteel 20µm number of cycles versus average crack length with maximum - minimum range

Figure 7 - 35 shows the total crack length, which started at 62.6mm at 500 cycles and increased to 129.2mm at 1,000 cycles (a rate of 66.6mm / 500 cycles); this reduced to 11.45mm / 500 cycles but at 2,000 cycles the rate increased again to 44mm / 500 cycles and at 2,500 reduced to 9.56mm / 500 cycles. The total crack length at the conclusion of the experiment was 243.95mm.

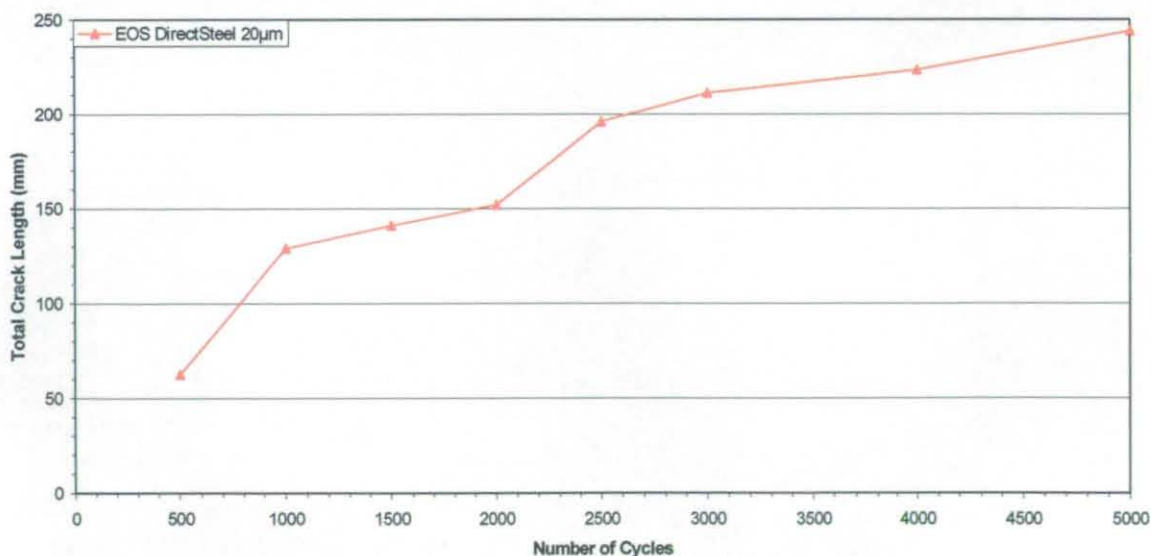


Figure 7 - 35 EOS DirectSteel 20µm number of cycles versus total crack length

Chapter 8: Post Thermal Fatigue Analysis

Optical and scanning electron microscopy (SEM) were employed to examine material microstructure, crack initiation sites and crack growth characteristics. Energy dispersive spectroscopy (EDS), otherwise known as energy dispersive x-rays (EDX) as discussed in chapter 3, section 3.7.6) allowed the material composition of the material and the composition of the crack surface to be determined.

8.1 Specimen Sectioning and Mounting

Specimens for the SEM examination required a flat surface. Initially the area of interest was cut from each specimen using a Struers Labotom cut-off machine with a Struers high quality cut-off wheel (34 TRE 250 x 1.5 x 32mm).

The next stage was to place specimens in a conductive mount (Buehler Konducto Met™ II aluminium conductive phenolic mounting compound) using a Struers Labopress-1 mounting machine.

Grinding was required to produce a flat surface; the first step was rough grinding using 220 wet and dry paper on a Metaserv polisher / grinder, model number C2345A. The specimen was washed with soapy water and rinsed prior to the next stage. Using a Metaserv hand grinder model C187 further grinding was carried out using successively finer grades (320, 400 and 600) of paper. To avoid carrying course grit to the finer papers the specimens were washed in soapy water and rinsed after each grade of paper had been used.

The next stage was to polish the specimens using a Metaserv universal polisher / grinder, model C25485, with variable speed settings. In this process, the first polishing stage used the wheel impregnated with 6µm diamond paste (Buehler, Medadi®); this was wetted with extender fluid (Buehler, Metadi®) for lubrication. The specimen was polished at 400rpm for two minutes, was then washed with soapy water and rinsed. The process was repeated using the wheel impregnated with 1µm diamond paste and the speed reduced to 200rpm and again the specimen was washed before the final polish. The final polish used a wheel impregnated with 0.05mm alumina (Buehler, Gamma Micropolish® number 3). The wheel was lubricated with distilled water and polishing occurred at 200rpm for two minutes. Finally, the specimen's surface was washed in soapy water, rinsed with water and then acetone or methanol before being thoroughly dried on a Metaserv specimen dryer model C210 and placed in a specimen dessicator with silica gel crystals to reduce the moisture level. All specimens were prepared in the same manner.

The specimens were then examined optically on a Nikon Optiphot with images taken using a JVC Colour Video Camera TK-C1481BEG and WinTV software. Images were also obtained using the SEM (Leo 1350 VP FEG) and EDS analysis (chapter 3, section 3.7.6).

After the initial examination, the specimens were etched to reveal the structure of the materials in more detail. Different etchants were used depending upon the material as some materials are resistant to certain chemicals. Metalcopy 5507, Metalcopy Janalloy and Metalcopy Cu were etched in acidic ferric chloride (5g FeCl_3 , 50ml HCl , 100ml H_2O). The Metalcopy 5507 was etched for 15 - 30 seconds, Metalcopy Janalloy for 30 seconds, Metalcopy Cu for 10 - 15 seconds. Amdry 790 was etched with 50% acetic acid and 50% nitric acid for 10 - 20 seconds and the remainder of the specimens were etched with 2% or 5% nitric acid (in alcohol) for 15 - 45 seconds dependent upon the depth of etch required. After etching the specimens were immediately rinsed in water followed by acetone or methanol and thoroughly dried on a Metaserv specimen dryer model C210 and placed in a specimen dessicator with silica gel crystals to reduce moisture level.

8.2 H13 Post Thermal Fatigue Results

8.2.1 Crack Initiation and Propagation

Optical examination of H13 specimens revealed a retained austenite tempered martensite structure with fine carbide precipitate. Figure 8 - 1 shows two cracks in specimen number 1, the crack seen in (A) is wide with smaller cracks propagating from the end of it.

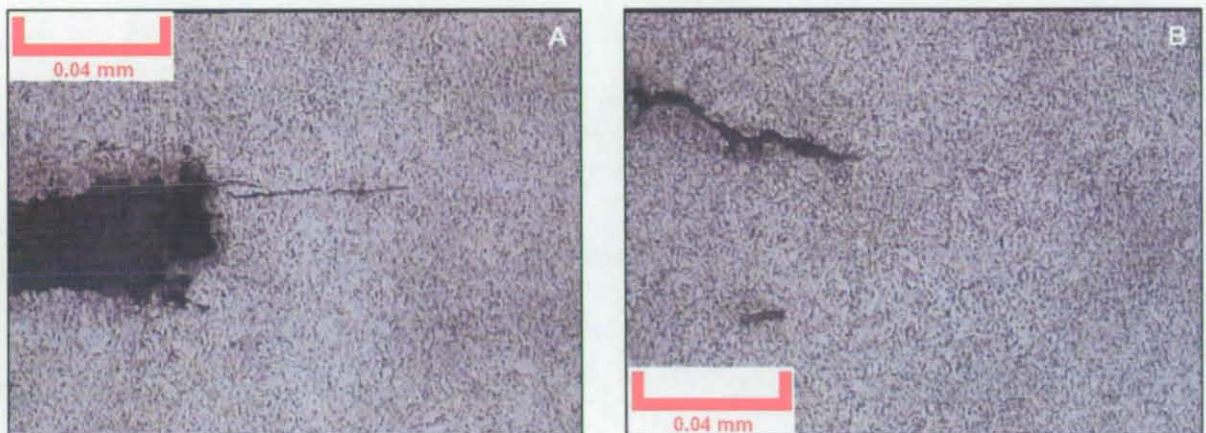


Figure 8 - 1 (A) H13-S1-300K-2-x40 crack tip; (B) H13-S1-300K-3-x40

The SEM examination of specimen 1 (Figure 8 - 2) revealed the propagation of two cracks causing a section of the material to fatigue and break away creating a larger void as seen in the enlarged image.

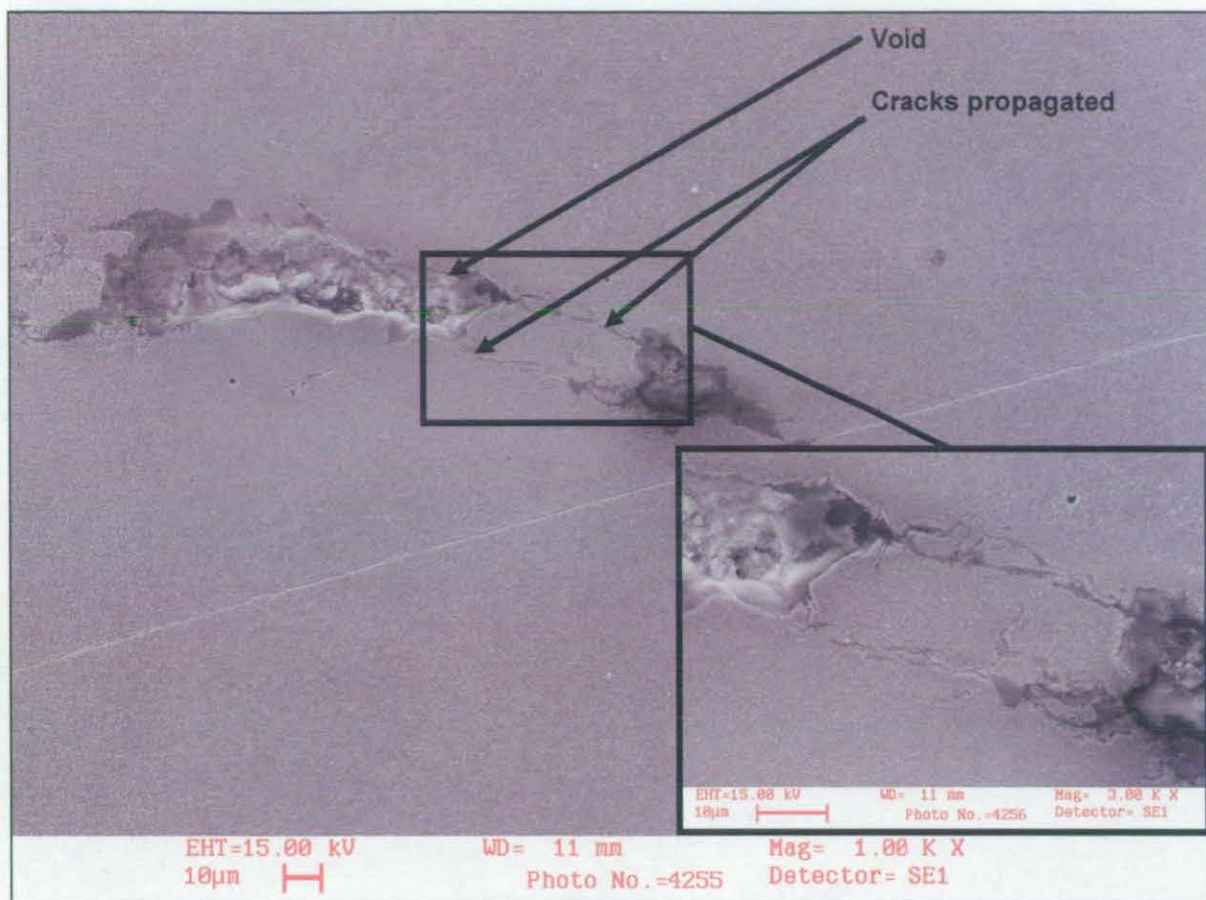


Figure 8 - 2 H13 specimen 1, S1-300K-1-x1000 (close up specimen 1, S1-300K-1-x3000)

8.2.2 EDX Analysis

Figure 8 - 3 shows an area of specimen 1 with a crack, under EDX analysis; it shows the crack area to have a higher concentration of vanadium, silicon, molybdenum, oxygen and aluminium. However, there was a reduced amount of chromium and iron, which suggested that it had either been removed or had fallen out during thermal fatigue test. The presence of oxygen suggested the presence of an oxide. The EDX results suggested that the crack favoured growth where the alloy was rich in the elements that form carbides in H13 steel, such as vanadium and molybdenum.

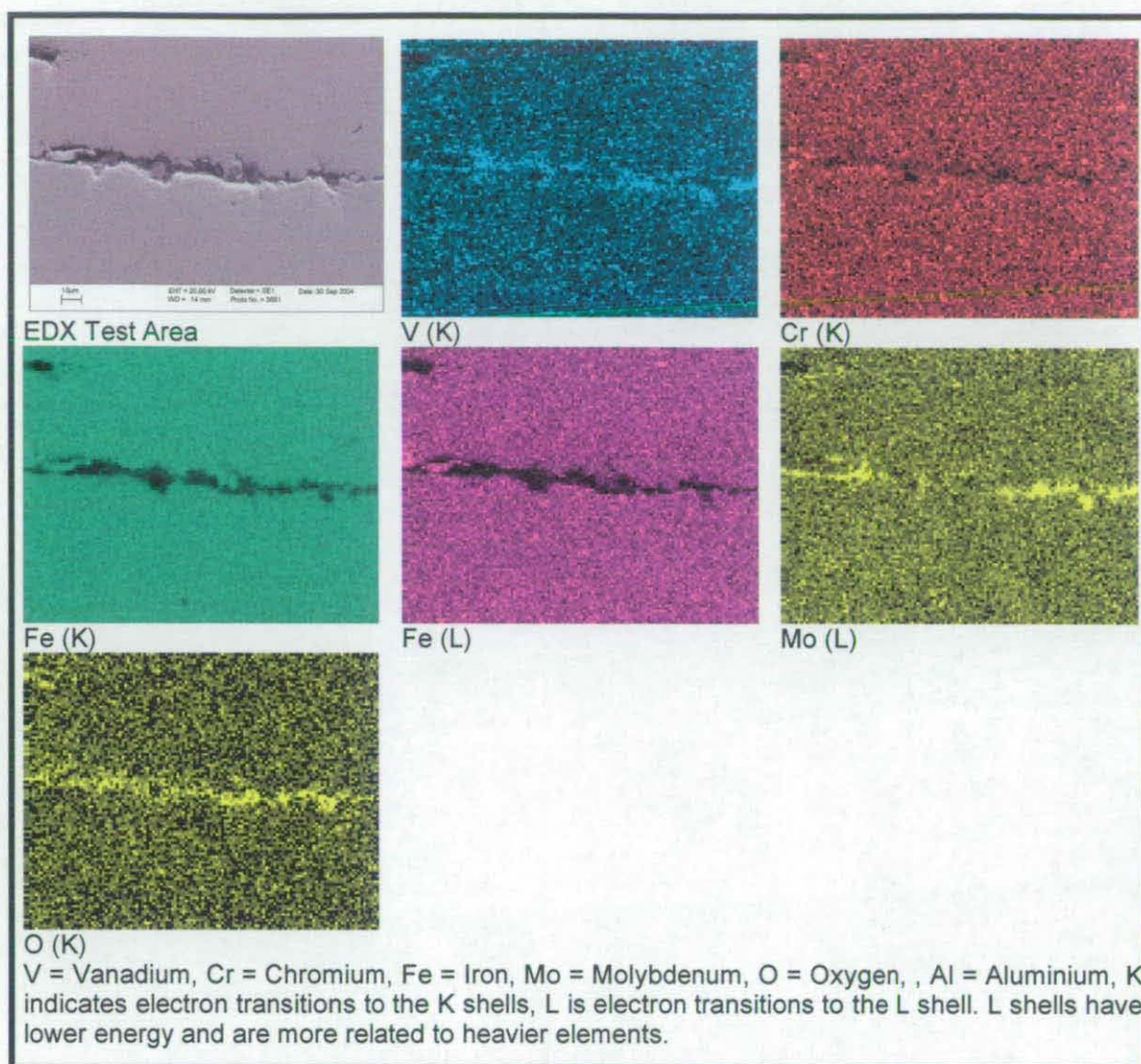


Figure 8 - 3 H13 EDX analysis

8.3 Metalcopy 5507 Post Thermal Fatigue Results

8.3.1 Crack Initiation and Propagation

Optical examination revealed that the cracks initiated in the matrix and at the outer radius of the specimen and then propagated through the matrix. The steel balls acted as crack arresters and the cracks could not propagate through them but were forced to go around them. Figure 8 - 4 shows a dark area running from left to right, which is a crack. It shows how the crack propagated through the matrix when subjected to a series of thermal fatigue cycles.

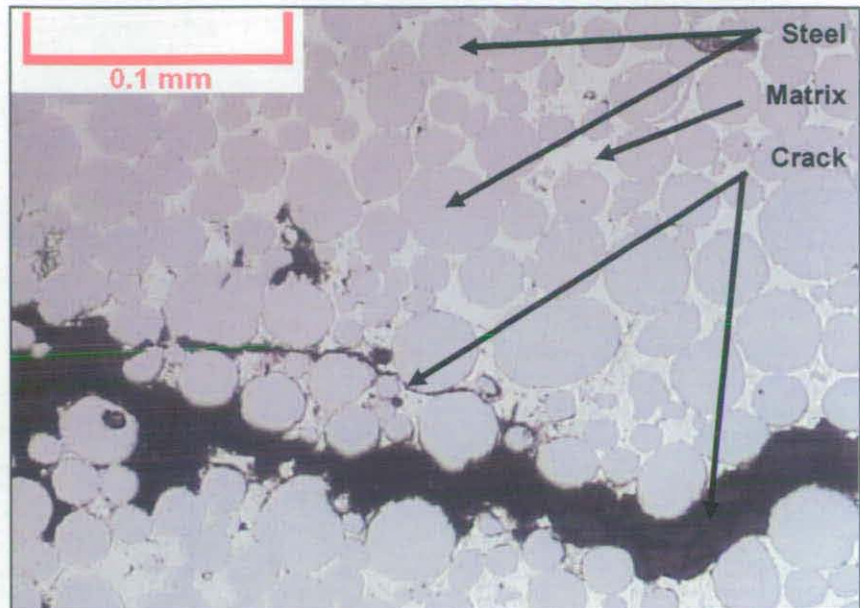


Figure 8 - 4 Metalcopy 5507 S3-25K-6-x20 showing crack propagating through matrix

Figure 8 - 5 shows the Metalcopy 5507 structure with a heavy etch revealing what appeared to be grain boundaries in the steel. The black areas in the matrix indicated areas, which had been over etched in order to reveal the structure of the steel.

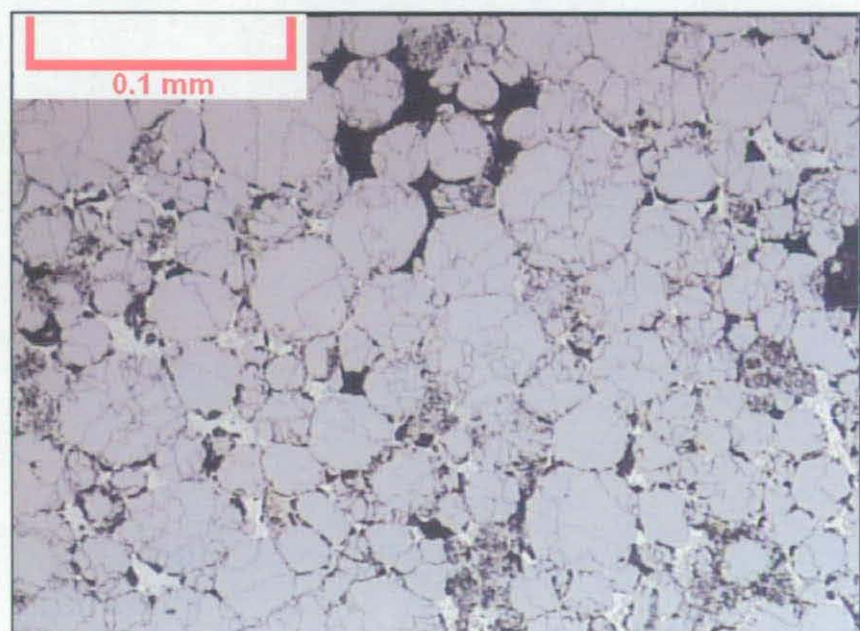


Figure 8 - 5 Metalcopy 5507 reference specimen S5-25K-3-x20 over etched to reveal structure in the stainless steel

SEM examination provided similar evidence with the crack originating from the edge of the specimen and running through the matrix (Figure 8 - 6).

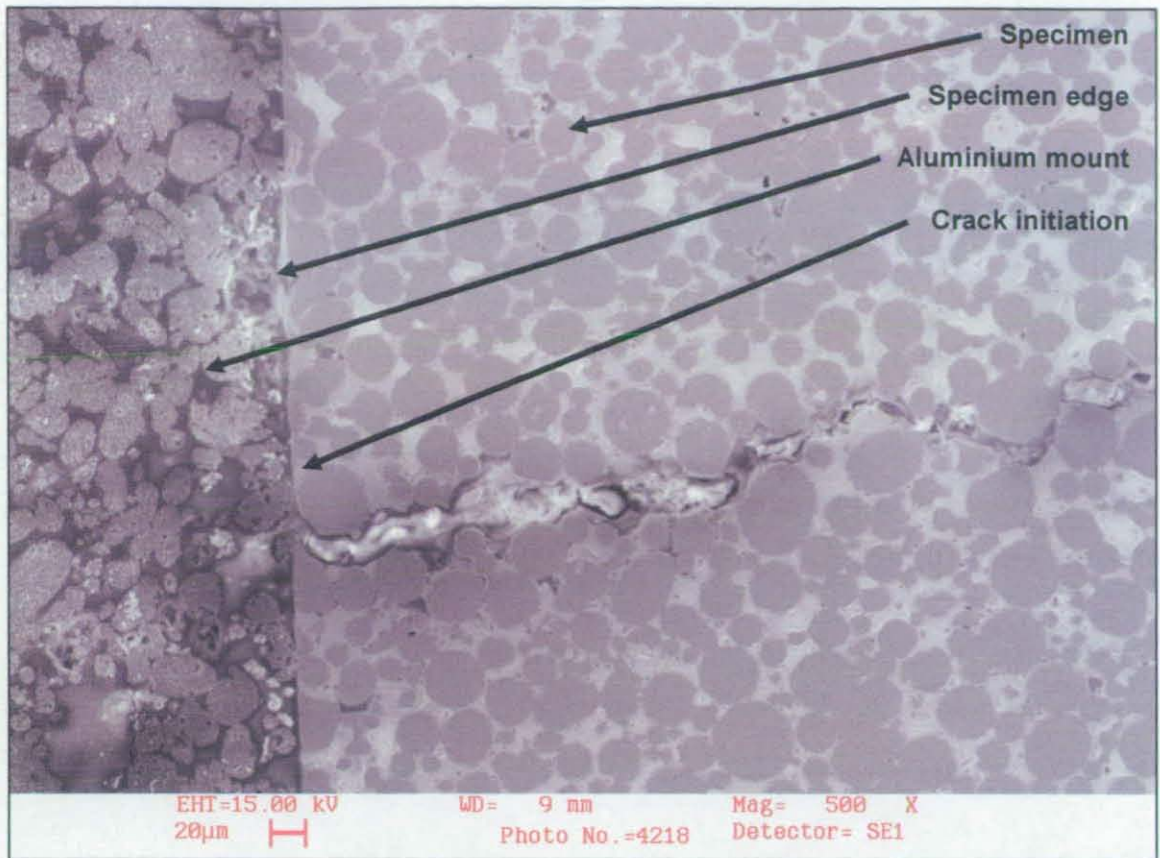


Figure 8 - 6 Metalcopy 5507 S3-25K-11-x500

However, at the end of one crack a different type of crack propagation was observed (Figure 8 - 7), where a crack was seen propagating through or along the grain boundary of a steel ball. In this instance the crack appeared to grow around the interface, through the matrix and through the powder. Additional unknown particles were also visible and the EDX analysis revealed these to be copper (Figure 8 - 10).

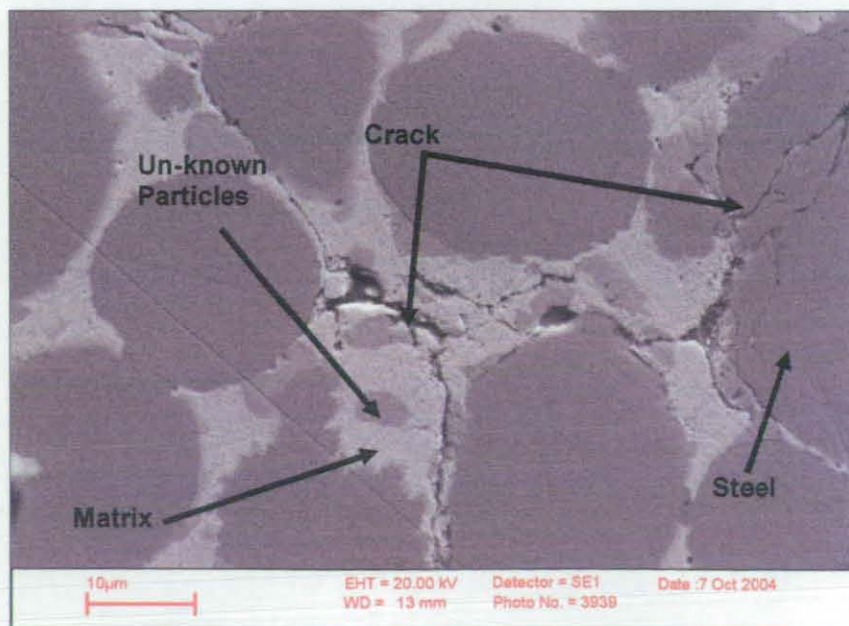


Figure 8 - 7 Crack tip showing growth in the matrix and through the steel

In the majority of cases the crack propagated in the matrix and circumnavigated the steel balls (Figure 8 - 8). The image also shows small dark areas in the steel balls, which spot analysis revealed to be chromium rich areas.

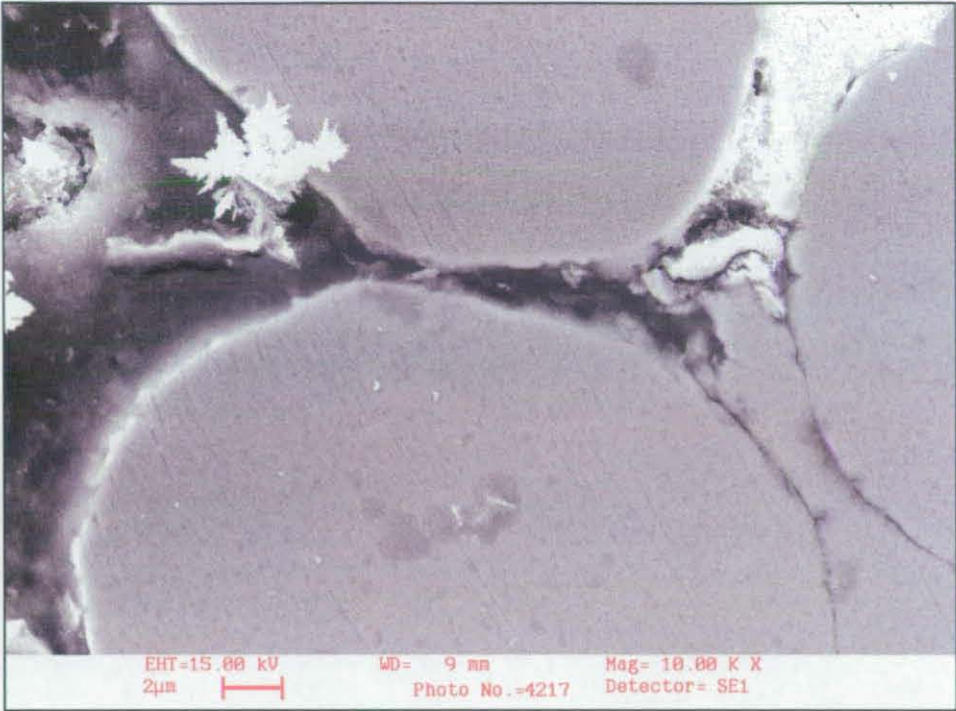


Figure 8 - 8 Metalcopy 5507 S3-25K-9-x10K

Figure 8 - 9 shows an area of Metalcopy 5507 specimen 3 with a crack propagating through it; this was subjected to EDX analysis and the results follow.

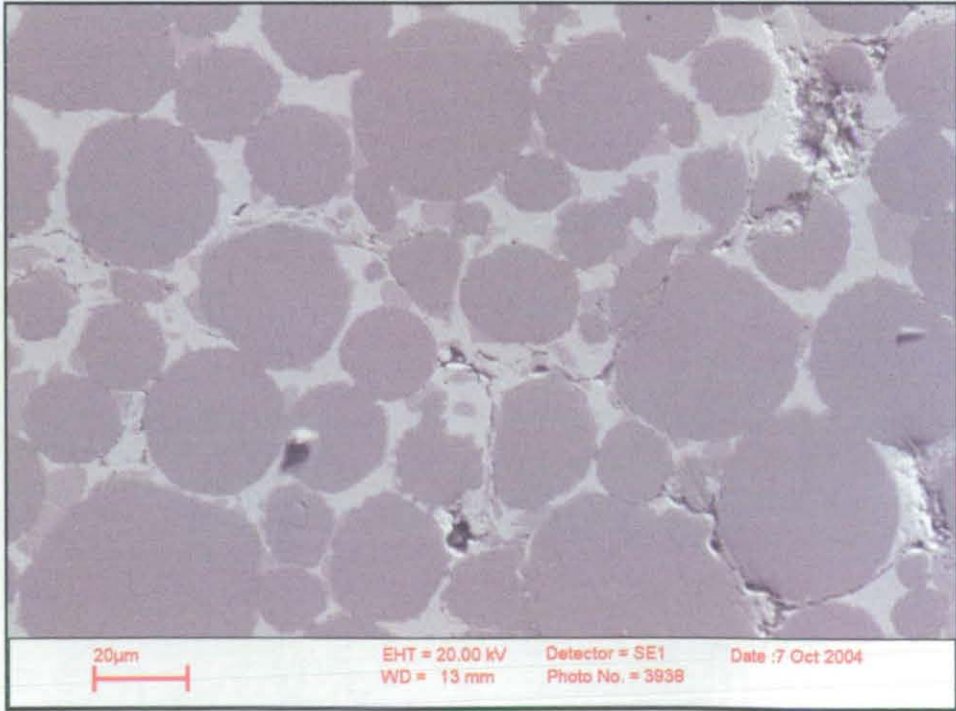


Figure 8 - 9 Metalcopy 5507-S3-25K-1

8.3.2 EDX Analysis

The EDX analysis showed that the matrix was an alloy of silver, copper and zinc in which balls having an iron, chromium, manganese, nickel, silicon and sulphur composition were insitu (Figure 8 - 10). It was apparent that there were areas in the matrix where copper and zinc were in greater concentrations (brighter areas). Also chromium, rich areas could be seen.

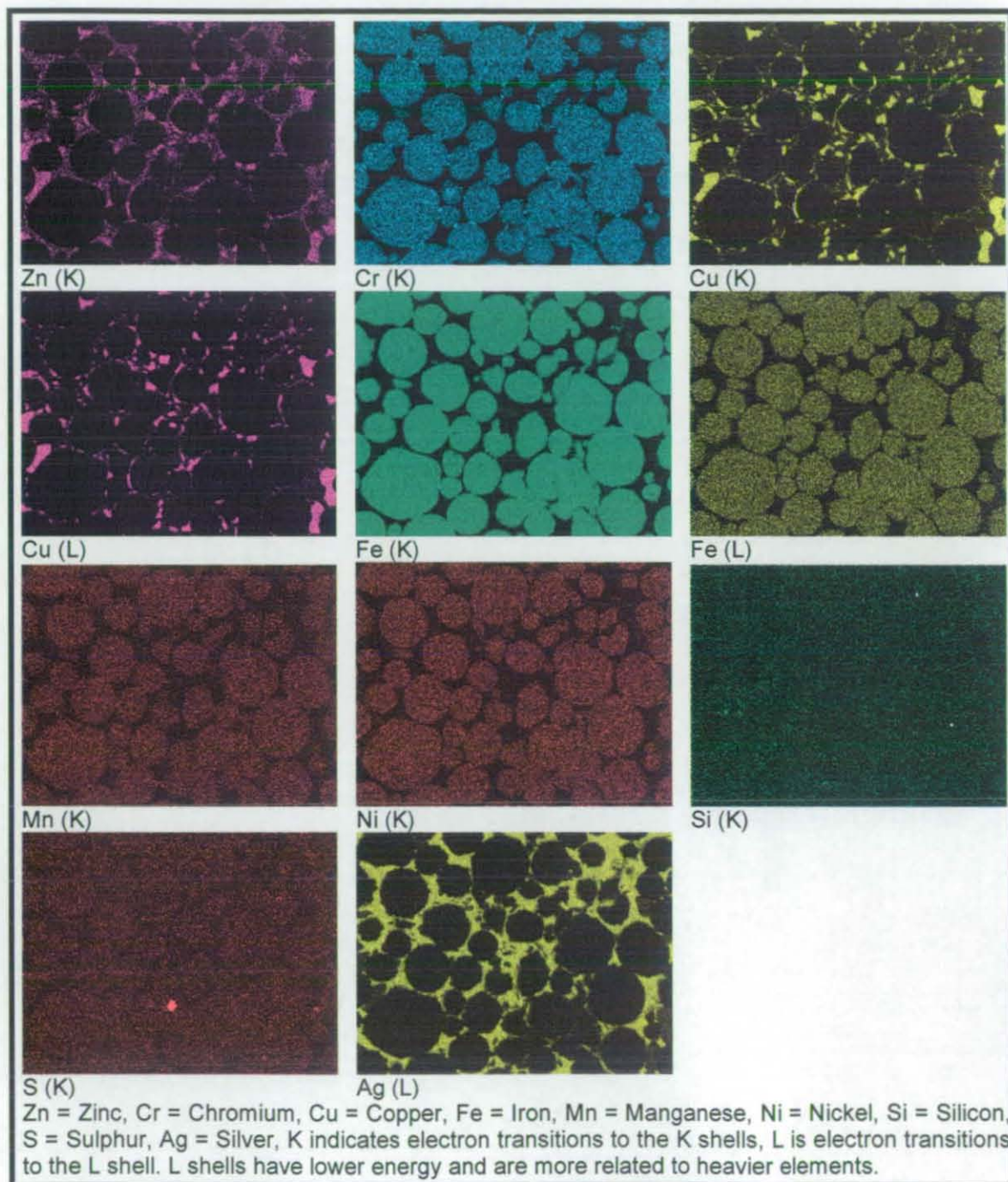


Figure 8 - 10 Metalcopy 5507 EDX analysis

8.4 Metalcopy Janalloy Post Thermal Fatigue Results

8.4.1 Crack Initiation and Propagation

Optical examination revealed that the specimen contained porosity, which would have been detrimental to the thermal fatigue resistance resulting in crack initiation and allowing a crack path to be easily developed (Figure 8 - 11). It is likely that the porosity was a result of gasses and carbon being trapped during the infiltration process of the specimen manufacture. This could also explain the crack number difference between specimens since the amount of porosity varied from one specimen to another.

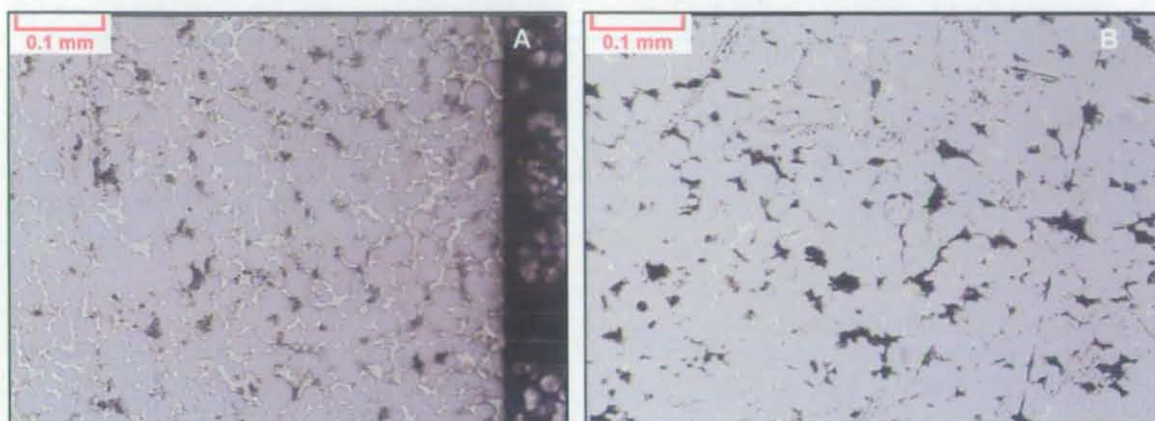


Figure 8 - 11 (A) Reference specimen S5-0K-2-x10 (not etched); (B) Specimen 3 S3-5K-8-x10 (not etched)

Figure 8 - 12 shows the Metalcopy Janalloy structure heavily etched revealing what appear to be the grain boundaries in the steel.

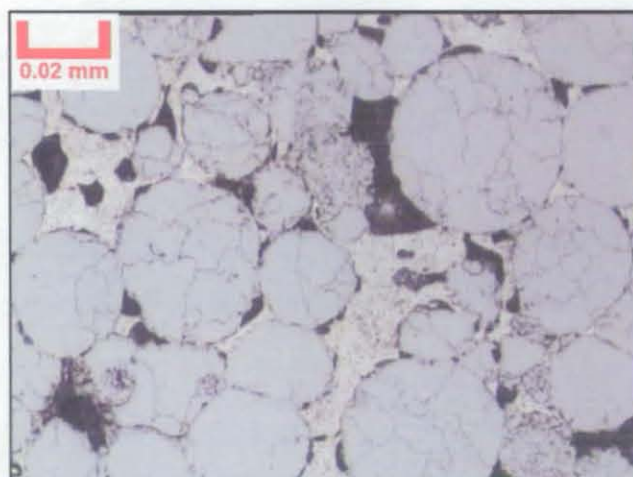


Figure 8 - 12 Reference specimen S5-0K-12-x40

SEM examination revealed that crack initiation occurred at the interface between the steel balls and the matrix with propagation along the passage of least resistance in the matrix (Figure 8 - 13).

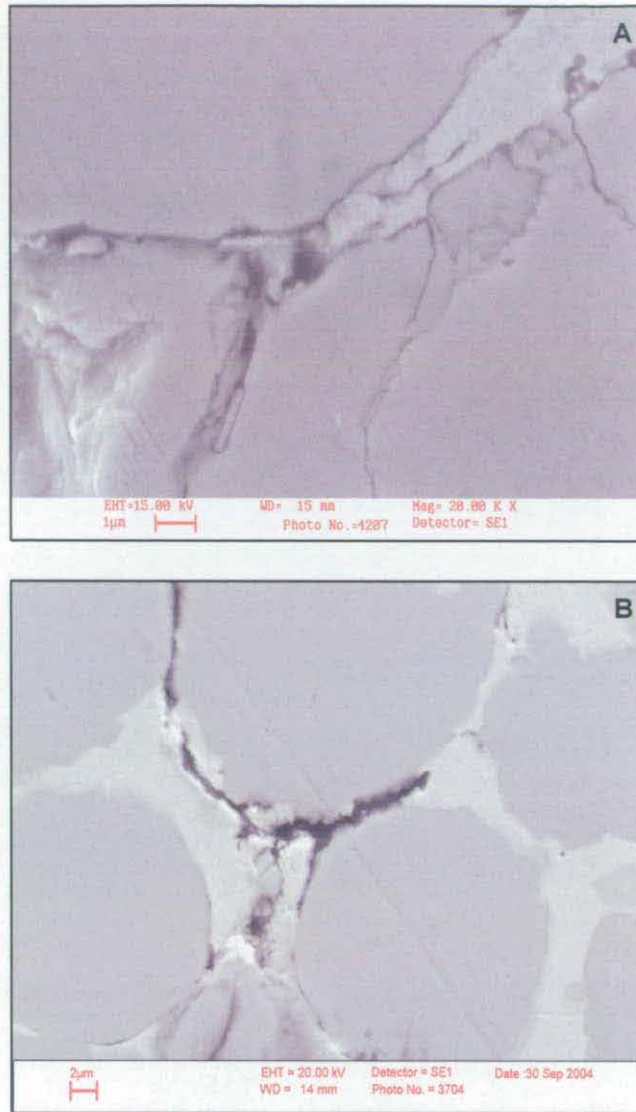


Figure 8 - 13 (A) Metalcopy Janalloy specimen 3 S3-5K-4-x20K; (B) Metalcopy Janalloy specimen 3 S3-5K-5

The Figure 8 - 14 (A) shows an interesting region of specimen 3 where the steel ball had broken at the periphery (chromium rich particles). It also showed that the matrix contained small particles, which showed up lighter on the image. Figure 8 - 14 (B) proved how the crack propagated though the matrix travelling from one ball / matrix interface to the next via areas of porosity.

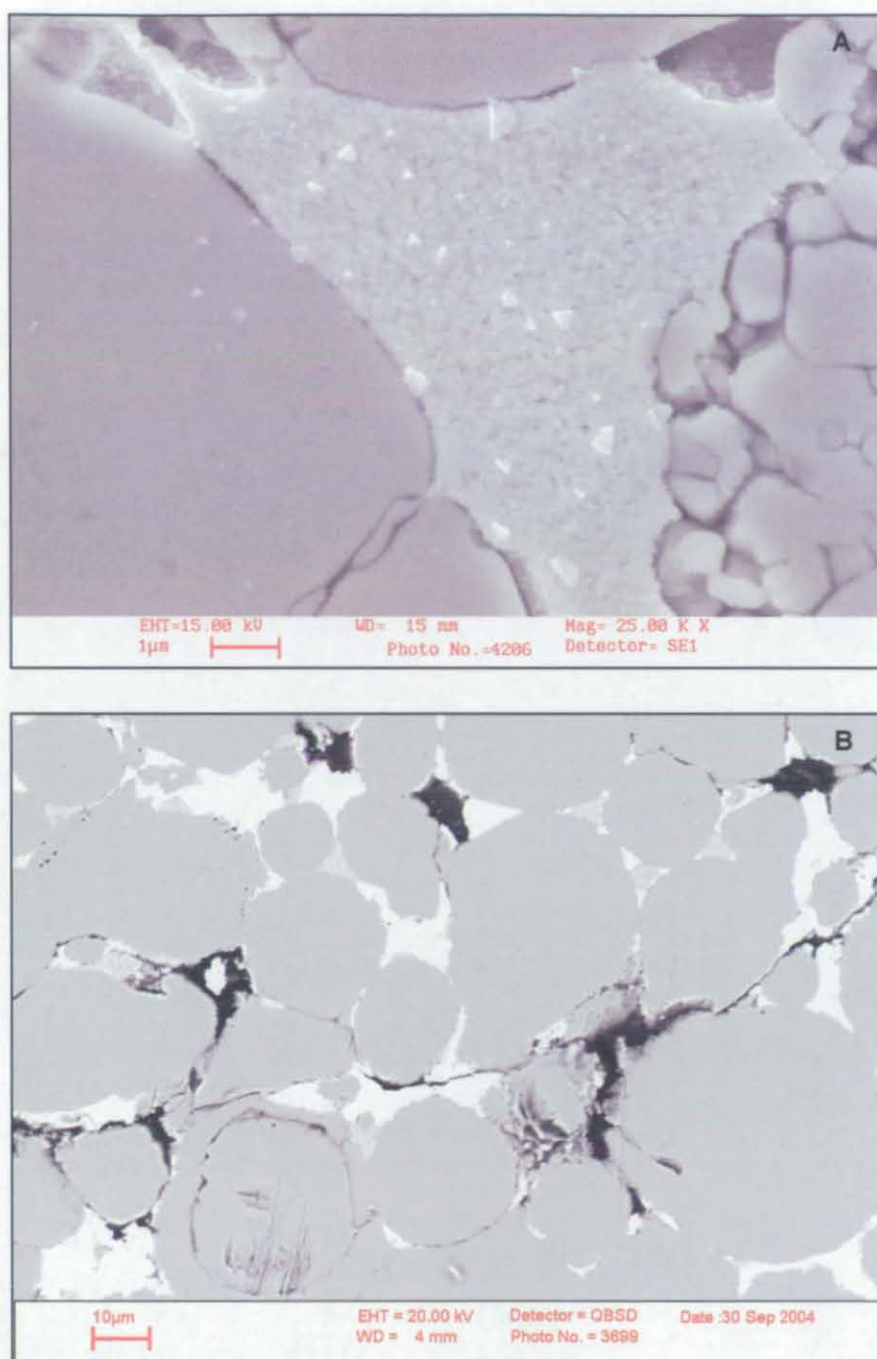


Figure 8 - 14 (A) Metalcopy Janalloy specimen 3 S3-5K-3-x25K; (B) Metalcopy Janalloy specimen 3 S3-5K-8

8.4.2 EDX Analysis

The EDX analysis of Figure 8 - 13 B is shown in Figure 8 - 15. It showed that the matrix was an alloy of silver, rhenium and copper, through which the crack propagated. Areas rich in copper were also visible (brighter areas on the EDX). The steel contained iron, dispersed vanadium, dispersed molybdenum, nickel and chromium with chromium rich areas at the boundary of the steel balls.

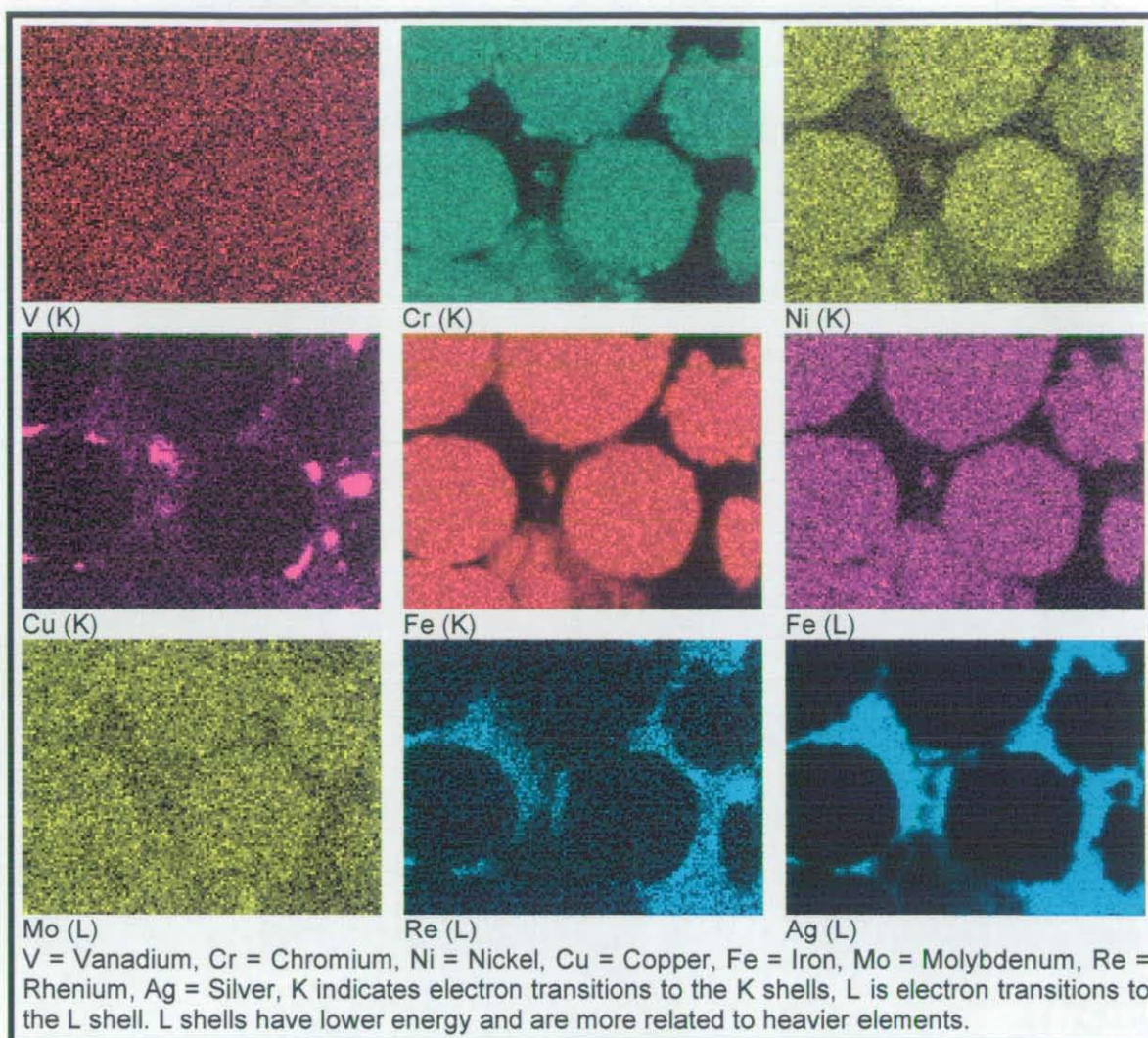


Figure 8 - 15 Metalcopy Janalloy EDX analysis

8.5 Metalcopy Cu Post Thermal Fatigue Results

8.5.1 Crack Initiation and Propagation

Optical examination showed some porosity in the specimens (Figure 8 - 16 (A)) and a heavy etch removed the bonding material and revealed particles in the steel balls (Figure 8 - 16 (B)).

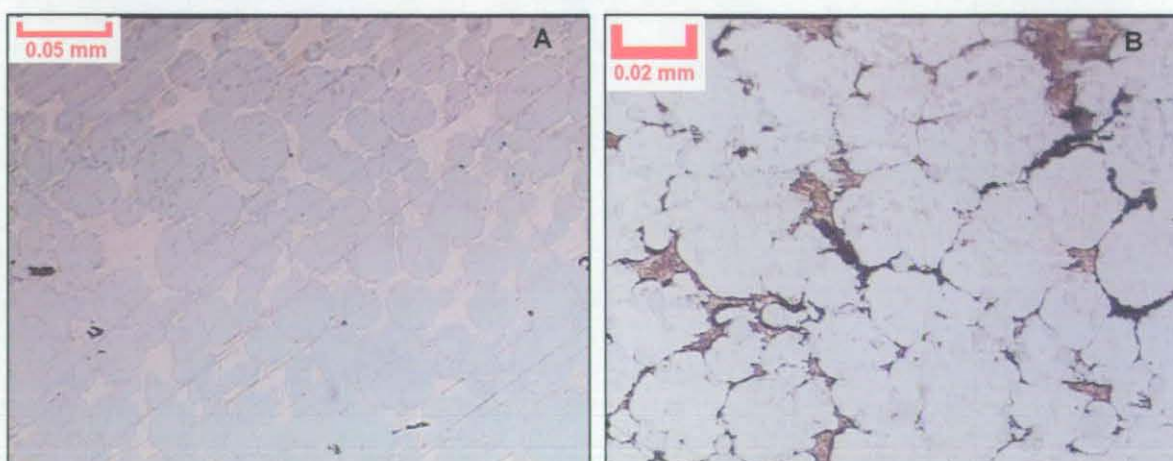


Figure 8 - 16 (A) Reference specimen 5 S5-0K-3-x20; (B) Specimen 1 S1-25K-8-x40

Further examination using SEM revealed that some steel balls did not appear to have wetted to the bonding material and were not bonded to the matrix (Figure 8 - 17).

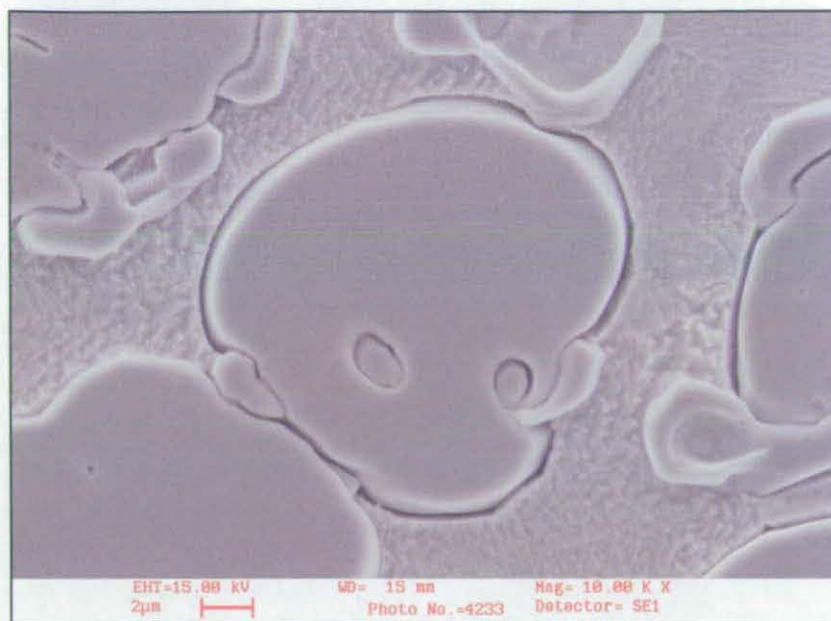


Figure 8 - 17 Reference specimen 5 S5-0K-13-x10K

As with the previous specimens the cracks initiated from the steel powder / matrix interface and tended to propagate through the matrix (Figure 8 - 18).

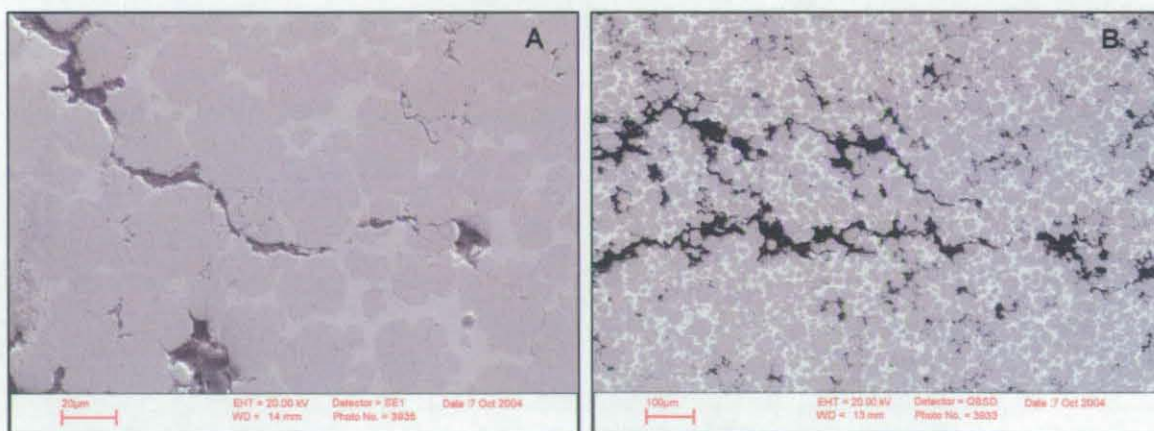


Figure 8 - 18 (A) Metalcopy Cu specimen 1 S1-25K-92; (B) Metalcopy Cu specimen 1 S1-25K-89

However, this was not always the case, Figure 8 - 19 shows a crack propagating through the matrix and also through the steel balls. In addition, the bonding problem was likely to have caused the void formation as the cracks propagated and the powder detached (Figure 8 - 19).

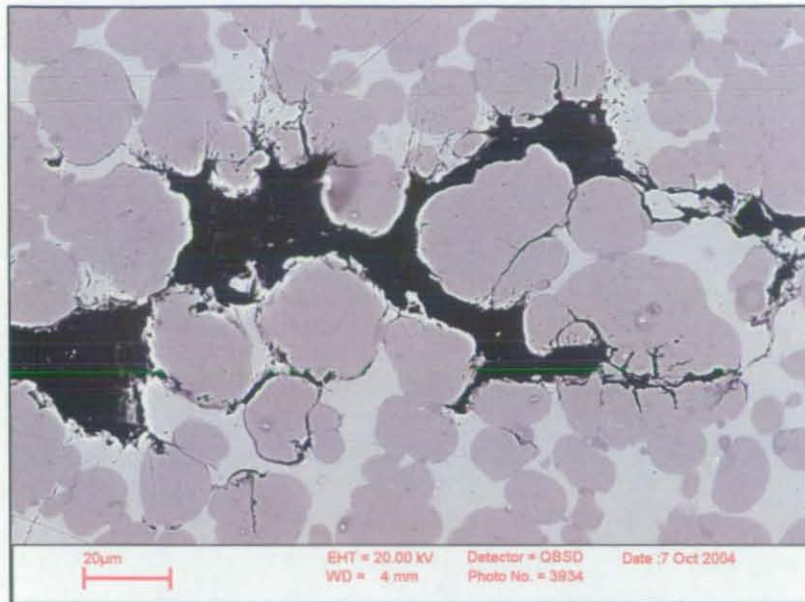


Figure 8 - 19 Metalcopy Cu specimen 1 S1-25K-91

8.5.2 EDX Analysis

Figure 8 - 20 shows EDX analysis, which was conducted on the area of Metalcopy Cu specimen 1 with a crack growing through the matrix. It was clear that the balls were steel made up of iron, chromium, molybdenum, nickel and manganese. Both the steel and some areas of the matrix contained chromium and manganese rich particles. It should also be noted that there were particles containing higher concentrations of molybdenum, especially in or near the crack area. The matrix appeared to be primarily copper with some chromium rich particles.

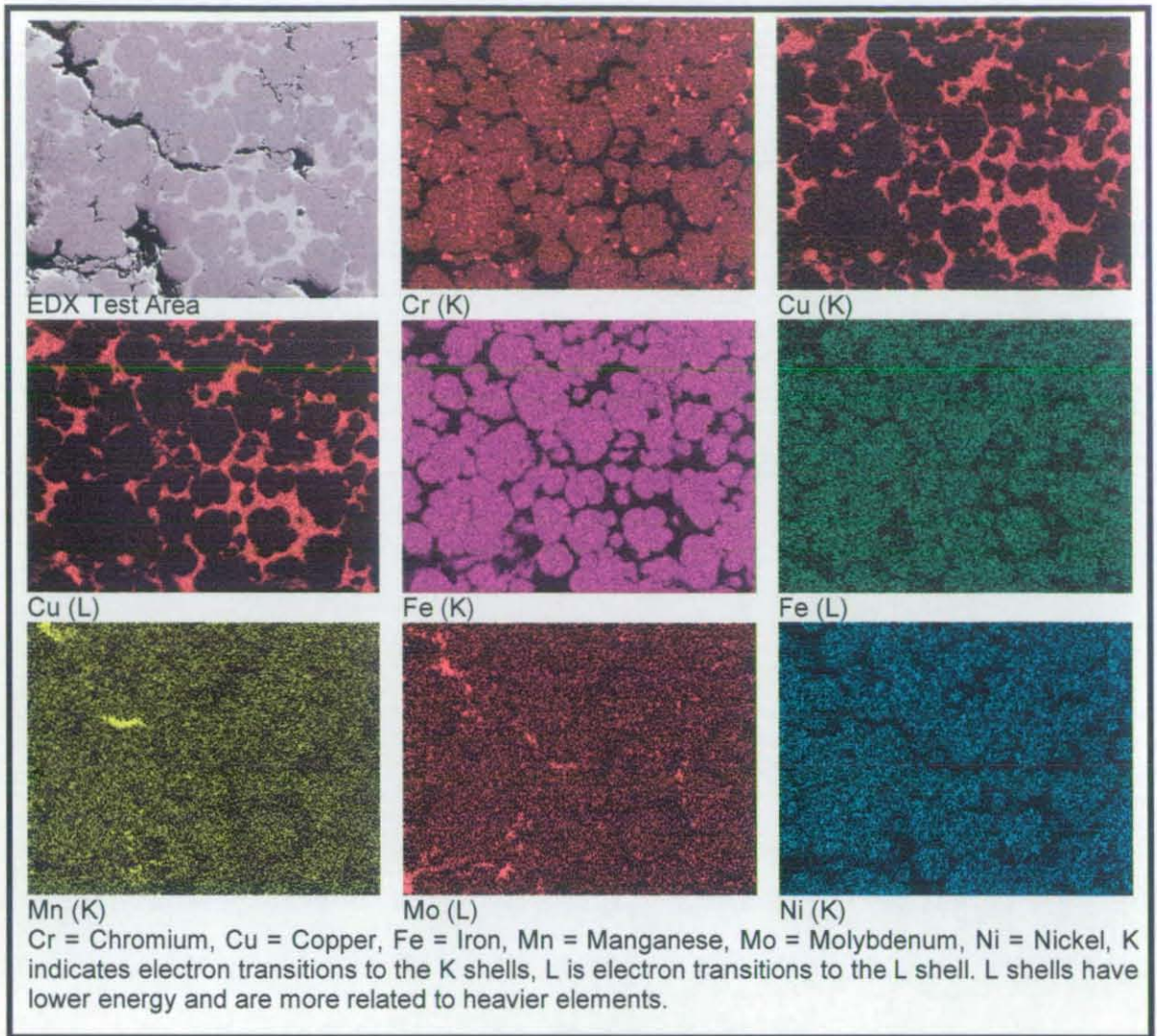


Figure 8 - 20 Metalcopy Cu EDX analysis

8.6 Vertical Laminate Post Thermal Fatigue Results

8.6.1 Crack Initiation and Propagation

From optical examination (Figure 8 - 21) it was clear that the braze had bonded well and diffusion had occurred. The EDX analysis showed the presence of chromium, iron, nickel, and silicon with the centre of the braze having a nickel rich phase.

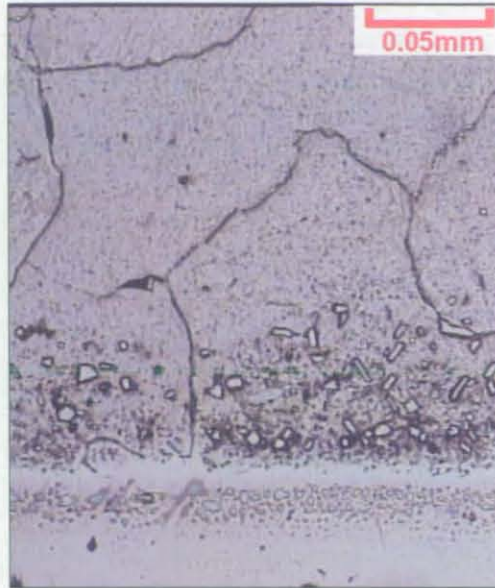


Figure 8 - 21 Vertical laminate reference specimen 5 S5-5K-4-x20

The braze structure had two phases, one of which tended to run down the centre (Figure 8 - 22 (A)). Porosity in the centre of the braze was also apparent in some of the specimens (Figure 8 - 22 (B)); this was probably caused because the gasses produced during the brazing process could not escape. Porosity was also a possible source of crack initiation.

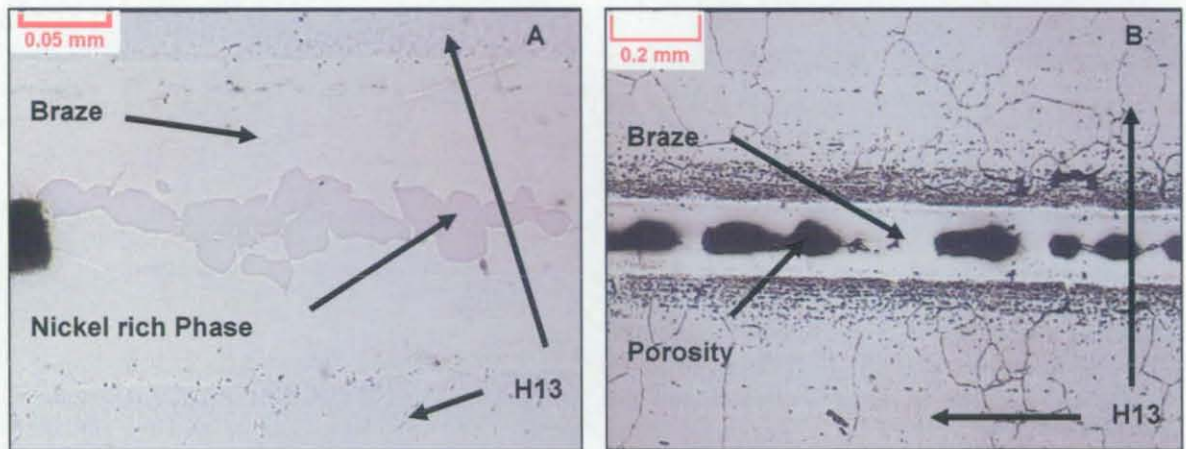


Figure 8 - 22 (A) Vertical laminate specimen 1 S1-5K-5-x20; (B) Vertical laminate reference specimen 5 S5-5K-5-x5

Figure 8 - 23 (A), shows a crack initiating from a void and working its way along the central phase of the braze. It was interesting to note that the crack went through the nickel rich phase and not down the boundary between phases. Figure 8 - 23 (B) also shows the crack propagating to the braze H13 interface and along the interface. All the cracks initiated in the braze that bonded the laminate structure together.

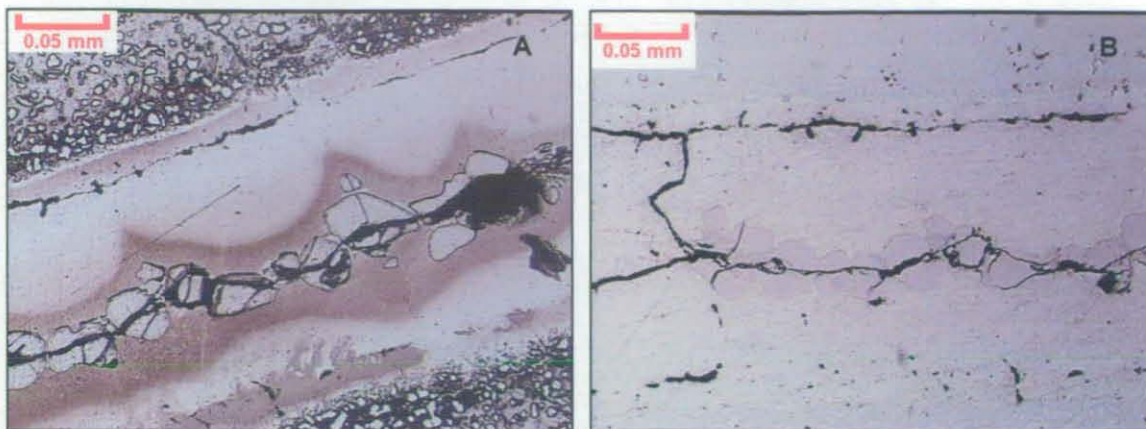


Figure 8 - 23 (A) Vertical laminate specimen 1 S1-5K-12-x20; (B) Vertical laminate specimen 1 S1-5K-4-x20

SEM showed the same crack formation, however, an area in the central phase suffered from craze cracking as shown in Figure 8 - 24 (A) and in a higher magnification in Figure 8 - 24 (B).

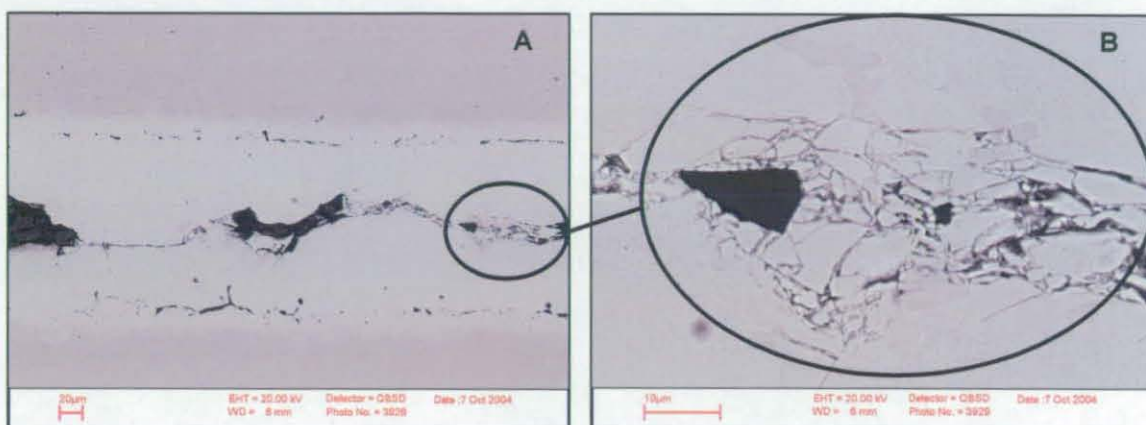


Figure 8 - 24 (A) Vertical laminate specimen 1 S1-5K-85; (B) Vertical laminate specimen 1 S1-5K-86

8.6.2 EDX Analysis

A 30 line spot test and an EDX was conducted to determine the elements in the braze. The spot test was repeated three times on different areas of the specimen across the braze (Figure 8 - 25) producing comparable data. The braze was richer in nickel and poorer in iron at the centre (Figure 8 - 26). EDX results confirmed this and Figure 8 - 27 shows the area over which EDX was conducted. The results (Figure 8 - 28) showed high concentrations of nickel and silicon in the centre. The chromium trace showed higher concentrations in the H13 as expected.

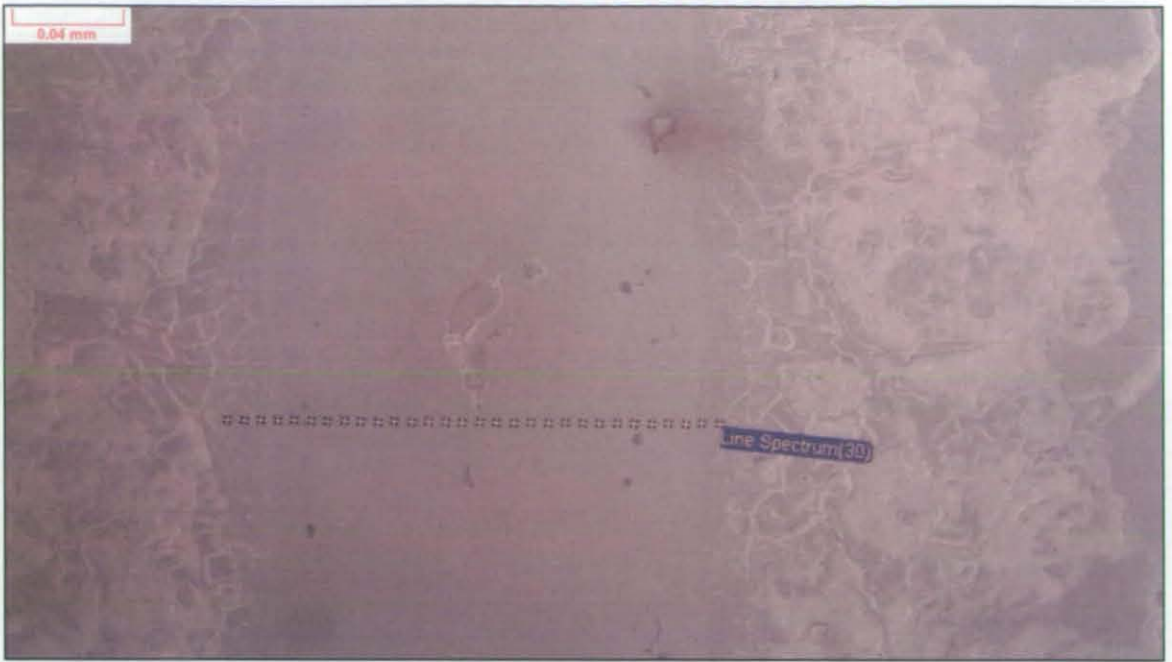


Figure 8 - 25 Vertical laminate SEM element spot line

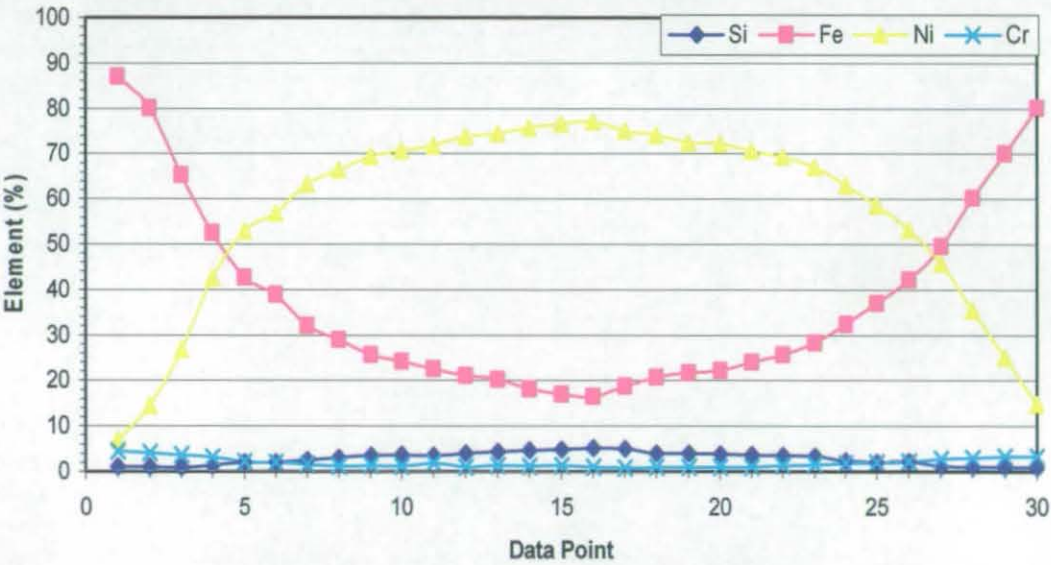


Figure 8 - 26 Vertical laminate elemental change across braze



Figure 8 - 27 Vertical laminate specimen 4 S4-5K-82

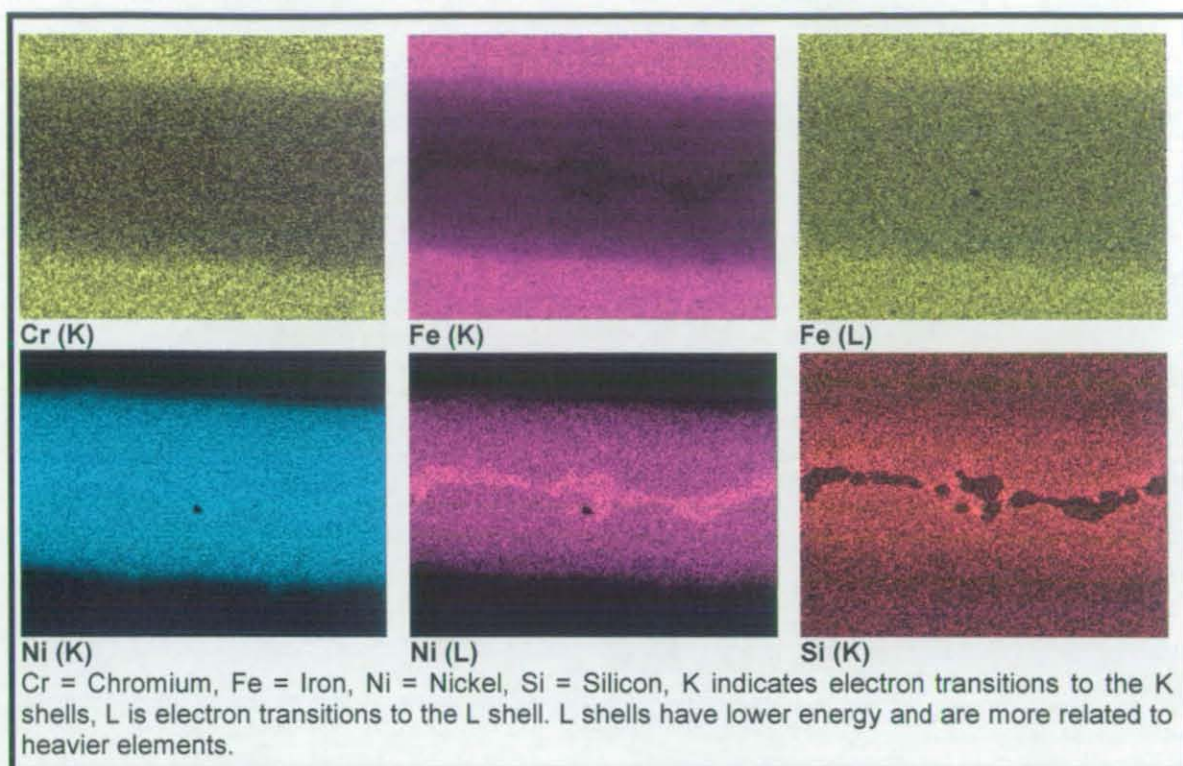


Figure 8 - 28 Vertical laminate EDX analysis

8.7 Horizontal Laminate Post Thermal Fatigue Results

8.7.1 Crack Initiation and Propagation

Optical examination revealed further detail of the mode of failure. Figure 8 - 29 shows an untested H13 braze interface. It shows how the H13 laminate thinned from 1mm thick to fractions of a mm thick. It should also be noted that the braze contained porosity.

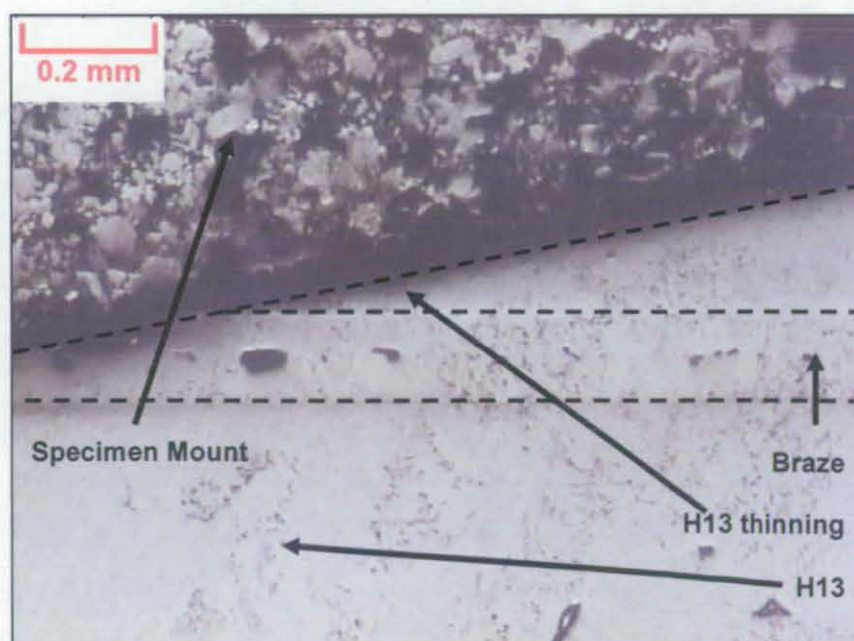


Figure 8 - 29 Horizontal laminate specimen 5 S5-5K-1-x5

Figure 8 - 30 shows a H13 braze interface after 5,000 cycles, where it can be seen that some of the braze has been removed, as a result of the constant expansion and contraction, leading to a thin unsupported / un-bonded section of H13 being exposed, which would eventually fatigue and fall off. As the test progressed this process continued and escalated. The mode of failure caused under cuts at the H13 braze interface that would be detrimental in a die, since the molten aluminium would be forced into the undercut, which when ejected would, either, cause adhesion (failure to eject), or removal of the undercut resulting in further die damage.

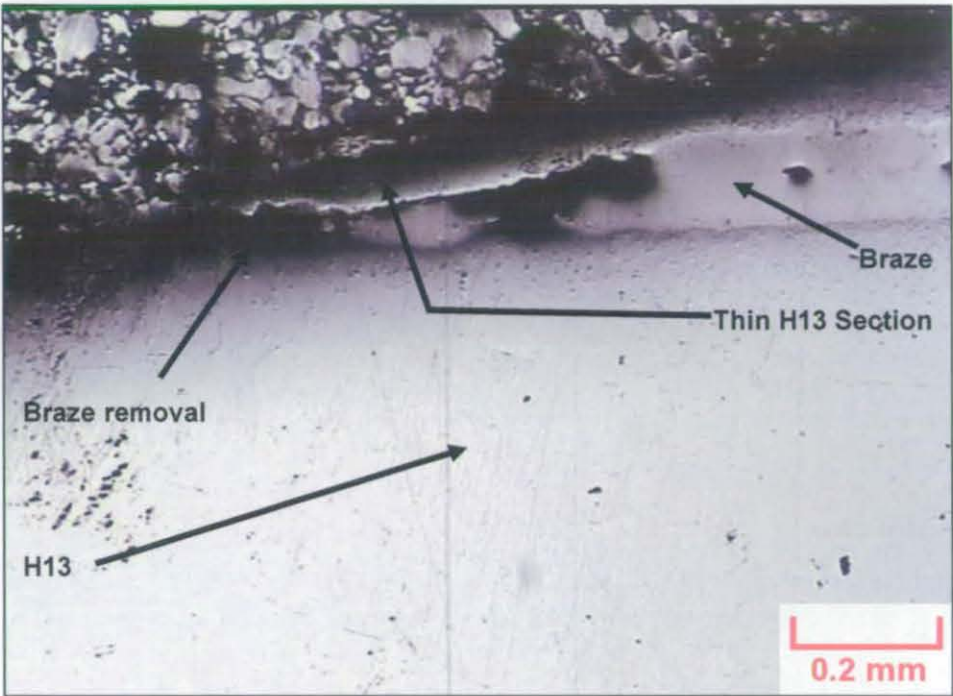


Figure 8 - 30 Horizontal laminate specimen 1 S1-5K-9-x5

Optical examination also revealed the same material structure (Figure 8 - 31) in the Horizontal laminate specimens as in the Vertical laminate specimens.

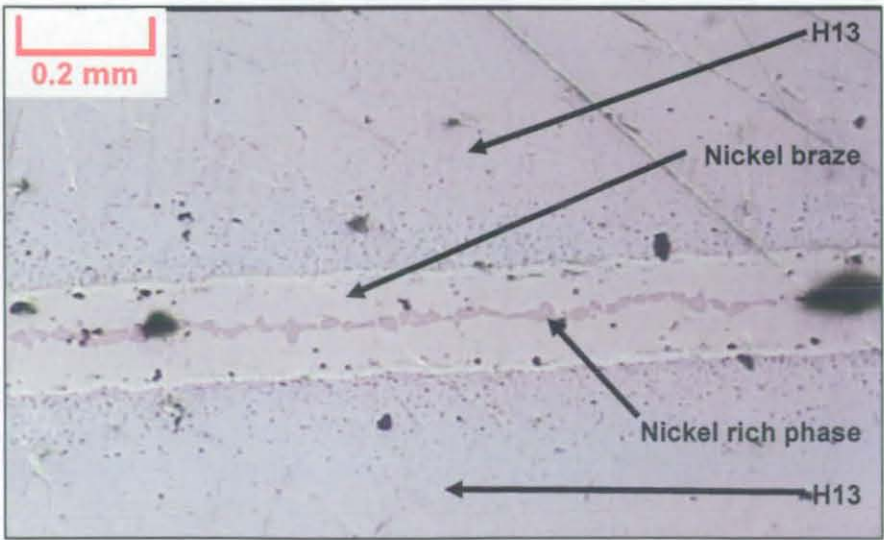


Figure 8 - 31 Horizontal laminate specimen 1 S1-5K-5-x5

8.7.2 EDX Analysis

SEM examination did not reveal any further information and the EDX analysis was the same for both Vertical and Horizontal laminate specimens.

8.8 Amdry 790 Post Thermal Fatigue Results

8.8.1 Crack Initiation and Propagation

Optically specimens 1 and 2 and the reference specimen were identical to each other containing a nickel and a silicon phase. The specimens, however, appeared to contain porosity but this could have been mistaken for nickel particles, which had been pulled out during polishing (Figure 8 - 32).

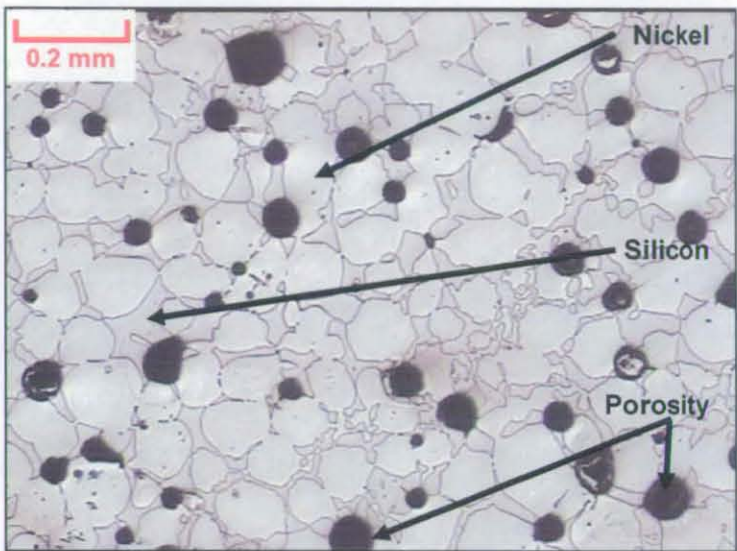


Figure 8 - 32 Amdry 790 specimen 1 S1-100K-1-x5

Etching the specimen revealed the structure in the silicon phase (Figure 8 - 33).

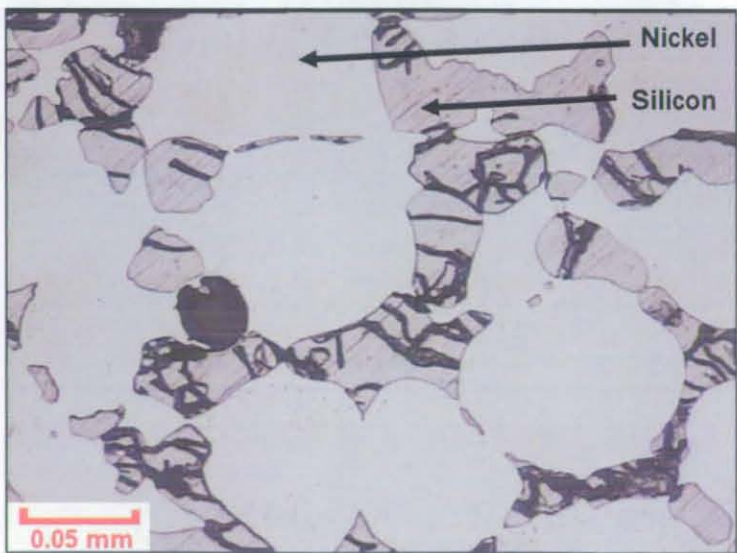


Figure 8 - 33 Amdry 790 specimen 1 S1-110K-2-x20

However, specimen 3 contained a eutectic structure (Figure 8 - 34) probably as a result of different element contents (poor mixing of the powder and the heavier elements sinking; it could also have occurred due to different cooling conditions). The difference in the structure and the increased quantities of silicon present may further explain the difference in hardness previously observed.

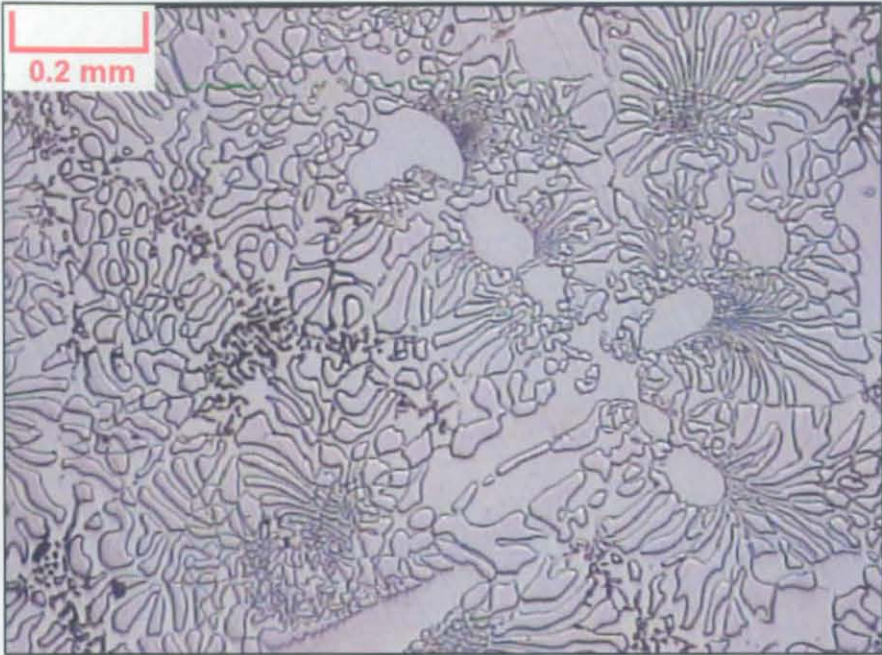


Figure 8 - 34 Amdry 790 specimen 3 S3-110K-1-x5

Figure 8 - 35 shows the structure in more detail, the nickel appeared to have a characteristic structure emanating from a circle of silicon.

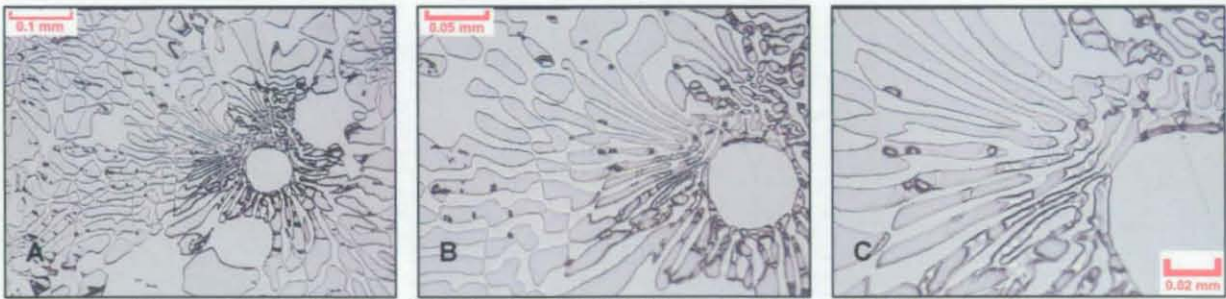


Figure 8 - 35 (A) S3-110K-1-x10; (B) S3-110K-1-x20; (C) S3-110K-1-x40

8.8.2 EDX Analysis

From the SEM (Figure 8 - 36 and Figure 8 - 37) and the EDX (Figure 8 - 38) analyses a clearer picture of specimen 3 emerged. Figure 8 - 36 shows a light area (A), which contained 99.97% nickel; area B was nickel containing small traces of sulphur and micro cracks; area C was silicon with nickel veins running through it.

Micro cracks initiated in area B propagated through it until they reached the interface of the nickel area B and area C. The cracks then propagated down thin veins of nickel in the silicon

until reaching another nickel rich area (B) (Figure 8 - 36). Figure 8 - 37 shows this propagation over a larger area.

The reason for this could be a function of the different rates of expansion between nickel and silicon, also nickel is ductile in comparison to silicon.

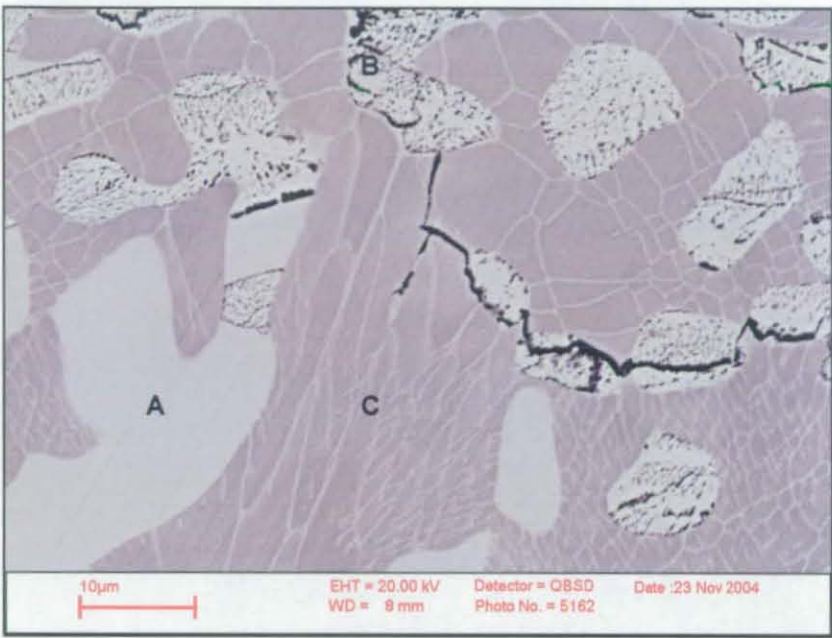


Figure 8 - 36 Amdry 790 specimen 3 S3-110K-3

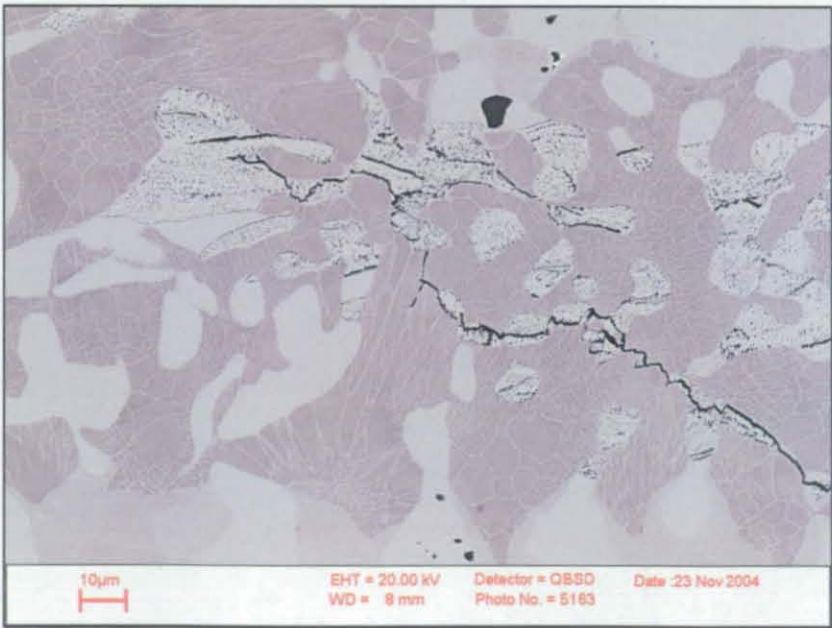


Figure 8 - 37 Amdry 790 specimen 3 S3-110K-4

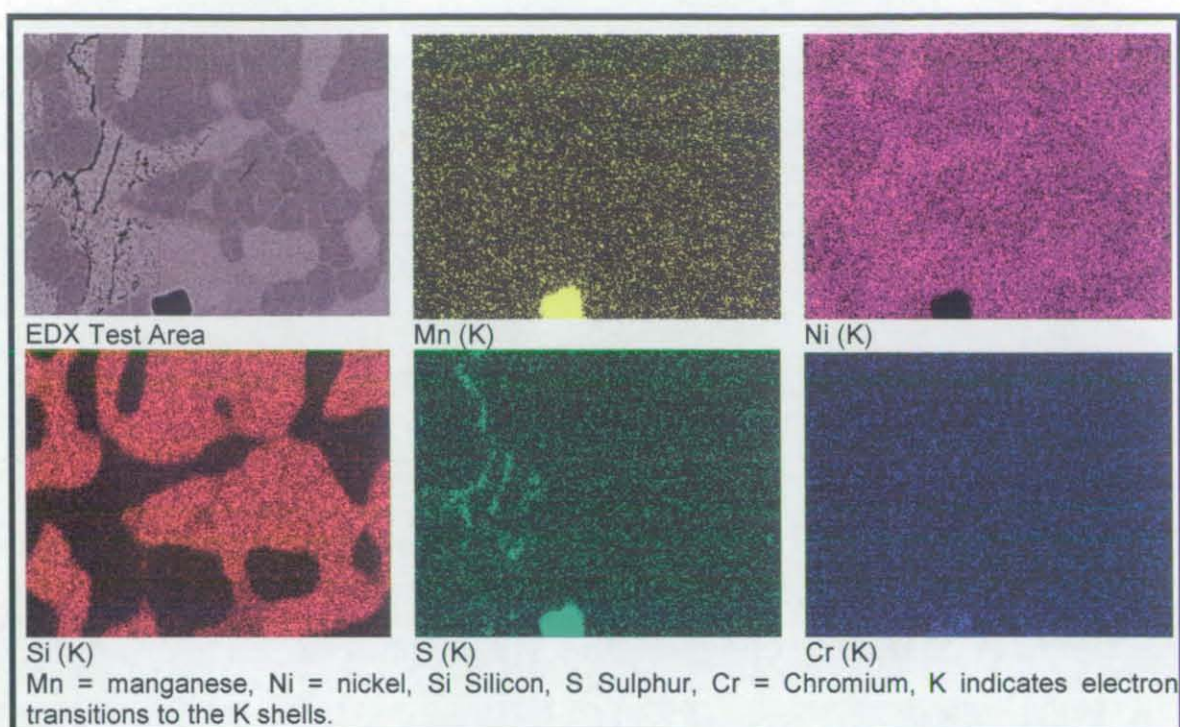


Figure 8 - 38 Amdry 790 specimen 3 EDX test 1

Although specimen 3 had a different structure to specimens 1 and 2, the SEM images showed similar crack initiation and crack propagation (Figure 8 - 39).

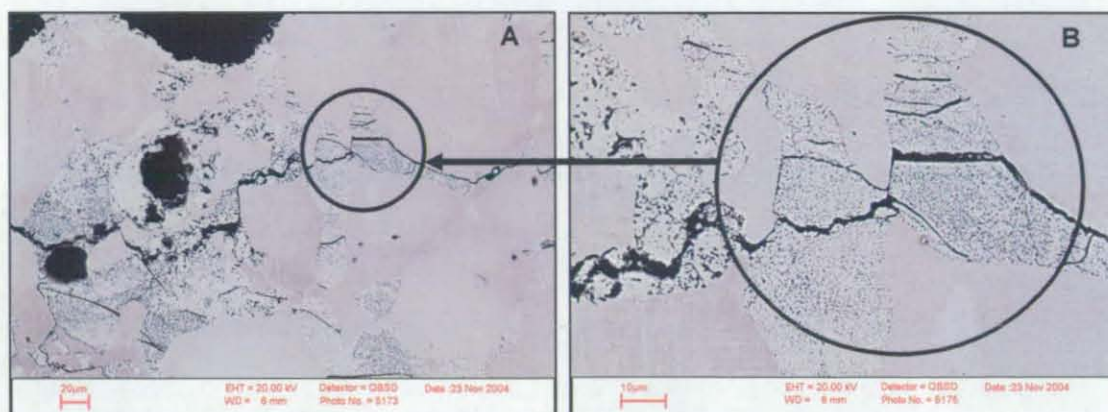


Figure 8 - 39 Amdry 790; (A) Specimen 1 S1-110K-14; (B) Specimen 1 S1-110K-16

8.9 Horizontal RapidSteel 2.0 Post Thermal Fatigue Results

8.9.1 Crack Initiation and Propagation

Optical examination revealed a structure similar to that exhibited by the Metalcopy materials (Metalcopy 5507, Metalcopy Janalloy, Metalcopy Cu). The material consisted of steel balls in a bronze matrix and most noticeable were dark areas of porosity in the specimens (Figure 8 - 40).

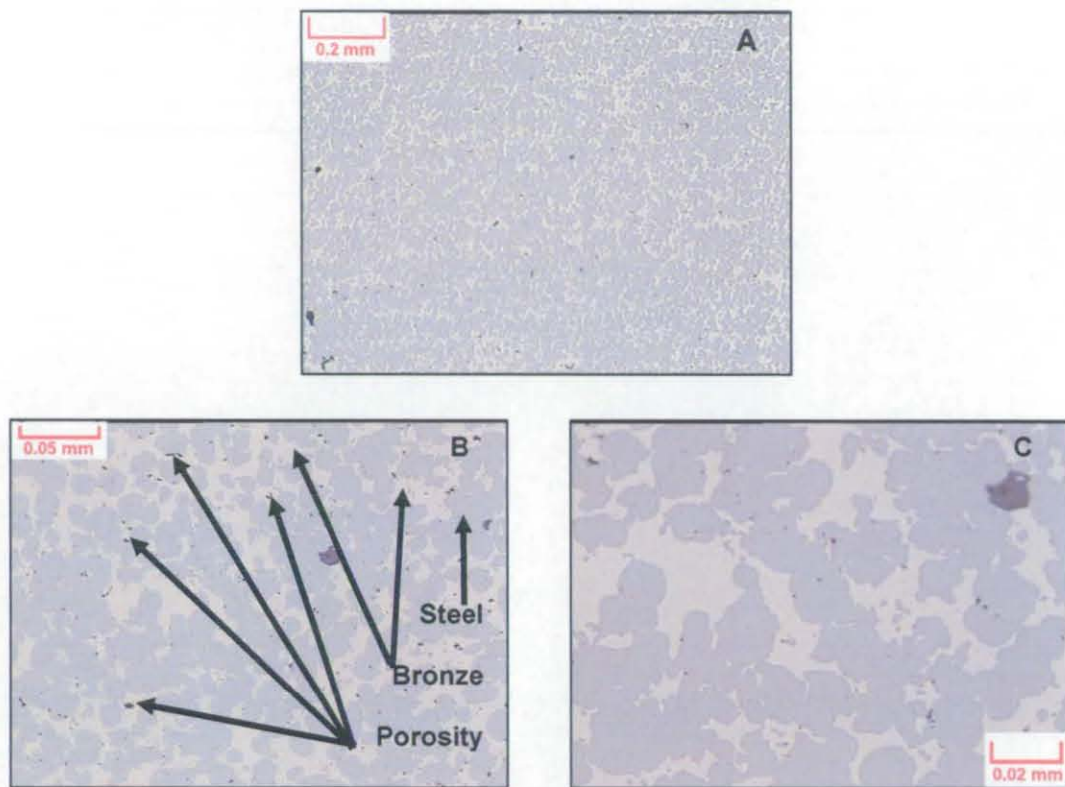


Figure 8 - 40 Reference specimen 5; (A) S5-0K-1-x5; (B) S5-0K-1-x20; (C) S5-0K-1-x40

Figure 8 - 41 shows specimen 5 with the steel heavily etched revealing smaller particles, which the EDX results indicated as chromium rich areas (Chromium rich precipitates, Uzunsoy et.al., 2002 and 2003).

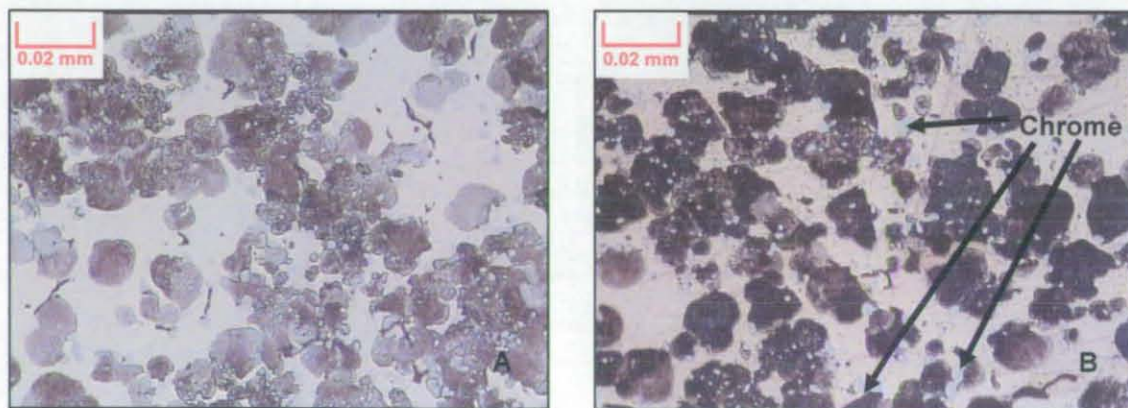


Figure 8 - 41 Specimen 5; (A) S5-0K-5-x40; (B) S5-0K-1-x40

Figure 8 - 42 shows that specimen 1 contained a greater amount of porosity, which may have accounted for the premature cracking observed.

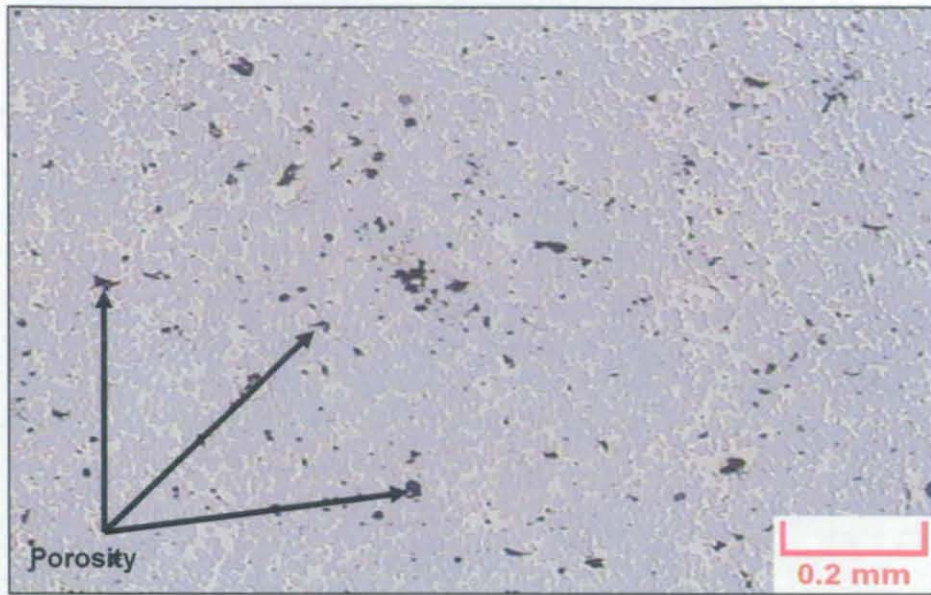


Figure 8 - 42 Horizontal RapidSteel 2.0 specimen 1 S1-100K-5-x5

Optical examination showed that there were potential crack initiation sites, for example, porosity and the matrix braze interface. The crack preferred direction of crack propagation was along the interfaces between the steel and the matrix. However, on occasions the crack propagated through the matrix and the steel balls (Figure 8 - 43) (Uzunsoy et.al., 2003).

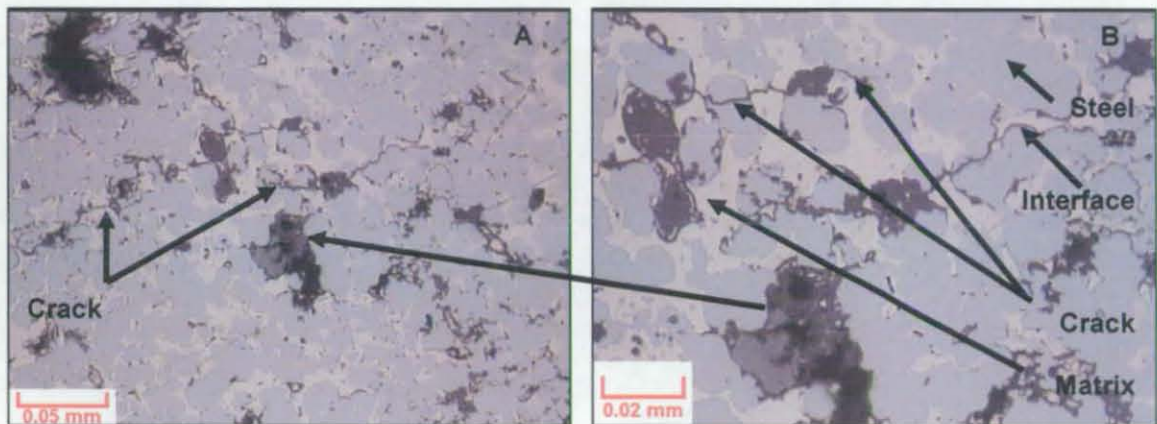


Figure 8 - 43 Horizontal RapidSteel 2.0 specimen 1; (A) S1-100K-6-x20; (B) S1-110K-7-x40

8.9.2 EDX Analysis

The SEM examination revealed oxide along the crack edges (Figure 8 - 44). The EDX analysis (Figure 8 - 45 and Figure 8 - 46) revealed what appears to be iron oxide forming down either side of the crack path. It also revealed that the bonding material (matrix) was a bronze material containing copper, silicon and tin and that the balls consisted of chromium rich steel. Particles with high chrome content were also revealed as were areas rich in tin (brighter areas).

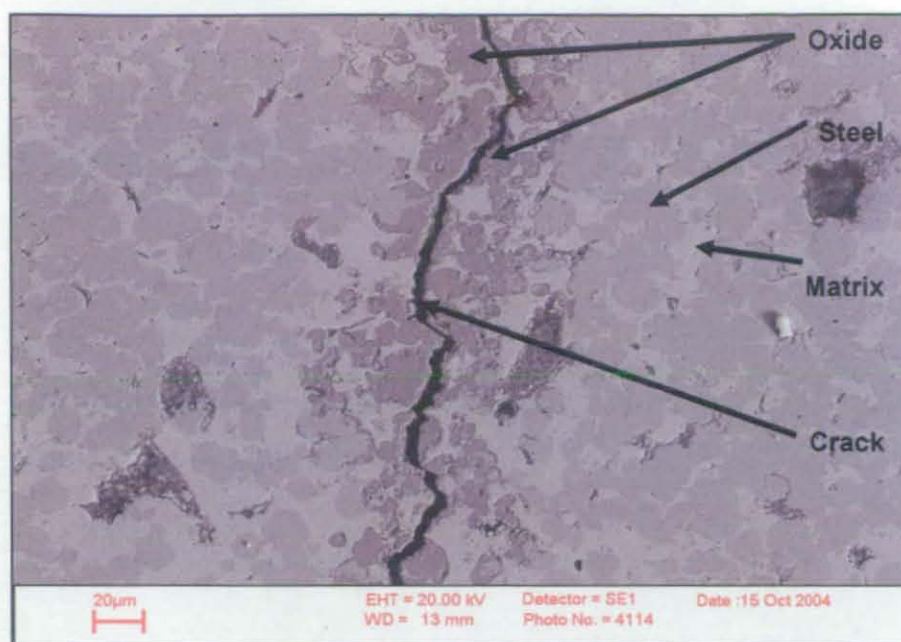


Figure 8 - 44 Horizontal RapidSteel 2.0 specimen 1 EDX analysis area test 1

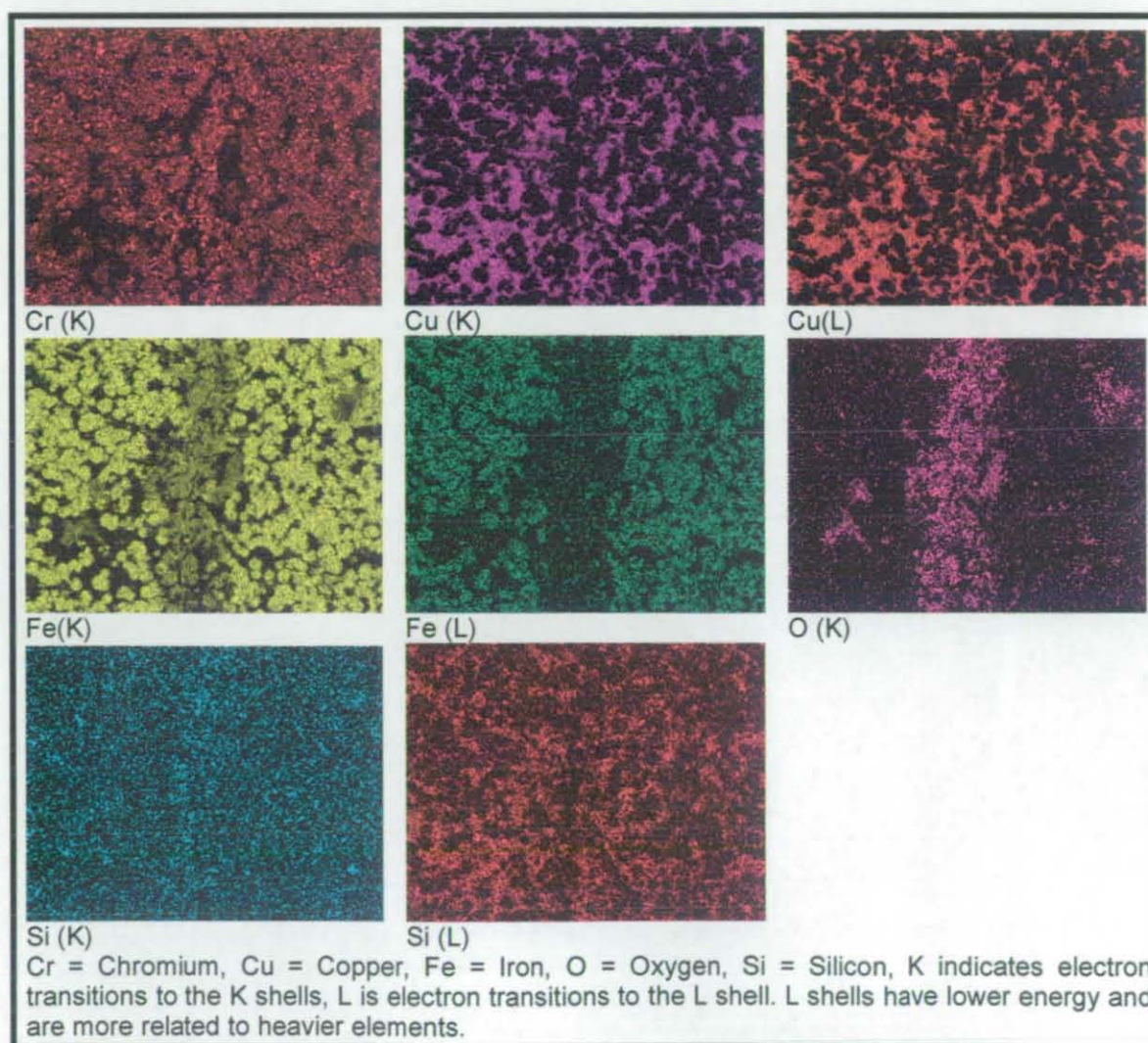


Figure 8 - 45 Horizontal RapidSteel 2.0 specimen 1 EDX analysis test 1

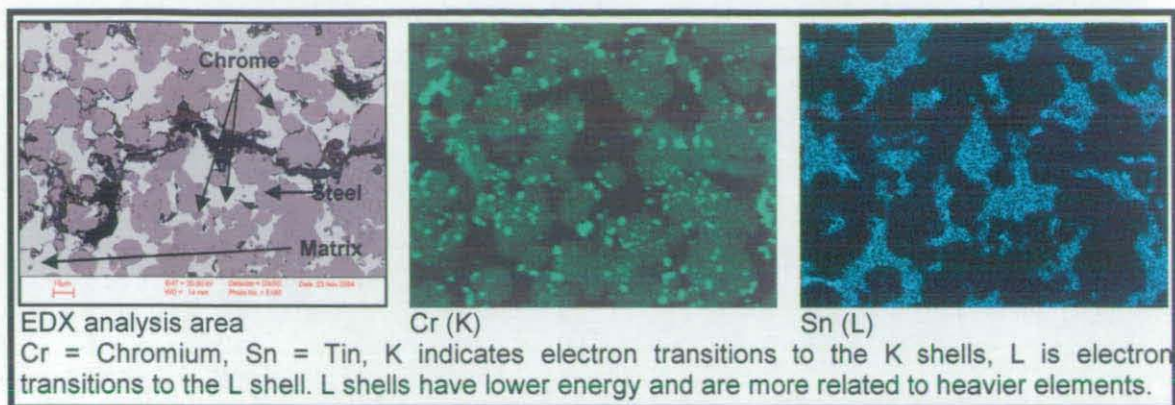


Figure 8 - 46 Horizontal RapidSteel 2.0 specimen 3 EDX analysis test 2

8.10 EOS DirectSteel 20 μ m Post Thermal Fatigue Results

8.10.1 Crack Initiation and Propagation

Optical examination revealed a structure similar to a series of welds layered one upon another (Figure 8 - 47), which was a reflection of the method of manufacture. It is likely that the darker areas were porosity, contaminants or inclusions from the bonding process. However, there appeared to be an underlying structure at 90° to the layers (Figure 8 - 47 and Figure 8 - 48) in the form of a needle like phase (columnar crystals) orientated in the direction of cooling, which the crack propagated down. Inclusions (contaminants, flux etc?) or porosity and an interface layer were also visible (Bassoli et.al., 2004).

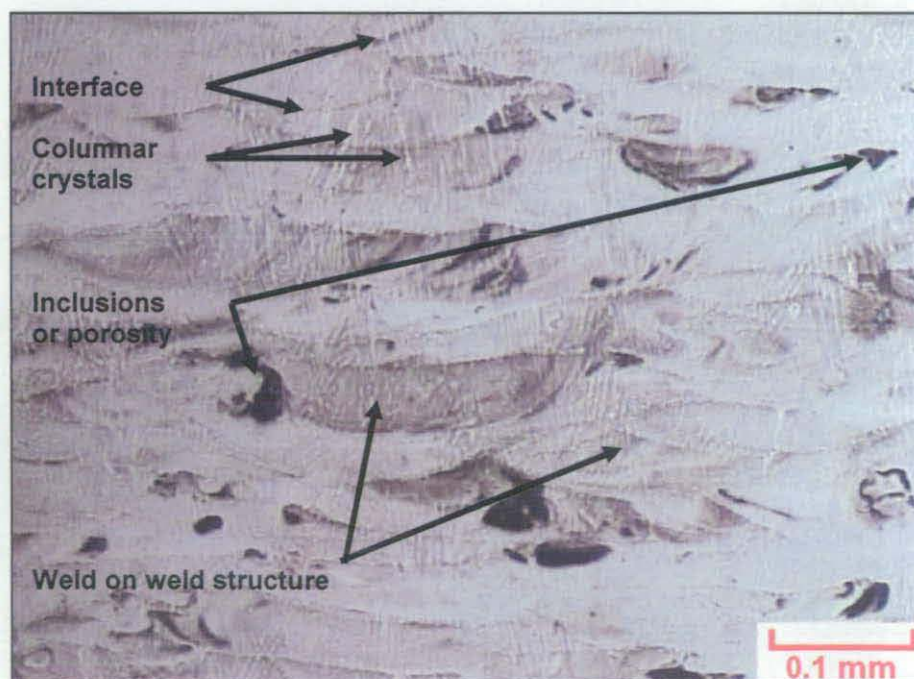


Figure 8 - 47 EOS DirectSteel 20 μ m specimen 5 S5-5K-4-x10



Figure 8 - 48 EOS DirectSteel 20μm specimen 5 S5-5K-3-x40

Although no specific cause of crack initiation was evident it was likely that initiation was either from an inclusion in the melt pool or poor wetting between melt pools. Examination showed that the cracks grew at 90° to the build direction and followed the columnar crystals (Figure 8 - 49).



Figure 8 - 49 EOS DirectSteel 20μm specimen 1 S1-5K-9-x10

8.10.2 EDX Analysis

The SEM examination did not reveal any additional information. The EDX (Figure 8 - 50 and Figure 8 - 51) showed that the material was made from iron, copper, nickel and phosphorous. It is clear from literature that the infiltrant is a nickel, copper and phosphorous alloy. However, phosphorous in a nickel alloy causes embrittlement.

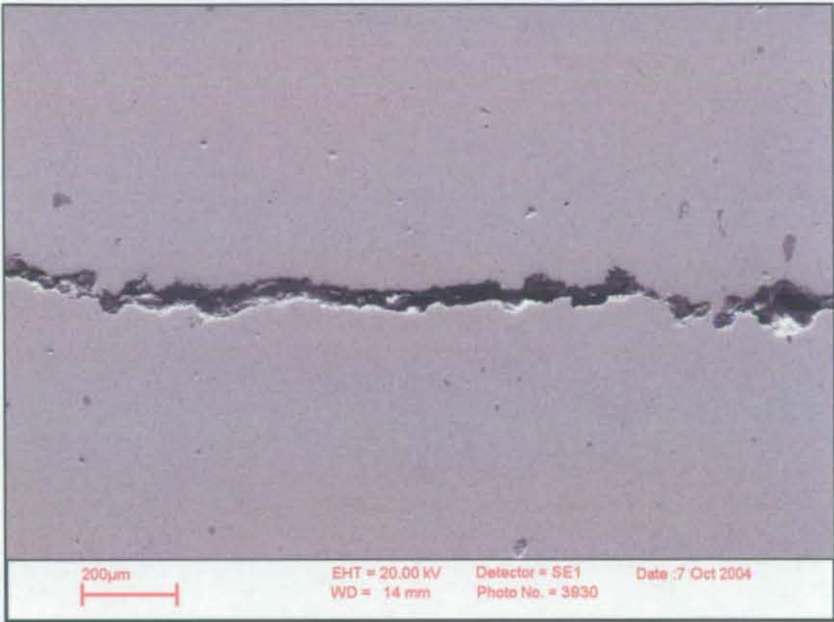


Figure 8 - 50 EOS DirectSteel 20µm specimen 1 S1-5K-87

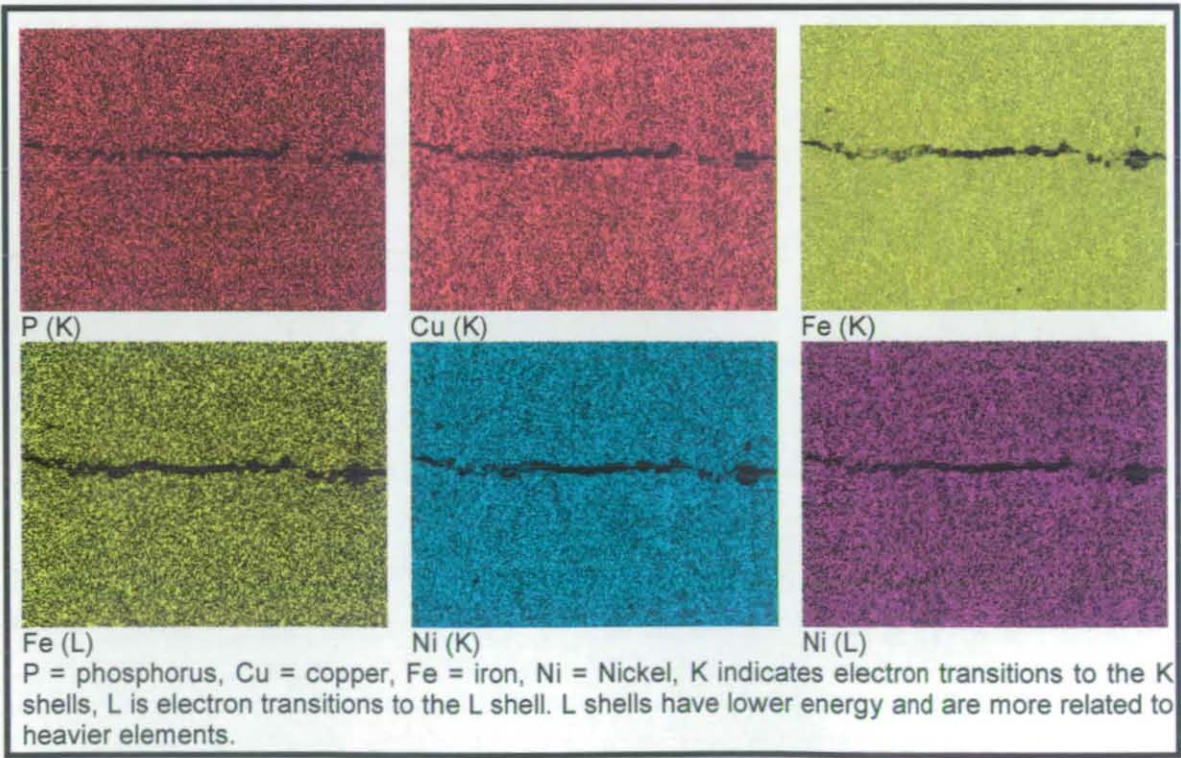


Figure 8 - 51 EOS DirectSteel 20µm EDX analysis

Chapter 9: Discussion

9.1 Overview

The aim of this work was to acquire an understanding of the mechanism of failure in rapid tooling materials that are subjected to harsh die casting environments and to determine material performance, mode of failure and suitability for the application. Hence, by carrying out this research it was expected to be possible to predict the life expectancy of materials and their failure mode leading to research to improve the thermal fatigue resistance of these materials.

Die casting and more importantly pressure die casting was selected as the process to simulate as the industry has a problem and requires a means of producing prototype components and short run tooling, the tooling could even lend itself for tooling for production die validation.

Chapter 1 describes the various common industrial die casting practices. The research showed pressure die-casting to be one of the most common and commercially used casting processes. The process has a fast cycle time (≈ 25 seconds) although dependent upon the alloy and casting size. Aluminium cold chamber pressure die casting tools have a shorter die life than magnesium and zinc due to the melting temperature of alloys and hence the thermal gradient and thermal shock the die is subjected to. Brass die casting is the only other pressure die casting process that has a higher melting temperature and thermal shock and shorter die life, but, the process was not chosen as it is not as common. Due to this aluminium pressure die cast was selected as the area of study.

In terms of the aluminium alloy to cast, research showed that in both America and Europe LM24 is most commonly cast alloy mainly due to its fluidity and castability. Due to this it was chosen as the material to be cast in the study.

Chapter 2 discussed the types of die used in the pressure die casting industry; this served a number of purposes. One was to determine the various features found in a die i.e. radius as small as 0.5mm, varying cross section etc. and to implement them in a specimen design. The second purpose was to determine what type of die to use to conduct the surface temperature trials to obtain a representative result. Finally it was necessary to establish current tooling practice which would allow alternative tooling manufacturing processes to be selected. Any new process must be able to match the current tooling methods.

In terms of comparing the tool materials it was important to have a direct comparison to an existing tooling material used commercially. The study revealed there are several commonly tried and tested materials and all are mainly hot work tool steels. The study showed H13 tends

to be the alloy of choice due to its hot work performance and was chosen as a suitable reference material.

Chapter 2 also discusses the heat treatment process for H13. It was important to establish how the material was heat treated in order to conduct the same heat treatment program on the reference specimens to obtain identical materials properties to that found in a die. This was important for accurate comparison between materials.

Chapter 3 assessed the modes of failure of a pressure die casting tool to determine what is most detrimental and how best to test the candidate materials to determine their suitability. The most detrimental was deemed to be thermal fatigue, although the other modes can contribute to crack initiation and a decline in fatigue life. It was decided thermal fatigue failure should be simulated to test a materials suitability and life expectancy for a pressure die cast tool. A study on fatigue and thermal fatigue was conducted to understand how cracks initiate, propagate and lead to failure. It was found that a material's fatigue life is affected by both its microstructure and mechanical properties.

The research revealed three equations (equations 3 - 2, 3 - 3 and 3 - 4) all similar to one another. From the formulas, it was apparent that yield strength, thermal conductivity, elastic modulus and coefficient of thermal expansion play a key role in thermal fatigue resistance. A high yield strength is important since thermal fatigue generally occurs in the elastic region, a high thermal conductivity is advantageous to reduce the thermal gradient and hence, the stress in the material, a low elastic modulus is of benefit since the plastic component of thermal fatigue is small and a low thermal expansion reduces stress in the material.

However, the research revealed several other material properties that are also beneficial such as hardness, resistance to tempering, good ductility etc. A complete list and explanation is shown in chapter 3, section 3.1. A major point that must be noted is that the formulas and the material properties which are deemed advantageous were created for alloy materials and may not be conclusive if used for rapid tooling materials. Moreover, many of the rapid tooling material properties are unknown and due to time constraints and material availability not all could be tested. Hence, the thermal fatigue test was required to determine the material suitability.

Chapter 3 also addresses types of thermal fatigue testing including two used to assess materials and material coatings for die casting. However, these tests are not representative of the die casting process for the reasons discussed in chapter 4, section 4.5.

Chapter 3 continues to identify methods for crack detection. Optical was considered the best solution for crack detection during the test programme as it was simple, cost effective and accurate to 0.1mm - 0.5mm. It also was the only practical method due to the facilities available. Post thermal fatigue analysis employed both optical microscopy and scanning electron

microscopy. The scanning electron microscopy has a better resolution (0.001mm) and was used to determine how the cracks initiated. Energy dispersive spectroscopy / energy dispersive X-ray (spectrometer) determined the mode of crack propagation through the material.

Once the die casting process, alloy, die types / die characteristics / die materials / die failure mode, the most detrimental failure mode, testing methods and evaluation methods etc. had been established it was possible to review possible rapid tooling solutions and materials. However, obtaining a complete set of materials proved difficult due to some processes being in their infancy or because of insufficient funds (It must be noted that several of the techniques discussed in chapter 4 did not exist at the commencement of the work).

When selecting a material to use as a die material for aluminium pressure die casting it is desirable to choose materials with similar properties to that of H13. However, the research was not trying to match a production die material, merely assess the potential of direct and indirect tooling materials for suitability for short run tooling (1 - 2000 components) for the manufacture of prototype components using the pressure die casting process. Due to this the materials were selected mainly on their temperature resistance and not purely on their mechanical properties.

One of the reasons the metal copy process was selected for was because they were an industrial collaborator during the research period. Their materials are a mixture of 316L stainless steel infiltrated with three infiltrant materials. As discussed in chapter 5, section 5.3, 316 stainless steel should withstand the temperatures of pressure die casting enabling castings to be produced. The material was chosen to determine which infiltrant material increased the performance of the material.

Keltool uses A6 tool steel and is infiltrated with 30% copper, but was not selected for testing as specimens could not be obtained and they were not a collaborator in the research.

The rapid solidification process (RSP) claims to be as good if not better than a H13 tool steel. The problem of the process is its limited size approximately Ø150mm x 100mm thick. Due to this and that they were not a collaborator; it was not selected as a suitable process as dies are generally larger.

The EcoTool process was not selected as specimens could not be obtained.

The direct tooling methods found in the literature were, laminate tooling, selective laser sintering, direct laser sintering, ProMetal, Solidica-Ultrasonic Consolidation, Laser Caving, CMB, ARCAM, Sprayform, Laser Engineered Net Shaping (LENS), Laser Consolidation.

Laminate tooling was selected due to previous research on unbonded tooling, however, it was unclear how a bonded tool would perform. The material is predominantly sheet H13 tool steel brazed together with a high temperature braze. It was selected as it is the only process that

uses a commercial tool material used in pressure die-casting and it was not clear how the brazed laminate structure would behave when subjected to thermal fatigue.

The direct laser sintered materials selected were DirectSteel 20 μ m and DirectSteel 50 μ m, as they both contained steel (alloy not divulged) as the base material and have a max operating temperature of 800°C. The DLS process has other materials such as DirectMetal 20 μ m; however, this is a bronze material with a maximum operating temperature of 400°C and lower mechanical properties than the steel based materials. In addition DirectMetal 20 μ m has higher thermal expansion which is detrimental to thermal fatigue. The manufacture of the DirectSteel 50 μ m specimens proved problematic due to cracking during manufacture preventing there testing; this left DirectSteel 20 μ m.

From the selective laser sintering process only one material was selected, RapidSteel 2.0 which replaced RapidSteel 1.0. The material is 60% 316 stainless steel infiltrated with 40% phosphor bronze (90%Cu, 10%Sn).

ProMetal, Solidica-Ultrasonic Consolidation, Laser Caving, CMB, ARCAM, Sprayform, Laser Engineered Net Shaping (LENS), Laser Consolidation process was not selected as specimens could not be obtained.

9.2 The Thermal Cycle of an Aluminium Pressure Die Casting Tool

Using thermocouples and temperature paints it was possible to obtain the temperature profile of an aluminium pressure die casting tool.

The results of this work showed that the surface temperature of the die reached between 400°C and 450°C and cooled to between 150°C and 200°C. Persson's (2003) research was on brass pressure die casting and not aluminium. Persson (2003), recorded the surface temperature of the die reaching 980°C but cooled rapidly to 750°C in 0.35 seconds then cooled to approximately 300°C over the remainder of the cycle (\approx 29.65 seconds). Despite Persson using brass, it was clear that there are similarities between the die temperature profile of a brass and aluminium die with the only difference being the higher temperatures (brass has a higher casting temperature than aluminium). Both experience rapid cooling as the molten metal hits the die surface and they have a similar cooling profile over the cycle time. Persson (2003), however, did estimate the surface of an aluminium die would reach 520°C. Srivastava (2003), also states that an aluminium pressure die casting tool surface reaches a maximum temperature of 457°C and cools down to 107°C. These results are in keeping with the tool temperature results of this work (450°C - 150°C).

In addition, the profile shown in Figure 6 - 31B is believed to be correct as research (Diecasting times, 2004) has shown a shot sleeve to reach an internal surface temperature of 480°C - 500°C with a significant amount of heat being lost by the molten metal (typically poured at 700°C) prior to injection. In turn, the tool surface temperature was recorded to reach 400°C to

450°C. Research has shown that as molten aluminium contacts the surface of the die a thin layer freezes instantaneously and the die never reaches the temperature of the molten material (Chen, 2003, Ghomashchi, 1995). The mass of the die draws the heat away rapidly during solidification. Upon die opening, ejection, mould spray etc. the die surface begins to cool more rapidly as shown in Figure 6 - 18.

9.3 Reproducing the Temperature Profile of an Aluminium Pressure Die Casting Tool

A new method of thermal fatigue testing was developed at the beginning of the work to establish a means of comparing materials and determining their suitability for tooling in aluminium pressure die casting.

At the commencement of the work, searches of the British and American standards revealed that no thermal fatigue test for this existed. This was thought to be due to the different variables involved that affect the materials thermal fatigue resistance. For example, the shape of the specimen, different heating and cooling mediums, the shape of the thermal cycle, the maximum and minimum temperatures etc. However, when undertaking a final search of the American standards during the writing up of the work a Japanese industrial standard (JIS Z 2278, 1992) and a Chinese standard GB/T 15824 - 1995 (1995) were identified. Despite the standard dates (1992 and 1995) they had only recently been placed in the American standards, hence, previous searches did not detect them (Chinese standard GB/T 15824 - 1995 still has a new tag on the American standards (2006) website).

Unfortunately, no information could be gained from the Chinese standard as it has not been translated. However, the Japanese industrial standard by coincidence is identical to the test method developed in this work. It employs the same specimen and edge radius, and employs an automated transfer system, however, it does not identify the means of heating or cooling with the exception of water. It does recommend that if cooling in water the temperature should be maintained below 30°C; this research maintained the water temperature below 20°C.

The thermal fatigue test methods discussed in chapter 3, section 3.5 were not considered to be a true representation of thermal fatigue in an aluminium pressure die casting so a new test was created. Although the new test does not reproduce the die casting temperature cycle exactly, the materials were subjected to the same minimum and maximum temperatures experienced in a die. The new test only considered thermal fatigue and not other contributing factors associated with die-casting such as pressure, erosion, wear, chemical attack etc. This allowed thermal fatigue resistance of materials to be compared.

Additional benefits over previous tests methods were that the apparatus was versatile in terms of the temperature range 25°C - 1200°C, heating and cooling medium and the cycle time could be easily controlled. The specimens were small, allowing several to be tested simultaneously and the geometry allowed easy measurement of cracks. The fatigue apparatus was robust and

reliable which was essential since many thousands of cycles were required. This test method could be adopted as a standard internationally for thermal fatigue testing.

9.3.1 Effect of Material Structure on Thermal Fatigue

The materials tested can be categorised into four types:

- 1) Alloy steel
- 2) Spherical powder infiltrated with a lower melting point alloy
- 3) Braze bonded laminates
- 4) Direct laser sintered

Category 1: The material tested in category 1 was H13 tool steel which was the experimental reference specimen. Literature has shown that a die in aluminium pressure die casting will exhibit cracking at approximately 100,000 - 150,000 (Clegg, 1999) cycles and Wallace's thermal fatigue experiment attempts to mirror this. However, his experiment incorporates other categories associated with die failure such as chemical attack which promotes crack initiation sites. The test in this work only considered thermal fatigue and hence, cracking did not occur in the H13 until later (180,000 - 220,000 cycles). The results from the H13 specimens were limited due to the overwhelming numbers of cracks that formed simultaneously, making cataloguing practically impossible. The crack patterns created are termed crazed cracking and are typical of the type of cracks seen on a thermally fatigued die surface. It was clear that a drop in hardness coincided with severe cracking. Persson, 2005 reported that gradual softening of his specimens also reduced the material's yield strength; a high yield strength increases thermal fatigue life. H13 is strengthened by carbide formation and this increases the materials resistance to repeated strains. It was noticed that the cracks in the H13 specimens tended to propagate through the areas rich in carbides and small cracks interlinked, which is endorsed by literature. Woodford and Mowbray's (1974) research showed that when a material containing carbides was subjected to thermal fatigue, the crack propagated from one carbide to another. The carbides may be a stress concentrator in the material and the source of crack initiation (Bendyk, et.al., 1970, Norström, 1982, Norström, 1989, Weroński and Hejwoski, 1991, Schwam et.al., 2004 Simons, 1972, Sjoström and Bergström 2004, Woodford and Mowbray's, 1974, Worbye, 1985).

Category 2: The materials tested in category 2 contained steel powder (spheres) in a low melting point alloy bonding material (silver, copper, phosphor bronze etc.). The tendency for the metalcopy materials was for a crack to initiate at the interface between the steel powder and the matrix. This was probably a result of poor wetting creating a void which was a defect and stress concentrator and this allowed a crack to initiate (Simons, 1972). In addition, the material had chrome and molybdenum rich areas (carbides) in the steel and at the powder / bonding material interface that could have caused a stress raiser. The crack then propagated from one interface to another through the matrix. This structure proved detrimental to thermal fatigue resistance since the interfaces are crack initiation sites. The literature (Weroński and Hejwoski, 1991)

showed that composition and structure is as influential in thermal fatigue as it is in mechanical fatigue. It was seen that the materials contained large chrome and molybdenum carbides in the steel powder and at the steel and at the powder / infiltrant interface that may have caused a stress raiser. Although literature states carbide formation and solid solution strengthening are mechanisms to increasing strength and thermal fatigue resistance (Weroński and Hejwoski, 1991), large carbides are detrimental and are crack initiators and also cracks propagate from one carbide to another (Bendyk, et.al., 1970, Norström, 1982, Norström, 1989, Weroński and Hejwoski, 1991, Schwam et.al., 2004 Simons, 1972, Sjoström and Bergström 2004, Woodford and Mowbray's, 1974, Worbye, 1985).

The thermal fatigue resistance of the Metalcopy materials was relatively poor and a major contributing factor was thought to be the inconsistency in the material manufacture with porosity and inclusions allowing ease of crack propagation. Another contributing factor was the alloying of the bonding material for Metalcopy 5507 and Metalcopy Janalloy. Both contained 316 stainless steel powder. However, the bonding materials were meant to be identical and contain silver, copper and zinc, but, the Metalcopy Janalloy bonding material was manufactured in-house, whereas the Metalcopy 5507 bonding material was made by a supplier. It was clear from the thermal fatigue results that Metalcopy Janalloy was inferior to Metalcopy 5507. The Metalcopy Janalloy bonding material did not contain any zinc, instead it contained rhenium. It is not clear if this was a contributing factor to the poor thermal fatigue resistance.

Metalcopy Cu tended to have better thermal fatigue characteristics than the other Metalcopy materials. Metalcopy Cu was infiltrated with copper whereas Metalcopy 5507 and Metalcopy Janalloy were an Ag, Cu, and Zn / Re alloy.

The RapidSteel 2.0 material also fell into category 2; this material contained 316 stainless steel powder in a matrix of phosphor bronze. This bonding alloy also has good material properties in comparison to others. From optical examination, the matrix and the 316 stainless steel powder exhibited better wetting than the Metalcopy materials. Literature showed that better wetting reduces crack initiation sites and aids thermal fatigue performance (ASM, 1996). The material contained porosity and the likely cause was gas entrapment during infiltration. Despite this the material had a good resistance to thermal fatigue. This may be due to better mechanical properties of the material and good wetting characteristics in comparison to the Metalcopy materials, reducing the possibility of crack initiation sites. It was unclear how the cracks initiated. Literature suggests that cracking may have initiated from the porosity and or the chromium rich (carbides) areas at the powder / bonding material interface as both are material flaws and stress concentrators (Simons 1972). The cracks propagated down the powder / bonding material interface and through the bonding material taking the easiest route from one interface to another. It was also noticed that the areas around the crack were oxidised. Literature states that oxides are detrimental as they produce a brittle oxide film which can crack, form pits, create a stress concentrator which can promote cracking. It should also be noted that the steel powder was 316 stainless steel and should not oxidise at the test temperatures since it has good oxide

resistance in intermittent service to 870°C (Azom, 2006). However, it did oxidise to some extent. It is likely the 316 stainless steel became sensitised during infiltration. Phosphor bronze melts at 830°C - 1020°C and when 316 stainless steel is heated to around 700°C, chromium carbide forms at the intergranular boundaries, depleting the grain edges of chromium, impairing their corrosion resistance. Steel in such condition is called sensitized. Chromium rich areas were also visible in the EDX analysis of RapidSteel 2.0 (chapter 8, section 8.9.2). It is however, possible to reclaim sensitized steel by heating it to above 1000°C and holding at this temperature for a given period of time, dependent on the mass of the piece, followed by quenching it in water. This process dissolves the carbide particles and then keeps them in solution. However, the manufacturing process of RapidSteel 2.0 does not involve water quenching (Wikipedia, 2006). Sensitised 316 stainless steel is susceptible to intergranular corrosion and chromium-depleted zones also act as local galvanic cells, causing local galvanic corrosion. In addition, RapidSteel 2.0 is manufactured from two materials one more noble than the other and this could have caused a galvanic cell. In turn, water may have travelled down the crack (capillary action) creating an electrolyte cell causing the oxidation seen along the crack (Wikipedia, 2006).

Amdry 790 is a braze material and although not bonded like the other category 2 materials, it had a similar microstructure with the nickel phase forming spheroid particles in a matrix of silicon (silicon is added to aid fluidity in the braze). However, the mode of crack initiation was different. It was unclear how the cracks initiated, however, sulphur was present in the nickel phase where micro cracking occurred. The sulphur may have caused embrittlement (Chen et.al., 2004). The crack propagated in this phase until it reached the silicon phase and then propagated down thin vanes of nickel (nickel / silicon grain boundaries) running through the silicon until it reached a nickel phase again. Once a crack is initiated it is common for it to propagate by de-cohesion along the grain boundary (ASM, 1996).

Category 3: Category three consisted of nickel braze (Amdry 790) bonded H13 tool steel (Horizontal laminate and Vertical laminate). It is clear from the micrographs that good wetting and diffusion bonding had occurred, which literature states increases thermal fatigue life (ASM, 1996). It was found that the braze had two phases, one near the laminates and the other which tended to run down the centre, it is believed that this can and did affect the thermal fatigue resistance. The braze was richer in nickel and poorer in iron at the centre. The braze also contained porosity, probably caused by the gasses produced during the brazing process which were not able to escape. Porosity was also the likely source of crack initiation (Simons 1972). The cracks initiated from voids and propagated down the central phase of the braze and not down the boundary between phases. Cracks on occasion initiated and propagated along the braze / H13 interface. All the cracks initiated in the braze that bonded the laminate structure together.

Category 4: The EOS DirectSteel 20µm material had a structure similar to a series of welds layered one upon another and these were caused by the method of manufacture. There appeared to be contaminants or inclusions in the material, which could be possible crack

initiators. This was also noted by Bassoli et.al, 2004. The material had a grain structure at 90° to the build / layer orientation, which appeared to be a needle like phase (columnar crystals). This was orientated in the direction of cooling and it was along this that the cracks propagated (grain boundary de-cohesion ASM, 1996).

No specific cause of crack initiation was identified but it was likely that initiation was either from an inclusion in the melt pool or from poor wetting between melt pools. A crack may also have initiated / propagated as a result of residual stress, created by the melt pool solidifying whilst being restrained by the surrounding material. In turn, weld structures have a heat affected zone which is undesirable as the crystal structure varies, as do the material properties, in that area.

9.4 Comparison of Material Performance

Prior to comparing the thermal fatigue resistance it is important to establish a ranking system so that the effects of material properties can be understood later. Ranking the fatigue resistance of the different materials was difficult as it is dependent upon how you view the data, for example:

- Is a material that initiated cracks first with a low rate of crack initiation thereafter better or worse than a material which initiated cracks later with a high rate of crack initiation thereafter?
- Is a material that initiated cracks first with a low crack length thereafter better or worse than a material which initiated cracks later with a high crack length thereafter?
- Is a material that initiated cracks first with a low crack growth rate better or worse than a material which initiated cracks later with a high crack growth rate thereafter?
- Is a material that initiated cracks first with many cracks but a low crack length better or worse than a material which initiated cracks later with few cracks but a high crack length?

The following sections discuss the order of fatigue resistance in terms of the number of cycles versus initial crack initiation, initial and final number of cracks, initial and final total crack length and initial and final average crack length. The effect of the material properties will be discussed later.

As the materials chosen for this research were mainly for low volume tools then the ranking was determined as follows:

- The lower the number of cycles for crack initiation, the worse the material is at resisting thermal fatigue
- The higher the number of cracks (initially and finally), the worse the material is at resisting thermal fatigue
- The higher the crack length (initially and finally), the worse the material is at resisting thermal fatigue

The H13 tool steel as expected out performed the rapid tooling materials in all cases, however, when cracking occurred the numbers were overwhelming and no sensible crack data could be obtained.

9.4.1 Initial Signs of Cracking

When comparing the order of thermal fatigue resistance in terms of the number of cycles to initiate cracks (Figure 9 - 1), it can be seen that EOS DirectSteel 20µm was the worst material initiating 11 cracks at 500 cycles. Horizontal RapidSteel 2.0 was the best rapid tooling material initiating 14 cracks at 50,000. As expected H13 out performed all the rapid tooling materials initiating cracking at 180,000 cycles.

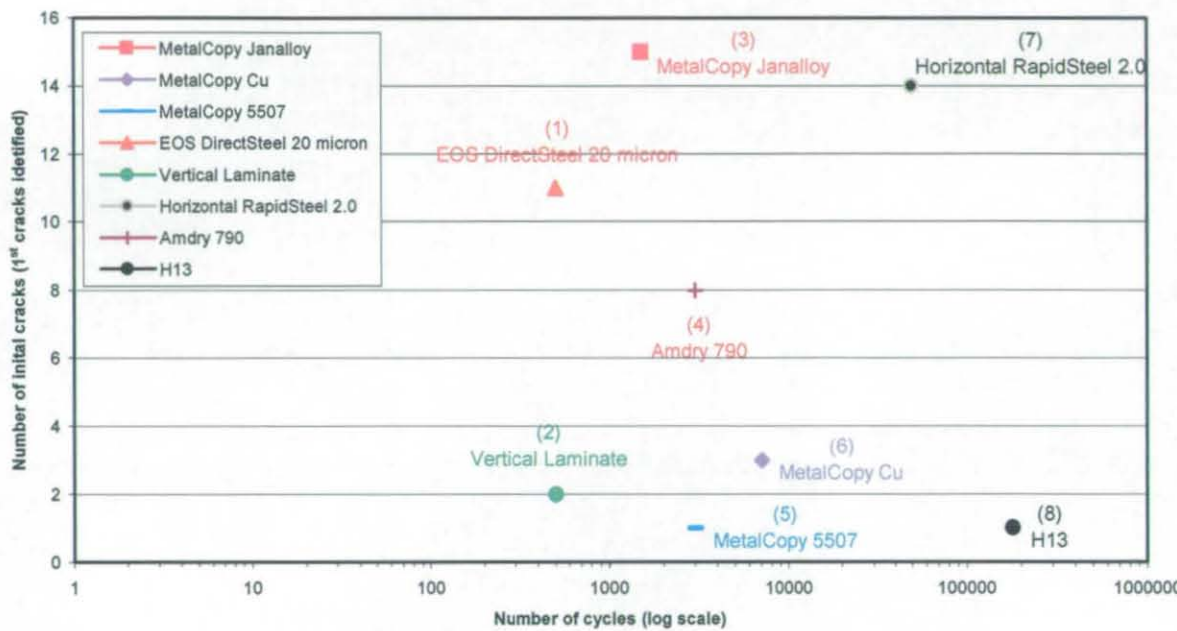


Figure 9 - 1 Number of cycles versus initial number cracks (log scale)

Previous aluminium pressure die-casting trials (Hague, 2001, Harris et.al., 2003^a, Harris et.al., 2003^b, Harris et.al., 2004, Norwood et.al., 2001, Norwood and Soar, 2001, Norwood et.al., 2004, Norwood and Dickens, 2005) showed that the rapid tooling materials (DirectSteel 20µm, RapidSteel 2.0, Metalcopy 5507, Vertical laminate) cracked earlier than predicted and severe cracking was evident after 500 cycles. It is probable that this was made worse by chemical attack of the infiltrant material by the molten aluminium. Factors such as chemical attack, adhesive wear, abrasive wear, erosion, oxidation, mechanical loading etc. promote crack initiation sites and propagation in these materials.

9.4.2 Number of Cracks

This section reviews the number of cycles versus the total number of cracks; this is the combined number of cracks on all the four specimens. The data shows how crack numbers increased for each material as the number of cycles increased.

It is important to compare the total number of initial cracks, the total number of final cracks and the number of cycles at which the cracks initiated. (i.e. some materials may develop a few cracks at a low number of cycles (EOS DirectSteel 20µm) and have a low initiation rate thereafter, however, some materials may start to initiate cracks later (Metalcopy Janalloy) but initiate many cracks). So when comparing two materials, initially EOS DirectSteel 20µm was worse than Metalcopy Janalloy as it initiated cracking at a lower number of cycles. However, finally it was better than Metalcopy Janalloy as it had less cracks at the same number of cycles (Figure 9 - 2).

The materials are ranked as follows: a material that cracks at a low number of cycles is worse than one which cracks at a higher number of cycles. If more than one material initiated cracking at the same number of cycles, the material with the highest total number of cracks is considered to be worse. For example, EOS DirectSteel 20µm is worse at 500 cycles than the Vertical laminate material (Figure 9 - 2).

Reviewing the initial results (again the higher the number of cracks) showed that EOS DirectSteel 20µm was the worst material with Horizontal RapidSteel 2.0 being the best (Figure 9 - 2).

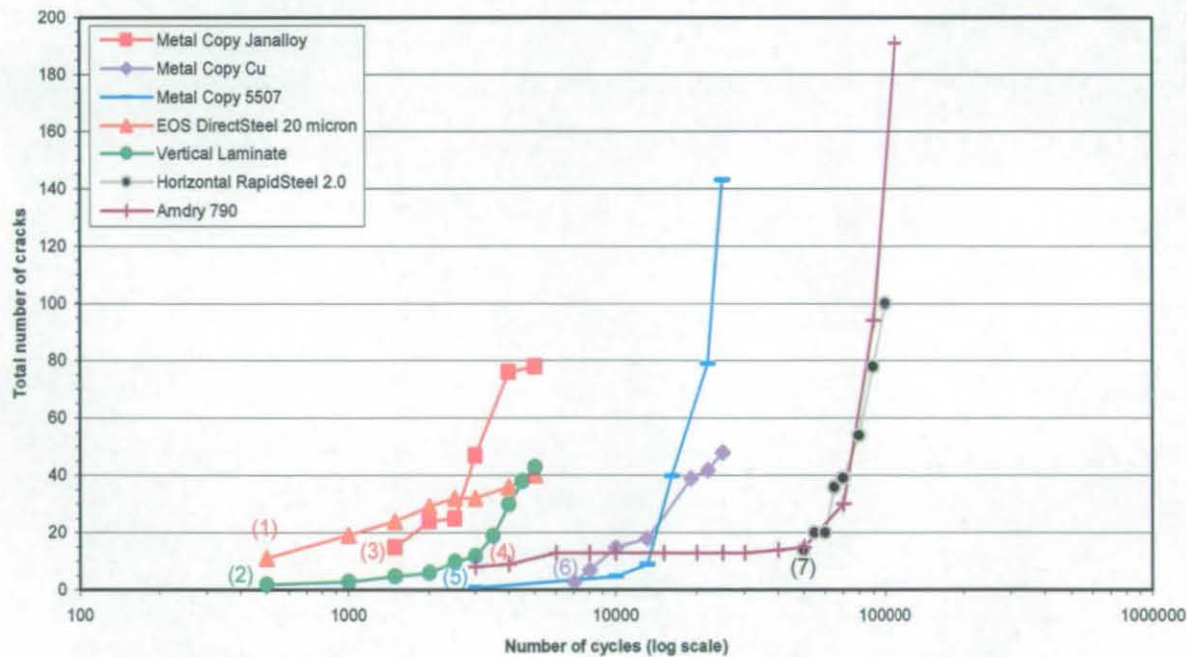


Figure 9 - 2 Number of cycles versus initial the total number of cracks (log scale)

Reviewing the final results (Figure 9 - 3) the materials are ranked as follows: a material with a low number of cycles at the end of testing is worse than one which cracked at a higher number of cycles. If more than one material initiated cracking at the same number of cycles, the material with the highest total number of cracks is considered to be worse.

Therefore, Metalcopy Janalloy was the worst because of the three materials that were stopped at 5,000 cycles it had the highest total number of cracks. RapidSteel 2.0 was the best material because it had a lower number of total cracks than Amdry 790 at 100,000 cycles.

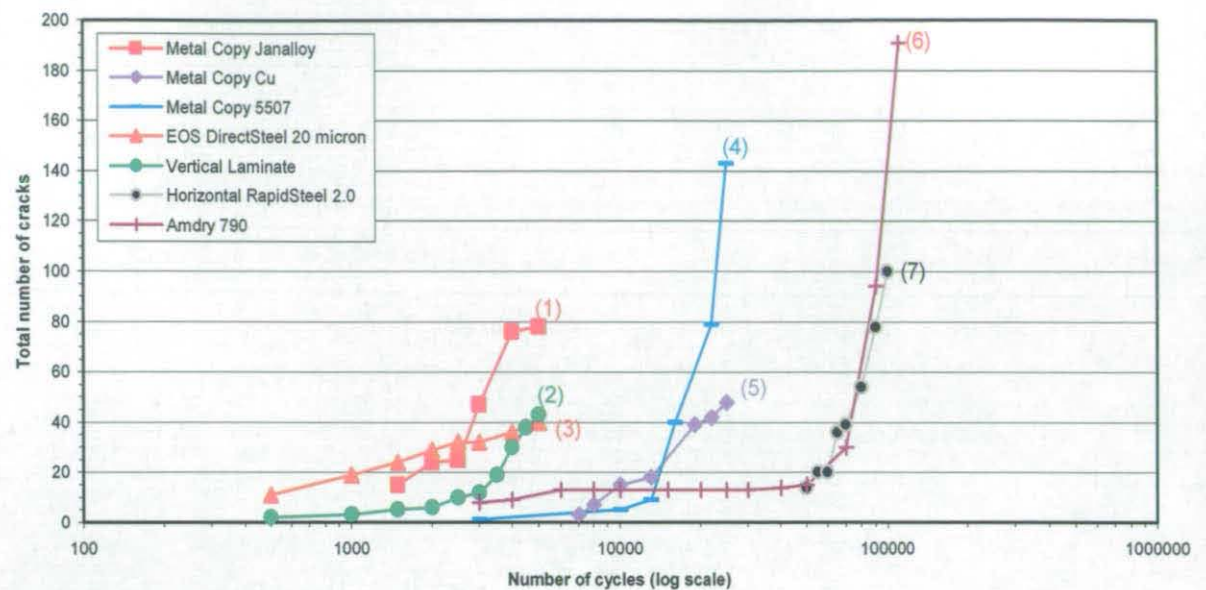


Figure 9 - 3 Number of cycles versus the final total number of cracks (log scale)

9.4.3 Crack Length

This section reviews the number of cycles versus the total crack length; this is the combined length of every crack on the specimens. The data shows how the crack length of each material increased as the number of cycles increased.

When ranking the number of cycles against crack length both the initial and final crack lengths have to be assessed. For example, a material that initiates cracking first and has a high crack length (EOS DirectSteel 20µm) is worse than a material that initiates cracking later (Metalcopy Janalloy) (Figure 9 - 4). However, a material that has a high final crack length (Metalcopy Janalloy) at the same number of cycles as a material with a lower final crack length (EOS DirectSteel 20µm) is worse (Figure 9 - 5).

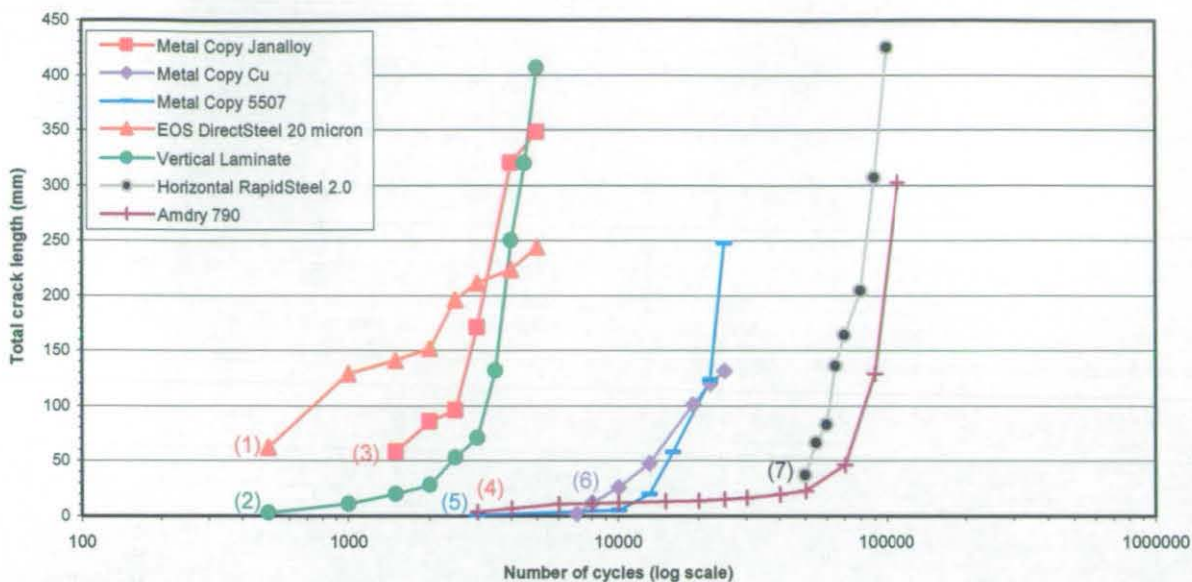


Figure 9 - 4 Number of cycles versus initial total crack length (mm) (log scale)

When comparing the specimens in terms of cycles versus total crack length the following was observed:

Initially EOS DirectSteel 20µm was the worst with Horizontal RapidSteel 2.0 being the best (Figure 9 - 4).

Finally the Vertical laminate specimens were the worst (Vertical laminate, Metalcopy Janalloy and EOS DirectSteel 20µm all completed 5,000 cycles) since they had the highest total crack length followed by Metalcopy Janalloy, EOS DirectSteel 20µm, Metalcopy 5507, Metalcopy Cu, Horizontal RapidSteel 2.0, Amdry 790 (Figure 9 - 5).

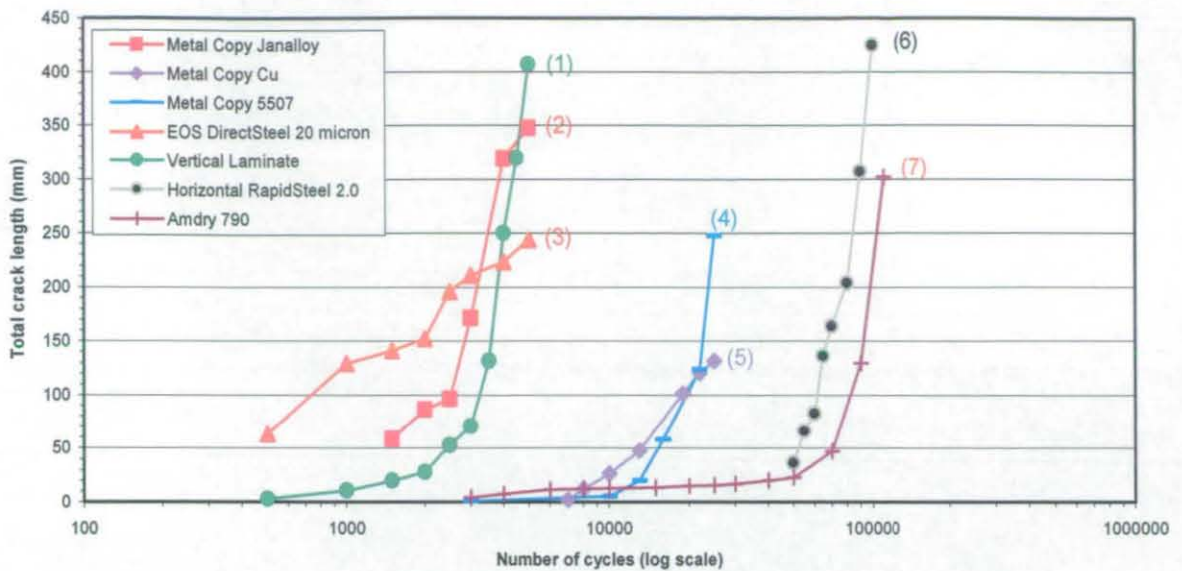


Figure 9 - 5 Number of cycles versus final total crack length (mm) (log scale)

9.4.3.1 Average Crack Length

The average crack length is the total crack length divided by the number of cracks.

A material which has a horizontal plot must be initiating and propagating cracks at a similar rate. Such as EOS DirectSteel 20µm and Metalcopy Janalloy. If the plot is increasing, the number of cracks must be low and the crack length and propagation higher (e.g. Vertical laminate) (Figure 9 - 6).

As with the previous ranking it is important to look at the initial average crack length and final average crack length against the number of cycles.

It is clear that initially EOS DirectSteel 20µm had the largest average crack length, with Horizontal RapidSteel 2.0 being the best (Figure 9 - 6).

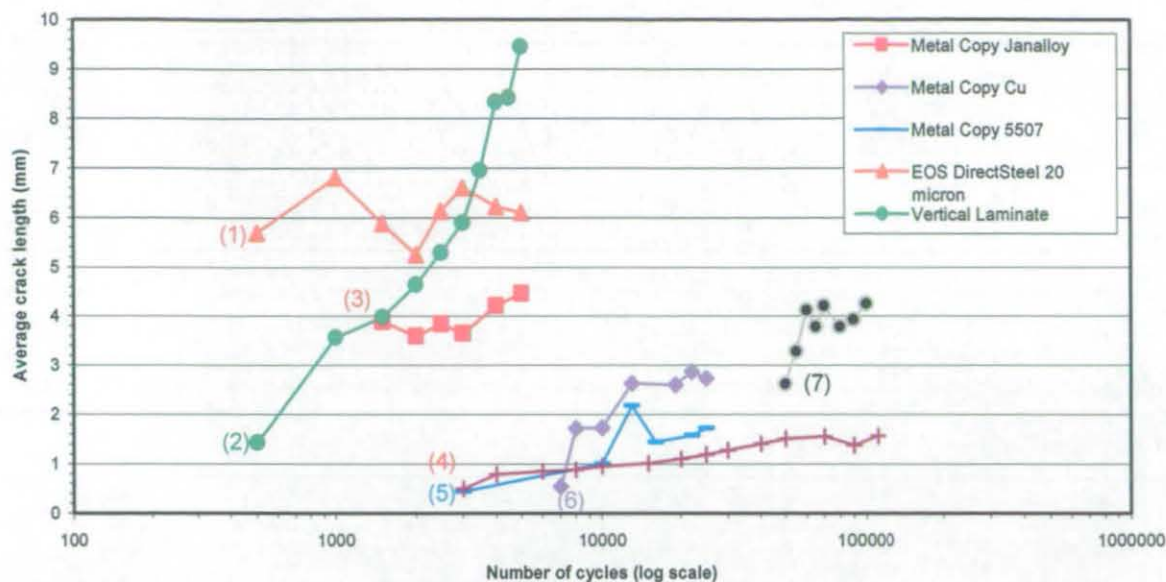


Figure 9 - 6 Number of cycles versus initial average crack length (mm) (log scale)

Figure 9 - 7 shows that finally the Vertical laminate material was the worst with Amdry 790 being the best.

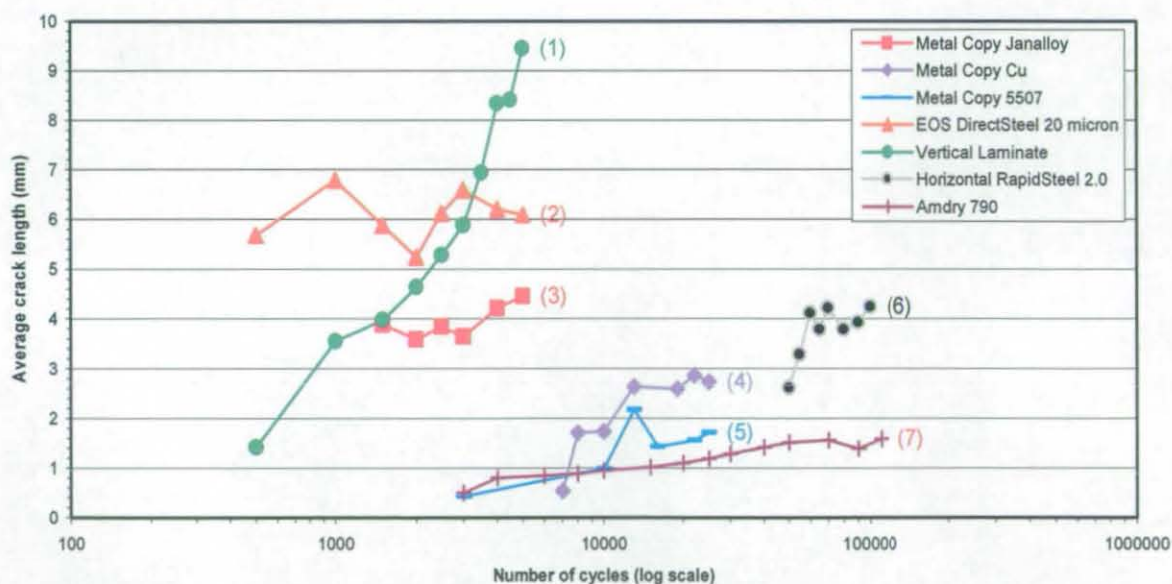


Figure 9 - 7 Number of cycles versus final average crack length (mm) (log scale)

As this research was investigating prototype tools, then initial results are more important than final results. Table 9 - 1 shows the overall initial material performance results. The lower the number the worse the material performance.

Material	Initial number of cracks	Initial total crack length	Initial average crack length	Overall
EOS DirectSteel 20µm	1	1	1	1
Vertical laminate	2	2	2	2
Metalcopy Janalloy	3	3	3	3
Amdry 790	4	4	4	4
Metalcopy 5507	5	5	5	5
Metalcopy Cu	6	6	6	6
Horizontal RapidSteel 2.0	7	7	7	7
H13	8	8	8	8

Table 9 - 1 Initial material performance

The main problem of cracking is the effect on surface finish of a part. In this case each of the three criteria have similar or equal importance. Therefore, each criteria was given the same importance.

If the demand for prototypes increased, as is often the case during product development, then the final material performance results would become important.

Table 9 - 2 shows the final material performance results. The lower the number the worse the material performance.

The severity of these factors will determine whether a part will stick in the tool cavity and therefore affect the usability of the die. This will depend greatly on the geometry of the part and therefore for this study each factor was assumed to have equal weighting.

Material	Final number of cracks	Final total crack length	Final average crack length	Overall
Vertical laminate	2	1	1	1.33
Metalcopy Janalloy	1	2	3	2.00
EOS DirectSteel 20µm	3	3	2	2.67
Metalcopy 5507	4	4	5	4.33
Metalcopy Cu	5	5	4	4.67
Horizontal RapidSteel 2.0	7	6	6	6.33
Amdry 790	6	7	7	6.67
H13	8	8	8	8

Table 9 - 2 Final material performance

By using both the initial and final results the following material performance was established (Table 9 - 3). Again the lower the number the worse the materials performance.

As the factors have been weighted equally and the materials have been promoted for small and medium volumes then the initial and final order were also weighted equally.

Material	Initial order	Final order	Order
Vertical laminate	2	1.33	1.67
EOS DirectSteel 20µm	1	2.67	1.84
Metalcopy Janalloy	3	2	2.50
Metalcopy 5507	5	4.33	4.67
Metalcopy Cu	6	4.67	5.34
Amdry 790	4	6.67	5.34
Horizontal RapidSteel 2.0	7	6.33	6.67
H13	8	8	8

Table 9 - 3 Overall thermal fatigue results

9.5 The Relationship between Material Properties and Thermal Fatigue Life

As discussed in the hypothesis in chapter 4 section 4.4 it was believed that the materials properties would be directly linked to thermal fatigue performance. This section will review the results against each of these material properties.

9.5.1 Hardness

Figure 9 - 8 shows the hardness of the specimens during thermal cycling. It is clear that the hardness remained reasonably constant.

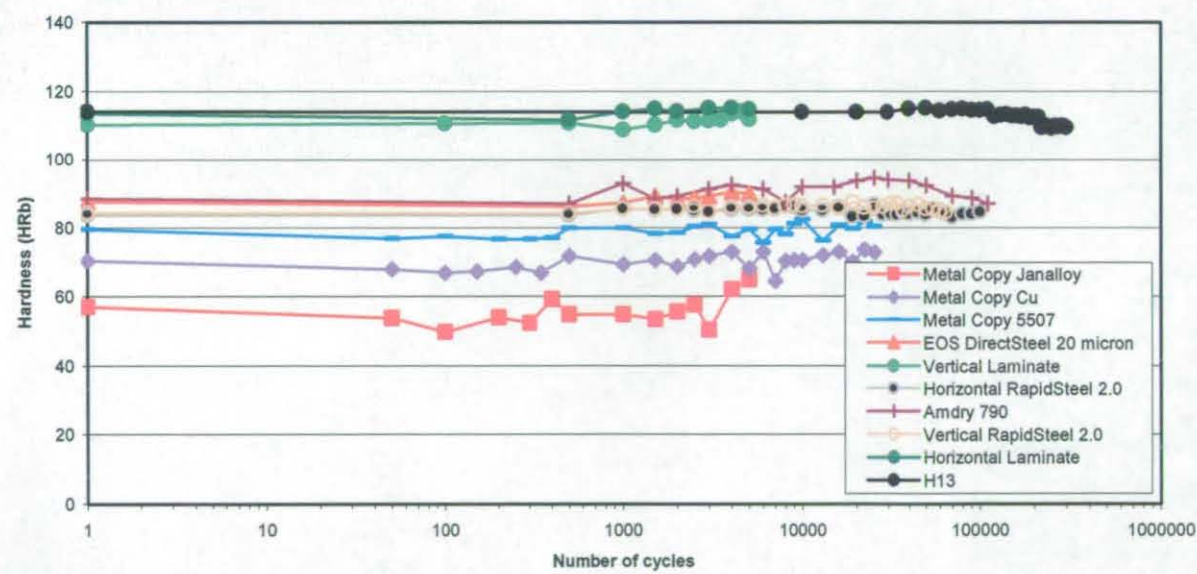


Figure 9 - 8 Number of cycles versus hardness (HRb) (log scale)

When comparing the experimental data of category 2 materials (Metalcopy Janalloy, Metalcopy Cu, Metalcopy 5507, Horizontal RapidSteel 2.0) with the exception of Amdry 790 (Amdry 790 is an alloy and not an infiltrated material) there appeared to be a correlation between hardness and thermal fatigue properties, i.e., the harder the material the better the thermal fatigue resistance in terms of crack initiation and life expectancy (Table 9 - 4, Table 9 - 5, Table 9 - 6).

No comparison (Table 9 - 4) between thermal fatigue resistance and hardness could be drawn for the EOS DirectSteel 20µm, Vertical laminate and Amdry 790 materials, as these are very different types of material.

Material	Hardness (HRb)	Fatigue Performance
EOS DirectSteel 20µm	89	Worst ↓ Best
Vertical laminate	111	
Metalcopy Janalloy	56	
Amdry 790	79	
Metalcopy 5507	70	
Metalcopy Cu	83	
Horizontal RapidSteel 2.0	86	
H13	104 - 120	

Table 9 - 4 Initial material performance versus hardness

Material	Hardness (HRb)	Fatigue Performance
Vertical laminate	111	Worst ↓ Best
Metalcopy Janalloy	56	
EOS DirectSteel 20µm	89	
Metalcopy 5507	70	
Metalcopy Cu	83	
Horizontal RapidSteel 2.0	86	
Amdry 790	79	
H13	104 - 120	

Table 9 - 5 Final material performance versus hardness

Material	Hardness (HRb)	Fatigue Performance
Vertical laminate	111	Worst ↓ Best
EOS DirectSteel 20µm	89	
Metalcopy Janalloy	56	
Metalcopy 5507	70	
Metalcopy Cu	83	
Amdry 790	79	
Horizontal RapidSteel 2.0	86	
H13	104 - 120	

Table 9 - 6 Overall material performance versus hardness

9.5.2 Density

Density is one of the material properties that may allow the prediction of thermal fatigue resistance. The higher the material's density the better it should be at resisting thermal fatigue.

No correlations for density and thermal fatigue resistance could be drawn for material performance (Table 9 - 7 - Table 9 - 9).

Material	Density (g/cm ³)	Fatigue Performance
EOS DirectSteel 20µm	7.91	Worst ↓ Best
Vertical laminate	7.73	
Metalcopy Janalloy	7.19	
Amdry 790	7.99	
Metalcopy 5507	8.05	
Metalcopy Cu	7.73	
Horizontal RapidSteel 2.0	7.82	
H13	7.8	

Table 9 - 7 Initial material performance versus density

Material	Density (g/cm ³)	Fatigue Performance
Vertical laminate	7.73	Worst ↓ Best
Metalcopy Janalloy	7.19	
EOS DirectSteel 20µm	7.91	
Metalcopy 5507	8.05	
Metalcopy Cu	7.73	
Horizontal RapidSteel 2.0	7.82	
Amdry 790	7.99	
H13	7.8	

Table 9 - 8 Final material performance versus density

Material	Density (g/cm ³)	Fatigue Performance
Vertical laminate	7.73	Worst ↓ Best
EOS DirectSteel 20µm	7.91	
Metalcopy Janalloy	7.19	
Metalcopy 5507	8.05	
Metalcopy Cu	7.73	
Amdry 790	7.99	
Horizontal RapidSteel 2.0	7.82	
H13	7.8	

Table 9 - 9 Overall material performance versus density

During thermal fatigue testing it was noted that cracks tended to initiate and propagate through the materials bonding material. When looking at the bonding material density, a pattern emerged. With the exception of Amdry 790 which is a braze and an alloy (not infiltrated / bonded) the remaining materials had improved thermal fatigue resistance as their bonding material density decreased (Table 9 - 7 - Table 9 - 9). This is a contradiction since a low density usually equals a low thermal fatigue resistance.

Material	Density (g/cm ³)	Fatigue Performance
Metalcopy Janalloy infiltrant	9.35	Worst ↓ Best
Amdry 790	7.99	
Metalcopy 5507 infiltrant	9.27	
Metalcopy Cu infiltrant	8.88	
Horizontal RapidSteel 2.0 infiltrant	8.78	

Table 9 - 10 Initial material performance versus infiltrant density

Material	Density (g/cm ³)	Fatigue Performance
Metalcopy Janalloy infiltrant	9.35	Worst ↓ Best
Metalcopy 5507 infiltrant	9.27	
Metalcopy Cu infiltrant	8.88	
Horizontal RapidSteel 2.0 infiltrant	8.78	
Amdry 790	7.99	

Table 9 - 11 Final material performance versus infiltrant density

Material	Density (g/cm ³)	Fatigue Performance
Metalcopy Janalloy infiltrant	9.35	Worst ↓ Best
Metalcopy 5507 infiltrant	9.27	
Metalcopy Cu infiltrant	8.88	
Amdry 790	7.99	
Horizontal RapidSteel 2.0 infiltrant	8.78	

Table 9 - 12 Overall material performance versus infiltrant density

However, this led to discovering that the difference in density between the powder material and bonding material is important. With a bonding material with a low density there is less difference with the powder material. So it is advisable to have a bonding material and powder material with similar densities to improve thermal fatigue life. Table 9 - 13 shows differences of up to 1.35g/cm³.

Material	Powder material	Bonding material	Difference	Fatigue Performance
Metalcopy Janalloy	316 SS (8g/cm ³)	Ag alloy (9.35g/cm ³)	1.35g/cm ³	Worst ↓ Best
Metalcopy 5507	316 SS 8(g/cm ³)	Ag alloy (9.27g/cm ³)	1.27g/cm ³	
Metalcopy Cu	316 SS (8g/cm ³)	Cu alloy (8.88g/cm ³)	0.88g/cm ³	
RapidSteel™ 2.0	316 SS (8g/cm ³)	Phosphor Bronze (8.78g/cm ³)	0.78g/cm ³	

Table 9 - 13 Powder material and bonding material densities and differences

The lower the difference in densities between the materials the better the thermal fatigue resistance.

9.5.3 Thermal Conductivity

Initial tests were conducted on all the candidate materials to assess their thermal conductivity.

It is generally considered that a high thermal conductivity equates to better fatigue resistance as there is a reduced temperature difference through a material and hence less stress.

All the materials analysed are made either from two alloys (e.g. Metalcopy 5507, 316 stainless steel and a silver alloy) or contain two main element's forming the alloy (e.g. EOS DirectSteel 20µm, Amdry 790). Each alloy / elements thermal conductivity was reviewed to determine if a correlation existed.

The initial material performance shows that there is a correlation between the composite material's thermal conductivity and the material's ability to resist thermal fatigue. (The higher the composite material thermal conductivity the better the thermal fatigue performance) (Table 9 - 14).

The final and overall material performance show a similar trend, the exceptions are EOS DirectSteel 20µm and Amdry 790. However, these are both alloys and not bonded materials so it is difficult to directly compare them. When comparing them to one another the rule still applies

(the higher the thermal conductivity of the material the better the material performance) (Table 9 - 15 - Table 9 - 16).

Another point to note is EOS DirectSteel 20µm contained two materials iron and nickel with thermal conductivities of 80.4W/mk and 90.0W/mk respectively. However, the material itself had a thermal conductivity of only ≈14W/mk. Microscopy revealed that the material contained large inclusions / porosity and poor wetting between the layers, which was the probable cause of its poor thermal conductivity.

Micrographs also showed that Amdry 790 contained porosity, which may have reduced the material's thermal conductivity.

No clear correlations were evident for material 1, material 2 or the thermal conductivity differences between the materials (Table 9 - 14 - Table 9 - 16).

Material	Thermal Conductivity (W/mk)				Fatigue Performance
	Composite Material	Material 1	Material 2	Difference	
EOS DirectSteel 20µm	13.93	Iron - 80.4	Nickel - 90.0	10.4	<div>Worst</div> <div>↓</div> <div>Best</div>
Vertical laminate	21.64	H13 - 25.82	Amdry - 25.78	0.04	
Metalcopy Janalloy	24.61	316 SS - 16.3	Ag alloy - 65.15	48.85	
Amdry 790	25.78	Nickel - 90.9	Silicon - 150	59.1	
Metalcopy 5507	27.17	316 SS - 16.3	Ag alloy - 62.66	46.36	
Metalcopy Cu	32.18	316 SS - 16.3	Cu alloy - 230.54	214.24	
Horizontal RapidSteel 2.0	34.34	316 SS - 16.3	Phosphor Bronze - 50	33.7	
H13		24.3			

Table 9 - 14 Initial material performance versus thermal conductivity

Material	Thermal Conductivity (W/mk)				Fatigue Performance
	Composite Material	Material 1	Material 2	Difference	
Vertical laminate	21.64	H13 - 25.82	Amdry - 25.78	0.04	<div>Worst</div> <div>↓</div> <div>Best</div>
Metalcopy Janalloy	24.61	316 SS - 16.3	Ag alloy - 65.15	48.85	
EOS DirectSteel 20µm	13.93	Iron - 80.4	Nickel - 90.0	10.4	
Metalcopy 5507	27.17	316 SS - 16.3	Ag alloy - 62.66	46.36	
Metalcopy Cu	32.18	316 SS - 16.3	Cu alloy - 230.54	214.24	
Horizontal RapidSteel 2.0	34.34	316 SS - 16.3	Phosphor Bronze - 50	33.7	
Amdry 790	25.78	Nickel - 90.9	Silicon - 150	59.1	
H13		24.3			

Table 9 - 15 Final material performance versus thermal conductivity

Material	Thermal Conductivity (W/mk)				Fatigue Performance
	Composite Material	Material 1	Material 2	Difference	
Vertical laminate	21.64	H13 - 25.82	Amdry - 25.78	0.04	<div>Worst</div> <div>↓</div> <div>Best</div>
EOS DirectSteel 20µm	13.93	Iron - 80.4	Nickel - 90.0	10.4	
Metalcopy Janalloy	24.61	316 SS - 16.3	Ag alloy - 65.15	48.85	
Metalcopy 5507	27.17	316 SS - 16.3	Ag alloy - 62.66	46.36	
Metalcopy Cu	32.18	316 SS - 16.3	Cu alloy - 230.54	214.24	
Amdry 790	25.78	Nickel - 90.9	Silicon - 150	59.1	
Horizontal RapidSteel 2.0	34.34	316 SS - 16.3	Phosphor Bronze - 50	33.7	
H13		24.3			

Table 9 - 16 Overall material performance versus thermal conductivity

9.5.4 The Effect of the Material Properties and Thermal Fatigue Properties

9.5.4.1 Crystal Structure

The bonding materials had the same crystal structure, face centre cubic (Shackelford and Alexander, 2001 and Gale and Totemeier 2004), and therefore, the same slip planes. This meant that the bonding material crystal structure of the materials chosen was not a factor in fatigue performance.

9.5.4.2 Thermal Expansion

A material with low thermal expansion is generally considered to have better thermal fatigue resistance. The thermal expansion data shown in Table 9 - 17 to Table 9 - 19 shows that no definite correlations can be drawn.

The Vertical laminate specimen was made from two materials laminated together with different coefficients of expansion (the coefficient of linear thermal expansion of nickel is $13.3\mu\text{m/m}^\circ\text{C}$ and H13 $1.04\mu\text{m/m}^\circ\text{C}$). It is likely this would induce expansion and contraction at different rates resulting in stress formation in the material. The braze also had a nickel rich centre through which the crack propagation occurred.

Material	Thermal Expansion m/m/°C			Fatigue Performance
	Material 1	Material 2	Difference	
EOS DirectSteel 20µm	Iron - 11.8×10^{-6}	Nickel - 13.3×10^{-6}	1.5×10^{-6}	Worst ↓ Best
Vertical laminate	H13 - 1.04×10^{-6}	Nickel - 13.3×10^{-6}	12.26×10^{-6}	
Metalcopy Janalloy	316 SS - 16.5×10^{-6}	Silver - 19.68×10^{-6}	3.18×10^{-6}	
Amdry 790	Nickel - 13.3×10^{-6}	Silicon - 4.2×10^{-6}	9.1×10^{-6}	
Metalcopy 5507	316 SS - 16.5×10^{-6}	Silver - 19.68×10^{-6}	3.18×10^{-6}	
Metalcopy Cu	316 SS - 16.5×10^{-6}	Copper - 16.5×10^{-6}	0	
Horizontal RapidSteel 2.0	316 SS - 16.5×10^{-6}	Phosphor Bronze - 18.4×10^{-6}	1.9×10^{-6}	
H13	1.04×10^{-6}			

Table 9 - 17 Initial material performance versus thermal expansion

Material	Thermal Expansion m/m/°C			Fatigue Performance
	Material 1	Material 2	Difference	
Vertical laminate	H13 - 1.04×10^{-6}	Nickel - 13.3×10^{-6}	12.26×10^{-6}	Worst ↓ Best
Metalcopy Janalloy	316 SS - 16.5×10^{-6}	Silver - 19.68×10^{-6}	3.18×10^{-6}	
EOS DirectSteel 20µm	Iron - 11.8×10^{-6}	Nickel - 13.3×10^{-6}	1.5×10^{-6}	
Metalcopy 5507	316 SS - 16.5×10^{-6}	Silver - 19.68×10^{-6}	3.18×10^{-6}	
Metalcopy Cu	316 SS - 16.5×10^{-6}	Copper - 16.5×10^{-6}	0	
Horizontal RapidSteel 2.0	316 SS - 16.5×10^{-6}	Phosphor Bronze - 18.4×10^{-6}	1.9×10^{-6}	
Amdry 790	Nickel - 13.3×10^{-6}	Silicon - 4.2×10^{-6}	9.1×10^{-6}	
H13	1.04×10^{-6}			

Table 9 - 18 Final material performance versus thermal expansion

Material	Thermal Expansion m/m/°C			Fatigue Performance
	Material 1	Material 2	Difference	
Vertical laminate	H13 - 1.04×10^{-6}	Nickel - 13.3×10^{-6}	12.26×10^{-6}	Worst ↓ Best
EOS DirectSteel 20µm	Iron - 11.8×10^{-6}	Nickel - 13.3×10^{-6}	1.5×10^{-6}	
Metalcopy Janalloy	316 SS - 16.5×10^{-6}	Silver - 19.68×10^{-6}	3.18×10^{-6}	
Metalcopy 5507	316 SS - 16.5×10^{-6}	Silver - 19.68×10^{-6}	3.18×10^{-6}	
Metalcopy Cu	316 SS - 16.5×10^{-6}	Copper - 16.5×10^{-6}	0	
Amdry 790	Nickel - 13.3×10^{-6}	Silicon - 4.2×10^{-6}	9.1×10^{-6}	
Horizontal RapidSteel 2.0	316 SS - 16.5×10^{-6}	Phosphor Bronze - 18.4×10^{-6}	1.9×10^{-6}	
H13	1.04×10^{-6}			

Table 9 - 19 Overall material performance versus thermal expansion

9.5.4.3 Modulus of Elasticity

The thermal fatigue resistance of a material is considered to increase if the material has a low modulus of elasticity. The modulus of elasticity investigated were bulk, rigidity and Young's.

Table 9 - 20 - Table 9 - 22 shows the material moduli of elasticity, at first glance there does not appear to be any correlations. However, when comparing Metalcopy Janalloy, Metalcopy 5507, Metalcopy Cu and RapidSteel 2.0 materials some correlations appear.

- 1) The thermal fatigue resistance increases as material 2 rigidity modulus increases
- 2) The thermal fatigue resistance increases as rigidity modulus difference decreases

Material	Modulus of Elasticity (GPa)											Fatigue Performance	
									Difference				
	Material 1	Bulk	Rigidity	Youngs	Material 2	Bulk	Rigidity	Youngs	Bulk	Rigidity	Youngs		
EOS DirectSteel 20µm	Iron	170	82	211	Nickel	180	76	200	10	6	11	Worst 	

Table 9 - 20 Initial material performance versus modulus of elasticity

Material	Modulus of Elasticity (GPa)											Fatigue Performance
									Difference			
	Material 1	Bulk	Rigidity	Youngs	Material 2	Bulk	Rigidity	Youngs	Bulk	Rigidity	Youngs	
Vertical laminate	H13	140	81	210	Nickel	180	76	200	40	5	10	Worst

Table 9 - 21 Final material performance versus modulus of elasticity

Material	Modulus of Elasticity (GPa)											Fatigue Performance
									Difference			
	Material 1	Bulk	Rigidity	Youngs	Material 2	Bulk	Rigidity	Youngs	Bulk	Rigidity	Youngs	
Vertical laminate	H13	140	81	210	Nickel	180	76	200	40	5	10	Worst <

Table 9 - 22 Overall material performance versus modulus of elasticity

9.5.4.4 Elongation

The percentage elongation at break of the bonding materials played a part in determining fatigue resistance. Generally, the higher the percentage elongation of material 2, the better the thermal fatigue resistance (Table 9 - 23 - Table 9 - 25).

Material	Elongation (%)			Fatigue Performance
	Material 1	Material 2	Difference	
EOS DirectSteel 20µm	Iron - ??	Nickel - 30 - 40	??	Worst ↓ Best
Vertical laminate	H13 - 9 - 10	Nickel - 30 - 40	20 - 30	
Metalcopy Janalloy	316 SS - 40	Silver - 50	10	
Amdry 790	Nickel - 30 - 40	Silicon - ??	??	
Metalcopy 5507	316 SS - 40	Silver - 50	10	
Metalcopy Cu	316 SS - 40	Copper - 60	20	
Horizontal RapidSteel 2.0	316 SS - 40	Phosphor Bronze - 70	30	
H13	9 - 10			

Table 9 - 23 Initial material performance versus elongation

Material	Elongation (%)			Fatigue Performance
	Material 1	Material 2	Difference	
Vertical laminate	H13 - 10	Nickel - 30 - 40	20 - 30	Worst ↓ Best
Metalcopy Janalloy	316 SS - 40	Silver - 50	10	
EOS DirectSteel 20µm	Iron - ??	Nickel - 30 - 40	??	
Metalcopy 5507	316 SS - 40	Silver - 50	10	
Metalcopy Cu	316 SS - 40	Copper - 60	20	
Horizontal RapidSteel 2.0	316 SS - 40	Phosphor Bronze - 70	30	
Amdry 790	Nickel - 30 - 40	Silicon - ??	??	
H13	9 - 10			

Table 9 - 24 Final material performance versus elongation

Material	Elongation (%)			Fatigue Performance
	Material 1	Material 2	Difference	
Vertical laminate	H13 - 10	Nickel - 30 - 40	20 - 30	Worst ↓ Best
EOS DirectSteel 20µm	Iron - ??	Nickel - 30 - 40	??	
Metalcopy Janalloy	316 SS - 40	Silver - 50	10	
Metalcopy 5507	316 SS - 40	Silver - 50	10	
Metalcopy Cu	316 SS - 40	Copper - 60	20	
Amdry 790	Nickel - 30 - 40	Silicon - ??	??	
Horizontal RapidSteel 2.0	316 SS - 40	Phosphor Bronze - 70	30	
H13	9 - 10			

Table 9 - 25 Overall material performance versus elongation

9.5.4.5 Ultimate Tensile Strength

A correlation is evident for Metalcopy Janalloy, Metalcopy 5507, Metalcopy Cu and RapidSteel 2.0 materials. As the ultimate tensile strength of material 2 (bonding material) increased, the resistance to thermal fatigue improved (Table 9 - 26 - Table 9 - 28).

No correlations were apparent for EOS DirectSteel 20µm, Vertical laminate and Amdry 790.

Material	Ultimate Tensile Strength (MPa)			Fatigue Performance
	Material 1	Material 2	Difference	
EOS DirectSteel 20µm	Iron - 180 - 210	Nickel - 400 - 600	220 - 390	Worst ↓ Best
Vertical laminate	H13 - 1990	Nickel - 400 - 600	1590 - 1390	
Metalcopy Janalloy	316 SS - 515	Silver - 140	375	
Amdry 790	Nickel - 400 - 660	Silicon - ??	??	
Metalcopy 5507	316 SS - 515	Silver - 140	375	
Metalcopy Cu	316 SS - 515	Copper - 210	305	
Horizontal RapidSteel 2.0	316 SS - 515	Phosphor Bronze - 455 - 1014	60 - 499	
H13	1990			

Table 9 - 26 Initial material performance versus ultimate tensile strength

Material	Ultimate Tensile Strength (MPa)			Fatigue Performance
	Material 1	Material 2	Difference	
Vertical laminate	H13 - 1990	Nickel - 400 - 600	1590 - 1390	Worst ↓ Best
Metalcopy Janalloy	316 SS - 515	Silver - 140	375	
EOS DirectSteel 20µm	Iron - 180 - 210	Nickel - 400 - 600	220 - 390	
Metalcopy 5507	316 SS - 515	Silver - 140	375	
Metalcopy Cu	316 SS - 515	Copper - 210	305	
Horizontal RapidSteel 2.0	316 SS - 515	Phosphor Bronze - 455 - 1014	60 - 499	
Amdry 790	Nickel - 400 - 660	Silicon - ??	??	
H13	1990			

Table 9 - 27 Final material performance versus ultimate tensile strength

Material	Ultimate Tensile Strength (MPa)			Fatigue Performance
	Material 1	Material 2	Difference	
Vertical laminate	H13 - 1990	Nickel - 400 - 600	1590 - 1390	Worst ↓ Best
EOS DirectSteel 20µm	Iron - 180 - 210	Nickel - 400 - 600	220 - 390	
Metalcopy Janalloy	316 SS - 515	Silver - 140	375	
Metalcopy 5507	316 SS - 515	Silver - 140	375	
Metalcopy Cu	316 SS - 515	Copper - 210	305	
Amdry 790	Nickel - 400 - 660	Silicon - ??	??	
Horizontal RapidSteel 2.0	316 SS - 515	Phosphor Bronze - 455 - 1014	60 - 499	
H13	1990			

Table 9 - 28 Overall material performance versus ultimate tensile strength

9.5.4.6 Yield Strength

A high yield stress is considered advantageous to resist thermal fatigue. A potential correlation may exist between yield stress and thermal fatigue resistance; however, there is not enough data to validate this (Table 9 - 29 - Table 9 - 31). Further testing would be required to determine this for certain. In addition, no material data could be sourced for the yield strength of silver or silicon so no correlations could be made.

Material	Yield Strength (MPa)			Fatigue Performance
	Material 1	Material 2	Difference	
EOS DirectSteel 20µm	Iron - 120 - 150	Nickel - 150 - 480	30 - 330	Worst ↓ Best
Vertical laminate	H13 - 1650	Nickel - 150 - 480	1500 - 1170	
Metalcopy Janalloy	316 SS - 205	Silver - ??	??	
Amdry 790	Nickel - 150 - 480	Silicon - ??	??	
Metalcopy 5507	316 SS - 205	Silver - ??	??	
Metalcopy Cu	316 SS - 205	Copper - 33.3	172	
Horizontal RapidSteel 2.0	316 SS - 205	Phosphor Bronze - 193	12	
H13	1650			

Table 9 - 29 Initial material performance versus yield strength

Material	Yield Strength (MPa)			Fatigue Performance
	Material 1	Material 2	Difference	
Vertical laminate	H13 - 1650	Nickel - 150 - 480	1500 - 1170	Worst ↓ Best
Metalcopy Janalloy	316 SS - 205	Silver - ??	??	
EOS DirectSteel 20µm	Iron - 120 - 150	Nickel - 150 - 480	30 - 330	
Metalcopy 5507	316 SS - 205	Silver - ??	??	
Metalcopy Cu	316 SS - 205	Copper - 33.3	172	
Horizontal RapidSteel 2.0	316 SS - 205	Phosphor Bronze - 193	12	
Amdry 790	Nickel - 150 - 480	Silicon - ??	??	
H13	1650			

Table 9 - 30 Final material performance versus yield strength

Material	Yield Strength (MPa)			Fatigue Performance
	Material 1	Material 2	Difference	
Vertical laminate	H13 - 1650	Nickel - 150 - 480	1500 - 1170	Worst ↓ Best
EOS DirectSteel 20µm	Iron - 120 - 150	Nickel - 150 - 480	30 - 330	
Metalcopy Janalloy	316 SS - 205	Silver - ??	??	
Metalcopy 5507	316 SS - 205	Silver - ??	??	
Metalcopy Cu	316 SS - 205	Copper - 33.3	172	
Amdry 790	Nickel - 150 - 480	Silicon - ??	??	
Horizontal RapidSteel 2.0	316 SS - 205	Phosphor Bronze - 193	12	
H13	1650			

Table 9 - 31 Overall material performance versus yield strength

9.5.4.7 Poisson's Ratio

Table 9 - 32 - Table 9 - 34 shows the thermal fatigue data and the material's Poisson's ratio.

There appears to be a general trend for Metalcopy Janalloy, Metalcopy 5507, Metalcopy Cu and RapidSteel 2.0 materials. As material 2 Poisson's ratio decreases the thermal fatigue performance increases. As the Poisson's ratio difference decreases the thermal fatigue resistance increases.

No conclusions could be drawn for EOS DirectSteel 20µm, Vertical laminate and Amdry 790.

Material	Poisson's Ratio			Fatigue Performance
	Material 1	Material 2	Difference	
EOS DirectSteel 20µm	Iron - 0.291	Nickel - 0.31	0.019	Worst ↓ Best
Vertical laminate	H13 - 0.3	Nickel - 0.31	0.01	
Metalcopy Janalloy	316 SS - 0.27 - 0.3	Silver - 0.37	0.1 - 0.07	
Amdry 790	Nickel - 0.31	Silicon - 0.42	0.11	
Metalcopy 5507	316 SS - 0.27 - 0.3	Silver - 0.37	0.1 - 0.07	
Metalcopy Cu	316 SS - 0.27 - 0.3	Copper - 0.343	0.073 - 0.043	
Horizontal RapidSteel 2.0	316 SS - 0.27 - 0.3	Phosphor Bronze - 0.34	0.07 - 0.04	
H13	0.3			

Table 9 - 32 Initial material performance versus poisson's ratio

Material	Poisson's Ratio			Fatigue Performance
	Material 1	Material 2	Difference	
Vertical laminate	H13 - 0.3	Nickel - 0.31	0.01	Worst ↓ Best
Metalcopy Janalloy	316 SS - 0.27 - 0.3	Silver - 0.37	0.1 - 0.07	
EOS DirectSteel 20µm	Iron - 0.291	Nickel - 0.31	0.019	
Metalcopy 5507	316 SS - 0.27 - 0.3	Silver - 0.37	0.1 - 0.07	
Metalcopy Cu	316 SS - 0.27 - 0.3	Copper - 0.343	0.073 - 0.043	
Horizontal RapidSteel 2.0	316 SS - 0.27 - 0.3	Phosphor Bronze - 0.34	0.07 - 0.04	
Amdry 790	Nickel - 0.31	Silicon - 0.42	0.11	
H13	0.3			

Table 9 - 33 Final material performance versus poisson's ratio

Material	Poisson's Ratio			Fatigue Performance
	Material 1	Material 2	Difference	
Vertical laminate	H13 - 0.3	Nickel - 0.31	0.01	Worst ↓ Best
EOS DirectSteel 20µm	Iron - 0.291	Nickel - 0.31	0.019	
Metalcopy Janalloy	316 SS - 0.27 - 0.3	Silver - 0.37	0.1 - 0.07	
Metalcopy 5507	316 SS - 0.27 - 0.3	Silver - 0.37	0.1 - 0.07	
Metalcopy Cu	316 SS - 0.27 - 0.3	Copper - 0.343	0.073 - 0.043	
Amdry 790	Nickel - 0.31	Silicon - 0.42	0.11	
Horizontal RapidSteel 2.0	316 SS - 0.27 - 0.3	Phosphor Bronze - 0.34	0.07 - 0.04	
H13	0.3			

Table 9 - 34 Overall material performance versus poisson's ratio

9.5.5 The Effect of Material Properties on Fatigue Resistance Overview

The results show that there are many factors (mechanical properties and material microstructure) which influence a material's thermal fatigue performance.

Since the materials are manufactured by different methods and have different structures it is difficult to do a direct comparison of the material's thermal fatigue performance and the material properties. It must also be noted that the list of desirable material properties obtained from the literature search are for alloy materials, no such list was able to be drawn for composite materials.

9.5.5.1 Category 1 H13 Tool Steel

As expected the H13 reference material showed superior thermal fatigue resistance when compared to the rapid tooling materials tested. The reason for this is that the material has been specifically designed for such an application.

9.5.5.2 Metalcopy Janalloy, Metalcopy 5507, Metalcopy Cu and RapidSteel 2.0 Materials

In the case of Category 2 materials it is possible to conclude important information when viewing the material properties. It was, however, clear from the research that the mechanical properties of the bonding material were key in the performance of the materials.

The literature showed (ASM, 2001, Bendyk, et.al., 1970, Novovic et.al., 2004, Schwam, et.al., 2004, Simons, 1972, Sjoström and Bergström 2004) that higher hardness leads to better thermal fatigue resistance and this has also been seen in this work.

A high density material also performs better (Rytz, 1996), however, no conclusions could be drawn since the densities were similar to one another. What does seem important to improve thermal fatigue resistance is a low difference in density between the steel powder and the infiltrant material.

Askeland, 1994, Norström, 1982, Olive, 2005, Schwam et.al., 2004, Weroński and Hejwoski, 1991 and Worbye, 1985 state that a high thermal conductivity improves fatigue performance and this work shows this to be true. However, a material constructed of dissimilar metals and different thermal conductivities it likely to induce internal / localised stress in the material (Schwam, et.al., 2004).

Norström, 1982, Schwam et.al., 2004, Weroński and Hejwoski, 1991 and Worbye, 1985 state that a low thermal expansion is considered beneficial, however, the results of this work are inconclusive.

Askeland, 1994, Norström, 1982, Schwam et.al., 2004 Weroński and Hejwoski, 1991 and Worbye, 1985 state that a low Young's modulus is advantageous. The bonding materials all had very low modulus when compared to the steel powder and it was evident that if the bonding material had a higher modulus it had better fatigue resistance, however, this is a contradiction, but it transpired that by reducing the modulus difference between the bonding material and the powder material increases fatigue resistance.

Bendyk, et.al., 1970, Norström, 1982, Norström, 1989, Weroński and Hejwoski, 1991, Simons, 1972, Sjoström and Bergström 2004, Worbye, 1985 stated that a high percentage elongation improves thermal fatigue resistance and the work found this to be the case for the bonding material.

Askeland, 1994, Bendyk, et.al., 1970, Norström, 1982, Weroński and Hejwoski, 1991, Simons, 1972, Sjoström and Bergström 2004, and Worbye, 1985 state that a high ultimate tensile strength improves fatigue performance and this work clearly shows that as the higher the bonding material UTS the better the thermal fatigue resistance (Table 9 - 26 - 9 - 28).

Badger Metals, 2001, Worbye, 1985, Schwam, et.al., 2004 state that is beneficial for a material to have a high yield strength. No conclusions could be drawn from this work.

Although no literature was found to suggest that Poisson's ratio has an affect on thermal fatigue resistance the results of the work showed that if the bonding material had a lower Poisson's ratio it had improved thermal fatigue resistance. A lower bonding material Poisson's ratio also reduces the difference between it and the powder material increasing the composites fatigue resistance.

The research has shown that several conclusions can be drawn for category 2 composite materials. It also showed it is beneficial to reduce the difference or have similar material properties for the powder and bonding material.

9.5.5.3 EOS DirectSteel 20 μ m, Vertical Laminate and Amdry 790 Materials

Due to the different structure of these materials and limited material data is proved difficult to compare the thermal fatigue performance against material properties. Few conclusions could be drawn.

Askeland, 1994, Norström, 1982, Olive, 2005, Schwam et.al., 2004, Weroński and Hejwoski, 1991 and Worbye, 1985 state that a high thermal conductivity improves fatigue resistance and this work shows this to be true. However, a material constructed of dissimilar metals and different thermal conductivities it likely to induce internal / localised stress in the material (Schwam, et.al., 2004).

Although no literature was found to suggest that Poisson's ratio has an affect on thermal fatigue resistance the results of the work showed that if the bonding material had a lower Poisson's ratio it had improved thermal fatigue resistance. A lower bonding material Poisson's ratio also reduces the difference between it and the materials increasing fatigue resistance.

It is clear that further material tests would need to be conducted to enable conclusions for EOS DirectSteel 20 μ m, Vertical Laminate and Amdry 790 Materials to be drawn.

9.6 Methods to Improve Thermal Fatigue Resistance

Using the information from this research and the information gained from the literature search the thermal fatigue resistance of rapid tooling materials that are composites may be improved using the following general guidelines.

- Reduce porosity / inclusions to decrease potential crack initiation sites
- Avoid having a element rich phase in the structure
- Avoid having materials with carbides or element rich phase at the powder bonding material interface to reduce crack initiation

- Ensure good wetting and bonding of materials to reduce potential crack initiation sites and propagation routes
- Avoid bonding materials that cause embrittlement

The research has shown, that all the rapid tooling materials have poor thermal fatigue characteristics, when compared to H13 tool steel because they contain multiple materials, have poor material microstructure and poor material properties. However, Metacopy 5507 and Metacopy Cu did not initiate cracking until 3,000 cycles and it may be possible to use these materials for prototype die casting tooling. Moreover, Horizontal RapidSteel 2.0 did not initiate cracking until 50,000 cycles and it may be used for prototype and low volume die cast tooling.

Chapter 10: Conclusions

This work has shown clearly the temperature at the surface of a typical aluminium pressure die casting tool and revealed the surface heats up to 400°C - 450°C and cools to 150°C - 200°C.

A new test method has been established enabling a materials thermal fatigue resistance to be identified. The test is robust, reliable and versatile. It has a large operating temperature range, (25°C - 1200°C), alternative heating and cooling mediums can be used. The cycle times and dwell times are adjustable.

An exact simulation of the aluminium die casting process could not be achieved using this method due to insufficient heating rate. However, materials can be compared and an approximate fatigue life for aluminium pressure die casting determined.

It was possible to determine how many thermal cycles a material could be subjected to prior to crack initiation and to determine the crack growth properties. Post thermal fatigue examination was able to determine the mechanism of crack initiation and propagation.

For the Metalcopy materials cracks initiated at the interface between the steel powder and the matrix, the material also had chrome and molybdenum rich areas (large carbides) in the steel and at the powder / infiltrant interface that may have caused a stress raiser. The cracks propagated from one interface to another through the matrix and the material was manufacture with porosity and inclusions allowed ease of crack initiation and propagation. Hence, the thermal fatigue resistance of the Metalcopy materials was relatively poor.

RapidSteel 2.0 was the best tooling material at resisting thermal fatigue as it had better powder / bonding material wetting than the Metalcopy materials but it did contain some porosity. There were large carbide rich areas at the powder / bonding material interface and the cracks propagated down the powder / bonding material interface and through the bonding material taking the easiest route from one interface to another. Oxide was also visible at the crack edges.

Amdry 790 resisted thermal fatigue in a similar manner to RapidSteel 2.0 but differed to the other materials in that it was a braze and not a bonded material. It was unclear how the cracks initiated, however, the presence of sulphur indicated embrittlement and could cause the observed micro cracking in the nickel. The cracks propagated from the micro cracks down thin vanes of nickel (grain boundary de-cohesion).

This material suffered from internal stresses possibly due to different thermal coefficients of expansion of the component materials. The presence of a rich phase at the centre of the bonding material is the likely cause of crack initiation and propagation through the rich phase. The presence of porosity in the bonding material increased crack initiation sites and reduced thermal fatigue resistance.

A weld like structure with columnar grains was observed with inclusions that would increase crack initiation sites and reduce thermal fatigue resistance. Poor wetting between layers which would also increase crack initiation sites and reduce thermal fatigue resistance. Cracks propagated at 90° to the build orientation and down (or along) the columnar grain structure (de-cohesion along the grain boundary).

It is important to note, before using the results and manufacturing a die-casting tool from any of the rapid tooling materials tested, that aluminium has an affinity for the bonding materials. It is likely that adhesion, wear, erosion will result from its use in die casting tooling. The thermal fatigue resistance will reduce because of the increased potential of crack initiation sites as observed in several tooling case studies conducted during the course of this work (Gibbons et.al. 2003, Harris et.al., 2003^a, Harris et.al 2003^b, Harris et.al 2004, Norwood, 2001, Norwood et.al., 2001, Norwood 2002^b, Norwood et.al., 2004).

The structure, alloying and material properties were found to have a big influence on how a material will behave when subjected to thermal fatigue.

From this work material properties clearly had an effect on the thermal fatigue performance. It has been shown that the hardness, UTS, elongation to break and thermal conductivity should be as high as possible. This work has shown for the first time the importance of Poisson's ratio and the difference of values between the infiltrant materials and the powders, also a similar situation is apparent for density. The key finding is reducing the difference between the values for the two materials improves fatigue performance. Large carbides, porosity, inclusions, poor wetting and element rich phases have been shown to provide crack initiation sites.

From the data obtained in this research it was clear that two materials performed better than the majority studied, namely Horizontal RapidSteel 2.0 and Amdry 790. The best in terms of resistance to crack initiation was Horizontal RapidSteel 2.0 and the best in terms of crack growth rate was Amdry 790. However, Amdry 790 is a braze material and was predominantly tested to understand how the braze behaved independently of a laminate structure (not bonded to form a H13 laminate structure). The research has shown Horizontal RapidSteel 2.0 to be the best material for resisting thermal fatigue.

Chapter 11: Recommendations for Further Work and the Contribution of this Work to the Body of Knowledge

11.1 Recommendations for Further Work

It would be useful to understand how different thermal cycles affect the performance of materials in order to establish their limitations and to predict their life expectancy in tooling applications. In addition, developing stress versus number of cycles curves (S – N curves) for the materials would be useful to enable finite element analysis to be conducted for life time predictions with different geometries and at varying stress levels.

This work identified that the mode of crack propagation in the EOS DirectSteel 20 μ m was at 90° to the build orientation. It would be of use to determine how altering the build orientation affects the crack propagation.

Metalcopy materials and Amdry 790 showed inconsistency in their microstructure, indicating that their manufacture was not consistent. Research into their manufacture and how it affects the microstructure and material properties will be necessary to improve the performance of the materials. Additionally, infiltration techniques need to be researched to reduce defects, such as inclusions and porosity.

Due to time restraints it was not possible to create a statistical / modelling approach to determine the thermal fatigue resistance of the materials using the materials mechanical properties of the materials. Creating such a model would be very advantageous.

An area of this research was concerned with bonded H13 laminates but research of different brazes, braze thickness or bonding methods could lead to improved thermal fatigue. Selecting a braze with the desired mechanical properties discussed in chapter 9) and similar thermal expansion properties to the material being bonded may improve fatigue life. In turn, it is unknown how varying the braze thickness will affect thermal fatigue resistance. Improving the brazing process may also reduce porosity and reduce crack initiation sites.

Thermal fatigue is only one aspect of aluminium pressure die-casting. Other aspects need to be investigated such as chemical attack, i.e. how aluminium reacts with rapid prototype materials; impact and how constant loading and unloading affect the die materials (die opening and closing).

It is necessary to conduct bulk elastic modulus testing on phosphor bronze to confirm that the thermal fatigue resistance of a material increases as bulk modulus increases.

It would also be advantageous to test the material mechanical properties, to gain an overall picture of how this affects thermal fatigue resistance.

11.2 Contribution to the Body of Knowledge

The knowledge gained from this research has enabled the suitability of currently available rapid tooling metallic materials for high temperature processes to be determined. It has also created a platform for thermal fatigue testing from which new materials may be developed and their performance compared.

The contribution has also been the generation of data to provide an understanding of temperatures in dies; it has provided a new thermal fatigue test method allowing comparisons between materials. The results have shown how thermal fatigue occurs in rapid tooling materials, and established guidelines on how a material may perform. In turn, the guide lines show how the rapid tooling materials should be improved in order to increase thermal fatigue resistance.

References

- 3D Systems, (2004), About 3D Systems, accessed 16-04-04, <http://www.3dsystems.com/company/index.asp>, 2004
- Accufusion (2006), accessed 25-05-06, <http://www.accufusion.com/> Accufusion Inc., 800 Collip Circle, London, Ontario, Canada, N6G 4X8, Tel: 519-430-7065
- Acheson Colloids Company, (2004), DeltaCast 333 release 3, Prince Rock Plymouth, PL4 0SP, UK, <http://www.achesonindustries.com/index.asp>, 2004
- Agarwala, M., Bourell, D., Beaman, J., Marcus, H., Barlow, J., (1995^a), Post-Processing of Selective Laser Sintered Metal Parts, Rapid Prototyping Journal, Volume 1, Number 2, 1995, pp 36 - 44, ISSN 1355 - 2546
- Agarwala, M., Bourell, D., Beaman, J., Marcus, H., Barlow, J.W., (1995^b), Direct Selective Laser Sintering of Metals, Rapid Prototyping Journal, Volume 1, Number 1, 1995, pp 26 - 36, ISSN 1355 - 2456
- Allsop, D.F. and Kennedy, D., (1983), Pressure Diecasting, Part 2: The Technology of the Casting and the Die, Pergamon Press Ltd, Oxford, 1983
- American standards (2006), ANSI e standards store search, accessed 06-02-06, <http://webstore.ansi.org/ansidocstore/find.asp?>, 2006
- Andarifar (2004), Private Correspondence, IPTME Loughborough University, Loughborough, Leicestershire, LE11 3TU, 2004
- Anter Corporation, (2004), 1700 Universal Road, Pittsburgh, PA 15235-3998, Principle Methods of Thermal Conductivity Measurements, accessed 29-09-04, <http://www.anter.com/TN67.htm>
- Anter Corporation, (2005), Principal Methods of Thermal Conductivity Measurements, accessed 27-06-05, <http://www.anter.com/TN67.htm>
- Armstrong Mould Corporation, (2004), RAPID Die-casting, accessed 28-04-04, <http://www.armstrongmold.com/pages/twosteparticle.html>

ASM International, (1975), Metals Handbook, Failure Analysis and Prevention, Volume 10, 8th Edition, 1975, prepared under the direction of the ASM Handbook Committee, Boyer, H.E., editor, American Society for Metals, Metals Park, Ohio, USA, 669/MET

ASM International, (1992), Engineering Properties of Steel, pp 469 - 481, August 1992, American Society for Metals, Metals Park, Ohio, USA M ISBN 0-87170-144-8

ASM International, (1989), Metals Handbook, Volume 17, Non Destructive Evaluation and Quality Control / prepared under the direction, American Society for Metals, Metals Park, Ohio, USA 1989, ISBN 0871700239

ASM international, (1996), Fatigue and Fracture, Volume 19, 1996, American Society for Metals, Metals Park, Ohio, USA, ISBN 0 - 87170 - 385 - 8

ASM International, (1997), Heat Resistant Materials, October 1997, pp 98 - 99, American Society for Metals, Metals Park, Ohio, USA ISBN 0 -87170 - 596 - 6

ASM International, (1998), Metals Handbook, Volume 1, 10th Edition, 1998, pp 793 - 800, American Society for Metals, Metals Park, Ohio, USA, 669/MET

ASM International, (2001), Advanced Material and Processes, Volume 159, Number 12, December 2001, p 83

ASTM B85-03, Standard Specification for Aluminium-Alloy Die Castings, ASTM International, 100 Barr Harbor Drive, West Conshohocken, Pennsylvania, USA. <http://www.astm.org/cgi-bin/SoftCart.exe/index.html E+mystore>

ASTM C177-04, Standard Test Method for Steady-State Heat Flux Measurements and Thermal Transmission Properties by Means of the Guarded-Hot-Plate Apparatus, ASTM International, 100 Barr Harbor Drive, West Conshohocken, Pennsylvania, USA. <http://www.astm.org/cgi-bin/SoftCart.exe/index.html E+mystore>

Askeland, D.R., (1994), The Science and Engineering of Materials Third Edition, PWS Publishing Company, 20 Park Plaza, Boston, MA 02116-4324, ISBN 0-534-93423-4

Avery, now Avery Berkel Ltd, Smethwick, Foundry Lane, Smethwick, Warley, West Midlands, B66 2LP, Tel +44 (0)870 905 0064, Fax +44 (0)870 900 0366, e-mail: info@averyberkel.com, Web site: www.averyberkel.com

Azom, (2006), Stainless Steels - Stainless 316 Properties, Fabrication and Applications, Supplier Data by Aalco, accessed 2005, <http://www.azom.com/details.asp?ArticleID=863>

- Badger Metals, (2001), accessed 24-01-05, <http://www.badgermetal.com/newsletters/1997-01.htm>
- Badger Metals, (2003), accessed 24-01-05, <http://www.badgermetal.com/newsletters/1997-03.htm>
- Bahrami, A., Mousavi, A.S.H., Golozar, M.A., Schamanian, M., Varahram, N., (2004), Effects of Conventional Heat Treatment on Wear Resistance of AISI H13 Tool Steel, International Journal of Wear, Volume 258, 2004, pp 846 - 851, ISSN 0043 - 1648
- Bak, D., (2003), Rapid Prototyping or Rapid Production? 3D Printing Processes Move Industry Towards the Latter, Journal of Assembly Automation, Volume 23, Number 4, 2003, pp 340 – 345, ISSN 0144 - 5154
- Bartley, R., (1992), British and European Aluminium Casting Alloys their Properties and Characteristics, Published by The Association of Light Alloys Refiners, Broadway House, Calthorpe Road, Five Ways, Birmingham, B15 1TN, 1992, pp 82 - 142
- Bassoli, E., Gatto, A., Iuliano, L., Atzeni, E., (2004), Direct Laser Sintering of Metal Parts: Characterisation and Evaluation of Joining Mechanisms, Materials Research Society (MRS) Fall Meeting, Hynes Conference Centre and Sheraton Boston Hotel, Boston, MA, USA, 2004
- Behrendt, U. and Shellabear, M., (1995), The EOS Rapid Prototyping Concept, International Journal of Computers in Industry, Volume 28, 1995, pp 57 - 61, ISSN 0166 - 3615/95
- Bendyk, J.C., Maracz, O.J., Wallace, J.F., (1970), Thermal Fatigue Behaviour of Die Materials for Aluminium Die Casting, The 6th SDCE International Die Casting Congress, Cleveland, Ohio, Paper Number 111, November 16th - 19th 1970, pp 1 - 20
- Bernard, A., Delplace, J.C., Perry, N., Gabriel, S., (2003), Integration of CAD and Rapid Manufacturing for Sand Casting Optimisation, Rapid Prototyping Journal, Volume 9, Number 5, 2003, pp 327 - 333, ISSN 1355 - 2546
- Bocking, C., Jacobson, D.M., Sangha S.P.S., Dickens, P.M., Soar, R., (1997), The Production of Large Rapid Prototype Tools using Layer Manufacturing Technology, The GEC Journal of Technology, Volume 14, Number 2, 1997, pp 110 - 114
- Bohler Special Steels, European Business Park, Taylors Lane, Oldbury, West Midlands, B69 2BN, United Kingdom, Tel +44 121 552 2575, Fax +44 121 552 0023

Bounds, S., (2000), An Experimental and Numerical Investigation into Thermal Behaviour of the Pressure Die Casting Process, Journal of Manufacturing Science and Engineering, Transactions of the ASME, Volume 122, 2000, pp 90 - 99

Bryden, B.G. and Pashby, I.R., (1999), Sequential Laminated Tooling, Joined by Brazing for Injection Moulding, Rapid Prototyping Journal, Volume 5, Number 2, 1999, pp 89 - 93, ISSN 1355 - 2546

Bryden, B.G., Pashby, I.R., Wimpenny, D.I., Adams, C., (2000), Laminated Steel Tooling in the Aerospace Industry, Journal of Materials and Design, Volume 21, 2000, pp 403 - 408.

Bryden, B.G., Wimpenny, D.I., Pashby, I.R., (2001), Manufacturing Production Tooling Using Metal Laminations, Rapid Prototyping Journal, Volume 7, Number 1, 2001, pp 52 - 59, ISSN 1355 - 2546

Bryden, B.G. and Pashby, I.R., (2001), Hot Platen Brazing to Produce Laminated Steel Tooling, Journal of Materials Processing Technology, Volume 110, 2001, pp 206 - 210

BS 874 - 2.1, (1986), Methods for Determining Thermal Insulating Properties, Tests for Thermal Conductivity and Related Properties. Guarded Hot-Plate Method, British Standards Institution, 389 Chiswick High Road, London, W44AL, United Kingdom, <http://www.bsi-global.com/index.xalter>

BS 874 - 3.1, (1987), Methods for Determining Thermal Insulating Properties. Tests for Thermal Transmittance and Conductance. Guarded Hot-Box Method, British Standards Institution, 389 Chiswick High Road, London, W44AL, United Kingdom, <http://www.bsi-global.com/index.xalter>

BS 1490, (1998), Specification for Aluminium and Aluminium Alloy Ingots and Castings for General Engineering Purposes, British Standards Institution, 389 Chiswick High Road, London, W44AL, United Kingdom, <http://www.bsi-global.com/index.xalter>

BS EN 60584-1, (1995), Thermocouple Voltages Conversion, British Standards Institution, 389 Chiswick High Road, London, W44AL, United Kingdom, <http://www.bsi-global.com/index.xalter>

Buehler, Saturn Building, 101 Lockhurst Lane, Coventry, CV6 5SF, Tel 024 7658 2158 Fax 024 7658 2159, <http://www.buehler.co.uk/index.asp>

Carbolite, Parsons Lane, Hope, Hope Valley, S33 6RB, England, Tel +44 (0)1433 620011 Fax +44 (0)1433 621198

Castelli, M.G. and Ellis, J.R., (1993), Improved Techniques for Thermo-Mechanical Testing in Support of Deformation Modeling, Thermo Mechanical Fatigue Behavior of Materials, ASTM STP 1186, American Society for Testing and Materials, Philadelphia, 1993, pp 195 - 211

Castle Island's, (2006), Worldwide Guide to Rapid Prototyping, Processes in Early Stages of Commercialization or Under Development, accessed 25-05-06, http://home.att.net/~castleisland/tl_222.htm

CERAM Research Ltd., (2003), Queens Road, Penkhull, Stoke-on-Trent, Staffordshire, ST4 7LQ, UK, <http://www.ceram.com/>

Chang, R., Morris, W.L., Buck, O., (1979), Journal of Scripta Metallurgica et Materialia (Scr. Metall.), Volume 27, 1979, pp 191

Chen, K., Zhao, L., Patnaik, P.C., (2004), The Role of First Principles Calculations in the Development of High Temperature materials for Aerospace Applications, Second International Symposium on Aerospace Materials and Manufacturing: Development and Life Issues - Honouring William Wallace, Hamilton, Ontario, Canada, Session 15, August 22 - 25, 2004

Chen, Z.W., Fraser, D.T., Jahedi, M.Z., (1999), Structures of Intermetallic Phases Formed During Immersion of H13 Tool Steel in an Al-11Si-3Cu Die Casting Alloy Melt, International Journal of Materials and Science Engineering, Volume A260, 1999, pp 188 - 196

Chen, Z.W. and Jahedi, M.Z., (1999), Die Erosion and its Effect on Soldering Formation in High Pressure Die Casting of Aluminum Alloys, Journal of Materials and Design, Volume 20, 1999, pp 303 - 309

Chen, Z.W., (2003), Skin Solidification during High Pressure Die Casting of Al-11Si-2Cu-1Fe Alloy, Journal of Materials Science and Engineering , Volume A348, 2003, pp 145 - 153

Chen, Z.W., (2005), Formation and Progression of Die Soldering During High Pressure Die Casting, International Journal of Materials Science and Engineering, Volume A397, 2005, pp 356 – 369, ISSN 0921 - 5093

Chinese Standard GB/T 15824-1995 (1995), Thermal fatigue testing method for hot die steel (Text of document is in Chinese, ICS 77.040.10

Cincinnati Machine, (2003), A UNOVA Company, 4701 Marburg Ave, Cincinnati, OH, 45209

Clegg, A.J., (1991), Precision Casting Processes, Pergamon Press Plc, New York, 1991, pp 42 - 43, ISSN 0 - 08 - 037878 - 1

- Coffey, J.M., (1980), The Measurement of Crack Length and Shape During Fracture Fatigue, Edited by Beevers, C.J., Engineering Materials Advisory Services, Warley, U.K., 1980, p 345
- Cottrell, A.H. and Hull, D., (1957), Proceedings of the Royal Society, (London), Volume A242, 1957, p 211
- CRDM, 2005, Steel Prototypes, Time Compression Technologies, Volume 13, Issue 1, 2005, p 37
- CSIRO, (2004), Manufacturing and Infrastructure Technology, Cast Tooling, accessed 26-04-04, <http://www.cmit.csiro.au/brochures/tech/casttooling/>
- Cussons Technology Ltd., 102 Great Clowes Street, Manchester, M7 1RH, UK, Tel +44 (0)161 833 0036, Fax +44 (0) 161 834 4688, e-mail sales@cussons.co.uk, <http://www.cussons.co.uk/>
- Dalgarno, K.W. and Stewart, T., (2001), Production Tooling For Polymer Moulding Using the RapidSteel™ Process, Rapid Prototyping Journal, Volume 7, Number 3, 2001, pp 173 - 179, ISSN 1355 - 2546
- Dalgarno, K.W. and Goodridge, R.D., (2004), Compression Testing of Layered Manufactured Metal Parts: The RAPTIA Compression Benchmark, Rapid Prototyping Journal, Volume 10, Number 4, 2004, pp 261 - 264, ISSN 1355 - 2546
- Dandy, A.B., (1995), Tools and Dies a Changing Industry Still Changing, Sheet Metal Industries, Volume 72, 1995, pp 35 - 36
- Danzer, R., Sturm, F., Schindler, A., Zieppnig, W., (1983), Thermal Fatigue Cracks in Pressure Die Casting Dies, Gisserei-Praxis, Volume 19 - 20, 1993, p 287
- Davey, K. and Hinduja, S., (1990), Modelling the Transient Thermal Behaviour of the Pressure Die-Casting Process with BEM, Journal of Applied Mathematical Modelling, Volume 14, Issue 8, 1990, pp 394 - 409
- Davis, J.R., (1995), ASM Speciality Handbook, Tool Materials, ASM International, Materials Park, Ohio, 1995, p 251, ISBN 0 - 87170 - 545 - 1
- DeGarmo, E.P., (1988), Material and Processes in Manufacturing 7th Edition Macmillan Publishing Company, New York, USA, 1988, pp 356 - 375, ISSN 0 - 02 - 328631 - 8
- Delcam, (2004), Small Heath Business Park, Birmingham, B10 OHJ, UK

Dickens, P.M., Stangroom, R., Greul, M., Holmer, B., Hon, K.K.B., Hovtun, R., Neumann, R., Noeken, S., Wimpenny, D., (1995), Conversion of RP Models to Investment Casting, Rapid Prototyping Journal, Volume 1, Number 4, 1995, pp 4 - 11, ISSN 1355 - 2546

Dickens, P.M., (1996), Laminated Tooling for Moulding Polyurethane Parts, Proceedings from the SME Rapid Prototyping and Manufacturing Conference, Dearborn, Michigan, April 22 - 25 1996

Dickens, P.M., (1997), Principles of Design for Laminate Tooling, International Journal Production Research, Volume 35, Number 5, 1997, pp 1349 - 1357

Dickens, P.M., (1999), Rapid Prototyping - Past Present and Future, Journal of the Institution of Engineering Designers, January 1999, pp 12 - 15, ISSN 0013 - 7858

Diecasting Times, (2004), Don't Let the Cracks Show, Die-casting Times, Volume 6, Number 1, December / January 2004, p 13, ISSN 1467 - 0240

Dimov, S.S., Pham, D.T., Lacan, F., Dotchev, K.D., (2001), Rapid Tooling Applications of the Selective Laser Sintering Process, Journal of Assembly and Automation, Volume 21, Number 4, 2001, pp 296 - 302, ISSN 0144 - 5154

DIN 52612, Testing of Thermal Insulating Materials; Determination of Thermal Conductivity by the Guarded Hot Plate Apparatus; Test Procedure and Evaluation, Deutsches Institut für Normung, Burggrafenstrasse 6. DE-10787 Berlin

DTM Corporation, (1999), The Sinterstation System, Guide to Materials: RapidSteel 2.0 DCN, 1999, 8002-10001-001

DTM Corporation, (2004), now 3D Systems, 1611 Headway Circle, Austin, Texas, USA 78754 (see 3D systems)

Dynacast (Alcester) Ltd., (2004), Tything Road, Alcester, Warwickshire, B49 6EW, ENGLAND, <http://www.dynacast.com/>, accessed 13-12-04

Dyson Ltd, Tetbury Hill, Malmesbury, SN16 0RP, <http://www.dyson.co.uk/>

EDAX UK, part of AMETEK, Inc., Process and Analytical Instruments Division, Wych End, Park Lane, Castle Camps, Cambs. CB1 6SR, GB, Tel +44 (0) 1799 584 934, Fax +44 (0) 1799 584 936

Efunda, (2005), Engineering Fundamentals, Thermal Conductivity of Iron, accessed 28-06-05, http://www.efunda.com/materials/elements/TC_Table.cfm?Element_ID=Fe

- Environmetal Chemistry, (2005), Environmetal, Chemistry and Hazardous Material Information and Resourses, Periodic Table of Elements, accessed 2005, <http://environmetalchemistry.com>
- EOS GmbH, (2005), Electro Optical Systems, Robert-Stirling-Ring 1, D-82152, Krailling / Munich, Germany, <http://www.eos-gmbh.de/pag/file/found.htm>
- Eurotherm Limited, Faraday Close, Durrington, Worthing, West Sussex BN13 3PL, Tel +44 (0) 1903 268500, Fax +44 (0) 1903 265982
- Ewing, J.A. and Humfrey (1903), The Fracture of Metals under Repeated Alternations of Stress, Philosophical transactions of the Royal society of London A, Volume 200, 1903, p 241
- Feenstra, F., Holmer, B., Pohl, H., Tromans, G., Moos, N., Mieritz, B., RP, (2002), RT, RM Trends and Development / Research Survey, RAPTIA, 17th September 2002, pp 1 - 42
- Fine, M. E. and Chung, Y. W., (1980), Fatigue Failure in Metals, Metall Transactions A, Volume 11A, March 1980, pp 368 - 379
- Fissolo, A., Marini, B., Nais, G., Wident, P., (1996), Thermal Fatigue Behaviour for a 316L Type Steel, Journal of Nuclear Materials, Volume 233 - 237, Part 1, 1996, pp 156 - 161, ISSN 0022 - 3115
- Forsyth, P. J. E., (1979), The Physical Basis of Metal Fatigue, Blackie, 1979
- Foseco Foundry International Limited, Tamworth, <http://www.foseco.com/>
- Frech U.K. Ltd., The Production Centre, Boundary Industrial Estate, Fordhouses, Wolverhampton, WV10 7EL, UK, <http://www.frech.com/>
- Gale, W.F. and Totemeier, T.C., (2004), Smithells Metals Reference Book, 8th Edition, Elsevier Butterworth Heineman, ISBN 0 - 7506 - 7509 - 8
- Gallenkamp, now Sanyo Gallenkamp PLC, Loughborough, Monarch Way, Belton Park, Loughborough, Leicestershire, LE11 5XG, Tel +44 (0)1509 265265, Fax +44 (0)1509 269770, e-mail: sanyogall@sgplc.co.uk, Web site: www.sanyogallenkamp.com
- GEC-Marconi Materials Technology Ltd., accessed 13-12-04, published on: 01-12-04, <http://www.marconi.com/Home>
- Ghomashchi, M.R., (1995), High Pressure Die Casting: Effect of Fluid Flow on the Microstructure of LM24 Die Casting Alloy, Journal of Materials Processing Technology, Volume 52, 1995, pp 193 - 206, ISSN 0924 - 0136/95

- Gibbons, G., Hansell, R., Dickens, P., Norwood, A.J., (2003), Rapid Laminate Die-cast Tooling, International Journal of Assembly Automation, Volume 23, Number 4, 2003, pp 372 – 381
- Gideon, (2004), Analytical Labs, Energy dispersive x-ray spectroscopy, <http://gideonlabs.com/sem-eds.htm>, accessed 28-09-04
- Gildemeister, (2004), DML 40: For complete machining of filigree mould-pieces, accessed 26-04-04, <http://www.gildemeister.com/en/ultrasonic---lasering-product-lines>
- Glenny, E., Northwood, J.E., Shaw, S.W.K., Taylor, T.A., (1959), A Technique for Thermal-Shock and Thermal-Fatigue Testing Based on the Use of Fluidised Solids, Journal of the Institute of Metals, Volume 87, 1959, pp 294 - 302
- Glozer, G.R., (1992), Laminate Tooling for Injection Moulding, Proceedings of the Institute of Mechanical Engineers, Volume 207, Part B1, December 1992, pp 9 - 15
- Goodfellow, (2005), material information, accessed 2005, www.goodfellow.com
- Gopal, S., Lakara, A., Shivpuri, R., (2000), Soldering in Die Casting: Aluminium Alloy and Die Steel Interactions, Die Casting Engineer, Volume 44, Number 3, May / June 2000, pp 70 - 81
- Green, D. and Munz, D., (1996), Thermal Fatigue Growth Experiments on Austenitic Steel Plates, International Journal Pressure Vessels and Piping, Volume 65, 1996, pp 369 - 378
- Gulizia, S., Jahedi, M.Z., Doyle, E.D., Chen, Z.W., (1999), Application of Duplex Surface Treatments for Aluminium High Pressure Die Casting Tools, Tooling 1999 conference Proceedings, Melbourne Institute of Materials Engineering, Australia, 1999, pp 205 - 210
- Gulizia, S., Jahedi, M.Z., Doyle, E.D., (2001), Performance Evaluation of PVD Coatings for High Pressure Die Casting, International Journal of Surface and Coatings Technology, Volume 140, 2001, pp 200 - 205, ISSN 0257 - 8972/01
- Hague, R. and Reeves, P., (2000), Rapid Prototyping, Tooling and Manufacture: An Overview, Rapra Review Reports, Volume 10, Number 9, Report 117, 2000, ISBN: 1 - 85957 - 203 - 0
- Hague, R., (2001), Rapid Tooling for Magnesium Die Cast Components, An investigation into Innovative Technologies and Processes for Ericsson Mobile Communication AB, Rapid Manufacturing Research Group Ericsson Die Casting Project, Consortium Members Report 2001, accessed 10-10-03, http://www.lboro.ac.uk/departments/mm/research/RapidManufacturing/consortium/project/Ericsson_DieCast.pdf

Hague, R., D'Costa, G., Dickens, P.M., (2001), Structural Design and Resin Drainage Characteristics of Quickcast 2.0, Rapid Prototyping Journal, Volume 7, Number 2, 2001, pp 66 - 72, ISSN 1355 - 2546

Halford, B., (1999), Rapid Tooling, Journal of the Institute of Engineering Designers, May 1999, pp 4 - 6

Hansen, S., (2006), Causes of Damage of Steckel Mill Drums during Hot Rolling of Steel Slab IPSCO Steel, Alabama Inc, Axis, AL 36505, USA, MPLUS No.: MC-03-008, <http://216.239.59.104/search?q=cache:bBAtaLLbfBAJ:www.ms.ornl.gov/programs/mplus/projects/stekelmills.doc+MPLUS+No.:+MC-03-008&hl=en&gl=uk&ct=clnk&cd=1>

Harris, R.A., Norwood, A.J., Dickens, P.M., Bjork, L., Zenker, E., (2003^a), The Use of Metal Powder Binder Rapid Tooling in Metal and Polymer Small Batch Manufacturing Techniques, 1st International Conference on Advanced Research in Virtual and Rapid Prototyping October 1st - 4th, 2003, pp 497 - 501, ISBN 972 - 99023 - 0 - 5, Leiria, Portugal

Harris, R.A., Norwood, A.J., Dickens, P.M., Bjork, L., Zenker, E., (2003^b), Metal Powder Tooling for Low Volume Manufacturing Processes, 8th User Forum, Rapid Product Development - Process and Process Chains In Hybrid Product Development, 17th September 2003, Fraunhofer IPA, Stuttgart, Germany

Harris, R.A., Norwood, A.J., Dickens, P.M., (2004), Metal Powder Binder Rapid Tooling for High Pressure Die-Casting, International Conference on Competitive Manufacturing - Progress in Innovative Manufacturing, 4th - 6th February, 2004, pp 223 - 228, ISBN 0 - 7972 - 1018 - 0, University of Stellenbosch, South Africa

Hartman, G., (1985), A Thermal Control System for Thermal Cycling, Journal of Test Evaluation, Volume 13, Number 5, 1985, pp 363 - 366

Hayashi, M., Enomoto, K., Saito, T., Miyagawa, T., (1998), Development of Thermal Fatigue Testing Apparatus with BWR Water Environment and Thermal Fatigue Strength of Austenitic Stainless Steels, Journal of Nuclear Engineering and Design, Volume 184, 1998, pp 113 - 122

Hertzberg, R., (1996), Deformation and Fracture Mechanics of Engineering Materials, 4th Edition, John Wiley and Sons, Inc., 1996, ISBN - 0471012149

Higgins, R.A., (1991), Materials for the Engineering Technician, Edward Arnold, Mill Road, Dunton Green, Sevenoaks, Kent, TN13 2YA, 1991, ISBN 0 - 3404 - 1476 - 6

Himmer, T., Nakagawa, T., Anzai, M., (1999), Lamination of Metal Sheets, International Journal of Computers in Industry, Volume 39, Number 1, 1999, pp 27 - 33

Himmer, T., Techel, A., Nowotny, S., Beyer, E., (2003), Recent Developments in Metal Laminated Tooling by Multiple Laser Processing, Rapid Prototyping Journal, Volume 9, Number 1, 2003, pp 24 - 29, ISSN 1355 - 2546

Howes, M.A.H., (1973), Evaluation of Thermal Fatigue Resistance of Metals Using the Fluidised Bed Technique, American Society Testing Materials, 1973, pp 242 - 254

Hypertextbook, (2003), Conduction, The Physics Hypertextbook™, accessed 17-06-03, <http://hypertextbook.com/physics/thermal/conduction/>

Induction Heating Systems (UK) Ltd, Bakewell Business Centre, Ashford Rd, Bakewell, Derbyshire, DE45 1GL, Tel 01629 812787

Isoma SA, 7 chemin des pinsons CH-2500 Bienne 7 / Switzerland, Tel +41 (0)32 366 00 20, Fax +41 (0)32 366 00 21, <http://www.isoma.ch/>

Jacobs, P., (1995), Rapid Tooling, Journal of World Class Design to Manufacture, Volume 2, Number 6, 1995, pp 42 - 50, ISSN 1352 - 3074

Jahedi, M.Z. and Fraser, D.T., (2001), Prevention of Soldering in High Pressure Die-Casting Dies Using Aluminium and Iron Oxide Surface Treatment, North American Die-Casting Association 2001 Transactions Congress Sessions, Cincinnati Convention Centre, Cincinnati, Ohio, 2001, pp 379 - 395

JIS Z 2278, (1992), Method of Thermal Fatigue Testing for Metallic Materials, Japanese Industrial Standards Association, 1-24, Akasaka 4, Minato-ku, Tokyo 107, Japan, 1992, UDC 620.178.37/.38 : 669

Joshi, V., Srivastava, A., Shivpuri, R., (2004), Intermetallic Formation and its Relation to Interface Mass Loss and Tribology in Die Casting Dies, International Journal of Wear, Volume 256, 2004, pp 1232 - 1235, ISSN 0043 - 1648

Juster, N.P., (1994), Rapid Prototyping using the Selective Sintering Process, Journal of Assembly Automation, Volume 14, Number 2, 1994, pp 14 - 17

JVC Professional Europe, Ullswater House, Kendal Avenue, London W3 0XA, <http://www.jvcpro.co.uk/>

Karapatis, N.P., Van Griethuysen, J.P.S., Glardon, R., (1998), Direct Rapid Tooling: A Review of Current Research, Rapid Prototyping Journal, Volume 4, Number 2, 1998, pp 77 - 89, ISSN 1355 - 2546

Kawamoto, M., Tanaka, T., Nakajima, H., (1966), Effect of Several Factors on Thermal Fatigue, Journal of Materials, Volume 1, Number 4, 1966, pp 719 - 758

Kemlows Diecasting Ltd., Charlton Mead Lane, Hoddesdon, Herts, EN11 0HB, Tel +44 (0) 1992 460671, Fax +44 (0) 1992 446 889

Khaing, M.W., Fuh, J.Y.H., Lu, L., (2001), DirectMetal Laser Sintering For Rapid Tooling Processing and Characterization of EOS Parts, Journal of Materials Processing Technology, Volume 113, 2001, pp 269 - 272

Kilingbeil, N.W., and Bontha, S., (2003), A Maximum Allowable Flaw Size For Debonding-Resistant Bimaterial Layers, International Journal of Engineering Fracture Mechanics, Volume 70, 2003, pp 2103 - 2114

Klarenfjord, B., (2005), The Necessity for Good Properties in High Pressure Dies, Diecasting World, Volume 14, Number 1, 2005, pp 10 - 11

Klocke, F., Celiker, T., Song, Y.A., (1995), Rapid Metal Tooling, Rapid Prototyping Journal, Volume 1, Number 3, 1995, pp 32 - 42, MCB University Press, ISSN 1355 - 2546

Knirsch, J., Folkestad, J., McHugh, K., (2002), RSP tooling – A Revolutionary New Process to Manufacture Die Cast Production Tooling in Prototype Timing, Die Casting Engineer, Volume 46, Number 3, 2002, pp 56 - 60, ISSN 0012 - 253X

Krauss, G., (1990), Steels: Heat Treatment and Processing Principles, ASM International, Materials Park Ohio, 1990, ISBN: 0 - 8717 - 0370 - X

Kulkarni, P. and Dutta, D., (1996), An Accurate Slicing Procedure for Layered Manufacturing, International Journal of Computer Aided Design, Volume 28, Number 9, 1996, pp 683 - 697, ISSN 0010 - 2285/96

Lafarge Refractories, (2004), now Lafarge Monolithics Ltd, 5-8 Ashfield Way, Whitehall Estate, Whitehall Road, Leeds, LS12 5JB, UK, Tel +44 113 263 62 68, Fax +44 113 279 05 39

Laserage Technology Corporation, (2004), 3021 Delany Road, Waukegan, IL 60087-1826, USA, Tel 847 249 5900, Fax 847 336 1103, <http://www.laserage.com/info.html>

Leo Electron Microscopy, now Carl Zeiss SMT Ltd, Nano Technology Systems Division 511 Coldhams Lane Cambridge CB1 3JS UK Tel +4412 23 / 414166 Fax +4412 23 / 412776, http://www.smt.zeiss.com/de/semicon/nts/home_e.nsf/

Lesuer, D.R., (1996), Mechanical Behaviour of Laminated Metal Composites Segregation to Boundaries and Interfaces in Solids, International Materials Reviews, Volume 41, Number 5, 1996, ISSN 0950 - 6608

Levy, G.N. and Schindel, R., (2002), Overview of Layer Manufacturing Technologies, Opportunities, Options and Applications for Rapid Tooling, Proceedings of the Institution of Mechanical Engineers, Volume 216, Part B: Journal of Engineering Manufacture, 2002, pp 1621 - 1634

Linseis, M., (1985), Measurement System Guide 1985, with complete TC Reference Tables, Linseis Worldwide Sales Organization, Linseis GmbH, P.O.Box 1404, 8672 Selb, West Germany (company catalogue, no ISBN number), http://www.linseis.net/html_en/home.php

Liu, G.W., Morsi, Y.S., Clayton, B.R., (2000), Characterisation of the Spray Cooling Heat Transfer Involved in a High Pressure Die Casting Process, International Journal of Thermal Sciences, Volume 39, 2000, pp 582 - 591

Maillot, V., Fissolo, A., Degallaix, G., Degallaix, S., (2005), Thermal Fatigue Crack Networks Parameters and Stability: An Experimental Study, International Journal of Solids and Structures, Volume 42, 2005, pp 759 - 769, ISSN 0022 - 7683

Marom, E. and Mueller, R.K., (1971), International Journal of Non-destructive Testing, Volume 3, Number 2, 1971, p 171

Material Testing Services, (2004), Physical Properties - Thermal Conductivity, accessed 13-12-04, [http://fp.uni.edu/rtrtc/mts/Thermal Conductivity.asp](http://fp.uni.edu/rtrtc/mts/Thermal%20Conductivity.asp)

Materialise, (2004), Materialise software homepage, accessed 15-04-04, <http://www.materialise.com>

MatWeb, (2004), Online Material Data Sheet, accessed 16-08-04, <http://www.matweb.com/search/SpecificMaterial.asp?bassnum=MSH13A>

Merola, M., Matera, R., Sevini, F., (1996), Experimental Results of the Thermal Fatigue Tests for I.A.E.A. Benchmark Components, Journal of Nuclear Materials, Volume 233 - 237, 1996, pp 620 - 625

Metaserv, Metallurgical Services, Betchworth, Surry, UK

Mitterer, C., Holler, F., Ustel, F., Heim, D., (2000), Application of Hard Coatings in Aluminium Die Casting – Soldering, Erosion and Thermal Fatigue Behaviour, International Journal of Surface and Coatings Technology, Volume 125, 2000, pp 233 - 239, ISSN 0257 - 8972/00

- Monolithics Ltd., 5-8 Ashfield Way, Whitehall Estate, Whitehall Road, Leeds, LS12 5JB, Tel +44 (0) 113 263 6268, Fax +44 (0) 113 279 0539
- Morgan Crucible, Part of Morganite Crucible Ltd, Norton Works, Woodbury Lane, Norton, Worcester, Worcestershire WR5 2PU, Tel +44 (0) 1905 728200, Fax +44 (0) 1905 767877
- Mowbray, D.F. and McConnelee, J.E., (1976), Nonlinear Analysis of a Tapered Disk Thermal Fatigue Specimen, Thermal Fatigue of Materials and Components, American Society for Testing and Materials (ASTM), 1976, pp 10 - 29
- Mueller, T., (1992), Stereolithography: A Rapid Way to Produce Prototype Die Castings, Die Casting Engineer, Volume 36, Number 3, 1992, pp 28 - 33, ISSN 0012 - 253X
- Mueller, T. and Thomas, J., (1992), Using Rapid Prototyping Techniques to Prototype Metal Castings, SAE Technical Paper Series, Number 921639, 1992, pp 1 - 5
- Mueller, T., (1996), Recent Developments in the Use of Rapid Prototyping Techniques to Prototype Die Cast Parts, Die Cast Engineer, 1996, Pages 1 - 7
- NADCA, 2006, FAQ about die casting, accessed 25-05-06, <http://www.diecasting.org/faq/>
- Nakagawa, T., (1985), Laser Cut Sheet Laminated Forming Dies by Diffusion Bonding, Proceedings of the 25th International MTDR Conference, Volume 4, 1985, pp 505 - 510
- National Instruments U.K. Corporation Ltd, Measurement House, Newbury Business Park, London Rd, Newbury, Berkshire RG14 2PS, Tel +44 (0) 1635 523545, Fax +44 (0) 1635 523 154, <http://digital.ni.com/worldwide/uk.nsf/main?readform>
- Nikon U.K. Limited, Nikon House, 380 Richmond Road, Kingston Upon Thames, Surrey, KT2 5PR, United Kingdom, Tel +44 (0) 2082 471 717, Fax +44 (0) 2085 414 584
- Norström, L.Å., (1982), Performance of Hot-Work Steels, Scandinavian Journal of Metallurgy, Volume 11, 1982, p 33
- Norwood, A.J., (2001), Rapid Prototyping and Tooling State of the Industry, Wohlers Report, Annual Worldwide Progress Report, Part 3, Laminate Tooling, 2001
- Norwood, A.J. and Soar, R., (2001), Current Rapid Tooling Technologies, Diecasting World, Volume 175, September 2001, pp 16 - 17

Norwood, A.J., Dickens, P., Soar, R., (2001), North America Die Casting Society, 2001 Transactions Congress Sessions, Bonded and Un-bonded Laminated Tooling for Rapid Tooling and Prototyping Within the Die Casting Industry, Cincinnati Convention Center, Cincinnati Ohio, October 29th - November 1st 2001, pp 415 - 422

Norwood, A.J., (2002^a), Rapid Prototyping and Tooling State of the Industry, Wohlers Report, Annual Worldwide Progress Report, Part 3, Laminate Tooling 2002

Norwood, A.J., (2002^b), Laminate Tooling, Working in Harmony, Diecasting Times, Volume 4, Number 1, 2002

Norwood, A.J., Dickens, P., Soar, R., Gibbons, G., Hansell, R., (2004), Analysis of Cooling Channels Performance, International Journal of Computer Integrated Manufacturing, Volume 17, Number 8, December 2004, pp 669 - 678

Norwood, A.J. and Dickens, P., (2005), Some Options for Rapid Tooling, Die-Casting World, Volume 14, Number 1, 2005, pp 12 - 13

Novovic, D., Dewes, R.C., Aspinwall, D.K., Voice, W., Bowen, P., (2004), The Effect of Machined Topography and Integrity on Fatigue Life, International Journal of Machine Tools and Manufacture, Volume 44, 2004, pp 125 - 134, ISSN 0890 - 6955

Oberg, E., Franklin, D.J., Holbrook, L., Henry, H.P., (1996), Machinery's Handbook 25th Edition, Industrial Press Inc, 200 Madison Avenue, New York, 1996, ISBN 0 - 8311 - 2575 - 6

Obikawa, T., (1999), Sheet Steel Lamination for Rapid Manufacturing, Journal of Materials Processing Technology, Volume 89 - 90, 1999, pp 171 - 176

ÓDonnchadha, B. and Tansey, A., (2004), A Note on Rapid Metal Composite Tooling by Selective Laser Sintering, Journal of Materials Processing Technology, Volume 152 - 154, 2004, pp 28 - 34

Olive, S., (2005), Long-Life Die Design, Diecasting World, Volume 14, Number 1, 2005, p 15

Optomec, (2006), LENS Applications, LaserEngineered Net Shaping, accessed 25-05-06, http://www.optomec.com/site/lens_home Optomec Advanced Applications Laboratory, 1000 Westgate Dr. , Suite 123, Saint Paul, MN 55114, Tel. (651) 641-2850

Persson, A., Bergstrom, J., Burman, C., Hogmark, S., (2001), Influence of Deposition Temperature and Time During PVD Coating of CrN on Corrosive Wear in Liquid Aluminium, International Journal of Surface and Coatings Technology, Volume 146 – 147, 2001, pp 42 - 47, ISSN 0257 - 8972/01

- Persson, A., (2003), Tool Failure in Die Casting, Doctoral Thesis, Uppsala University, Department of Materials Science, 2003
- Persson, A., (2004), Strain-Based Approach to Crack Growth and Thermal Fatigue Life of Hot Work Tool Steels, Scandinavian Journal of Metallurgy, Volume 33, Issue 1, February 2004, p 53
- Persson, A., Hogmark, S., Bergstrom, J., (2004^a), Simulation and Evaluation of Thermal Fatigue Cracking of Hot Work Tool Steels, International Journal of Fatigue, Volume 26, 2004, pp 1095 - 1107, ISSN 0142 - 1123
- Persson, A., Hogmark, S., Bergstrom, J (2004^b), Temperature Profiles and Conditions for Thermal Fatigue Cracking in Brass Die Casting Dies, Journal of Materials Processing Technology, Volume 152, 2004, pp 228 - 236
- Persson, A., Hogmark, S., Bergstrom, J., (2005), Thermal Fatigue Cracking of Surface Engineered Hot Work Tool Steels, International Journal of Surface and Coatings Technology, Volume 191, 2005, pp 216 - 227, ISSN 0257 - 8972
- Pham, D.T., Dimov, S., Lacan, F., (1999), Selective Laser Sintering: Applications and Technological Capabilities, Proceedings of the Institution of Mechanical Engineers, Volume 213, Part B, 1999, pp 435 - 449
- Pham, D.T., Dimov, S.S., Lacan, F., (2000), The Rapid Tool Process: Technical Capabilities and Applications, Proceedings of the International Journal of Mechanical Engineers, Volume 214, Part B, 2000, pp 107 - 116
- POM, (2006), DMD™ (Direct Metal Deposition), accessed 25-05-06, Advanced Product Development Centre, 2350 Pontiac Road, Auburn Hills, Michigan 48326, Tel.: 248-409-7900 Fax. 248-409-7901
- Proctor and Gamble EMEA Service Centre, Cobalt 12, Silver Fox Way, Cobalt Business Park, Newcastle Upon Tyne, Tyne and Wear, NE27 0QJ
- ProMetal, (2006), Equipment, accessed 25-05-06, <http://www.prometal.com/equipment.html>
- Prototal AB, Instrumentvägen 6, SE-553 02, Jönköping, info@prototal.se
- Radstok, E., (1999), Rapid Tooling, Rapid Prototyping Journal, Volume 5, Number 4, 1999, pp 164 - 168, MCB University Press, ISSN 1355 - 2546
- Ramsell SMC, now Ramsell-Naber Ltd, Vigo Place, Aldridge, Walsall, West Midlands, WS9 8YB, Tel +44 (0)1922 455521, Fax +44 (0)1922 455277, <http://www.ramsell-naber.co.uk/>

Ray, M.S., (1987), The Technology and Applications of Engineering Materials, Prentice-Hall International (UK) Ltd., 1987, ISBN 0 - 1390 - 2099 - 3 or ISBN 0 - 1390 - 2081 - 0

Reimann, W.H. and Brisbane, A.W., (1973), Improved Fracture Resistance of 7075 Through Thermomechanical Processing, Engineering Fracture Mechanics, Volume 5, Issue 1, 1973, pp 67 - 78

Roberts, G., Krauss, G., Kennedy, R., (1998), Tool Steels, 5th Edition, ASM International, Materials Park, Ohio, 1998

Rooks, B., (2002^a), Rapid Tooling for Casting Prototypes, Journal of Assembly Automation, Volume 22, Number 1, 2002, pp 80 - 45, ISSN 0144 - 5154

Rooks, B., (2002^b), Rapid Manufacturing Advances at Loughborough, Journal of Assembly Automation, Volume 22, Number 4, 2002, pp 333 - 336, ISSN 0144 - 5154

RS Components, Lenton Lane, Nottingham, NG7 2NR, Tel 0115 986 6422, Fax 0115 986 6604, <http://rswww.com>

RSP Tooling, (2004), RSP Tooling, LLC 30555 Solon Industrial Parkway, Solon, OH, <http://www.rsptooling.com/index.htm>

Rutz, H., Murphy, T., Cimino T., (1996), The Effect of Microstructure on Fatigue Properties of High Density Ferrous P/M materials, PM-EC 1996 World Congress, June 16th - 21st 1996, Washington D.C.

Sandmeyer Steel Company, (2005), 1 Sandmeyer Lane, Philadelphia, PA 19116, 300 Series Austenitic Stainless Steel, accessed 2005

Schwartz, M.M., (1990), American Society for Metals (ASM) International, Brazing, November 1990, ISBN 0 - 8717 - 0246 - 0

Schwam, D., Wallace, J.F., Birceanu, S., (2004), Effect of Design Factors on Thermal Fatigue Cracking of Die Casting Dies, Final Report, Department of Materials Science, Case Western Reserve University, Cleveland, Ohio, Project number DE-FC07-00ID138486, US Department of Energy, Washington DC, October, 2004

Segal, J.I., and Cambell, R.I., (2001), A Review of Research into the Effects of Rapid Tooling on Part Properties, Rapid Prototyping Journal, Volume 7, Number 2, 2001, pp 90 - 98, MCB University Press, ISSN 1355 - 2546

- Shackelford, J.F. and Alexander, W., (2001), CRC Material Science and Engineering Handbook, 3rd Edition, CRC Press, London, UK, 2001, ISBN 0 - 8493 - 2696 - 6
- Shanker, S. and Apelian, D., (1997), Die Soldering – A Metallurgical Analysis of the Molten Metal / Die Interface Reactions, Proceedings of the 19th International Die casting Congress, North American Die-Casting Association Transactions, North American Die-Casting Association, November 1997, pp 245 - 251
- Shanker, S. and Apelian, D., (1999), Investigation of Die Soldering in Aluminium Die Casting, Progress Report, Aluminium Casting Research Laboratory, Metal Processing Institute (MPI) - Worcester Polytechnic Institute (WPI), Worcester, MA, 01609, December 1999
- Shanker, S., (2000^a), Soldering Tendencies of Alternate Non-Ferrous Die Materials, North American Die-Casting Association transactions, Rosemont, Illinois, November 2000
- Shanker, S., (2000^b), A Study of the Interface Reaction Mechanism between Molten Aluminium and Ferrous Die Materials, Doctoral Dissertation, WPI, Worcester, MA, 01609, April 2000
- Simons, E.N., (1972), Metal Fatigue, David and Charles, Newton Abbot, Devon - TQ12 1XD, pp 11 - 12, ISBN 0 - 7153 - 5526 - 0
- Sjöström, J. and Bergström, J., (2004), Thermal Fatigue Testing of Chromium Martensitic Hot Work Tool Steel After Different Austenitising Treatments, Journal of Materials Processing Technology, Volume 153 - 154, 2004, pp 1089 - 1096, ISSN 0924 - 0136
- Soar, R.C. and Dickens, P.M., (1996), Design of Laminate Tooling for High Pressure Die Casting, Proceedings of the 1996 Photonics East Conference, Boston, Massachusetts, USA, Volume 2910, 18th - 19th November 1996, pp 198 - 210, ISBN 0 - 8194 - 2312 - 2
- Soar, R.C. and Dickens, P.M., (1998^a), Rapid Prototyping Opportunities: Laminated Tooling for Aluminium Die Casting, Proceedings of the Aluminium 98 Conference, Messe Essen, Germany, September 1998, pp 23 - 24
- Soar, R.C. and Dickens, P.M., (1998^b), The Use of Laminated Tooling for the Production of Prototype Pressure Die-Cast Dies, Proceedings of the Time Compression Technologies Conference, October 1998, pp 331 - 340
- Soar, R.C., (2000), An Examination of the Feasibility and Design Limitations of Laminate Tooling for Pressure Die Casting, PhD Thesis, De-Montfort University, Leicestershire, 2000

Soar, R.C. and Dickens, P.M., (2001), Design Limits of Un-Bonded Laminate Tooling for Pressure Die-Casting, Proceedings of the Institution of Mechanical Engineers Part B, Journal of Engineering Manufacture, Volume 215 (B4), March 2001, pp 531 - 545, ISSN 0954 - 4054

Srivastava, A., (2003), A Multilayer Coating Architecture to Reduce Heat Checking of Die Surfaces, International Journal of Surface and Coatings Technology, Volume 163 - 164, 2003, pp 631 - 636

Srivastava, A., Joshi, V., Shivpuri, R., (2004), Computer Modelling and Prediction of Thermal Fatigue Cracking in Die-Casting Tooling, International Journal of Wear, Volume 256, 2004, pp 38 - 43

Stanton Instruments Ltd., 119 Oxford Street, London, W1

Starling, C.M.D. and Branco, J.R.T., (1997), Thermal Fatigue of Hot Work Tool Steel with Hard Coatings, International Journal of Thin Solid Films, Volume 308 - 309, 1997, pp 436 - 442, ISSN 0040 - 6090/97

Stewart, T.D., Dalgarno, K.W., Childs, T.H.C., (1999), Strength of the DTM RapidSteel™ 1.0 Material, Journal of Material and Design, Volume 20, Number 2 - 3, 1999, pp 133 - 138, ISSN 0261 - 3069/99

Storch, S., Nellessen, D., Schaefer, G., Reiter, R., (2003), Selective Laser Sintering: Qualifying Analysis of Metal Based Powder Systems for Automotive Applications, Rapid Prototyping Journal, Volume 9, Number 4, 2003, pp 240 - 251, ISSN 1355 - 2546

Street, A.C., (1986), The Die Casting Book, Second Edition, Portcullis Press Ltd., Queensway House, 2 Queensway, Surrey, 1986, ISBN 0 - 8610 - 8235 - 4

Struers Ltd., Erskine Ferry Road, Old Kilpatrick, Glasgow, G60 5EU, Strathclyde, Tel 01389 877222, Fax 01389 877600, www.struers.com

Sulzer Metco (UK) Ltd., (1998), Westmead, GB-Farnborough, Hants, GU14 7LP, Braze Products, July 1998

Sundqvist, M. and Hogmark, S., (1993), Effects of Liquid Aluminium on Hot-Work Tool Steels, Journal of Tribology International, Volume 26, 1993, p 129

Sundqvist, M., Bergstrom, T., Bjork, T., Westergard, R., (1997), Corrosive Wear of Duplex Coatings in Die Casting of Aluminium, Transactions 19th International Die-Casting Congress and Exposition, North America Die Casting Association, Minneapolis, 1997, p 325

Taira, M., Fujino, M., Ohtani, R., (1979), Collaborative study on Thermal Fatigue Properties of High Temperature Alloys in Japan, Journal of Fatigue and Fracture Engineering Materials and Structures, Volume 1, 1979, pp 495 - 508

Tata, K., Fadel, G., Bagchi, A., Aziz, N., (1998), Efficient Slicing for Layered Manufacturing, Rapid Prototyping Journal, Volume 4, Number 2, 1998, pp 151 - 167, ISSN 1355 - 2546

Taylor Hobson Ltd., PO Box 36, 2 New Star Road, Leicester, LE4 9JQ, <http://uk.multimap.com/p/browse.cgi?pc=LE49JQ&scale=100000Leicestershire>, Tel 0116 276 3771, Fax 0116 246 0579, www.taylor-hobson.com

Taylor Special Steels, Oldbury, West Midlands, B69 2RA, UK Tel +44 121 5522741, Fax +44 121 5111240

TC Ltd., (2003), Units 1 - 6, Brimington Road North, Chesterfield, S41 9BD, UK. Tel 01895 252 222, Fax 01895 273 540, www.tc.co.uk

Techne Ltd., Barloworld Scientific Ltd, Beacon Road, Stone, Staffordshire, ST15 0SA, United Kingdom, Tel +44 (0)1785 812121, Fax +44 (0)1785 813748

Tempilaq®, Walters and Walters Ltd, Unit 16, Orchard Road, Royston, Herts, SG8 5HA, UK

Timkin Latrobe Steel, (2004), A Timkin Company Subsidiary, accessed March 2004, http://www.timken.com/products/specialtysteel/engineering/tech_info/PDF_Files/air_melt/HotWorkToolSteels/TLS%20H13%20PQ.pdf

Trumpf, (2006), Direct Metal Deposition, accessed 26-05-06, http://www.trumpf.com/scripts/redirect2.php?domain=www.trumpf.com&nr=3&content=3.laserforming_dmd.html, GmbH + Co. KG, Johann-Maus-Straße 2, D-71254 Ditzingen, Germany

Tyberg, J. and Bohn, J.H., (1998), Local Adaptive Slicing, Rapid Prototyping Journal, Volume 4, Number 3, 1998, pp 118 - 127, ISSN 1355 - 2546

UKAS, (United Kingdom Accreditation Service), 21 - 47 High Street, Feltham, Middlesex, TW13 4UN, UK, Tel +44 (0)208917 8400, Fax +44 (0) 20 89178500, <http://www.ukas.org/>

University of Groningen, (2006), Fatigue crack initiation, accessed 15-01-06, <http://www.rug.nl/msc/research/groups/mimec/research/fatigueCrackInitiation>, Materials Science Centre, University of Groningen, Nijenborgh 4, NL-9747 AG Groningen, The Netherlands

Upcraft, S. and Fletcher, R., (2003), The Rapid Prototyping Technologies, Journal of Assembly Automation, Volume 23, Number 4, 2003, pp 318 - 330, ISSN 0144 - 5154

Uzunsoy, D., Chang, I.T.H., Bowen, P., (2002), Microstructural Evolution and Mechanical Properties of RapidSteel 2.0, International Journal of Powder Metallurgy, Volume 45, number 3, 2002, pp 251 – 254

Uzunsoy, D., Chang, I.T.H., Bowen, P., (2003), Fracture Behaviour of Selective Laser Sintered RapidSteel 2.0 Under Static Dynamic Loading, International Journal of Material Science and Technology, Volume 19, 2003, pp 897 - 901

Van Heerden, C., Nobel, A.P.P., Van Krevelen, D.W., (1953), Mechanism of Heat Transfer in Fluidized Beds, Industrial and Engineering Chemistry, 1953, Volume 45, Number 6, p 1237.

Vectstar Furnaces, now Vecstar Furnaces, Units 11 and 12, Foxwood Road, Dunston Trading Estate, Chesterfield, S41 9RF, Tel 01246 260094, Fax 01246 450213, Email: enquiries@vecstar.co.uk, <http://www.vecstar.co.uk/>

Venkataraman, G., Nakansone, Y., Chung, Y.W., Mura, T., (1990), Journal of Acta Metallurgica, Volume 38, 1990, p 31

Venkataraman, G., Chung, Y.W., Mura, T., (1991), Journal of Acta Metallurgica, Volume 39, 1991, pp 2621 and 2631

Walczyk, D.F. and Hardt, D.E., (1994), A New Rapid Cooling Method for Sheet Metal Forming Dies. Fifth International Conference on Rapid Prototyping, June 12th - 15th 1994, edited by Chartoff, R.P., Lightman, A.J., Schenk, J.A., (Sponsored by The Rapid Prototype Development Laboratory, The Management Development Centre, The University of Dayton), pp 275 - 289

Walczyk, D.F. and Hardt, D., (1996), Recent Developments in Profiled-Edge Lamination Dies for Sheet Metal Forming, Proceedings of the Seventh Solid Freeform Fabrication Symposium, Austin, Texas, August 12th - 14th, 1996, pp 215 - 226

Walczyk, D.F., (1998), Rapid Tooling for Sheet Metal Forming Using Profiled Edge Laminations - Design Principles and Demonstration, Transactions of the ASME Journal of Manufacturing Science and Engineering, Volume 120, Number 4, November 1998, pp 746 - 754

Wallace, J.F., Wang, Y., Schwam, D., (1997), Effect of Composition and Processing on the Thermal Fatigue and Toughness of High Performance Die Steels, Die Casting Engineer, Volume 41, September - October 1997, pp 26 - 32, ISSN 0012 - 253x

Wallace, J F; Schwam, D., (1999) Control of die steels and processing to extend die life, 20th International Die Casting Congress, NADCA Congress; Cleveland, OH; USA; 1st - 4th Nov. 1999. pp. 351 - 357.

Wallace, J.F., Xiaofeng, S.U., Schwam, D., (2000), Die Materials of Critical Applications and Increased Production of Castings, Die Casting Technology for the New Century 2000 Transactions, Rosemont, Illinois, USA, North America Die Casting Association (NADCA), 6th - 8th November, 2000

Wang, W., Conley, J.G., Stoll, H.W., (1999), Rapid Tooling for Sand Casting Using Laminated Object Manufacturing Process, Rapid Prototyping Journal, Volume 5, Number 3, 1999, pp 134 - 140, ISSN 1355 - 2546

Weroński, A. and Hejwoski, T., (1991), Thermal Fatigue, Thermal Fatigue of Metals, Published by Marcel Dekker inc., USA, 1991, pp 108 - 135, ISBN 0 - 8247 - 7726 - 3

White, D., (2005), Private Correspondence, Soldica, Inc. 3941 Research Park Drive Suite C, Ann Arbor, MI, 48108, Tel (734) 222 4680

Wiba AB, Grännavägen 24, 561 32 Huskvarna, Schweden, Tel +46 36 38 72 04, Fax +46 36 143038

Wimpenny, D.I., Bryden, B., Pashby, I.R., (2003), Rapid Laminated Tooling, Journal of Materials Processing Technology, Volume 138, 2003, pp 214 - 218

Wikipedia, (2006^a), Stainless steel, accessed 02-05-06, http://en.wikipedia.org/wiki/Stainless_steel#Intergranular_corrosion

Wohler, T., (2002), New Developments and Trends, Worldwide Advances in Rapid and High-Performance Tooling, EuroMold 2002, Exhibition Center Frankfurt, Frankfurt, Germany; 6th Decenber, 2002

Wohlers, T., (2003), Wohlers Report 2003 - Rapid Prototyping and Tooling State of the Industry Annual Worldwide Progress Report, Published by Wohlers Associates Inc., USA, Part 5, Asia and Europe, Sweden section, p 139

Wohlers, T., (2004), Wohlers Report 2004 - Rapid Prototyping and Tooling State of the Industry Annual Worldwide Progress Report, Published by Wohlers Associates Inc., USA

Wohlers, T., (2005), Wohlers Report 2005 - Rapid Prototyping and Tooling State of the Industry Annual Worldwide Progress Report, Published by Wohlers Associates Inc., USA

Woodford, D.A. and Mowbray, D.F., (1974), Effect of Material Characteristics and Test Variables on Thermal Fatigue of Cast Superalloys, Journal of Material Science Engineering, Volume 16, 1974, pp 5 - 43

Worbye, J., (1985), New Information Points the Way to Longer Die Casting Die Life, Die Casting Engineer, Volume 29, Part 4, 1985, pp 42 – 54

Wordreference, (2006), English Dictionary accessed 05-04-06http://www.wordreference.com/definition/modulus_of_rigidity,a

Xiaoxia, H., Hua, Y., Yan, Z., Fuzhen, P., (2004), Effect of Si on the Interaction Between Die Casting Die and Aluminium Alloy, Journal of Material Letters, Volume 58, 2004, pp 3424 - 3427

Yan, X. and Gu, P., (1996), A Review of Rapid Prototyping Technologies and Systems, International Journal of Computer Aided Design, Volume 28, Number 4, 1996, pp 307 - 318, ISSN 0010 – 4485

Yokoi, H., Suzuki, T., Suzuki, K., Nakagawa, T., (1984), Manufacture of Blanking Tool and its Die-Set by Laminate Laser-Cut Steel Sheets, Proceedings of the 12th North American Metalworking Research Conference (NAMRC), Houghton, Michigan, May 1984, pp 372 - 378

Yu, M., Shivpuri, R., Rapp, R.A., (1995), Effects of Aluminium on H13 Dies and Coatings, Journal of Materials Engineering and Performance, Volume 4, Number 2, 1995, p 175

Zhou, J.G. and He, Z., (1999), A New Rapid Tooling Technique and its Special Binder Study, Rapid Prototyping Journal, Volume 5, Number 2, 1999, pp 82 - 88, ISSN 1355 - 2546

Zhu, H., Guo, J., Jia, J., (2002), Experimental Study and Theoretical Analysis on Die Soldering in Aluminium Die Casting, Journal of Material Processing Technology, Volume 123, 2002, pp 229 - 235, ISSN 0924 - 0136

Zhu, Y., Schwam, D., Wallace, J.F., Birceanu, S., (2003), Evaluation of Soldering, Washout and Thermal Fatigue Resistance of Advanced Metal Materials for Aluminium Die-Casting Dies, International Journal of Materials Science and Engineering A, Volume 379, 2004, pp 420 - 431, ISSN 0921 - 5093

Appendix i

Material Thermal Conductivity and Density

H13 tool steel results													
Mass of Water (M)	Specific Heat of Water (S)	Test Duration (s)	Water Temp Out (T _{out})	Water Temp In (T _{in})	Change in Water Temp T _{out} - T _{in} (ΔT)	Water Flow (m)	Heat Conducted m ³ S ³ Δt (Q)	Distance Between Thermocouples (L)	Thermocouple One (T ₁)	Thermocouple Two (T ₂)	Temp Change Over Length T ₁ - T ₂ (ΔT)	Specimen Cross Sectional Area (A)	Thermal Conductivity (L(m ³ S ³ Δt))/(AXΔT) (K)
Litres (l)	Joules (J)	Seconds (s)	(°C)	(°C)	(°C)	(l/s)	Watts (W)	Mertres (m)	(°C)	(°C)	(°C)	(m ²)	(w/m °K)
0.7545	4186	615	31.72	21.90	9.82	0.00123	50.43	0.025	112.30	211.72	99.42	0.00049	25.88
0.7355	4186	615	31.23	21.60	9.63	0.00120	48.21	0.025	107.88	200.58	92.70	0.00049	26.53
0.7279	4186	615	31.12	21.83	9.29	0.00118	46.01	0.025	108.28	200.65	92.37	0.00049	25.42
0.7289	4186	615	31.37	21.92	9.45	0.00119	46.89	0.025	109.75	202.52	92.77	0.00049	25.79
0.7360	4186	615	31.18	21.98	9.20	0.00120	46.09	0.025	110.72	203.00	92.28	0.00049	25.48
Average													25.82

Appendix i Table 1 H13 thermal conductivity data

Metal copy 5507													
Mass of Water (M)	Specific Heat of Water (S)	Test Duration (s)	Water Temp Out (T _{out})	Water Temp In (T _{in})	Change in Water Temp T _{out} - T _{in} (ΔT)	Water Flow (m)	Heat Conducted m ³ S ³ Δt (Q)	Distance Between Thermocouples (L)	Thermocouple One (T ₁)	Thermocouple Two (T ₂)	Temp Change Over Length T ₁ - T ₂ (ΔT)	Specimen Cross Sectional Area (A)	Thermal Conductivity (L(m ³ S ³ Δt))/(AXΔT) (K)
Litres (l)	Joules (J)	Seconds (s)	(°C)	(°C)	(°C)	(l/s)	Watts (W)	Mertres (m)	(°C)	(°C)	(°C)	(m ²)	(w/m °K)
0.6175	4186	600	32.20	21.90	10.30	0.00103	44.37	0.025	115.63	203.47	87.84	0.00047	26.80
0.6119	4186	600	32.08	21.72	10.37	0.00102	44.25	0.025	112.47	203.77	91.30	0.00047	25.72
0.6240	4186	600	32.48	22.00	10.48	0.00104	45.64	0.025	122.55	212.65	90.10	0.00047	26.87
0.6167	4186	600	31.90	21.38	10.52	0.00103	45.25	0.025	118.45	207.72	89.27	0.00047	26.89
0.6107	4186	600	32.00	21.75	10.25	0.00102	43.67	0.025	120.82	199.20	78.38	0.00047	29.56
Average													27.17

Appendix i Table 2 Metal copy 5507 thermal conductivity data

Metal copy 5507 Infiltrant													
Mass of Water (M)	Specific Heat of Water (S)	Test Duration (s)	Water Temp Out (T _{out})	Water Temp In (T _{in})	Change in Water Temp T _{out} - T _{in} (ΔT)	Water Flow (m)	Heat Conducted m*S*Δt (Q)	Distance Between Thermocouples (L)	Thermocouple One (T ₁)	Thermocouple Two (T ₂)	Temp Change Over Length T ₁ - T ₂ (ΔT)	Specimen Cross Sectional Area (A)	Thermal Conductivity (L(m*S*Δt))/(AXΔT) (K)
Litres (l)	Joules (J)	Seconds (s)	(°C)	(°C)	(°C)	(l/s)	Watts (W)	Mertres (m)	(°C)	(°C)	(°C)	(m ²)	(w/m °K)
0.6073	4186	600	31.60	21.12	10.48	0.00101	44.41	0.025	171.65	209.57	37.92	0.00047	62.15
0.6572	4186	610	30.80	20.88	9.92	0.00108	44.73	0.025	171.28	209.15	37.87	0.00047	62.67
0.6445	4186	600	31.03	21.17	9.87	0.00107	44.36	0.025	168.57	206.25	37.68	0.00047	62.46
0.5907	4186	630	32.30	21.40	10.90	0.00094	42.78	0.025	169.43	206.97	37.54	0.00047	60.47
0.6605	4186	600	31.30	21.75	9.55	0.00110	44.01	0.025	173.65	209.28	35.63	0.00047	65.53
Average													62.66

Appendix i Table 3 Metal copy 5507 infiltrant thermal conductivity data

Metal copy Janalloy													
Mass of Water (M)	Specific Heat of Water (S)	Test Duration (s)	Water Temp Out (T _{out})	Water Temp In (T _{in})	Change in Water Temp T _{out} - T _{in} (ΔT)	Water Flow (m)	Heat Conducted m*S*Δt (Q)	Distance Between Thermocouples (L)	Thermocouple One (T ₁)	Thermocouple Two (T ₂)	Temp Change Over Length T ₁ - T ₂ (ΔT)	Specimen Cross Sectional Area (A)	Thermal Conductivity (L(m*S*Δt))/(AXΔT) (K)
Litres (l)	Joules (J)	Seconds (s)	(°C)	(°C)	(°C)	(l/s)	Watts (W)	Mertres (m)	(°C)	(°C)	(°C)	(m ²)	(w/m °K)
0.6377	4186	600	32.60	22.80	9.80	0.00106	43.60	0.025	109.80	206.60	96.80	0.00047	23.90
0.6415	4186	600	32.63	22.55	10.08	0.00107	45.12	0.025	113.67	208.12	94.45	0.00047	25.34
0.6396	4186	600	32.90	22.53	10.37	0.00107	46.27	0.025	107.93	206.95	99.02	0.00047	24.79
0.6304	4186	600	32.12	22.38	9.73	0.00105	42.81	0.025	113.77	205.40	91.63	0.00047	24.79
0.6334	4186	600	32.47	22.60	9.87	0.00106	43.60	0.025	104.90	200.48	95.58	0.00047	24.20
Average													24.61

Appendix i Table 4 Metal copy Janalloy thermal conductivity data

Metal copy Janalloy infiltrant													
Mass of Water (M)	Specific Heat of Water (S)	Test Duration (s)	Water Temp Out (T _{out})	Water Temp In (T _{in})	Change in Water Temp T _{out} - T _{in} (Δt)	Water Flow (m)	Heat Conducted m*S*Δt (Q)	Distance Between Thermocouples (L)	Thermocouple One (T ₁)	Thermocouple Two (T ₂)	Temp Change Over Length T ₁ - T ₂ (ΔT)	Specimen Cross Sectional Area (A)	Thermal Conductivity (L(m*S*Δt))/(AXΔT) (K)
Litres (l)	Joules (J)	Seconds (s)	(°C)	(°C)	(°C)	(l/s)	Watts (W)	Mertres (m)	(°C)	(°C)	(°C)	(m ²)	(w/m °K)
0.6342	4186	600	30.92	21.27	9.65	0.00108	42.69	0.025	172.98	209.32	36.34	0.00047	62.34
0.6211	4186	600	30.60	20.70	9.90	0.00104	42.90	0.025	171.98	208.65	36.67	0.00047	62.08
0.6172	4186	600	30.90	20.97	9.93	0.00103	42.77	0.025	170.95	207.25	36.30	0.00047	62.52
0.6160	4186	600	31.00	21.20	9.80	0.00103	42.11	0.025	170.15	205.22	35.07	0.00047	63.72
0.6508	4186	600	31.25	21.47	9.78	0.00108	44.42	0.025	173.35	204.73	31.38	0.00047	75.11
Average													65.15

Appendix i Table 5 Metal copy Janalloy infiltrant thermal conductivity data

Metal copy Cu													
Mass of Water (M)	Specific Heat of Water (S)	Test Duration (s)	Water Temp Out (T _{out})	Water Temp In (T _{in})	Change in Water Temp T _{out} - T _{in} (Δt)	Water Flow (m)	Heat Conducted m*S*Δt (Q)	Distance Between Thermocouples (L)	Thermocouple One (T ₁)	Thermocouple Two (T ₂)	Temp Change Over Length T ₁ - T ₂ (ΔT)	Specimen Cross Sectional Area (A)	Thermal Conductivity (L(m*S*Δt))/(AXΔT) (K)
Litres (l)	Joules (J)	Seconds (s)	(°C)	(°C)	(°C)	(l/s)	Watts (W)	Mertres (m)	(°C)	(°C)	(°C)	(m ²)	(w/m °K)
0.7004	4186	600	31.37	21.60	9.77	0.00117	47.73	0.025	117.27	212.78	95.51	0.00047	26.51
0.7949	4186	600	31.95	21.90	10.05	0.00132	55.73	0.025	128.93	203.30	74.37	0.00047	39.76
0.7981	4186	600	30.78	21.60	9.18	0.00133	51.11	0.025	118.88	208.50	89.62	0.00047	30.26
0.7932	4186	600	31.78	21.78	10.00	0.00132	55.34	0.025	122.63	203.08	80.45	0.00047	36.50
0.7646	4186	600	32.25	22.20	10.05	0.00127	53.61	0.025	123.18	217.00	93.82	0.00047	30.32
Average													32.18

Appendix i Table 6 Metal copy CU thermal conductivity data

Metal copy Cu Infiltrant													
Mass of Water (M)	Specific Heat of Water (S)	Test Duration (s)	Water Temp Out (T _{out})	Water Temp In (T _{in})	Change in Water Temp T _{out} - T _{in} (Δt)	Water Flow (m)	Heat Conducted m ³ S*Δt (Q)	Distance Between Thermocouples (L)	Thermocouple One (T ₁)	Thermocouple Two (T ₂)	Temp Change Over Length T ₁ - T ₂ (ΔT)	Specimen Cross Sectional Area (A)	Thermal Conductivity (L(m ³ S*Δt))/(AXΔT) (K)
Litres (l)	Joules (J)	Seconds (s)	(°C)	(°C)	(°C)	(l/s)	Watts (W)	Mertres (m)	(°C)	(°C)	(°C)	(m ²)	(w/m °K)
0.8004	4186	600	31.50	22.00	9.50	0.00133	53.05	0.025	195.03	207.28	12.25	0.00047	229.77
0.7752	4186	600	31.50	21.68	9.82	0.00129	53.09	0.025	195.72	208.02	12.30	0.00047	229.01
0.7706	4186	600	31.22	21.55	9.67	0.00128	51.97	0.025	191.75	203.77	12.02	0.00047	229.46
0.7568	4186	600	31.42	21.60	9.82	0.00126	51.83	0.025	192.57	204.97	12.40	0.00047	221.78
0.8528	4186	600	30.95	21.42	9.53	0.00142	56.72	0.025	197.00	209.40	12.40	0.00047	242.69
Average													230.54

Appendix i Table 7 Metal copy CU infiltrant thermal conductivity data

Vertical Laminate													
Mass of Water (M)	Specific Heat of Water (S)	Test Duration (s)	Water Temp Out (T _{out})	Water Temp In (T _{in})	Change in Water Temp T _{out} - T _{in} (Δt)	Water Flow (m)	Heat Conducted m ³ S*Δt (Q)	Distance Between Thermocouples (L)	Thermocouple One (T ₁)	Thermocouple Two (T ₂)	Temp Change Over Length T ₁ - T ₂ (ΔT)	Specimen Cross Sectional Area (A)	Thermal Conductivity (L(m ³ S*Δt))/(AXΔT) (K)
Litres (l)	Joules (J)	Seconds (s)	(°C)	(°C)	(°C)	(l/s)	Watts (W)	Mertres (m)	(°C)	(°C)	(°C)	(m ²)	(w/m °K)
0.6545	4186	600	31.18	22.10	9.08	0.00109	41.48	0.025	110.55	211.48	100.93	0.00049	20.93
0.6470	4186	600	31.70	22.40	9.30	0.00108	41.98	0.025	107.83	207.83	100.00	0.00049	21.38
0.6403	4186	600	31.43	22.30	9.13	0.00107	40.79	0.025	106.02	201.17	95.15	0.00049	21.87
0.5223	4186	600	31.98	21.65	10.33	0.00087	37.65	0.025	117.27	205.05	87.78	0.00049	21.88
0.8600	4186	1020	29.50	21.00	8.50	0.00084	30.00	0.025	65.00	134.00	69.00	0.00049	22.14
Average													21.64

Appendix i Table 8 Vertical Laminate thermal conductivity data

Horizontal Laminate													
Mass of Water (M)	Specific Heat of Water (S)	Test Duration (s)	Water Temp Out (T _{out})	Water Temp In (T _{in})	Change in Water Temp T _{out} - T _{in} (Δt)	Water Flow (m)	Heat Conducted m ³ S ³ Δt (Q)	Distance Between Thermocouples (L)	Thermocouple One (T ₁)	Thermocouple Two (T ₂)	Temp Change Over Length T ₁ - T ₂ (ΔT)	Specimen Cross Sectional Area (A)	Thermal Conductivity (L(m ³ S ³ Δt))/(AXΔT) (K)
Litres (l)	Joules (J)	Seconds (s)	(°C)	(°C)	(°C)	(l/s)	Watts (W)	Mertres (m)	(°C)	(°C)	(°C)	(m ²)	(w/m °K)
0.7208	4186	600	31.58	23.06	8.53	0.00120	42.89	0.025	110.75	214.12	103.37	0.00049	21.13
0.5984	4186	600	31.90	22.62	9.28	0.00100	38.75	0.025	105.42	202.10	96.68	0.00049	20.41
0.5838	4186	600	31.73	22.23	9.50	0.00097	38.69	0.025	104.77	200.73	95.96	0.00049	20.54
0.6188	4186	600	31.12	22.10	9.02	0.00103	38.93	0.025	103.77	200.70	96.93	0.00049	20.45
0.6078	4186	600	31.38	22.20	9.18	0.00101	38.94	0.025	103.90	201.05	97.15	0.00049	20.41
Average													20.59

Appendix i Table 9 Horizontal Laminate thermal conductivity data

Amdry (790)													
Mass of Water (M)	Specific Heat of Water (S)	Test Duration (s)	Water Temp Out (T _{out})	Water Temp In (T _{in})	Change in Water Temp T _{out} - T _{in} (Δt)	Water Flow (m)	Heat Conducted m ³ S ³ Δt (Q)	Distance Between Thermocouples (L)	Thermocouple One (T ₁)	Thermocouple Two (T ₂)	Temp Change Over Length T ₁ - T ₂ (ΔT)	Specimen Cross Sectional Area (A)	Thermal Conductivity (L(m ³ S ³ Δt))/(AXΔT) (K)
Litres (l)	Joules (J)	Seconds (s)	(°C)	(°C)	(°C)	(l/s)	Watts (W)	Mertres (m)	(°C)	(°C)	(°C)	(m ²)	(w/m °K)
0.7730	4186	600	31.12	22.47	8.65	0.00129	46.65	0.025	111.83	206.90	95.07	0.00047	26.02
0.7748	4186	600	30.85	22.40	8.45	0.00129	45.68	0.025	107.45	200.03	92.58	0.00047	26.16
0.7685	4186	600	30.78	22.45	8.33	0.00128	44.66	0.025	105.23	204.30	99.07	0.00047	23.91
0.7645	4186	600	31.08	22.60	8.48	0.00127	45.25	0.025	113.80	202.90	89.10	0.00047	26.93
0.6586	4186	600	31.72	21.92	9.80	0.00110	45.03	0.025	109.45	201.73	92.28	0.00047	25.88
Average													25.78

Appendix i Table 10 Amdry (790) thermal conductivity data

Vertical RapidSteel 2.0													
Mass of Water (M)	Specific Heat of Water (S)	Test Duration (s)	Water Temp Out (T _{out})	Water Temp In (T _{in})	Change in Water Temp T _{out} - T _{in} (ΔT)	Water Flow (m)	Heat Conducted m ³ S*Δt (Q)	Distance Between Thermocouples (L)	Thermocouple One (T ₁)	Thermocouple Two (T ₂)	Temp Change Over Length T ₁ - T ₂ (ΔT)	Specimen Cross Sectional Area (A)	Thermal Conductivity (L(m ³ S*Δt))/(AXΔT) (K)
Litres (l)	Joules (J)	Seconds (s)	(°C)	(°C)	(°C)	(l/s)	Watts (W)	Metres (m)	(°C)	(°C)	(°C)	(m ²)	(w/m °K)
0.8283	4186	600	31.87	22.22	9.65	0.00138	55.77	0.025	111.65	205.82	94.17	0.00047	31.40
0.8510	4186	605	30.90	21.68	9.22	0.00141	54.27	0.025	107.87	202.82	94.95	0.00047	30.31
0.8255	4186	600	31.25	21.60	9.65	0.00138	55.58	0.025	123.93	214.65	90.72	0.00047	32.49
0.8197	4186	600	31.12	21.62	9.50	0.00137	54.33	0.025	119.18	209.32	90.13	0.00047	31.98
0.8657	4186	640	31.60	21.97	9.63	0.00135	54.54	0.025	117.05	206.25	89.20	0.00047	32.43
Average													31.72

Appendix i Table 11 Vertical RapidSteel 2.0 thermal conductivity data

Horizontal RapidSteel 2.0													
Mass of Water (M)	Specific Heat of Water (S)	Test Duration (s)	Water Temp Out (T _{out})	Water Temp In (T _{in})	Change in Water Temp T _{out} - T _{in} (ΔT)	Water Flow (m)	Heat Conducted m ³ S*Δt (Q)	Distance Between Thermocouples (L)	Thermocouple One (T ₁)	Thermocouple Two (T ₂)	Temp Change Over Length T ₁ - T ₂ (ΔT)	Specimen Cross Sectional Area (A)	Thermal Conductivity (L(m ³ S*Δt))/(AXΔT) (K)
Litres (l)	Joules (J)	Seconds (s)	(°C)	(°C)	(°C)	(l/s)	Watts (W)	Metres (m)	(°C)	(°C)	(°C)	(m ²)	(w/m °K)
0.8537	4186	600	31.77	22.13	9.64	0.00142	57.40	0.025	123.20	206.07	82.87	0.00047	36.73
0.8450	4186	600	31.27	22.13	9.14	0.00141	53.87	0.025	119.25	206.60	87.35	0.00047	32.70
0.8440	4186	600	31.33	22.10	9.23	0.00141	54.37	0.025	118.45	205.37	86.92	0.00047	33.17
0.8750	4186	600	30.93	21.63	9.30	0.00146	56.77	0.025	112.97	203.02	90.05	0.00047	33.43
0.8585	4186	600	31.20	21.60	9.60	0.00143	57.50	0.025	116.93	202.40	85.47	0.00047	35.67
Average													34.34

Appendix i Table 12 Horizontal RapidSteel 2.0 thermal conductivity data

Vertical EOS DirectSteel 50μm													
Mass of Water (M)	Specific Heat of Water (S)	Test Duration (s)	Water Temp Out (T _{out})	Water Temp In (T _{in})	Change in Water Temp T _{out} - T _{in} (ΔT)	Water Flow (m)	Heat Conducted m ³ S*Δt (Q)	Distance Between Thermocouples (L)	Thermocouple One (T ₁)	Thermocouple Two (T ₂)	Temp Change Over Length T ₁ – T ₂ (ΔT)	Specimen Cross Sectional Area (A)	Thermal Conductivity (L(m ³ S*Δt))/(AXΔT) (K)
Litres (l)	Joules (J)	Seconds (s)	(°C)	(°C)	(°C)	(l/s)	Watts (W)	Mertres (m)	(°C)	(°C)	(°C)	(m ²)	(w/m °K)
0.5349	4186	625	30.40	21.42	8.98	0.00086	32.18	0.025	92.28	208.88	116.60	0.00047	14.64
0.4998	4186	600	30.48	21.60	8.88	0.00083	30.96	0.025	96.10	207.72	111.62	0.00047	14.71
0.4328	4186	600	31.80	21.90	9.90	0.00072	29.89	0.025	91.52	206.78	115.26	0.00047	13.75
0.4324	4186	600	31.78	21.77	10.02	0.00072	30.21	0.025	93.02	207.50	114.48	0.00047	13.99
0.4295	4186	600	31.03	21.63	9.40	0.00072	28.17	0.025	86.35	206.32	119.97	0.00047	12.45
Average													13.91

Appendix i Table 13 Vertical EOS DirectSteel 50µm thermal conductivity data

Horizontal EOS DirectSteel 50µm													
Mass of Water (M)	Specific Heat of Water (S)	Test Duration (s)	Water Temp Out (T _{out})	Water Temp In (T _{in})	Change in Water Temp T _{out} - T _{in} (Δt)	Water Flow (m)	Heat Conducted m ³ S*Δt (Q)	Distance Between Thermocouples (L)	Thermocouple One (T ₁)	Thermocouple Two (T ₂)	Temp Change Over Length T ₁ – T ₂ (ΔT)	Specimen Cross Sectional Area (A)	Thermal Conductivity (L(m ³ S*Δt))/(AXΔT) (K)
Litres (l)	Joules (J)	Seconds (s)	(°C)	(°C)	(°C)	(l/s)	Watts (W)	Mertres (m)	(°C)	(°C)	(°C)	(m ²)	(w/m °K)
0.4061	4186	600	31.12	21.00	10.12	0.00068	28.66	0.025	88.53	203.93	115.40	0.00047	13.17
0.4782	4186	600	30.72	21.07	9.65	0.00080	32.20	0.025	92.70	207.88	115.18	0.00047	14.82
0.4851	4186	600	30.27	21.40	8.87	0.00081	30.01	0.025	92.03	201.90	109.87	0.00047	14.48
0.4807	4186	600	30.72	21.20	9.52	0.00080	31.91	0.025	89.62	205.67	116.05	0.00047	14.58
0.4564	4186	600	31.83	21.60	10.23	0.00076	32.58	0.025	95.03	206.37	111.34	0.00047	15.52
Average													14.52

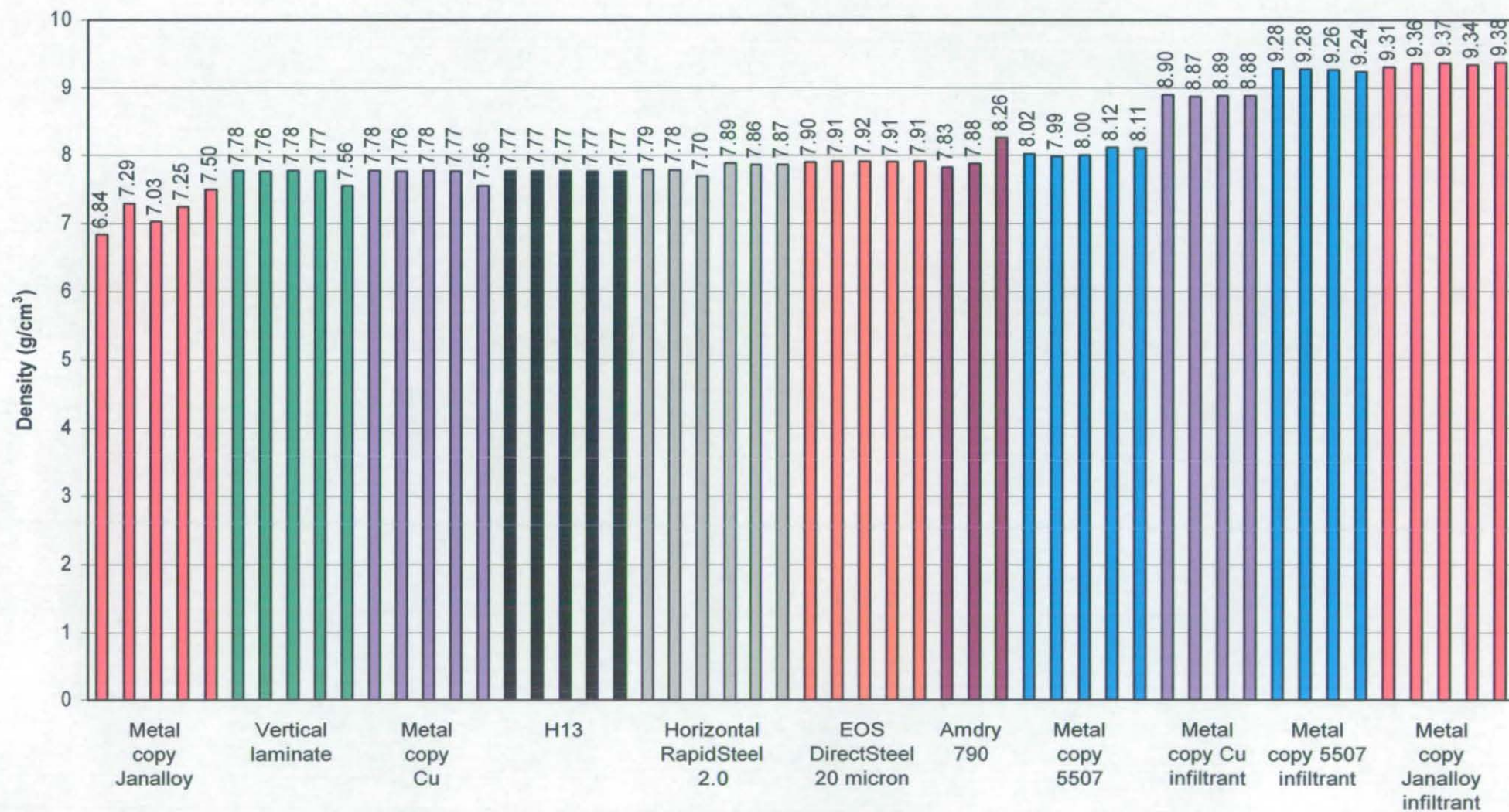
Appendix i Table 14 Horizontal EOS DirectSteel 50µm thermal conductivity data

Vertical EOS DirectSteel 20µm													
Mass of Water (M)	Specific Heat of Water (S)	Test Duration (s)	Water Temp Out (T _{out})	Water Temp In (T _{in})	Change in Water Temp T _{out} - T _{in} (Δt)	Water Flow (m)	Heat Conducted m ³ S*Δt (Q)	Distance Between Thermocouples (L)	Thermocouple One (T ₁)	Thermocouple Two (T ₂)	Temp Change Over Length T ₁ - T ₂ (ΔT)	Specimen Cross Sectional Area (A)	Thermal Conductivity (L(m ³ S*Δt))/(AXΔT) (K)
Litres (l)	Joules (J)	Seconds (s)	(°C)	(°C)	(°C)	(l/s)	Watts (W)	Mertres (m)	(°C)	(°C)	(°C)	(m ²)	(w/m °K)
0.4378	4186	600	31.45	21.87	9.58	0.00073	29.26	0.025	98.68	208.28	109.60	0.00047	14.16
0.4400	4186	600	31.07	21.77	9.30	0.00073	28.55	0.025	93.10	202.93	109.83	0.00047	13.79
0.4510	4186	600	32.52	22.30	10.22	0.00075	32.15	0.025	92.57	212.25	119.68	0.00047	14.24
0.4240	4186	600	32.02	23.70	8.32	0.00071	24.60	0.025	89.35	208.07	118.72	0.00047	10.99
0.4261	4186	600	32.05	22.45	9.60	0.00071	28.54	0.025	93.63	204.50	110.87	0.00047	13.65
Average													13.36

Appendix i Table 15 Vertical EOS DirectSteel 20µm thermal conductivity data

Horizontal EOS DirectSteel 20µm													
Mass of Water (M)	Specific Heat of Water (S)	Test Duration (s)	Water Temp Out (T _{out})	Water Temp In (T _{in})	Change in Water Temp T _{out} - T _{in} (Δt)	Water Flow (m)	Heat Conducted m ³ S*Δt (Q)	Distance Between Thermocouples (L)	Thermocouple One (T ₁)	Thermocouple Two (T ₂)	Temp Change Over Length T ₁ - T ₂ (ΔT)	Specimen Cross Sectional Area (A)	Thermal Conductivity (L(m ³ S*Δt))/(AXΔT) (K)
Litres (l)	Joules (J)	Seconds (s)	(°C)	(°C)	(°C)	(l/s)	Watts (W)	Mertres (m)	(°C)	(°C)	(°C)	(m ²)	(w/m °K)
0.5797	4186	600	29.62	21.55	8.07	0.00097	32.63	0.025	93.93	211.12	117.19	0.00047	14.76
0.4807	4186	600	30.73	21.40	9.33	0.00080	31.29	0.025	98.75	203.52	104.77	0.00047	15.84
0.4223	4186	600	31.97	22.00	9.97	0.00070	29.36	0.025	94.60	203.73	109.13	0.00047	14.27
0.4384	4186	605	31.57	21.67	9.90	0.00072	30.02	0.025	94.20	206.32	112.12	0.00047	14.20
0.4310	4186	600	31.45	21.80	9.65	0.00072	29.01	0.025	92.85	208.00	115.15	0.00047	13.36
Average													14.49

Appendix i Table 16 Horizontal EOS DirectSteel 20µm thermal conductivity data



Appendix i Figure 1 Material density

Appendix ii

Thermocouple, Temperature Paint Calibration and H13 Heat Treatment

Appendix ii: Thermocouple Calibration

A calibrated mineral insulated K type thermocouple (12-k-500-125-1.5-2l-3p2L-100mm A30KX) from TC Ltd was used.

Appendix ii Table 1 shows the calibration data obtained from TC Ltd., (TC Ltd, 2003).

Measured temperature (°C)	Measured voltage (mV)	Equivalent IEC value (°C)	Error (°C)
19.80	787	19.7	-0.10
700.67	29153	700.54	-0.13
1000.55	41210	998.30	-2.25

Appendix ii Table 1 Temperature and micro voltage readings

The thermocouple was calibrated by comparison with two reference resistance thermometers and two reference type R thermocouples. All measurements are traceable to recognised national standards. Calibration was carried out using a stirred liquid bath and a triple zone furnace. The thermocouple wires were referenced to 0°C. The resistance and voltage outputs were measured on a precision digital multi-meter. All tests were carried out in a controlled environment using devices having known and traceable values. The temperature measurements were traceable to ITS-90. The thermocouple voltages were converted using BS EN 60584-1:1995 and Linseis, (1985).

The depth of immersion of the thermocouple was to a minimum of 125mm. The overall uncertainty of measurement was $\pm 0.3^{\circ}\text{C}$ at 20°C , $\pm 1.5^{\circ}\text{C}$ at 700°C and $\pm 2.5^{\circ}\text{C}$ at 1000°C . The reported expanded uncertainty is based on a standard uncertainty multiplied by a coverage factor of $K = 2$, providing a level of confidence of approximately 95%. The uncertainty evaluation has been carried out in accordance with UKAS requirements (TC Ltd., 2003).

The calibrated K type thermocouple was used as a reference for all other temperature measuring equipment used in this project. The thermocouples were placed in a Carbolite furnace (Model number: MFHT 1.1400 Prog) set at 700°C . A calibrated digital volt meter was used to record the micro volts output of each of the thermocouples, which were compared to reference values to obtain the temperature (Appendix ii Table 2). These values were then compared with the calibrated thermocouple.

Thermocouple	Furnace set temperature (°C)	Volt meter reading (mV)	Reference temperatures from micro volt readings (°C)
Calibrated	700	29270	703.4
1	700	29180	701.2
2	700	29145	700.4
3	700	29240	702.7
4	700	29210	702
5	700	29190	701.5
6	700	29120	699.8
7	700	29060	698.4
8	700	29210	702
9	700	29290	703.9
10	700	29140	700.3

Appendix ii Table 2 Results of Carbolite furnace thermocouple micro volt calibration at 700°C

In Appendix ii Table 2 the deviation of the micro-volts reading from the reference thermocouple can be seen to be between +0.5°C and -5°C. When measuring the temperature in the tool it was necessary to use a compensating cable to connect the thermocouples to a multi channel recorder. As a result of using this procedure the calibration test was repeated using the compensating cable. When connected to a multi-channel digital reader, through compensating cables, the deviations were greater, between +9.9°C and -5.4°C (Appendix ii Table 3).

Thermocouple	Furnace set temperature (°C)	Digital reader temp (°C)	Reference temperatures from micro volt readings (°C)	Difference (°C)
Calibrated	700	695	703.4	8.4
1	700	695	701.2	6.2
2	700	694	700.4	6.4
3	700	694	702.7	8.7
4	700	694	702	8
5	700	693	701.5	8.5
6	700	693	699.8	6.8
7	700	693	698.4	5.4
8	700	694	702	8
9	700	694	703.9	9.9
10	700	694	700.3	6.3

Appendix ii Table 3 Thermocouple digital readout calibration at 700°C

The results show that there can be a total variation of $\approx 15^{\circ}\text{C}$ when recording temperatures around 700°C . A second test was conducted to assess the performance of the thermocouples at lower temperatures. A water tank was chilled to 10°C and the procedure used for the high temperature comparisons were followed.

From Appendix ii Table 4 it can be seen that the micro volt deviation from the reference thermocouple was between +1°C and -1.7°C.

Thermocouple	Tank set temperature (°C)	Volt meter reading (mV)	Reference temperatures from micro volt readings (°C)
Calibrated	10	390	9.8
1	10	395	9.9
2	10	395	9.9
3	10	415	10.5
4	10	320	8.1
5	10	355	8.9
6	10	390	9.8
7	10	430	10.8
8	10	385	9.7
9	10	415	10.5
10	10	360	9.1

Appendix ii Table 4 Thermocouple micro volt calibration at 10°C

When connected to a multi-channel digital reader, through compensating cables, the deviation was between +1.5°C and -0.9°C (Appendix ii Table 5). It is clear from the data that the thermocouples were more accurate at lower temperatures.

Thermocouple	Tank set temperature (°C)	Digital reader temp (°C)	Reference temperatures from micro volt readings (°C)	Difference (°C)
Calibrated	10	10	9.8	-0.2
1	10	10	9.9	-0.1
2	10	9	9.9	0.9
3	10	9	10.5	1.5
4	10	9	8.1	-0.9
5	10	9	8.9	-0.1
6	10	9	9.8	0.8
7	10	10	10.8	0.8
8	10	10	9.7	-0.3
9	10	10	10.5	0.5
10	10	10	9.1	-0.9

Appendix ii Table 5 Thermocouple digital readout calibration at 10°C

ii.i Thermal Paints Furnace Test

ii.i.i Aim

Temperature sensitive paints made by Tempilaq® were used to validate the maximum temperature recorded by the thermocouples. However, the tolerance range and accuracy of these paints had to be assessed as did their suitability for use with molten aluminium. In order

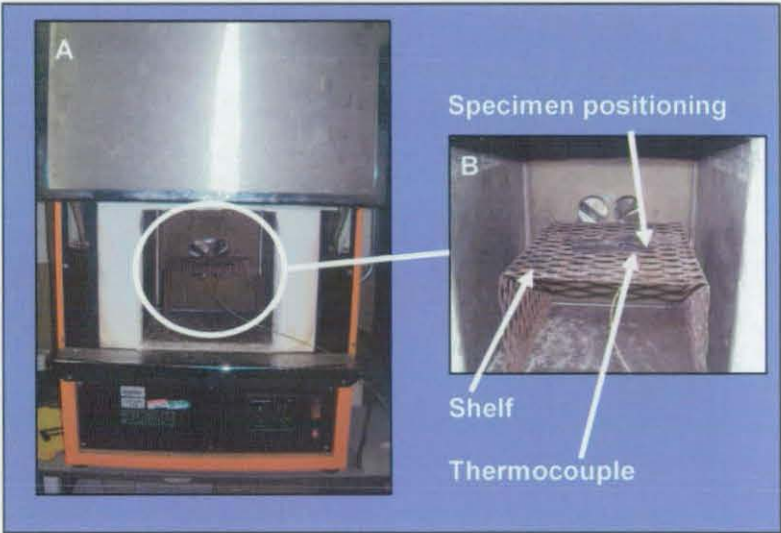
to make this assessment, appropriate tests were conducted. Appendix ii Table 6 shows the temperatures at which they should burn off.

Paint Number	1	2	3	4	5	6	7	8	9	10	11
Temperature (°F)	225	400	475	700	750	850	950	1022	1100	1200	1300
Temperature (°C)	107	204	246	371	399	454	510	550	593	649	704

Appendix ii Table 6 Temperature paint range

ii.i.ii Methodology

The first test used was the furnace trials. A muffle furnace (**Error! Reference source not found.**, Vectstar SP700) was calibrated at each of the test temperatures using a calibrated thermocouple and reader. A shelf was constructed to position the specimen in the centre of the furnace and a calibrated thermocouple placed alongside to ensure that the correct temperature was attained (Appendix ii Figure 1).



Appendix ii Figure 1 (A) Vectstar muffle furnace; (B) Specimen positioning

Five specimens were assessed at each test temperature by applying one paint type to each of five H13 steel strips (1mm thick x 20mm width x 80mm long) in a similar manner shown in Appendix ii Figure 2. The specimens were placed on the shelf in the furnace until the temperature at which the paint burns off was shown by the thermocouple. The specimens were then immediately removed from the furnace.



Appendix ii Figure 2 Temperature paints and test strips

ii.i.iii Results

- Temperature paint 107°C: 10°C below the specified temperature the paint was clearly visible. At the specified temperature half of the paint had burned off and at 10°C above the specified temperature all the paint had burned off. Giving a temperature range of 97°C - 117°C
- Temperature paint 204°C: 10°C below the specified temperature the paint was clearly visible. At the specified temperature half of the paint had burned off. 10°C above the specified temperature only small traces of paint remained. 20°C above the specified temperature all the paint had been removed. Giving a temperature range of 194°C - 224°C
- Temperature paint 246°C: 10°C below the specified temperature the paint was visible. At the specified temperature half of the paint had burned off. 10°C above the specified temperature only traces of paint remained. 20°C above the specified temperature all the paint had been removed. Giving a temperature range of 236°C - 266°C
- Temperature paint 371°C: 20°C below the specified temperature the paint was clearly visible. 10°C below the specified temperature the paint had dulled. 10°C above the specified temperature all the paint had been removed. Giving a temperature range of 351°C - 381°C
- Temperature paint 399°C: 20°C below the specified temperature the paint was clearly visible. 10°C below the specified temperature the paint had dulled. At the specified temperature all the paint had been removed. Giving a temperature range of 379°C - 409°C
- Temperature paint 454°C: 10°C below the specified temperature the paint was visible. At the specified temperature half of the paint had burned off. 10°C above the specified temperature all the paint had been removed. Giving a temperature range of 444°C - 464°C

- Temperature paint 510°C: 10°C below the specified temperature the paint was visible. 10°C above the specified temperature all the paint had been removed. Giving a temperature range of 500°C - 520°C
- Temperature paint 550°C: 10°C below the specified temperature the paint was visible. At the temperature half the paint had burned off. 20°C above the specified temperature all the paint had been removed. Giving a temperature range of 540°C - 570°C
- Temperature paint 593°C: 50°C below the specified temperature the paint was visible. 40°C below the specified temperature half the paint had burned off. 30°C below the specified temperature only traces of paint remained, from 10°C below the specified temperature, and above, all the paint had been removed. Giving a temperature range of 543°C - 583°C
- Temperature paint 649°C: 30°C below the specified temperature a quarter of the paint had burned off. 20°C below the specified temperature half the paint had burned off. 10°C below the specified temperature half the paint had burned off. At the specified temperature and 10°C above the specified temperature only traces of the paint remained. 20°C above the specified temperature all the paint had been removed. Giving a temperature range of 619°C - 669°C
- Temperature paint 704°C: 10°C below the specified temperature the majority of the paint was visible. At the specified temperature two thirds of the paint had burned off. 10°C above the specified temperature all the paint had been removed. Giving a temperature range of 694°C - 714°C

ii.i.iv Conclusion

It is important to apply an even layer of paint to avoid confusing results. However, the paints do work at approximately their set temperature. The furnace trials showed the temperature paints had a variable tolerance. The test determined at what temperature the paints were visible and visa versa, allowing them to be used as a cross reference in the die temperature experiment. However, it was not clear if the paints would respond in the same manner when subjected to molten aluminium, so additional tests were conducted.

ii.ii Casting Test One

ii.ii.i Aim

The casting trials were used to establish how the temperature paints behaved when molten aluminium at 700°C was poured onto them.

ii.ii.ii Methodology

Casting trial one was a simple test, which was repeated three times to assess the reproducibility of the results. Six specimens (H13 steel strips 1mm thick x 20mm width x 80mm long) were each painted with the 11 temperature paints as shown in Appendix ii Figure 3.



Appendix ii Figure 3 Painted specimens

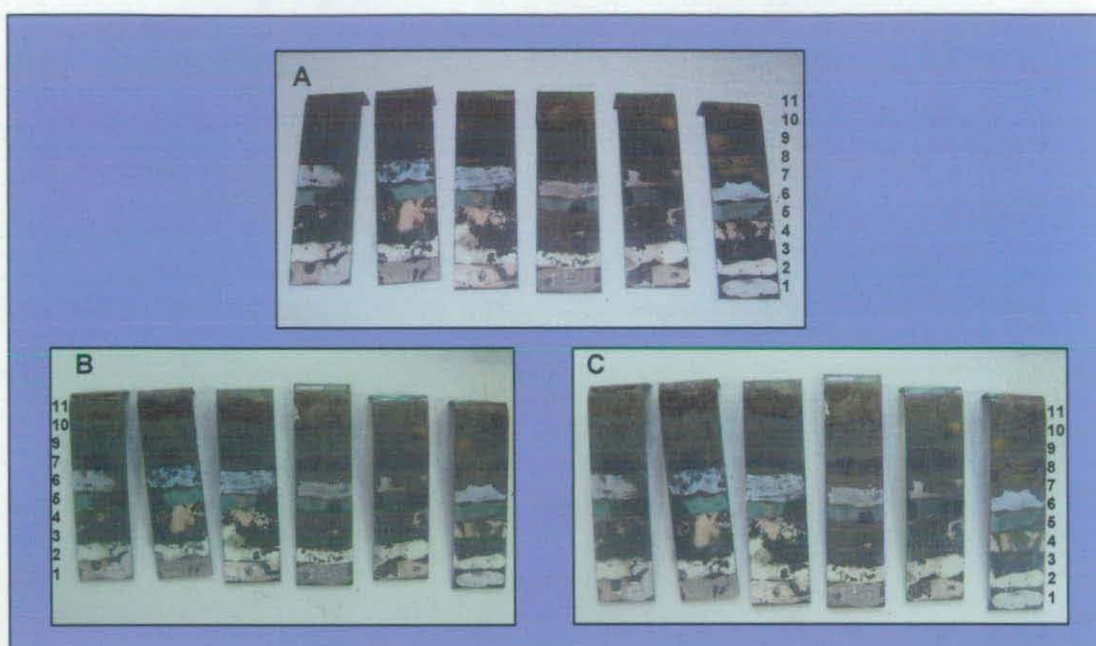
The test was set up as shown in Appendix ii Figure 4 and aluminium LM24 was heated in a ceramic crucible to 800°C using an induction furnace (Induction heating Systems (UK) Ltd., 100KW, 700 V, 199 A, 800 - 1200 Hz, weight 700kg). The molten aluminium was cooled in still air to 700°C; this was verified using a calibrated thermocouple. The aluminium was then poured onto the surface of the painted test specimens for 3 seconds ensuring the aluminium coated the specimens as shown in Appendix ii Figure 4, and allowed to cool.



Appendix ii Figure 4 Aluminium being cast on the specimens

ii.ii.iii Results

Once cool the aluminium was removed from the surface of the test specimens and the results are shown in Appendix ii Figure 5. The aluminium was also inspected and no sign of the paint was visible. The specimens showed that the higher temperature paints 1 - 6 (702°C - 454°C) were still visible but paints 7 - 11 (399°C - 107°C) had burnt off.



Appendix ii Figure 5 Casting specimens after casting (A) test 1; (B) test 2; (C) test 3

The test showed that some of the paints burn off when in contact with molten aluminium. However, the test also showed that the aluminium cooled rapidly when poured onto the H13 steel surface, which was at 20°C - 25°C. This was seen visually during the experiment and the paints showed that the H13 specimens never reached 700°C. The lowest visible paint from all the tests was the blue paint (paint 6), which was designed to burn off at 454°C; this occurred because the small quantity of aluminium poured formed a skin almost instantaneously on contact with the painted specimens.

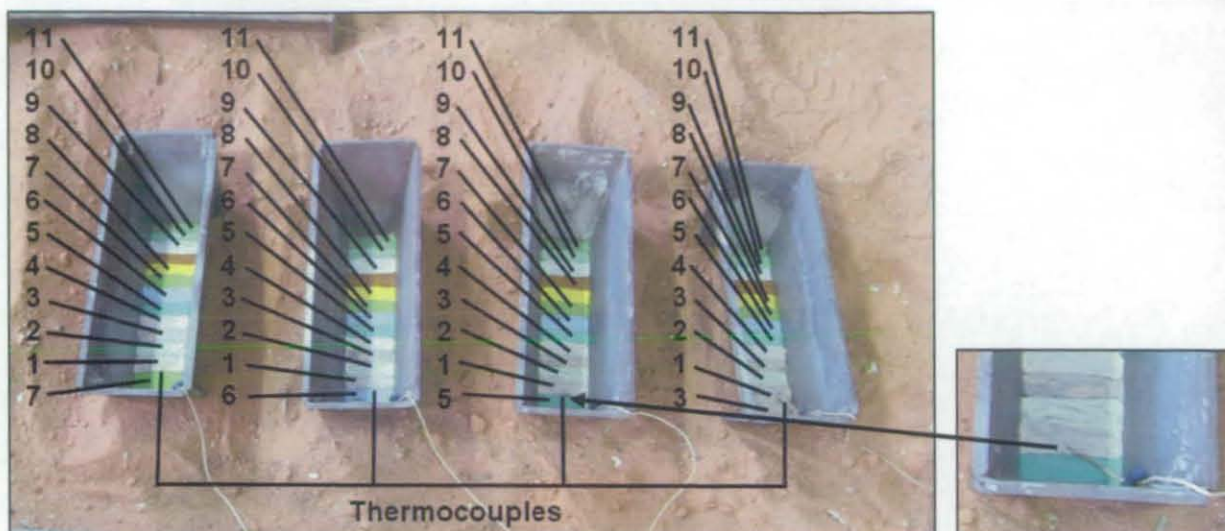
ii.iii Casting Test Two

ii.iii.i Aim

There was some concern that the results of the previous test may have been affected by the small amount of aluminium used and, therefore, resulted in a rapid cooling rate. A new test was designed to assess the affects of a large volume of aluminium on the paints.

ii.iii.ii Methodology

The paints (1 - 11) were applied to the bottom of four ingot moulds and where space allowed additional paints (7, 6, 5, 3) were added (Appendix ii Figure 6). A thermocouple was placed at the end of each ingot to verify the temperature of the aluminium. The ingots were constructed from 5mm mild steel plate and were at 20°C - 25°C.

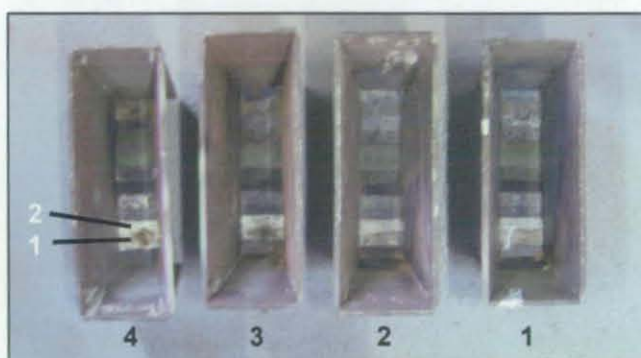


Appendix ii Figure 6 Ingot moulds with temperature paint and thermocouple locations

The aluminium (LM24) was melted in a gas furnace (Morgan Crucible model MIN), when molten it was removed from the furnace and its temperature measured using a calibrated thermocouple. Each ingot received the same quantity of aluminium LM24 measured in a ladle (495ml), the ladle was then left to cool to 700°C prior to pouring. During the pouring process the maximum temperature was recorded using a thermocouple. The aluminium was allowed to cool and then removed.

ii.iii.iii Results

Although it could be seen where all the paints had been applied (Appendix ii Figure 7), there were only two paints remaining, paint 1 (704°C) and paint 2 (649°C); this agreed with the maximum temperatures recorded during the casting process, as shown in Appendix ii Table 7.



Appendix ii Figure 7 Cast ingots after casting (white text = paint number; Black text = ingot number)

Ingot	Maximum temperature (°C)
1	640.58
2	630.54
3	621.6
4	618.2

Appendix ii Table 7 Ingot casting test maximum thermocouple temperatures

Temperature paint 3 had burned off completely indicating that the temperature reached 603°C but temperature paint 2 remained indicating that it did not exceed 649°C.

The casting trials proved that the paints operated at the predicted temperatures within the tolerances discussed in section 6.1.2.3 and worked with a larger volume of molten aluminium. The paint experiments would be able to confirm the thermocouple temperature recorded during the aluminium pressure die casting process.

ii.iv H13 Heat treatment

Hardening profile for trial 1		
Furnace set to 750°C		
Argon shield, flow rate 20 Litres/min		
Notes	Time (mins)	Temperature (°C)
Specimen placed in furnace	0	573
Furnace ramped up to 1040°C	30	750
	55	1000
	60	1015
Removed at	70	1018
Specimen withdrawn from furnace and cooled in still air		25
Tempering 1 profile for trial 1		
Furnace set at 630°C	0	616
	5	630
	20	630
Specimen withdrawn from furnace and cooled in still air		25
Tempering 2 profile for trial 1		
Furnace set at 660°C	0	645
	5	660
	20	660
Specimen withdrawn from furnace and cooled in still air		25

Appendix ii Table 8 H13 hardness and tempering trial one

Hardening profile for trial 2		
Furnace set to 750°C		
Argon shield, flow rate 20 Litres/min		
Notes	Time (mins)	Temperature (°C)
Specimen placed in furnace	0	602
Furnace ramped up to 1030°C	20	750
	50	1000
Removed at	65	1015
Specimen withdrawn from furnace and cooled in still air		25
Tempering 1 profile for trial 2		
Furnace set at 650°C	0	500
	20	650
	35	653
Specimen withdrawn from furnace and cooled in still air		25
Tempering 2 profile for trial 2		
Furnace set at 650°C	0	495
	20	650
	35	651
Specimen withdrawn from furnace and cooled in still air		25

Appendix ii Table 9 H13 hardness and tempering trial two

Hardening profile for trial 3		
Furnace set to 750°C		
Argon shield, flow rate 20 Litres/min		
Notes	Time (mins)	Temperature (°C)
Specimen placed in furnace	0	612
	10	725
	25	750
Furnace ramped up to 1040°C	45	1000
Removed at	60	1027
Specimen withdrawn from furnace and cooled in still air		25
Tempering 1 profile for trial 3		
Furnace set at 645°C	0	565
	5	623
	20	645
Specimen withdrawn from furnace and cooled in still air		25
Tempering 2 profile for trial 3		
Furnace set at 645°C	0	565
	5	620
	20	645
Specimen withdrawn from furnace and cooled in still air		25

Appendix ii Table 10 H13 hardness and tempering trial three

Trial 1	Hardening at 1040°C hardness (HRc)	Temper 1 at 630°C hardness (HRc)	Temper 2 at 660°C hardness (HRc)
Side 1	46.5	45.5	41
	44.8	46.0	40.8
	46.5	47.2	40.5
	44.8	44.3	42.0
Side 2	46.5	45.3	38.9
	45.2	46.5	40.8
	46.8	44.9	42.0
	44.8	45.8	40.5
Average	45.74	45.69	40.81
Trial 2	Hardening at 1030°C hardness (HRc)	Temper 1 at 650°C hardness (HRc)	Temper 2 at 650°C hardness (HRc)
Side 1	43.5	42.5	41.2
	44.8	43	42.5
	44.1	40.8	41.5
	47.5	43	42
Side 2	42.0	42.2	42.5
	44.0	42.0	42
	42.0	41.8	41.8
	43.0	42.4	42
Average	43.86	42.21	41.94
Trial 3	Hardening at 1040°C hardness (HRc)	Temper 1 at 645°C hardness (HRc)	Temper 2 at 645°C hardness (HRc)
Side 1	50	44	45.1
	50.1	45.2	43.8
	50.1	42.5	44.1
	50.5	44.7	43.4
Side 2	48	43.2	46
	50	43.5	44
	46.8	42.6	42.8
	48.4	43.3	43.4
Average	49.24	43.62	44.075

Appendix ii Table 11 Hardness values (Rockwell Scale C) from hardness and tempering trials

Appendix iii

Bonded Laminate Manufacture

Appendix iii: Vertical Laminate and Horizontal Laminate Specimen Manufacture

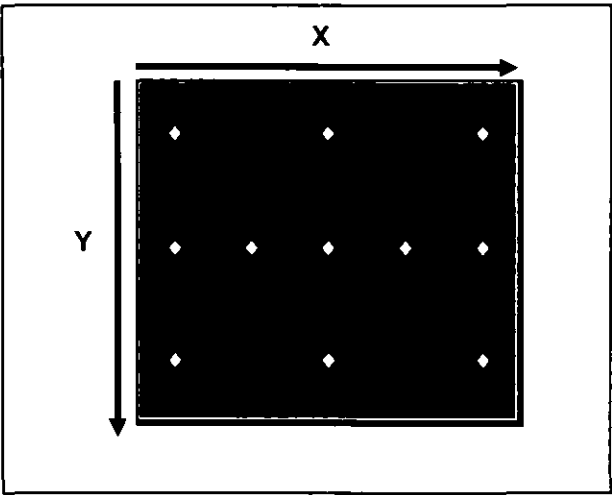
iii.i Sheet Thickness

The sheet as supplied was specified to have a thickness of 1mm +/- 0.11mm. Five sheets measuring 2m x 1m x 1.05mm were measured using a digital vernier to establish the sheets tolerance (Appendix iv Table 1 to Appendix iv Table 5). All sheets measured were within the specified tolerance.

iii.ii Cutting and Affect on Flatness and Microstructure

iii.ii.i Flatness

The sheet flatness was tested, with specimens selected randomly from several sheets. The guillotined and laser cut specimens were de-burred while a third set of specimens were laser cut, de-burred and finished. The specimen size was 100mm x 100mm and these were tested individually at the same location on a surface plate. The surface plate had a flatness tolerance of +/- 0.0001mm. A dial gauge moved across the surface of the specimen and measurements were taken at 25mm - 50mm increments (Appendix iii Figure 1). To achieve uniform braze thickness and stack height it was important to ensure that the sheets remained as flat as possible (Appendix iii Table 1).



Appendix iii Figure 1 Location of measurements for flatness test (♦ = measurement point)

Process condition	Distance from edge (mm) (Y Axis)	Distance from edge (mm) (X Axis)				
		0	25	50	75	100
Guillotined Specimen 1	0	0		0.09		0.01
	50	-0.012	0.068	0.08	0.048	-0.02
	100	-0.03		0.065		-0.05
Guillotined Specimen 2	0	0		-0.05		-0.02
	50	0.021	0.06	0.055	0.04	0.08
	100	-0.02		-0.05		-0.05
Guillotined Specimen 3	0	0		0.05		-0.05
	50	0.045	0.048	0.045	0.045	0.02
	100	-0.015		-0.05		-0.01
Guillotined Specimen Point Ave.	0	0		0.03		-0.02
	50	0.018	0.059	0.06	0.044	0.025
	100	-0.022		-0.012		-0.037
Laser Cut Specimen 1	0	0		0.02		0.015
	50	0.032		0.03		0.01
	100	0.18		-0.03		0
Laser Cut Specimen 2	0	0		0.035		0.03
	50	0.05		0.025		0.024
	100	-0.01		0.03		0.01
Laser Cut Specimen 3	0	0		0.045		0.02
	50	0.04		0.07		0.035
	100	0.01		0.04		0.05
Laser Cut Specimen Point Ave.	0	0		0.033		0.022
	50	0.041		0.042		0.023
	100	0.06		0.013		0.02
Linished Specimen 1	0	0		-0.06		-0.075
	50	0.05	0.03	0.03	0.025	0.015
	100	0.03		0.01		0.01
Linished Specimen 2	0	0		0.032		0.04
	50	-0.02	0.01	0.015	0.01	0.015
	100	-0.012		0.02		0.03
Linished Specimen 3	0	0		-0.03		-0.05
	50	-0.02	-0.051	-0.01	-0.015	-0.03
	100	-0.015		-0.02		-0.051
Linished Specimen Point Ave.	0	0		-0.019		-0.028
	50	0.003	-0.004	0.012	0.0067	0
	100	0.001		0.003		-0.004

Appendix iii Table 1 Flatness test results

The guillotined specimens had a large deviation in flatness, probably, caused by the cutting forces bending the specimen. The maximum deviation of flatness was 0.97mm (the shape of the specimen can be seen in Appendix iv Figure 1). The laser cut specimen had an improved flatness with an average maximum deviation of 0.06mm (Appendix iv Figure 2) whereas the laser cut and linished specimens had an average maximum deviation of 0.048mm (Appendix iv Figure 3).

iii.ii.ii Microstructure

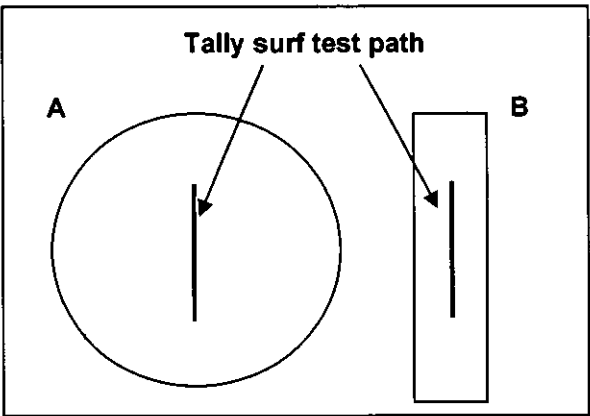
The laminates were all cut oversize to allow for machining, which would have removed the laser cut portion from the laminates. In turn the specimens would be heat treated, which would also change the structure.

iii.iii Surface Finish of Laminates

The surface roughness of a random selection of laminates was measured, to ensure that they had similar surfaces, which would enable consistent bonding (Appendix iii Figure 2). The tests were conducted with a Taylor - Hobson Talysurf 10 with the following:

- 50mm recording length
- 2000 x magnification
- Ra meter ranges: full scale 0.5µm

The Individual surface roughness (µm Ra) of laminates was controlled via linishing (Appendix iii Table 1). In addition, to controlling the surface roughness of the laminates, linishing de-burrs, de-oxidises, de-greases and helps flatten the laminates. The as rolled and linished specimens were 1mm x Ø65mm and 1mm x 15mm x 65mm cut randomly from the H13 sheets. As expected the as rolled surface roughness was good with an average of 0.25µm Ra in comparison to the linished specimens with an average of 0.48µm Ra.



Appendix iii Figure 2 Tally surf test paths; (A) 1mm Ø65mm horizontal profile; (B) 1mm x 15mm x 65mm vertical profile

Specimen	Sheet as Rolled (µm Ra)	Sheet Linished (µm Ra)
1	0.28	0.51
2	0.21	0.48
3	0.23	0.4
4	0.29	0.46
Average	0.25	0.46

Appendix iii Table 2 Laminate surface roughness

iii.iv Bonding Methods

Bonding can be categorised into several domains such as adhesive bonding, melt bonding, infiltration bonding, diffusion bonding, reaction bonding and deformation bonding (Lesuer, 1996).

Aluminium laminates have been bonded with epoxy resin and solders. Epoxy adhesives produce an extremely high interfacial bond strength and when tested to failure the material did not de-laminate (Lesuer, 1996). An epoxy bonded aluminium structure does make a relatively good short run rapid tool for injection moulding. Employing this method of construction would make it a production tool of limited life because the more aggressive polymers, such as glass filled nylon, would erode both the epoxy bond and the aluminium laminates rapidly.

The major draw back with adhesive bonding is that it cannot operate above 250°C (Soar and Dickens, 1996). Although it is possible to load the resin with ceramic powder, the resin is still the weak link. However, it is feasible to operate these adhesives at the average temperature of a die casting tool for a short period. Alternatives are inorganic adhesives that can operate up to and beyond 990°C (Soar and Dickens, 1996). However, wear, tensile strength and differences in thermal expansion again limit these tools to short run tools only.

Brazing and soldering are cost effective, simple and commonplace engineering joining / bonding techniques and both methods have been employed to produce mould tools. Work conducted with silver solders has been successful in low temperature applications (<450°C) and can be employed for laminated injection mould tools (Soar and Dickens, 1996).

Brazing produces high strength joints with a melting point higher than aluminium but lower than H13 steel. The braze material can be applied between laminates in the form of a foil, paste, powder or spray. This process is commonly used in the aerospace industry for bonding honeycomb structures (Soar and Dickens, 1996). The thickness of the braze must be accounted for when slicing a CAD model to produce individual laminate slices, in order for the tool to meet its overall dimensions.

The high temperature and strength characteristics of brazing are very attractive and important when considering its application for the construction of a die casting tool. Selecting the correct braze is crucial, factors such as chemical composition of the substrate and the material to be cast, have to be considered. Other considerations include resistance to debond (Kilingbeil, and Bontha, 2003), distortion, wear and heat treatment of a laminate structure. The reason for selecting a particular brazing alloy was based on the hardening curve of H13. H13 is heat-treated between 995°C - 1025°C with quenching in still air, inert gas or salt. Nickel brazing alloys have a melting temperature between 950°C - 1010°C (Sulzer Metco (UK) Ltd, 1998). This enables bonding at the same stage as heat treatment hence eliminating a process.

Nickel chromium brazes, termed as 'super alloys', have been developed for high temperature service and are suitable for use under moderate to high loading in the temperature range of 540°C to 1100°C. Nickel brazes have been used in the aerospace industry for the construction of gas turbine engines and hot airframe components (Schwartz, 1990).

Heat resistant alloys are generally brazed in an inert environment or in high vacuum furnaces using nickel based metals. Most brazing processes may be used on nickel alloys. The most common are torch, furnace, induction and resistance brazing.

A selection of nickel braze alloys supplied by Sulzer Metco (UK) Ltd are shown In Appendix iii Table 3, they have good corrosion resistance, good bond strength, good oxidation resistance and excellent machinability.

Braze	Alloying elements (% Wt.)							
	Ni	Fe	Re	Cu	Cr	B	Mn	Si
Amdry 936	Bal.		0.03	4		1	19	6
Amdry 775	Bal.				15	3.5		
Amdry 780	Bal.					3		4.5
Amdry 100	Bal.				19			10
Amdry 790	Bal.	1.5				2		3.5

Appendix iii Table 3 Nickel based brazes (Sulzer Metco, 1998)

Nickel brazes are brazed at high temperatures and the affect on the base metal should be taken into account. Non heat treatable alloys will suffer moderate strength losses due to grain growth during brazing (Schwartz, 1990).

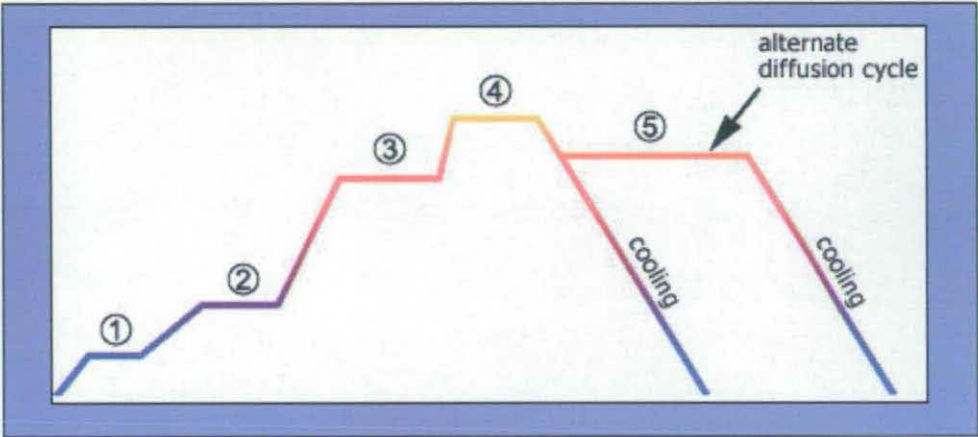
In order to obtain good braze coverage and uniform thickness it was important to select a suitable method of depositing it onto the base material. For the purpose of laminate tooling it was also necessary to control the braze thickness in order to maintain the tolerance of the tool. This could be achieved, by tape, spray, powder or paste. It is possible to automate spray or paste forms, improving process control and consequently maintaining the tool tolerance.

Surface preparation was crucial to achieve a good bond, base materials must have oxide layers and grease removed by machining, pickling and de-greasing. Each laminate specimen was manufactured as outlined in Appendix iii Table 4.

Stage	Activity	Process
1	Rough machining	Machined individual profiles with a CO ₂ laser to + 1mm of finish specification.
2	Linishing	Linished individual laminates to 0.48µm Ra on a de-burring and finishing machine.
3	De-grease	Isopropanol alcohol followed by rinse and dry.
4	Assemble	Assembled the laminates with powder / paste braze between them.
5	Braze	In an inert argon atmosphere.
6	Finish machining	Turn external surfaces on CNC lathe.

Appendix iii Table 4 Manufacturing process for bonded laminates

The furnace temperature is dependent upon the composition of the braze material and can go up to 1150°C. Appendix iii Figure 3 (Sulzer Metco, 1998) shows a typical brazing cycle.



Appendix iii Figure 3 Typical heating and cooling cycle for brazing (Sulzer Metco, 1998)

The first hold (1) is between 150°C - 260°C for 10 - 15 minutes to allow the solvents or water in the powder / paste / binder to outgas from the braze alloy; this also reduces porosity in the braze and restores the atmosphere, which can be degraded by the gasses. The second hold (2) is at 540°C for 10 - 15 minutes to allow the organics (not liquids) in the braze sufficient time to become gaseous and to be pumped out. Hold number three (3) is for 10 minutes at 10 °C - 38°C below the braze alloy solidus temperature to allow stabilisation. The temperature is then increased as fast a possible to the brazing temperature (4) and held for 1 hour to allow sufficient time for the braze to melt and flow into the joints. One of two ramp down methods can be chosen for the final stage:

- 1) Allows the braze to solidify then quenching can take place below the solidus temperature of the braze

- 2) Hold at 1066°C - 1150°C (5) for 2 - 4 hours to allow boron to diffuse and raise the re-melt temperature of the braze alloy

Bryden and Pashby, (1999) conducted research on laminate tooling, which was joined by brazing for injection moulding. Using a heated platen, individual bonded joints were produced.

Lap shear specimens of two laminate gauges (0.8mm and 1.6mm) were produced to evaluate the tensile strengths of the bonded laminates. At optimum conditions, which is the least time taken for highest tensile strength to be attained, the 0.8mm laminate withstood a load of 4.7kN after 120 seconds heating time and the 1.6mm laminate averaged 9.3kN after 210 seconds heating time.

Like brazing, soldering has a lower melting point than the materials to be joined and will form a bond even if the surfaces are not even. A diffusion soldering technique was developed by GEC-Marconi Materials Technology Ltd. The solder was based on copper, silver, gold and tin. Each laminate required electro-plating. The layers were stacked and subjected to 3 MPa and 525°C for 1 hour in a vacuum. The process produced a diffused solder joint of primarily silver. Like the brazing technique it was necessary to have an accurate thickness of electro-plated solder material to ensure tool accuracy was maintained; this process produced shear strengths approaching 100MPa and was capable of withstanding temperatures approaching 962°C due to the phase changes that occurred during the soldering process (Bocking et.al., 1997).

Obikawa, 1999, described a similar process where 0.2mm steel laminates were coated with 40µm of U-alloy, a low melting point solder (90°C) (Obikawa, 1999). A laminate structure was built up layer-by-layer and each layer was bonded to the next using an induction heater to heat the press. Once bonded the laminate was laser cut and the process repeated until the component was complete.

Diffusion bonding removes the need for a material, such as a braze or solder, to be placed between the laminates. Instead the edges of each individual laminate are electron beam welded in a vacuum. The laminate structure is then placed in a hot isostatic press (HIP) where it is subjected to a temperature of 1100°C and a pressure of 6MPa. The thesis author, in conjunction with CERAM, has successfully hot isostatically pressed H13 tool steel and stainless steel producing a complete solid. This method, however, is time consuming and requires an expensive hot isostatic press.

Nakagawa, 1985, overcame this by employing a process of pressure bonding of tool steel (Hot rolled SK5) laminate sheets (Nakagawa, 1985). The process began with a stack of assembled laminates that were subjected to 1100°C in an atmosphere of dissociated ammonia ($N_2 + 3H_2$). This was then removed and immediately pressed (30MPa) between two flat dies in air for up to

a minute. Once the pressing cycle was complete it was cooled in the furnace to prevent oxidation.

Additional bonding methods include: explosive welding, friction welding, ultrasonic welding and resistance welding (DeGarmo, 1988). However, possible problems of bonded tools are:

- The heat treatment process for a bonded laminate structure will be different to that of a conventionally manufactured die, which is heat treated after machining. H13 is hardened at 1020°C and double tempered at 640°C to achieve a hardness of 43HRc - 48HRc. The bonding material has a higher melting point than 730°C (aluminium casting temperature) to prevent melting during the casting process. In order to bond the laminates it is also important that the bonding material has a melting point similar to or higher than the hardening temperature of the laminates to achieve bonding and hardening. The laminates then require finishing in their hardened state
- A bonded laminated structure may have different rates of thermal conductivity and this can cause hot spots / cool spots within the tool and its structure; this may cause increased stress and heat cracking and / or thermal fatigue, which in turn would cause premature failure
- Differing coefficients of expansion between the laminate and bonding material could create stress in the tool and premature failure
- Clamping / ejection forces may cause de-lamination of the tool
- Erosion / wear of bond during the tool life
- Thermal fatigue / hot cracking of a bonded laminate structure
- Subjecting the die to abnormal tensile loading, (if a component seizes), would result in possible composite structure failure

iii.v Bonding of Laminates

The brazing process has several variables, such as:

- Time (controlled by furnace cycle)
- Temperature (controlled by furnace cycle)
- Heat cooling profile (controlled by furnace cycle)
- Pressure (controlled by a dead weight on the laminate stack)

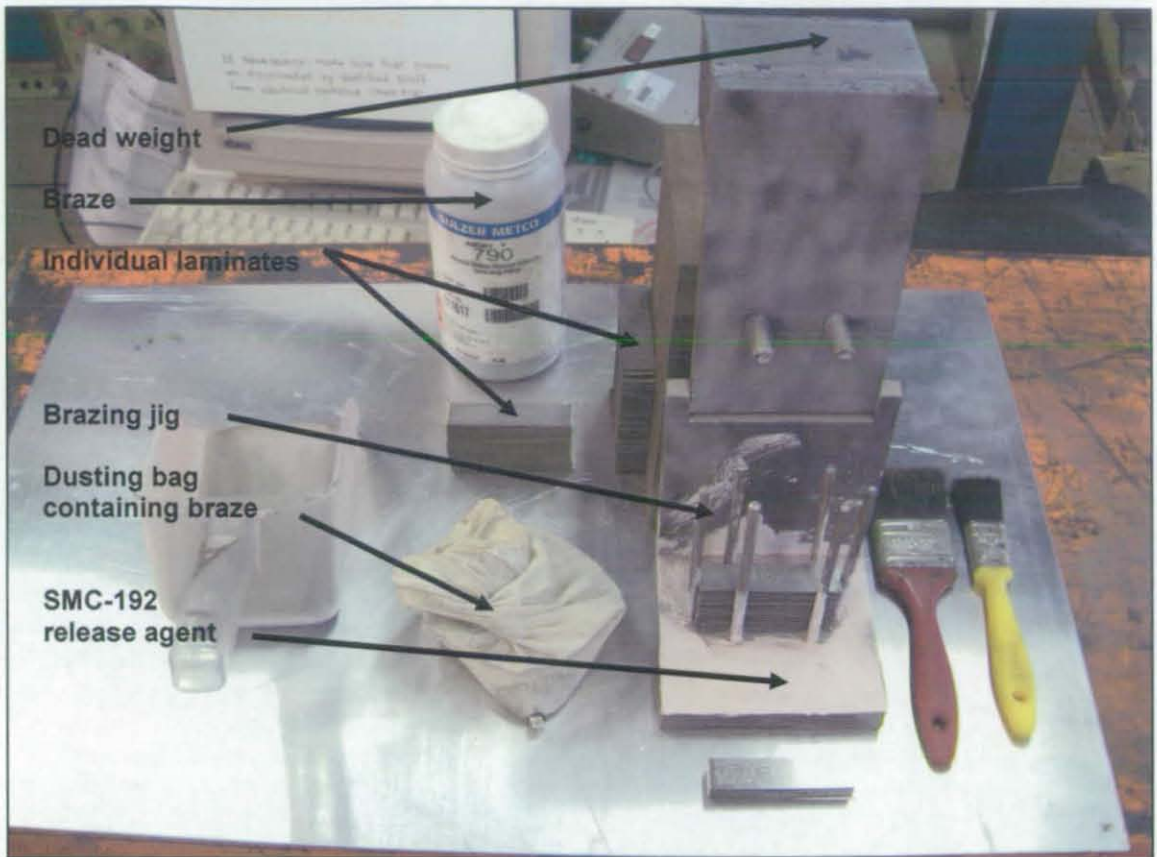
By using a programmable furnace it was possible to control the brazing temperature, time and heating profile. During the brazing process equal pressure, laminate alignment and braze thickness were achieved by using jigs with dead weights applying a load on the top of the laminate stack. Appendix iii Figure 4 shows the horizontal (A) and vertical jigs (B); five of each type were manufactured.



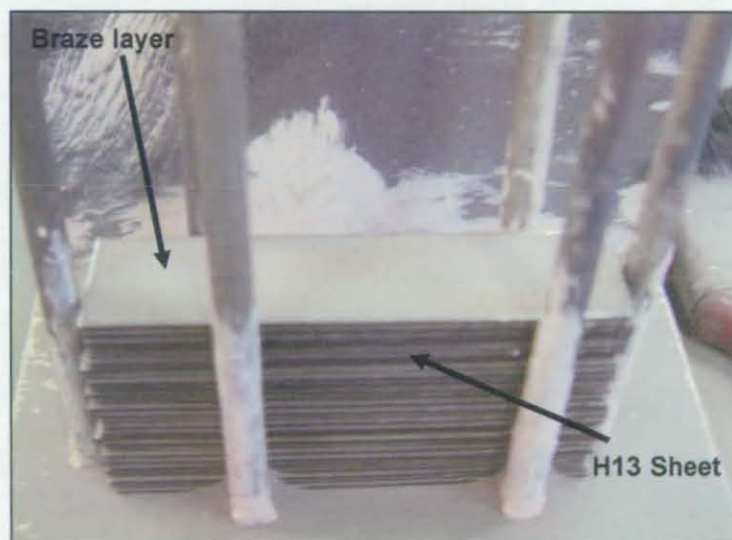
Appendix iii Figure 4 (A) Horizontal laminate jig; (B) Vertical laminate jig

A nickel braze (Amdry 790, supplied by Sulzer Metco (UK) Ltd) was used in the brazing process. The jigs were coated with a foundry coating (SMC-192, Foseco Foundry International Ltd) to assist the release of the laminate stack after brazing. The stacks were assembled by placing an individual laminate in the fixture and dusting it with the braze powder (Appendix iii Figure 5 and Appendix iii Figure 6), then the next laminate was placed on top and the process repeated until the desired height was achieved (note: during brazing the process stack would compress so it was important to compensate for this). Finally a bar was placed at the top of the stack to distribute the load applied from the jig evenly across the laminate stack.

The braze thickness was controlled by the weight of the top part of the fixture. When the braze was molten, excess would flow out of the joint resulting in a uniform braze thickness. This technique was taken from previous work (Bryden and Pashby, 1999).

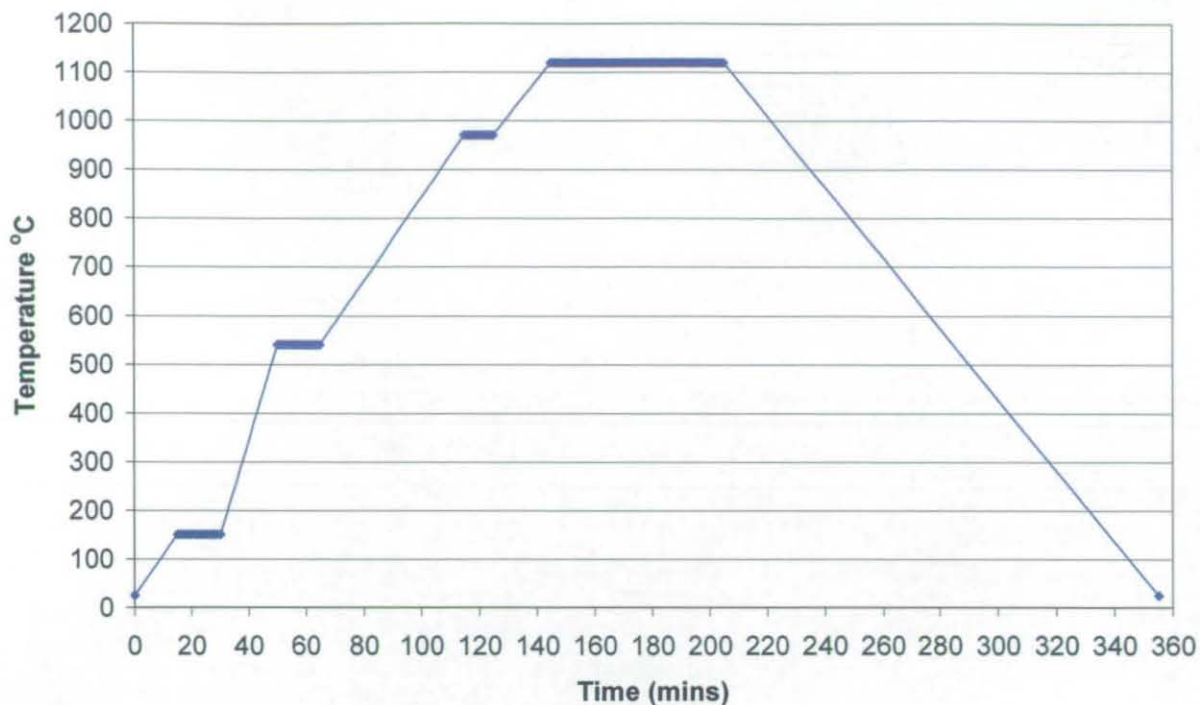


Appendix iii Figure 5 Laminate stack braze assembly



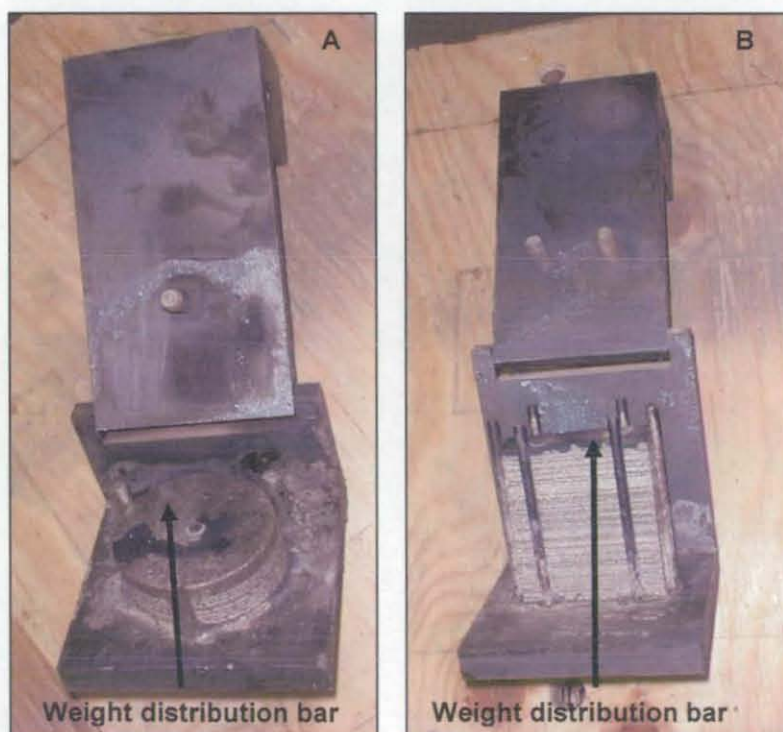
Appendix iii Figure 6 Laminate stack with dusting of braze (Amdry 790)

All the assemblies were placed in the furnace, which was purged with argon for 20 minutes at a rate of 30 litres/minute; this was then reduced to 10 litres / minute throughout the brazing cycle. Brazing was conducted in an inert atmosphere to avoid surface oxidation and embrittlement. Appendix iii Figure 7 shows the time / temperature profile for the brazing process.



Appendix iii Figure 7 Brazing furnace profile (Sulzer Metco, 1998)

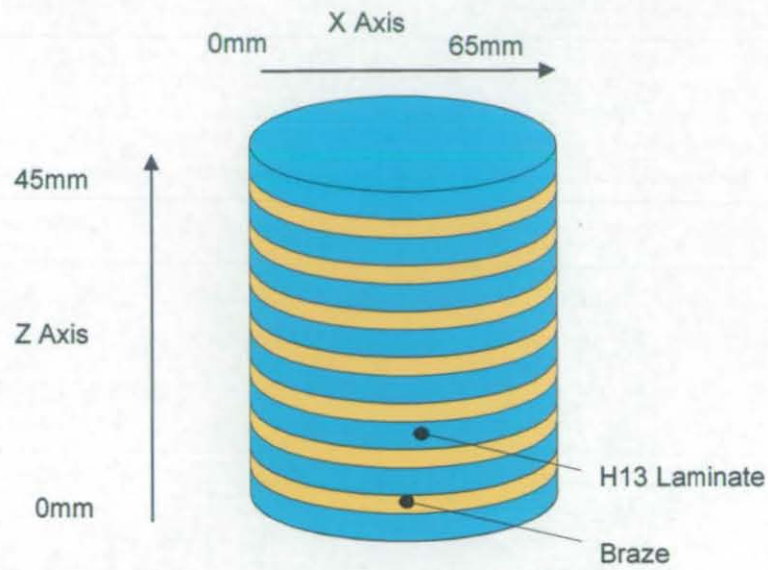
Appendix iii Figure 8 shows the Horizontal and Vertical laminate stacks in the jigs after brazing. The brazed laminates were then removed from the jigs to await machining.



Appendix iii Figure 8 Jigs and braze bonded laminates after removal from furnace; (A) Horizontal laminate specimens; (B) Vertical laminate specimens

iii.vi **Braze Thickness**

After rough machining the laminate stacks were examined (Appendix iii Figure 9). The specimen edges were inspected with a microscope, fitted with micrometers, at 50x magnification.



Appendix iii Figure 9 Bonded structure

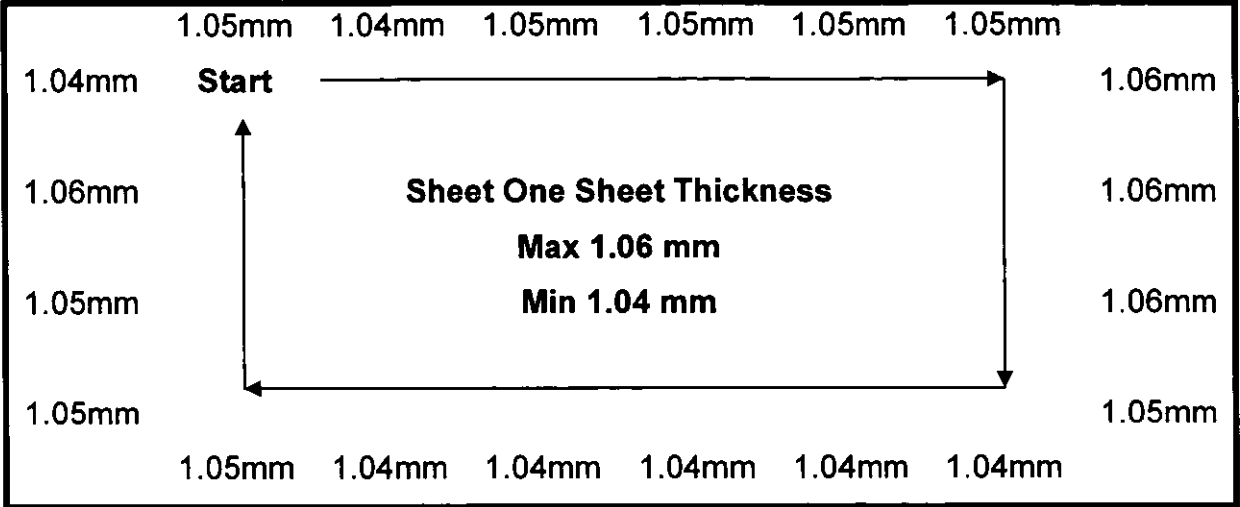
The braze thickness was, on average, found to be 0.15mm, a maximum of 0.16mm and a minimum of 0.11mm (Appendix iii Table 5).

Braze number	Braze thickness (mm) (X Axis)			Average
(Z axis measurement points)	0mm	25mm	50mm	
1 (0mm)	0.14	0.14	0.16	0.15
2 (5mm)	0.13	0.14	0.16	0.14
3 (10mm)	0.15	0.12	0.14	0.14
4 (15mm)	0.18	0.18	0.11	0.16
5 (20mm)	0.13	0.16	0.14	0.14
6 (25mm)	0.14	0.15	0.17	0.15
7 (30mm)	0.14	0.13	0.13	0.13
8 (45mm)	0.15	0.16	0.17	0.16
9 (40mm)	0.14	0.14	0.15	0.14

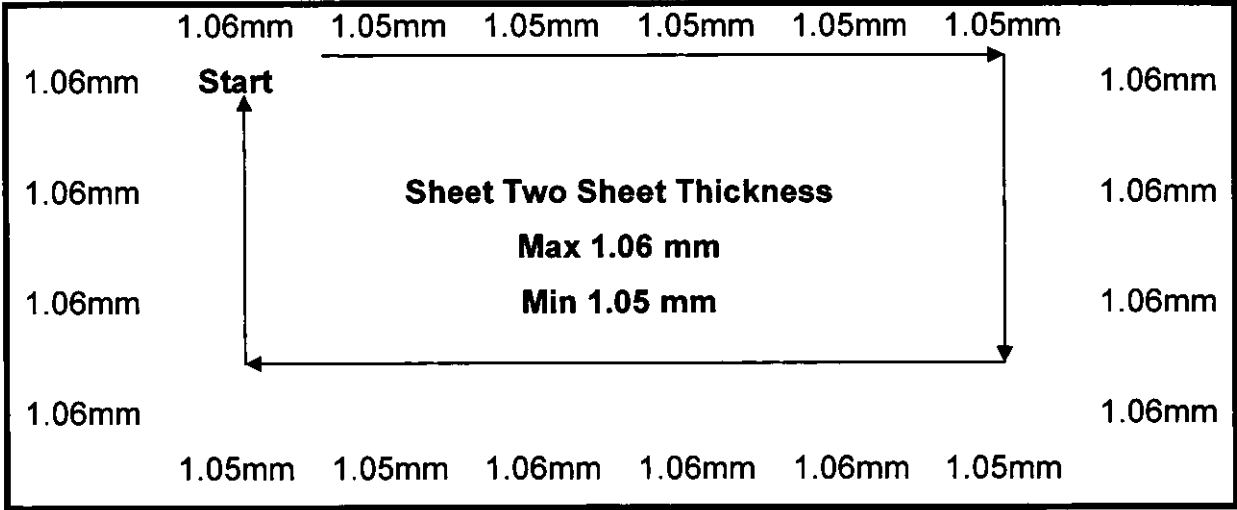
Appendix iii Table 5 Braze thickness

Appendix iv

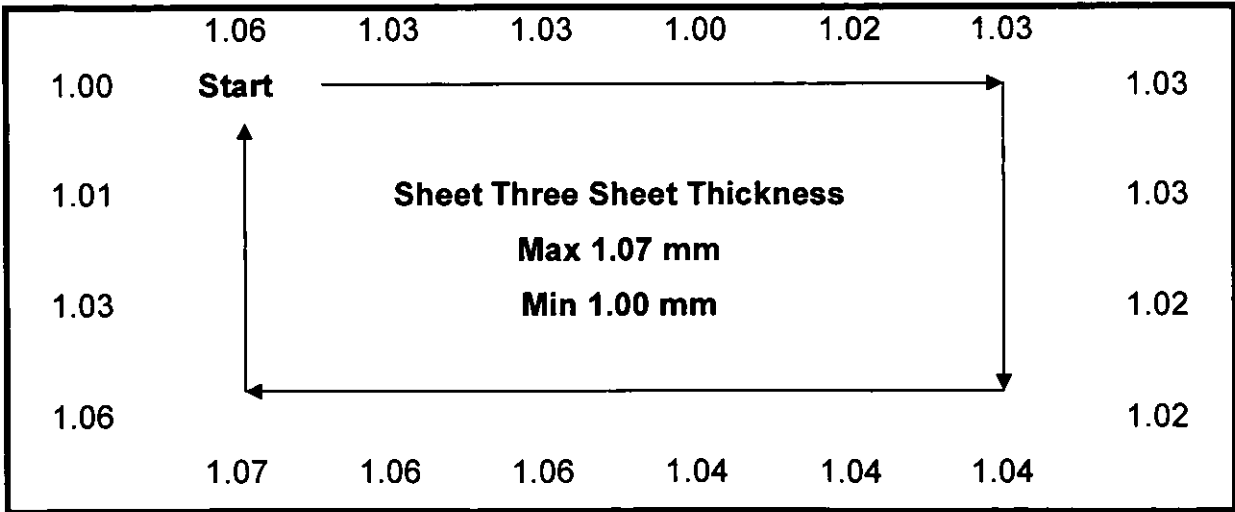
Material Flatness



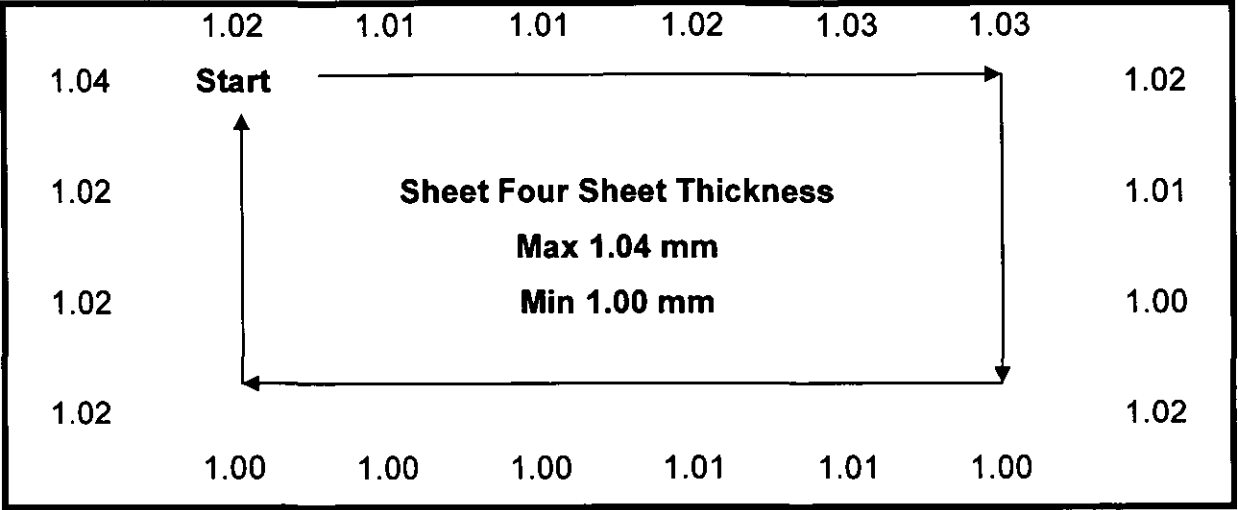
Appendix iv Table 1 Sheet 1 thickness



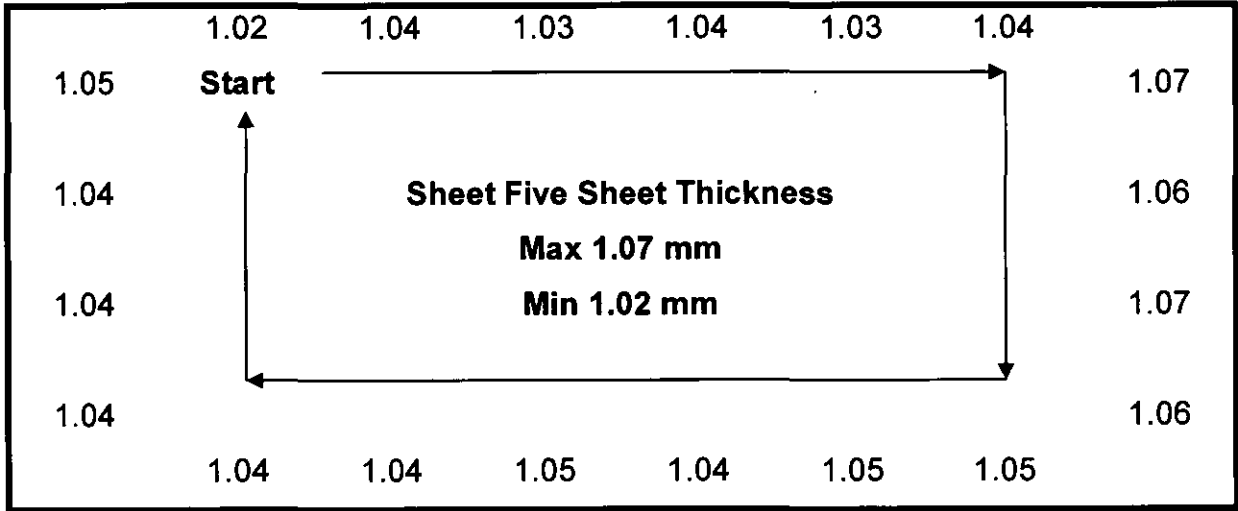
Appendix iv Table 2 Sheet 2 thickness



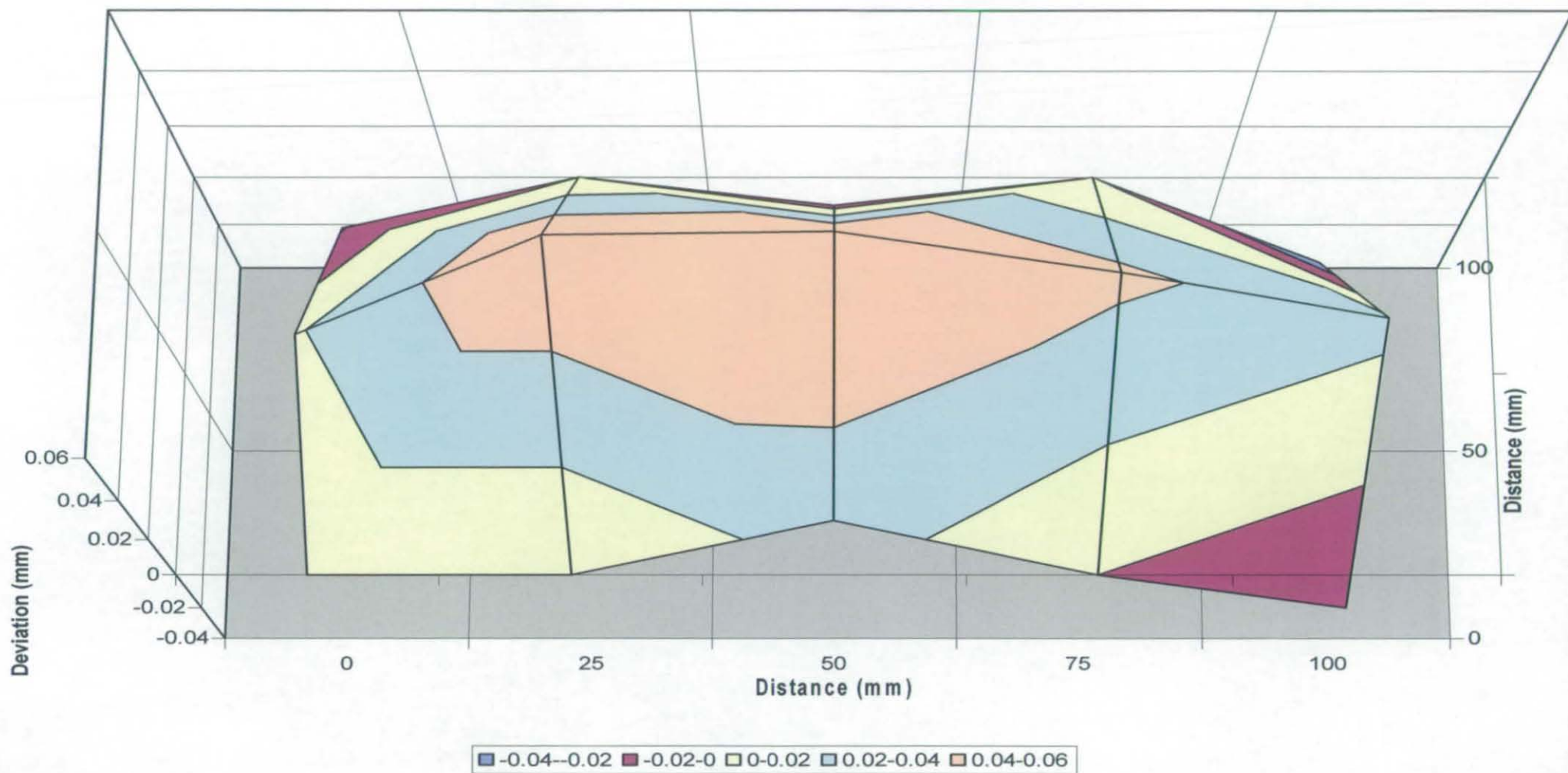
Appendix iv Table 3 Sheet 3 thickness



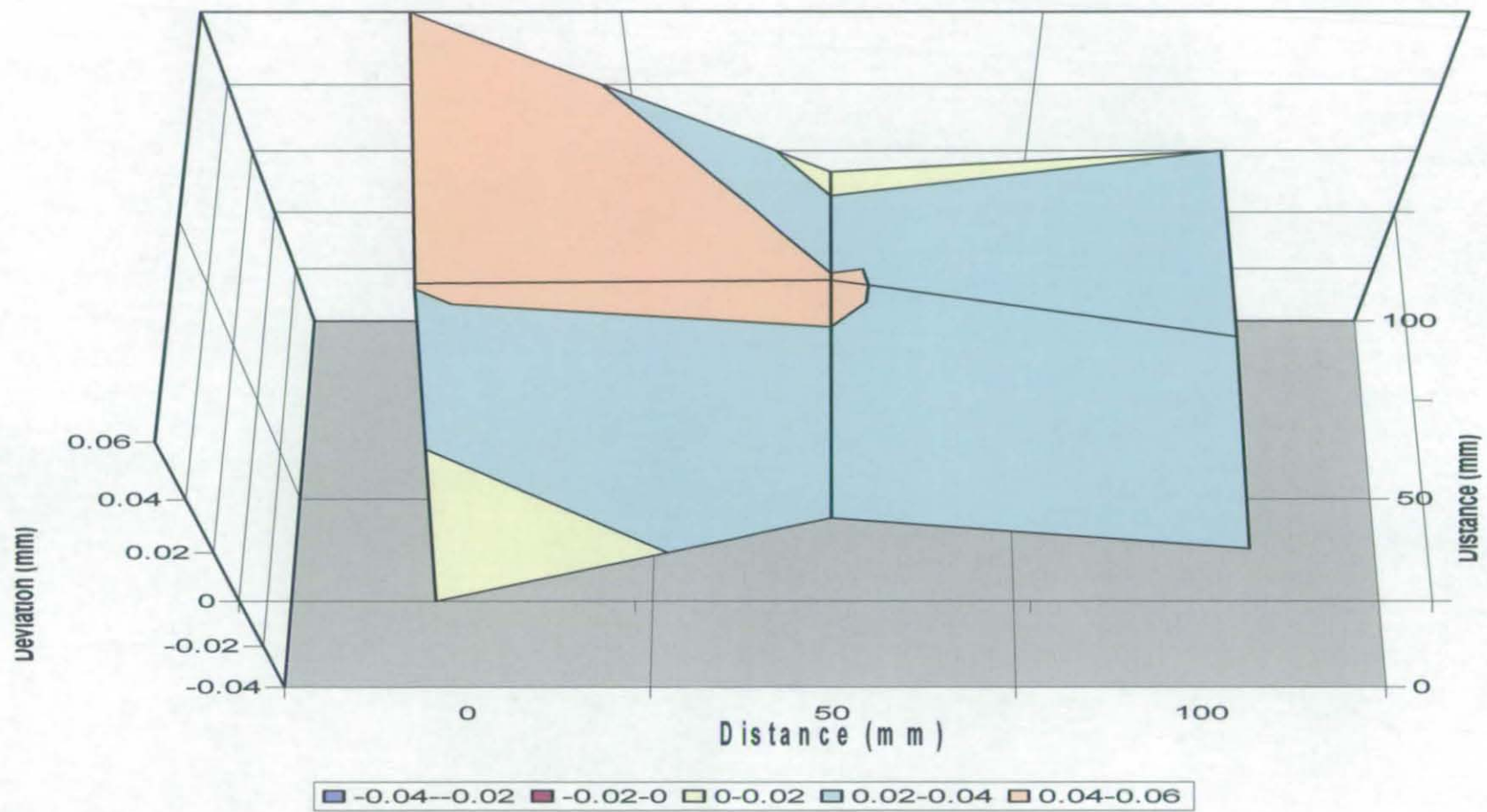
Appendix iv Table 4 Sheet 4 thickness



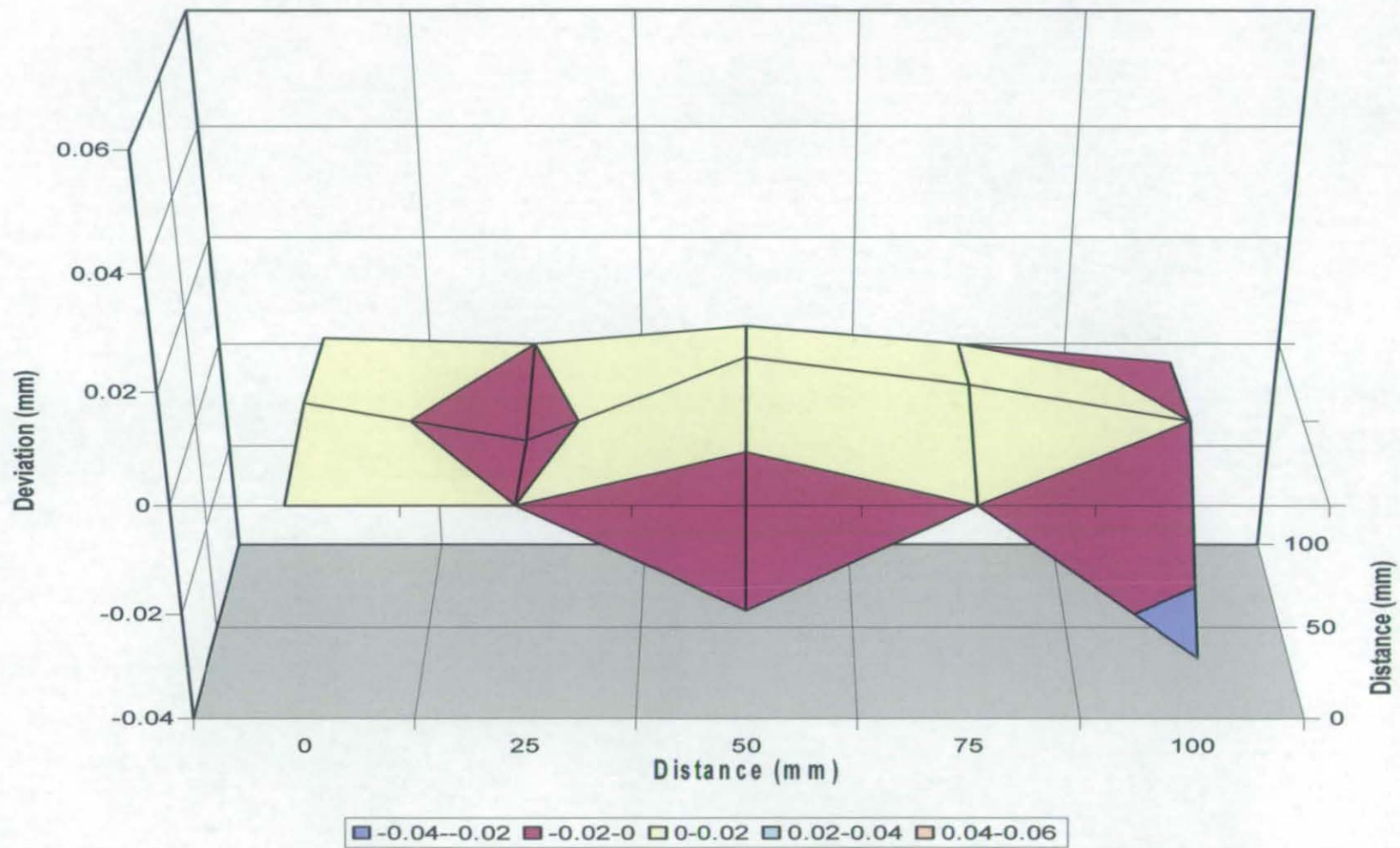
Appendix iv Table 5 Sheet 5 thickness



Appendix iv Figure 1 Average guillotined specimen surface flatness



Appendix iv Figure 2 Average laser cut specimen surface flatness



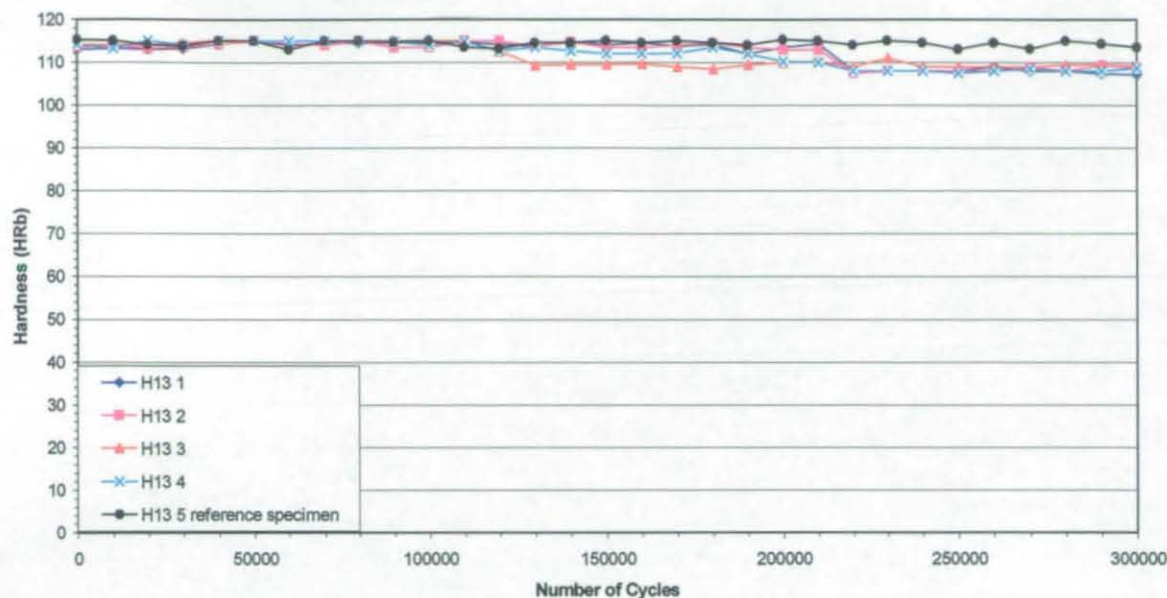
Appendix iv Figure 3 Average finished specimen surface flatness

Appendix v

Thermal Fatigue Experiment Graphs

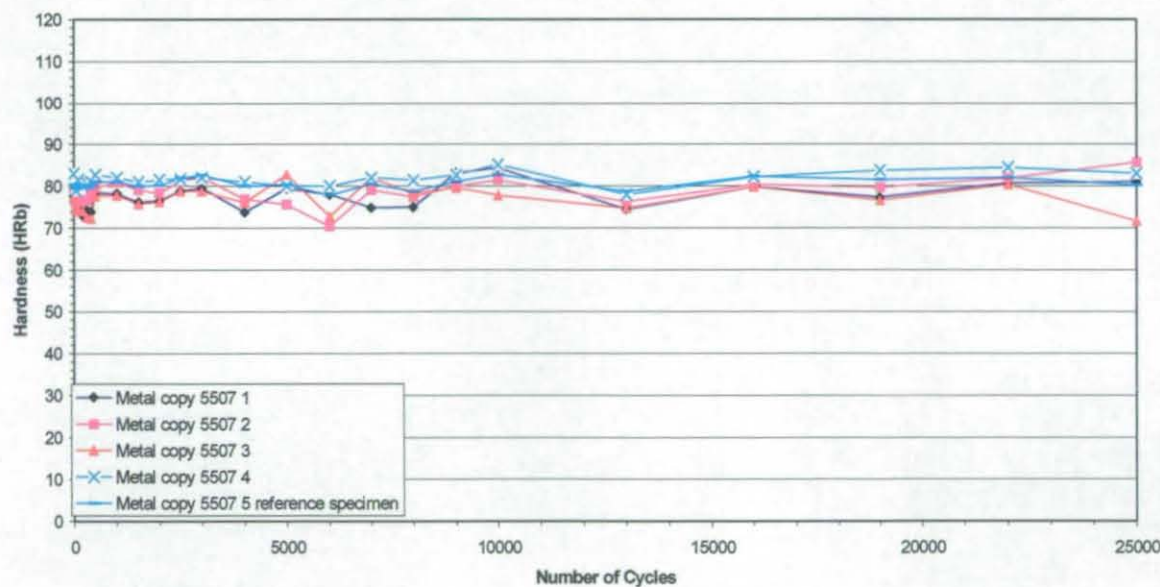
Appendix v: Thermal Fatigue Experiment Graphs

v.i H13 Thermal Fatigue Material Data

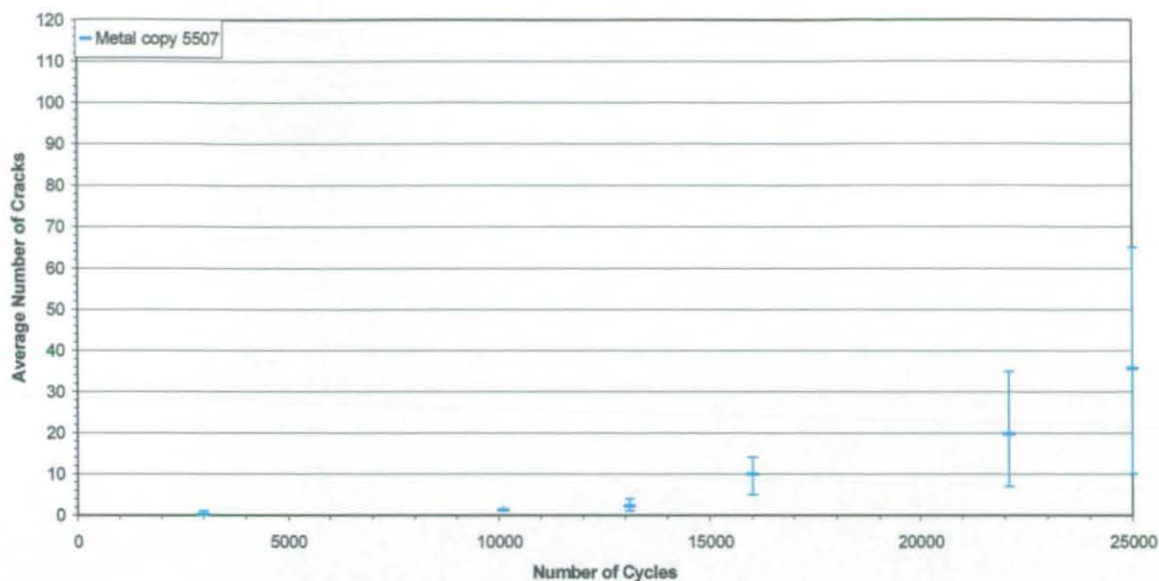


Appendix v Figure 1 H13 number of cycles versus hardness

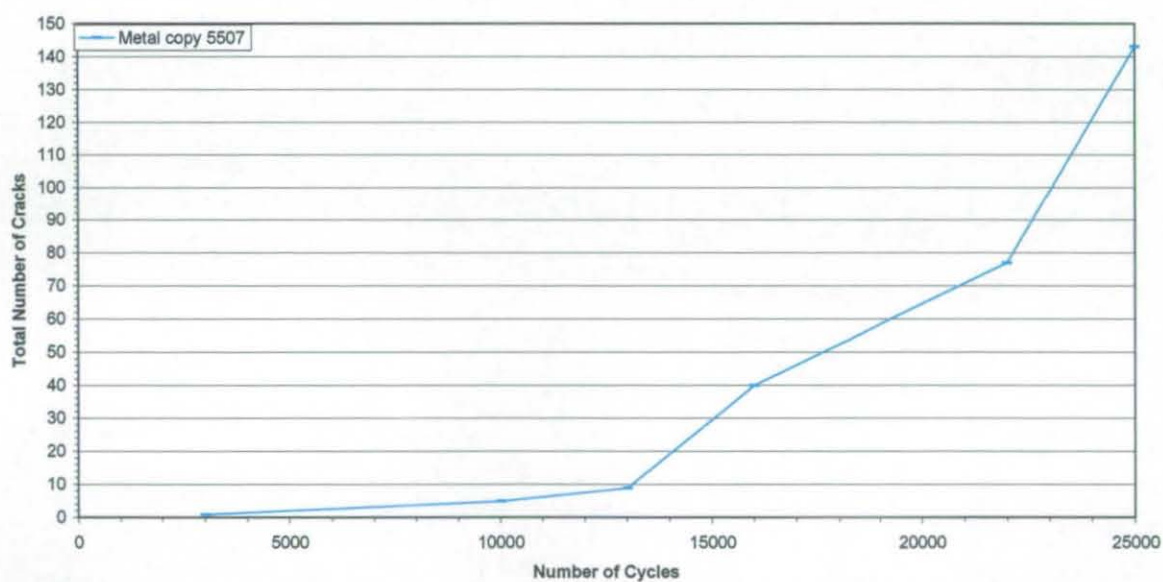
v.ii Metalcopy 5507 Thermal Fatigue Material Data



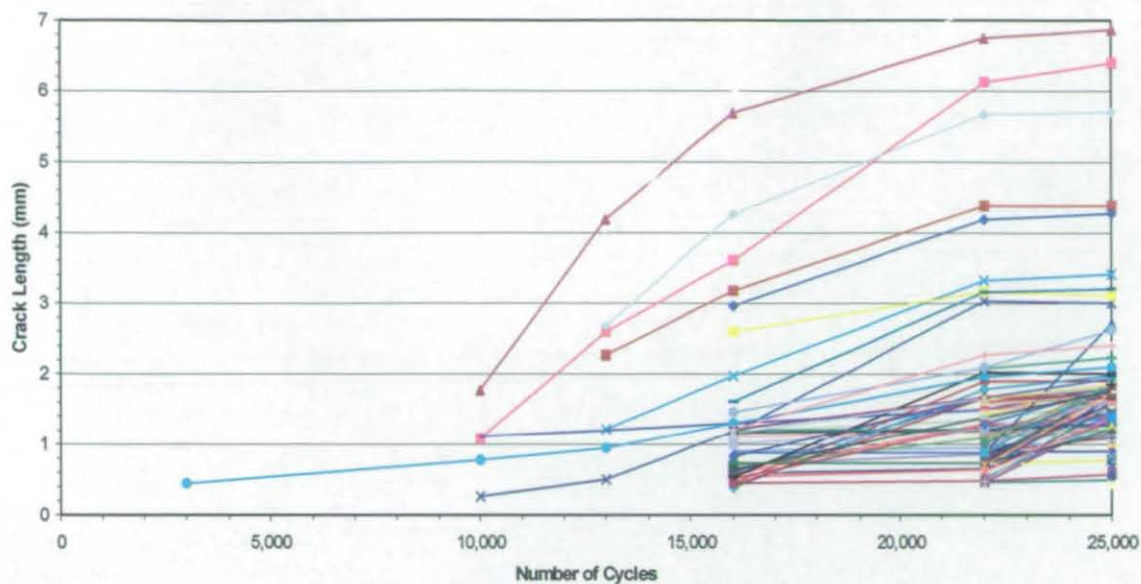
Appendix v Figure 2 Metalcopy 5507 number of cycles versus hardness



Appendix v Figure 3 Metalcopy 5507 number of cycles versus specimen average number of cracks with maximum - minimum range

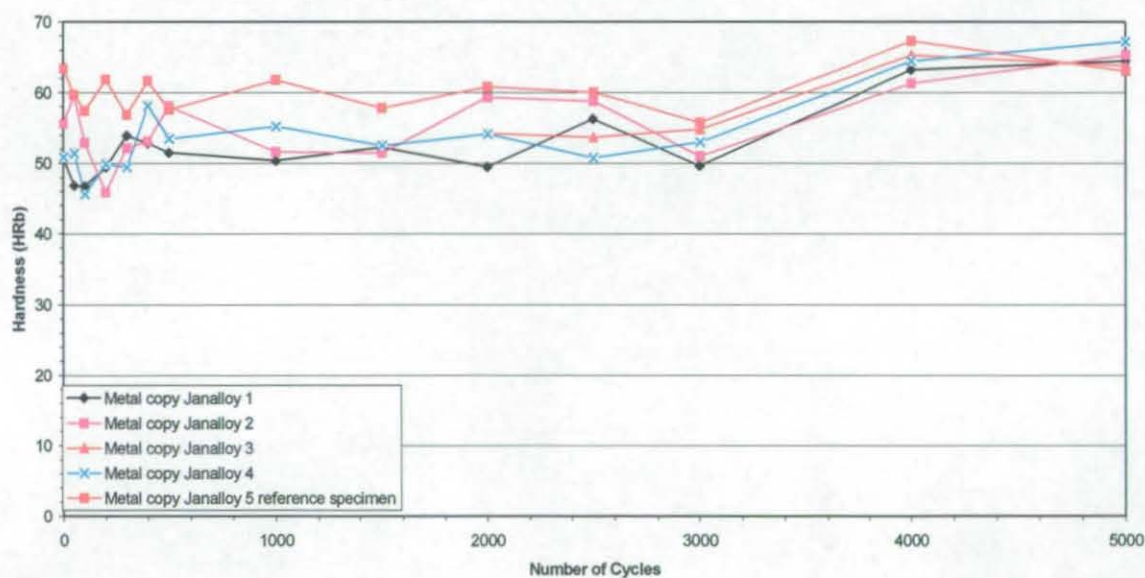


Appendix v Figure 4 Metalcopy 5507 number of cycles versus total number of cracks

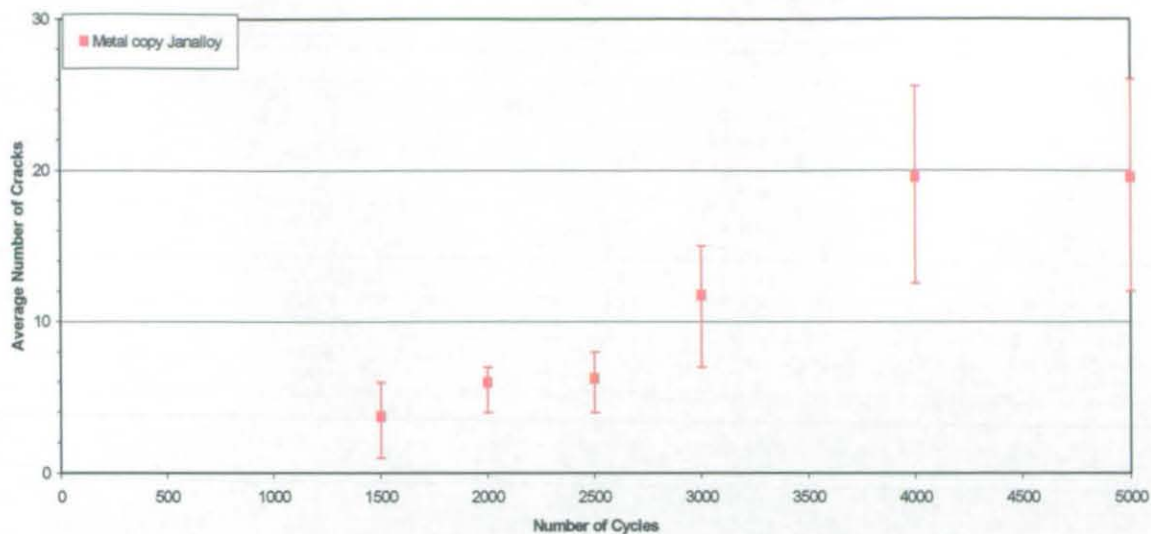


Appendix v Figure 5 Metalcopy 5507 number of cycles versus individual crack length

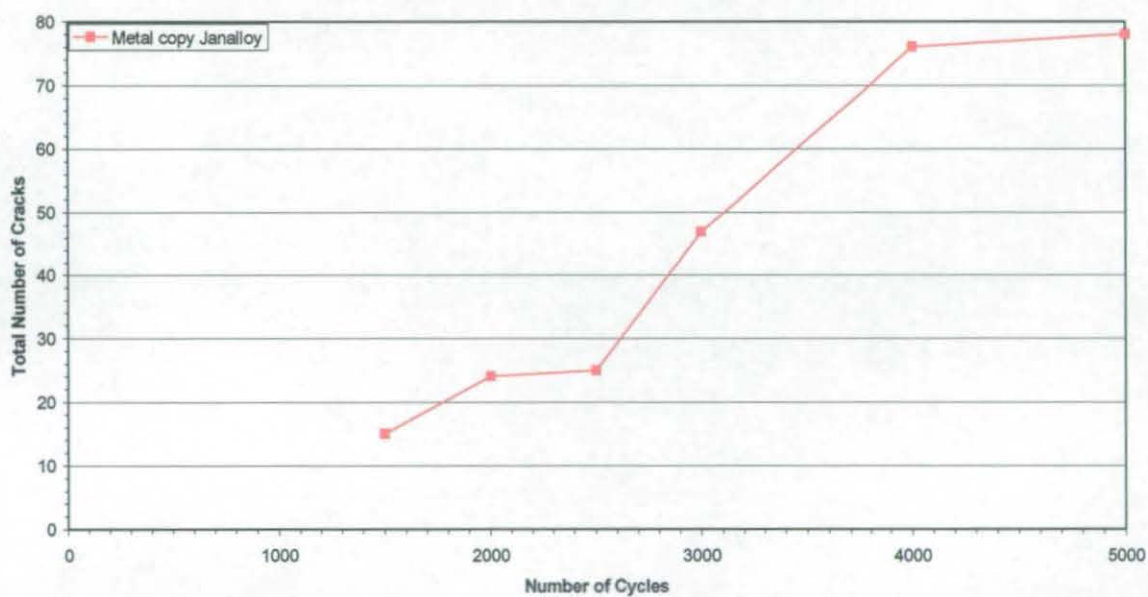
v.iii Metalcopy Janalloy Thermal Fatigue Material Data



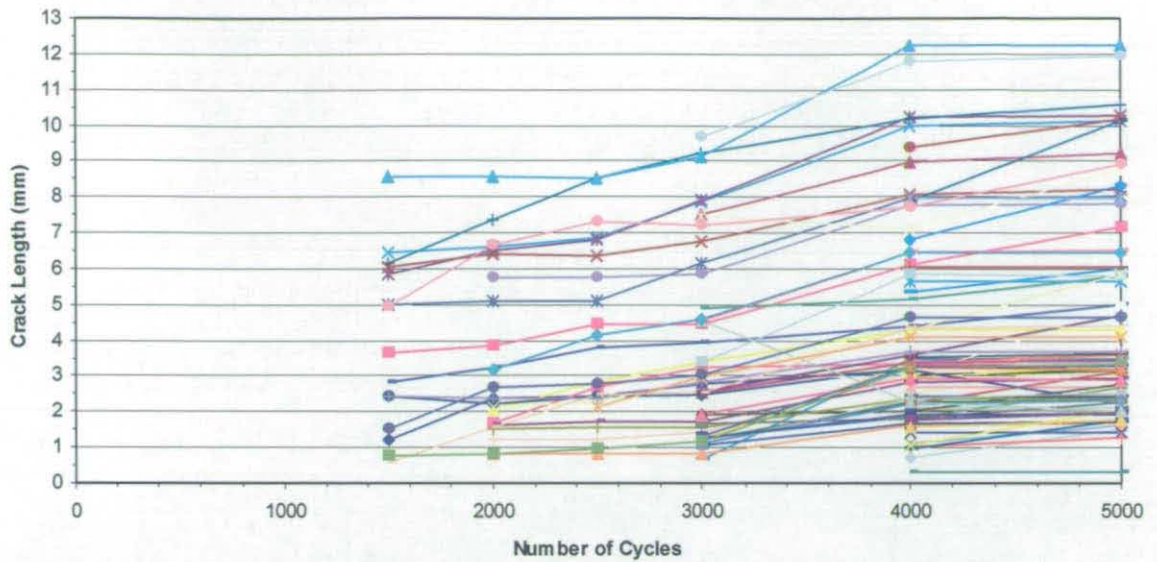
Appendix v Figure 6 Metalcopy Janalloy number of cycles versus hardness



Appendix v Figure 7 Metalcopy Janalloy number of cycles versus specimen average number of cracks with maximum - minimum range

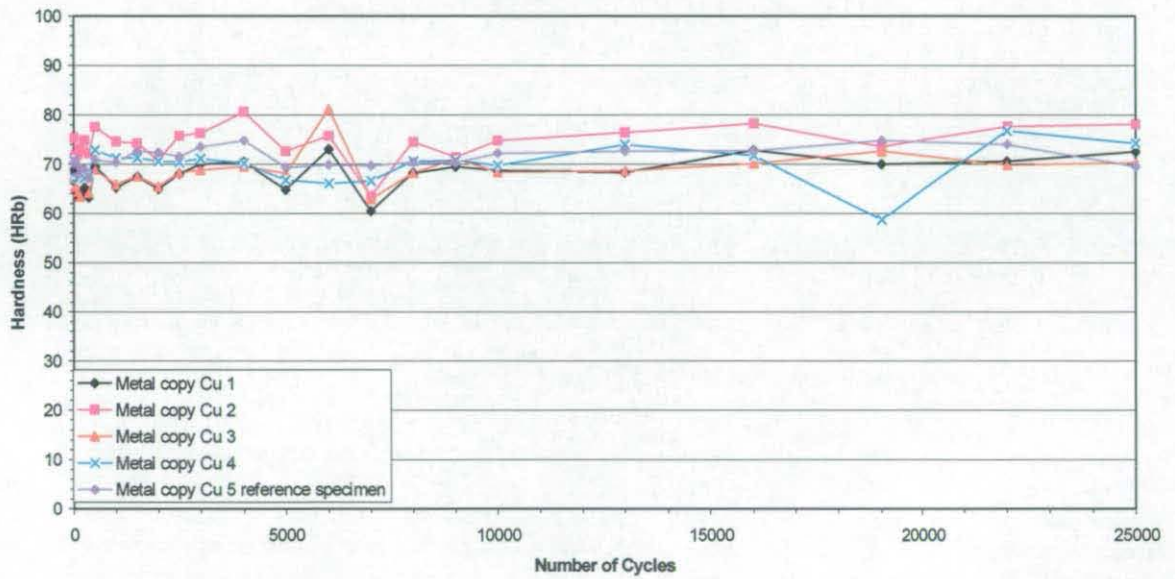


Appendix v Figure 8 Metalcopy Janalloy number of cycles versus total number of cracks

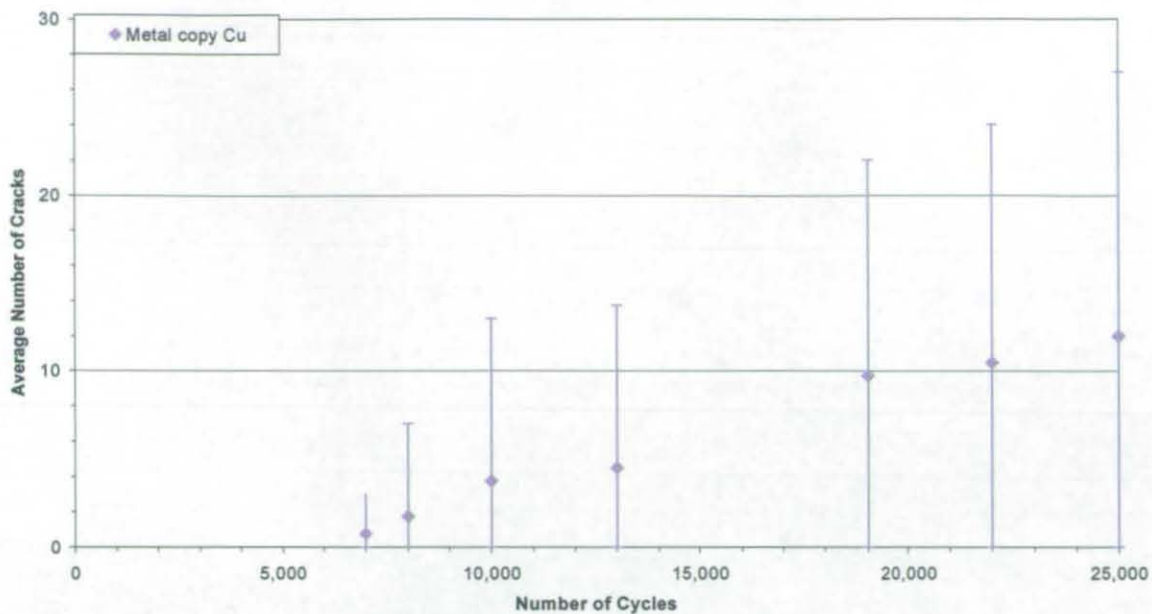


Appendix v Figure 9 Metalcopy Janalloy number of cycles versus individual crack length

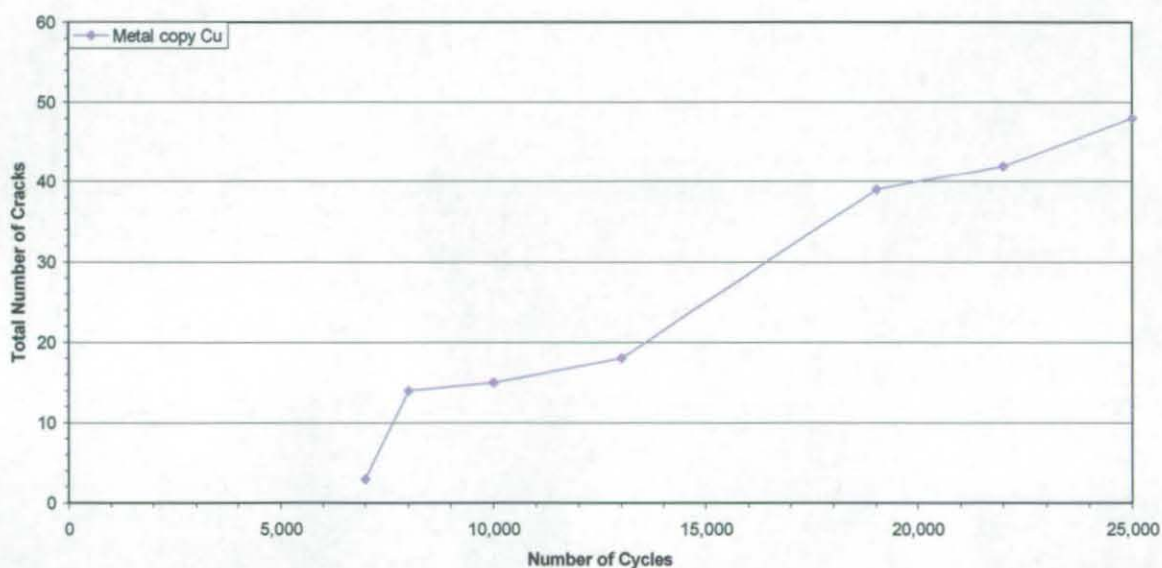
v.iv Metalcopy Cu Thermal Fatigue Material Data



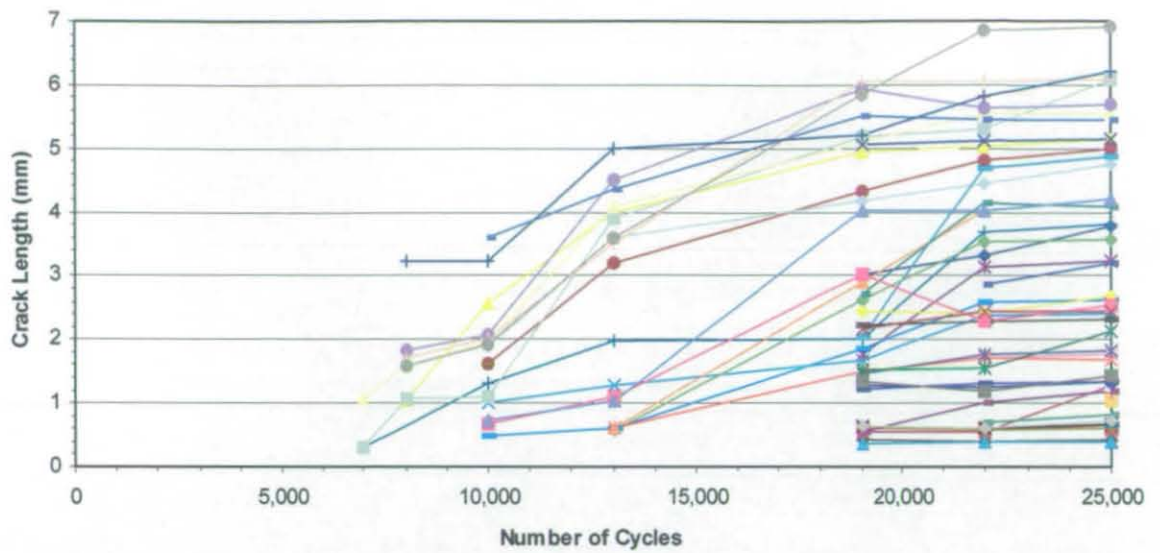
Appendix v Figure 10 Metalcopy Cu number of cycles versus hardness



Appendix v Figure 11 Metalcopy Cu number of cycles versus specimen average number of cracks with maximum - minimum range

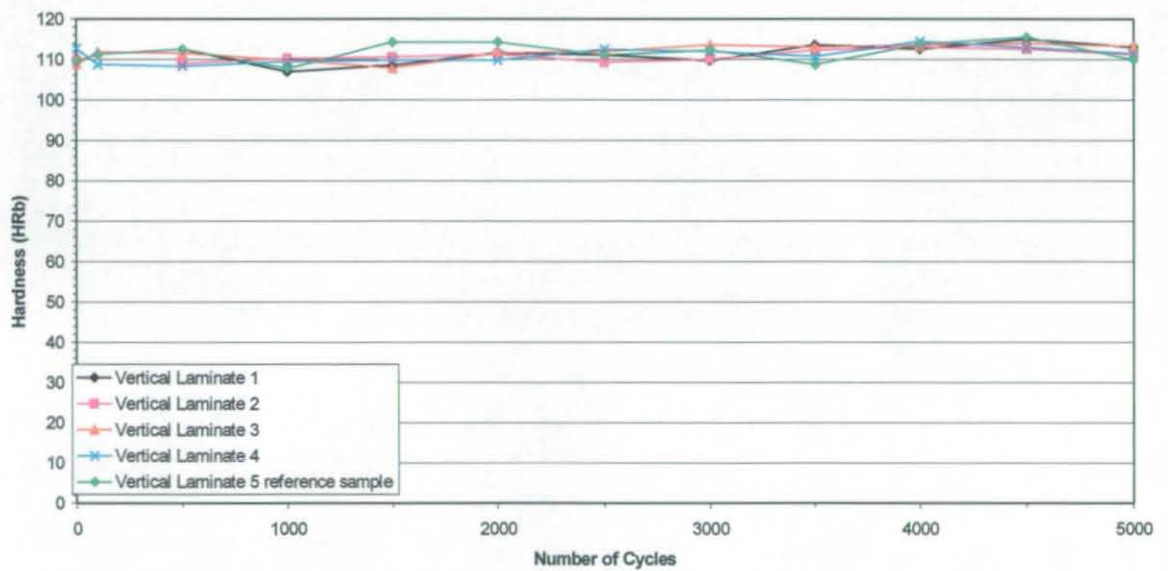


Appendix v Figure 12 Metalcopy Cu number of cycles versus total number of cracks

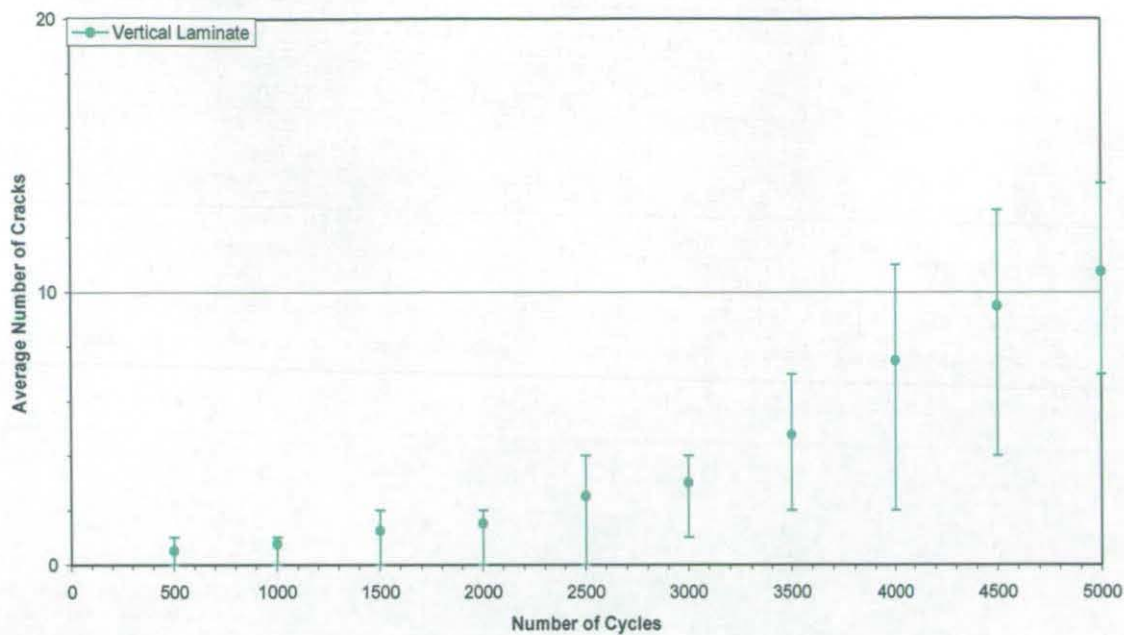


Appendix v Figure 13 Metalcopy Cu number of cycles versus individual crack length

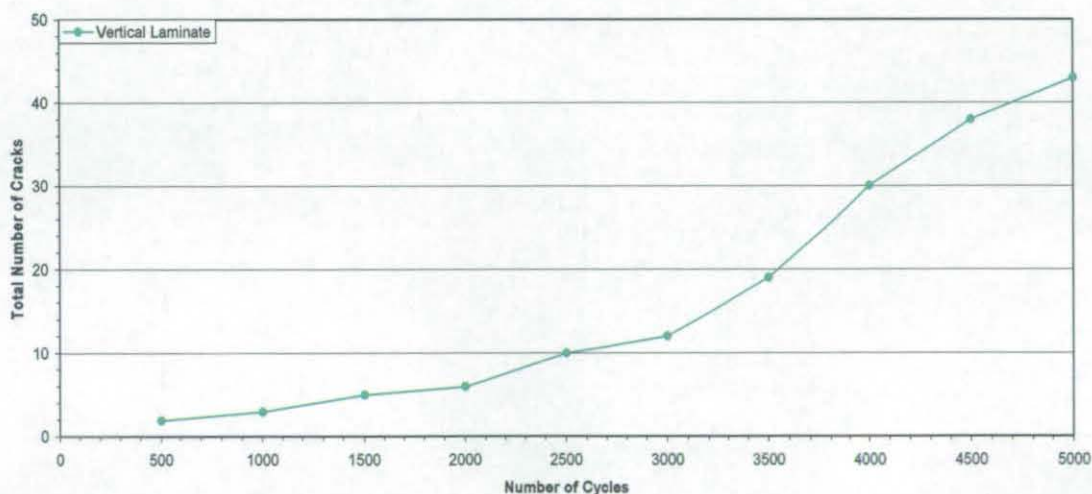
v.v Vertical Laminate Thermal Fatigue Material Data



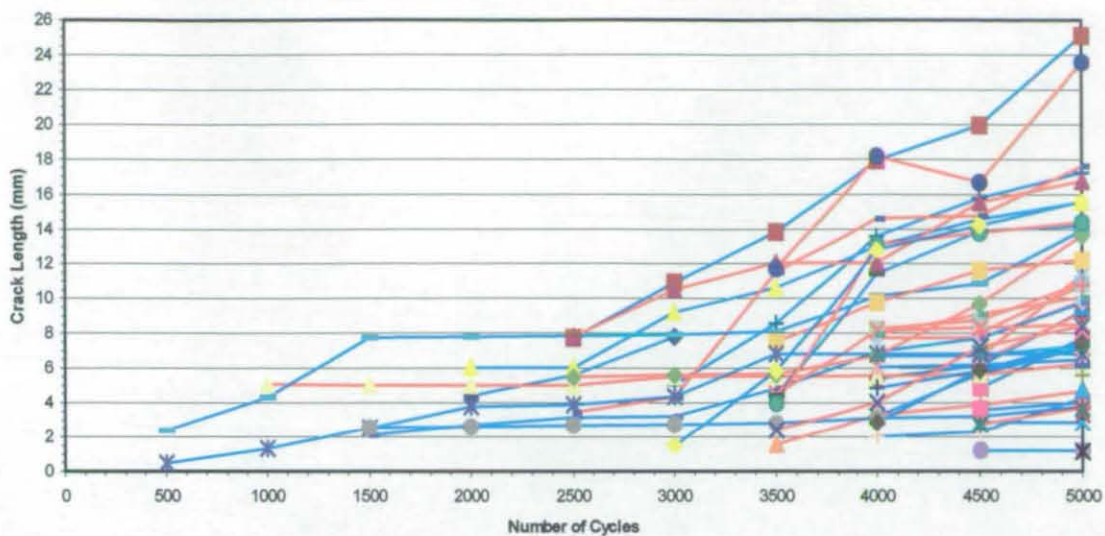
Appendix v Figure 14 Vertical laminate number of cycles versus hardness



Appendix v Figure 15 Vertical laminate number of cycles versus specimen average number of cracks with maximum - minimum range

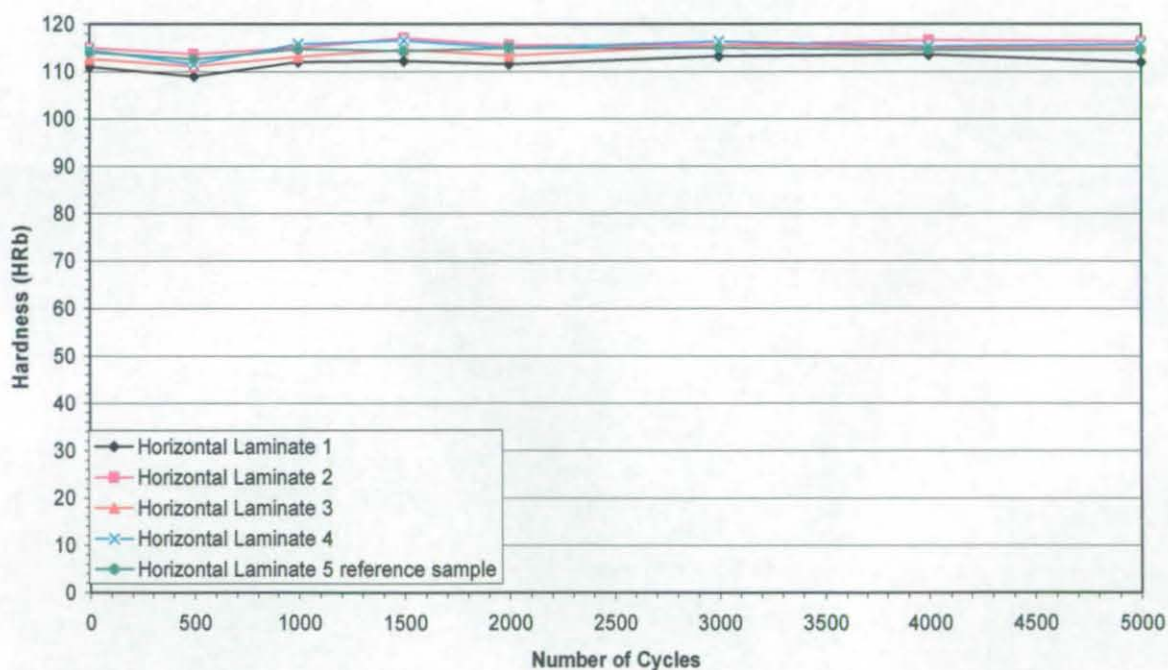


Appendix v Figure 16 Vertical laminate number of cycles versus total number of cracks

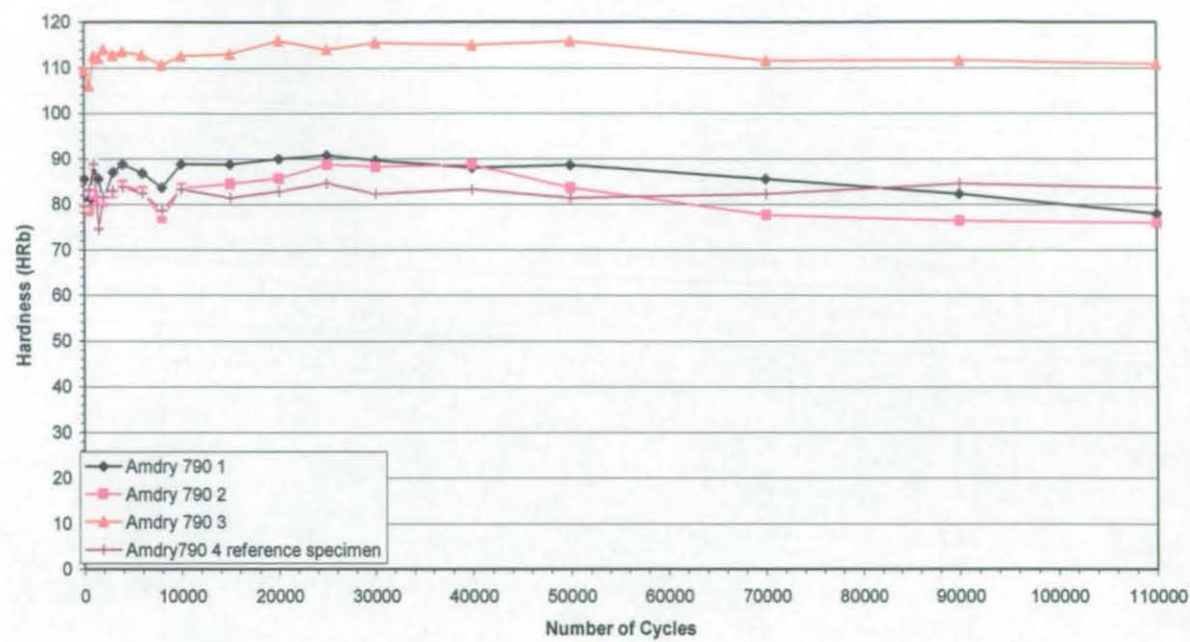


Appendix v Figure 17 Vertical laminate number of cycles versus individual crack length

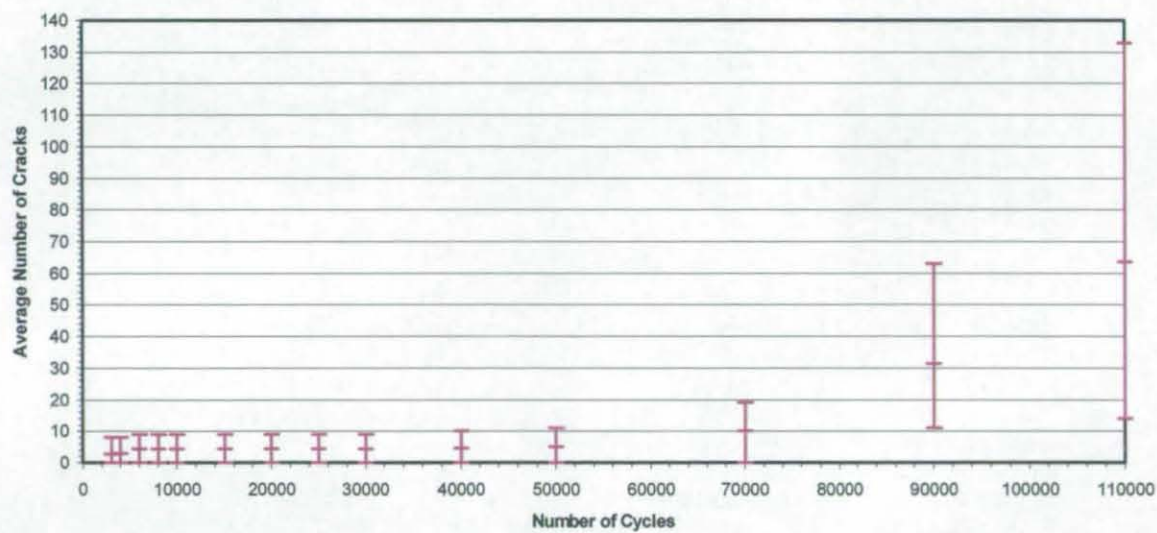
v.vi Horizontal Laminate Thermal Fatigue Material Data



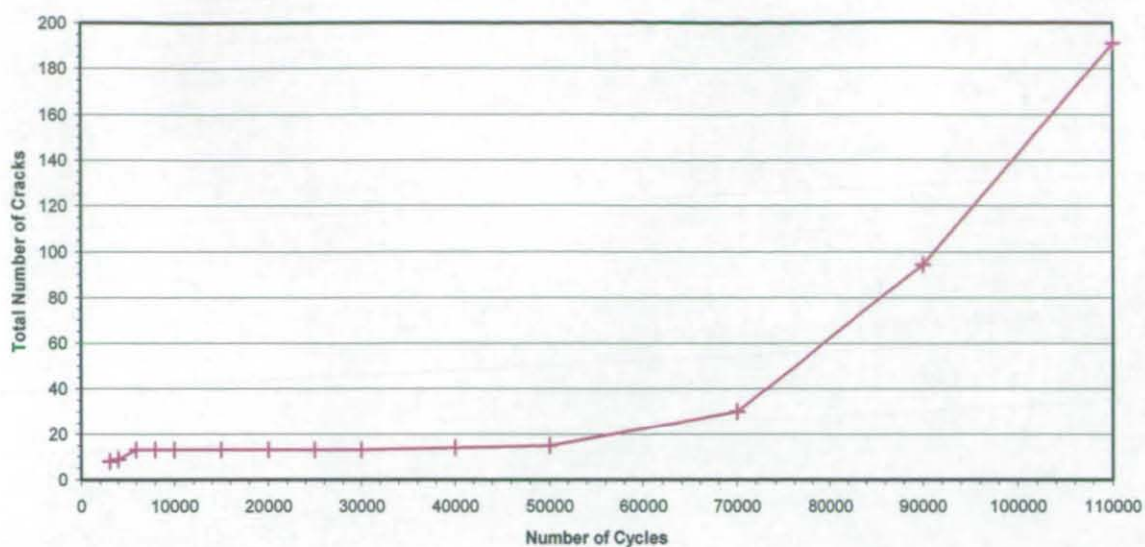
Appendix v Figure 18 Horizontal laminate number of cycles versus hardness



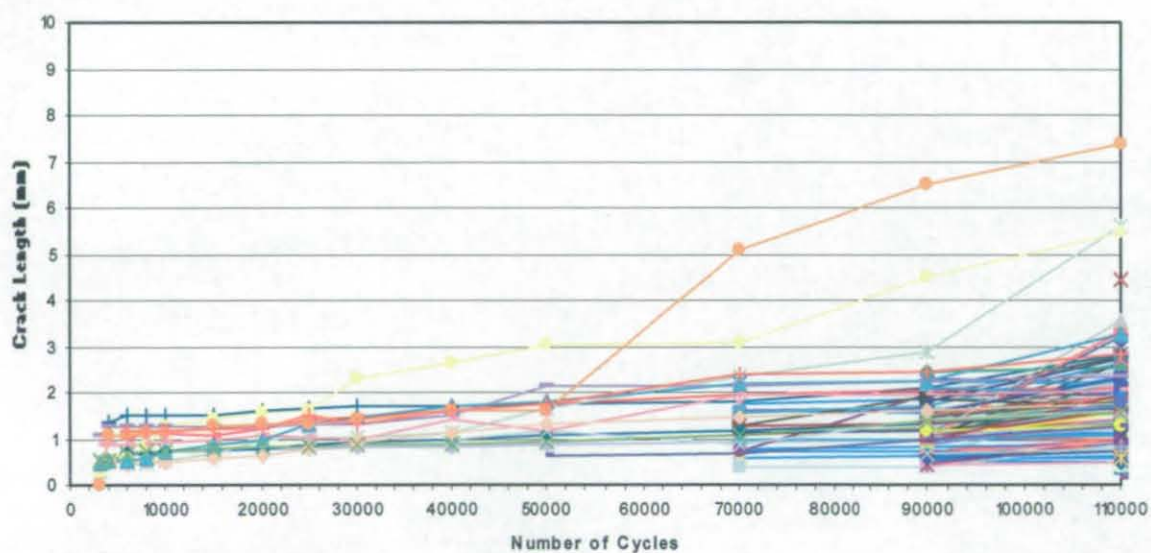
Appendix v Figure 19 Amdry 790 number of cycles versus hardness



Appendix v Figure 20 Amdry 790 number of cycles versus average number of cracks with maximum - minimum range

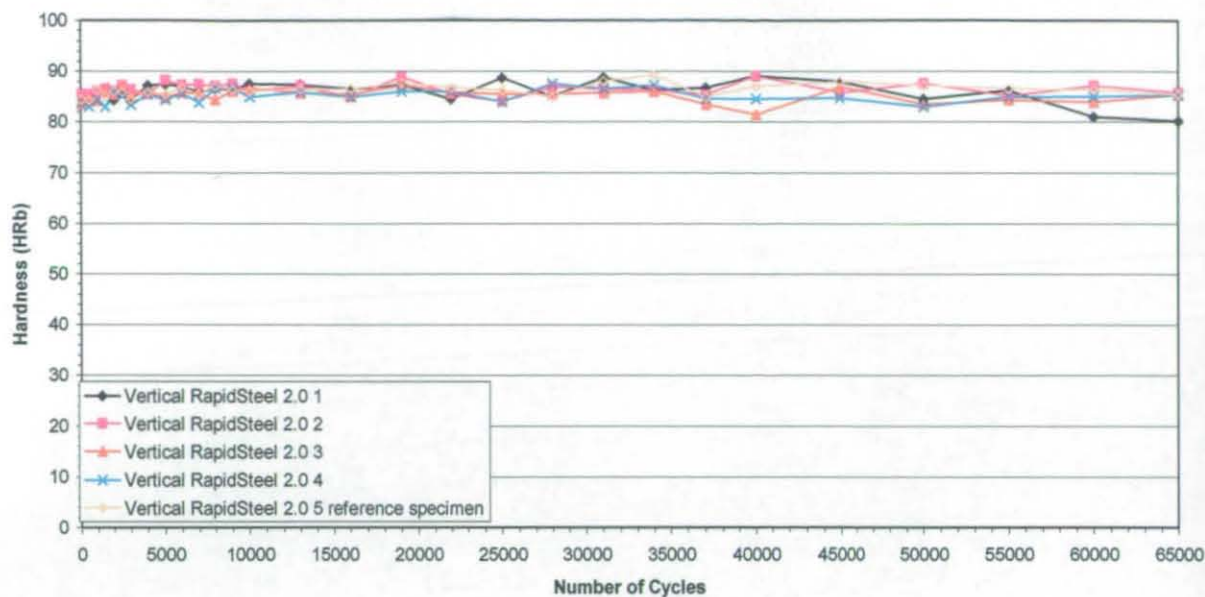


Appendix v Figure 21 Amdry 790 number of cycles versus total number of cracks



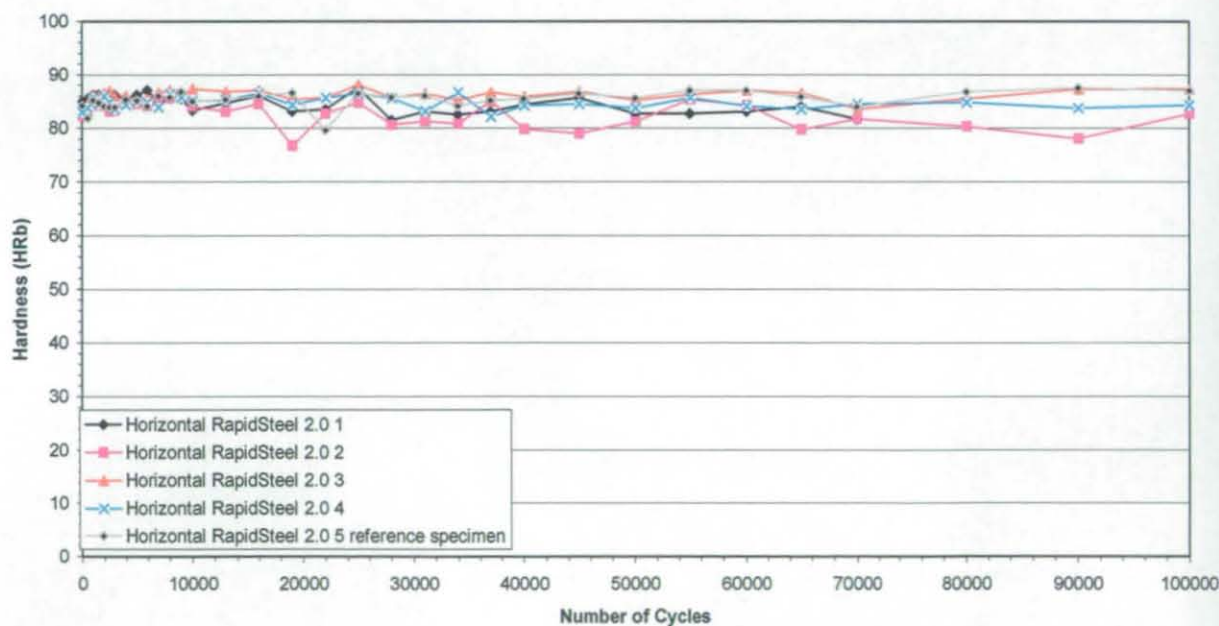
Appendix v Figure 22 Amdry 790 number of cycles versus individual crack length

v.viii **Vertical RapidSteel 2.0 Thermal Fatigue Material Data**

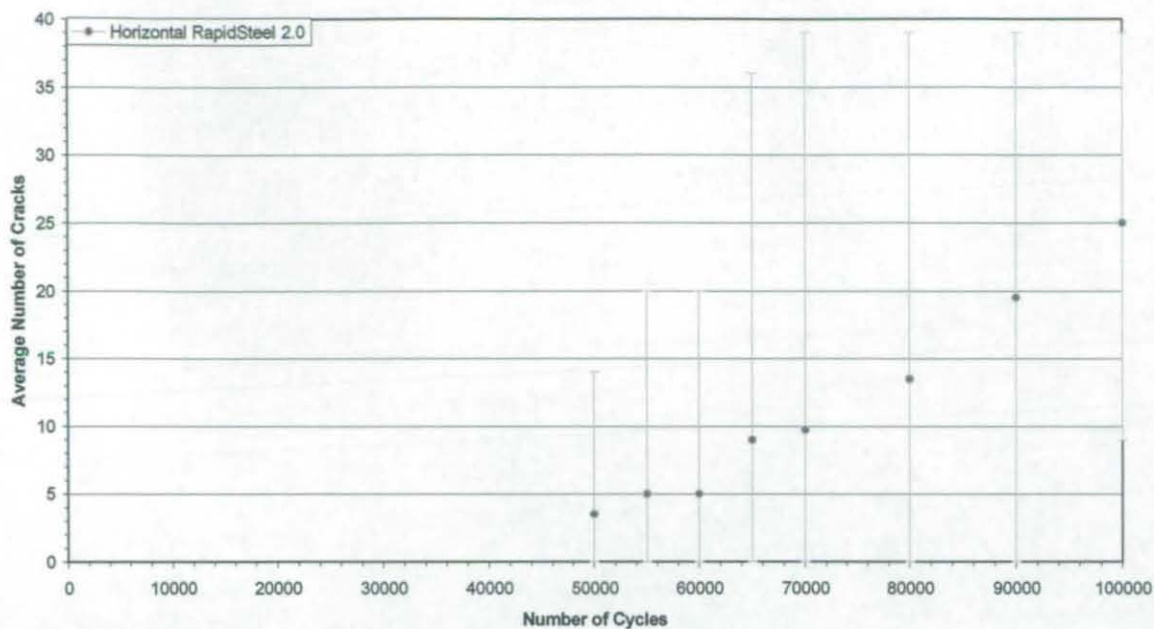


Appendix v Figure 23 Vertical RapidSteel 2.0 number of cycles versus hardness

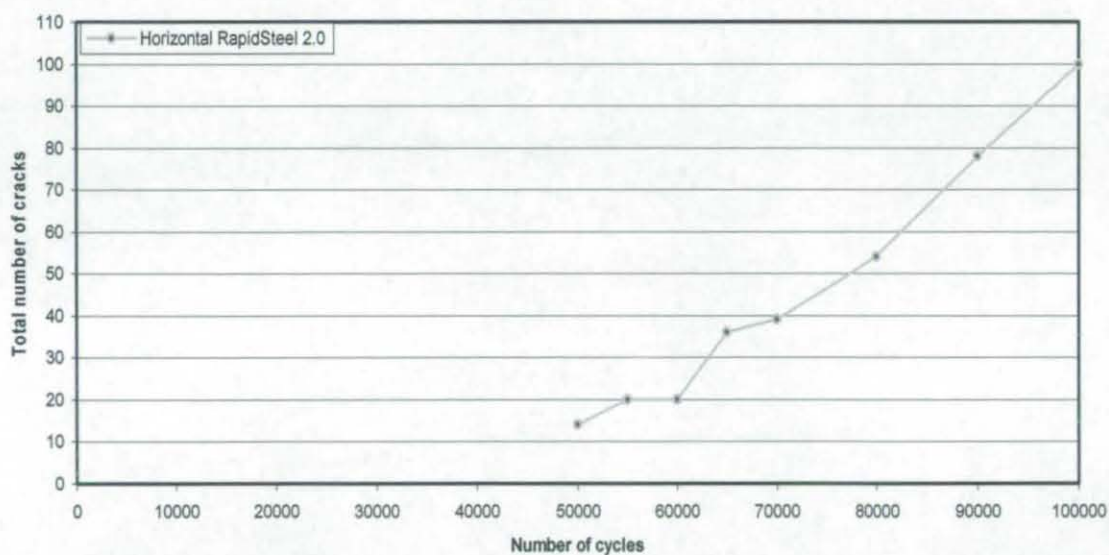
v.ix **Horizontal RapidSteel 2.0 Thermal Fatigue Material Data**



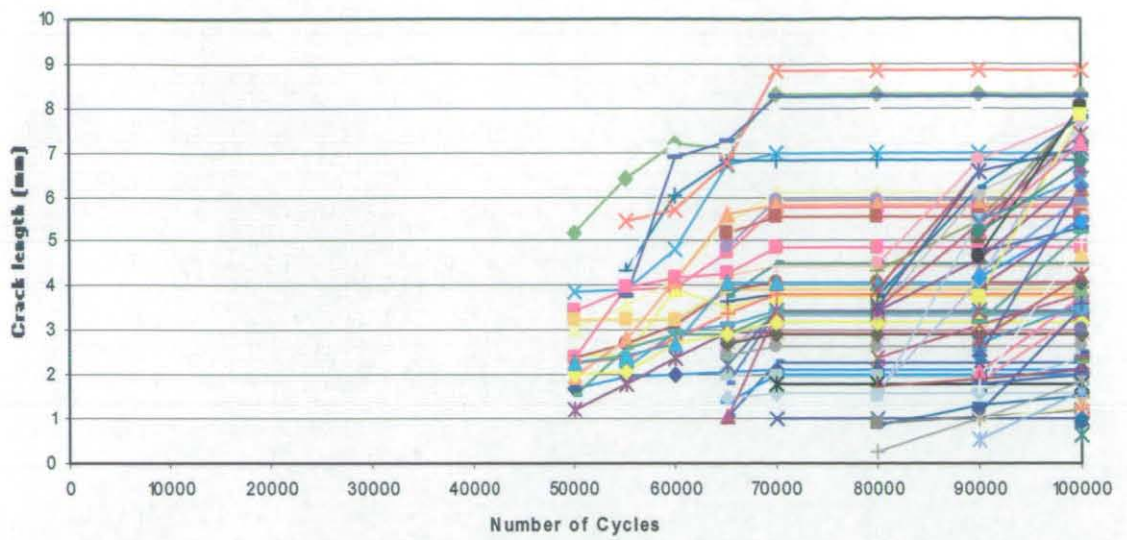
Appendix v Figure 24 Horizontal RapidSteel 2.0 number of cycles versus hardness



Appendix v Figure 25 Horizontal RapidSteel 2.0 number of cycles versus average number of cracks with maximum - minimum range

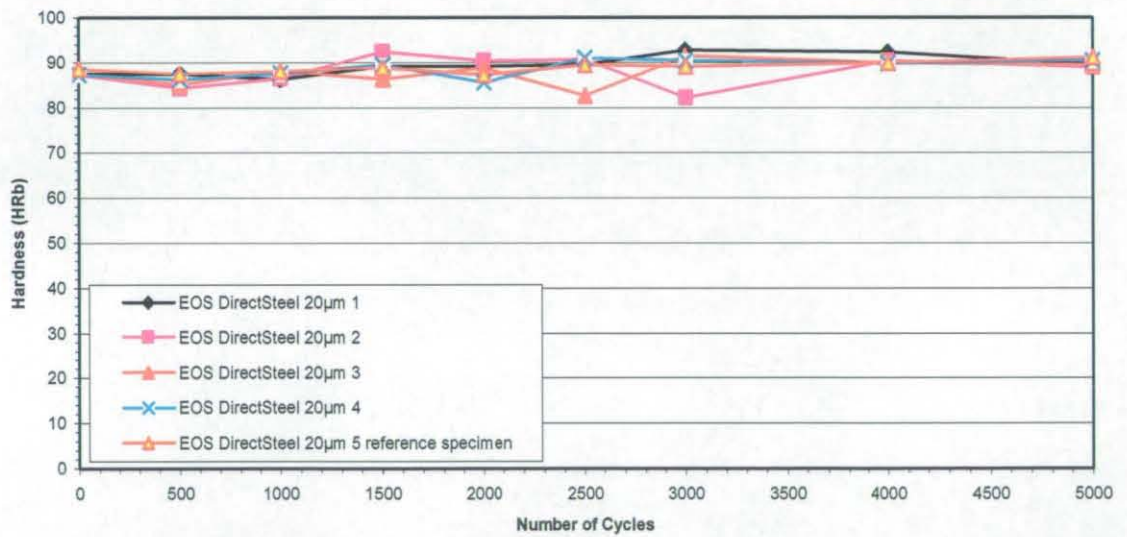


Appendix v Figure 26 Horizontal RapidSteel 2.0 number of cycles versus total number of cracks

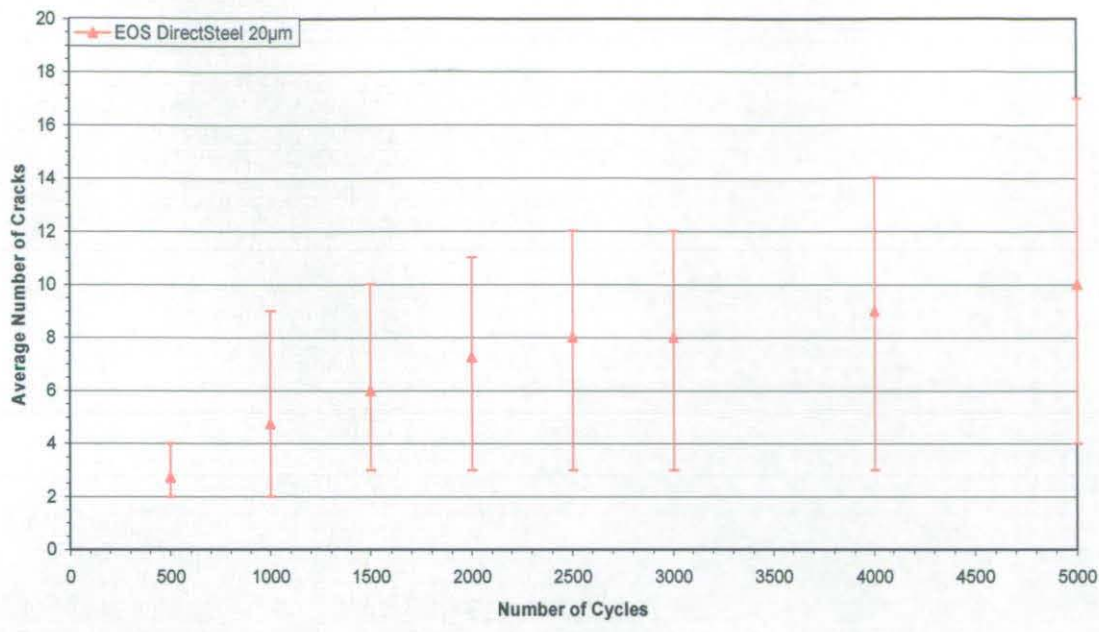


Appendix v Figure 27 Horizontal RapidSteel 2.0 number of cycles versus individual crack length

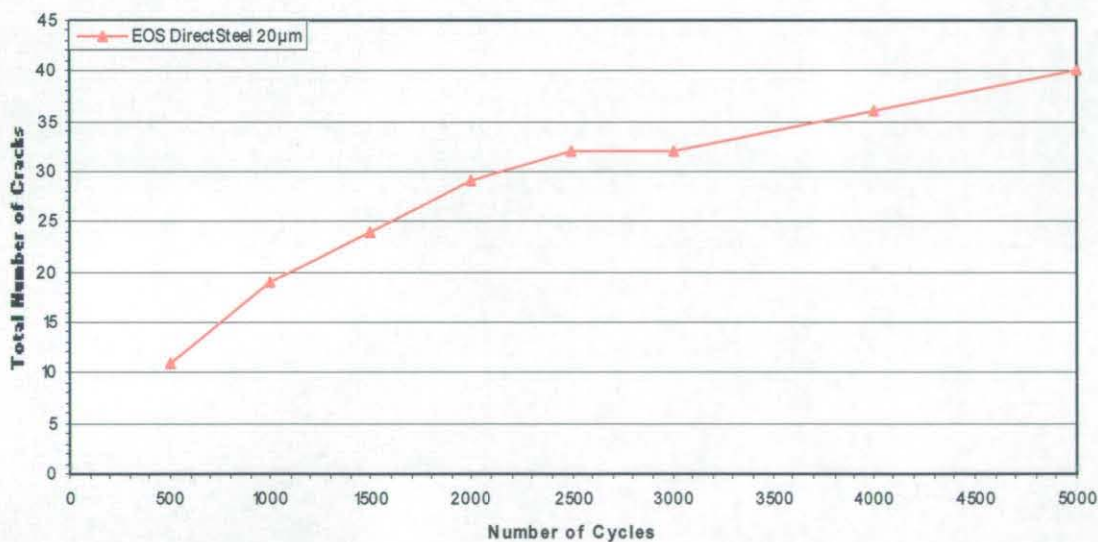
v.x EOS DirectSteel 20 μ m Thermal Fatigue Material Data



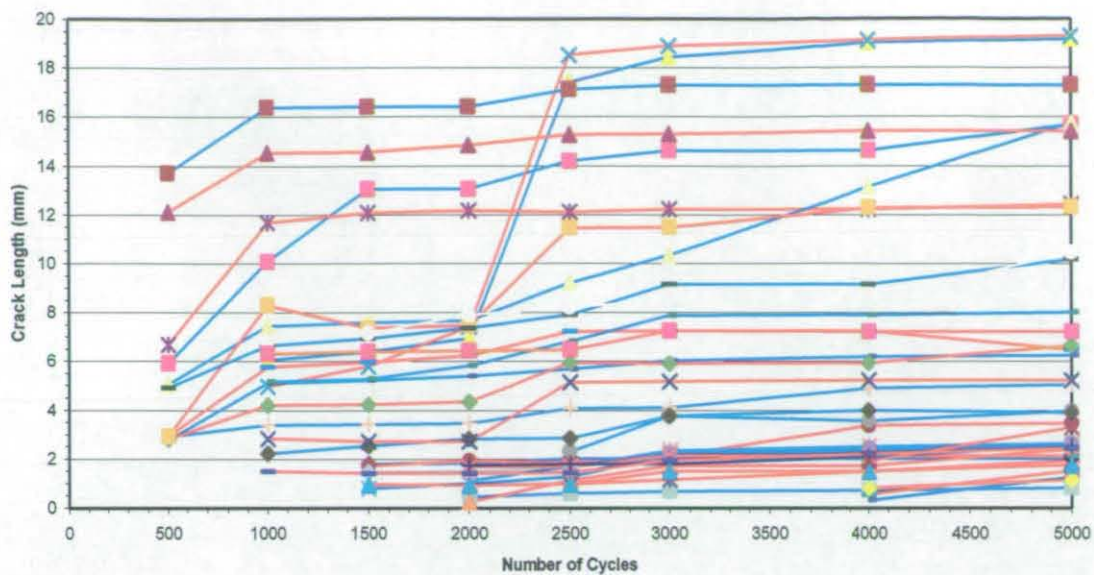
Appendix v Figure 28 EOS DirectSteel 20 μ m number of cycles versus hardness



Appendix v Figure 29 EOS DirectSteel 20µm number of cycles versus specimen average number of cracks with maximum - minimum range



Appendix v Figure 30 EOS DirectSteel 20µm number of cycles versus total number of cracks



Appendix v Figure 31 EOS DirectSteel 20μm number of cycles versus individual crack length

Appendix vi

Papers

THE USE OF METAL POWDER BINDER RAPID TOOLING IN METAL & POLYMER SMALL BATCH MANUFACTURING TECHNIQUES

Dr R. A. Harris ¹, Mr A. J. Norwood ¹, Professor P. M. Dickens ¹, Mr L. Bjork ² & Dr E. Zenker ³

¹ Rapid Manufacturing Research Group, Loughborough University, UK – R.A.Harris@lboro.ac.uk

² IVF Industrial Research and Development Corporation, Sweden ³ Ensinger TecaRIM, Austria

Abstract

Manufacturing industry is continuously searching for new and more competitive methods to produce tooling, especially where low production volumes are concerned where time and flexibility is of the essence. Within this 'rapid tooling' field of research there are several methods being developed. Each method has advantages and limitations and are based on varying techniques.

An area of such development involves the use of powder binder mixtures to produce metal tooling. This paper describes research into the use of a metal powder mixture tooling system utilised in plastic & metal part manufacturing processes.

The work describes the evaluation, identification of difficulties & failure modes, and subsequent attempts at tooling process improvement, in plastic injection moulding, high-pressure aluminium die-casting and sheet metal forming through evaluation by experimentation and case studies. The evaluation criteria includes: tool accuracy, mechanical & surface properties of tools, number & quality of parts, manufacturing time & cost, tool life and production process cycle time.

Keywords

High pressure die-casting, Metal powder mixture rapid tooling, Plastic injection moulding, Sheet metal forming, Small batch manufacturing.

Introduction

A technique to form solid geometries from a metal powder has been developed jointly by the Swedish company Prototal AB (previously known as Wiba AB) and IVF institute [1]. The process provides the opportunity to create tooling inserts as a rapid tooling technique. This technique is commercially termed 'MetalCopy'. The end product consists largely of steel with a low melting point alloy infiltrant material.

The MetalCopy process involves the following steps: A primary master of the tool is created, typically by an accurate rapid prototyping system. A silicone negative is cast from the master. The silicone negative is used to produce a 'green' part which consists of a mixture of steel powder and binder. The green part is sintered and the pores between the metal powder grains are filled by a low melting point alloy metal.

It is possible to utilise these products as tooling inserts for manufacturing processes. Depending on geometrical complexity, the technique may provide time and cost advantages as compared to traditional tool production techniques. Should the technique be further developed the tooling may be tailored to its purpose with respect to material properties due to the opportunities presented by its powder mixture nature.

The aim of the work is to assess the technique's suitability as a tooling process for different manufacturing processes: plastic injection moulding, high-pressure aluminium die-casting and sheet metal forming.

Methodology

High pressure die casting methodology The test piece that was used in die-casting trials is the 'dyson' geometry, as shown in Figure 1.



Approx size 300 x 17 mm

Figure 1 - CAD image of 'dyson' geometry

The tooling design produced 4 parts simultaneously and consisted of 5 separate inserts. One of these tooling inserts was produced by the MetalCopy process and was assembled in the tool along with conventional steel inserts. The tool half concerned and the gating arrangement is illustrated in Figure 2.



Figure 2 - MetalCopy & steel inserts in die-casting tool

The accuracy of the MetalCopy insert was compared with the stl file (the form of CAD data used to manufacture the master) that was supplied to Prototab AB by comparing measurements of different features. The surface roughness (Ra) of an area within the casting cavity was measured before and after die casting. This area is illustrated in Figure 3.

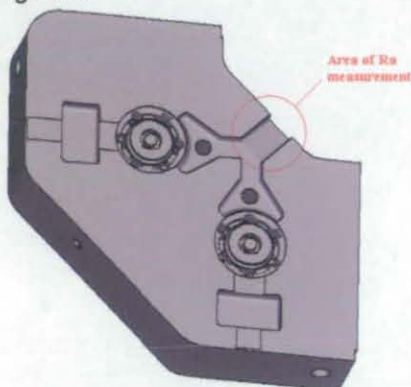


Figure 3 - Area of surface roughness analysis

LM24 aluminium was utilised as the die-casting material.

Injection moulding methodology

The test piece that was used in die-casting trials is the geometry shown in Figure 4. This geometry is a scaled down version of a valve cover for a single cylinder engine, provided by Rotax Bombardier.



Figure 4 – CAD image of valve cover geometry

The 2 part tool consisted of one half manufactured by the MetalCopy process, and the other half was machined in aluminium. The tool inserts can be viewed in Figure 5.



Figure 5 – MetalCopy insert (left) & aluminium insert (right)

The accuracy of the MetalCopy insert was again compared with the .stl file (the form of CAD data used to manufacture the master) that was supplied to Prototab AB by comparing measurements of different features.

The material utilised in the injection moulding was PA66 with a 35% glass content.

Sheet metal forming methodology

The geometry utilised in the sheet metal forming trials was taken from part of an exhaust manifold assembly provided by Rotax Bombardier. The whole assembly is shown Figure 6.



Figure 6 – CAD image of exhaust manifold assembly

The tooling consisted of three parts: the punch, the die, and the blank holder. The punch was manufactured using the MetalCopy process, the die by direct metal powder laser sintering (EOSint) and the blank holder by wire spark erosion of steel. The die and punch are shown in Figure 7. Prior to use the cavity surfaces were polished.



Figure 7 – Sheet metal forming die (right) & punch (left)

The sheet forming material was 1.5mm thick stainless steel.

Results

High pressure die casting results

The tool was used to produce 500 parts. This quantity had previously identified by the project partners in represent a 'low volume' production run. The process cycle time taken to produce one part was 25 seconds utilising the same process parameters used by a complete steel tool.. Initial signs of cracking in the Protocal AB insert began after approximately the 50 parts. This propagated from the central boss feature and continued to progress during continued production.

These cracks became clearly visible after approximately 200 parts. As production progressed to the 500th part this cracking became more extreme and ablative. This cracking is shown in Figure 8.



Figure 8 - Damage inflicted on MetalCopy insert after die casting 500 parts

Some these effects were quantified by measuring the surface roughness of the tool before and after die- casting. Prior to casting, the area of tool shown in Figure 3 measured an average surface roughness of $4.8\mu\text{m}$, while after casting it measured $7.8\mu\text{m}$.

The comparative accuracy measurements are shown in Figure 9.

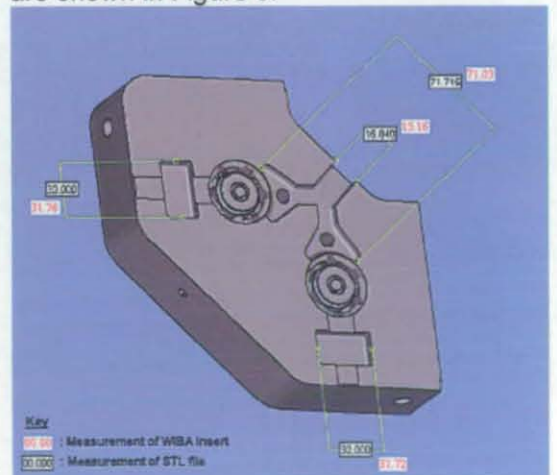


Figure 9 - Comparative measurement of MetalCopy insert & STL file

Injection moulding results

The tool successfully produced 840 parts without any signs of wear. All parts were

deemed to be of acceptable quality and dimensions.

The accuracy measurements of the MetalCopy insert in comparison to the CAD data yielded similar results to those from the die-casting trials, the inserts were ~0.2mm undersized.

Sheet metal forming results

The tool begins to show signs of severe wear after on a few sheets were formed; production was ceased after only 17 sheets were formed. The area of wear occurred on the edge curvature on the die edge. This area is illustrated in Figure 10.

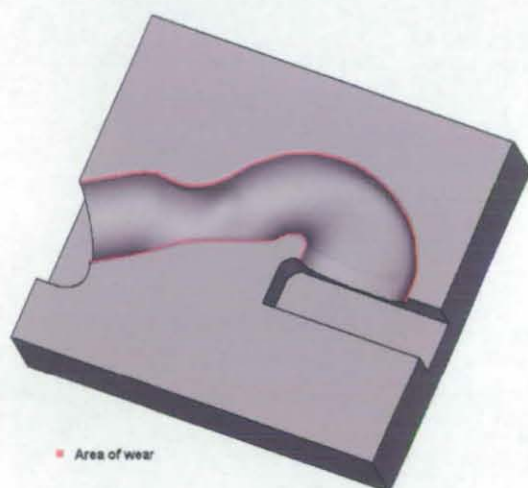


Figure 10 – Area of wear on die

Conclusions

High pressure die casting conclusions

The results show that the MetalCopy insert is undersized in comparison with the supplied .stl file. The process concerns multiple translation steps. The comparative accuracy of the translation needs to be examined after each step in order to determine at which points there is a change. Subsequently attempts to compensate for the under-sizing may be made.

The progression of MetalCopy material for die casting hinges upon improving its resistance to the cracking experienced in these trials. The repeated expansion and contraction of the tool material, caused by this heating & cooling, leads to the development of internal stresses. These stresses result in cracks appearing in the tooling material which ultimately lead to its failure [2]. In order to facilitate these improvements the following work in the project will be instrumental. A thermal fatigue test has been designed by Loughborough

University to evaluate tooling materials for high pressure die-casting. The experiment involves a repeated thermal shock treatment by exposing the sample to the temperature conditions that would be experienced in die-casting. The sample is exposed to very high temperatures, then a rapid decrease in temperature is induced to an ambient level. These conditions are repeated for 1000's of cycles. The experiment simulates the continued rise and fall in temperature that would be experienced by a tool in die-casting. The experiment is designed to assess the effects of this thermal fatigue by simulating these conditions and thus being able to assess its sole effects by eliminating other variables experienced during physical die-casting (ie. part release forces etc). The experiment is designed to ascertain a materials resistance to thermal fatigue and its suitability for use as a die-casting tooling material. The experiment will be utilised to quantify the suitability and facilitate improvements to powder binder mixture materials.

Injection moulding conclusions

In this particular application, the MetalCopy inserts demonstrated themselves to be very suitable for use as plastic injection moulding tooling. In a cost comparison it was demonstrated that the economical advantage over conventional machined tooling increased in relation to increasing geometrical complexity.

However, the use of MetalCopy inserts in plastic injection moulding did exhibit conditions that may lead to part anomalies. The mould was utilised at ambient temperature i.e. neither heated or cooled. The different heat transfer characteristics of the MetalCopy material and aluminium lead to a difficulty in maintaining the different mould sides at the same temperature prior to polymer injection. Previous work [3] has shown that the heat transfer characteristics of a tool during injection moulding are a highly influential factor that controls the resultant structure and characteristics of crystalline polymers, such as the material used in this case.

Sheet metal forming conclusions

The wear occurred on the die, which was manufactured by direct metal laser sintering. However, the work investigating the use of MetalCopy for sheet metal forming tooling will not be continued for reasons of economic viability. The use of MetalCopy to

produce tooling is only advantageous when the required geometry is complex. Due to the process nature of sheet metal forming only simple geometries can be produced. Therefore MetalCopy would never be able to compete economically with conventional tool production techniques.

Acknowledgements

This research was conducted collaboratively between 6 industrial, 3 research & 1 academic institutions situated throughout Europe. The work constitutes part of the IMS RPD 2001 project which is funded by the European Union.

References

- [1] B. Holmer & T. Wohlers, Wohlers Report 2003 - Rapid Prototyping & Tooling State of the Industry Annual Worldwide Progress Report, Published by Wohlers Associates, Inc. USA, Part 5: Asia & Europe, Sweden section. Page 139.
- [2] Bendyk, J.C. Maracz, O.J. Wallace, J.F., Thermal Fatigue Behaviour of Die Materials for Aluminium Die Casting, The 6th SDCE International Die Casting Congress, Cleveland, Ohio, November 16th – 19th 1970, Paper Number 111, Pages 1-20
- [3] R. A. Harris & P. M. Dickens, 'Determining, Understanding & Controlling the Morphology of Injection Moulded parts produced in Stereolithography Moulds', ANTEC 2003, May 4-8, Nashville, Tennessee, USA, Society of Plastics Engineers

Biography



Russ Harris has a first degree in Manufacturing Engineering, and a PhD in Rapid Prototyping & Polymers. He is currently a Research Fellow in the Rapid Manufacturing Research Group at Loughborough University, UK.



Andy Norwood has a first degree in Materials Engineering, and is currently studying for his PhD. He is currently a Research Associate in the Rapid Manufacturing Research Group at Loughborough University, UK.



Phill Dickens is Professor of Manufacturing Technology, Associate Dean of Research and head of the Rapid Manufacturing Research Group at Loughborough University, UK.



Lennart Björk has an M.Sc in material science and is active at the IVF Production Engineering Research Inst. in Sweden. His topics are prototype tools and material science.



Edmund Zenker has a PhD in Plastics Technology. He is currently General Manager of the Ensinger-TecaRIM Division located in Linz, Austria.

Metal Powder Binder Rapid Tooling for High Pressure Die-Casting

Dr R. A. Harris, Mr A. J. Norwood & Professor P. M. Dickens

Rapid Manufacturing Research Group, Wolfson School of Mechanical & Manufacturing Engineering, Loughborough University, Leicestershire, UK

ABSTRACT

The pressure die-casting industry is searching for new and more competitive methods to produce tooling, especially where low production volumes are concerned where time and flexibility is of the essence. Within this 'rapid tooling' field of research there are several methods being developed. Each method has advantages & limitations and are based on varying techniques.

An area of such development involves the use of powder binder mixtures to produce metal tooling. This paper describes research into the use of a metal powder mixture tooling system used for high-pressure die-casting of aluminium.

The work describes the identification of difficulties & failure modes through case studies. Subsequent tool material evaluation will be made by the development of a concise & quantitative experimental method. The results may lead to the further development of a metal powder binder material which is more suited to the conditions experienced in high-pressure die-casting. This work constitutes part of the IMS RPD 2001 project which is funded by the European Union.

Keywords

Rapid Prototyping & Tooling, Small batch manufacturing, High-pressure die-casting.

1. INTRODUCTION

A technique to form solid geometries from a metal powder has been developed by the Swedish company Protocal AB (previously known as Wiba AB). The process provides the opportunity to create tooling inserts as a rapid tooling technique. This technique is commercially termed 'MetalCopy' [1]. The end product consists largely of steel with a low melting point alloy infiltrant material. The MetalCopy process involves the following steps:

1. A primary master of the tool is created, typically by an accurate rapid prototyping system.
2. A silicone negative is cast from the master.
3. The silicone negative is used to produce a 'green' part which consists of a mixture of steel powder and binder.
4. The green part is sintered and the pores between the metal powder grains are filled by a low melting point alloy metal.

It is possible to utilise these products as tooling inserts for manufacturing processes. Depending on geometrical complexity, the technique may provide time and cost

advantages as compared to traditional tool production techniques. Should the technique be further developed the tooling may be tailored to its purpose with respect to material properties due to the opportunities presented by its powder mixture nature.

The aim of the work is to assess the technique's suitability as a tooling process for high-pressure aluminium die-casting and sheet metal forming.

The work began with a case study which revealed several weaknesses of the MetalCopy process to the application for high pressure die casting. The particular characteristics of the flaws were examined using differing examination techniques. This work is described in section 2.

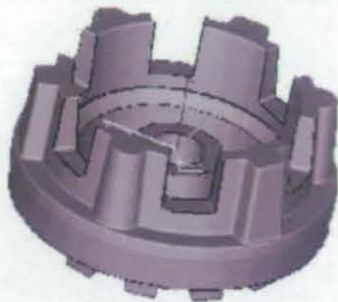
In order to conduct more concise material evaluation, an experimental apparatus and procedure has been developed by the authors. This experiment simulates the detrimental thermal conditions experienced by the tool material in high-pressure aluminium die casting. This allows a material's suitability for pressure die casting to be assessed without the complications of the other extra variables experienced (flow

characteristics due to particular part geometry etc). This work is described in section 3.

2. CASE STUDY

2.1. CASE STUDY METHODOLOGY

The test piece that was used in die-casting trials is the 'dyson' geometry, as shown in Figure 1.



Approx size 30x17mm

Figure 1 CAD image of 'dyson' geometry

The tooling design produced 4 parts simultaneously and consisted of 5 separate inserts. One of these tooling inserts was produced by the MetalCopy process and was assembled in the tool along with conventional steel inserts. The tool half concerned and the gating arrangement is illustrated in Figure 2.

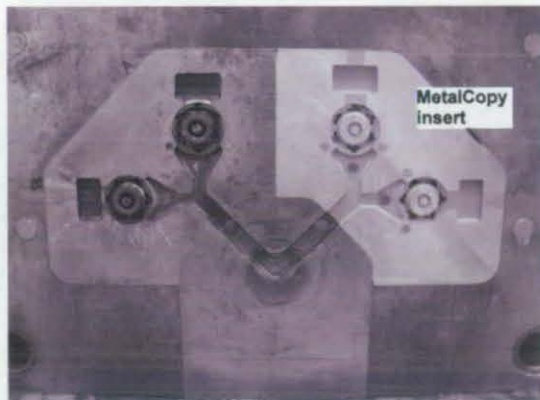


Figure 2 MetalCopy & steel inserts in die casting tool

The accuracy of the MetalCopy insert was compared with the .stl file (the form of CAD data used to manufacture the master) that was supplied to Protocal AB by comparing measurements of different features. The surface roughness (Ra) of an area within the casting cavity was measured before and after die casting. This area is illustrated in Figure 3.

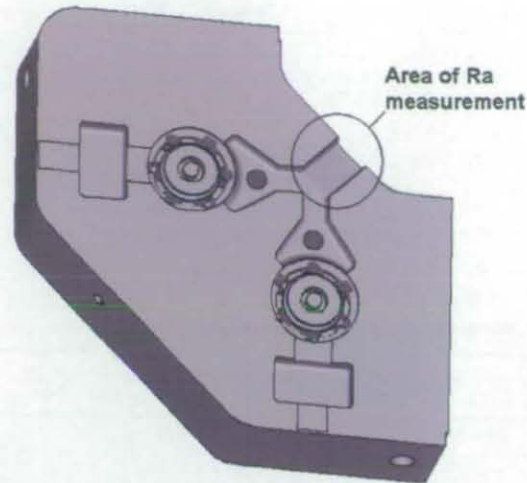


Figure 3 Area of surface roughness analysis

LM24 aluminium was utilised as the die-casting material.

2.2. CASE STUDY RESULTS

The tool was used to produce 500 parts. This quantity had previously identified by the project partners in represent a 'low volume' production run. The process cycle time taken to produce one part was 25 seconds utilising the same process parameters used by a complete steel tool. Initial signs of cracking in the MetalCopy insert began after approximately the 50 parts. This propagated from the central boss feature and continued to progress during continued production. These cracks became clearly visible after approximately 200 parts. As production progressed to the 500th part this cracking became more extreme and ablative. This cracking is shown in Figure 4.

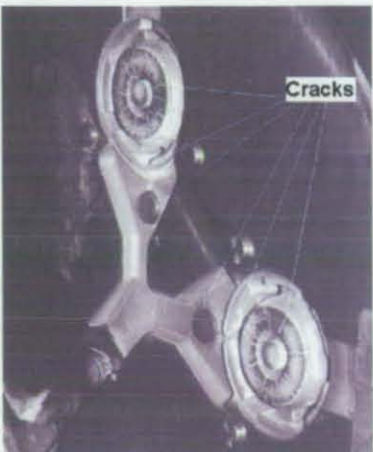


Figure 4 Damage inflicted on MetalCopy insert after die casting 500 parts

Some these effects were quantified by measuring the surface roughness of the tool before and after die- casting. Prior to casting, the area of tool shown in Figure measured an average surface roughness of $4.8\mu\text{m}$, while after casting it measured $7.8\mu\text{m}$.

The comparative accuracy measurements are shown in Figure 5.

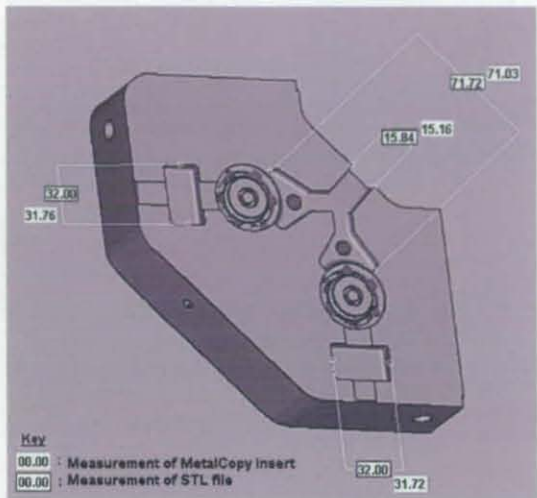


Figure 5 Comparative measurement of MetalCopy insert & STL file

Analysis was conducted to establish the characteristics of MetalCopy's structure that may have lead to the cracking failures experienced in the case study. Sections were taken from MetalCopy inserts before and after casting to allow magnified optical analysis of the structure and hardness testing at differing positions.

The optical analysis also indicated a level of porosity that was present in the MetalCopy inserts as they were received and also the variation on steel particle size. This is shown in Figure 6.

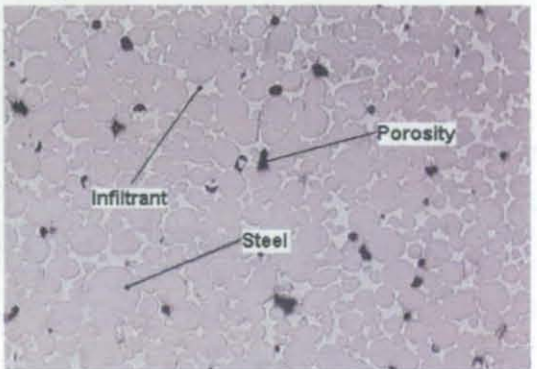


Figure 6 Illustration of MetalCopy structure

The cracks that were created by the high pressure die casting were investigated optically. This showed that the cracks propagated along lines of infiltrant material. This is shown in Figure 7.



Figure 7 MetalCopy crack post casting

3. THERMAL FATIGUE EXPERIMENTS

The progression of MetalCopy material for die casting hinges upon improving it's resistance to the cracking experienced in these trials. The repeated expansion and contraction of the tool material, caused by this heating & cooling, leads to the development of internal stresses. These stresses result in cracks appearing in the tooling material which ultimately lead to its failure [2]. In order to facilitate these improvements the following work in the project will be instrumental. A thermal fatigue test has been designed by Loughborough University to evaluate tooling materials for high pressure die-casting. The experiment involves a repeated thermal shock treatment

by exposing the sample to the temperature conditions that would be experienced in die-casting. The sample is exposed to very high temperatures, then a rapid decrease in temperature is induced to an ambient level. These conditions are repeated for 1000's of cycles. The experiment simulates the continued rise and fall in temperature that would be experienced by a tool in die-casting. The experiment is designed to assess the effects of this thermal fatigue by simulating these conditions and thus being able to assess it's sole effects by eliminating other variables experienced during physical die-casting (i.e. part release forces etc). The experiment is designed to ascertain a materials resistance to thermal fatigue and its suitability for use as a die-casting tooling material. The experiment will be utilised to quantify the suitability and facilitate improvements to powder binder mixture materials.

Thermal fatigue is the main cause in the reduction of a die's life and consequently it is important to understand how a material behaves. There are no standard test procedures. This has lead to researchers [3,4,5,6] developing and conducting their own experiments. The technique developed by Loughborough takes into account the findings of these prior works, leading to a hybrid technique. To conduct the thermal fatigue experiment a heated medium, a cooling medium and automated transfer system was required between the hot & cool mediums. A furnace containing molten aluminium and a cooling medium of water and die lubricant tank provided these mediums. The cooling medium tank was constructed from galvanised sheet steel and is designed to have constant cooling. The cooling medium temperature is controlled by a series of pipes circling the edge of the tank, which is connected to a chillier system. In order to obtain a constant level of water a simple float valve was positioned at the top of the water tank. The transfer rig consisted of X and Z axis operated by pneumatic pistons and controlled by reed switches and a CPU. This apparatus is shown in Figure 8.

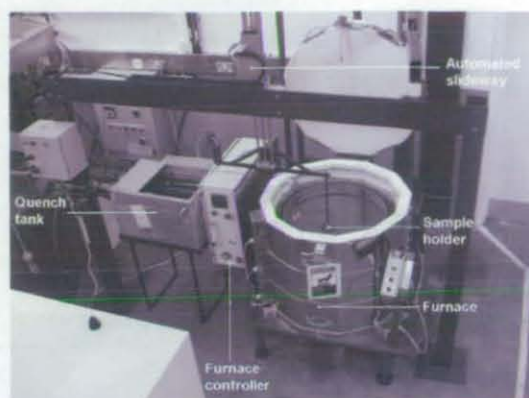


Figure 8 Thermal fatigue experimental apparatus

The CPU programme was constructed using Pneu Alpha Visual Basic software. Two timing delays were employed to enable separate control of heating and cooling times and a counter was used to enable automatic shut down after controlled number of cycles. A disc shaped specimen (Figure 9) was utilised which allows for easy crack measurement. The sample holder employed allows four separate samples to be analysed at once.

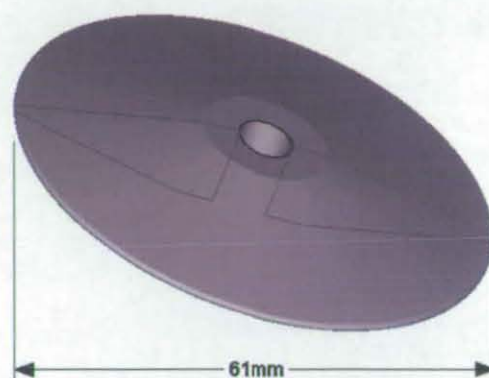


Figure 9 Specimen geometry

In order to ensure that these simulation tests represented the exact thermal conditions experienced by a high pressure die casting tool, it was necessary to perform some tests to exactly quantify these conditions. These tests were conducted to establish the exact temperatures of an aluminium pressure die-casting tool surface at production speeds and temperatures. The temperature profiles experienced would be replicated in the temperatures and cycle time of the thermal fatigue experiment. The temperature profiles were measured by a combination of two calibrated k-type 0.25mm diameter thermocouples and temperature sensitive paints in the runner system of the die

casting tool utilised in section 2. This is illustrated in Figure 10.

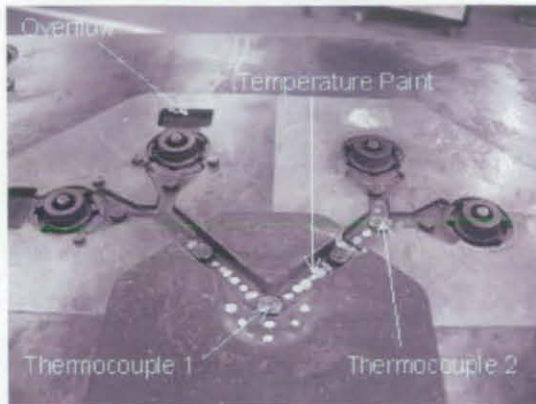


Figure 10 Temperature measurement in tool

The pressure die-casting test was conducted with the same casting parameters as in section 2. These were:

- The aluminium melt temperature was 710°C
- The die was preheated to 100°C – 150°C using a gas lance
- 50 shots ran prior to test initiation
- Cycle time 20s - 24s (production speeds)
- Die lubrication (delta cast 333 Release 3) sprayed every two shots
- Water cooling of overflow area and plunger tip

As shown in Figure 11, the thermocouple readings showed that the die surface temperature typically increased to 440°C when the aluminium was injected. The temperature paints confirmed this with the 399°C paint disappearing the 454°C paint partly removed and the 510°C paint unblemished. Upon removal of the casting and die cooling the surface temperature fell to 100°C – 150°C.

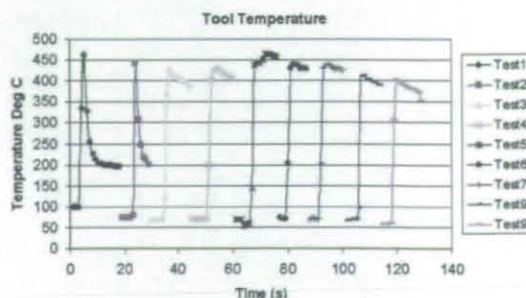


Figure 11 Tool temperature readings from thermocouples

As a result of the findings, the same temperature profile has been replicated in the thermal fatigue experiment by altering the temperature of the cooling & heating mediums (19°C & 730°C respectively), and the time of exposure (cooling: 0.9 sec, heating: 0.5 sec).

4. CONCLUSIONS

The results show that the MetalCopy insert is undersized in comparison with the supplied .stl file. The process concerns multiple translation steps. The comparative accuracy of the translation needs to be examined after each step in order to determine at which points there is a change. Subsequently attempts to compensate for the under-sizing may be made.

The results have shown that the infiltrant material is a weak point of the process when utilised as high pressure die casting. It has been shown that the cracks propagate along through this material avoiding the steel particles. The inherent porosity that has been demonstrated may also lend to this failure mode.

It is hoped that the thermal fatigue experiment described in this paper will allow for a better understanding of the failure mode which will in turn lead to material improvements. The experiment will be utilised to further quantify the process' suitability for high-pressure die casting tooling and facilitate improvements to powder binder mixture materials. The results of these experiments will be available in due course.

5. ACKNOWLEDGEMENTS

This work constitutes part of the project 'IMS RPD 2001' which is funded by the European Union.

6. REFERENCES

- [1] B. Holmer & T. Wohlers, Wohlers Report 2003 - Rapid Prototyping & Tooling State of the Industry Annual Worldwide Progress Report, Published by Wohlers Associates, Inc. USA, Part 5: Asia & Europe, Sweden section. Page 139.
- [2] Bendyk, J.C. Maracz, O.J. Wallace, J.F., Thermal Fatigue Behaviour of Die Materials for Aluminium Die Casting, The 6th SDCE International Die Casting Congress, Cleveland, Ohio, November 16th - 19th 1970, Paper Number 111, Pages 1-20
- [3] Glenny, E. Northwood, J.E. Shaw, S.W.K. Taylor, T.A. (1959), A Technique for Thermal-Shock and Thermal-Fatigue Testing Based on the Use of Fluidised Solids, Journal of the Institute of Metals, Volume 87, 1959, Pages 294-302
- [4] Howes, M.A.H. (1973), Evaluation of Thermal Fatigue Resistance of Metals Using the Fluidised Bed Technique, American Society Testing Materials, 1973, Pages 242-254
- [5] Wallace, J.F. Wang, Y. Schwam, D. (1997), Effect of Composition and Processing on the Thermal Fatigue and Toughness of High Performance Die Steels, Die Casting Engineer, Volume 41, Sep - Oct 1997, Pages 26-32, ISSN 0012-253x
- [6] Mowbray D.F. & McConnelee J.E. (1976), Nonlinear Analysis of a Tapered Disk Thermal Fatigue Specimen, Thermal Fatigue of Materials and Components, American Society for Testing and Materials (ASTM), 1976, Pages 10-29

7. BIOGRAPHY



Russ Harris has a first degree in Manufacturing Engineering, and a PhD in Rapid Prototyping & Polymers. He is currently a Research Fellow in the Rapid Manufacturing Research Group at Loughborough University, UK.



Andy Norwood has a first degree in Materials Engineering, and is currently studying for his PhD. He is currently a Research Associate in the Rapid Manufacturing Research Group at Loughborough University, UK



Phill Dickens is Professor of Manufacturing Technology, Associate Dean of Research and head of the Rapid Manufacturing Research Group at Loughborough University, UK.

Analysis of Cooling Channels Performance

A. J. Norwood^{1*}, P. M. Dickens¹, R. C. Soar¹, R. Harris¹ G. Gibbons², R. Hansell²

¹The Rapid Manufacturing Research Group, Wolfson School of Mechanical and Manufacturing Engineering, Loughborough University, Leicestershire, LE11 3TU, UK

²Warwick Manufacturing Group, Advanced Technology Centre, University of Warwick, Coventry, CV4 7AL, UK

ABSTRACT

The die casting industry is under increasing pressure to improve production rates to enable greater productivity. Employing conformal cooling channels could potentially improve a die performance through the reduction of solidification times. The paper reviews simulated solidification results from a traditional cooling channel design and a conformal cooling channel design. The paper continues by describing the construction of bonded laminate insert with integrated cooling channels. Casting trials were conducted using the inserts to validate the simulated results. Work to date has demonstrated the ability to manufacture laminate inserts quickly, the accuracy of Finite element analysis and the importance of designing conformal cooling channels.

KEYWORDS

Rapid tooling, laminate tooling, pressure die-casting, conformal cooling.

INTRODUCTION

The cooling of mould tools is crucial to the performance of tooling; it affects both production rates and component quality (Xu 2001 & Wayde 2000). Various methods exist to produce tools; such as laser sintering, spray metal tooling (Halford 1999), laser caving, wiba & keltool etc. However, laminate tooling could offer higher strength and toughness than the materials currently used in traditional layered manufacturing (Obikawa 1999). Laminate tooling is a typical layer-by-layer manufacturing process requiring a 3D STL CAD file, which is then sliced into layers. This sliced data is used to laser cut the individual laminates from sheet tool steel, these are then brazed together to form a die. The die surfaces are finished by either electrical discharge machining or high speed machining to remove the stepping effect created by layer manufacturing. Laminate tool manufacture allows a die to be constructed from die steel with the benefit of integrated conformal cooling as appose to a

solid H13 die where only straight cooling channels can be machined.

The rapid prototyping industry employs layer methods of manufacturing that allow virtually any geometry to be physically constructed (Dickens 1999). Due to this versatility, engineers are able to design and build complex components with internal features such as conformal cooling channels. Conformal cooling is achieved by creating a cooling channel that follows the exact contours of the mould cavity. By having the cooling channels uniformly located around the cavity, the risk of hot spots is virtually eliminated since the die is uniformly cooled this has been reported to produce less stressed parts in injection moulding. The increased effect of conformal cooling also helps to reduce cycle times, which in turn results in increased production rates. Conformal cooling lines of high complexity can be created (Xu 2001). Currently tooling is cooled through straight interconnecting channels. This traditional method is less than optimal because the passages can only be directed at right angles and cannot be optimally placed next to those strategic areas that need cooling. The result is a slower cycle time for the production of parts.

Software such as MAGMASOFT® now offer the die designer the ability to model tools and predict areas of concern and calculate mould fill times. The introduction of conformal cooling channels within tool design reduces the constraints / compromises made regarding cooling, as they can be placed exactly where required (Xu 2001).

AIMS AND OBJECTIVES

It is the intention of this research to explore the benefits conformal cooling may have on aluminium (LM24) pressure die-casting cycle times.

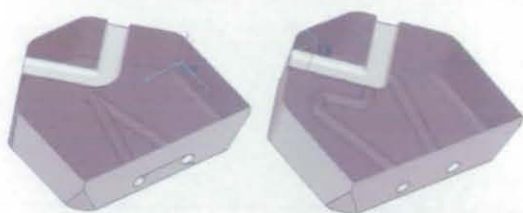


Figure 3 Designs for traditional cooling (left) and conformal cooling (right)

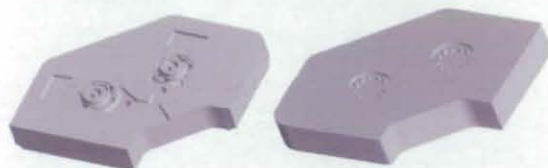


Figure 4 Male and female STL CAD of inserts

CONFORMAL COOLING DESIGN

The potential to decrease the cycle time is of great significance to the pressure die casting industry. A small reduction in the cycle time can significantly improve production rates.

STL CAD die insert files were created using Materialise Magics software and are shown in figure 3, one traditional cooled and the other conformal cooled. The diameters of the cooling lines in both were 10mm. The conformal cooling channel design shown in figure 3 had a 'M' profile following the runner and biscuit area. By introducing a larger cooled area in the biscuit region (1½ times larger) it was envisaged that the inserts cooling efficiency would increase due to the increased surface area of the cooling channel and water volume.

MAGMASOFT SIMULATION

Simulation was used to determine if a difference in time to solidification could be determined between the two cooling designs.

Analysis of the die was conducted using MAGMASOFT® software. The STL CAD files were combined to create two stl files, one with traditional cooling and the other with conformal cooling shown in Figure 5. These were then imported into the MAGMASOFT® pre-processor.



Figure 5 3D CAD models of the inserts and shot sleeve used for simulation

Half the model was removed, as the die was symmetrical allowing a reduction in processing time, the model was then meshed. Die cycling temperature and water-cooling were simulated. Figure 6 shows ten theoretical thermocouples that were positioned in the model, starting at the plunger tip spaced evenly through the insert, casting and cooling channel. The simulation was cycled 10 times to achieve 'near' steady state. The temperature of each thermocouple was recorded on the 11th cycle in a graphical format showing the time taken for the component to solidify. Approximately 8.5 temperature readings were recorded / thermocouple / second. Thermocouple 1 was located at the end of the plunger tip stroke, thermocouple 2, 3, 4 were located in the biscuit area of the casting, thermocouple 5, 6, 7, 8 were located in the insert and thermocouple 9, 10 were located in the cooling channel.

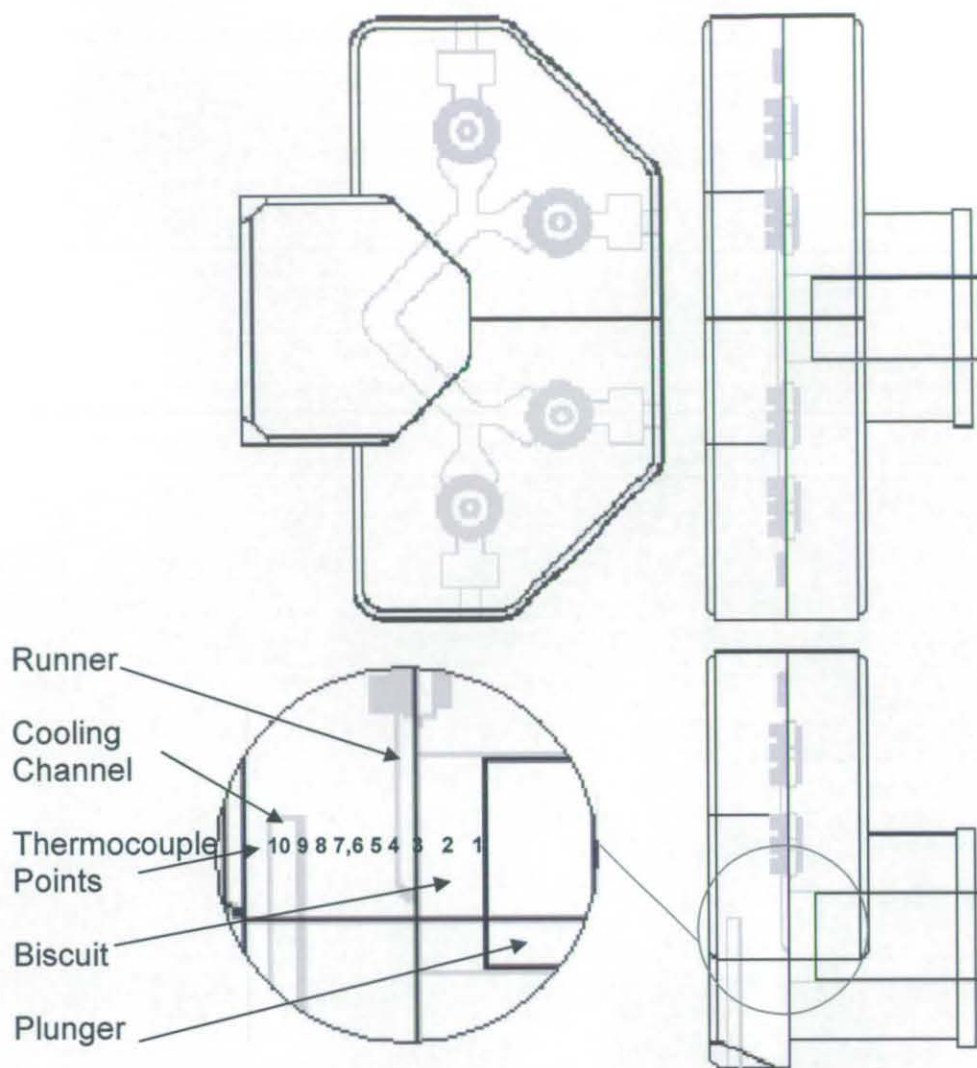


Figure 6 Section through the tool showing the location of thermocouple points.

CASTING VALIDATION

The experiment was designed to achieve a burst biscuit. A burst biscuit is where a casting has had insufficient time to fully solidify shown in Figure 7. In pressure die casting the biscuit is situated at the start of the runner system shown in Figure 8 and is usually the thickest part of a casting and hence the last area to solidify. By decreasing the solidification time it is possible to create what is called a "burst biscuit" which is where molten metal in the centre of the biscuit forces its way through a skin of solidified material. By achieving a burst biscuit the minimum amount of time to solidification can be determined. The lower the solidification time the faster the cycle time and better the productivity, as shown in Figure 9.

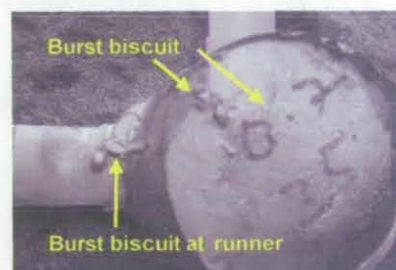


Figure 7 Burst biscuit

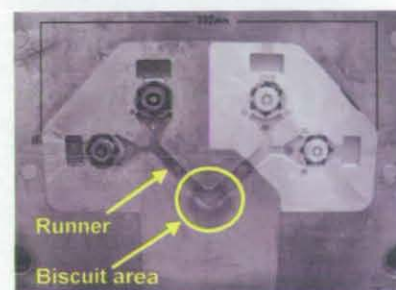


Figure 8 Insert location

Operator Starting cycle 1-2 sec	Die Close 1sec	Ladling 5-8 sec	Injection 1 sec	Solidification 3 sec	Die Open 3 sec	Ejection 2 sec	Release Agent 3 sec
Operator Starting cycle 1-2 sec	Die Close 1sec	Ladling 5-8 sec	Injection 1 sec	Solidification 7 sec	Die Open 3 sec	Ejection 3 sec	Release Agent 3 sec

Figure 9 Typical cycle time of the die

LAMINATE DIE INSERT MANUFACTURE

The STL CAD file of each insert was sliced in order to generate the 2D DXF CAD data. These contained the profiles that defined each cutting path of the laser, to produce the individual laminates. Using Delcam's PowerShape 3D Package the STL CAD files were sliced with a layer thickness of 1mm, the thickness of the steel sheet. This was a subroutine that enabled automatic slicing of

the 3D tool and output individual 2D, DXF files and produced a total of 90 profiles.

The profiles were then transferred directly to a 1200 Watt Photon Versa CO₂ continuous gas laser cutter where the H13 steel laminates were cut. The laminates were then grit blasted with a nickel alloy abrasive at 620 kPa to remove burrs, oxide layer and then degreased with isopropyl alcohol ((CH₃)₂ CHOH). The laminates were bonded using Amdry 936 supplied by Sulzer Metco in powder form (Table 1). The laminates were placed and each joint coated with Amdry 936 in a purpose built fixture to prevent excessive movement during the brazing process. The nickel braze was used due to its high melting temperature and ease of machinability.

	AMDRY 936
Recommended braze temperature	970-1010°C (1775-1850°F)
Recommended gap size	0.013mm - 0.1mm (0.0005" - 0.004")
Composition	Nickel Balance. – 19 Magnesium – 6Silicon – 1Boron – 4Copper – 0.03Rhenium

Table 1 Braze details

The inserts were brazed in a furnace with an inert Argon atmosphere. The furnace was purged with Argon at 100kPa and 30 l/m flow for 20 minutes prior to the start of the brazing cycle shown in Figure 10. The Argon was then reduced to 100kPa and 20l/m flow when the brazing process commenced. The first temperature hold at 150°C for 15 minutes was to allow solvents or water in the braze and furnace to outgas. This helped to prevent porosity in the braze and allowed time for the atmosphere to replenish. The

second hold at 540°C for fifteen minutes allowed organics in the braze sufficient time to become gaseous and to be pumped out and again time for the inert atmosphere to return. At 960°C there was a stabilisation hold for ten minutes. The temperature was then held at 1010°C for one hour to allow sufficient time for the alloy to melt and flow into the joint.

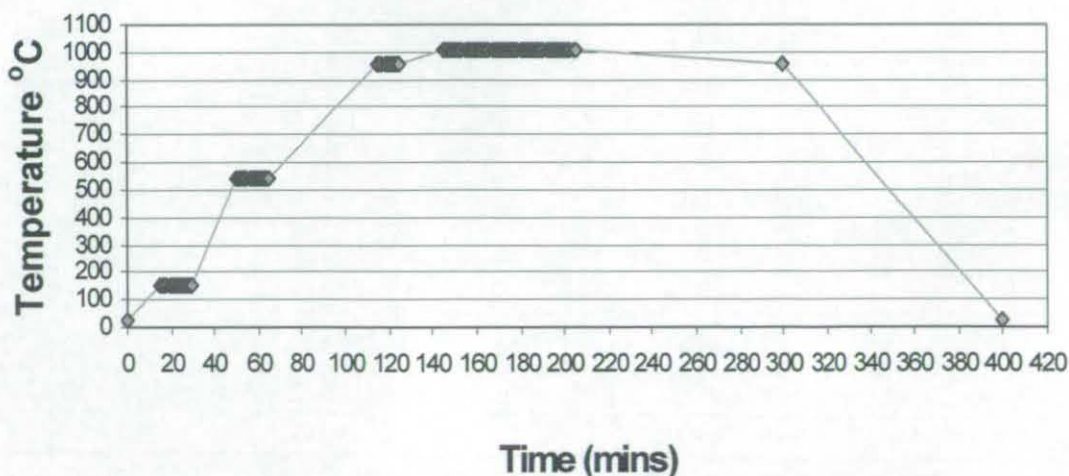


Figure 10 Heating and cooling profile of the brazing process

The inserts were allowed to cool in the furnace below the solids temperature of the braze at approximately 960°C at which point they were removed from the furnace and air quenched. Figure 11 shows the traditional insert after final machining of the exterior, runner, ejector holes etc.

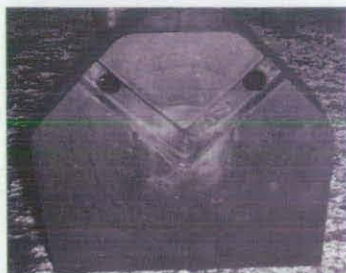


Figure 11 Insert after machining

CASTING PROCEDURE

The experiments involved a series of casting trials which were conducted at production speeds to maintain a representative die temperature.

The cooling channels were tested to ensure no leaks were present. This was achieved by simply blocking the outlet of the water channel, connecting the inlet to mains water (400 kPa) and checking for leaks.

The casting was conducted on a Frech 125 DAK SDV cold chamber die-casting machine which was modified to allow the solidification time to be adjusted below 3 Seconds. This is not a standard procedure due to the danger involved with opening a die whilst aluminium is potentially molten. To safe guard against injury the area was sealed off and machine guards put in place.

The die casting machine was set up as previously shown in figure 9. The cycle time was set at approximately 170 shots per hour (21 second cycle) with a solidification time of 3 seconds. The die was initially heated with a gas lance for 1½ hours and then 150 shots cast to achieve the dies working temperature of 200°C – 250°C. Thereafter, samples were taken every 10 shots and the cooling time for each shot recorded. After every 10 shots the cooling time was decreased by 0.1 of a second until there were signs of a biscuit burst shown in figure 7.

RESULTS

SIMULATION RESULTS

Thermal images show the rate at which solidification occurs in Figure 12 & Figure 13.

The conformally cooled thermal image shows the majority of the casting had solidified after 2 seconds and is similar to the traditionally cooled image with the exception of the biscuit area. The centre of the traditionally cooled biscuit takes approximately 10 seconds to fully solidify in comparison to 9 seconds for the conformally cooled image.



Figure 12 Traditionally cooled solidification time

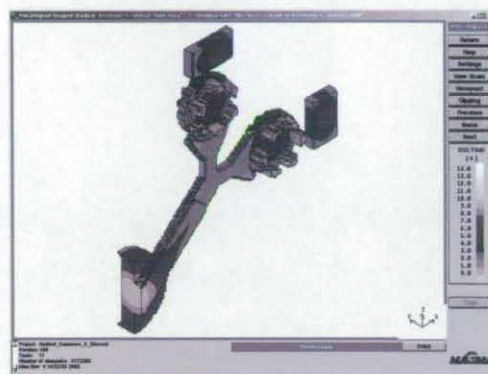


Figure 13 Conformal cooling solidification time

This is confirmed when comparing the raw data from thermo couple points 2, 3 & 4 shown in Figure 14. Aluminium LM24 solidifies between 520°C and 580°C, which is where crystallisation begins and ends this, is termed latent heat of fusion. Thermo couple 2 and 3 are located in the centre of the biscuit and solidification begins after 1 second and ends after approximately 8 seconds. For both the traditionally cooled and conformally cooled insert there is no significant difference between the solidification times. Thermocouple 4 is located at the edge of the runner near the die surface and is naturally is the first area to solidify, starting at 0.3 of a second and finishing at approximately 5 seconds.

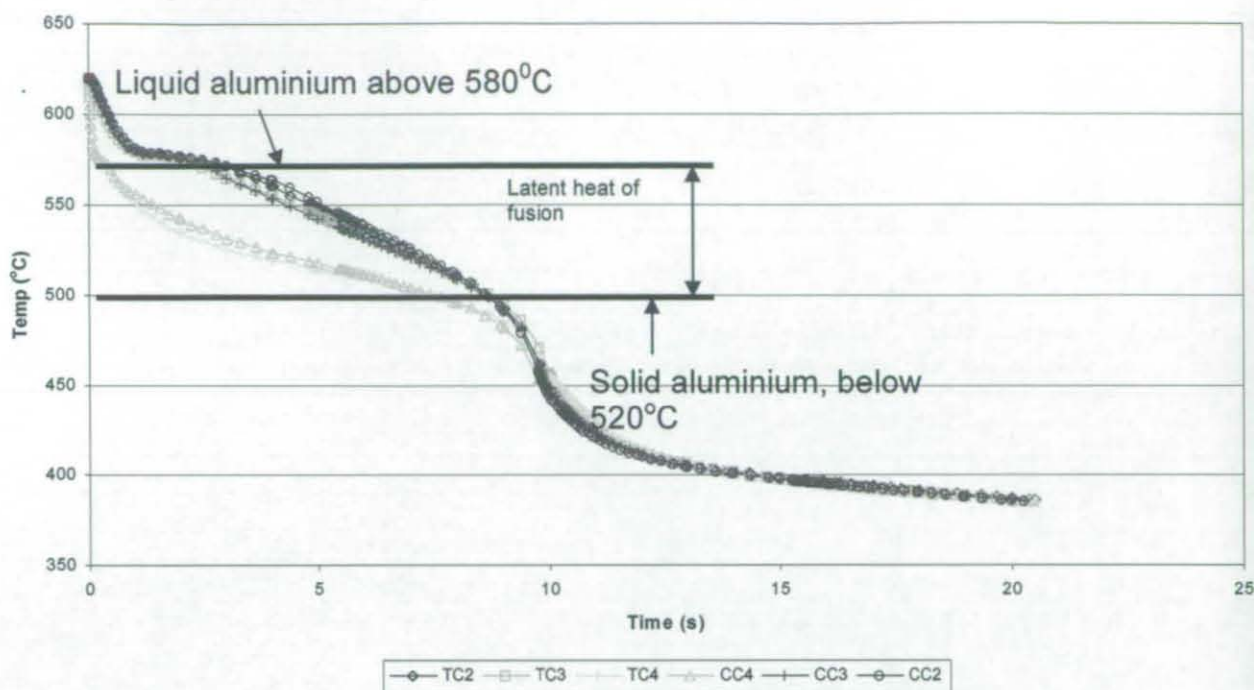


Figure 14 Traditional cooling (TC) verses conformal cooling (CC) (thermocouples 2-4)

Figure 14 shows little difference between the traditionally cooled (TC) and conformally cooled (CC) insert solidification time.

Thermocouples 5, 6, 7 & 8 were situated in the insert and as one would expect the closer to the die surface the thermocouple was, the greater the temperature recorded.

This can be seen in Figure 15 where traditionally cooled thermocouple 5 (TC5) is approximately 55°C hotter than traditionally

cooled thermocouple 8 (TC8) the same is true of conformally cooled thermocouple 5 and 8 (CC5 & CC8).

When comparing the traditional and conformal thermocouple points it can be seen that the conformally cooled insert is typically 20°C cooler than that of the traditionally cooled insert for each thermocouple location (Figure 15, TC7 and CC7 for example).

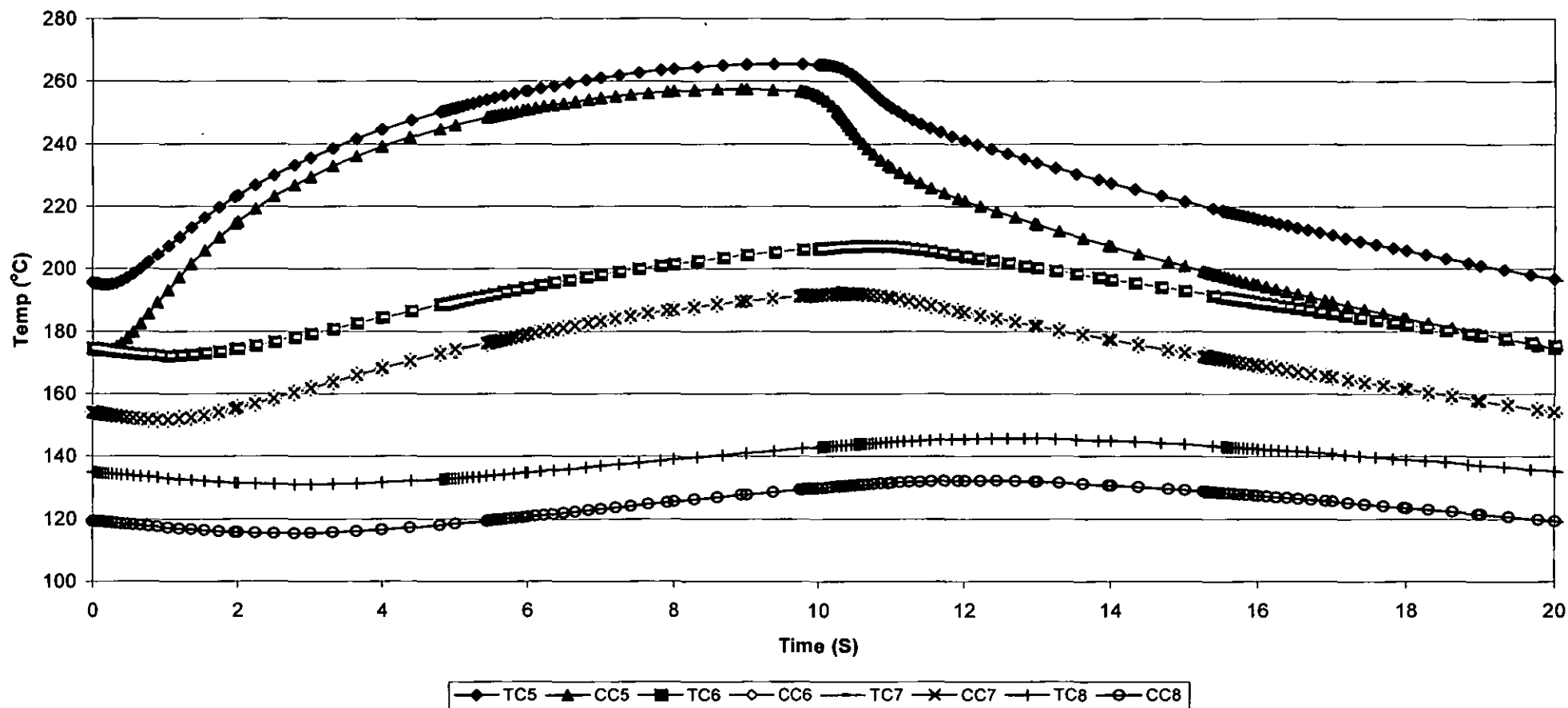


Figure 15 Traditional cooling (TC) verses conformal cooling (CC) (thermocouples 5-8)

RESULTS FROM CASTING

The results from both the traditional and conformal cooled tool were the same. During the casting trials the components were visually examined for signs of a burst biscuit. In both the traditionally and conformally cooled inserts the solidification time could be reduced from 3.5 seconds down to 1 second. The lowest time before failure of the biscuit and casting occurred was 0.7 seconds. Failure was determined as a burst biscuit or the biscuit being semi molten and separating from the runner/casting during ejection.

DISCUSSION

The Magmasoft simulation shows the conformally cooled insert to be approximately 20°C cooler than the traditionally cooled insert, shown in figure 15. The simulation however does not show an improved solidification time of the casting, shown in figure 14. When comparing the two simulations there is little difference in the cooling performance of the channel designs.

This was verified by the casting trials, proving that the simulation is accurate at predicting solidification rates. It is clear that the design of a conformal cooling channel is crucial since both the simulation and physical casting experimentation showed no reduction in solidification time.

The casting trials showed that solidification must happen quicker than predicted by the simulation since the die could be opened at 1 second with no signs of a burst biscuit. At 0.7 seconds the biscuit failed and separated from the rest of the casting upon die opening. This is achievable as the outermost surface of the casting created a skin trapping the remaining semi molten aluminium inside which allowed the die to be opened whilst the centre of the biscuit was semi molten. However the simulation shows no evidence of this, predicting that it takes the runner and biscuit area 8-10 seconds to solidify, as shown in figure 12 & figure 13.

Although the conformal cooled channel had 1½ times the surface area and volume it evidently was not enough to remove the heat. Both the simulation and casting trials showed no reduction in solidification time. In hindsight it would have been practical to conduct the finite analysis prior to the manufacture of the insert and casting trials.

CONCLUSIONS

The results showed that the simulation was accurate at predicting no differences between the channel designs. This was verified by the casting trials. This proves that by simply increasing the length of a channel does not necessarily improve cooling performance in a aluminium pressure die casting tool.

The simulation and casting trials do differ in how solidification takes place in the biscuit area. This area is the last area to solidify, as you would expect. However, the casting trials showed the die could be opened after one second with no signs of a burst biscuit. The simulation begs to differ. It clearly shows the biscuit still solidifying after 8 seconds even at the edge of the runner. If this were the case the die wouldn't have been able to open. The research has outlined the importance of conformal cooling geometry and placement, as conformal cooling did not reduce the solidification time in this case.

This may be due to the shape, surface area, volume, flow rate and or location of the cooling channels being inadequate. Changing the shape and increasing the water/ tool contact area should allow increased heat transfer from the tool to the water in the channel. Increasing the volume of the channel may allow greater heat dissipation in the water. Experimentation with flow rate, turbulent flow versus laminar flow and good placement of the channels may improve cooling performance.

The second stage of this research will be to conduct further finite element analysis with different conformal cooling channel designs to improve the cooling of the biscuit area. From this data the most efficient conformal cooling design will be manufactured and the simulated results validated by casting trials.

ACKNOWLEDGEMENTS

The authors would like to thank the following for supporting this work:

Foresight Vehicle Programme
The Engineering and Physical Sciences
Research Council (EPSRC)
Delcam International
Dyson Ltd
Kemlows Die Casting Products Ltd for their
support and casting trials.
MAGMA for running the thermal the finite
element simulations.

REFERENCES

DeGarmo E.P., 1998, Material and Processes in Manufacturing 7th Edition Collier Macmillan Publishers, Pages 356 – 375, ISSN 0-02-328631-8

Dickens P.M., 1999, Rapid Prototyping – Past, Present & Future. Journal of The Institute of Engineering Designers, pages 12-15, ISSN 0013-7858

Halford B., 1999, Rapid Tooling, Journal of the Institute of Engineering Designers May, pages 4-6, ISSN 0013-7858

Obikawa T., 1999, Sheet Steel Lamination for Rapid Manufacturing, Journal of Materials Processing Technology, Volume 89-90, pages 171-176

Soar, R.C., 2000, An Examination of the Feasibility and design Limitations of Laminate Tooling for Pressure Die Casting, PhD, De-Montfort University

Wayde R., 2000, Schmidt, Ronald D. White, Connie E. Bird, Joseph V. Bak, Conformal cooling vs. conventional cooling: an injection moulding, case study with 3-dimensional printing. Solid Freeform and Additive Fabrication, Materials Research Society Publications, Volume 625, pages 51 – 56, ISBN: 1-55899-533-1

Xu X., 2001, Emanuel Sachs, Samuel Allen, The design of conformal cooling channels in injection mould tooling, Polymer and Engineering Science, Volume 41, Number 7, pages 1265-1279

Norwood, A.J., and Soar, R.

LAMINATE TOOLING

Laminate tooling can be considered a direct tooling technique and is probably one of the simplest processes to design, manufacture and implement. The key attractions are low cost, scalability, robustness, lead time < 1 week, deep cavities, design verification and conformal heating and cooling channels.

Laminate tooling has been employed in applications, beginning with Professor Nakagawa's work in Japan in the late 1970's. Much of the early work was based around the fabrication of tooling for deep drawing and blanking tools with horizontally stacked laminates. This initial work has led to increased research into many tooling domains incorporating conformal cooling and heating channels. An additional benefit is the scale of the tooling is not limited unlike many rapid prototyping processes that are limited to the size of the machine platform.

The manufacture of a laminate tool is similar to Laminate Object Manufacturing (LOM) process where sheets of paper are replaced with steel sheets. The process starts like many other rapid prototyping methods, with an STL CAD model. The model is sliced as an offset function and each slice is saved as a DXF file. The DXF files are nested and define the cutting path for a profiling machine (Water jet, laser, plasma etc.) Here in lies the limiting factor for the size of tool, the size of the profiling bed. However, there are many companies who perform profiling work of three meters square. Each individual laminate is assembled in order by physical clamping or bonding. Like many rapid prototyping methods stepping occurs and the tool requires finishing, employing EDM or high speed machining achieves the desired tool finish. The dies can also be heat treated however; this is dependent upon the tool and bonding material.

Laminate tooling research is increasing and development work can be split into two categories (a) un-bonded for design verification, prototyping and short run tooling. These tools are mechanically clamped together usually employing nuts and bolts. (b) Bonded for long run tooling, adhesives, solder, brazing, friction welding etc. can be employed. Bonding prevents deflection of the individual laminates and

seals conformal channels preventing leakage.

Laminate tooling has been successfully employed for injection moulding, press tools, punch and die sets etc. and is beginning to emerge in industrial applications. Recent development work has led to tools for aluminium gravity die-casting and pressure die casting where the working environment is extremely aggressive.

GRAVITY DIE-CASTING DIES

De Montfort University and Warwick University is currently running an EPSRC project with industrial partners and have developed a simple brazed laminate tool for aluminium gravity die casting, to evaluate erosion, chemical attack, heat checking, delamination etc.

The tool was constructed from, cold rolled H13 sheet which was laser cut, de-burred and brazed with Amdry 936 supplied by Sulzer Metco and machined to remove stepping.

The die produced 2,000 components with out failure. Although the die was simple and under no external forces (die open/close) it proved that the composite material could tolerate the aggressive environment. In addition it produced a significant number of components making the process suitable for short run production tooling.

The next stage was to produce a larger more complex tool both bonded and un-bonded for aluminium gravity die-casting. A production brake master cylinder provided by TRW was the chosen component.

The tools were produced in the same manor, as before however, consideration for clamping and laminate orientation of the un-bonded tool had to be considered. Due to the components profile one insert was produced horizontally and the other vertically (Figure 1).

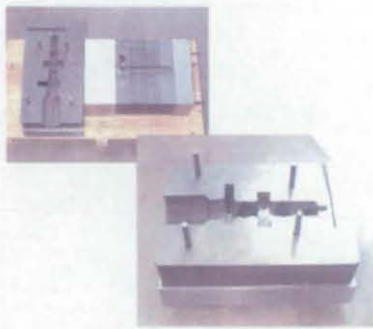


Figure 1 Pre Machined Inserts

Machining the un-bonded inserts caused the laminates to burr and several de-burring operations were carried out in order to maintain tolerance. To overcome this extra clamping was required (or high speed machining could have been employed), as the cutting forces could have been reduced.

PRESSURE DIE-CASTING DIES

The pressure die-casting process has more issues to address than that of gravity die casting. It works at much higher pressures and clamping forces up to 3000 tonnes are required to insure the mould remains closed, it has a 3 stage injection cycle, faster cycle times which means the die has a rapid heating and cooling, and channels have to be integrated into the die.

The majority of wear on a pressure die casting tool occurs in the gating system (where the biscuit is formed. This is due to the molten aluminium being forced into the runner system and rapidly changing direction by 90° . This is followed by pressure as the die continues to fill and solidify.

Horizontal and vertical bonded laminated gating Inserts were produced for a four impression aluminium (LM24) production tool. These were designed to incorporate conformal and traditional cooling channels. The benefits of conformal channels are that a designer is able to place cooling or heating where it is needed within a die. This is only feasible by producing a tool in a layer by layer approach.

A direct comparison between the bonded laminate inserts and the solid H13 inserts can be made. The test was designed to enable an evaluation of wear rates, thermal fatigue, failure mode, life expectancy and observe all the cycle times with conformal cooling and traditional cooling (Figure 2).

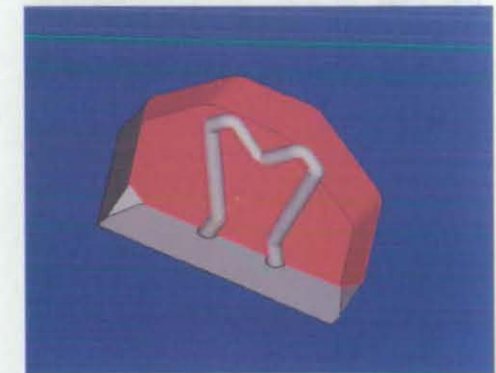
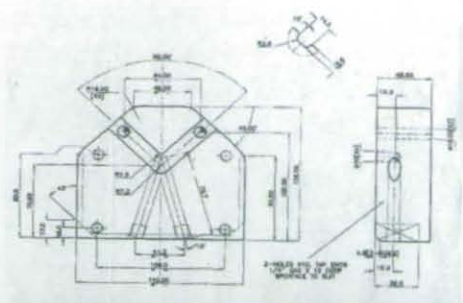


Figure 2 Traditional and Conformal Cooling Channels Designs for Inserts

Recent experiments have been produced encouraging results, using the conformal cooled gating insert, reduced the solidification time from 3 seconds to 0.7 seconds increasing production rate by approximately 11%. The trials will continue to determine the life expectancy of the insert.

The next stage will be to produce a bonded and un-bonded laminate pressure die-casting tool and compare them to a production die. This will enable us to evaluate the merit of laminate tools as an alternative method of producing prototype / production tooling for the die casting industry.

This tool will be designed to make comparisons between bonded, un-bonded and the production tool e.g. address performance characteristics of horizontal vs. vertical laminate orientations, costing, time to market profiles and die life comparisons.

It has been decided to use electro discharge machining (EDM) to remove any stepping and finish the tool due to the deep cavities on both sides of the die. EDM was chosen to determine whether it was a suitable finishing process for bonded and un-bonded structures i.e. would the braze wear faster than the H13 tool steel, how would the electrodes wear, what finish was achievable, etc. The EDM tooling are to be produced via electroplated SLA and EOS rapid prototyping methods.

The stereolithography process (SLA) employs a laser, which scans an image on the surface of a vat of UV curable resin. A thin layer of liquid resin becomes solid and the cross section is lowered and the next layer scanned on to the resin. The layering process continues until the part is built.

SUMMARY

Many of the tools discussed are beginning trials in industrial environments.

The research to date is primarily associated with the manufacture of a laminate tool for the die casting industry.

Un-bonded laminate tools are able to withstand the pressure die casting environment, however, it is not always possible to place clamping bolts where required due to component geometry. This causes uneven clamping pressures with associated distortion. It is also important at the design stage to select the correct laminate orientation in order to prevent un-clampable island/features.

Finishing via high speed machining can cause lifting and burring of laminates. Causing the tool to be disassembled and rebuilt increasing time and costs. Hence, EDM is the preferred finishing technique.

Bonded tools eliminate the problems associated with an un-bonded die i.e. uneven clamping, burring, leaks from cooling channels etc.

Heat treatment can also be conducted without the risk of laminates distorting. The brazing process is conducted at 1020°C, H13 Hardening temperature this is then tempered to 43Rc.

Initial problems arose when machining the brazed laminate structure, laminates would peel off due to lack of wetting. An increased soak time at the brazing stage reduced this problem. However, EDM was employed to prevent this recurring.

Our initial trials of the bonded gravity tool have proved promising with the brazed structure withstanding the temperature (730°C) involved with aluminium (LM24) gravity die-casting. The tool has shown no signs of erosion heat checking/fatigue or delamination to date.

It is envisaged that laminate tooling could be employed as a method of manufacturing prototype tooling to validate die design for the die casting industry. In addition it could be considered for short run tooling.

Further Industrial trials are to be conducted in order to validate the dies failure mode, life expectancy, effects of conformal cooling etc.

The direction is leading towards the construction of composite laminate tool allowing incorporation different metals and mechanical properties where required. It is envisaged that this will move towards mixed metal matrix and foils increasing tool detail and properties.

DIRECT METAL LASER SINTERING (DMLS)

Laminate tooling offers potential solutions to die-casters where sizes $\geq 500 \times 500 \times 500 \text{mm}$, weight removal and conformal cooling are the main decisions on tooling selection. DMU are also addressing Rapid Tooling solutions for HPDC where tooling is required for sizes $< 500 \times 500 \times 500 \text{mm}$. One particular process centres on the application of the laser sintering process currently available. EOS Finland are currently performing trials with DMU for their new 20 μm DMLS DirectSteel material (DS20 v1). Much of the laser sintered materials prior to this development have made good inroads into the injection moulding industries but so far have struggled where HPDC is concerned. DS20 v1 is a very promising material in that it has far higher detail than the previous 50 μm material and DMU have already demonstrated this material for injection moulding applications.

Direct Metal Laser Sintering (DMLS) is the term coined by EOS GmbH to describe their metal laser sintering process. Its true definition is actually 'Liquid Phase Sintering'. Distinctions are often drawn between the DTM and EOS process, the main being that the DTM process uses a polymer coated metal powder to form 'Green' parts that are subsequently sintered and infiltrated. This is opposed to the EOS process that produces a fully sintered part in one stage. There is often a misconception that the EOS process uses a more powerful laser to fuse the metal powders that are loaded into the machine.

This is not quite correct as the process actually relies on a blend of powdered metal that contains a low melting point and high melting point powder. As the laser scans each layer of deposited powder it is the low melting point powder that binds the remaining powder into the desired shape. In this respect there is some similarity in the two processes as they both rely on a secondary material to melt and bind a more robust metal powder.

So why doesn't DTM used lower melting point alloys to bind its powder? Besides the patent issues, the EOS powders have one more trick up their sleeve. They are very unusual in that they exhibit a volume expansion as they cool. Under normal conditions one the biggest problems with trying to get a fully dense metal part out of such a machine is the stresses that are set up as the powder is melted. Not only is there a volume change but also the material will try to shrink as it cools. The EOS materials (developed by Electrolux) expand as they cool thus negating some of the stresses that would otherwise hamper this process.

Of key interest to the HPDC industry is DMU's recent application of this process to produce both magnesium and aluminium die-casting dies that were run in the production environment. DMU were able to demonstrate the production of 500 Ericsson mobile phone chassis, some of which were assembled into working phones. Based on the success of this project a new project was set-up that drew on the die-casting skills of Kemlows Die-casting Ltd and the Dyson Ltd who donated a high production HPDC tool used to for producing a clutch housing mechanism for their vacuum cleaner. One of the inserts in this tool was replaced by a DS20 v1 insert, with integral heating and cooling lines. This tool was then run under full production conditions by Kemlows Die-casting Ltd and the castings sampled and measured for accuracy / tolerances etc. Dyson were able to confirm that the castings were within tolerance and the tool was run for 500 shots.

500 shots in Aluminium LM24 is a very promising number and certainly proves the concept for prototype tooling, bridge tooling or even short run tooling. The run was terminated after 500 casting based on time constraints and a frozen casting but the tool showed no signs of degradation and is awaiting to be run on to destruction.





2001 congress & exposition

| Tooling for Rapid Tooling and | Industry

Andrew Norwood, Research Fellow, De Montfort University, Leicester, UK

Phillip Dickens, Professor of Manufacturing Technology, De Montfort University, Leicester, UK.

Rupert Soar, Lecturer, De Montfort University, Leicester, UK.

Presented by:

North American Die Casting Association

Abstract

The need to produce components employing the desired casting material, tooling and process in order to evaluate a die design and its components is invaluable. This method of die manufacture has the ability to produce complex dies in a short lead-time and at a reduced cost. This paper addresses a novel method of manufacturing bonded and un-bonded laminate dies for use in aluminium die-casting.

The process involves several stages, they are, generation of a 3-D CAD model of the tool, slicing the model, laser beam cutting the individual slices in H13 tool steel, laminating them to form the die profile with stepping, brazing or clamping. This is followed by electrical discharge machining (EDM) or high speed machining to remove stepping.

The technique allows conformal cooling to be integrated and can allow die features to be altered, added or removed. Due to the composite structure of the die it is also feasible to integrate high strength materials where needed.

Several experimental dies were manufactured for gravity and high pressure die-casting applications to address tool wear, heat checking/thermal fatigue and the effects of conformal cooling.

Introduction

The rapid prototyping industry has created new methods of manufacturing allowing virtually any geometry to be physically constructed (Dickens 1999). Due to the versatility and layer technology engineers are able to design and easily build complex components. However, for validation of geometry and physical testing of components the prototypes need to be manufactured with the specified material and process.

This has led to spin-offs from the traditional methods of rapid prototyping, such as laminated tooling (Soar 2000) which employs the Laminated Object Manufacture (LOM) process however; metal sheet replaces resin bonded paper.

Various methods exist to produce tools, such as selective laser sintering, spray metal tooling (Halford 1999), laser caving. However, Laminated tooling is a good option since sheet metals have higher strength and toughness than the materials used for traditional layer manufacturing. (Obikawa T. 1999).

Laminate tooling is in its infancy although, several tools have been developed for different applications, example's are:

Blanking tool and die set (Yokoi 1994)
Polyurethane foam moulding tool (Dickens 1996)
Metal Forming dies (Walczyk 1994, 1998),
Injection Moulding dies (Glozer 1992, Bryden 1999)
Aluminium die casting tool (Soar 1998¹).

Injection mould tools have been manufactured and tested with favourable results (Glozer 1992). Glozer's moulding trials were conducted using polypropylene as it flows relatively easily and required a low injection pressure. The machine was set to have fill time of 1.56 second cycle and it had a maximum pressure of 67MPa on the screw. The mould produced over 400 components and showed no sign of wear or fatigue. He estimated the mould life to be in its thousands and would only be limited due to the softness of the aluminium laminates. Glozer (1992) also concluded "under the conditions used in this test that the polymer was not capable of forcing the laminates apart during injection".

The next logical transition was to transfer the technology to high pressure die casting (HPDC). However there are additional problems associated with the die-casting process.

- Injection speeds and forces
- Thermal shock.
- Ingress

History

Laminate tooling for the manufacture of high-pressure die-casting dies has several advantages:

It is feasible to produce tools in a time and cost effective manner. Deep narrow geometry's could be produced. Die geometry could be altered quickly and cost effectively. It is likely that tool repair would be rapid and cost effective. Production of laminates may be faster and cheaper than billet tools. For volumes over 500mm x 500mm x 500mm, sheet steel is cheaper than billet. (Soar, 2000). There is usually a shorter lead time on sheet as it's an off the shelf item. Evaluation of a component that has been produced using the desired production route and material.

Scale is not limited (Soar & Dickens 1998^b) as tool size is determined by the bed size of the laminate cutting and finishing processes. Both Male and female halves can be manufactured simultaneously. Inclusion of conformal cooling channels increases production and running speeds. (Himmer, 1999).

It may also be advantageous to produce hollow tools, to increase cooling/heating efficiency and reduce the die weight.

Harder die materials could be employed (Walczyk 1998) as different manufacturing processes are employed to manufacture a laminate tool. This would extend die life and reduce component cost since a greater number of components could be produced without the need for tool repairs or even a tool change. Cost effective short run tooling is achievable.

It's only in recent years that laminated tooling has been researched with aluminium die-casting and high pressure die casting in mind (Soar 2000).

The pioneering work conducted by Dr Rupert Soar (Soar 2000) was based upon investigating ingress of molten aluminium (LM24 alloy) between laminates, i.e. would the individual laminates deflect when subjected to the injection forces of the pressure die casting process and allow aluminium to enter between them.

Soar constructed a cold chamber laminate die-casting tool (Figure1) employing 1mm H13 steel sheet. The tool contained ramp features increasing in height. These went up in increments of 0.5mm, 1mm, 2mm, 3mm, 4mm, 5mm and 6mm.

The significance of the array of eight laminate heights above the ramp feature, was to determine the range which ingress of molten aluminium (LM24) would occur between the laminates caused by deflection on the protruding features (Figure 2).

Soar concluded (Soar 2000):

Un-bonded laminate tools are able to endure the conditions found in high pressure die casting and can be used for short runs for design verifications. Ingress between laminates did not occur where isolated 1mm thick laminates protrude less than 6mm.

For ingress of LM25 aluminium to occur the laminates must be deflected 0.05mm. For any die design laminates are more likely to deflect the closer they are to the inlet gate.

Removing a seized casting can damage the effectiveness of the laminates in a laminate die to resist deflection and hence ingress.

This research showed that un-bonded laminate tools are able to withstand the aggressive environment of the pressure die-casting process. However, problems exist such as:

- Laminate deflection at the shut of face
- Deflection of protruding features near to the gate due to high pressures in this area
- Possible deflection of individual laminates greater than 6mm
- Clamping of the laminates
- Laminate Alignment
- Cooling channels may leak

These factors hinder tool design and the complexity of an un-bonded pressure die casting tool is limited. The solution may be found in a bonded, and what could be termed composite laminate tool.

Process Technology

The initial stages of construction of a laminate tool are identical to that of a billet tool. A CAD model of the desired component is created and material shrinkage calculated, the model is then modified accordingly. This is easily achieved with modern CAD packages due to the fact the model can be offset and or scaled to achieve a 3D representation of what will become the tool cavity. It is then necessary to determine the parting line and orientation of the component. At this stage a number of factors should be considered; gating, undercuts, draft angles, witness marks, shrinkage on to features etc.

Again with the help of modern CAD systems the 3D model complete with split line can be subtracted from a solid cube, creating 3D models of both male and female halves simultaneously.

At this stage the design of a laminate tool deviates from that of a billet tool.

Features have to be reviewed such as; through holes running the length of the tool for clamping purposes/locating dowels, core pins for upright features and conformable cooling channels.

When the tool features have been finalised the two halves can be sliced in order to

generate the 2D CAD data required for cutting the profiles on each laminate. This is achieved by importing one half at a time into software such as Delcam's Power-Shape 3D Package. They have developed a slicing subroutine that enables automatic slicing of the 3D tool and outputs individual 2D, DXF or IGES files. Prior to running the subroutine it is important to know the slice thickness which is determined by the sheet from which the laminate is to be cut.

The 2D data can then be transferred directly to any automated cutting process, water Jet, laser, plasma etc. The selected process requires material type and dimensions to be inputted in order for the correct cutting parameters to be determined. The machine will then determine nesting to optimise the material.

Some processes such as plasma create a burr when cutting which must be removed hence, laser or water jet cutting are favoured. However, the laminates require cleaning prior to assembly, this can be effectively achieved by finishing or tumbling. Both processes are quick although finishing allows the laminate stack order to be maintained.

Once clean the laminates are stacked, aligned and either brazed or bolted together, the tool can then be checked to insure accuracy has been maintained.

The final procedure is to finish the tool in order to remove stepping, common to most rapid prototyping methods and the incorporation of the ejectors. Depending upon the tool geometry, electro discharge machining (EDM) or high speed machining can be employed.

The authors are involved in a collaborative project with Warwick University and several industrial partners funded by the UK Science & Engineering Council.

The project partners chose to employ the brazing method to bond individual laminates due to a number of reasons. Brazing is a traditional bonding method with high strength, high temperature properties and it is cost effective.

The high temperature and strength characteristics of brazing is very attractive and important when considering it for the construction of a aluminium die casting tool. Die surfaces are subjected to $\approx 730^{\circ}\text{C}$

(LM24 molten temperature). It is apparent that HIPing is the only other suitable method to fabricate a laminate structure capable of withstanding the aggressive aluminium die casting environment. However, this is an expensive method of manufacture and the author believes that brazing has the desired properties at a fraction of the cost, therefore making it a cost-effective solution and an alternative to billet tools.

Selecting the correct braze is crucial, factors such as chemical composition of the substrate and in our case the material to be cast (aluminium) have to be considered. Additional considerations are distortion, wear and heat treatment of a laminate structure. The rationale behind selecting a brazing alloy was based on the hardening curve of H13. H13 is heat-treated between 995°C – 1025°C with quenching in still air, inert gas or salt. Nickel brazing alloys have a melting temperature between 950°C – 1010°C (Sulzer Metco 1998). This potentially enables bonding at the same stage as heat treatment eliminating a process.

Nickel chromium brazes termed as "super alloys" have been developed for high temperature service and are suitable for use under moderate to high loading in the temperature range from 540°C to 1100°C. Nickel brazes have been used in the aerospace industry for the construction of gas turbine engines and hot airframe components. (Schwartz 1990).

Heat resistant alloys generally are brazed in a hydrogen environment or high vacuum furnaces with nickel base or special filler metals. Most brazing processes may be used on Nickel and high Nickel alloys. The most common are torch, furnace, induction and resistance brazing.

Nickel braze alloys were supplied by Sulzer Metco (UK) Ltd, The brazes (table1) have been selected as they have good corrosion resistance, bond strength, oxidation resistance and excellent machinability.

Nickel brazes, braze at high temperatures and the effect on the base metal should be taken into account. Non heat treatable alloys will suffer moderate strength losses due to grain growth during brazing. (Schwartz 1990).

By employing a humped back hydrogen belt furnace at 1000°C it is possible to bond and heat-treat multiple layers of H13 tool steel.

In order to obtain good braze coverage and uniform thickness it is important to select a suitable method of depositing it on the base material. For the purpose of laminate tooling it is necessary to control the braze thickness in order to maintain the tools tolerance. This may be achieved by tape, spray or paste where a known deposit thickness is applied to the base material prior to brazing. It is possible to automate spray or paste forms, improving process control and consequently the tool tolerance is maintained.

Surface preparation is crucial to achieving a good bond; base materials require oxide layers and grease removing which can be achieved by machining, pickling and de-greasing.

Gravity Die-Casting Tool

De Montfort University and Warwick University have developed a simple brazed laminate tool for aluminium gravity die casting, to evaluate erosion, chemical attack, heat checking, de-lamination etc.

The tool was constructed from, cold rolled H13 sheet which was laser cut, de-burred and brazed with Amdry 936 supplied by Sulzer Metco and machined to remove stepping.

The die produced 2,000 components with out failure. Although the die was simple and under no external forces (die open/close) it proved that the composite material could tolerate the aggressive environment. In addition it produced a significant number of components making the process suitable for short run production tooling.

The next stage was to produce a larger more complex tool both bonded and un-bonded for aluminium gravity die-casting. A production brake master cylinder provided by TRW was the chosen component (Figure 3).

The tools were produced in the same manner, as before however, consideration for clamping and laminate orientation of the un-bonded tool had to be considered. Due to the components profile one insert was produced horizontally and the other vertically (figure 4 & 8).

Machining the un-bonded inserts caused the laminates to burr and several de-burring operations were carried out in order to

maintain tolerance. To overcome this extra clamping was required (or high speed machining could have been employed), as the cutting forces could have been reduced.

Pressure Die-Casting Tool

The pressure die-casting process has more issues to address than that of gravity die casting. It works at much higher pressures and clamping forces up to 3000 tonnes are required to insure the mould remains closed, it has a 3 stage injection cycle, faster cycle times which means the die has a rapid heating and cooling, and channels have to be integrated into the die.

The majority of wear on a pressure die casting tool occurs in the gating system (where the biscuit is formed. This is due to the molten aluminium being forced into the runner system and rapidly changing direction by 90°. This is followed by pressure as the die continues to fill and solidify.

Horizontal and vertical bonded laminated Inserts were produced for a production tool (Figure 5). These were designed to incorporate conformal and traditional cooling channels. The benefits of conformal channels are that a designer is able to place cooling or heating where it is needed within a die. This is only feasible by producing a tool in a layer by layer approach.

A direct comparison between the bonded laminate inserts and the solid H13 inserts can be made. The test was designed to enable an evaluation of wear rates, thermal fatigue, failure mode, life expectancy and observe all the cycle times with conformal cooling and traditional cooling (Figure 6 & 7).

Sintered inserts produced via selective laser sintering were also chosen as an alternative solution for incorporating conformal cooling.

The next stage will be to produce a traditional, bonded / un-bonded laminate pressure die casting tool to evaluate its merit as an alternative method of producing prototype / production tooling for the die casting industry.

This tool will be designed to allow comparisons to be made between the bonded, un-bonded and the production tool e.g. address performance characteristics of horizontal vs. vertical laminate orientations, costing, time to market profiles and die life comparisons.

It has been decided to use electro discharge machining (EDM) to remove any stepping and finish the tool due to the deep cavities on both sides of the die. EDM was chosen to determine whether it was a suitable finishing process for bonded and un-bonded structures i.e. would the braze wear faster than the H13 tool steel, how would the electrodes wear, what finish was achievable, etc. The EDM tooling are to be produced via electroplated SLA and EOS rapid prototyping methods.

The stereolithography process (SLA) employs a laser, which scans an image on the surface of a vat of UV curable resin. A thin layer of liquid resin becomes solid and the cross section is lowered and the next layer scanned on to the resin. The layering process continues until the part is built.

The metal sintering machine (EOS) is a similar process in that a laser sinters a layer of metal powder the bed drops and the process repeats itself until the part is built.

Summary

Many of the tools discussed are beginning trials in industrial environments.

The research to date is primarily associated with the manufacture of a laminate tool for the die casting industry.

Un-bonded laminate tools are able to withstand the pressure die casting environment, however, it is not always possible to place clamping bolts where required due to component geometry. This causes uneven clamping pressures with associated distortion. It is also important at the design stage to select the correct laminate orientation in order to prevent un-clampable island/features.

Finishing via high speed machining can cause lifting and burring of laminates. Causing the tool to be disassembled and rebuilt increasing time and costs. Hence, EDM is the preferred finishing technique.

Bonded tools eliminate the problems associated with an un-bonded die i.e. uneven clamping, burring, leaks from cooling channels etc.

Heat treatment can also be conducted without the risk of laminates distorting. The brazing process is conducted at 1020°C, H13 Hardening temperature this is then tempered to 43HRC.

Initial problems arose when machining the brazed laminate structure, laminates would peel off due to lack of wetting. An increased soak time at the brazing stage reduced this problem. However, EDM was employed to prevent this recurring.

Our initial trials of the bonded gravity tool have proved promising with the brazed structure withstanding the temperature (730°C) involved with aluminium (LM24) gravity die-casting. The tool has shown no signs of erosion heat checking/fatigue or delamination to date.

It is envisaged that laminate tooling could be employed as a method of manufacturing prototype tooling to validate die design for the die casting industry. In addition it could be considered for short run tooling.

Further Industrial trials are to be conducted in order to validate the dies failure mode, life expectancy, effects of conformal cooling etc.

References

- Bryden B.G., (1999) Sequential Laminated tooling, joined by brazing for injection moulding, *Rapid Prototyping Journal*, Volume 5, Number 2, 1999, Pages 89 – 93, ISSN 1355-2546
- Dickens, P.M., (1996) Laminated Tooling for Moulding Polyurethane Parts, *Proceedings from the SME Rapid Prototyping and Manufacturing Conference*, Dearborn, Michigan, April 22-25, 1996
- Dickens P.M, (1999) Rapid Prototyping – Past, Present & Future, *Journal of The Institute of Engineering Designers*, January 1999, Pages 12-15
- Glozer G.R. (1992) Laminate Tooling for Injection Moulding, *Proceedings of the Institute of Mechanical Engineers*, Volume 207, Part No. B1, December 1992, Pages 9-15
- Halford B. (1999), *Rapid Tooling*, *Journal of the Institute of Engineering Designers*, May 1999, Pages 4-6
- Himmer T. (1999), *Lamination of Metal Sheets*, *Computers in Industry*, Volume 39, 1999, Pages 27-33
- Obikawa T. (1999), *Sheet Steel Lamination for Rapid Manufacturing*, *Journal of Materials Processing Technology*, Volume 89-90, 1999, Pages 171-176
- Schwartz, M. M. (1999), *American Society for Metals (ASM) International, Brazing*, November 1990, ISBN 0-87170-246-0
- Soar, R.C; Dickens P. (1998a), *Rapid Prototyping Opportunities: Laminated Tooling for Aluminium Die Casting*, *Proceedings from the Aluminium 98 Conference*, Messe Essen, Germany, 23-24 September 1998
- Soar, R.C; Dickens P. (1998b), *Proceedings from the Time Compression Technologies Conference, The Use of Laminated Tooling for the Production of Prototype Pressure Die-Cast Dies*, October 1998, Pages 331-340
- Soar, R.C. (2000), *An Examination of the Feasibility and design Limitations of Laminate Tooling for Pressure Die Casting*, PhD, De-Montfort University, 2000
- Sulzer Metco (UK) Ltd, (1998) Westmead, GB-Farnborough, Hants, GU14 7LP, Braze Products, July 1998
- Yokoi H. (1994), *Manufacture of Blanking Tool and its Die-Set by Laminate Laser-Cut Steel Sheets*, *Proceedings of the 12th North American Manufacturing Research Conference (NAMRC)*, Univ. of Florida Hotel and Conference Center Gainesville, Florida 1984, Pages 372-378
- Walczyk D.F. (1994), *A New Rapid Tooling Method For Sheet Metal Forming Dies*, *Proceedings of the 4th International Conference for Rapid Prototyping*, 1994, Pages 275-289
- Walczyk D.F. (1998), *Rapid Tooling for Sheet Metal Forming Using Profiled Edge Laminations – Design Principles and demonstration.*, *Transactions of the ASME*, Volume 120, November 1998, Pages 746-754

FIGURES

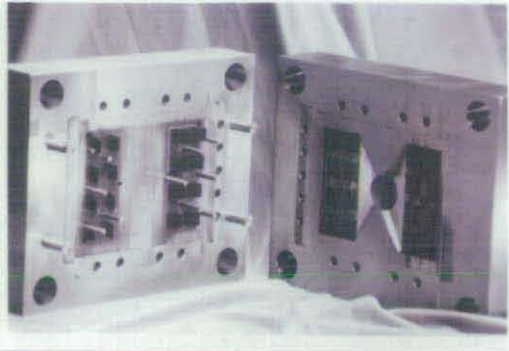


Figure 1 Laminate Die-casting Tool, Courtesy of Dr Rupert Soar (Soar 2000)

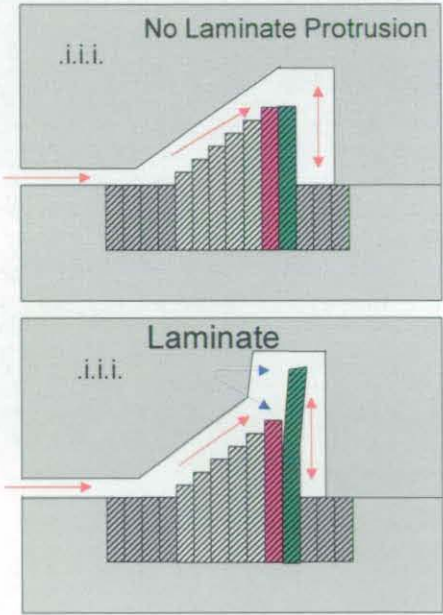


Figure 2 Schematic showing potential movement of laminates in a die (Soar 2000)

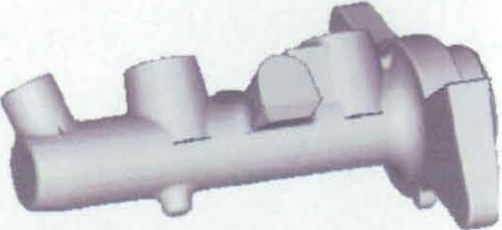


Figure 3 TRW Brake Master Cylinder (187mm in length)



Figure 4 Pre Machined Inserts



Figure 5 Pre Machined Bonded Horizontal and Vertical Inserts

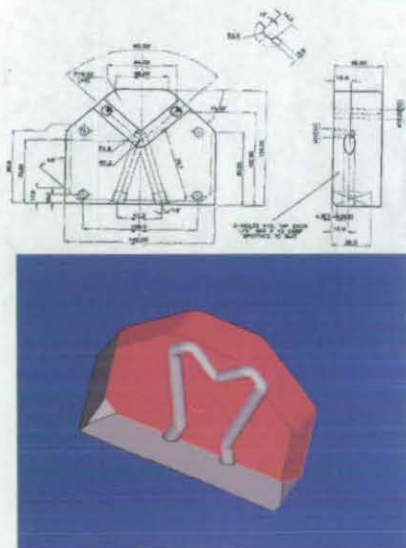


Figure 6 Traditional and Conformal Cooling Channels Designs for Inserts

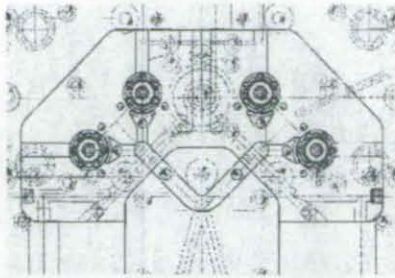


Figure 7 Schematic of the Die Showing the Insert location



Figure 8 Analysis Data

Un-bonded Brake Master Cylinder Gravity Die Cast Bolster and Inserts

Tables

Braze	Alloying elements						
	Ni	RE	Cu	Cr	B	Mn	Si
Amdry 936	Bal.	0.03	4		1	19	6
Amdry 775	Bal.			15	3.5		
Amdry 780	Bal.				3		4.5
Amdry 100	Bal.			19			10
Amdry 790	Bal.				2		3.5

Table 1 Nickel based brazes supplied by Sulzer Metco

